

# INDIAN JOURNAL OF PHYSICS

VOL. 36

AND

## PROCEEDINGS

OF THE

Indian Association for the Cultivation of Science, Vol. 44

*(Published in Collaboration with the Indian Physical Society)*

( With Ten Plates )

Printed by Kalipada Mukherjee, Eka Press, 204/1, B. T. Road, Calcutta  
and published by the Registrar, Indian Association for the Cultivation  
of Science, Jadavpur, Calcutta 32

**1962**

## BOARD OF EDITORS

K. BANERJEE	D. S. KOTNARI
D. M. BOSE	S. K. MITRA
S. N. BOSE	B. D. NAG CHAUDHURI
S. D. CHATTERJEE	K. R. RAO
P. S. GILL	D. B. SINHA
S. R. KHASTGIR	S. C. SIKKAR ( <i>Secretary</i> )
B. N. SRIVASTAVA	

## EDITORIAL COLLABORATORS

PROF. R. K. ASUNDI, Ph.D., F.N.I.
PROF. D. BASU, Ph.D.
PROF. J. N. BHAR, D.Sc., F.N.I.
PROF. V. G. BHIDE, Ph.D. (Nag), Ph.D. (Lond).
PROF. A. BOSE, D.Sc., F.N.I.
PROF. S. K. CHAKRABARTY, D.Sc., F.N.I.
DR. J. S. CHATTERJEE
DR. K. DAS GUPTA, Ph.D.
PROF. N. N. DAS GUPTA, Ph.D., F.N.I.
DR. J. DHAR, D.Phil. (So)
PROF. A. K. DUTTA, D.Sc., F.N.I.
PROF. C. S. GHOSH, M.Sc., S.M., F.N.I., M.I.E.E.

PROF. S. GHOSH, D.Sc., F.N.I.
PROF. S. N. GHOSH, D.Sc.
PROF. S. GUPTA, M.Sc., F.N.I.
PROF. D. N. KUNDU, Ph.D., F.N.I.
PROF. R. C. MAJUMDER, Ph.D., F.N.I.
PRINCIPAL Y. G. NAIK, Ph.D.
PROF. S. R. PALIT, D.Sc., F.R.I.C., F.N.I.
PROF. H. RAKSHIT, D.Sc., F.N.I.
PROF. A. SAHA, D.Sc., F.N.I.
DR. VIKRAM A. SARABHAI, M.A., Ph.D., F.N.I.
DR. A. K. SENGUPTA, D.Sc.
PROF. NAND LAL SINGH, D.Sc.
DR. M. S. SINHA, D.Sc., F.N.I.
PROF. N. R. TAWDE, Ph.D., F.N.I.
DR. P. VENKATESWARLU

## NOTICE

### TO INTENDING AUTHORS

Manuscripts for publication should be sent to the Assistant Editor, Indian Journal of Physics, Jadavpur, Calcutta-32.

The manuscripts submitted must be type-written with double space on thick foolscap paper with sufficient margin on the left and at the top. The original copy, and not the carbon copy, should be submitted. Each paper must contain an abstract at the beginning.

All references should be given in the text by quoting the surname of the author, followed by year of publication, e.g., (Ghosh, 1954). The full reference should be given in a list at the end, arranged alphabetically, as follows; Ghosh, D. K., 1954, *Ind. J. Phys.*, 28, 485.

Line diagrams should be drawn on white Bristol board or tracing paper with black India ink, and letters and numbers inside the diagrams should be written neatly in capital type with India ink. The size of the diagrams submitted and the lettering inside should be large enough so that it is legible after reduction to one-third the original size. A simple style of lettering such as gothic, with its uniform line width and no serifs should be used, e.g.,

A·B·E·F·G·M·P·T·W·

Photographs submitted for publication should be printed on glossy paper with somewhat more contrast than that desired in the reproduction, and should, if possible, be mounted on thick white paper.

Captions to all figures should be typed in a separate sheet and attached at the end of the paper.

The mathematical expressions should be written carefully by hand. Care should be taken to distinguish between capital and small letters and superscripts and subscripts. Repetition of a complex expression should be avoided by representing it by a symbol. Green letters and unusual symbols should be identified in the margin. Fractional exponents should be used instead of root signs.

*Annual Subscription—*

Inland Rs. 25.00

Foreign £ 2-10-0 or \$ 7.00



# INDIAN JOURNAL OF PHYSICS VOL. 36, 1962

## CONTENTS

### No. 1. January

	PAGE
1. On the Minimisation of Boolean Functions—A. K. Choudhury and M. S. Basu . . . . .	1
2. Various Approximations for the Isotopic Thermal Diffusion Factor. II. Application to Hydrogen Isotopes—S. C. Saxena and P. A. Pardeshi . . . . .	13
3. Efficacy of the Parabolic Interpolation Technique in the Derivation of Molecular Constants—N. R. Pawde, N. Sreedhara Murthy and (Miss) Sharada Hedge . . . . .	25
4. A Note on the Calculation of the Density of States—T. C. Roy . . . . .	29
5. On Detection of Group Invariance or Total Symmetry of a Boolean Function—A. K. Choudhury and M. S. Basu . . . . .	31
6. Lattice Expansion and Debye Temperature of $\alpha$ -Phase AgCd Alloys—Md. A. Quader and B. N. Dey . . . . .	43

#### LETTERS TO THE EDITOR

1. A Peculiar Phenomenon in the Electrolysis of a Flowing System—Santi R. Palit . . . . .	55
---	----

### No. 2. February

7. Raman and Infrared Spectra of some Fluorinated Toluenes in Different States—K. K. Deb . . . . .	59
8. Capture Rates of Negative Muons by Nuclei—Prakash Chand and B. K. Agarwal . . . . .	71
9. Dislocation Damping in $\alpha$ -AgCd Alloy—Md. Abdul Quader . . . . .	71
10. The Emission Band Spectra of SbF and BiF—T. A. Prasada Rao and P. Tiruvenganna Rao . . . . .	85
11. A Triple Coincidence Proton Scintillation Spectrometer—R. K. Mohindra and H. S. Hans . . . . .	93
12. On the Validity of the Revised Rotational Constants ( $C \rightarrow X$ ) Band System of ZrO—N. Sreedhara Murthy . . . . .	101

#### LETTERS TO THE EDITOR

2. Ejection of a $\text{Li}^0$ -‘Hammer’ Track—G. C. Deka and K. M. Pathak . . . . .	105
3. Symmetry of the Crystalline Electric Field on $\text{Yb}^{1+}$ -Ion in $\text{Yb}_2(\text{SO}_4)_3 \cdot 8\text{H}_2\text{O}$ Crystal—A. Mookherjee and D. Neogy . . . . .	107

**No. 3. March**

	PAGE
13. Asymmetric Shape Effects in Dia- and Paramagnetic Crystals—Manju Majumdar . . . . .	111
14. Vertical Transport of Electrons During Pre-Sunrise F-Layer "Splitting"—P. Bandyopadhyay and S. K. Chatterjee . . . . .	124
15. Number of $N_2^+$ , $N^+$ , $N^{++}$ and $O_2^+$ , $O^+$ , $O^{++}$ Ions Produced by Solar Protons in the Earth's Atmosphere—S. N. Ghosh and B. N. Srivastava . . . . .	129
16. Fluxmeter Studies of Slow Electric Field-Changes Due to Moving Thunder clouds—S. R. Khastgi and R. S. Srivastava . . . . .	137
17. Influence of Ultraviolet Absorption Frequencies on the Intensities of Raman Lines—A. K. Chakravorty . . . . .	151
18. On the Influence of Different Solvents on the Singlet→Triplet Absorption in some Halogenated Toluenes—J. K. Roy . . . . .	156
19. Influence of Solvents on Hydrogen Bonding in Ortho- and Para-nitrophenol—S. B. Banerjee and G. S. Kastha . . . . .	163

**No. 4 April**

20. Characteristics of the Ion-Source of the Calcutta 37-Inch Cyclotron—P. K. Dutt, A. P. Patro, B. Basu and A. Chatterjee . . . . .	169
21. On the Evaluation of $\alpha_c$ and $\alpha_c v_c$ from Three Constant Potential Energy Functions—M. R. Katti . . . . .	180
22. Scattering of Positrons by Six-Fold Ionized Uranium—Bhajan Singh and Brojendra K. Ghia . . . . .	189
23. Mutual Diffusion of Binary Mixtures of Ammonia with He, Ne and Xe—I. B. Srivastava . . . . .	193
24. Nonlinearity of Thermal Expansion of Solids with Temperature—G. B. Mitra and S. K. Mitra . . . . .	200

LETTERS TO THE EDITOR

4. Ultraviolet Absorption of $NO_2$ Ion—A. Mookherji and S. P. Tandon . . . . .	211
5. The New Ultraviolet Absorption Spectrum of Para-Fluorotolubenzene—Achuta Rao, Iyyanki . . . . .	213

**No. 5. May**

25. Magnetic Studies on $Co^{++}$ Ion in Pink and Blue Solution of $CoCl_2$ —T. Mookherji . . . . .	215
26. Certain Operational Characteristics for C.E.C. 21-103C Mass Spectrometer Using Boron Trifluoride—K. N. Bhide and S. C. Saxena . . . . .	224
27. Solar and Terrestrial Relationships of Daily Variation of Cosmic Rays During the I.G. Y—R. P. Kane . . . . .	237

# Contents

iii

## No. 6. June

	PAGE
28. Low Energy Scattering of Electron by Variational Method—S. C. Mukherjee and N. C. Sil . . . . .	283
29. On the Raman and Infrared Spectra of 1, 4-Dichlorobutane and Propionyl Chloride in Different States—K. K. Deb . . . . .	290
30. Electronic Spectra of $\beta$ -Chloronaphthalene in different States—T. N. Misra . . . . .	302
31. Maximum Superheat of Binary Liquid Mixtures—A. K. Jahiduddin and D. B. Sinha . . . . .	312
32. On Classification of Switching Functions Part I—A. K. Choudhury and M. S. Basu . . . . .	317
33. Internal Friction in Au-Ni Alloy—M. A. Quader . . . . .	330

## No. 7. July

34. Construction and Working Principles of the Banerjee Camera for Studying Small Angle Scattering of X-Rays—G. B. Mitra and J. C. Maity . . . . .	335
35. Light Absorption in $\text{NO}_2$ Ion in State of Solution Part I—300m $\mu$ Band—A. Mukherji and S. P. Tandon . . . . .	344
36. Helmholtz Instability in Hydromagnetics—S. P. Talwar . . . . .	351
37. On the Determination of Activation Energy of Diffusion through Dislocations—A. L. Laskar . . . . .	359
38. Grid Control of Gas-Tube Noise—K. K. Bose and P. L. Dasgupta . . . . .	364
39. A Twin-Tuned R-C Network—S. C. Dutta Roy . . . . .	369
BOOK REVIEWS . . . . .	379

## No. 8 August

40. On Classification of Switching Functions Part II—A. K. Choudhury and M. S. Basu . . . . .	383
41. Elastic Scattering of Fast Protons by Deformed Nucleus—S. K. Dutta and N. C. Sil . . . . .	408
42. Intensity of Fluorescence of Dye-stuffs in Solution—Jugal Kishore, M. K. Machwe, K. Gopala Krishnan and K. D. Chaudhuri . . . . .	415
43. Mossbauer Scattering of Low Energy Gamma-Rays—B. S. Sood . . . . .	419
44. Second Virial and Zero Pressure Joule-Thomson Coefficients of Non-polar Quasi-Spherical Molecules—S. C. Saxena and K. M. Joshi . . . . .	422

### LETTERS TO THE EDITOR—

6. Effect of Surface Recombination Velocity on Carrier Lifetime for Cylindrical Geometry—P. Das . . . . .	431
7. A Composite Modulator for Compatible Single Sideband—N. B. Chakrabarti . . . . .	435
BOOK REVIEWS . . . . .	436

**No. 9. September**

	PAGE
45. Indirect Spin Coupling in Magnetic Garnets—K. P. Sinha and M. K. Sinha .. .. .	439
46. Infrared Study of Hydrogen Bonding in Isomeric Toluidines in Different Environments—K. C. Medhi, S. B. Banerjee and G. S. Kastha .. .. .	457
47. Multicomponent Diffusion in the Systems $^{85}\text{Kr}-\text{Ne}-\text{Kr}$ and $^{85}\text{Kr}-\text{A}-\text{Kr}$ —Ranjit Paul .. .. .	464
48. A Method of Determining the Terminal Impedances and Transfer Function of General Multimesh Ladder Networks Containing two kinds of Elements only—S. C. Dutta Roy .. .. .	469
49. A Natural Occurrence of Beta form of Iron Oxy hydroxide—K. C. Chandy .. .. .	484
50. The Correlation of Spread on one Night and the Successive Nights—M. S. V. Gopal Rao and B. Ramachandra Rao .. .. .	490

LETTER TO THE EDITOR—

8. Unit Cell and Space Group of Thiodiglycolic Acid—Sukla Roy ..	493
BOOK REVIEW .. .. .	495

**No. 10. October**

51. Periodicity and Structural Development in Nuclei—A. K. Dutta, B. Pal, A. Das Gupta and N. Choudhury .. .. .	497
52. Luminescence Spectra of 2,4-Dichloro- and 3,4-Dichlorotoluene in the Solid State at $-180^\circ\text{C}$ —J. K. Roy .. .. .	507
53. $\text{F}^{19}$ Free Induction Decay in Polycrystalline $\text{MgF}_2$ —S. K. Sinha, S. K. Ghosh, J. Lahiri and A. Roychoudhury .. .. .	513
54. On Adaptation of the Grouping Chart and Simplification of Multiple output Switching Functions—A. K. Choudhury, M. S. Basu and Sunil Ranjan Das .. .. .	521
55. On the Absorption of 3.18-cm Microwaves in Aniline and Substituted Anilines—T. J. Bhattacharyya .. .. .	533

LETTERS TO THE EDITOR

9. A General Method of Finding the Principal Crystalline Susceptibilities of Triclinic Crystals—U. S. Ghosh and R. N. Bagchi .. .. .	538
10. Election Temperature in Air Under Low Frequency Electric Discharges Exerted by External Sleeve Electrodes—D. P. Jatar and K. R. Chandrakar .. .. .	541
11. The Infrared Spectrum of Cyclohexyl Benzene—R. N. Bapat .. .. .	543
BOOK REVIEWS .. .. .	545

No. 11. November

	PAGE
56. Response Function of a Degenerate Electron Gas—P. Misra and D. Misra .. .. .	549
57. Raman and Infrared Spectra of Isoquinoline, $\alpha$ -Fluoro- and $\alpha$ -Chloro-naphthalene in Different States—Krishna Kumar Deb .. .. .	557
58. Linear Polarization of $5.12mc^2$ Gamma Rays Rayleigh Scattered from K-Electrons in Mercury—B. S. Sood .. .. .	569
59. Electron Capture by Alpha-Particle Passing Through Helium Atom—S. C. Mukherjee and N. C. Sil .. .. .	573
60. Ultrasonic Velocity in Liquid Binary Mixtures—M. V. Kaulgud .. .. .	577
61. Some Peculiarities in Current Conduction during Electrolysis of a Flowing Electrolyte—Santi R. Palit .. .. .	586
62. The Total Cross-Sections for the Nuclear Scattering of High Energy Nucleons—G. Z. Shah and B. M. Thaker .. .. .	595

LETTERS TO THE EDITOR—

12. A Short Note on the Magnetic Anisotropy and Susceptibility of $Cu^{2+}$ Ion—R. Chatterjee and U. S. Ghosh .. .. .	600
13. Preliminary X-Ray Study of Crystal Structure of Cedrelone—B. Chaudhury, I. M. Das and A. N. Talukdar .. .. .	602
14. A Note on Kihara's Theory of Radiofrequency Discharge—S. N. Sen and A. K. Ghosh .. .. .	605

No. 12. December

63. The Spectrum of CoBr in the Visible ( $\lambda 1300$ - $\lambda 4700 \text{ \AA}$ )—S. V. Krishna Rao and P. Tiruvenganna Rao .. .. .	609
64. Ultrasonic Studies in Aqueous Solutions of Electrolytes—M. G. Seshagiri Rao and B. Ramachandra Rao .. .. .	613
65. Resonance in Electron Capture by Proton Passing through Hydrogen Atoms—S. C. Mukherjee and N. C. Sil .. .. .	622
66. Intensity Measurement in Bands and Rotational Temperature—N. R. Tawde and M. I. Savadatti .. .. .	630
67. Elastic Scattering of Fast Protons by Spheroidal Nuclear Potential with Diffuse Boundary—S. K. Dutta and N. C. Sil .. .. .	633
68. On the Relation between Dissociation Energy and Molecular Constants—B. B. Laud .. .. .	639
69. The Crystal Structure of 3,5-Dibromo Para-Amino Benzoic Acid—A. K. Pant .. .. .	650

	PAGE
LETTERS TO THE EDITOR—	
15. The Crystal Structure of 1,8-Dihydroxy Anthraquinone—Anand Prakash .. . . .	654
16. Study of Silver Fulminate by X-Ray Diffraction—S. N. Pandey ..	657
17. A Short Note on the Nature of the Crystalline Electric Field in Triva- lent Vanadium Alum—R. Chatterjee .. . . .	660
BOOK REVIEW .. . . .	662

# AUTHOR INDEX

AUTHOR	SUBJECT	PAGE
Agarwal, B. K.	See Chand, Prakash	
Bagchi, R. N.	See Ghosh, U. S.	
Bandyopadhyay, P. and Chatterjee, S. K.	Vertical transport of electrons during pre-sunrise F-layers 'Splitting'	124
Banerjee, S. B.	See Medhi, K. C.	
Banerjee, S. B. and Kastha, G. S.	Influence of solvents on hydro- gen bonding in ortho- and paranitrophenol	163
Bapat, R. N.	The infrared spectrum of cyclohexyl benzene (L)	543
Basu, B.	See Dutta, P. K.	
Basu, M. S.	See Choudhury, A. K.	
Bhattacharyya, T. J.	On the absorption of 3.18 -cm mi- crowaves in aniline and subs- tituted anilines	533
Blide, K. N. and Saxena, S. C.	Certain operational characteristics for C E C-21-103C mass spectrometer using boron tri- fluoride	224
Bose, K. K. and Dasgupta, P. L.	Grid control of gas-tube noise	364
Chakrabarti, N. B.	A composite modulator for compa- tible single sideband (L)	435
Chakravorty, A. K.	Influence of ultraviolet absorption frequencies on the intensities of Raman lines	151
Chand, Prakash and Agarwal, B. K.	Capture rates of negative muons by nuclei	71
Chandrakar, K. R.	See Jatar, D. P.	
Chandy, K. C.	A natural occurrence of beta form of iron oxyhydroxide	484
Chatterjee, R.	A short note on the nature of crys- talline electric field in trivalent vanadium alum (L)	660
Chatterjee, R. and Ghosh, U. S.	A short note on the magnetic aniso- tropy and susceptibility of $\text{Cu}^{2+}$ ion (L)	600
Chatterjee, S. K.	See Bandyopadhyay, P.	

AUTHOR	SUBJECT	PAGE
Choudhury, A. K. and Basu, M. S.	On the minimisation of Boolean functions	1
	On detection of group invariance or total symmetry of a Boolean function	31
	On classification of switching functions. Part I	317
	On classification of switching functions. Part II	383
Choudhury, A. K., Basu, M. S. and Das, Sumit Ranjan	On adaptation of the grouping chart and simplification of multiple output switching functions	521
Chaudhury, B., Das, I. M. and Talukdar, A. N.	Preliminary X-ray study of crystal structure of cedrelone (L)	602
Chaudhuri, K. D.	See Kishore, Jugal	
Chaudhury, N.	See Dutta, A. K.	
Das, I. M.	See Chaudhury, B.	
Das, P.	Effect of surface recombination velocity on carrier lifetime for cylindrical geometry (L)	431
Das, Sumit Ranjan	See Choudhury, A. K.	
Dasgupta, P. L.	See Bose, K. K.	
Das Gupta, B.	See Dutta, A. K.	
Deb, K. K.	Raman and infrared spectra of some fluorinated toluenes in different states	59
	On the Raman and infrared spectra of 1, 4-dichlorobutane and propionyl chloride in different states	290
	Raman and infrared spectra of isoquinoline, $\alpha$ -fluoro and $\alpha$ -chloronaphthalene in different states	557
Deka, G. C. and Pathak, K. M.	Ejection of a $\text{Li}^0$ 'Hammer' track (L)	105
Dey, B. N.	See Quader, Md.A.	
Dutta, A. K., Pal, B., Das Gupta, A. and Chaudhury, N.	Periodicity and structural development in nuclei	497
Dutta, S. K. and Sil, N. C.	Elastic scattering of fast protons by deformed nucleus	408
	Elastic scattering of fast protons by spheroidal nuclear potential with diffuse boundary	633



# Author Index

ix

AUTHOR	SUBJECT	PAGE
Dutt, P. K., Patro, A. P., Basu, B. and Chatterjee, A. Dutta Roy, S. C.	Characteristics of the ion-source of the Calcutta 37-inch cyclotron A twin-tuned R-C network A method of determining the ter- minal impedances and transfer function of general multimesh ladder networks containing two kinds of elements only	169 369 469
Ghosh, A. K.	See Sen, S. N.	
Ghosh, S. K.	See Sinha, S. K.	
Ghosh, S. N. and Srivastava, B. N.	Number of $N_2^+$ , $N^+$ , $N^{++}$ and $O_2^+$ , $O^+$ , $O^{++}$ ions produced by solar protons in the earth's atmos- phere	129
Ghosh, U. S.	See Chatterjee, R.	
Ghosh, U. S. and Bagchi, R. N.	A general method of finding the principal crystalline suscepti- bilities of triclinic crystals (L)	538
Guha, Brojendra K.	See Singh, Bhajan	
Hans, H. S.	See Mohindra, R. K.	
Hogde, (Miss) Sharada	See Tawde, N. R.	
Iyyanki, Achuta Rao	The near ultraviolet absorption spectrum of para-fluoronitro- benzene (L)	213
Jalaluddin, A. K. and Sinha, D. B.	Maximum superheat of binary liquid mixture	312
Jatar, D. P. and Chandrakar, K. R.	Electron temperature in air under low frequency electric dis- charges excited by external sleeve electrodes (I)	541
Joshi, K. M.	See Saxena, S. C.	
Kane, R. P.	Solar and terrestrial relationships of daily variation of cosmic rays during the I.G.Y.	237
Kastha, G. S.	See Banerjee S. B. ; Medhi, K. C.	
Katti, M. R.	On the evaluation of $\alpha_e$ and $w_e x_e$ from three constant potential energy functions	180
Kaulgud, M. V.	Ultrasonic velocity in liquid binary mixtures	577
Khastgir, S. R. and Srivastava, R. S.	Fluxmeter studies of slow electric field-changes due to moving thunder clouds	137

AUTHOR	SUBJECT	PAGE
Kishore, Jugal, Machwe, M. K., Krishnan, Gopala, K. and Chaudhuri, K. D.	Intensity of fluorescence of dyestuffs in solutions	415
Krishnan, Gopala K.	See Kishore, Jugal.	
Lahiri, J.	See Sinha, S. K.	
Laskar, A. L.	On the determination of activation energy of diffusion through dislocations	359
Laud, B. B.	On the relation between disso- ciation energy and molecular constants	639
Machwe, M. K.	See Kishore, Jugal	
Mazumdar, Manju	Asymmetric shape effects in dia- and paramagnetic crystals	11
Maitra, J. C.	See Mitra, G. B.	
Medhi, K. C., Banerjee, S. B. and Kastha, G. S.	Infrared study of hydrogen bond- ing in isomeric toluidines in different environments	457
Misra, D.	See Misra, P.	
Misra, P. and Misra, D.	Response function of degenerate electrons gas	549
Misra, T. N.	Electronic spectra of $\beta$ -chlorona- phthalene in different states	302
Mitra, G. B. and Mitra, S. K.	Nonlinearity of thermal expansion of solids with temperature	200
Mitra, G. B. and Maitra, J. C.	Construction and working prin- ciples of the Banerjee camera for studying small angle scatter- ing of X-rays	335
Mitra, S. K.	See Mitra, G. B.	
Mohindra, R. K. and Hans, H. S.	A triple coincidence proton scintil- lation spectrometer	93
Mookherjee, A. and Neogy, D.	Symmetry of the crystalline elec- tric field on $\text{Yb}^{+++}$ ion in $\text{Yb}_2(\text{SO}_4)_3 \cdot 8\text{H}_2\text{O}$ crystal (L)	107
Mookherji, A. and Tandon, S. P.	Light absorption in $\text{NO}_3$ ions in state of solutions Part I -- 300m $\mu$ band	344
	Ultraviolet absorption of $\text{NO}_2$ ion (L)	211
Mookherji, T.	Magnetic studies on $\text{Co}^{+}$ ion in pink and blue solution of $\text{CoCl}_2$	215

AUTHOR	SUBJECT	PAGE
Mukherjee, S. C. and Sil, N. C.	Low energy scattering of electrons by variational method	283
	Electron capture by alpha-particle passing through helium atom	573
	Resonance in electron capture by proton passing through hydro- gen atoms	622
Neogy, D.	See Mookherjee, A.	
Pal, B.	See Dutta, A. K.	
Palit, Santi R.	A peculiar phenomenon in the elec- trolysis of a flowing system (L)	55
	Some peculiarities in current con- duction during electrolysis of a flowing electrolyte	586
Pandey, S. N.	Study of silver fulminate by X-ray diffraction (L)	657
Pant, A. K.	The crystal structure of 3,5-dibro- mo para-amino benzoic acid	650
Pardeshi, P. A.	See Saxena, S. C.	
Pathak, K. M.	See Deka, G. C.	
Patro, A. P.	See Dutt, P. K.	
Paul, Ranjit	Multicomponent diffusion in the systems <sup>86</sup> Kr-Ne-Kr and <sup>86</sup> Kr- Ar-Kr	464
Prakash, Anand	The crystal structure of 1,8-dihy- droxy anthraquinone (L)	654
Quader, M. Abdul	Dislocation damping in $\alpha$ -AgCd alloy	77
	Internal friction in Au-Ni alloy	330
Quader, M. D. and Dey, B. N.	Lattice expansion and Debye tem- perature of $\alpha$ -phase AgCd alloys	43
Rao, Gopal V. and Rao, Ramachandra B.	The correlation of spread on one night and the successive nights	490
Rao, Krishna, S. V. and Rao, Tiruvenganna P.	The spectrum of CoBr in the visible ( $\lambda$ 4300- $\lambda$ 4700Å)	609
Rao, Prasada, T. A. and Rao, Tiruvenganna P.	The omission band spectra of SbF <sup>3</sup> and BiF <sup>3</sup>	85
Rao, Ramachandra, B.	See Rao, Gopal V. : also Rao, Seshagiri, M. G.	
Rao, Seshagiri, M. G. and Rao, Ramachandra, B.	Ultrasonic studies in aqueous solu- tions of electrolytes	613

AUTHOR	SUBJECT	PAGE
Rao, Tiruvenganna P	See Rao, Prasada, T. A. ; also Rao, Krishna, S. V.	
"          "          "		
Roy, J. K.	On the influence of different solvents on the singlet→triplet absorption in some halogenated toluenes	156
	Luminescence spectra of 2, 4-dichloro- and 3, 4-dichloro- toluene in the solid state at—180°C	507
Roy, Sukla	Unit cell and space group of thiodiglycolic acid (L)	493
Roy, T. C.	A note on the calculation of the density of states	29
Roychoudhury, A.	See Sinha, S. K.	
Savadatti, M. I.	See Tawde, N. R.	
Saxena, S. C.	See Bhide, K. N.	
Saxena, S. C. and Joshi, K. M.	Second virial and zero pressure Joule-Thomson coefficients of non-polar quasi-spherical molecules	422
Saxena, S. C. and Pardeshi, P. A.	Various approximations for the isotopic thermal diffusion factor. II. Application to hydrogen isotopes	13
Sen, S. N. and Ghosh, A. K.	A note on Kihara's theory of radio-frequency discharge (L)	605
Shah, C. Z. and Thaker, B. M.	The total cross-sections for the nuclear scattering of high energy nucleons	595
Sil, N. C.	See Dutta, S. K. ; Mukherjee, S. C.	
Singh, Bhajan and Guha, Brojendra K.	Scattering of positrons by six-fold ionised uranium	189
Sinha, D. B.	See Jalaluddin, A. K.	
Sinha, K. P. and Sinha, M. K.	Indirect spin coupling in magnetic garnets	439
Sinha, M. K.	See Sinha, K. P.	
Sinha, S. K., Ghosh, S. K., Lahiri, J. and Roychoudhury, A.	F <sup>19</sup> free induction decay in polycrystalline MgF <sub>2</sub>	513

AUTHOR	PAGE
Sood, B. S.	Mossbauer scattering of low energy gamma-rays 419
	Linear polarization of $5.12\text{mc}^2$ gamma rays Reyleigh scattered from $k$ -electrons in mercury 569
Sreedhara Murthy, N.	On the validity of the revised rota- tional constants $\alpha(\text{C} \rightarrow \text{X})$ band system of $\text{ZrO}$ 101
	Also see Tawde, N. R.
Srivastava, B. N.	See Ghosh, S. N.
Srivastava, I. B.	Mutual diffusion of binary mixtures of ammonia with He, Ne, and Xe 193
Srivastava, R. S.	See Khastgir, S. R.
Talukdar, A. N.	See Chaudhury, B.
Talwar, S. P.	Helmholts instability in hydro- magnetics 351
Tandon, S. P.	See Mookherji, A.
Tawde, N. R., Sreedhara Murthy, N. and Hegde, (Miss) Sharada	Efficacy of the parabolic interpolation technique in the derivation of mole- cular constants 25
Tawde, N. R. and Savadatti, M. I.	Intensity measurement in bands and rotational temperature 630
Thaker, B. M.	See Shah, C. Z.



# SUBJECT INDEX

SUBJECT	AUTHOR	PAGE
Absorption of 3.18 cm microwaves in aniline and substituted anilines. On the	T. J. Bhattacharyya	533
Activation energy of diffusion through dislocations. On the determination of	A. J. Laskar	359
Asymmetric shape effects in dia- and paramagnetic crystals	Manju Majumdar	111
Banerjee camera for studying small angle scattering of X-rays. Construction and working principles of the	G. B. Mitra and J. C. Maatra	335
Capture rates of negative muons by nuclei	Prakash Chand and B. K. Agarwal	71
Composite modulator for compatible single sideband. A (L)	N. B. Chakrabarti	435
Correlation of spread on one night and the successive nights. The	M. S. V. Gopal Rao and B. Ramachandra Rao	490
Crystal structure of 2, 8-dihydroxy anthraquinone. The (L)	Anand Prakash	654
Crystal structure of cedrelone. Preliminary X-ray studies of (L)	B. Choudhury, I. M. Das and A. N. Talukdar	602
Crystal structure of 3, 5-dibromo para-amino benzoic acid. The	A. K. Pant	650
Crystalline electric field on Yb <sup>+++</sup> ion in Yb <sub>2</sub> (SO <sub>4</sub> ) <sub>3</sub> · 8H <sub>2</sub> O crystal. Symmetry of the (L)	A. Mookherjee and D. Neogy	107
Current conduction during electrolysis of a flowing electrolyte. Some peculiarities in	Santi R. Palit	586
Daily variation of cosmic rays during the I.G.Y. Solar and terrestrial relationships of	R. P. Kane	237
Density of states. A note on the calculation of the	T. C. Roy	29
Dislocation damping in $\alpha$ -AgCd alloy	Md. Abdul Quader	77

SUBJECT	AUTHOR	PAGE
Elastic scattering of fast protons by spheroidal nuclear potential with diffuse boundary	S. K. Dutta and N. C. Sil	633
Elastic scattering of fast protons by deformed nucleus	S. K. Dutta and N. C. Sil	408
Electron capture by alpha-particle passing through helium atom	S. C. Mukherjee and N. C. Sil	573
Electron temperature in an under low frequency electric discharges excited by external sleeve electrodes (L)	D. P. Jatar and K. R. Chandrakar	541
Electrolysis of a flowing system. A peculiar phenomenon in the (L)	Santi R. Palit	55
Ejection of a $\text{Li}^9$ 'hammer' track (L)	G. C. Deka and K. M. Pathak	105
Evaluation of $\alpha_e$ and $w_e x_e$ from three constant potential energy function On the	M. R. Katti	180
$\text{F}^{19}$ free induction decay in polycrystalline $\text{MgF}_2$	S. K. Sinha, S. K. Ghosh, J. Lhhiri and A Roychoudhury	513
Grid control of gas-tube noise	K. K. Bose and P. L. Dasgupta	364
Grouping chart and simplification of multiple output switching functions. On adaptation of the	A. K. Choudhury, M. S. Basu and Sunil Ranjan Das	521
Group invariance or total symmetry of Boolean function. On detection of	A. K. Choudhury and M. S. Basu	31
Helmholtz instability in hydromagnetics	S. P. Talwa	351
Hydrogen bonding in ortho- and para-nitrophenol Influence of solvents on	S. B. Banerjee and G. S. Khastha	163
Indirect spin coupling in magnetic garnets	K. P. Sinha and M. K. Sinha	439
Internal friction in Au-Ni alloy	M. A. Quader	330
Intensity of fluorescence of dyes in solution	Jugal Kishore, M. K. Machwe, K. Gopala Krishnan and K. D. Chaudhuri	415
Intensity measurement in bands and rotational temperature	N. R. Tawde and M. I. Savadatti	630
Ion-source of the Calcutta 37-inch cyclotron. Characteristics of the	P. K. Dutt, A. P. Patro, B. Basu and A. Chatterjee	169



# Subject Index

xvii

SUBJECT	AUTHOR	PAGE
Isotopic thermal diffusion factor. II. Application to hydrogen isotopes. Various approximations for the	S. C. Saxena and P. A. Pardeshi	13
Kihara's theory of radiofrequency discharge. A note on (L)	S. N. Sen and A. K. Ghosh	605
Lattice expansion and Debye tempera- ture of $\alpha$ -phase AgCd alloys	M. A. Quader and B. N. Dey	43
Light absorption in $\text{NO}_3$ ion in state of solution Part I—300m $\mu$ band	A. Mookherji and S. P. Tandon	344
Linear polarization of 5.12 mc <sup>2</sup> gamma rays Rayleigh scattered from K-elec- trons in mercury	B. S. Sood	569
Low energy scattering of electrons by variational method	S. C. Mukherjee	283
Magnetic anisotropy and susceptibility of $\text{Cu}^{2+}$ ion. A short note on the (L)	R. Chatterjee and U. S. Ghosh	600
Magnetic studies on $\text{Co}^{+4}$ ion in pink and blue solution of $\text{CoCl}_2$	T. Mookherji	215
Mass spectrometer using boron trifluoride Certain operational characteristics for C.E.C. 21-103C	K. N. Blude and S. C. Saxena	224
Maximum superheat of binary liquid mixtures	A. K. Jalaluddin and D. B. Sinha	312
Minimization of Boolean functions. On the	A. K. Choudhury and M. S. Basu	1
Mössbauer scattering of low energy gamma rays	B. S. Sood	419
Multicomponent diffusion in the sys- tems $^{85}\text{Kr}$ -Ne-Kr and $^{86}\text{Kr}$ -Ar-Kr	Ranjit Paul	464
Mutual diffusion of binary mixture of ammonia with He, Ne and Xe	I. B. Srivastava	193
Natural occurrence of beta form of iron oxyhydroxide. A	K. C. Chandy	484
Nature of the crystalline electric field in trivalent vanadium alum. A short note on the (L)	R. Chatterjee	660
Nonlinearity of thermal expansion of solids with temperature	G. B. Mitra and S. K. Mitra	200

SUBJECT	AUTHOR	PAGE
Nuclear scattering of high energy nucleons. The total cross-section for the	G. Z. Shah and B. M. Thaker	595
$N_2^+$ , $N^+$ , $N^{++}$ and $O_2^+$ , $O^+$ , $O^{++}$ ions produced by solar protons in the earth's atmosphere. Number of	S. N. Ghosh and B. N. Sivastava	129
Parabolic interpolation technique in the derivation of molecular constants. Efficacy of the	N. R. Tawde, N. Sreedhara Murthy and (Miss) Sharada Hegde	25
Periodicity and structural development in nuclei	A. K. Dutta, B. Pal, A. Das Gupta and N. Chaudhury	497
Principal crystalline susceptibilities of triclinic crystals. A general method of finding the (L)	U. S. Ghosh and R. N. Bagehi	538
Relation between dissociation energy and molecular constants. On the	B. B. Laid	639
Resonance in electron capture by proton passing through hydrogen atoms	S. C. Mukherjee and N. C. Sil	622
Response function of a degenerate electrons gas	P. Misra and D. Misra	549
Scattering of positrons by six-fold ionized uranium	Bhajan Singh and Brojendra K. Guha	189
Second virial and zero pressure Joule-Thomson coefficients of non-polar quasi-spherical molecules	S. C. Saxena and K. M. Joshi	422
Slow electric field-changes due to moving thunder clouds. Fluxmeter studies of	S. R. Khastgir and R. S. Srivastava	137
Singlet-triplet absorption in some halogenated toluenes. On the influence of different solvents on the	J. K. Roy	156
Surface recombination velocity on carrier lifetime for cylindrical geometry. Effect of (L)	P. Das	431
SPECTRA :		
Electronic spectra of chloronaphthalene in different states	T. N. Misra	302
Emission band spectra of SbF and BiF. The	T. A. Prasada Rao and P. Tiruvenganna Rao	85

# Subject Index

iii

SUBJECT	AUTHOR	PAGE
Infrared spectrum of cyclohexyl benzene. The (L)	R. N. Bapat	543
Infrared study of hydrogen bonding in isomeric toluidines in different environments	K. C. Medhi, S. B. Banerjee and G. S. Kastha	457
Intensities of Raman lines. Influence of ultraviolet absorption frequencies on the	A. K. Chakravorty	151
Luminescence spectra of 2, 4-dichloro and 3, 4-dichlorotoluene in the solid state at $-180^{\circ}\text{C}$	J. K. Roy	507
Near ultraviolet absorption spectrum of para-fluoronitrobenzene. The (L)	Achuta Rao, Iyyanki	213
Raman and infrared spectra of 1, 4-dichlorobutane and propionyl chloride in different states. On the	K. K. Deb	290
Raman and infrared spectra of some fluorinated toluenes in different states	K. K. Deb	59
Raman and infrared spectra of isoquinoline, fluoro- and $\alpha$ -chloronaphthalene in different states	Krishna Kumar Deb	557
Spectrum of CoBr in the visible ( $\lambda 4300-\lambda 4700 \text{ \AA}$ ). The	S. V. Krishna Rao and P. Tiruvenganna Rao	609
Switching function Part I. On classification of	A. K. Choudhury and M. S. Basu	317
Switching function Part II. On classification of	A. K. choudhury and M. S. Basu	383
Triple coincidence proton scintillation spectrometer. A	R. K. Mohindra and H. S. Hans	93
Terminal impedances and transfer function of general multimesh ladder networks containing two kinds of elements only. A method of determining the	S. C. Dutta Roy	469
Twin-tuned R-C network. A	S. C. Dutta Roy	369
Ultrasonic velocity in liquid binary mixtures	M. V. Kaulgud	577

SUBJECT	AUTHOR	PAGE
Ultrasonic studies in aqueous solutions of electrolytes	M. G. Seshagiri Rao and B. Ramachandra Rao	613
Ultraviolet absorption of $\text{NO}_2$ ion (L)	A. Mookherji and S. P. Tandon	211
Unit cell and space group of thio- diglycollic acid (L)	Sukla Roy	493
Validity of the revised rotational constants $\alpha(\text{C} \rightarrow \text{X})$ band system of $\text{ZrO}$ . On the	N. Sreedhara Murthy	101
Vertical transport of electrons during pre-sunrise F-layer 'Splitting'	P. Bandyopadhyay and S. K. Chatterjee	124
X-ray diffraction. Study of silver fulminate by (L)	S. N. Pandey	657
Book Reviews	379, 436, 495, 545 and 662	

## ON THE MINIMISATION OF BOOLEAN FUNCTIONS

A. K. CHOUDHURY AND M. S. BASU

INSTITUTE OF RADIO PHYSICS AND ELECTRONICS,  
UNIVERSITY OF CALCUTTA*(Received July 15, 1961)*

**ABSTRACT** A systematic procedure for finding out all the minimal forms of a Boolean function is presented in this paper. A grouping chart has been devised for determining the prime implicants and identifying the essential prime implicants. A convenient feature of the chart is that it can be easily mechanised.

## INTRODUCTION

In the design of switching circuits using diodes as logical elements, it becomes necessary to find out an arrangement which will require the minimum number of diodes for any specified switching operation for economy of components. Application of Boolean algebra for this purpose is quite common. The output performance of the switching circuit is specified in terms of a Boolean function of the input variables. Then by applying Boolean algebra the minimal form of the function as sum of the products is found out. By minimal form we mean an expression of the Boolean function which involves the smallest number of literals. This will generally correspond to the utilisation of the smallest number of diodes in the design of the switching circuit.

## GENERAL OUTLINE OF AVAILABLE METHODS

In all the available methods of minimisation, one basic principle is applied. If a Boolean function is true for  $X \cdot Y$  and also true for  $X \cdot \bar{Y}$ , then both these statements are included in the simple statement that the function is true for  $X$ . Expressed algebraically, the theorem is  $XY \mid X\bar{Y} = X$ . Therefore, if two terms of any Boolean function differ by only one variable, the two terms can be combined to form a new term eliminating that particular variable.

Thus in an actual procedure suggested by Quine (Quine, 1952) the different terms of the given Boolean function are compared amongst themselves and new terms are formed, whenever possible, in the above mentioned way. The newly formed terms are again compared amongst themselves and elimination of one more variable is done, whenever possible. This procedure is continued till no further elimination is possible. All the new terms thus obtained and also the original terms that could not be combined with others are known as prime implicants of the function. Some of the prime implicants may be essential and they

must be included in the final expression of the minimal form. Otherwise, some of the terms of the original Boolean function will remain uncovered. Out of the other non-essential prime implicants, only those are chosen for inclusion in the final expression which will most economically cover all the other terms of the original function. Thus in any method of minimisation the three steps to be performed are (1) determining the prime implicants, (2) finding out the essential prime implicants, if any, and (3) finding out the most economical coverage for the terms not included by the essential prime implicants.

In the present paper, a method is presented in which the labour involved in the first two steps is very greatly reduced by taking help of a chart which can be called "The Grouping Chart." By visual inspection of the chart the terms of the original function which are related by one change of variable, are readily determined and the prime implicants and the essential prime implicants, if any, are quickly found out. A systematic procedure for the third step is suggested which leads to the determination of all the minimal forms of the function.

#### THE GROUPING CHART

The Grouping Chart, as the name suggests, furnishes all the informations regarding groupings amongst the different terms of any given Boolean function.

The variables of a Boolean function as well as the function itself are binary in nature. Any term or state of a binary function  $f(x_{n-1}, x_{n-2}, \dots, x_0)$  of  $n$ -variables can be expressed by an equivalent decimal number. The term or state as derived from any row of a truth table is a binary number and is equivalent to a decimal number  $K$  where

$$K = \sum_{i=0}^{n-1} x_i 2^i$$

$x_i$  is the  $(i+1)$ th digit of the binary number. Thus in a four variable function, the term 1010 is equivalent to  $1 \times 2^3 + 0 \times 2^2 + 1 \times 2^1 + 0 \times 2^0 = 10$ .  $K$  can have  $2^n$  values, viz., 0, 1, 2, ...,  $2^n - 1$ . One can, therefore, write a Boolean function

$$f(x_{n-1}, x_{n-2}, \dots, x_0) = \phi(k)$$

With each term of an  $n$ -variable function are associated  $n$  other terms which are related by one change of variable. As an example, in a five-variable function, the term 0 is related to the terms 1, 2, 4, 8 and 16 by one change of variable. Similarly, each of the terms 0 to 31 of a five variable function is related to five other terms by one change of variable. The terms which are related by one change of variable can be grouped together and in their representation by Boolean variables, elimination of one variable will result. Thus 2 and 3 can be grouped together and is represented by  $x_4 x_3 x_2 \bar{x}_1$  after elimination of the variable  $x_0$ . These groups of two terms can be combined to form groups of four terms provided two groups of two terms are again related by one change of variable. Thus groups of two

terms (0-1) can be grouped with (2-3), or (4-5) or (8-9) or (16-17) to form groups of four terms — (0-1-2-3) or (0-1-4-5) and so on. In their representation, elimination of two variables results. It is very easy to know which variable is to be eliminated when two groups of two terms are combined to form a group of four terms. If the leading terms of the two groups differ by  $2^i$ , then the variable  $x_i$  is to be eliminated. Thus in the formation of 0-1-4-5 by combining 0-1 and 4-5, 1 and 5 differ by  $2^2$ , and hence the variable to be eliminated is  $x_2$ .

The total number of terms related by one change of variable to any term of the given Boolean function, as well as the groupings of the terms of the function, the prime implicants and essential prime implicants, if any, can be very easily found from the grouping chart.

The chart is constructed in the following manner. A squared paper is taken. Numbers 0, 1, 2, 3, 4, ...  $(2^n - 1)$  which represent different terms of Boolean functions are written at the top as column headings. Similarly, the rows are also marked by the same numbers 0, 1, 2, 3, 4, ...  $(2^n - 1)$ . The total number of rows or columns in a chart for  $n$  variables will be  $2^n$ . Any square on the graph is designated by its row and column numbers. Now let us take up the row 0. We know that the term 0 differs by one variable from the terms 1, 2, 4, 8 and 16. The squares 0-0, 0-1, 0-2, 0-4, 0-8 and 0-16 are marked by dots at the centre. The term 1 is related similarly to 0, 3, 5, 9 and 17. So the squares 1-0, 1-1, 1-3, 1-5, 1-9 and 1-17 are marked by dots. In this way all the different

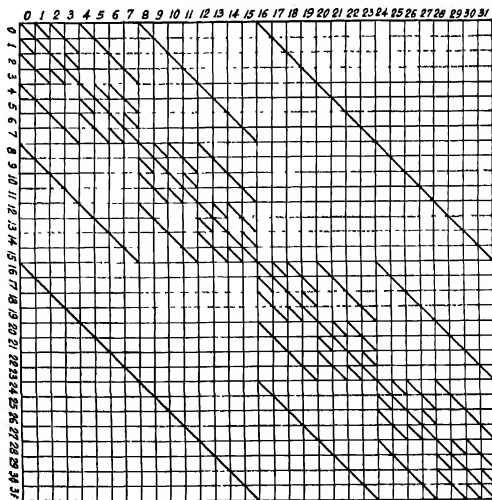


Fig. 1 Grouping chart for five variables.

rows are considered. Oblique line is drawn through each dot in any square and the consecutive oblique lines are joined. A chart for five variables is shown in Fig. 1. There is one continuous diagonal line and other off diagonal oblique lines in shorter or longer sections.

It will be seen from the chart that if we move along any row or any column, there will be  $n$  intersections with off diagonal oblique lines. The row and column numbers by which those squares are designated also give the terms which can form groups of two. Thus if we move along row 8, we find that there are intersections with oblique sections on squares 8-0, 8-9, 8-10, 8-12, etc., which means that the terms 8-0, 8-9, 8-10, etc., can form groups of two. Again, if we move along two rows or two columns, headed by terms which differ by one variable, the intersections in these two rows or columns with the off diagonal oblique continuous sections are terms which can form a group of four. For example, if we move along columns 8 and 10, there are intersections on off diagonal continuous line at 12-8 and 14-10. This means 8-10-12-14 can form a group of four.

The different uses of the chart will now be illustrated by an actual example. Let us say that the terms of a given Boolean function are twelve in number, viz ,

$$0, 2, 4, 6, 8, 10, 11, 12, 13, 14, 16, 18$$

We draw vertical and horizontal lines on the grouping chart through all those points. There will be  $12^2$  i.e., 144 points of intersections. But only those intersection points which fall on off diagonal lines will be significant for us. A chart with vertical and horizontal lines drawn through the given terms is shown in Fig. 2.

If we move along the horizontal line through 0, in the chart, it is observed that there are intersection marks at 2, 4, 8 and 16 in addition to the intersection mark at 0 on the diagonal line. This indicates that for the given function the term 0 differs from four terms (2, 4, 8, 16) by one variable and in a minimisation problem we can form groups of 2 like 0-2, 0-4, 0-8, 0-16 resulting in the elimination of one variable. Again, if we move downwards along verticals through, say, 0 and 2, it is found that there are intersection marks on the same oblique line at squares (4-0) and (6-2). This indicates that 0-2-4-6 can form a group of 4 and elimination of two variables is possible. Similarly, all the other groups of 4 that can be formed by the term 0 can be found out. It will be found from the chart that vertical lines through (0 and 2) have intersection marks with oblique lines at (8-0), (10-2) and (16-0), (18-2) squares. Other groups of four with 0-2 are (0-2, 8-10) and (0-2, 16-18).

If we move downwards along vertical lines through 0, 2, 4 and 6, we find that there are intersection marks at 8, 10, 12, 14 on the same oblique line. This means that a group of eight can be formed with 0-2-4-6-8-10-12-14. Essential prime implicants, if present, can also be easily detected by the help of the



chart. Let us suppose that in a Boolean function, a term is found to differ by one variable from only three other terms of the function. Now, if that term can be included in a group of eight as explained above, then it is quite obvious that any further grouping with higher number of terms is not possible. Hence the prime implicant formed by the elimination of three variables will be an essential prime implicant with respect to the term. The number of other terms of a function which differ by one variable from a particular term will be called the weight of the latter term (Svoboda, 1957). So, in general, we can say that in an  $n$ -variable function if the weight of a term is  $k$  and if it is included in a group of  $2^k$  terms of the function, then the resulting prime implicant will be an essential one and it will most economically cover the term in question. In our example, the terms 4 and 8 have weight 3 and hence the group (0-2-4-6-8-10-12-14) will be an essential prime implicant with respect to the terms 4 and 8.

In one more respect the Grouping Chart reduces unnecessary labour. While considering any term of a Boolean function, it is only necessary to think of its groupings with other terms which will come to the right of the diagonal line. For example, let us say that we are considering the term 10. Then we need only to think of its groupings with 11, 14 and 26. All relevant informations regarding its groupings with 2 and 8 must have been already obtained while considering the terms 2 and 8 as we are proceeding systematically from lower to higher order terms. This considerably reduces the labour by eliminating the possibility of the recurrence of the same groupings again and again.

The chart can be mechanised very easily. A method of mechanisation of the grouping chart is described in a later section of this paper.

#### SYSTEMATIC PROCEDURE FOR MINIMISATION

The suggested procedure for minimisation of a given Boolean function utilising the grouping chart can be outlined as follows

(a) Vertical and horizontal lines are drawn on the grouping chart through all the terms of the given Boolean function.

(b) A table is made. In the first column of the table all the terms of the given function are entered starting from the term designated by the smallest decimal number and then proceeding in the ascending order. In the second column, the weights corresponding to each term as read out from the chart are entered.

(c) The first term of the table is taken up. All the groups of two that it can form combining with one other term is noted in column 3 of the table. Similarly, all the groups of 4, 8, 16, etc., that can be formed by the term with other terms of the function, are entered in columns 4, 5, 6, etc., of the table. These can be very easily found out from a glance at the grouping chart.

(d) If the weight of the term happens to be  $k$  and a group of  $2^k$  terms can be formed by it as read out from the chart then that becomes an essential prime

implicant with respect to the term. If the weight of the term does not satisfy this condition, then it will not be an essential prime implicant with respect to the term and we will have to see whether this is so with respect to any other term or not

(c) A survey of the weights of all the terms present in the largest group of the first term is made. If any of them satisfies the condition mentioned in step (d), then they are marked with a cross and they need not be considered any further. The group is also marked to denote that it is an essential prime implicant.

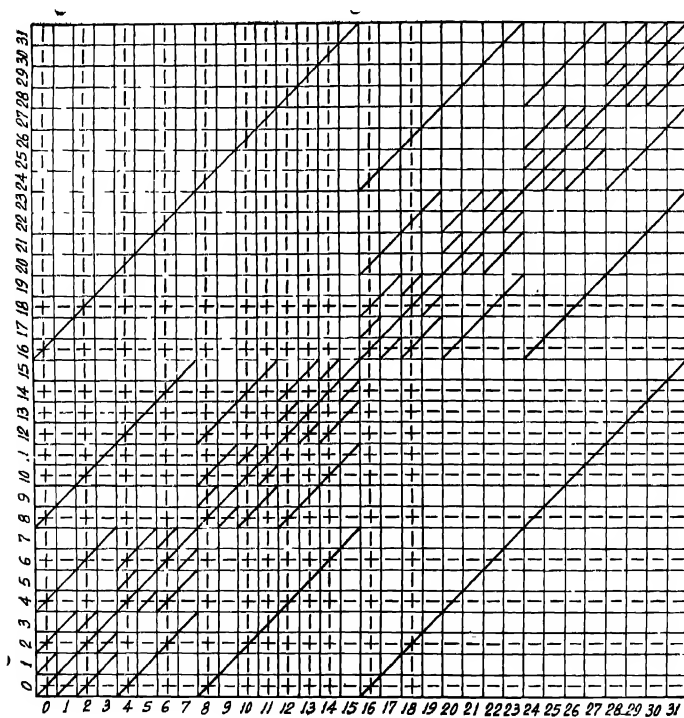


Fig. 2 Grouping chart with the function  $f = \Sigma(0, 2, 4, 6, 8, 10, 11, 12, 13, 14, 16, 18)$  plotted on it.

(1) The next uncrossed term is then taken up. The procedure mentioned in step (c) is repeated for this also. In this way all the terms are examined and a search for essential prime implicants is made. All the essential prime implicants are marked and the terms which are covered by them are crossed out.

While considering any particular term, we need concentrate on finding its grouping with higher order terms only. That is, we need only to look horizontally to the right of the diagonal line on the grouping chart. After finding out the essential prime implicants and crossing out the terms covered by them, we are left with a number of non-essential prime implicants and also the remaining terms which are still to be covered. The next part of the problem is to choose out the prime implicants which will give most economical coverage to all those terms. In order to achieve this we start from any one of the terms and a prime implicant which can cover that term is taken up. Then other prime implicants are grouped with it, keeping in mind that no term will be covered more than once. Ultimately a stage will be reached when it will be found that some term or terms

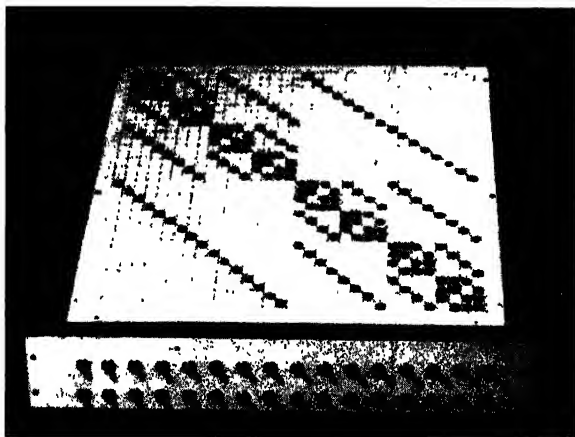


Fig. 3 A mechanised grouping chart for five variables.

are remaining uncovered and they cannot be covered without making some other term covered twice. All the different ways of doing this are tried and the minimal forms are selected out. The systematic procedure is best explained by taking an actual example.

#### EXAMPLE

To find out the minimal forms of the following 4-variable Boolean function :

$$f = \Sigma(3, 4, 5, 6, 8, 9, 10, 13, 14, 15).$$

(a) Vertical and horizontal lines are drawn on the grouping chart through the given terms of the function.

(b)-(e) The following table is made and entries are done in the different columns by utilising the grouping chart :

TABLE I

Terms	Weight	Group of 1	Group of 2	Group of 4
$\times 3$	0	(3)	Nil	Nil
4	2		4-5, 4-6	--do-
5	2		5-13	--do-
6	2		6-14	--do-
8	2		8-9, 8-10	--do-
9	2		9-13	--do-
10	2		10-14	--do-
13	3		13-15	--do-
14	3		14-15	--do-
15	2			--do-

The weight of the term 3 is 0 and as such the term 3 is an essential prime implicant. The term 3 is crossed out and the group 3 is marked by a circle. It is found that, no group of 4 can be formed by the terms. So the groups of two as entered in the last but one column are the prime implicants. Now we are to find out the most economical coverage for the other terms excepting the term 3 utilising these prime implicants. We can start from any term. Let us start from the term 4. We see that it can be covered either by the prime implicant 4-5, or 4-6. Let us take (4-5) and combine one more prime implicant with it so that there may not be any repetition and four terms will be covered. All the different ways of doing this are noted down as below :

(4-5), (6-14)

(4-5), (8-9)

(4-5), (8-10)

(4-5), (9-13)

(4-5), (10-14)

(4-5), (13-15)

(4-5), (14-15)

Now we will combine another prime implicant so that again there may not be any repetition and six terms may be covered :

(4-5), (6-14), (8-9)	
(4-5), (6-14), (8-10)	
(4-5), (6-14), (9-13)	
(4-5), (6-14), (13-15)	
<hr/>	
(4-5), (8-9) (10-14)	
(4-5), (8-9), (13-15)	
(4-5), (8-9), (14-15)	
<hr/>	
(4-5), (8-10), (9-13)	
(4-5), (8-10), (13-15)	
(4-5), (8-10), (14-15)	
<hr/>	
(4-5), (9-13), (10-14)	
(4-5), (9-13), (14-15)	
<hr/>	
(4-5), (10-14), (13-15)	
<hr/>	

The horizontal lines are drawn for dividing into groups, the members of which differ amongst themselves only in the last prime implicant. While searching for another prime implicant which can be included, comparison is made among members of the same group.

We can proceed one step further and include one more prime implicant covering eight terms without any repetition .

	terms remaining uncovered
(4-5), (6-14), (8-9), (13-15)	10
(4-5), (6-14), (8-10), (9-13)	15
(4-5), (6-14), (8-10), (13-15)	9
<hr/>	
(4-5), (8-9), (10-14), (13-15)	6
<hr/>	
(4-5), (8-10), (9-13), (14-15)	6
<hr/>	

It is now evident that it is not possible to proceed any further in the same way and the terms which are remaining uncovered cannot be covered without making any repetition.

If we start from the last expression, we can see by consulting Table I that 6 can be included either by taking the prime implicant (4-6) or (6-14). In a similar way we can find out all the coverages for the remaining terms 9, 10 and 15. All the different expressions that are obtained are written down.

- |  |               |
|--|---------------|
| (a) (4-5), (4-6), (8-10), (9-13), (14-15)  |               |
| (b) (4-5), (6-14), (8-10), (9-13), (14-15) | includes 6    |
| (c) (4-5), (4-6), (8-9), (10-14), (13-15)  |               |
| (d) (4-5), (6-14), (8-9), (10-14), (13-15) | J             |
| (e) (4-5), (6-14), (8-9), (8-10), (13-15)  | includes 9    |
| (f) (4-5), (6-14), (8-10), (9-13), (13-15) |               |
| (g) (4-5), (6-14), (8-9), (8-10), (13-15)  | } includes 10 |
| (h) (4-5), (6-14), (8-9), (10-14), (13-15) |               |
| (i) (4-5), (6-14), (8-10), (9-13), (13-15) | } includes 15 |
| (j) (4-5), (6-14), (8-10), (9-13), (14-15) |               |

It is found by inspection that (e) and (g) are identical.

(d) and (h) are identical.

(f) and (i) are identical.

(b) and (j) are identical.

So, (g), (h), (i), (j) are cancelled out. We are left with the following (after including the essential term)

- |   |     |
|---|-----|
| (a) 3, (4-5), (4-6), (8-10), (9-13), (14-15)  |     |
| (b) 3, (4-5), (6-14), (8-10), (9-13), (14-15) |     |
| (c) 3, (4-5), (4-6), (8-9), (10-14), (13-15)  |     |
| (d) 3, (4-5), (6-14), (8-9), (10-14), (13-15) | (A) |
| (e) 3, (4-5), (6-14), (8-9), (8-10), (13-15)  |     |
| (f) 3, (4-5), (6-14), (8-10), (9-13), (13-15) |     |

All the above six expressions are the alternative minimal forms of the original Boolean function as each of them is composed of six prime implicants and the dimensions of the non-essential prime implicants are all equal.

It may be recalled that we started with the term 4 which is covered by the prime implicants (4-5) and (4-6). We chose (4-5) as our starting point and arrived at the above six minimal forms. Instead of that we could have as well started from (4-6) and that would have given us the other minimal forms.

Those can be found out following exactly the same procedure. The other minimal forms are four in number, viz. .

- (g) (3), (4-6), (5-13), (8-10), (9-13), (14-15)
- (h) (3), (4-6), (5-13), (8-9), (10-14), (13-15)
- (i) (3), (4-6), (5-13), (8-9), (8-10), (14-15)
- (j) (3), (4-6), (5-13), (8-9), (10-14), (14-15).

It may be mentioned that the example chosen here to illustrate the method is rather simple in the sense that all the prime implicants are groups of 2 and there are no groups of four or higher order groups present. But even when all the prime implicants are not of the same order, the method will still be applicable. The labour involved in finding out all the minimal forms may be somewhat more in certain cases.

#### MECHANISATION OF THE GROUPING CHART

A grouping chart for five variables can be easily mechanised in the following manner. On the front face of a wooden board a grouping chart for five variables is painted with prominent lines. The thirty-two rows and columns of the chart are marked by numbers 0 to 31. On the back side of the board thirty-two vertical and thirty-two horizontal wires are fixed up which are all insulated from each other. Small holes are made on the centres of those squares of the grouping chart through which oblique lines pass and a lamp is placed at the back side of each of such squares, so that the glow of the lamps can be viewed from the front side of the board through the holes. The terminals of the lamp at the back of any square are connected to the vertical and horizontal wires passing through that square. There are 32 switches numbering from 0 to 31. The function of any switch is to connect a battery between the corresponding vertical and horizontal wires. So, if we make switch number 5 on, the lamp on the diagonal line at the crossing of row 5 and column 5 will glow. While considering any Boolean function, it is only necessary to make those switches on whose numbers are same as the term numbers of the function. Lamps at all the significant intersection points of the grouping chart will glow and at a glance all necessary information regarding groupings can be found out. The labour involved in having vertical and horizontal lines drawn on the chart every time a new function is handled is entirely eliminated in this way. In plate No. 1, the mechanised chart is shown.

#### CONCLUSION

A method for finding out all the minimal forms of a Boolean function has been presented in this paper. The mechanised grouping chart, as explained in the paper, renders the task of finding out the prime implicants and detection of the essential prime implicants extremely easy. The procedure for finding out the minimal forms is quite straightforward.

## ACKNOWLEDGMENT

The authors wish to express their indebtedness to Professor J. N. Bhar, D.Sc., F.N.I., for guidance and keen interest in the work

## REFERENCES

- Caldwell, S. H., 1958, *Switching Circuits and Logical Design*, John Wiley & Sons, New York
- Karnaugh, M., 1953, *Trans. A.I.E.E.*, **72**, Part I, Nov.
- McCluskey E. J. Jr., 1956, *Bell System Tech. Jour.*, **35**, 1417-1444
- Quine, W. V., 1952, *The American Mathematical Monthly*, **59**, No. 8, pp. 521-531.
- Svoboda, A., Proceedings of an International Symposium on the Theory of Switching, 1957, Part I, Annals 29, Harvard University Press, Cambridge, Massachusetts, 1959.
- Troye, N. C. de, 1959, *Phillips Research Reports* 14.
- Urbano, R. H., and Mueller, R. K., 1956, *J.R.E. Trans. on Electronic Computer EC-5*, September.



# VARIOUS APPROXIMATIONS FOR THE ISOTOPIC THERMAL DIFFUSION FACTOR. II. APPLICATION TO HYDROGEN ISOTOPES

S. C. SAXENA\* AND P. A. PARDESHI

ATOMIC ENERGY ESTABLISHMENT TROMBAY, BOMBAY

(Received August 18, 1961)

**ABSTRACT.** Numerical calculations are performed for the thermal diffusion factor of hydrogen isotopes in conjunction with the various theoretical formulae. New formulae are derived for the two limiting concentrations of the binary mixtures. These formulae are further simplified by expanding in terms of the reduced mass and also as ratio of the two molecular masses. The accuracies of these approximate formulae are estimated by comparison against the rigorous formulae for several interesting binary mixtures of hydrogen isotopes. Approximate calculations are done to estimate the quantum corrections.

## INTRODUCTION

The task of determining the intermolecular forces from experimental thermal diffusion data requires knowledge of the accurate theoretical expression for the thermal diffusion factor,  $\alpha_T$ . This is not always readily available, as the infinite series representing  $\alpha_T$  has a poor convergence and requires to be investigated for the specific cases, Chapman-Cowling (1953). In the hope to have faster convergence, Kihara (1949) developed another version of this infinite series which has been considerably extended and applied by Mason (1957), and Saxena and Mason (1958). Kihara scheme does not always yield accurate results (Mason and Saxena, 1959), and the only alternative is to perform these laborious calculations for the individual gases to arrive at the right conclusion.

Thermal diffusion factor, at least in lower approximations, is better represented by an expansion in terms of the reduced mass. For the case of heavy isotopes, where the reduced mass is small, consideration up to the first power is usually sufficient. However, if the reduced mass is not small, terms of higher powers have significant contribution. Thus, Saxena and Pardeshi (1961) found it essential to consider the expansion up to second power of the reduced mass for helium. In this paper the relative adequacy of the various expressions of  $\alpha_T$  has been investigated for the hydrogen isotopes. Hydrogen has a stable isotope, deuterium, and a radioactive isotope, tritium; both chemically exchange with the normal hydrogen and produce more species. Numerical computations have been performed and new formulae are developed for the various isotopic mixtures which

---

\*Present Address: Reader in Physics, Rajasthan University, Jaipur

are likely to be present in actual experiments. The mixtures where the heavier component may be in trace are given special attention in view of their practical importance.

#### FORMULAE FOR $\alpha_T$

According to the rigorous Chapman-Enskog kinetic theory of gases, the  $m$ -th Chapman-Cowling approximation for  $\alpha_T$  is, Chapman and Cowling (1953),

$$[\alpha_T]_m^{m,0} = \frac{5}{2} \left[ X_1 X_2 A_{00}^{(m)} \right]^{-1} \left[ X_1 A_{01}^{(m)} \left( \frac{M_1 + M_2}{2M_1} \right)^{\frac{1}{2}} + X_2 A_{0-1}^{(m)} \left( \frac{M_1 + M_2}{2M_2} \right)^{\frac{1}{2}} \right], \quad \dots (1)$$

where  $X_1$  and  $X_2$  are the mole fractions of the two components of molecular weights  $M_1$  and  $M_2$  respectively. The quantity  $A^{(m)}$  is a determinant of  $(2m+1)$  order, the general term of which is  $a_{ij}$  where  $i$  and  $j$  range from  $-m$  to  $+m$  including zero. The minor of  $A^{(m)}$  obtained by deleting the row and column containing  $a_{ij}$  is denoted by the symbol  $A_{ij}^{(m)}$ . To the first approximation, Eq. (1) can be cast into the following familiar form

$$[\alpha_T]_1^{1,0} = \frac{(6C^* - 5)(X_1 S_1 - X_2 S_2)}{X_1^2 Q_1 + X_2^2 Q_2 + X_1 X_2 Q_{12}}, \quad \dots (2)$$

where all the quantities are as previously defined by Saxena and Pardeshi (1961).

Chapman (1941) expanded Eq. (2) in powers of the reduced Mass,  $M$ . His result is

$$[\alpha_T]_1^{1,0} = [\alpha_0]_1^{1,0} [1 - \gamma M (X_1 - X_2)] M, \quad \dots (3)$$

in which

$$[\alpha_0]_1^{1,0} = \frac{15(6C^* - 5)(2A^* + 5)}{2A^*(16A^* - 12B^* + 55)}, \quad \dots (4)$$

and

$$\gamma = \frac{3(5 - A^*)}{2(5 + 2A^*)} - \frac{2(12B^* + 5)}{(16A^* - 12B^* + 55)}, \quad \dots (5)$$

$A^*$ ,  $B^*$  and  $C^*$  have their usual meaning. The limiting case,  $X_1 \rightarrow 0$ , is of special interest and Eq. (1) gets considerably simplified. We have then

$$[\alpha_T]_1^{m,0} = -(6C^* - 5)(S_2/Q_2),$$

$$= -(6C^* - 5) \cdot \frac{[(1-M)(1+M) - \frac{1}{2}A^* - (1-M^2)A^* - (15/4)M(1+M)]}{[(1+M) - \frac{1}{2}A^* \{(\frac{5}{2} - \frac{5}{2}B^*)(1-M)^2 + 3(1+M)^2 + \frac{1}{2}A^*(1-M^2)\}]} \quad (6)$$

$$[\alpha_T]_1^{1,0} = [\alpha_0]_1^{1,0} [1 + \gamma M] M. \quad \dots (7)$$

and

$$[\alpha_T]_2^{ms} = \frac{5}{2} \left( \frac{M_1 + M_2}{2M_1} \right)^{\frac{1}{2}} \left[ \frac{(a_{10} a'_{22} - a_{20} a'_{12})}{(a'_{11} a'_{22} - a'_{12} a'_{22})} \right] + \frac{5}{2} \left( \frac{M_1 + M_2}{2M_2} \right)^{\frac{1}{2}} \left[ \frac{(a_{-10} a''_{-2-2} - a_{-20} a''_{-1-2})}{(a''_{-2-2} a''_{-1-1} - a''_{-1-2} a''_{-1-2})} \right]$$

$$+ (a'_{11} a'_{22} - a'_{12} a'_{22})^{-1} (a''_{-2-2} a''_{-1-1} - a''_{-1-2} a''_{-1-2})^{-1}$$

$$\{ (a_{20} a'_{12} - a_{10} a'_{22}) (a''_{-2-2} a_{-11} - a_{1-2} a''_{-1-2})$$

$$+ (a_{10} a'_{12} - a_{20} a'_{11}) (a''_{-2-2} a_{-12} - a_{-22} a''_{-1-2}) \} \quad (8)$$

The various  $a_{ij}$  are as defined by Mason (1954). Eq. (8) was derived by Saxena and Dave (1961). Keeping in view the relative magnitudes of the various terms we have put Eq. (8) in terms of  $M$ . The result is

$$[\alpha_T]_2^{iso} = \frac{5}{2} M \left\{ \frac{A}{A_1} \left( \frac{A_2}{A} - \frac{A_3}{A_1} - 1 \right) + \frac{A_4}{A_5} + \frac{3}{2} \left( 1 + \frac{M}{4} - \frac{M^2}{24} + \frac{M^3}{64} + \dots \right) \right.$$

$$\left. \left( \frac{A_0 + A_1 M}{A_5} \right) + \frac{1}{A_1 A_5} \{ A_7 (A_8 - 5A_0/2) - A(A_{10} - A_{11}/2) + (A_{12} A_0 - A_2 A_{11}) \right.$$

$$\left. - (A_3/A_1)(A_7 A_0 - A A_{11}) \} \right\} \quad \dots \quad (9)$$

The various  $A_i$  of Eq. (9) are given in the Appendix.

Saxena and Dave (1961) have also expanded Eq. (1) in powers of  $(M_2/M_1)$ . The final results, as applicable to isotopic mixtures, are

$$[\alpha_T]_1^{M'} = \frac{5(6C^* - 5)}{4\sqrt{2} A^*} \left[ 1 - \frac{M_2}{M_1} \left( \frac{3}{2} + \frac{2\sqrt{2}}{15} A^* \right) + \frac{M_2^2}{M_1^2} \left\{ \frac{1}{24} \right. \right.$$

$$\left. \left. - \frac{2\sqrt{2}}{15} A^* + \frac{2}{5} B^* + \frac{8}{15} A^* \left( 1 + \frac{2\sqrt{2}}{15} A^* \right) \right\} \right] \quad \dots \quad (10)$$

and

$$[\alpha_T]_2^{M'} = \frac{(6C^* - 5)}{96\sqrt{2} A^*} \frac{1}{(b - c^2)} \left[ 120(b + 4cd) - \{ 16\sqrt{2} A^* (b - c^2) + 180b \right.$$

$$\left. + 1200cd \} \frac{M_2}{M_1} \{ 16\sqrt{2} g A^* (b - c^2) - 2100cd - 225b + 4be + 128fc \} \frac{M_2^2}{M_1^2} \right] \quad \dots \quad (11)$$

The various quantities of Eq. (11) are defined by Saxena and Dave (1961) except the various subscripts characterizing the molecular species are all the same for isotopic mixtures.

The expressions for the other limiting end, viz.  $X_2 \rightarrow 0$ , have also been worked out by Saxena and Dave (1961a). We finally get

$$|\alpha_T|_1^{mix} = (6E^* - 5)(S_1/Q_1), \quad \dots \quad (12)$$

$$|\alpha_T|_1^{iso} = |\alpha_0|_1^{iso} [1 - \gamma M] M, \quad \dots \quad (13)$$

and

$$\begin{aligned} |\alpha_T|_2^{mix} = & \frac{5}{2} \left( \frac{M_1 + M_2}{2M_1} \right)^2 \left\{ [(a'_{-1-1} a'_{-2-2} - a'^2_{-1-2})^{-1} (a''_{-1-1} a''_{-2-2} - a''^2_{-1-2})^{-1}] \right. \\ & \{ (a_{10} a''_{2-2} - a''_{12} a_{02}) (a'_{-1-1} a'_{-2-2} - a'^2_{-1-2}) \\ & + (a_{1-1} a''_{-2-2} - a''_{12} a_{2-1}) (a_{-20} a'_{-1-2} - a_{-10} a'_{-2-2}) \\ & \left. + (a_{1-2} a''_{2-2} - a''_{12} a_{2-1}) (a_{-10} a'_{-1-2} - a_{-20} a'_{-1-1}) \right\} \\ & + \frac{5}{2} \left( \frac{M_1 + M_2}{2M_2} \right)^2 \left( \frac{a_{-10}}{a_{-1-1}} \right) \left( 1 - \frac{a_{-20} a'_{-1-2}}{a_{-10} a'_{-1-2}} \right) \left( 1 - \frac{a'^2_{-1-2}}{a_{-1-1} a'_{-2-2}} \right)^{-1} \quad \dots \quad (14) \end{aligned}$$

On Kihara approximation scheme only the first and second approximations have been worked out. The results on this scheme are primed in this paper to distinguish from Chapman-Cowling results. The general expressions for  $|\alpha_T'|_1^{mix}$  and  $|\alpha_T'|_1^{iso}$  are given by Saxena and Pardeshi (1961). The second approximation is

$$|\alpha_T'|_2^{mix} = |\alpha_T'|_1^{mix} (1 + K'_1) + K'_2, \quad \dots \quad (15)$$

where  $K'_1$  and  $K'_2$  are given by Mason (1957). For the particular case when  $X_1 \rightarrow 0$  we get

$$|\alpha_T'|_1^{mix} = -(6E^* - 5)(S_2/Q'_2), \quad \dots \quad (16)$$

$$|\alpha_T'|_1^{iso} = |\alpha_0'|_1^{iso} [1 + \gamma' M] M, \quad \dots \quad (17)$$

where the defining equations for  $Q'_2$ ,  $|\alpha_0'|_1^{iso}$  and  $\gamma'$  are given by Saxena and Pardeshi (1961).  $|\alpha_T'|_1^{mix}$  is again given by Eq. (15) except  $K'_1$  and  $K'_2$  have different expressions and these are given by Saxena and Dave (1961). These expressions are considerably simplified by expanding in powers of the reduced mass. Thus,

$$K'_1 = -1 (8E^* - 7)^2 + \frac{Z_{12}^{'2}}{Z'_{11} Z'_{22}} \left[ 1 + M \left\{ \frac{U_{-2}}{4Z'_{22}} - \frac{5}{2} \frac{Z_{00}}{Z'_{11}} - \frac{Z''_{12}}{Z'_{12} - 2} \right\} \right],$$

and

$$\begin{aligned}
 & K_2' - \frac{5}{2} M \left[ \frac{Z_{01} Z'_{12}{}^2}{Z'_{11} Z''_{11} Z'_{22}} \left\{ 2 - \frac{7}{8} \frac{Z_{00}}{Z'_{12}} (6C^* - 5) \right\} \right. \\
 & - \frac{Z_{01} Z'_{12} Z'_{12}}{Z'_{11} Z''_{11} Z'_{22}} + \frac{Z_{01} Z''_{12}}{2 Z'_{11} Z''_{11} Z'_{22}} - \frac{Z_{01} Z'_{12} Z''_{12}}{Z'_{11} Z''_{11} Z'_{22}} \\
 & \left. \left\{ 2 + \frac{7}{4} \frac{Z'_{11}}{Z'_{22}} + \frac{7}{8} \frac{Z_{00}}{Z'_{12}} (6C^* - 5) \right\} + \frac{Z_{02} Z''_{12}}{Z'_{11} Z'_{22}} \right. \\
 & \left. + \frac{Z_{02} Z'_{12}}{Z''_{11} Z'_{22}} \left\{ \frac{7}{8} \frac{Z_{00}}{Z'_{12}} (6C^* - 5) + \frac{5}{2} \frac{Z_{00}}{Z'_{11}} \right\} \right. \\
 & \left. - \frac{1}{2} \frac{Z_{02} Z'_{12}}{Z'_{11} Z'_{22}} + \frac{Z_{02} Z''_{12}}{Z'_{11} Z''_{22}} \left\{ 4 + \frac{7}{4} \frac{Z'_{11}}{Z'_{22}} \right\} \right]. \quad \dots (18)
 \end{aligned}$$

Here the various  $Z_{ij}$  are obtained from the corresponding  $c_{ij}$  and  $a_{ij}$  of Mason (1954) by putting  $M_1 = M_2$  and assuming the various subscripts referring to the molecular species to be the same. On expanding the rigorous expressions in powers of  $M_2/M_1$  we get following Saxena and Dave (1961) :

$$\begin{aligned}
 [\alpha_{T'}]_1^{M'} = \frac{5(6C^* - 5)}{4\sqrt{2}A^*} \left[ 1 - \left( \frac{3}{2} + \frac{2\sqrt{2}}{15} A^* \right) \frac{M_2}{M_1} + \left\{ \frac{13}{24} \right. \right. \\
 \left. \left. - \frac{2\sqrt{3}}{15} A^* + \frac{8}{15} A^* \left( 1 + \frac{2\sqrt{2}}{15} A^* \right) \right\} \frac{M_2^2}{M_1^2} \right], \quad \dots (19)
 \end{aligned}$$

and

$$\begin{aligned}
 [\alpha_{T'}]_2^{M'} - [\alpha_T]_1 \left\{ 1 + \frac{(8E^* - 7)^2}{42} \right\} + \frac{5}{42\sqrt{2}} \frac{(6C^* - 5)(8E^* - 7)}{A^*} \\
 \left\{ 1 - \frac{3(5 - 4B^*)}{4(6C^* - 5)} \right\} + \left[ \frac{(6C^* - 5)(8E^* - 7)^2}{252} \right. \\
 + \frac{5(6C^* - 5)}{4\sqrt{2}A^*} \left\{ \frac{5}{21} (8E^* - 7) \left( 1 - \frac{3}{4} \frac{(5 - 4B^*)}{(6C^* - 5)} \right) \right\} \frac{M_2}{M_1} \\
 + \left[ \frac{(6C^* - 5)(8E^* - 7)(1 - \frac{8}{15} A^*)}{252} + [\alpha_T]_1 \frac{21}{125} (6C^* - 5)^2 \right. \\
 + \frac{5(6C^* - 5)}{4\sqrt{2}A^*} \left\{ \frac{5}{12} (8E^* - 7) \left( 1 - \frac{3(5 - 4B^*)}{4(6C^* - 5)} \right) - \frac{21(6C^* - 5)^2}{125} \right. \\
 \left. \left. - \frac{4}{315} (8E^* - 7)(2A^*(8E^* - 7) - 7(6C^* - 5)) \right\} \right] \frac{M_2^2}{M_1^2}. \quad \dots (20)
 \end{aligned}$$

The various quantities are as defined by Saxena and Dave (1961) after suitably modifying them to suit for isotopic mixtures.

Saxena and Dave (1961a) have also worked out the expressions for the other end of the composition, viz.,  $X_2 \rightarrow 0$   $[\alpha_T']_2^{mix}$  is again given by Eq. (15) where

$$K_1' = \frac{C''_{-1-1} C''_{-2-2}}{C''_{-1-1} C''_{-2-2}} + \frac{C''_{12}^2}{C''_{11} C''_{22}}$$

and

$$\begin{aligned} K_2^1 = & \frac{5}{2} \left( \frac{M_1}{2M_2} \right)^{\frac{1}{2}} \left[ \frac{a_{10} C'_{1-2} C''_{-1-2}}{C''_{11} C''_{-1-1} C''_{-2-2}} - \frac{a_{10} C'_{-1-2} C''_{12}}{C''_{11} C''_{-1-1} C''_{-2-2}} \right. \\ & + \frac{C'_{-12} C''_{0-1} C'_{12}}{C''_{22} C''_{-1-1} C''_{11}} - \frac{C'_{2-2} C''_{1-2} C''_{0-1} C'_{12}}{C''_{22} C''_{-2-2} C''_{-1-1} C''_{11}} - \frac{a_{0-2} C'_{1-2}}{C'_{11} C''_{-2-2}} \\ & \left. + \frac{a_{0-1} C'_{1-1} C''_{1-2}}{C''_{11} C''_{-1-1} C''_{-2-2}} - \frac{a_{20} C'_{12}}{C''_{11} C''_{22}} + \frac{a_{-20} C'_{2-2} C''_{12}}{C''_{11} C''_{22} C''_{-2-2}} \right] \\ & - \frac{5}{2} \left( \frac{M_1}{2M_2} \right)^{\frac{1}{2}} \left[ \frac{a_{0-2} C''_{1-2}}{C'_{-1-1} C''_{-2-2}} + \frac{a_{0-1} C''_{12}}{C''_{11} C''_{22} C''_{-1-1}} \right], \quad \dots (21) \end{aligned}$$

Further

$$[\alpha_T']_1^{mix} = (6C_1^* - 5)(S_1/Q_1), \quad \dots (22)$$

$$[\alpha_T']_1^{iso} = [\alpha_0']_1^{iso} [1 - \gamma' M/M], \quad \dots (23)$$

#### $\alpha_T$ VALUES FOR HYDROGEN ISOTOPES

All the theoretical  $\alpha_T$  values are calculated according to the modified Exp-Six potential for which, parameters are assigned by Mason and Rice (1954). The experimental data of Heath, Ibbs and Wild (1941) giving the composition dependence of  $\alpha_T$  for  $H_2$ - $D_2$  system at 316.4°K are recorded in Table I. For this system the formulae in terms of the reduced mass are preferable to those in terms of the ratio of the molecular masses, and therefore the latter formulae are not used for computation. We find that the Chapman-Cowling approximation formulae have a poor convergence and the second approximation is about 4% greater. Simple Eq. (4) is inadequate in as much as it fails to predict the composition dependence of  $\alpha_T$  contrary to the experimental evidence. The formula given by Eq. (3) is quite good and is preferable for approximate work both from the viewpoint of simplicity and accuracy.

Kihara approximation scheme gives better results and has a better and satisfactory convergence. The difference between the first and second approxima-

tion is small but relatively increases for mixtures having either of the component in trace. Even for such mixtures the probable error because of the neglect of higher approximations is likely to be much smaller than the experimental errors. The shortcomings of the formulae for  $[\alpha_T']_1^{iso}$  and  $[\alpha_T']_1'^{iso}$  are similar to those of the corresponding formulae on Chapman-Cowling scheme.  $[\alpha_T']_1^{mix}$  formula is quite adequate for most of the work at this temperature and has the advantage of being much simpler than  $[\alpha_T']_2^{mix}$ .

The theoretical values, however, are only in approximate agreement with the experimental values. The calculated values are consistently lower than the experimental values. We feel that this discrepancy should be attributed partly to the experimental errors and partly to the lack in the appropriateness of the potential form chosen for calculation. This inadequacy of the potential is more evident in this work because of the greater sensitivity of the thermal diffusion factor to the law of molecular model.

Table II lists the experimental  $\alpha_T$  data of Grew, Johnson and Neal (1954) for  $H_2$ - $D_2$  system as a function of temperature. At lower temperatures the classically calculated values will be in error because of the quantum corrections and we will consider them in detail in the next section. At high temperatures we find that the differences between  $[\alpha_T']_1^{mix}$  and  $[\alpha_T']_2^{mix}$  values are small. The agreement between  $[\alpha_T']_2^{mix}$  and the experimental values is reasonable, the experimental values in this case are systematically lower unlike the previous case, Table I. The difference at high temperatures is much more than the estimated uncertainties in the experimental data, and this gives support to the postulate that the Exp-Six potential is inadequate to precisely represent the potential energy between two hydrogen molecules.  $[\alpha_T]_1^{mix}$  values are also tabulated in Table II and are appreciably different from  $[\alpha_T']_1^{mix}$  values. These calculations also confirm the view that  $[\alpha_T']_1^{mix}$  formula is adequate for all approximate work. The error involved because of the neglect of higher approximations may be in between 2 to 3% but  $[\alpha_T']_1^{mix}$  formula is preferable from the viewpoint of computational labour.

Some interest centres in the  $\alpha_T$  values of  $H_2$ - $D_2$  mixtures with either of the component present in trace. Such values of  $\alpha_T$  are recorded in Tables III and IV as a function of temperature. In Table III are recorded the rigorous  $[\alpha_T]_2^{mix}$  and  $[\alpha_T']_2^{mix}$  values, as well as the values obtained from the simpler expressions in terms of the reduced mass. The listings indicate that these simpler expressions (Eqs. (9) and (18)) are quite adequate from the point of accuracy. Here also Kihara approximation results are preferable. If in the mixtures  $H_2$  is in trace results of Table IV apply and which again suggest preference for Kihara approximation formulae. In Table V are reported the  $\alpha_T$  values as a function of temperature, for  $H_2$ -HD and HD- $D_2$  systems with the heavier component in trace and calculated according to Kihara approximation scheme. The second approxi-

mation formula expressed in terms of the reduced mass is used in these calculations.

For  $H_2-T_2$  system with  $T_2$  in trace the calculated values are presented in Table VI. Here, the formula in terms of the ratio of molecular masses are preferable to those expressed in powers of the reduced mass. An examination of the rigorous first and second approximation  $\alpha_T$  values of Table VI reveals that the convergence for both the approximation schemes is of the same order but is worse than for  $H_2-D_2$  mixtures. Kihara approximation is slightly preferable. The simpler formula up to the second power of  $(M_2/M_1)$  is as adequate as the rigorous formula and should be used in view of its simplicity. For  $H_2-HT$  system the results of  $H_2-D_2$  system apply as both have identical molecular weights and intermolecular forces. For  $HT-T_2$  system with  $T_2$  in trace the calculated values of  $[\alpha_T']_2^{1/2}$  given in Table V are according to the formula involving reduced mass. For  $H_2-T_2$  system with  $H_2$  in trace values may be calculated according to the expressions given by Saxena and Dave (1961a). As these values are of little practical importance no tabulations are presented in this paper.

#### APPROXIMATE QUANTUM MECHANICAL CALCULATION OF $\alpha_T$

At present it is not possible to perform rigorous quantum mechanical calculations of  $\alpha_T$  for realistic intermolecular potentials though attempts in this direction have started. Choi and Ross (1960). We will, therefore, adopt an approximate procedure suggested by de Boer and Bird (1954) and applied for the case of He by Saxena, Kelley and Watson (1961). This calculation is valid only for the reduced temperature greater than five and is according to a simple inverse twelfth power potential. Following de Boer and Bird (1954) it can be shown that

$$A_{qu}^* = A_{cl}^* \frac{[1 + \{C^{(2,2)}\Lambda^{*2}/T^{*5/6}\}]}{[1 + \{C^{(1,1)}\Lambda^{*2}/T^{*5/6}\}]}, \quad (24)$$

and

$$C_{qu}^* = C_{cl}^* \frac{[1 + \{C^{(1,2)}\Lambda^{*2}/T^{*5/6}\}]}{[1 + \{C^{(1,1)}\Lambda^{*2}/T^{*5/6}\}]}, \quad (25)$$

Here  $\Lambda^* = h/\sigma(2\mu\epsilon)^{1/2}$ ,  $h$  is the Planck's constant,  $\epsilon$  and  $\sigma$  are the potential parameters and  $\mu = (M_1 M_2)/N_0(M_1 + M_2)$ ,  $N_0$  being the Avogadro's number. The values of  $C^{(i,j)}$  used are those given by Saxena, Kelley and Watson (1961). We will use the first approximation Kihara formula for  $\alpha_T$  and the following simple potential

$$\phi(r) = 4\epsilon(\sigma/r)^{12}, \quad (26)$$

where  $\phi(r)$  is the potential energy between two molecules at a separation distance  $r$ ,  $\epsilon$  and  $\sigma$  are the potential parameters and for our present work we have taken their values as  $37.3^\circ K$  and  $3.337 \text{ \AA}$  respectively, following Mason and Rice (1954).



TABLE I

Experimental and calculated values of  $\alpha_T$  for the  $H_2$ - $D_2$  system at 316.4°K.

% of $D_2$	Chapman-Cowling approximation scheme					Kihara approximation scheme			
	$\alpha_T$ Eq. (1)	$[\alpha_T]^{iso}_1$ Eq. (4)	$[\alpha_T]^{iso}_1$ Eq. (3)	$[\alpha_T]^{mix}_1$ Eq. (2)	$[\alpha_T]^{mix}_2$ Eq. (1)	$[\alpha_T']^{iso}_1$ Eq. (1)	$[\alpha_T']^{iso}_1$ Eq. (1)	$[\alpha_T']^{mix}_1$ Eq. (1)	$[\alpha_T']^{mix}_2$ Eq. (15)
100	—	0.164	0.155	0.147	0.153	0.169	0.163	0.157	0.155
90	0.161	0.164	0.157	0.149	—	0.169	0.161	0.158	0.157
80	0.166	0.164	0.159	0.149	0.156	0.169	0.165	0.159	0.157
70	0.170	0.164	0.161	0.152	—	0.168	0.167	0.160	0.160
60	0.173	0.164	0.163	0.154	—	0.169	0.168	0.161	0.161
50	0.173	0.161	0.164	0.156	0.162	0.169	0.169	0.162	0.163
40	0.173	0.161	0.166	0.158	—	0.169	0.170	0.164	0.165
30	0.177	0.164	0.168	0.161	—	0.169	0.172	0.166	0.167
20	0.176	0.164	0.170	0.163	—	0.169	0.173	0.167	0.169
10	0.187	0.164	0.172	0.166	0.169	0.169	0.174	0.169	0.172
0	—	0.164	0.174	0.169	0.174	0.169	0.176	0.171	0.174

TABLE II

Experimental and calculated values of  $\alpha_T$  for an equimolar mixture of  $H_2$ - $D_2$  as a function of temperature.

T °K	$\alpha_T$ Exptl*	$[\alpha_T]^{mix}_1$ Eq. (2)	$[\alpha_T']^{mix}_1$	$[\alpha_T']^{mix}_2$ Eq. (15)
29.3	0.0050	0.0058	0.0059	+0.0008
46.5	0.063	0.027	0.028	0.024
73.6	0.102	0.076	0.079	0.076
118.7	0.132	0.117	0.122	0.119
185	0.146	0.143	0.149	0.147
293	0.152	0.155	0.161	0.162
465	0.152	0.158	0.164	0.166

\*Values refer to a binary mixture consisting of 49.7%  $D_2$  and 50.3%  $H_2$ .

TABLE III

Calculated values of  $\alpha_T$  for  $H_2-D_2$  in trace ( $X_1 \rightarrow 0$ ).

T °K	Chapman-Cowling approximation scheme				Kihara approximation scheme			
	$[\alpha_T]_1^{mix}$ Eq. (6)	$[\alpha_T]_1^{iso}$ Eq. (7)	$[\alpha_T]_2^{mix}$ Eq. (8)	$[\alpha_T]_2^{iso}$ Eq. (9)	$[\alpha_T']_1^{mix}$ Eq. (16)	$[\alpha_T']_1^{iso}$ Eq. (17)	$[\alpha_T']_2^{mix}$	$[\alpha_T']_2^{iso}$ Eq. (18)
185	0.156	0.161	0.159	0.162	0.157	0.161	0.150	0.160
316	0.169	0.174	0.174	0.178	0.171	0.176	0.175	0.175
465	0.171	0.176	0.177	0.176	0.173	0.177	0.177	0.178
900	0.168	0.172	0.173	0.173	0.170	0.174	0.174	0.175

TABLE IV

Calculated values of  $\alpha_T$  for  $H_2-D_2$  system with  $H_2$  in trace ( $X_2 \rightarrow 0$ ).

T °K	Chapman-Cowling approximation scheme			Kihara approximation scheme		
	$[\alpha_T]_1^{mix}$ Eq. (12)	$[\alpha_T']_2^{iso}$ Eq. (13)	$[\alpha_T]_2^{mix}$ Eq. (14)	$[\alpha_T']_1^{mix}$ Eq. (22)	$[\alpha_T']_1^{iso}$ Eq. (23)	$[\alpha_T']_2^{mix}$ Eq. (21)
185	0.134	0.111	0.139	0.143	0.150	0.140
316	0.147	0.155	0.153	0.157	0.163	0.155
465	0.149	0.156	0.156	0.158	0.165	0.158
900	0.147	0.155	0.154	0.156	0.162	0.156

TABLE V

Calculated values of  $\alpha_T$  for various systems with the heavier component present always in trace ( $X_1 \rightarrow 0$ ).

T °K	$H_2-HD$	$HD-D_2$	$HT-T_2$
185	0.0956	0.0681	0.0957
316	0.1035	0.0747	0.1037
465	0.1050	0.0758	0.1043
900	0.1051	0.1122	0.1020

TABLE VI

Calculated values of  $\alpha_T$  for  $H_2$ - $T_2$  system where  $T_2$  is in trace ( $X_1 \rightarrow 0$ ).

T °K	Chapman-Cowling approximation scheme				Kihara approximation scheme			
	$[\alpha_T]_1^{mix}$ Eq. (6)	$[\alpha_T]_1^{M'}$ Eq. (10)	$[\alpha_T]_2^{mix}$ Eq. (8)	$[\alpha_T]_2^{M'}$ Eq. (11)	$[\alpha_T]_1^{mix}$ Eq. (16)	$[\alpha_T]_1^{M'}$ Eq. (19)	$[\alpha_T]_2^{mix}$ Eq. (20)	$[\alpha_T]_2^{M'}$ Eq. (20)
185	0.232	0.238	0.237	0.255	0.233	0.240	0.237	0.238
465	0.255	0.261	0.263	0.284	0.256	0.264	0.264	0.265
900	0.251	0.257	0.259	0.278	0.252	0.260	0.259	0.260

These calculations are therefore valid for temperatures only above 185°K. At 185°K the quantum mechanical  $[\alpha_T]_1^{mix}$  value for an equimolar mixture of  $H_2$ — $D_2$  is about 1.7% greater than the corresponding classical value. If the rigorous calculations are performed for a realistic intermolecular potential the correction will be probably larger. This view gets support from the treatment of low temperature diffusion data, Saxena (1960), and from the work of Cohen *et al.* (1956).

## ACKNOWLEDGMENT

The authors are thankful to Mr. H. N. Sethna and Dr. J. Shankar for their interest and encouragement in this work.

## REFERENCES

- Chapman, S., 1941, *Proc. Roy. Soc.*, **A177**, 38.  
 Chapman, S. and Cowling, T. G., 1953, *The Mathematical Theory of Non-Uniform Gases*, Cambridge University Press, England.  
 Chou, S. and Ross, J., 1960, *J. Chem. Phys.*, **33**, 1324.  
 Cohen, E. G. D., Offerhaus, M. J., Van Leeuwen, J. M. J., Ross, B. W. and de Boer, J., 1956, *Physica*, **22**, 791.  
 de Boer, J. and Bird, R. B., 1951, *Phys. Rev.*, **83**, 1259, 1954, *Physica*, **20**, 185.  
 Grew, K. E., Johnson, F. A., and Neal, W. E. J., 1954, *Proc. Roy. Soc.*, **A224**, 513.  
 Heath, I. R., Ibbot, T. L., and Wild, N. E., 1941, *Proc. Roy. Soc.*, **A178**, 380.  
 Hirschfelder, J. O., Curtiss, C. F., and Bird, R. B., 1954, *The Molecular Theory of Gases and Liquids*, John Wiley and Sons, Inc., New York.  
 Kihara, T., 1949, *Imperfect Gases*, Originally published in Japanese (Asakusa Book Store, Tokyo) and translated into English by the U. S. office of Air Research, Wright-Patterson Air Force Base; See also 1953, *Rev. Mod. Phys.*, **25**, 831.  
 Mason, E. A., 1954, *J. Chem. Phys.*, **22**, 169.  
 Mason, E. A., 1957, *J. Chem. Phys.*, **27**, 75, 782.  
 Mason, E. A. and Rice, W. E., 1954, *J. Chem. Phys.*, **22**, 522.  
 Mason, E. A., and Saxena, S. C., 1959, *J. Chem. Phys.*, **31**, 511.  
 Saxena, S. C., 1960, *Physica*, **26**, 730.  
 Saxena, S. C., and Dave, S. M., 1961, *Rev. Mod. Phys.*, **33**, 148.  
 Saxena, S. C., and Dave, S. M., 1961a, In course of preparation.  
 Saxena, S. C., Koley, J. G. and Watson, W. W., *Phys. Fluids*, to be published.  
 Saxena, S. C., and Mason, E. A., 1958, *J. Chem. Phys.*, **28**, 623.  
 Saxena, S. C. and Pandey, P. A., 1961, *Ind. J. Phys.*, **35**, 55. (paper 1).

## APPENDIX

The defining relations for  $A_i$  which occur in connection with Eq. (9) are as follows :

$$A = Z_{01}Z'_{22} - Z_{02}Z'_{12},$$

$$A_1 = Z_{11}Z'_{22} - Z_{12}^2,$$

$$A_2 = Z_{01}(Z_{22}' - Z_{22}'' - C_3) - (Z_{02}'/2)(2Z_{12}' - 3Z_{12}'' - 2C_2),$$

$$C_2 = \frac{1295}{64} \Omega^{(1,1)*} - \frac{1827}{32} \Omega^{(1,2)*} + \frac{285}{4} \Omega^{(1,3)*} - \frac{75}{2} \Omega^{(1,4)*}$$

$$C_3 = \frac{7805}{512} \Omega^{(1,1)*} - \frac{5439}{64} \Omega^{(1,2)*} + \frac{2319}{16} \Omega^{(1,3)*}$$

$$- \frac{525}{4} \Omega^{(1,4)*} + \frac{225}{4} \Omega^{(1,5)*} - \frac{35}{8} \Omega^{(2,2)*}$$

$$- 14 \Omega^{(2,3)*} + 10 \Omega^{(2,4)*} + 3 \Omega^{(3,3)*},$$

$$A_3 = Z'_{11}(2Z'_{22} - Z''_{22} - C_3) - Z_{22}'\{(Z'_{11}/2) + S_{11}\} - Z'_{12}(4Z'_{12} - 3Z''_{12} - 2C_2),$$

$$S_{11} = \frac{45}{8} \Omega^{(1,1)*} - \frac{45}{2} \Omega^{(1,2)*} + 18 \Omega^{(1,3)*},$$

$$A_4 = Z_{02}Z''_{12},$$

$$A_5 = Z_{11}''Z_{22}'' - Z''_{12}^2,$$

$$A_6 = Z_{02}Z''_{12} - Z_{01}Z''_{22},$$

$$A_7 = Z_{01}Z'_{12} - Z_{02}Z'_{11},$$

$$A_8 = Z''_{12}(Z'_{22} - Z_{22}''),$$

$$A_9 = Z''_{12}Z'_{22} - Z''_{22}Z'_{12},$$

$$A_{10} = Z''_{12}(Z'_{12} - Z''_{12}),$$

$$A_{11} = Z''_{12}(Z'_{12} - Z''_{12}) - Z''_{22}(Z'_{11} - Z''_{11}),$$

$$A_{12} = Z_{01}\{3Z'_{12} - (3/2)Z''_{12} - C_2\} - Z_{02}\{Z'_{11} - (Z''_{11}/2) - S_{11}\}.$$

# EFFICACY OF THE PARABOLIC INTERPOLATION TECHNIQUE IN THE DERIVATION OF MOLECULAR CONSTANTS

N. R. TAWDE, N. SREEDHARA MURTHY\* AND (Miss) SHARADA HEGDE

DEPARTMENT OF PHYSICS, KARNATAK UNIVERSITY, DHARWAR

(Received November 13, 1961)

**ABSTRACT** The molecular constants  $\nu_0$ ,  $(B'_v - B''_v)$ , and  $(D'_v - D''_v)$  of  $(1\Sigma^+ \rightarrow {}^1\Pi)$  system of MgO have been recalculated from the  $Q(J)$  measurements of Lagerqvist and Uhler (1949), using the parabolic interpolation method of Logunov (1959) in place of the graphical procedure adopted by Lagerqvist and Uhler. The constants thus revised have been tested for precision in relation to graphical method and it is found that they reflect the experimental data many times better than the graphical method.

## INTRODUCTION

Recently Logunov (1959) has given a procedure for evaluating the molecular constants of a band system by correctly processing the data mathematically with the use of least square technique (Chebyshev). He has illustrated this method in the case of (11, 2) band of BeO ( ${}^1\Pi \rightarrow {}^1\Sigma$ ) system obtained with a spectral dispersion of 2 Å/mm. As the method has given a set of constants with a fair amount of accuracy even under such inadequate dispersion and less number of measured lines, we thought it desirable to examine the method for better accuracy, if any, by using larger number of measurements, and those too, under high dispersion. The bands chosen are those of MgO ( ${}^1\Sigma^+ \rightarrow {}^1\Pi$ ) system for which the measurements of rotational lines under a dispersion of 1.2 Å/mm are available from the work of Lagerqvist and Uhler (1949) and for which molecular constants have been evaluated by them using the usual graphical method.

## PROCEDURE

The following is the expression for the wave numbers of the rotational lines of a  $Q$  branch.

$$\nu = Q(J) = \nu_0 + (B'_v - B''_v)J(J+1) - (D'_v - D''_v)J^2(J+1)^2 + \quad (1)$$

where  $\nu_0$  = zero line of a band,  $B'_v$ ,  $D'_v$  and  $B''_v$ ,  $D''_v$  are the rotational constants of the upper and lower states respectively. Logunov has evaluated  $(B'_v - B''_v)$  and  $(D'_v - D''_v)$  according to the least square technique of the orthogonal Chebyshev functions by solving the normal equations employing Doolittle scheme. The values of powers and sums of powers of  $J(J+1)$  are given by Logunov up to  $J = 50$ .

\*On leave of absence from the Central College, Bangalore

TABLE I  
Molecular constants for MgO ( $\Sigma^* \rightarrow {}^1\Pi$ ) system

Band $\nu', \nu''$	$\nu_0$ cm <sup>-1</sup>		$B', -B'',$ cm <sup>-1</sup>		$(D_1', -D_1'')$ 10 <sup>6</sup> cm <sup>-1</sup>	
	Parabolic method	Graphical method (L & U)	Parabolic method	Graphical method (L & U)	Parabolic method	Graphical method (L & U)
2,0	18120.04 ± 0.01	18119.8 <sub>6</sub>	0.067231 ± 0.000007	0.06755	-0.0013 ± 0.0007	0.03
1,0	17314.855 ± 0.007	17314.8 <sub>5</sub>	0.072086 ± 0.000004	0.07215	-0.0030 ± 0.0005	0.00
0,0	16500.28 ± 0.01	16500.2 <sub>9</sub>	0.07692 ± 0.00001	0.07665	-0.006 ± 0.001	-0.03
0,1	15843.67 ± 0.01	15843.6 <sub>7</sub>	0.08157 ± 0.00001	0.08125	0.005 ± 0.003	-0.03
0,2	15194.81 ± 0.01	15194.8 <sub>7</sub>	0.08615 ± 0.00001	0.0839	0.004 ± 0.002	-0.02

L & U: Lagerqvist and Uhler

TABLE II

Band 0,0			Band 0,2		
J	(O-C) Parabolic present study	(O-C) Graphical L. & U	J	(O-C) Parabolic present study	(O-C) Graphical L. & U
74	-0.03	0.74	63	0.02	0.57
75	-0.05	0.72	64	0.03	0.50
76	0.00	0.76	65	0.01	0.57
77	-0.03	0.74	66	-0.04	0.53
78	0.05	0.81	67	-0.02	0.55
79	0.05	0.80	68	0.01	0.59
80	0.03	0.78	69	0.00	0.58
81	0.05	0.80	70	0.05	0.63
82	-0.01	0.73	71	0.02	0.60
83	-0.03	0.70	72	0.00	0.58
			73	-0.04	0.53
			74	-0.07	0.51
			75	0.02	0.59
			76	0.10	0.67
			77	-0.07	0.49

L. &amp; U.—Lagerqvist &amp; Uhler

only. As some of the bands have rotational lines as high as  $J = 97$ , we have extended these computations to  $J = 100$ . The  $Q(J)$  measurements of Lagerqvist and Uhler have been adopted, but in making use of them, their asterisked values have not been taken into account, because of uncertainty in the accuracy of their measurements as a result of overlapping.

## RESULTS

The molecular constants evaluated correct to the third approximation for the 5 bands of MgO (red system) for which  $Q(J)$  measurements are available are shown in Table I. Along with these, the results of Lagerqvist and Uhler by graphical method are also given for comparison.

## DISCUSSION

The parabolic procedure is adopted only for a  $Q$  branch, and only  $(B'_v - B''_v)$  and  $(D'_v - D''_v)$  are obtained, whereas for obtaining  $B'_v$ ,  $B''_v$  and  $D'_v$ ,  $D''_v$  individually, one has to analyse  $P$  and  $R$  branches by the method of combination differences. The least square technique given by Loginov, as adopted here, is found simple and convenient for estimating their accuracy by the method of Gauss. Further, as can be seen from Table I, an accuracy of a much better order in molecular constants is obtainable here, by the application of the parabolic method than by the graphical method. The correctness of the rotational constants is determined by finding out the values of  $v$  from the expression (1) for both sets of constants in Table I. Such a comparison in the case of (0,0) and (0,2) bands for high  $J$  values is given in Table II, and compared with the measured values of  $Q(J)$ . To make the two methods comparable,

the value of  $B''_c$  is calculated from the knowledge of the average value  $B''_v \left( = \frac{B''_c + B''_d}{2} \right)$  and  $(B''_c - B''_d)$  given by Lagerqvist and Uhler. As a result of  $\lambda$ -type doubling, the  $Q$  branch involves the use of  $B''_c$ , and this value is used for the calculation of  $(O - C)$  (difference between the observed and calculated values) in the case of graphical method. It is quite evident from a comparison of  $(O - C)$  under parabolic and graphical methods that the calculated values given by the former method agree very closely with the measured values, whereas in the case of graphical method, the calculated values differ appreciably and this is much more so at high  $J$  values where the deviation reaches as much as  $0.81 \text{ cm}^{-1}$ . In the case of least square technique, it does not exceed  $0.1 \text{ cm}^{-1}$  i.e. 1/8th the measure obtained from the graphical method. The same is also verified to be true in the case of other bands too, of this system. There is a considerable difference in the values of  $(D'_v - D''_v)$  obtained from the parabolic procedure and the graphical method. This is partly responsible for the comparatively large difference  $(O - C)$ , arising from the graphical method, particularly at the high  $J$  values, where the term involving  $(D'_v - D''_v)$  becomes more important. It may safely be concluded from this observation that the constants evaluated here by the parabolic method reflect the experimental data with much greater precision than those obtained by Lagerqvist and Uhler using the graphical method. Thus there should be as much stress laid on the mathematical processing of the observational data, as it is on the precision in measurement.

Because of the presence usually of small systematic perturbations, either in the upper or lower or in both the states, it is generally preferable to use the method of combination differences (either through graphical or least square evaluation). However, in the present MgO (red) system under study, Lagerqvist and Uhler have not noticed any perturbations in the two states of it, and if at all present, they may be too small to be detected in the vibrational levels of  $\Sigma^*$  investigated. This offers a justification for the use of parabolic method to give better accuracy of molecular constants in such cases.

#### ACKNOWLEDGMENTS

One of the authors (N.S.M.) is grateful to the National Institute of Sciences of India for permission to work on this particular piece in the general research programme. He is also thankful to Dr. K. S. Rao for helpful discussions on the subject. Miss Hegde expresses her gratitude to the Ministry of Education, Government of India for the award of a Research Training Scholarship.

#### REFERENCES

- Logunov, V. A., 1950, *Optics and Spectroscopy*, **6**, 197  
 Lagerqvist, A., and Uhler, U., 1949, *Arkiv f. Fys.*, **21**, 459



# A NOTE ON THE CALCULATION OF THE DENSITY OF STATES

T. C. ROY

PHYSICS DEPARTMENT,  
JADAVPUR UNIVERSITY, CALCUTTA, INDIA

(Received October 4, 1961)

**ABSTRACT.** An analysis had been made here about the number of states per unit energy interval in the final state. The calculation has been made in the cases where there is no external field and when there is an external field independent of time.

The calculation of matrix element for scattering cross section with the help of  $S$ -matrix formalism has now a days been greatly facilitated by the use of Feynman graphs and by using the renormalisation techniques. As a result the remaining job i.e., set of rules for calculating the density of states seems to be of worth consideration.

Let us suppose that we have a number of incoming particles which after collision (1) freely or (2) in a time independent external field get scattered with or without change of the total number of particles. Let the total number of particles be  $n$  in the final state. Then the general results of quantum field theory state that in case (1) both the total momentum and total energy will be conserved and in case (2) simply the total energy will be conserved. This really means that out of the  $3n$  components of moments of the  $n$  particles, in case (1) there will be 4 relations among them and in case (2) there will be only one. Thus the number of degrees of freedom will be either (1)  $3n - 4$  or it will be (2)  $3n - 1$ . Since now we are to calculate the number of states inside the energy shell of thickness unity we do not let the final energy be constant but rather use it as a parameter. Thus we have now either (1)  $3(n - 1)$  or (2)  $3n$  degrees of freedom, that is, we might use the momenta co-ordinates of all the (1)  $(n-1)$  particles or (2)  $n$  particles for our description.

Let now the unimportant co-ordinate space volume be unity, which really goes out in cross section calculation, then using polar co-ordinates in momentum space we have an element of volume in phase space as,  $p^2 dp d\Omega$ , so that the number of states in  $dE_f$  is,

$$(1) \frac{p_1^2 p_2^2 \dots p_{n-1}^2 dp_1 \dots dp_{n-1} d\Omega_1 \dots d\Omega_{n-1}}{(2\pi\hbar c)^3 (n-1)}$$

$$(2) \frac{p_1^2 p_2^2 \dots p_n^2 dp_1 \dots dp_n d\Omega_1 \dots d\Omega_n}{(2\pi\hbar c)^3 n}$$

But now we have got to choose having the physical phenomenon in mind any (1)  $3n-4$  or (2)  $3n-1$  co-ordinates say, (1)  $\alpha_1, \alpha_2, \dots, \alpha_{3n-4}$  or 2)  $\alpha_1 \dots \alpha_{3n-1}$  and the last co-ordinate should always be  $dE_f$ .

The expression then of  $\rho_f$  will be,

$$(1) \quad \rho_f dE_f = \rho d\alpha_1 \dots d\alpha_{3n-4} dE_f = \frac{p_1^2 \dots p_{n-1}^2 dp_1 \dots dp_{n-1} d\Omega_1 \dots d\Omega_{n-1}}{(2\pi\hbar c)^{3(n-1)}}$$

$$(2) \quad \rho_f dE_f = \rho d\alpha_1 \dots d\alpha_{3n-1} dE_f = \frac{p_1^2 \dots p_n^2 dp_1 \dots dp_n d\Omega_1 \dots d\Omega_n}{(2\pi\hbar c)^{3n}}$$

Therefore,

$$(1) \quad \rho = \frac{p_1^2 \dots p_{n-1}^2}{(2\pi\hbar c)^{3(n-1)}} \frac{d(p_1 \dots p_{n-1} \Omega_1 \dots \Omega_{n-1})}{d(\alpha_1 \dots \alpha_{3n-4}, E_f)}$$

$$(2) \quad \rho = \frac{p_1^2 \dots p_n^2}{(2\pi\hbar c)^{3n}} \frac{d(p_1 \dots p_n \Omega_1 \dots \Omega_n)}{d(\alpha_1 \dots \alpha_{3n-1}, E_f)}$$

The method will be illustrated by giving two classic examples. For case (1) let us consider the case of Compton scattering. Here  $n=2$  and we may take the  $3n-4=2$   $\alpha$ 's as  $d\Omega$  of the photon momentum, thus,

$$\rho = \frac{k^2}{(2\pi\hbar c)^3} \frac{d(k, \Omega)}{d(E_f, \Omega)} = \frac{k^2}{(2\pi\hbar c)^3} \left( \frac{dk}{dE_f} \right) \Omega$$

Hence the density per unit energy interval is,

$$\rho_f = \frac{k^2 d\Omega}{(2\pi\hbar c)^3} \left( \frac{dk}{dE_f} \right) \Omega$$

As an example of case (2) we consider the case of Brem-strahlung. Here also,  $n=2$  and we may take the  $3n-1=5$   $\alpha$ 's as  $dk d\Omega d\Omega_k$ ; thus

$$\begin{aligned} \rho &= \frac{p^2 k^2}{(2\pi\hbar c)^6} \frac{d(p, k, \Omega, \Omega_k)}{d(E_f, k, \Omega, \Omega_k)} \\ &= \frac{p^2 k^2}{(2\pi\hbar c)^6} \left( \frac{dp}{dE_f} \right) \Omega, k \\ &= \frac{p E k^2}{(2\pi\hbar c)^6} \end{aligned}$$

Hence the density per unit energy interval is,

$$\rho_f = \frac{p E k^2}{(2\pi\hbar c)^6} d\Omega d\Omega_k dk$$

# ON DETECTION OF GROUP INVARIANCE OR TOTAL SYMMETRY OF A BOOLEAN FUNCTION

A. K. CHOUDHURY AND M. S. BASU

INSTITUTE OF RADIO PHYSICS AND ELECTRONICS,  
CALCUTTA UNIVERSITY

(Received September 4, 1961)

**ABSTRACT.** A systematic procedure of finding out the group invariance or total symmetry of a switching function is presented in this paper. By interpreting the terms of any  $n$ -variable function as vertices of an  $n$ -dimensional unit cube, the relative distances of each term with respect to the other terms of the function are computed. The knowledge of these distances enables one to locate the terms among which re-ordering will be possible under permutation or priming operations which will keep the transmission matrix unaltered.

## INTRODUCTION

As a rule a Boolean function is altered if some of the variables are permuted or primed. There are however certain functions which, for some permutations or priming operations, remain unaltered. That is, the same terms are again obtained after the permutation or priming operations are done and the transmission remains unchanged. This is expressed by saying that the function has group invariance for those particular operations. There is yet another class of functions which remains unaltered for all possible permutation of the variables. Such functions are said to exhibit total symmetry. Different authors (Caldwell, 1954; McCluskey, 1956) have suggested methods of finding the group invariance and total symmetry of switching functions. In this paper a method is presented for finding out the group invariance or total symmetry by utilising the geometrical concept of the function.

## BASIC PRINCIPLE UNDERLYING THE METHOD

The total number of permutations and priming operations that can be applied to an  $n$ -variable Boolean function is  $n!2^n$ . Under some of these operations the function may remain unaltered. When the function remains unaltered, the only change that can take place in the transmission matrix of the function under these permutations and priming operations is that some of the rows may interchange places. In the Table I(a) is given the transmission matrix of a Boolean function  $T = \Sigma(0, 1, 2, 7, 11, 13)$

In Table I(b) is shown the effect of permutation of variables  $X_3$  and  $X_4$ . It will be seen that due to this operation transmission matrix has remained unchanged with re-ordering between rows 7 and 11.

TABLE 1

(a)					(b)				
	$X_4$	$X_3$	$X_2$	$X_1$		$X_3$	$X_4$	$X_2$	$X_1$
0	0	0	0	0	0	0	0	0	0
1	0	0	0	1	1	0	0	0	1
2	0	0	1	0	2	0	0	1	0
7	0	1	1	1	11	1	0	1	1
11	1	0	1	1	7	0	1	1	1
13	1	1	0	1	13	1	1	0	1

If two columns of a transmission matrix are identical then it is obvious that those two columns can be interchanged without changing the transmission matrix in any way. In Table II (a) is given the transmission matrix of a Boolean function  $T = \Sigma(0, 1, 2, 3, 12, 13, 14)$ .

TABLE II

(a)					(b)				
	$X_1$	$X_3$	$X_2$	$X_4$		$X_3$	$X_1$	$X_2$	$X_4$
0	0	0	0	0	0	0	0	0	0
1	0	0	0	1	1	0	0	0	1
2	0	0	1	0	2	0	0	1	0
3	0	0	1	1	3	0	0	1	1
12	1	1	0	0	12	1	1	0	0
13	1	1	0	1	13	1	1	0	1
14	1	1	1	0	14	1	1	1	0

In Table II(b) is shown the effect of permutation of variables  $X_3$  and  $X_4$ . It will be seen that due to these operations the transmission matrix has remained unaltered without any re-ordering between the rows.

Any term of a given  $n$ -variable Boolean function may be represented as a vertex of an  $n$ -dimensional unit cube. Each term of the given function is related to other terms by certain changes of variables. Geometrically this means that the vertex is separated by certain distances from other vertices corresponding to the given function. For any given term of the function, if we calculate the number of terms related to it by one change of variable, by two changes of variables etc., and arrange these numbers one after another we get an array of numbers which we call the distance vector of the term. Permutation and priming of the variables

are equivalent to re-numbering the vertices of the  $n$ -dimensional unit cube. It follows, therefore, that if due to any permutation and priming operation the function is to remain unchanged with re-ordering among certain rows, then this re-ordering can only take place between rows which are identically related regarding mutual separation between the different vertices, i.e., amongst rows having identical distance vectors.

In the Table III is given the function of Table I(a) with the distance vector of the individual terms.

TABLE III

	$X_4$	$X_3$	$X_2$	$X_1$	$\omega_1$	$\omega_2$	$\omega_3$	$\omega_4$
0	0	0	0	0	2	0	3	0
1	0	0	0	1	1	4	0	0
2	0	0	1	0	1	3	0	1
7	0	1	1	1	0	4	1	0
11	1	0	1	1	0	4	1	0
13	1	1	0	1	0	3	1	1

$w_1, w_2, \dots$  etc. denote weight of order 1, weight of order 2 etc. for any particular term. By weight of order  $K$  of any term is meant the total number of terms in the function which differ by  $K$  changes of variables from the term in question.

It will be seen from the Table III that only terms 7 and 11 have identical distance vectors. Hence re-ordering can take place between 7 and 11. By computing the distance vector of each term of a given function we can at once find the possible re-ordering among the rows of the transmission matrix if the function has to remain invariant under permutation and priming operations. Once we have thus spotted rows which can be re-ordered amongst themselves, it is an easy matter to find out the specific operations which will convert one into the other. Considering the effect of those operations on the other rows of the transmission matrix we can determine the group invariance of the function.

#### ILLUSTRATION OF THE METHOD AS APPLIED TO DIFFERENT TYPES OF FUNCTIONS

While searching for group invariance we may come across the following different types of functions :

(I) The function may be such that none of the distance vectors of the terms are identical, i.e., no re-ordering between the rows is possible but some of the columns of the transmission matrix may be identical and it is possible to interchange those columns without altering the transmission. It is extremely easy to find out such group invariances. In the Table IV is given the transmission matrix with the distance vectors of each term of a function  $T = \Sigma(0, 1, 6, 15)$ .

TABLE IV  
 $T = \Sigma(0, 1, 6, 15)$

	$X_4$	$X_3$	$X_2$	$X_1$	$\omega_1$	$\omega_2$	$\omega_3$	$\omega_4$
0	0	0	0	0	1	1	0	1
1	0	0	0	1	1	0	2	0
6	0	1	1	0	0	2	1	0
15	1	1	1	1	0	1	1	1

It will be seen that no two rows have identical distance vector. Hence no re-ordering between rows is possible. But columns  $X_3$  and  $X_2$  are identical. Hence  $X_3$  and  $X_2$  can be permuted amongst themselves without affecting the transmission.

(II) The function may be such that it has a row consisting of only 0's or only 1's and that the distance vector of that particular row is different from the distance vectors of all other rows. Hence it is obvious that any priming operation will alter the function. In detecting group invariance of such a function only permutation operations have to be considered.

In the Table V is given the transmission matrix with distance vectors of each term of a function  $T = \Sigma(0, 1, 6, 10, 12)$ .

TABLE V

	$X_4$	$X_3$	$X_2$	$X_1$	$\omega_1$	$\omega_2$	$\omega_3$	$\omega_4$
0	0	0	0	0	1	3	0	0
1	0	0	0	1	1	0	3	0
6	0	1	1	0	0	3	1	0
10	1	0	1	0	0	3	1	0
12	1	1	0	0	0	3	1	0

It will be seen that first row has entry 0 at all columns positions and distance vector of this term is distinct from all other terms. Hence all priming operations will alter the function. It will be seen that terms 6, 10, 12 have identical distance vectors. Hence re-ordering between 6, 10, 12 is possible. Any permutation of variables  $X_4, X_3, X_2$  will keep the function invariant.

(III) The function may be such that it may have group invariance under both priming and permutation operations.

In the Table VI is given the transmission matrix with distance vector of each terms of a function  $T = \Sigma(0, 3, 5, 9, 14)$ .

TABLE VI

	$X_4$	$X_3$	$X_2$	$X_1$	$\omega_1$	$\omega_2$	$\omega_3$	$\omega_4$
0	0	0	0	0	0	3	1	0
3	0	0	1	1	0	3	1	0
5	0	1	0	1	0	3	1	0
9	1	0	0	1	0	3	1	0
14	1	1	1	0	0	0	4	0

It will be seen from the table that distance vector of the last term is different from all other terms and remaining terms (0 3, 5, 9) can be re-ordered amongst themselves.

The column positions  $X_4$ ,  $X_3$ ,  $X_2$  are identical in the last term. Therefore  $X_4$ ,  $X_3$ ,  $X_2$  can be permuted amongst themselves without altering the last term. We find that these permutations effect the re-ordering between (3, 5, 9). In order to make re-ordering of terms 3, 5 or 9 with the term 0 possible, certain priming operations will be necessary. Since the last term cannot be changed, it will require two priming operations and  $X_1$  must be one of them. Hence the only priming operations possible are  $X_1$  and  $X_2$ ,  $X_1$  and  $X_3$ , and  $X_1$  and  $X_4$  and after priming, the columns must be permuted to keep the transmission unchanged. It will be observed that certain priming operation becomes necessary for re-ordering between 0 and other terms 3, 5, 9 because the number of 1's in the row (0) is different from number of 1's present in the other rows (3,5, 9). In situations where the rows among which re-ordering is possible (as indicated by their having identical distance vectors) are found to contain different number of 1's, then certain priming operations will be necessary to effect the re-orderings.

(IV) The function may be such that re-ordering between groups of terms is possible. Indication about this possibility is obtained if a certain system is followed in arranging the transmission matrix. The weights of the order one of all the terms of the function is found out and the terms are then arranged in order of non-ascending weights. Horizontal lines are drawn to subdivide the function into groups of terms having identical values of  $\omega_1$ . The groups are again subdivided into subgroups on the basis of interconnection of the terms to form 1-cells. This is illustrated in the Table VII which gives the transmission matrix with the distance vectors of each term of the function  $T = \Sigma(0, 1, 2, 13, 14, 15)$ .

TABLE VII

	$X_4$	$X_3$	$X_2$	$X_1$	$\omega_1$	$\omega_2$	$\omega_3$	$\omega_4$
0	0	0	0	0	2	0	2	1
15	1	1	1	1	2	0	2	1
1	0	0	0	1	1	2	1	1
2	0	0	1	0	1	2	1	1
13	1	1	0	1	1	2	1	1
14	1	1	1	0	1	2	1	1

It will be observed that 0 and 15 have same value of  $\omega_1$  and they are placed in the same group. Similarly, 1, 2, 13, 14 form another group. Terms 1 and 2 both differ by one change of variable from the term 0 and similarly, terms 13 and 14 both differ by one change of variable from the term 15. Hence the dotted line is drawn to subdivide the group into two subgroups. Observation of the distance vectors will reveal that re-ordering between (0 and 15) and (1, 2, 13 and 14) are possible. Since the relationship of the terms 1 and 2 with the term 0 is same as that of the terms 13 and 14 with the term 15, the group of terms 1 and 2 will be re-ordered with the group formed by 13 and 14 when 0 is re-ordered with 15.

#### SYSTEMATIC PROCEDURE FOR DETERMINATION OF GROUP INVARIANCE

##### Step I.

In first step we find out the weight of order one of each term i.e., the number of terms with which it is related by one change variable. Then arrange the terms in non-ascending weight, and write down binary equivalents of each decimal number. Against each term we write the distance vector of the term. Horizontal lines are drawn to subdivide the terms into groups having identical weights of order one.

##### Step II.

Next in the transmission matrix we search for identical columns. Permutation of identical columns obviously keeps the transmission matrix invariant. Hence the function has those group invariances.

##### Step III

(i) We look in the distance vectors of the terms. If there is a row having 1 or 0 at all positions and it has a distinct distance vector, the transmission will change under any priming operation.



(ii) If there are no two rows having identical distance vectors, the function will alter under any permutation and priming operation, excepting those obtained in the *Step II*.

(iii) Generally the function will be found to be composed of a number of groups of terms such that the distance vectors of the members of each group are identical. We choose the smallest or one of the smallest of these groups. If it consists of only one term, we make a list of all the permutation and priming operations which will keep that particular term unaltered. By observing the effect of those operations on the other terms of the function, the group invariances are found out. If the smallest group chosen is composed of two terms, then all the operations are listed which will effect re-ordering between those two terms and also those which keep the terms unaltered. The rest of the procedure is same as stated in the previous case. By some easy inspections (e.g., counting the number of 0's and 1's in each column of the transmission matrix) we can discard some of the operations listed and thereby reduce the labour involved in observing the effect of the listed operations on the other terms for finding out group invariances. If the smallest group chosen consists of more than two terms, we make a list of the operations which will keep the first term unaltered and at the same time re-order the other terms of the group and also of the operations which will effect the re-orderings between the first term and each of the other terms of the group. Then we proceed as stated previously. The total number of group invariances present cannot exceed the total number of re-orderings that can be effected. The systematic procedure as stated above is illustrated by the example below.

*Example.*

Detect the group invariances of the function

$$T = \Sigma(4, 5, 7, 8, 9, 11, 30, 33, 49)$$

We first follow the procedure stated in *Step I*. The transmission matrix along with the distance vectors is given below in *Table VIII*.

*Step 2.*

In the transmission matrix there are no two identical columns.

*Step 3.*

We observe that the distance vectors of the terms 5 and 9 are identical and the distance vectors of terms (4, 7, 8, 11) are identical. The group (4, 7, 8, 11) can be divided into two subgroups (4, 7) and (8, 11). Hence re-ordering between (5 and 9), (4 and 7), and (8 and 11) and between groups (4, 7) and (8, 11) are possible.

TABLE VIII

	$X_0$	$X_5$	$X_4$	$X_3$	$X_2$	$X_1$	$\omega_1$	$\omega_2$	$\omega_3$	$\omega_4$	$\omega_5$	$\omega_6$
5	0	0	0	1	0	1	2	2	3	1	0	0
9	0	0	1	0	0	1	2	2	3	1	0	0
4	0	0	0	1	0	0	1	2	3	2	0	0
7	0	0	0	1	1	1	1	2	3	2	0	0
8	0	0	1	0	0	0	1	2	3	2	0	0
11	0	0	1	0	1	1	1	2	3	2	0	0
33	1	0	0	0	0	1	1	2	4	0	0	1
49	1	1	0	0	0	1	1	0	2	4	1	0
30	0	1	1	1	1	0	0	0	5	1	1	1
	$\frac{2}{3}$	$\frac{2}{3}$	$\frac{1}{3}$	$\frac{1}{3}$	$\frac{2}{3}$	$\frac{2}{3}$						

We choose the term 30 as our smallest group since it has got a distinct distance vector. The following operations are listed which will keep the term unaltered :

- All permutations between the variables  $X_2, X_3, X_4, X_5$ .
- Permutation between variables  $X_1$  and  $X_0$ .
- Priming of  $X_1$  and any one of  $X_2, X_3, X_4, X_5$  and subsequent permutation.
- Priming of  $X_0$  and any one of  $X_2, X_3, X_4, X_5$  and subsequent permutation.
- Priming of  $X_1$  and  $X_0$  and any two from the other variables and subsequent permutation.

By inspecting all the columns of the matrix we discard the following operations

- Permutation of  $X_2$  with any one of  $X_3, X_4, X_5$ .
- Permutation of  $X_5$  with any one of  $X_2, X_3, X_4$ .
- Permutation between  $X_0$  and  $X_6$ .
- Priming of  $X_1$  and any one of  $X_3, X_4, X_5$  and subsequent permutation.
- Priming of  $X_0$ .

Hence the only operations permitted are:

- Permutation of variables  $X_3$  and  $X_4$ .
- Priming of  $X_1$  and  $X_2$  and then permuting. These are the only group invariances.

Incidentally it may be noted that the operation (A) re-orders the terms 5 and 9 and the group (4, 7) with (8, 11). The operation (B) brings about the re-ordering between 4 and 7 and between 8 and 11. Hence these are the only group invariances present in the function. It may be noted that in cases where none of

the groups contain more than two terms as in the present example, the procedure for finding group invariances can be simplified very much. In such cases much labour is saved if we find out only those operations which effect the re-orderings suggested by the distance vectors.

#### DETECTION OF SYMMETRIC FUNCTIONS

The method given for detection of group invariance can very easily be applied for detection of total symmetry of a function by utilising certain properties of symmetric functions. The required properties are

(i) If an  $n$ -variable function is totally symmetric with  $a$ -number of the function equal to  $a_j$ , then total number of true states in the function must be equal to  ${}^nC_{a_j}$ , where  $a_j$  is any number between 0 and  $n$ , inclusive. Since the function is invariant under all permutation operation, any re-ordering between rows of the function must be possible. Total number of 1's in each of the rows of the function must be equal to  $a_j$ . The dimension of the body of any  $n$ -variable symmetric function is  $n$ , except in the trivial case when the function is composed of a single term. In other words, in a symmetric function there cannot be any column containing only 1's or only 0's.

(ii) The sum of two symmetric functions is a symmetric function. The  $a$ -number of the sum of  $K$  symmetric functions will have  $K$  different values. The total number of true states of the function will be  ${}^nC_{a_{j_1}} + {}^nC_{a_{j_2}} + {}^nC_{a_{j_3}} + \dots + {}^nC_{a_{j_k}}$ ; where  $a_{j_1}, a_{j_2}, a_{j_3}, \dots, a_{j_k}$  are the  $a$ -numbers of the component functions. Since the function is invariant under all permutation operation, it must be possible to find out groups consisting of  ${}^nC_{a_{j_1}}, {}^nC_{a_{j_2}}, {}^nC_{a_{j_3}}, \dots, {}^nC_{a_{j_k}}$  terms. In the group having  ${}^nC_{a_{j_k}}$  terms, the number of 1's in each row must be  $a_{j_k}$ . All re-orderings between the terms of any one group amongst themselves will be possible.

(iii) Besides the above properties of a symmetric function, we will take cognisance of one property of the distance vectors of the terms of the functions. Due to any permutation and priming of the variables of the function, terms of the function may alter but the distance vector of the changed terms will be identical to the corresponding terms of the original function. In other words, the distance vector of a term remains invariant under all permutation or priming operations.

Again the ratio  $\frac{(\text{Number of rows containing odd number of 1's})}{(\text{Number of rows containing even number of 1's})}$  remains unaltered

for even number of priming operations and become inverted for odd number of priming operations.

#### METHOD FOR DETECTION OF SYMMETRIC FUNCTIONS

(i) Procedure stated in *Step I* for detection of group invariance is followed.

(ii) Total number of terms in each group that can be re-ordered amongst themselves is found out. If the number of terms in the groups satisfy the condition for total symmetry as stated previously, then we count total number of 1's in the rows of each group. If they are all equal to the number then we know that the function is totally symmetric. If the number of 1's in the rows of each group differ then we try suitable priming operation which will make the number of 1's in the rows of the groups identical with the corresponding  $\alpha$ -number. The method is illustrated by an example.

To determine what symmetric function, if any, is represented by

$$T = \Sigma(0, 5, 6, 9, 10, 15, 19, 20, 24, 29, 30)$$

The transmission matrix and the distance vector of each terms is given in the table below:

TABLE IX

	$X_5$	$X_4$	$X_3$	$X_2$	$X_1$	$\omega_1$	$\omega_2$	$\omega_3$	$\omega_4$	$\omega_5$
0	0	0	0	0	0	0	6	1	3	0
5	0	0	1	0	1	0	6	1	3	0
6	0	0	1	1	0	0	6	1	3	0
9	0	1	0	0	1	0	6	1	3	0
10	0	1	0	1	0	0	6	1	3	0
15	0	1	1	1	1	0	6	1	3	0
19	1	0	0	1	1	0	0	10	0	0
20	1	0	1	0	0	0	6	1	3	0
24	1	1	0	0	0	0	6	1	3	0
29	1	1	1	0	1	0	6	1	3	0
30	1	1	1	1	0	0	6	1	3	0

By looking into distance vectors we observe that the function can be divided into two groups. In one group there is only one term and the other group has 10 terms. The total number of terms is sum of  ${}^5C_0 + {}^6C_2$ , or  ${}^5C_0 + {}^6C_3$ , or  ${}^5C_5 + {}^5C_2$ , or  ${}^5C_5 + {}^5C_3$ . The ratio of rows containing odd number of 1's to rows containing even number of 1's is 1/10. Therefore, the possible  $\alpha$ -numbers of the function are (0, 3), or (2, 5). We first find out what is the priming operation that must be applied on the row which singly forms a group to make the number of one's in that row equal to zero. This can be done by priming the variables  $X_1$ ,  $X_2$  and  $X_5$  and this makes the number of one's in all rows of the other group equal to 3. Hence the function can be written as  $S_{0,3}(X_5'X_4X_3X_2'X_1')$ . Alterna-

tively, if we prime the variables,  $\bar{X}_4$  and  $\bar{X}_3$  we find that the term in the group with single term has 1 in all positions and the other group has two in all rows. Hence the function can be written as  $S_{5,2}(X_5X'_4X'_3X_2X_1)$ .

## A SPECIAL CASE

The given function may be such that it can be expressed as a sum of two symmetric functions which belong to the same equivalence class and one is derived from the other by priming all the variables. The distance vectors of all the terms of such a function will be identical. That the function can be split up into two functions for detection of total symmetry will thus not be quite apparent. But an indication to this will be obtained by observing that the weight of the order  $n$  for all the terms will be same, i.e., 1. The procedure for collecting the terms of the function into two distinct groups will be as follows. We take any one term and place it in one group and the term which is related by  $n$  changes of variables with this will be placed in the other group. In this way half of the total number of terms will come in one group and the other half in the other group. We should, however, keep in mind that the dimension of the body of each of the two newly formed functions must be  $n$ . Also in each group, all the rows will contain either odd number of 1's or even number of 1's. The following table gives the transmission matrix and the distance vectors of each term of the function

$$T = \Sigma(0, 3, 5, 6, 9, 10, 12, 15)$$

TABLE X

	$X_1$	$X_3$	$X_2$	$X_4$	$w_1$	$w_2$	$w_3$	$w_4$
0	0	0	0	0	0	6	0	1
3	0	0	1	1	0	6	0	1
5	0	1	0	1	0	6	0	1
6	0	1	1	0	0	6	0	1
9	1	0	0	1	0	6	0	1
10	1	0	1	0	0	6	0	1
12	1	1	0	0	0	6	0	1
15	1	1	1	1	0	6	0	1

There is one term with only 0's and one term with only 1's. The other six terms have two 1's in each row. As  ${}^4C_2 = 6$ , we can write the number of terms as  ${}^4C_0 + {}^4C_2 + {}^4C_4$  and obviously the function is a symmetric function with  $a$ -numbers 0, 2, and 4, i.e., the function can be written as  $S_{0,2,4}(X_4X_3X_2X_1)$ . Again, we can split up the function into two groups as follows according to the procedure already suggested because we find that the value of  $w_4$  is 1 for all the terms.

TABLE XI.

	$X_4$	$X_3$	$X_2$	$X_1$
0	0	0	0	0
3	0	0	1	1
5	0	1	0	1
9	1	0	0	1
15	1	1	1	1
12	1	1	0	0
10	1	0	1	0
6	0	1	1	0

If we prime the variable  $X_1$ , the terms of one group contain one 1 in each row and the terms of the other group contain three 1's in each row. As  ${}^4C_1 = 4$  and  ${}^4C_3 = 4$ , obviously the function is totally symmetric and can be written as

$$S_{1,3}(X_4X_3X_2X'_1)$$

#### CONCLUSION

A method for detection of group invariance and total symmetry of a function utilising geometrical properties of an  $n$  variable Boolean function has been presented. By the application of the method group invariance and total symmetry of any function can be very easily detected.

#### ACKNOWLEDGMENT

The authors wish to express their indebtedness to Professor J. N. Bhar, D.Sc., F.N.I., for guidance and keen interest in the work.

#### REFERENCE

- Caldwell, S. H., 1954, *Trans. A.I.E.E.* **73**, Part 1 pp. 142-149.  
 Caldwell, S. H., 1958, *Switching Circuits and Logical Design*, John Wiley & Sons, Inc., N. Y.  
 Lee, C. Y., 1954, *Trans. A.I.E.E., Part I*, pp. 289-291.  
 McCluskey, E. J. (Jr.), 1956, *Bell System Tech. Jour.*, Vol. **35**, p. 1445.  
 Marcus, M. P., 1956 *I.R.E., Transactions on Electronic Computers*, Vol. **ED-5** pp. 237-239.  
 Shannon, C. E., 1949, *Bell System Tech. Jour.*, Vol. **28**, pp. 59-98.

# LATTICE EXPANSION AND DEBYE TEMPERATURE OF $\alpha$ -PHASE AgCd ALLOYS

MD. A. QUADER AND B. N. DEY

INDIAN ASSOCIATION FOR THE CULTIVATION OF SCIENCE, CALCUTTA.

(Received November 14, 1961)

**ABSTRACT.** The lattice parameters of three  $\alpha$ -phase silver cadmium alloys with 24.3, 29.3 and 33.8 atomic per cent cadmium have been measured upto 500°C by taking X-ray powder diffraction photographs in the high temperature camera. The linear thermal expansion coefficient has been calculated for all the alloys and the results compared with Gruneisen's theory by drawing the "Gruneisen plots". For the alloys the Debye characteristic temperature,  $\theta$ , was obtained from the measurement of the temperature variation of intensity of the high angle diffraction lines. For the above three alloys  $\theta = 183^\circ\text{K}$ ,  $183^\circ\text{K}$ , and  $178^\circ\text{K}$ , were obtained.

## INTRODUCTION

The normal thermal expansion of solids due to anharmonicity of interatomic forces and the calculation of thermal expansion is often based on a simple phenomenological parameter,  $\gamma$ , known as 'Gruneisen's constant' as an average measure of the anharmonicity. The Gruneisen theory of thermal expansion (Gruneisen, 1912, 1926) is based on the simple Debye model of monatomic solid and implies a simple relation between the value of the constant,  $\gamma$ , (defined by  $\gamma = \frac{\alpha V}{C_v K}$ , where  $\alpha$  is the coefficient of volume expansion,  $C_v$  and  $V$  are the specific heat and volume and  $K$  the compressibility of the solid) and the sum of the exponents in the attractive and repulsive terms of the interatomic potential for central forces between atoms of Mie-Lennard-Jones type. Gruneisen theory was shown to represent the correct type of expansion, at least, at temperatures above the characteristic temperature  $\theta$ , by a number of workers (Gruneisen, 1912, 1926; Nix MacNair, 1941; Hume-Rothery, 1945). However, the valuable low temperature work of Bijl and Pullan (1954, 1955), Rubin *et al.* (1954) and Figgins *et al.* (1956) revealed that the simple Gruneisen's theory breaks down at temperatures below  $0.3 \theta$ ,  $\gamma$  no longer remaining constant but increasing, and the thermal expansion becoming larger than the value predicted by the law. In a rigorous treatment Barron (1955) tried to explain the variation of  $\gamma$  with temperature in an analogous way to that done by Blackman (1934) for  $\theta$ , though the agreement is not satisfactory.

\* Present address : National Metallurgical Lab., Jamshedpore, India.

While the low temperature measurements of expansivity are needed for the theoretical development of lattice dynamics, the high temperature data for the alloys are required to test the validity of Gruneisen theory of thermal expansion in case of alloys.

The Debye temperature  $\theta$  is another parameter of solids which enters into a number of solid state problems because of its inherent relation with lattice vibration. For majority of metals  $\theta$  values are known but for alloys  $\theta$  is mostly unknown. The direct way of obtaining  $\theta$  is by the measurement of specific heat. However, according to Debye-Waller theory, the measurement of integrated intensity of diffracted X-rays with temperature presents an alternative method for obtaining  $\theta$ . Such measurements have been made for Cu, Al and Au by Owen and Williams (1947) for Ag by Spreadborough and Christian (1959b) and Haworth (1960) and for Al, Pb and  $\beta$ -brass by Chipman (1960).

In the present work we have measured the lattice parameter of three  $\alpha$ -phase silver-cadmium alloys by recording X-ray powder diffraction photographs in a high temperature camera and also measured their Debye temperatures from the microphotometric measurement of the variation of X-ray intensity of Bragg reflections with temperatures. Following the measurements of lattice parameters we have calculated the Gruneisen plots by Fischmeister (1956) method for comparison with Gruneisen theory.

#### EXPERIMENTAL PROCEDURE

Silver-cadmium alloys with 24.8, 29.3 and 33.8 atomic per cent cadmium were prepared from spectroscopically pure mattey metals by melting appropriate quantities of the metals in evacuated pyrex tubes as described earlier (Quader, 1960). From the homogeneous alloys filings were made with a file, displaced through 200 and 300 mesh sieves and then sealed in evacuated pyrex tubes and annealed at 650°C for 6 hours, thereby yielding strain-free powders with stable grain sizes. This long time annealing at a high temperature was necessary to have stable grain sizes so that no further grain growth occurred during subsequent heating in the high temperature camera. For the high temperature powder camera small specimens, about 3 mm in length and 0.3 mm in diameter, were prepared by taking the annealed powder in thin-walled pyrex capillaries and sealing both ends. A long specimen was always avoided because some distillation of cadmium occurred from it due to thermal gradient in the camera chamber. It has also been observed that the powders get oxidised at temperatures above 300°C if the seal gets broken, even though the camera is evacuated during heating. Therefore, every precautions was taken to guard against these difficulties during the preparation of the specimen. Every specimen was mounted in another glass capillary which in turn was mounted on the specimen holder of the camera. This practice was adopted to avoid the loss of heat of the specimen to the specimen holder by conduction.



High temperature photographs up to 522°C were recorded in Unicam 19 cm. high temperature camera using copper  $K\alpha$  radiations from a Philips sealed off X-ray tube. The temperature of the specimen was controlled manually to within  $\pm 1^\circ\text{C}$  and could be read by two Pt—PtRh thermocouples. The thermocouples of the high temperature camera were calibrated by measuring the lattice parameter of pure silver.

For the measurement of variation of intensity of the X-ray diffraction lines with temperature, exposures were given at a constant voltage of 36 kV and 20mA for four hours. All the films were developed simultaneously in the same bath along with a standard wedge photograph, and the intensity of the high angle (511) and (422) lines were obtained microphotometrically.

## RESULTS AND DISCUSSIONS

### (a) Lattice parameter and thermal coefficient of linear expansion

The lattice parameter of the alloys was calculated from the high angle lines and corrected by the standard extrapolation method (Taylor and Sinclair, 1945). These values are recorded in Table I and are probably correct to within  $\pm 0.0005\text{\AA}$ . Fig. 1 shows the plot of the lattice parameter against temperature. It will be

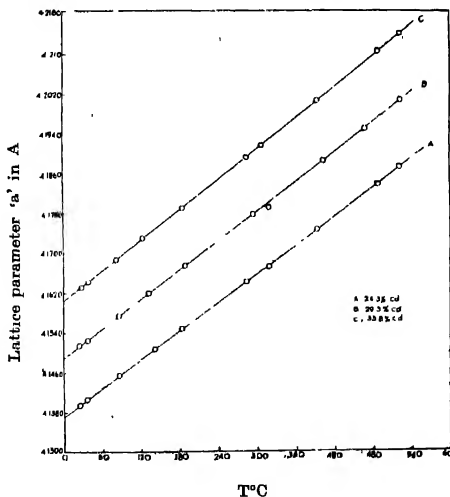


Fig. 1. Lattice spacing-temperature for  $\alpha$ -phase AgCd alloys.

seen that the points lie on curves which deviate only slightly from a straight line. The linear thermal expansion coefficient  $\alpha = \frac{1}{a} \cdot \frac{da}{dT}$  was calcu-

lated at four different temperatures and the values are recorded in Table II and plotted in Fig. 2.

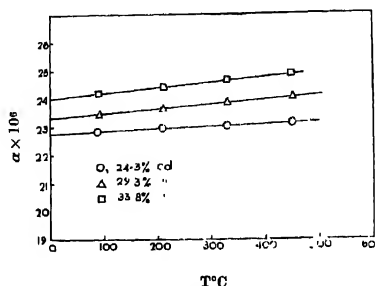


Fig. 2 Variation of linear thermal expansion co-efficient with temperature for the AgCd alloys.

TABLE I  
Lattice parameter of pure silver and silver cadmium alloys

Pure Silver*		24.3% Cd alloy		29.3% Cd alloy		33.8% Cd alloy	
Temp. °C	Lattice parameter Å	Temp. °C	Lattice parameter Å	Temp. °C	Lattice Parameter Å	Temp. °C	Lattice Parameter Å
16	4.0854	25	4.1395	26	4.1513	27	4.1631
22	4.0858	37	4.1406	37	4.1524	38	4.1642
134	4.0960	86	4.1454	86	4.1574	81	4.1686
257	4.1066	140	4.1506	131	4.1610	123	4.1728
327.5	4.1131	184	4.1548	189	4.1674	184	4.1790
399	4.1184	284	4.1643	295	4.1778	284	4.1894
459	4.1231	319	4.1676	319	4.1793	311	4.1926
552	4.1312	394	4.1746	404	4.1885	394	4.2006
596	4.1360	480	4.1827	468	4.1950	490	4.2106
717	4.1477	522	4.1873	522	4.2006	522	4.2140
846	4.1624						
943	4.1739						

The linear thermal expansion coefficient of the Ag-Cd  $\alpha$ -phase alloys was studied by Owen and Roberts (1939) using a high temperature powder camera. They reported a mean value of  $\alpha$  over the temperature range of 0°C to 300°C which are about 5% lower than those obtained in the present measurements. It is evident that the expansion coefficient increases with increase of cadmium concentration.

TABLE II

Linear thermal expansion coefficient,  $\alpha$ , of AgCd alloys at different temperatures

Composition of alloy at. % Cd	$\alpha \times 10^6$ at the temperature of				Extrapolated $\alpha \times 10^6$ at 0°C
	90°C	210°C	330°C	450°C	
24.3	22.84	22.95	23.05	23.15	22.78
29.3	23.48	23.61	23.85	24.08	23.35
33.8	24.21	24.35	24.67	24.85	24.02

(b) Comparison with Gruneisen theory

An approximate theory of the thermal expansion, based on the Debye model of monatomic solids with a single characteristic temperature,  $\theta$ , has been developed by Gruneisen (1912, 1926). It will be interesting to see how far this theory is applicable in  $\alpha$ -phase alloys where the lattice structure is the same as that of the solvent. For a crystal whose atoms exert nearly harmonic vibrations in an asymmetrical force field, Gruneisen theory predicts a volume expansion according to the relation

$$3 \frac{a_T - a_0}{a_0} = \frac{V_T - V_0}{V_0} = \frac{E/Q}{1 - pE/Q} \quad \dots (1)$$

where  $E$  is the vibrational energy given by the integral  $\int_0^T C_p dT'$  and  $Q, p$  are constants. These latter can be estimated from other properties of the crystal and are given by

$$Q = \frac{V_0}{\gamma K_0} \quad \dots (2)$$

where  $V_0$  and  $K_0$  are respectively the molar volume and the compressibility both at absolute zero, and  $\gamma$  is another constant known as 'Gruneisen constant; and

$$p = \frac{m+n+3}{6} \quad \dots (3)$$

where  $m$  and  $n$  are the powers of the Mie potential function  $\phi = \frac{A}{r^m} - \frac{B}{r^n}$ ,  $r$  being

the interatomic distance. The above two constants  $Q$  and  $p$  can be obtained graphically using the inverted form of Eq. (1) :

$$\frac{a_0}{a_T - a_0} = \frac{3Q}{E} - 3p \quad \dots (4)$$

The left side of (4) is the reciprocal of the dilatation referred to 0°K; to calculate this from the available expansion data which are referred to 273°K it is necessary to know  $(a_{273} - a_0)/a_0$ . This quantity can be estimated from the low temperature approximation to Eq. (4) as done by Fischmeister (1956):

$$3 \frac{a_{273} - a_0}{a_0} = \left( \frac{E}{Q} \right)_{273} = \frac{3\alpha_{273} \cdot E_{273}}{C_{v273}} \quad (5)$$

since the approximation  $Q = \frac{U_v}{3\alpha}$  is applicable at low temperatures. For determining  $a_0$ , the lattice parameter at 0°K, with the help of this relation  $\alpha_{273}$  and  $a_{273}$  was taken from our measurements and are recorded in Table III.

TABLE III  
Data for Calculation of ' $a_0$ '

Materials	$a_{273}$ Å	$\alpha_{273} \times 10^6$	$C_{v273}$ cal mol <sup>-1</sup> °C <sup>-1</sup>	$E_{273}$ cal mole	' $a_0$ ' Å
Pure Ag	4.0840	20.0	5.88	1195	4.06760
24.3% alloy	4.1371	22.78	5.87	1227.5	4.11796
29.3% "	4.1488	23.35	5.87	1228.3	4.12907
33.8% "	4.1604	24.02	5.87	1228.8	4.14000

For the alloys the  $C_p$  values from zero to 300°K were estimated from the experimentally measured specific heat data of pure silver and cadmium (N.B.S. monograph No. 21, 1960) with the help of Neumann-Kopp's approximate rule. From the  $C_p$  thus obtained the  $C_v$  values were calculated from the relation

$$C_p - C_v = 0.0214 \left( \frac{T}{T_m} C_p^2 \right)$$

where  $T_m$  is the melting point of the alloys in °K. Finally, the values of

$E_T = \int_0^T C_v \cdot dT$  were obtained from the area of the graphs of  $C_v$  against temperature.

Fig. 3 shows the 'Grüneisen plot' obtained with Eq. (4) i.e.  $\frac{a_0}{a_T - a_0}$  vs  $\frac{1}{E_T}$  for the three  $\alpha$ -phase AgCd alloys and pure silver; the data for Fig. 3 are given in Table IV. The lattice parameters of pure silver were taken from Spreadborough and Christian (1959a). It is obvious that the Grüneisen plot for the alloys and pure silver are straight lines similar to those obtained by Fischmeister (1956) for alkali halides. But following a similar procedure Mitra and Mitra (1957) obtained non-linear curves for Cu, Ag, Al and Pt.

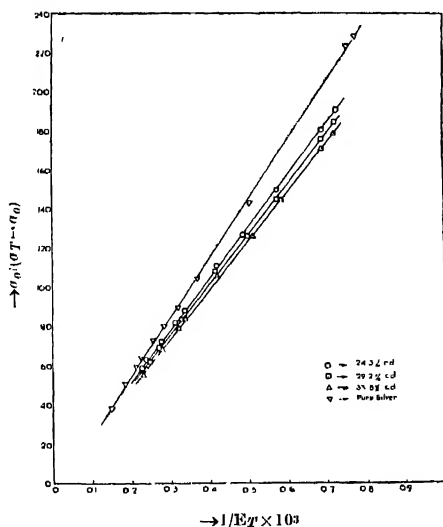


Fig. 3 Grüneisen plots for the  $\alpha$ -phase AgCd alloys and pure silver

The constants  $Q$  and  $p$  as obtained from Fig. 3 are listed in Table V. The  $Q$  values for the alloys are probably correct to within 10 per cent. For silver the  $Q$  value is lower than the best value as suggested by Hume-Rothery (1945) viz. 108010 which would be obtained if  $\alpha_{273} = 19.0 \times 10^{-6}$  was used for silver for the calculations of ' $a_0$ '. This shows that the  $\alpha_{273}$  value affects  $Q$  and  $p$  to a great extent, but the curves still remain rectilinear within the limits of experimental error. Unfortunately, for the alloys  $Q$  values are not available for comparison nor can they be calculated from relation (2) because the Grüneisen constant  $\gamma$  and compressibility are not known. However, it appears that the Grüneisen relation is valid for solid solutions.

TABLE IV  
Data for Gruneisen plot of AgCd alloys

Pure Silver		24.3% Cd alloy		29.3 Cd alloy		33.8% Cd alloy	
$\frac{1}{E_T} > 10^3$	$\frac{u_0}{a_T - a_0}$	$\frac{1}{E_T} > 10^3$	$\frac{u_0}{a_T - a_0}$	$\frac{1}{E_T} \times 10^3$	$\frac{u_0}{a_T - a_0}$	$\frac{1}{E_T} \times 10^3$	$\frac{u_0}{a_T - a_0}$
775	228.5	727	191.17	724	185.74	720	179.22
755	223.4	692	181.88	691	176.98	688	171.07
504	143.2	576	150.07	576	145.74	586	145.77
368	104.2	487	127.72	50	126.93	512	126.21
319	89.4	418	111.77	413	108.28	418	106.15
281	80.07	336	88.48	329	84.73	330	84.31
255	73.2	314	82.95	314	83.87	319	79.61
224	63.9	276	72.70	271	69.47	276	68.65
211	59.4	239	63.60	246	62.62	238	58.64
183	50.75	228	59.38	228	58.04	228	55.94
147	38.2						

TABLE V

Materials	Q from Fig. 3	p from Fig. 3	$\theta_{100}^\circ$ K	$\theta_{111}$ K	*
Pure Silver	102200	2.3	191*	225*	
24.3% alloy	88700	1.5	183		
29.3% "	86000	1.5	183		
33.8% "	84000	1.5	178		

\*Spredborough and Christian (1959b).

(c) *Debye temperature from the temperature variation of the intensity of X-ray diffraction*

From the Debye-Waller theory, the temperature dependence of the intensity of an X-ray reflection is given by the factor  $\exp(-2M)$  (following James, 1948) when

$$M = \frac{6h^2T}{mk\theta_M^2} \cdot \frac{\sin^2 \theta}{\lambda^2} \left\{ \phi(x) + \frac{x}{4} \right\} \quad \dots (1)$$

and

$$x = (\theta/T)$$

the other symbols have their usual meanings

If it is assumed that there is a single Debye-characteristic temperature  $\theta$  which does not vary with temperature, and if the small effect due to change of Bragg angle  $\theta$  with temperature is neglected, the Debye-Waller theory leads to an expression

$$\frac{\lambda^2}{\sin^2\theta} \ln \left( \frac{\rho_T}{\rho_{T_0}} \right) = \frac{12h^2}{mk\theta^2} \left\{ T_0\phi \left( \frac{\theta}{T_0} \right) - T\phi \left( \frac{\theta}{T} \right) \right\}. \quad \dots (2)$$

where  $\rho_{T_0}$  and  $\rho_T$  are the integrated intensities of a Bragg reflection at temperatures  $T_0$  and  $T$  respectively,  $\phi$  is the Debye integral function and the other symbols have their usual meaning. Using Cu K  $\alpha$  radiation the integrated intensity of the two high angle (511) and (422)  $\alpha_1$  lines of the alloys was measured at various temperatures as stated earlier. From Eq. 2 it follows that  $(\lambda/\sin \theta)^2 \log_{10} (\rho_T/\rho_{T_0})$  (where  $T_0$  is the room temperature) should vary linearly with temperature, since  $\{\phi(x) - x/4\}$  is approximately unity for all temperatures greater than  $\theta$ . The observed decrease in intensity is however greater than the theoretical decrease as has been found by other workers while testing Debye-Waller theory at high temperatures. The main error in Eq. 2 arises from the assumption that the volume of the crystal remains constant as the temperature changes. Paskin (1957) has given a method of correcting for the volume changes which is easier to apply than the earlier method of Zener and Bilinsky (1936). His thermodynamical derivation of the variation of  $\theta$  (regarded as a temperature dependent parameter  $\theta_T$ ) with volume leads to a Debye temperature  $\theta_T$ , which for an isotropic crystal obeying Grüneisen's expansion equation is related to the Debye temperature by the relation

$$\theta_T/\theta_0 = \left( \frac{V_0}{V_T} \right)^\gamma \quad \dots (3)$$

where  $V_T$  and  $V_0$  are the atomic volumes at temperatures  $T$  and 0°K and  $\gamma$  is the Grüneisen constant. Thus plotting  $\frac{\lambda^2}{\sin^2\theta} \log_{10} (\rho_T/\rho_0)$  against a modified temperature  $T^1$  given by

$$\frac{T^1}{T} = \left( \frac{V_T}{V_0} \right)^{2\gamma}$$

where  $V_{T_0}$  is the atomic volume at reference temperature  $T_0$  a straight line would be obtained. The Paskin correction has been applied by Spreadborough and Christian (1959b) and Haworth (1960) in case of silver who got linear plots of Eq. 2 from the slope of which  $\theta$  was calculated. In the present measurements with  $\alpha$ -AgCd alloys Paskin's correction was not applied as the value of Grüneisen constant  $\gamma$  is not known. Therefore, for these alloys we have plotted

$\log_{10} \left( \frac{\rho_T}{\rho_{T_0}} \right) \times \frac{\lambda}{\sin^2\theta}$  against the temperature  $T$ , taking room temperature as

the reference temperature  $T_0$ . The plot is shown in Fig. 4 and the necessary data are given in Table VI. The points lie on curves the tangents to which through the reference temperature represent the Debye Waller theoretical line (James, 1948). From the slope of these lines the Debye characteristic temperature  $\theta$  at room temperature was obtained. These values are given in Table V and are correct to within  $\pm 10^\circ\text{K}$ .

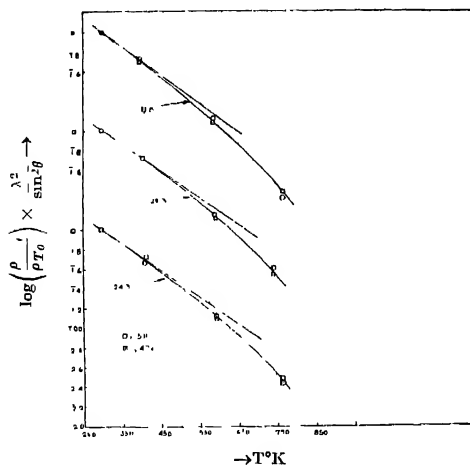


Fig. 4. Variation of  $\log_{10}(\rho_T/\rho_{T_0}) \times \frac{\lambda^2}{\sin^2 \theta}$  with temperature for  $\alpha\text{-Ag Cd}$  alloys

According to Zener and Bimsky (1936) the  $\theta$  value from the X-ray measurements should be higher than that obtained from specific heat measurements because of the different ways of averaging the lattice vibration frequencies in the two cases. The measurements of Owen & Williams (1947) and of Chipman (1960) also showed that  $\theta$  values from X-ray are 3 to 5% higher than those from specific heat measurements. However, by X-ray method Spreadborough & Christian (1959b) and Haworth (1960) have got 191 and  $197^\circ\text{K}$  respectively for the room temperature value of  $\theta$  for silver which are lower than  $225^\circ\text{K}$  deduced from specific heat measurements (Corak *et al.*, 1955). In a theoretical calculation of the X-ray Debye temperature for a face-centred-cubic lattice, based on the known vibrational spectrum, Blackman (1957) finds  $\theta = 189^\circ\text{K}$ . According to Blackman, if the actual vibrational spectrum has the Debye form,  $\theta$  from X-ray measurements should be equal to  $\theta$  from specific heat measurements. Thus the effect of taking the actual spectrum into account is to lower the X-ray value in comparison to the specific heat value.



TABLE VI

Alloy Composition at. % Cd.	Temperature °K	$\left[ \log_{10} \left( \frac{\rho_T}{\rho_{T_0}} \right) \times \frac{\lambda^2}{\sin^2 \theta} \right]_{\theta 11}$	$\left[ \log_{10} \left( \frac{\rho_T}{\rho_{T_0}} \right) \times \frac{\lambda^2}{\sin^2 \theta} \right]_{\theta 22}$
24.3	298	0	0
	413	1.681	1.720
	529	1.123	1.101
	762	2.440	2.482
29.3	299	0	0
	404	1.720	1.725
	592	1.139	1.090
	741	2.585	2.518
33.8	300	0	0
	396	1.721	1.690
	584	1.120	1.080
	763	2.319	2.381

In our present measurements we find for the alloys at the room temperature  $\theta = 178$  to  $183^\circ\text{K}$  which values are lower than that for pure silver. Unfortunately,  $\theta$  for these alloys are not known from specific heat measurements for comparison, and hence the conclusion drawn by Blackman and others could not be verified.

## ACKNOWLEDGMENT

The authors are grateful to Prof. B. N. Srivastava, D.Sc., F.N.I., for kindly suggesting the present work and guidance throughout its progress.

## REFERENCES

- Barron, T. H. K., 1955, *Phil. Mag.*, **46**, 720.  
 Bijl, D. and Pullan, H., 1954, *Phil. Mag.* **45**, 290; (1955) *Physica*, **21**, 285.  
 Blackman M., 1957, *Handbuch der physik*, **71**, 325.  
 Blackman, M., 1934, *Proc. of the Royal Soc.*, Vol. A148, 365  
 Chipman, D. R., 1960, *J. App. Phys.*, **31**, 2012.  
 Corak, W. S., Garfunkel, M. P., Sattarthwaite, C. B. and Wexler, A., 1955, *Phys. Rev.* **98**, 1699.  
 Corruccini, R. J., and Gniewek J. J. 1960, N. B. S. Monograph No 21  
 Figgins, B. F., Jones, G. O. and Riley, D. P. 1956, *Phil. Mag.*, **1**, 747.  
 Fischmeister, H. F. 1956, *Acta Cryst.*, **9**, 416.  
 Grunosen, E., 1912, *Ann. Phys. Leipzig*, **39**, 279; 1926 *Handbuch der physik*, **10**, 1.  
 Haworth, C. W., 1960, *Phil. Mag.* **5**, 1229.  
 Hume-Rothery, W., 1945, *Proc. Phys. Soc.*, **57**, 209.

- James, R. W., 1948, Optical Principles of X-ray diffraction  
 Mitra, G. and Mitra, S., 1957, *Nature*, **179**, 1295.  
 Nix, F. C. and Mc.Nun, D., 1941, *Phy Rev.*, **60**, 597.  
 Owen, E. A. and Roberts, E. W., 1939, *Phil. Mag.*, **27**, 294.  
 Owen E. A. and Williams, R. W., 1947, *Proc. Roy Soc A* **188**, 509.  
 Paskin, A., 1957, *Acta Cryst*, **10**, 667.  
 Quader, A., 1960 *Ind Jour. Phys.*, **34**, 506.  
 Rubin, T., Altman, H. W. and Johnston, H. L., 1951, *J. Am Chem. Soc.*, **76**, 5289.  
 Sinclair, H. and Taylor, A., 1945, *Proc. Phy. Soc.*, **57**, 108, 126.  
 Spreadborough, J. and Christian, J. W., 1959a, *J. Sc. Inst* **36**, 116.  
 1959b *Proc Phys Soc (Lond)* **74**, 609.  
 Zenor, C. and Bilinsky 1936, *Phy Rev*, **50**, 101.

# Letters to the Editor

The Board of Editors will not hold itself responsible for opinions expressed in the letters published in this section. The notes containing reports of new work communicated for this section should not contain many figures and should not exceed 500 words in length. The contributions must reach the Assistant Editor not later than the 15th of the second month preceding that of the issue in which the letter is to appear. No proof will be sent to the authors.

## 1

### A PECULIAR PHENOMENON IN THE ELECTROLYSIS OF A FLOWING SYSTEM

SANTI R. PALIT

INDIAN ASSOCIATION FOR THE CULTIVATION OF SCIENCE, CALCUTTA-32,

(Received December 28, 1961)

On applying a definite voltage between two electrodes immersed in a solution of an electrolyte, the current is somewhat unsteady presumably owing to polarisation, evolution of bubbles and other disturbances. The observation has been made that if the electrolyte is made to flow, the current decreases through the applied voltage is maintained constant, and above a critical velocity of flow of the electrolyte the current drops down to a steady value independent of any further increase of velocity of flow of the electrolyte. The difference in current strength,  $\Delta i = i' - i$ , where  $i'$  is the rather unsteady value of the current passing through the stationary electrolyte and  $i$  is the steady current through the flowing electrolyte at the same voltage, is generally from a few per cent to as high as one hundred per cent of  $i$  but its accurate measurement is generally not possible due to the difficulty of a precise measurement of  $i'$ . This remarkable behaviour however, is shown by both A. C. as well as D. C. but it is experimentally easier to study it with D. C. as the observation in question can be demonstrated with D.C. at a very low current strength where complication due to heating effect of the current is negligible

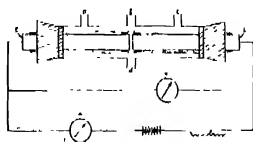


Fig. 1. Electrolytic cell with flowing electrolyte.

The above phenomenon can be simply demonstrated with the help of the arrangement shown in Fig. 1. The electrolyte enters the electrolytic cell made

of a tube of about 15 mm diameter through any one of the side tubes *a*, *b*, *c* and *d* and leaves through any of the remaining three, the two idle side tubes being kept closed. A thermometer is introduced through a central hole (not shown in the Fig. ) to read temperature. The two electrodes, *E*, *E*, are ordinary carbon rods 8 to 12 mm in diameter introduced through stoppers from the two ends of the tube. The carbon rods may be sheathed with a close-fitting glass tube cemented to the carbon electrode leaving only the face free for bearing current. For a ready demonstration running tap water can be used as the flowing electrolyte. As the D. C. source a lead battery (12 volts) with a rheostat and suitable arrangement for measuring current and applied voltage is used. With the electrolyte flowing through the cell, the current may be conveniently adjusted in the vicinity of 10 milliamperes by adjusting the applied voltage. On suddenly stopping the flow of the electrolyte, the ammeter needle shows a rapid drift of gradually decreasing intensity to a higher value which may be as high as ten to hundred per cent or so under suitable conditions. On reversing the above procedure, i.e. on first establishing the current with the electrolyte stationary and then letting the electrolyte flow, an immediate 'kick' of the milliammeter needle to a lower value is observed.

The two most important factors governing the magnitude of the 'kick',  $\epsilon$ , appear to be the distance between the two electrodes and the conductivity of the electrolyte. The nearer are the two electrodes, the higher is the 'kick', so much so, that with the above arrangement the 'kick' with very dilute electrolytes is one hundred per cent, from one steady value to another, if the distance between the two faces of the electrodes is about 1 mm. At a constant separation between the two electrodes, the lower the conductivity of the electrolyte, the higher is the difference,  $\Delta i$ , between the 'non-flow' current and the 'flow' current. Hence distilled water shows a higher value of  $\Delta i$  than many other electrolytes and in fact  $\Delta i/i$  versus concentration curve shows a maximum round  $N/1000$  for many electrolytes. Further, D.C. voltage above decomposition voltage are more effective than A. C. voltage of the same value. Platinum, carbon and stainless steel electrodes have been found to behave in the same pattern.

A remarkable property of the above behaviour however is that the current-voltage curve with A.C. of the flowing electrolyte appears to be linear passing through the origin which in effect means that the flowing electrolyte behaves as an ohmic resistance over quite a long range. The results of some preliminary experiments illustrating the above behaviour are shown in Fig. 2. Thus all disturbances due to polarisation seem to disappear by the simple expedient of making the electrolyte flow at a sufficiently high speed, though, strangely enough more brisk stirring of the electrolyte is unable to do the same.

It is rather difficult to understand the mechanism of the above behaviour. A reduction of polarisation by the flow of the electrolyte can not explain the ob-

served behaviour as that would result in an increase of current. That the flow of the electrolyte helps in migration of the ions can not also be a possible expla-

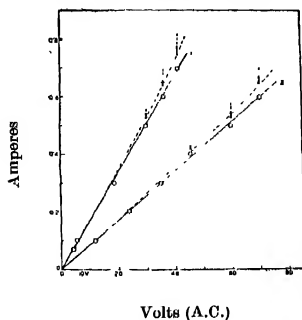


Fig. 2. Current-voltage curve of (1) M/5  $\text{MgSO}_4$  and (2) M/10  $\text{MgSO}_4$ . The dotted line is for 'stationary' electrolyte, the current drifting to higher value with time as indicated by the arrows; the bold line is for the flowing electrolyte.

nation because the observed effect is not an increase but is a decrease, and the latter is independent of the direction of flow of the current or the electrolyte, and is more easily produced if the flow of the electrolyte is at right angles to the electrodes. It is difficult to associate the observation in question with the deformation of the ion atmosphere of the migrating ions because of the weak flow necessary to cause the phenomenon. It however, seems more likely that the reported observation is due to the production of some highly conducting charged species near the electrodes which move in the line of the current, and the flow of the electrolyte merely removes these disturbing entities. In this connection the following observation is significant. If the electrolysis of a nonflowing electrolyte is stopped and a little potassium iodide solution is immediately added, iodine is liberated as is shown by its blue color with starch sol; however, very little or no iodine is liberated if the iodide solution is added after about ten minutes, which discounts the possibility of hydrogen peroxide being responsible for the iodine liberation. A correct theory however has to wait until more facts are known, and to this end further experiments are in progress, the results of which will be reported later.



# RAMAN AND INFRARED SPECTRA OF SOME FLUORINATED TOLUENES IN DIFFERENT STATES\*

K. K. DEB

OPTICS DEPARTMENT,

INDIAN ASSOCIATION FOR THE CULTIVATION OF SCIENCE,  
CALCUTTA-32.

(Received December 4, 1961)

## Plate I

**ABSTRACT.** The results of investigations on the Raman and infrared spectra of a few fluorinated toluenes in different states and in different environments have been discussed. Tentative assignments of some of the vibrational frequencies of the molecules in the low-frequency region have been proposed. The changes in some of the intramolecular oscillations observed in the Raman and infrared spectra have been discussed on the hypothesis of intermolecular coupling through fluorine atoms of the substances. Some of the new Raman lines appearing in the low-frequency region in the Raman spectra of the substances in the solid state at  $-180^{\circ}\text{C}$  have been assigned to some of the vibrational modes of the molecules perpendicular to the planes of the benzene ring.

## INTRODUCTION

The Raman spectra of benzene and a large number of substituted benzenes in the solid state at low temperatures have been studied earlier by many workers. Generally, chlorine or bromine substituted benzene compounds yield intense and numerous new low-frequency Raman lines in the solid state at low temperatures. The results of investigation on the Raman spectra of some simple fluorine substituted benzene compounds in the solid state (Mukherjee, 1960; Deb, 1961) also indicated the dependence of the number of low-frequency Raman lines on the substituent atom. It has been observed that fluorobenzene yields only one new low-frequency line in the solid state while chlorobenzene gives five such lines. This difference has been attributed to the strong chemical affinity of the fluorine atom in the molecules of such compounds (Mukherjee, 1960, Deb, 1961) resulting in the formation of strongly associated dimers. In order to find out how the numbers and intensity of the low-frequency Raman lines depend on the position of the fluorine atom in a disubstituted molecule containing a single fluorine atom, the Raman spectra of ortho- and metafluorotoluenes have been studied in the solid state at  $-180^{\circ}\text{C}$  and compared with the spectra of the substances in the liquid state. Since it would be interesting to find out how the spectra would be modified if the fluorine atom were transferred from the benzene ring to a substituent group,

\* Communicated by Prof. S. C. Sirkar.

the Raman spectra of benzonitrile in the liquid state and in the solid state at  $-180^{\circ}\text{C}$  have also been studied.

The infrared absorption spectra of all the compounds in the liquid state and of their solutions in some aliphatic solvents have been investigated in order to find out the effect of environment on the vibrational frequencies of the molecules. The results have been compared with those reported by previous workers in the case of similar substituted benzene compounds and the changes observed have been discussed.

#### EXPERIMENTAL

The liquids ortho- and metafluorotoluenes were obtained from Dr. Theodor Schwachardt, Germany and the liquid benzonitrile was supplied by Eastman Kodak Co., U.S.A. The liquids were of chemically pure quality and they were further purified by repeated distillations under reduced pressure before each exposure. The experimental arrangement and procedure in recording the Raman spectra in the solid state were the same as those used by Biswas (1954). The spectra were photographed on Ilford Zenith plates with the help of a Fuess glass spectrograph having a dispersion of about  $11 \text{ \AA/mm}$  in the region  $4047 \text{ \AA}$ .

The infrared absorption spectra of the compounds were recorded with a Perkin Elmer Model 21 spectrophotometer with NaCl optics. Absorption cells of thickness  $0.05 \text{ mm}$  were used in recording the spectra of the solutions and a much thinner films were used in the case of the pure liquids. Suitable compensation cells containing the solvents were used in the reference beam while recording the spectra of the solutions.

#### RESULTS

The spectrograms are reproduced in Figs. 1, 2 and 3, Plate I. The observed Raman shifts of the molecules in the liquid state and in the solid state at  $-180^{\circ}\text{C}$  are tabulated in Tables I, II and III respectively. The Raman frequencies for the compounds in the liquid state reported by previous workers are also included in the tables for comparison.

The infrared absorption spectra of the compounds in the liquid state and of their solutions in  $\text{CCl}_4$ ,  $\text{CS}_2$  and *n*-hexane are shown in Figs. 4, 5 and 6 and the wave numbers of the absorption bands are tabulated in Tables I, II and III respectively. The frequencies of the bands due to the compounds in the liquid state reported by previous workers are also included in the corresponding tables for comparison.



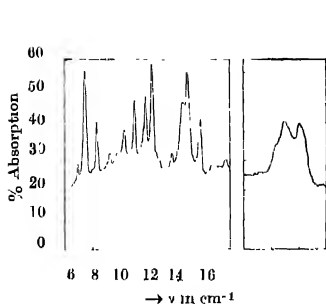


Fig. 4(a) Infrared spectrum of ortho-fluorotoluene (liquid at 26°C).

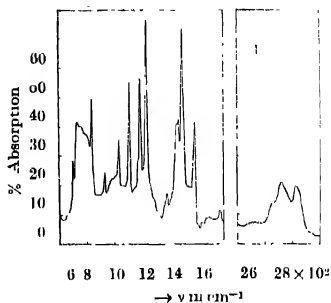


Fig. 4(b) Infrared spectrum of 5% solution of ortho-fluorotoluene in carbon tetrachloride.

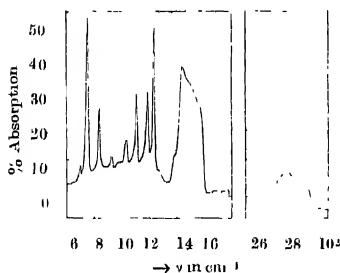


Fig. 4(c) Infrared spectrum of solution of ortho-fluorotoluene in carbon bisulphide.

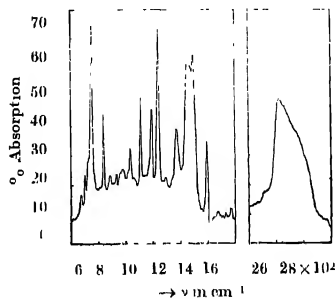


Fig. 4(d) Infrared spectrum of 5% solution of ortho-fluorotoluene in *n*-hexane.

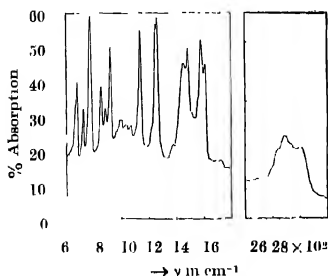


Fig. 5(a) Infrared spectrum of meta-fluorotoluene (liquid at 26°C)

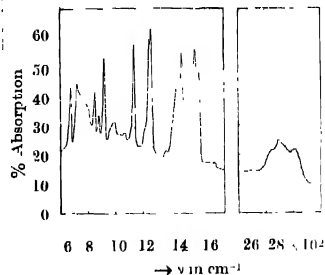


Fig. 5(b) Infrared spectrum of 5% solution of meta-fluorotoluene in carbon tetrachloride.

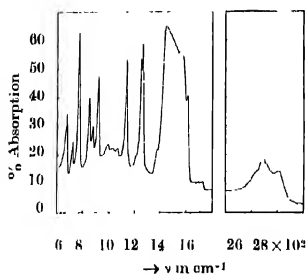


Fig. 5(c) Infrared spectrum of 5% solution of metafluorotoluene in carbonbisulphide.

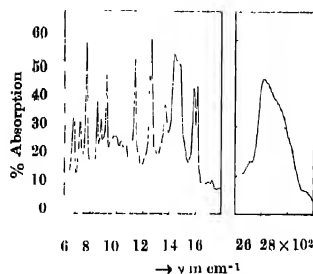


Fig. 5(d) Infrared spectrum of 5% solution of metafluorotoluene in *n*-hexane.

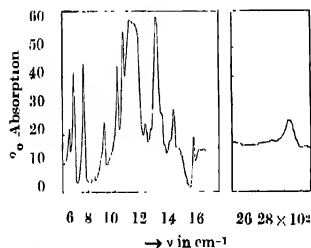


Fig. 6(a) Infrared spectrum of benzotrifluoride (liquid at 26°C)

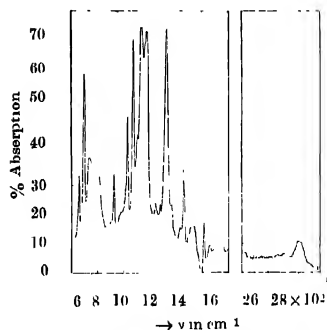


Fig. 6(b) Infrared spectrum of 5% solution of benzotrifluoride in carbon tetrachloride.

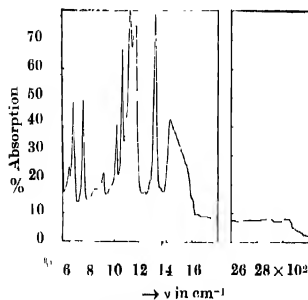


Fig. 6(c) Infrared spectrum of 5% solution of benzotrifluoride in carbonbisulphide.

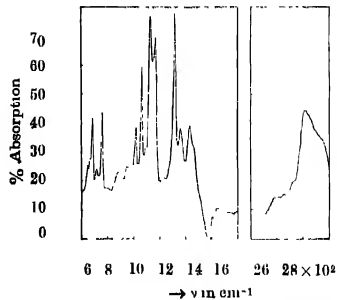


Fig. 6(d) Infrared spectrum of 5% solution of benzotrifluoride in *n*-hexane.

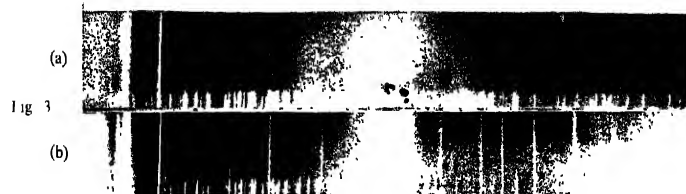
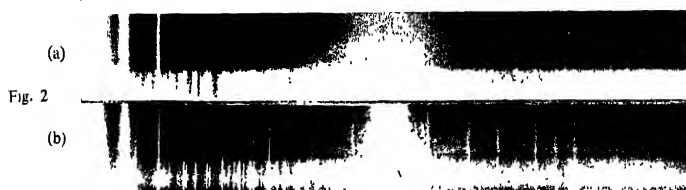
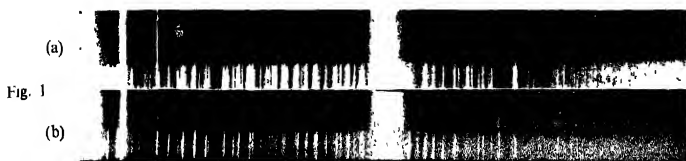


Fig. 1 (a) Orthofluorotoluene solid at  $-180^{\circ}\text{C}$   
 (b) „ liquid at  $26^{\circ}\text{C}$   
 Fig. 2 (a) Metafluorotoluene liquid at  $26^{\circ}\text{C}$   
 (b) „ solid at  $-180^{\circ}\text{C}$   
 Fig. 3 (a) Benzotrifluoride liquid at  $26^{\circ}\text{C}$   
 (b) „ solid at  $-180^{\circ}\text{C}$



TABLE I

Raman and infrared spectra of orthofluorotoluene,  $\nu$  in  $\text{cm}^{-1}$ ,

Raman shifts			Infrared bands					
Liquid		Solid ( $-180^\circ\text{C}$ )	Pure liquid	Solutions (Present author)				
Thomson and Temple (1948)	Present author	Present author	Thomson and Temple (1948)	Present author	in carbon tetra- chloride	in carbon bisulph- ide	in <i>n</i> - hexane	
		73 (4) 96 (2) 170 (2) 202 (5)						
185 (6)D	190 (6b)							
275 (5)D	272 (6b)	274 (3)						
428 (1)								
526 (4)D	526 (3b)	528 (1)	528 $\mu$					670 w
576 (5)P	578 (4)	578 (2)	578 s					700 w
747 (10)P	744 (12)	745 (10)	703 s	700 vw	700 w	700 w		755 vs
			752 vs			750 vs		
			807 w	800 vw				
848 (0)			842 vs		835 s	835 ms	835 s	
			850 ms					
			886 s	900 vw		880 w	880 w	
986 (2) P	986 (0b)	986 (0b)	934 s	932 w	930 w	930 w	930 w	
			985 ms	980 w	976 vw	978 w	978 w	
1037 (8)P	1039 (0)	1039 (0)	1037 vs	1032 ms	1033 ms	1032 w	1032 w	
			1072 vw					
1155 (3b)	1156 (1b)		1108 vs	1108 vs	1110 s	1110 s	1110 s	
			1145 vw	1120 vw			115 w	
			1172 vs	1172 ms	1173 ms	1185 s	1170 w	
			1193 vs	1186 vs	1190 s		1190 s	
1233 (8)P	1234 (8)	1231 (6)	1233 vs	1235 vs	1235 vs	1232 vs	1238 vs	
1277 (2)	1276 (2)		1275 ms	1265 w				
			1298 vw	1290 vw	1290 vw	1290 vw	1290 w	
1381 (3)P	1380 (0)	1378 (0)	1382 ms	1385 w	1385 w			
1441 (1)D			1445 vs	1415 w	1415 w			
				1450 vs	1455 ms			
			1465 vs	1465 vs				
1583 (2)	1586 (2)		1500 vs	1490 vs	1490 vs			
			1580 s	1582 s	1578 s			1590 ms
1618 (5)D	1615 (6)	1614 (2)	1600 w	1610 vw	1615 vw			1615 vw
				1690 vw	1688 vw			1688 vw
				1760 w				
				1770 w	1770 vw			
				1890 w	1895 vw			1895 vw
				1930 vw	1930 vw			1930 vw
				2830 s	2840 w	2835 w		
				2900 ms	2915 ms	2900 ms		
		2017 (4)						
2926 (3b)	2929 (4b)	2950 (2) 3064 (3)						
				3010 ms	3025 ms	3010 ms		
3069 (4b)	3064 (10b)	3070 (5)		3040 ms	3052 ms	3040 ms		

TABLE II

Raman and infrared spectra of metafluorotoluene,  $\nu$  in  $\text{cm}^{-1}$ 

Raman shifts			Infrared bands				
Liquid		Solid ( $-180^{\circ}\text{C}$ )	Pure liquid		Solutions (Present author)		
Thomson and Temple (1948)	Present author	Present author	Thomson and Temple (1948)	Present author	in carbon tetra- chloride	in carbon bisulphide	in <i>n</i> - hexane
<hr/>							
		88 (8b)					
212 (1b) D	212 (2)						
243 (3b)	245 (5b)	252 (3)					
290 (0)	294 (0)						
450 (0)							
512 (2)P	513 (4)	518 (2)	518 ms				
527 (3)P	528 (8)	528 (2)	532 ms				
552 (1)D	556 (2)	550 (0)					
			685 vs	680 s	680 ms	678 ms	678 ms
728 (5)P	727 (15)	729 (8)	730 s	725 ms		725 ms	725 w
775 (0)			778 vs	772 vs		772 vs	772 vs
843 (0)			857 s	850 s	850 ms	852 ms	853 ms
			888 s	880 w	882 w	880 w	880 w
			922 vs	922 vs	922 s	922 s	925 ms
			968 w	960 w			950 w
			995 w	995 w	998 w	995 w	990 w
1003 (6)P	1002 (15)	1002 (10)	1004 ms				
			1039 w	1030 w	1030 w	1030 w	1032 w
1078 (1b)P	1082 (3)	1082 (0)	1075 ms	1070 w	1070 w	1072 w	1075 w
1160 (0)D	1161 (1)	1158 (0)	1143 vs	1140 vs	1140 vs	1142 vs	1140 vs
				1220 w	1220 w	1220 w	1220 w
1250 (2) P	1256 (5)	1255 (1b)	1255 vs	1250 vs	1250 vs	1250 s	1250 s
1266 (2) P	1272 (6)	1272 (1b)		1260 vs	1265 vs	1267 vs	1267 vs
1379 (1) D	1381 (4)	1383 (2)	1376 ms	1380 w	1380 w	1378 w	
1437 (0)			1445 vs	1450 vs	1440 ms		1440 s
1437 (0)			1465 vs	1482 vs	1450 ms		1455 s
			1486 vs		1490 vs		1485 s
			1515 vw	1510 w	1540 ms		
1590 (0)	1590 (0b)	1590 (0b)	1590 vs	1555 ms	1555 ms		
				1582 vs	1585 vs		1588 ms
1618 (2) D	1619 (8)	1618 (2)	1610 s	1606 vs	1615 s	1610 ms	1615 ms
			1655 vw	1650 vw	1650 vw		
				1730 vw	1730 w	1725 vw	1730 vw
				1835 vw			
				1920 vw	1920 vw	1915 vw	1920 vw
				2310 vw			
				2840 w	2840 w	2840 w	
				2890 ms	2900 ms	2890 w	
2925 (3b)	2920 (0b)	2926 (5b)		2930 w	2935 w	2930 w	
2961 (0)							
						3005 w	
3060 (3b)P	3060 (8b)	3060 (3b)					
3081 (2b) P	3078 (4b)	3080 (2b)					

TABLE III

Raman and infrared spectra of benzotrifluoride,  $\nu$  in  $\text{cm}^{-1}$ 

Raman shift			Infrared bands				
Liquid		Solid ( $-180^\circ\text{C}$ )	Pure liquid		Solutions	(Present author)	
Narasimham <i>et al</i> (1957)	Present author	Present author	Thomson and Temple (1948)	Present author	in carbon tetra- chloride	in carbon bisulphide	in <i>n</i> - hexane
1	2	3	4	5	6	7	
		98 (8)					
139 (s) (7)	138 (10b)	120 (1)					
		145 (2)					
199 (vvw)D	200 (0h)	185 (ob)					
235 (vvw)							
321 (vw)D	323 (0)						
339 (m)P	336 (6)	336 (2)					
400 (w)D	400 (oh)	384 (0b)					
485 (vvw)D							
583 (vvw)			599 s				
618 (m) D	618(5)	618 (1)		655 ms	655 ms	652 w	655 w
657 (w) P			661 s	665 w	660 w	668 w	668 ms
			676 ms				
			699 s	692 vs	692 vs		690 ms
769 (s) P	774 (10)	774 (8)	771 s	770 vs			
						762 ms	765 ms
800 (vw) P	797 (0)						
844 (vw)D	846 (0b)		844 vw	840 vw		840 vw	840 vw
			900 w	900 w			
925 (vw)D			923 s	920 ms	922 ms	918 w	915 w
972 (vw)P			970 w	985 w	975 w		975 w
991 (w)			992 vw				
1003.5 (vs)P	1002 (15)	999 (10)	1005 w				
1027 (m) P	1029 (4)	1022 (2)	1027 s	1027 vs	1027 s	1025 ms	1025 ms
1071 (w) P	1070 (0h)		1065 s	1070 vs	1070 vs	1065 s	1070 s
			1080 vs				
1127 (vvw)P				1100 vs	1100 s	1097 w	1098 ms
				1125 vs	1130 vs		1132 vs
1161 (w) D	1158 (1)		1150 vs	1160 vs	1160 vs	1160 vs	1160 s
1187 (w) P	1189 (1)		1183 vs	1170 vs	1172 vs	1175 vs	1170 vs
1239 (vvw)			1238 ms	1240 ms	1240 w	1235 vw	1240 w
			1290 w	1282 w	1278 w	1275 vw	
1324 (m)P	1323 (6)	1323 (0h)	1325 vs	1322 vs	1322 vs	1322 vs	1320 vs
1365 (vvw)			1360 ms	1365 ms		1362 vw	
1389 (vvw)			1390 vw	1390 w			
1427 (vvvw)	1425 (2)		1412 vw	1425 w	1425 w		1422 w
			1430 w				
1458 (vw)D			1455 s	1452 s	1452 ms		1445 ms
				1500 w	1505 w		
1593 (w)D	1590 (2)	1590 (0)	1540 vw				
1610 (w)D	1612 (4)	1616 (4)	1615 s	1610 w	1610 w		1610 vw
1662 (vvw)				1650 vw			
1687 (vvw)				1690 vw			
				1720 vw	1720 vw		1715 vw
				1760 vw			
				1800 vw			
1841 (vvw)				1890 vw	1890 vw		1890 vw
				1900 vw			
1940 (vvvw)							
1981 (vvvw)							
2204 (vvvw)							
2265 (vvvw)							

TABLE III—(contd.)

2321 (vvvw)			2610 vw	2615 vw	
2461 (vvw)					
2741 (vvw)D					
2913 (vvw)D			2900 vw	2895 vw	2900 vw
2926 (vvw)					
2952 (vvvw)			2950 vw	2950 vw	
2995 (w) P	2990 (1)	2990 (1)			
3022 (w) P	3024 (1)	3024 (1)			
			3040 ms	3040 ms	304 w
3076 (s) P	3070 (4)	3070 (3)			
	3082 (10)	3086 (8)	3095 w	3090 w	3090 vw
3183 (w) P					
3218 (w) P					

## DISCUSSION

## 1. Raman spectra

The Raman frequencies observed in the case of the substances in the liquid state agree with those reported by previous authors except in the case of benzotrifluoride, the Raman spectrum of which reported by Narasimhan *et al.* (1957) show many more very very weak Raman lines which have not been observed in the present investigation. On examining the spectrum, it is found that the lines 2913, 2926 and 2952  $\text{cm}^{-1}$  are definitely absent although they were reported by the authors mentioned above. A spectrogram obtained with a filter to cut off 4047 Å line of Hg show the lines 1158 and 1189  $\text{cm}^{-1}$  excited by the 4358 Å line with undiminished intensity. Hence the lines 2926 and 1956  $\text{cm}^{-1}$  excited by the 4047 Å line are not superposed on these lines. The spectrogram also show the CH lines excited by the 3650 Å group of Hg lines in the vicinity of the Hg line 4108 Å. The line 485  $\text{cm}^{-1}$  may be superposed on it, but there is no such line excited by the 4358 Å line in the spectrogram.

*Changes in the Raman spectra with solidification*

With solidification of the liquids some changes in the spectra are observed. When orthofluorotoluene is solidified and cooled to  $-180^{\circ}\text{C}$ , the line 190  $\text{cm}^{-1}$  splits up into two lines 170 and 200  $\text{cm}^{-1}$  and the line 2929  $\text{cm}^{-1}$  is split up into two lines 2917 and 2950  $\text{cm}^{-1}$  respectively. In this case also two more new lines of Raman shifts 73 and 96  $\text{cm}^{-1}$  appear in the spectrum of the solid. Similarly, in the case of metafluorotoluene the line 212  $\text{cm}^{-1}$  becomes very weak and a new strong and broad line 88  $\text{cm}^{-1}$  appears in the spectrum of the solid. Also the line 245  $\text{cm}^{-1}$  appear to shift to 252  $\text{cm}^{-1}$  under similar conditions.

In order to understand these changes it is necessary to identify the modes of vibration which give rise to these lines. As several depolarised lines are observed with values of  $\Delta\nu$  less than 400  $\text{cm}^{-1}$  it is difficult to assign the lines unequivocally without comparing the spectra of all the single halogen substituted toluenes with



each other. The Raman frequencies of such depolarised lines are listed in Table IV. In this connection it has to be mentioned that the Raman spectrum of *p*-fluorotoluene was photographed again in order to find out whether the line  $152\text{ cm}^{-1}$  actually disappears as reported earlier (Deb, 1961) or it appears with feeble intensity. It was found that the line shifts to  $162\text{ cm}^{-1}$  and becomes much weaker. Hence, this line has been included in Table IV.

TABLE IV

	Mode		Mode $\nu_{11}$	
	$\nu_{10}(a,b)$			
	Raman shifts in $\text{cm}^{-1}$		Raman shifts in $\text{cm}^{-1}$	
	Liquid	Solid	Liquid	Solid
<i>o</i> -Fluorotoluene <sup>a</sup>	272	274	190	170 202
<i>o</i> -Chlorotoluene <sup>b</sup>	247	243	163	102 186
<i>o</i> -Bromotoluene <sup>c</sup>	239	247	152	100 172
<i>m</i> -Fluorotoluene <sup>a</sup>	245	252	212	88
<i>m</i> -Chlorotoluene <sup>d</sup>	222	218	187	50 129
<i>m</i> -Bromotoluene <sup>d</sup>	200	203	173	33 130
<i>p</i> -Fluorotoluene <sup>e</sup>	333	103 353	152	127 162
<i>p</i> -Chlorotoluene <sup>b</sup>	307	50 390	100 <sup>g</sup>	85 130
<i>p</i> -Bromotoluene <sup>e</sup>	242	52 162	80 <sup>g</sup>	91 103
<sup>a</sup> Present work			<sup>d</sup> Biswas, 1955	
<sup>b</sup> Sanyal, 1953			<sup>e</sup> Deb, 1961	
<sup>c</sup> Biswas, 1954				

It can be seen from column 2 of this table that a depolarised Raman line of frequency-shift ranging from 203 to  $333\text{ cm}^{-1}$  appears in the spectra of all the single halogen substituted toluenes. Evidently, this frequency is due to an  $A''$  mode. There are two such modes which can be identified with  $\nu_{10}(\epsilon_g^-)$  and  $\nu_{11}(\alpha_{1u})$  of benzene (Sponer and Kirby Smith, 1941) and these involve bending of the C—H and C—R bonds at right angles to the plane of the ring. The frequency of  $\nu_{10}$  is expected to be higher than that of  $\nu_{11}$ . The latter mode is allowed in the Raman effect in monosubstituted benzenes and disubstituted ortho- and meta compounds. On examining the Raman frequencies of such compounds, it is found that a line having Raman frequency ranging from  $214\text{ cm}^{-1}$  to  $184\text{ cm}^{-1}$  appears in the spectra

of toluene, chlorobenzene and bromobenzene, but it either becomes extremely weak or vanishes when a similar substituent atom replaces the hydrogen atom in the para position of the benzene ring. Hence this line can be assigned to the mode  $\nu_{11}$  which is forbidden in the centro-symmetrical disubstituted benzenes. In the present case the line  $190\text{ cm}^{-1}$  of *o*-fluorotoluene and  $212\text{ cm}^{-1}$  of meta fluorotoluene are assigned to  $\nu_{11}$ .

There is another totally depolarised line with the Raman frequency ranging from  $255$  to  $340\text{ cm}^{-1}$  in the spectra of the mono substituted benzenes mentioned above. There is also a third such line in the neighbourhood of  $800\text{ cm}^{-1}$ . These frequencies can be assigned to the modes corresponding to  $\nu_{10(a)}$  and  $\nu_{10(b)}$  mentioned above. In the spectra of ortho and meta-fluorotoluene the corresponding frequencies are  $272\text{ cm}^{-1}$  and  $245\text{ cm}^{-1}$  respectively. The lines  $526\text{ cm}^{-1}$  and  $556\text{ cm}^{-1}$  can similarly be assigned to the mode  $\nu_{17}$  which is allowed in the cases of these two molecules and is almost forbidden in the case of *p*-fluorotoluene which shows a very weak depolarised line  $498\text{ cm}^{-1}$ .

Table I shows that the line  $190\text{ cm}^{-1}$  splits up into two lines at  $202\text{ cm}^{-1}$  and  $170\text{ cm}^{-1}$  respectively and the line  $272\text{ cm}^{-1}$  remains almost unchanged when orthofluorotoluene is solidified and cooled to  $-180^\circ\text{C}$ . The splitting of the former line is small and this may be due to weak intermolecular coupling of different strengths with different neighbouring molecules in the lattice. The splitting of the line  $2929\text{ cm}^{-1}$  due to the  $\text{CH}_3$  group shows that such coupling takes place between the fluorine atom and the  $\text{CH}_3$  group of the neighbouring molecule.

In the case of the meta compound the changes in the spectrum with solidification of the liquid appear to be more drastic. The line  $212\text{ cm}^{-1}$  disappears and a strong broad line appears at  $88\text{ cm}^{-1}$ . The line  $245\text{ cm}^{-1}$  shifts to  $252\text{ cm}^{-1}$  and becomes weaker and sharper. These changes may be due to stronger intermolecular coupling between the fluorine atom and the neighbouring benzene ring in the crystal. Probably the line  $252\text{ cm}^{-1}$  is due to a configuration of  $\nu_{10}$  in which the coupled fluorine atom remains stationary and the  $\text{CH}_3$  group along with CH groups executes bending oscillation. The other component of  $\nu_{10}$  may have a frequency near about  $90\text{ cm}^{-1}$  and the new broad line  $88\text{ cm}^{-1}$  may thus be due to the two modes  $\nu_{10}$  and  $\nu_{11}$  in such coupled molecules.

In the case of the ortho compound there are two more new low-frequency lines  $73$  and  $96\text{ cm}^{-1}$  respectively. In this case the mode  $\nu_{10}$  is allowed and in coupled molecules the frequency is expected to be lower than that due to  $\nu_{11}$ . Hence the two lines  $73$  and  $96\text{ cm}^{-1}$  may be due to  $\nu_{10(a)}$  and  $\nu_{10(b)}$  respectively.

When benzotrifluoride is solidified and cooled to  $-180^\circ\text{C}$  the line  $138\text{ cm}^{-1}$  arising from a bending of the  $\text{C}-\text{CF}_3$  bond (Nelson and Thieme, 1957) splits into three lines  $98$ ,  $120$  and  $145\text{ cm}^{-1}$  respectively. The line  $400\text{ cm}^{-1}$  shifts to  $384\text{ cm}^{-1}$  and the line  $200\text{ cm}^{-1}$  shifts to  $185\text{ cm}^{-1}$  with the solidification of the liquid. The line  $138\text{ cm}^{-1}$  can be assigned to a mode corresponding to  $\nu_{11}$  of benzene and

the line  $200\text{ cm}^{-1}$  to  $\nu_{10(b)}$ . The splitting of the line  $138\text{ cm}^{-1}$  into three components may be due to weak linking of the  $\text{CF}_3$  group with the hydrogen atom of the neighbouring molecule, the strength of the linking being different along the three axes.

The line  $400\text{ cm}^{-1}$  has been assigned to rocking of the  $\text{CF}_3$  group. The shift of this line to lower frequency in the solid state at  $-180^\circ\text{C}$  may be due to the formation of weak linkage between the fluorine atoms and the neighbouring molecules. It has to be pointed out, however, that toluene also shows a depolarised line at  $405\text{ cm}^{-1}$  and this may be due to  $\nu_{10(a)}$  which gives a weak line in the spectrum of benzene.

## II. Infrared spectra

The infrared spectra of the substances in the liquid state were reported earlier upto  $1600\text{ cm}^{-1}$  (Thomson and Temple, 1948). Also the infrared absorption spectrum of liquid benzotrifluoride in the vapour state has been studied upto  $3100\text{ cm}^{-1}$  (Narasimham *et al.*, 1957). In the present investigation the absorption spectra of the liquids in the pure state and in the solutions of various aliphatic solvents have been recorded upto  $3600\text{ cm}^{-1}$ . Tables I, II, and III show that most of the infrared bands of the compounds agree closely with those reported by previous workers. In the case of ortho-fluorotoluene the strong bands  $703$  and  $886\text{ cm}^{-1}$  reported by previous workers appear very weakly in the present investigation and a new band  $1415\text{ cm}^{-1}$  has been recorded. In the case of meta-fluorotoluene one broad band  $998\text{ cm}^{-1}$  has been observed in place of two bands  $995$  and  $1004\text{ cm}^{-1}$  reported by previous workers and two extra bands  $1220$  and  $1260\text{ cm}^{-1}$  have been recorded. Similarly, in the case of benzotrifluoride the bands  $771\text{ cm}^{-1}$  and  $1183\text{ cm}^{-1}$  reported by previous workers appear as doublets with components  $750$  and  $770\text{ cm}^{-1}$  in the first case and  $1160$  and  $1170\text{ cm}^{-1}$  in the second case.

### *Infrared spectra of solutions compared to the spectra due to pure liquids*

The records of the absorption spectra reproduced in figures 4, 5 and 6 show some changes in the strengths of absorption and positions of some of the bands with dissolution in certain solvents. Figure 4 shows that the band  $1032\text{ cm}^{-1}$  becomes much weaker when the substance is dissolved in  $\text{CS}_2$  and it is slightly weaker in the case of the solution in *n*-hexane. Similarly, the band  $1250\text{ cm}^{-1}$  of *m*-fluorotoluene becomes much weaker in the solution in *n*-hexane and slightly weaker in solution in carbon disulphide. These lines are probably some modes which involve the simultaneous stretching of C-H, C-CH<sub>3</sub> and C-F bonds of the molecules. The weakening of the bands indicates that the fluorine atom is weakly linked with the solvent molecules in both the cases.

In the case of benzotrifluoride (Fig. 6) the band  $1027\text{ cm}^{-1}$  becomes much weaker in solutions in  $\text{CS}_2$  and in *n*-hexane. This line has been assigned to the

C—F stretching mode in the  $\text{CF}_3$  group (Narasimham *et al.*, 1957) and in this case also the results indicated weak coupling of the fluorine atoms with the solvent molecules.

#### ACKNOWLEDGMENT

The author wishes to acknowledge his ever grateful indebtedness to Professor S. C. Sirkar, D.Sc., F.N.L. for his kind help and inspiring guidance throughout the progress of the work. Thanks are due to Dr. G. S. Kastha, D.Sc. for helpful discussions in connection with this work.

#### REFERENCES

- Biswas, D. C., 1954a, *Ind. J. Phys.*, **28**, 54  
Biswas, D. C., 1954b, *Ind. J. Phys.*, **28**, 423.  
Biswas, D. C., 1955, *Ind. J. Phys.*, **29**, 257.  
Deb, K. K., 1961, *Ind. J. Phys.*, **35**, 16  
Mukherjee, D. K., 1960, *Ind. J. Phys.*, **34**, 402  
Narasimham, *et al.*, 1957, *J. Chem. Phys.*, **27**, 740  
Sanyal, S. B., 1953, *Ind. J. Phys.*, **27**, 417  
Sponer, H. and Kirby Smith, J. S., 1941, *J. Chem. Phys.*, **9**, 667  
Thomson, H. W. and Temple, R. B., 1948, *J. Chem. Soc.*, p. 1432.

# CAPTURE RATES OF NEGATIVE MUONS BY NUCLEI

PRAKASH CHAND AND B. K. AGARWAL

DEPARTMENT OF PHYSICS, UNIVERSITY OF ALMAHABAD, INDIA

(Received November 27, 1960)

**ABSTRACT** Using recent muon mass and radius of nuclear charge distribution  $R = 1.2A \times 10^{-13}$  cm, the Wheeler's  $Z_{eff}$  has been calculated employing hydrogen-like wave functions for different nuclei. Substituting these values of  $Z_{eff}$  in Primakoff's formula the capture rates of mesons by various nuclei have been evaluated. The results of present calculations are in good agreement with experimental data.

## 1. INTRODUCTION

When a  $\mu$  meson gets an opportunity to be slowed down by ionizing collisions to nearly thermal velocity, being a Dirac particle, it falls into a hydrogen-like 'Bohr orbit' around the nucleus. It may now be captured by a nucleus according to the process

$$\mu^- + p \rightarrow n + \nu \quad (1)$$

The other competing process is the radioactive decay into an energetic electron and two neutrinos

$$\mu \rightarrow e^- + 2\nu \quad \dots (2)$$

At about  $Z = 10$ , the lifetime for nuclear absorption is approximately equal to the lifetime of the decay of slow mesons and only when  $Z$  decreases below 10, process (1) loses out very rapidly to process (2). Wheeler (1949) has shown that the probability of nuclear absorption, process (1) is sensitive to the atomic number of the nucleus. The probability per second of absorption is

$$\Lambda \propto \sum_{\text{all protons}} |\psi_{\mu}(\text{at each proton})|^2 \quad \dots (3)$$

Assuming that all protons can interact independently with the  $\mu$ -mesons in the  $K$  orbit, and the nucleus is a point, we have

$$\Lambda \propto \sum |\psi_{\mu}(0)|^2 \propto Z |\psi_{\mu}(0)|^2 \quad \dots (4)$$

where  $\psi_{\mu}(0)$  is the ground state wave function evaluated at the origin and  $a_{\mu 0}$  is the muon Bohr radius. If, for  $Z = Z_0$ , the absorption and decay probabilities are equal, the decay lifetime  $\tau_0$  is given by

$$\frac{1}{\tau_0} = \text{constant} \times Z_0^4$$

Eq. (4) can now be written as

$$\Lambda = \frac{1}{\tau_0} \left( \frac{Z}{Z_0} \right)^4 \quad \text{constant} \propto Z^4$$

Obviously, this is a very crude estimate, especially for high  $Z$  where the radius of muon orbit is comparable to the nuclear radius. For a finite size nucleus with a continuous charge distribution, Wheeler (1949) writes the probability per second of absorption as

$$\Lambda = \text{constant} \propto (Z_{\text{eff}})^4 \quad \dots (5)$$

where  $Z_{\text{eff}}$  is defined by

$$Z_{\text{eff}} = \left\{ \frac{\alpha \mu_0^3}{\frac{4}{3} \left( \frac{e^2}{2m_\mu} \right)^3} \right\}^{1/4} \left[ \frac{Z}{A} \frac{\int_0^R |\psi_\mu(q)|^2 d^3q}{\int_0^\infty |\psi_\mu(q)|^2 d^3q} \right]^{1/4} \quad \dots (6)$$

Using  $m_\mu = 210m_e$  the constant term in (6) outside the square brackets comes out to be 47.1. With  $m_\mu = 206.86m_e$  it comes out to be 46.0, a value which we will employ in our calculation.

## 2. CALCULATION OF $Z_{\text{eff}}$

Wheeler has evaluated (6) for several nuclei, using ground state wave functions of the three dimensional isotropic oscillator, and connected them by an empirical formula

$$Z_{\text{eff}} = Z \left[ 1 + \left( \frac{Z}{37.2} \right)^{1.54} \right]^{-1.54} \quad \dots (7)$$

which yields nearly a straight line for the absorption probability vs.  $Z_{\text{eff}}$  graph. Recently, several workers [Keuffel and Meyer (1957), Sens *et al.* (1957), Astbury *et al.* (1958), Gilboy and Tennent (1959), Sens (1959)] have measured the capture probability of elements like Fe, Hg, Cu, Sb, Bi, Pb, etc. and have found that experimental points do not fall on the curve predicted by Wheeler's theory, even if powers occurring on the right hand side of Eq. (7) are readjusted. Thus Keuffel and Meyer (1957) and Sens (1959) find that points for Tl, Pb, Bi, Hg and U show considerable departure from the straight line obeying Eq. (7) for  $Z_{\text{eff}}$ . Kennedy (1952) has tried to explain the discrepancy for Pb by arguing that for it the nuclear structure is of closed shell and thus is responsible for the effect. However, this fails to account for the cases of Bi and Hg. Also, Kennedy (1952) has calculated the ratio of capture rate by Pb and Ca as 1.6, the value from Wheeler's calculations comes out to be 1.14, while the recent experimental values of Sens (1959) is 1:4.6.

To remove the strong disagreement between the  $Z_{eff}$  values given by Wheeler's formula (7) and those desired from observed values, we have undertaken to cal-

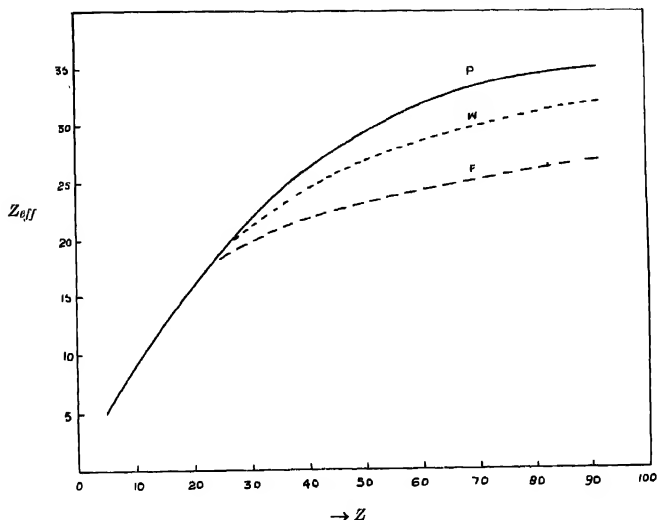


Fig. 1. The plot of  $(Z_{eff})$  against  $Z$ . W due to Wheeler, F due to Ferrari and Villi; P due to present calculations.

culate  $Z_{eff}$  from Eq. (6) using hydrogen-like wave functions (for the method of calculation see Appendix 1). The integral occurring in the numerator of (6) has been cut off at,

$$R = (1.2 \pm 0.03)A^{1/3} \times 10^{-13} \text{ cm.} \quad (8)$$

which is the latest experimental value for the radius of the uniform distribution of charge within the finite volume of the nucleus. This value of  $R$  seems to be the most reliable one (Fitch and Rainwater, 1953; Ford and Hill, 1955). Results of our calculations, taking  $R = 1.2 \pm 0.03 \times 10^{-13} \text{ cm.}$  are plotted in Fig. 1, which also shows the values of  $Z_{eff}$  calculated by Wheeler's formula (7), and by Ferrari and Villi (1954).

### 3. EVALUATION OF CAPTURE RATE

The capture of meson by nuclei involves a weak interaction between half-spin particles. It is now believed that universal Fermi interaction is responsible for the process (1). On this basis Primakoff (1959) has estimated the transition matrix element for the reaction (1), by means of the closure approximation taking into account the Pauli principle and assuming that those

states which are not energetically possible do not contribute very much to the result. The results are given in the form

$$\text{Capture rate} = \Lambda^\mu_{ap}(A, Z) = \gamma \Lambda^\mu_{cap}(1, 1) \left\{ 1 - \frac{A-Z}{2A} \delta \right\} \quad \dots (9)$$

when terms of order  $1/A$  are neglected. Estimated values of parameters are  $\delta = 3.15$ ,  $\gamma \Lambda^\mu_{cap}(1, 1) = 188 \text{ sec.}^{-1}$ . We have calculated the capture rate from Eqs. (6), (8) and (9). The calculated curve for capture rate has been plotted in Fig. 2, against  $Z$ . The figure also contains the curves according to the calculations of Wheeler (1949) and Ferrari and Villi (1954) together with the available experimental data. The agreement between our calculations and experimental values

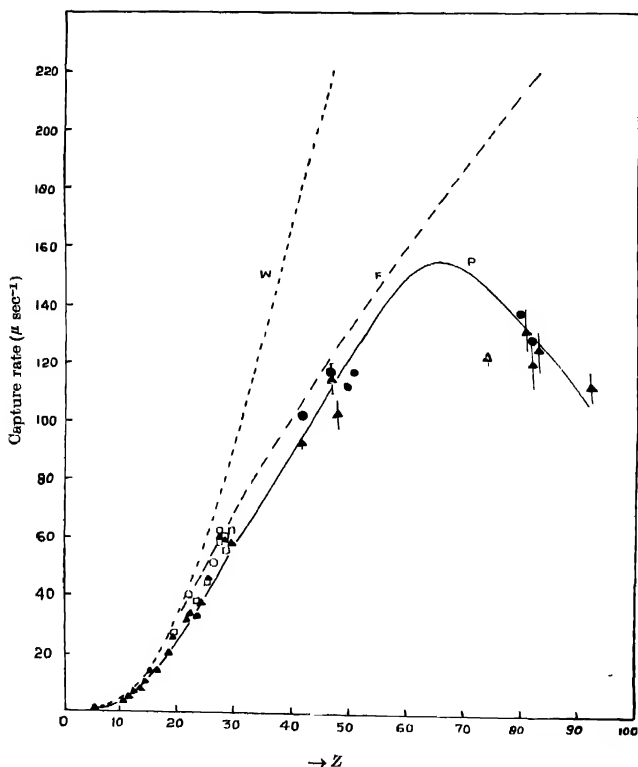


Fig. 2. The capture rate for  $\mu^-$  mesons as a function of  $Z$ . Calculated curves are W due to Wheeler, F due to Ferrari and Villi, and P due to present calculations.

Experimental points:  $\Delta$  Souda,  $O$  Astbury et al.,  $\square$  Gibbo et al.,  $\bullet$  Kouffol & Moyer



is fairly good. The ratio  $\Lambda_{\text{cap}}^{\mu}(_{82}\text{Pb}^{208})/\Lambda_{\text{cap}}^{\mu}(_{20}\text{Ca}^{40})$  comes out to be 1:4.43 which is close to the experimental value  $1.459 \pm .21$  (Sens, 1959). It will be worthwhile to look for the isotope effect experimentally. For Ca our calculated values give

$$\Lambda_{\text{cap}}^{\mu}(_{20}\text{Ca}^{48})/\Lambda_{\text{cap}}^{\mu}(_{20}\text{Ca}^{40}) = 1/3.4$$

#### 4. CONCLUSION

It appears from our calculations that Eq. (8) for the radius,  $R$ , to calculate  $Z_{\text{eff}}$  is a sufficiently good approximation and it is not necessary to employ Fermi-type or other functions to represent the charge distributions for various nuclei. To further test the validity of our calculation measurements of capture rates of muons by nuclei of rare earths (with targets of known  $A$  value) will be desirable. It should be noted that at higher  $Z$  our calculated curve shows that capture probability should decrease with increase in  $Z$ . This appears to be confirmed by the experimental data of Kenfelf and Meyer (1957) who find that capture probability in Pb is lower than that in Hg although the  $Z$  value of the former is greater than that of the latter. The low capture probability for U observed by Sens (1959) further confirms the downward trend of our calculated curve at higher  $Z$ .

#### ACKNOWLEDGMENTS

One of us (Prakash Chand) is grateful to the Department of Atomic Energy, Government of India, for the financial aid given. We would like to express our thanks to Mr. R. N. Bhargava for helpful discussions. Prakash Chand is thankful to Professor M. G. K. Menon for his kind encouragement.

#### APPENDIX I

The Schrodinger wave function in a hydrogen-like atom is

$$\psi_{nl} = \frac{1}{2\sqrt{\pi}} \left\{ \frac{4Z^3}{n^2 a_{\mu_0}^3} \frac{(n-l-1)!}{[(n+l)!]^3} \right\}^{\frac{1}{2}} e^{-\rho/2} \rho^l L_{n+l}^{2l+1}(\rho)$$

with

$$\rho = \frac{2Zr}{na_{\mu_0}}, \quad a_{\mu_0} = \frac{\hbar^2}{m_{\mu}e^2} \quad (\Delta 1)$$

For the  $K$  orbit, we have

$$|\psi_{\mu}| = \frac{1}{\sqrt{\pi}} \left( -\frac{Z}{a_{\mu_0}} \right)^{3/2} e^{-\left( \frac{Z}{a_{\mu_0}} \right) \cdot r}$$

Therefore,

$$Z^4_{eff} \propto \int r^2 \psi_\mu^2 dr \int \tilde{r}^2 \tilde{\psi}_\mu^2 d\tilde{r}$$

$$\propto \int_0^R r^2 e^{-br} dr \int_0^\infty \tilde{r}^2 e^{-b\tilde{r}} d\tilde{r}, \quad \text{where } b = \frac{2Z}{a\mu_0}$$

which can be easily evaluated.

#### REFERENCES

- Astbury, A., Kemp, M. A. R., Lipman, N. H.  
 Fermi, E. and Ylli, C., 1954, *Phys. Rev.*, **96**, 1159  
 Fitch, V. L. and Rainwater, J., 1953, *Phys. Rev.*, **92**, 789  
 Gilboy, W. B. and Tennent, R. M., 1959, *Phil. Mag.*, **4**, 1055  
 Kennedy, J. M. 1952, *Phys. Rev.*, **86**, 953  
 Kuffel, J. W. and Meyer, A. J., 1957 (See Fowler, G. N. and Wollendale, A. W., 1958, *Progress in Elementary Particle and Cosmic Ray Physics*, North Holland Publishing Company, Vol. IV, 107).  
 Munthead, H., Voss, R. G. P., Zaugg, C. and Kuk, A., 1958, *Proc. Phys. Soc.*, **A72**, 494.  
 Primakoff, H., 1959, *Rev. Mod. Phys.*, **31**, 802  
 Sells, J. U., 1959, *Phys. Rev.*, **113**, 679  
 Sells, J. U., Swanson, R. A., Telegh, V. L. and Yovanovitch, D. D., 1957, *Phys. Rev.*, **107**, 1464  
 Wheeler, J. A., 1949, *Rev. Mod. Phys.*, **21**, 133

# DISLOCATION DAMPING IN $\alpha$ -AgCd ALLOY

MD. ABDUL QUADER\*

INDIAN ASSOCIATION FOR THE CULTIVATION OF SCIENCE, CALCUTTA-32.

INDIA

(Received November, 14, 1961)

**ABSTRACT.** The effect of heat treatment on the dislocation damping is studied in 29.3 atomic per cent cadmium silver-cadmium alloy. A hardening effect is observed, analogous to that found by previous workers in pure gold. The furnace cooled specimen shows more hardening effect than the water quenched one, but the amplitude independent internal friction is higher in water quenched specimen. Thus, the results for this alloy are contradictory in regard to the quench hardening effects. The observed effects are interpreted in terms of the pinning of dislocations by vacancies and discussed in the light of Granato and Lucke theory.

## INTRODUCTION

The dislocations in metals are known to execute oscillatory motions under the applied alternating stress (Nowick, 1953) and thereby produce damping that accounts for the relatively high damping of high purity metals. This part of the damping is strongly dependent on the amplitude of vibration due to the breaking away of dislocations from their pinning points (Granato and Lucke, 1956). The fact that impurity atoms and point defects such as vacancies are capable of pinning dislocations has been demonstrated by various effects of addition of small amounts of impurities (Maddin and Cottrell, 1955) and of irradiation (Jamison and Blewitt, 1953) on mechanical properties. The quench hardening effect as observed by Li, Washburn and Parker (1953) in Zn crystals and by Maddin and Cottrell (1955) in Al crystals is, according to them, due to the pinning of dislocations by the quenched in excess vacancies. The latter workers also related the age-hardening phenomena as due to the room temperature migration of quenched-in vacancies to dislocations.

That the quenching has marked effects on internal friction has been shown by Levy and Metzger (1955) in aluminium and also Roswell and Nowick (1957) in pure gold. They have observed that the amplitude dependent internal friction was considerably lower in air quenched specimen than the furnace cooled ones, while the damping of water quenched specimen was practically independent of the strain amplitude. Further, the observations of Weertmann and Salkovitz (1953) in lead and Caswell (1958) and Beshers (1959) in copper revealed that both

---

\*Present address : National Metallurgical Lab. Jamshedpur

the amplitude dependent and amplitude independent internal friction decreased on increasing the impurity concentration. These results are in agreement with the theoretical predictions of Granato and Lucke (1956) that the excess vacancies trapped in the metal by quenching from a higher temperature and also the impurity atoms pin the dislocation thereby reducing the loop length and hence the decrease in internal friction. According to the theory the internal friction in alloys with high solute concentrations should be independent of amplitude at least in the low and moderate amplitude of vibration.

It is clear from the above accounts that all the observations on dislocation damping are limited to either pure metals or very dilute alloys where the Granato and Lucke theory holds good. In the present investigation we have studied the quenching effects on dislocation damping in an alloy where the solute is present in large quantities i.e., 29.3 atomic per cent cadmium of silver-cadmium alloy. Attempts have been made to interpret the results in the light of Granato and Lucke theory.

#### EXPERIMENTAL METHOD

The silver-cadmium alloy specimen used in these experiments was prepared from spectroscopically pure metals. The details of the preparation of the alloy and the specimen for use in the torsional pendulum was given earlier (Quader, 1961). The specimens of the 29.3% alloy were sealed in evacuated Pyrex tubes and given a six-hours anneal at 650°C followed by either furnace cooling or water quenching. Internal friction measurements were made at room temperature by means of a torsional pendulum vibrating at a frequency of about one cycles per second. The quenched sample was mounted in the pendulum and tested within 15 min. of the quench. After that the specimen was allowed to stay at room temperature in the pendulum undisturbed and internal friction was measured with time. In a similar way the furnace cooled specimen was tested. In one case internal friction at 72 and 120°C was obtained with the water quenched specimen after 5 days stay at room temperatures when it had attained a steady value of internal friction.

The vibration of the pendulum was recorded photographically on a rotating drum. Hence, from a single run internal friction at all amplitudes of strain was obtained. The measure of internal friction herein adopted was the log decrement divided by  $\pi$ . The strain amplitude was calculated from the relation  $\epsilon_0 = \frac{\theta r}{l}$  when  $\epsilon_0$  is the strain amplitude,  $\theta$  the angle of twist,  $r$  the radius of the specimen wire and  $l$  its length.

#### EXPERIMENTAL RESULTS

Internal friction measurements were obtained for strain amplitudes of 1 to  $5 \times 10^{-5}$  and are shown in Fig 1. The full curves, representing the internal friction

measured within 15 min of mounting, show a strong amplitude dependence. While the water quenched specimen shows approximately amplitude independent internal friction below a strain amplitude of about  $2 \times 10^{-5}$ , the constant value being  $1.28 \times 10^{-3}$ , the furnace cooled specimen shows no such amplitude independent internal friction even at a strain amplitude of  $1.4 \times 10^{-5}$ . However, in furnace cooled alloy, the internal friction drops very rapidly below the strain amplitude of  $2 \times 10^{-5}$  and probably it would be even lower than the constant amplitude independent part in the water quenched specimen. The curves are similar in nature to those obtained by Wert (1949) in Zn and indicate considerable amount of irreversible amplitude dependence of the internal friction, being more in furnace cooled specimen. This shows that the measurement itself is affecting the condition of the material. However, no definite information about the hysteresis in any of these curves could be obtained with the torsional pendulum. One more thing is clear viz., that the amplitude dependent internal friction is higher in the case of furnace cooled specimen.

Internal friction data for the solid curves of Fig. 1, as stated earlier were obtained within 15 min of mounting the specimen in the pendulum. Upon standing, there is a tendency for these internal frictions to decrease. This effect is

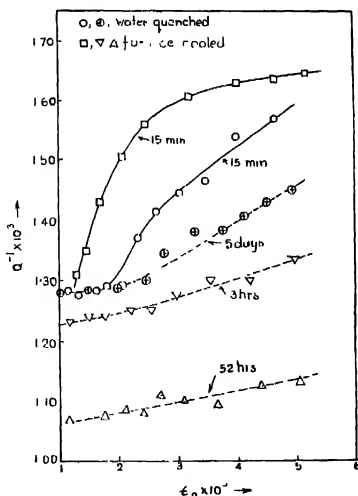


Fig. 1. The variation of internal friction with strain amplitude as a function of initial heat treatment (solid curves) and as a function of time (broken curves).

greatest for the furnace cooled sample and is illustrated by the broken curves of Fig. 1. After standing for three hours the internal friction of the furnace cooled alloy decays to values lower than that for the quenched one. The water quenched

sample, on the other hand, shows a slow decay of the amplitude dependent damping during the first few hours of ageing after which its variation becomes negligibly small. However, the amplitude independent part of the damping remains practically constant in all times. This is evident from the curve obtained after 5 days of ageing.

The decay of internal friction on standing might be interpreted as an age-hardening effect as Levy and Metzger (1955) have done for aluminium. Roswell and Nowick (1957) have observed a similar effect in pure gold and interpreted the decay as due to the elimination of the effects of handling in the mounting of the specimen. We also suspected a similar cause for the decay and performed some handling experiments in which both the furnace cooled and water quenched specimens were allowed to stand in the pendulum for 5 days after which they were disassembled and remount in the pendulum and the internal friction measured. The results are given in Table I and show that mere dismounting of the specimen and subsequent mounting always bring the internal friction back to its original

TABLE I

Effect of handling on the internal friction (at strain amplitude of  $4 \times 10^{-5}$ )  
of furnace cooled and water quenched samples

Handling treatment of the specimen	Initial $Q^{-1} \times 10^3$	Standing time	Final $Q^{-1} \times 10^3$
<i>A Furnace cooled</i>			
Original mount	1.62	3 hours 52 hours	1.30 1.12
Disassembled and remount	1.65	3 hours	1.31
Disassembled and remount	1.63	4 hours	1.25
<i>B Water Quenched</i>			
Original mount.	1.52	3 hours 5 days	1.43 1.40
Disassembled and remount	1.54	3 hours	1.45

value before decay. These results show, therefore, that the decay in time is the elimination of handling effects that takes place during mounting the specimen on the pendulum. The furnace cooled specimen shows more rapid increase in internal friction (both amplitude dependent and amplitude independent) with handling and rapid decay, while the water quenched specimen shows increase only in the amplitude dependent internal friction with handling and slow decay. Another interesting point to note is that the amplitude independent internal friction in water quenched specimen is higher than that for the furnace cooled alloy after the handling effects have decayed out which is opposite the case of pure gold as observed by Roswell and Nowick (1957).

## DISCUSSION

The results of the present measurements may be summarised as follows :

(1) The room temperature internal friction of the 29.3% Ag-Cd alloy depends on the initial heat treatment. Also the internal friction is strongly amplitude dependent and decays on standing. (2) The existence of the handling effect on the internal friction has been demonstrated, whereby the furnace cooled sample is the most sensitive to handling. These results will now be discussed.

In quenching experiments no types of disorder other than vacancies can be expected to be trapped, in the crystals. Thus a high density of vacancies attached to the dislocation is expected. Also the excess vacancies trapped in the lattice migrate to the dislocations and pin them further. These account for the increased hardness in quenched metals. However, with regard to the quenching effects in the AgCd alloy the results are contradictory. The amplitude independent room temperature internal friction, after the handling effects decayed out, is higher in water quenched specimen than that of the furnace cooled one. This might indicate that the hardness of the alloy depends on the rate of cooling, being more hard on slow cooling or in other words no quench hardening. On the other hand, the water quenched sample is less susceptible to handling effects. According to Roswell and Nowick (1957) the quench hardening in pure gold manifests itself primarily in terms of susceptibility of the specimen to handling, i.e., the lesser the handling effects the greater is the hardening. According to the above conclusion, the AgCd alloy is showing quench hardening to some extent.

The results of Levy and Metzger (1953) for Al and of Roswell and Nowick for gold illustrate that both the amplitude dependent and amplitude independent internal friction of metals are reduced by quenching from a high temperature, and usually the faster the quenching, the greater the reduction. The main change of state produced by quenching a metal is to introduce vacancies, the concentration being greater the higher the initial temperature and the faster the rate of quenching. These vacancies pin the dislocations and thus reduce the loop length and so also the internal friction. In case of pure gold, Roswell and Nowick further assumed that in quenched specimen most probably the dislocations are pinned by clusters of vacancies which form an atmosphere about the partial dislocation in the metal. But in the case of AgCd alloy we find that both the amplitude dependent and amplitude independent internal friction are higher in case of water-quenched alloy. This may be due either to a high density of dislocation in the quenched specimen or some peculiarity of the dislocation. But since the nature of the dislocation in this alloy is not known no definite conclusions can be drawn.

The small amount of cold working during the handling of the specimen tore off some of the dislocations from their tightly bound configuration and made them free. These freed dislocations execute oscillatory motion under the applied alternating stress producing high damping. On standing the vacancies again

move to the dislocation and pin them thereby decreasing the internal friction. It is well known (Mott, 1952) that the stress required to pull a dislocation line free of a row of pinning points increases with increasing number of pinning points per unit length of the dislocation line. Thus, with regards to the handling effects we conclude that the larger sensitivity of the furnace cooled sample to handling may be related to the fact that this sample has the greatest separation between the pinning points along the dislocation line. Also it may be due to the circumstance that the pinning points in furnace cooled sample are mostly single vacancies whereas in a water quenched alloy they are cluster of vacancies. The above conclusion also accounts for the rapid decay of the handling effects in the furnace cooled alloy because a single vacancy is highly mobile in the lattice. It may also be that the quenching stresses also play some part in reducing handling effect in the quenched specimen.

Now in the present measurement we find that the damping is composed of two parts, i.e.,

$$\Delta = \Delta_1 + \Delta_H \quad (1)$$

where  $\Delta$  is the total damping,  $\Delta_1$  is the amplitude independent damping and  $\Delta_H$  is the amplitude dependent damping. According to Granato and Lucke (1956), all the amplitude dependent data can be expressed in the form

$$\Delta_H = C_1/c_0 \exp(C_2/c_0) \quad \dots (2)$$

where  $c_0$  is the shear strain and  $C_1$  and  $C_2$  are constant for a given metal. Therefore, if the experimental data are plotted in the form

$$\log(c_0 \Delta_H) \text{ against } 1/c_0$$

a straight line plot would be obtained. The slope of the line is given by

$$C_1 = \frac{Kc'a}{L_e} \quad \dots (3)$$

where  $c'$  is the Cottrell misfit parameter, i.e., the fractional difference in the sizes of the solute (impurity) and solvent atoms, 'a' is the lattice constant,  $K$  is a factor depending on the orientation and anisotropy of the specimen and  $L_e$  is the characteristic impurity pinned dislocation length. That this is true has been shown by a number of measurements (Niblett and Wilks, 1960)

Granato and Lucke plots have been drawn here for the water quenched specimen by taking the amplitude independent background for  $\Delta_1$ , the data for which are given in Table II. Fig. 2 shows that the plots are straight lines and also that the line falls appreciably on standing at



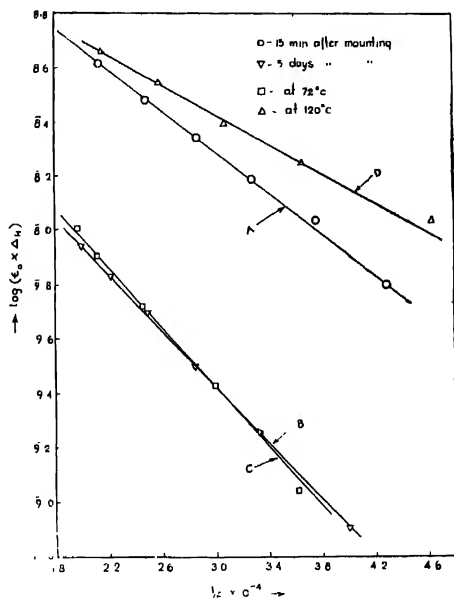


Fig. 2. Granato and Lucke plots for the water-quenched sample as a function of time (curves A & B) and as a function of temperature (Curves C & D).

TABLE II  
Data for Granato-Lucke plot of the water quenched silver-cadmium  
29.3% alloy

15 min after mounting		5 days after mounting		at 120°C			
$\frac{1}{\epsilon_0} \times 10^{-4} \log(\epsilon_0 \times \Delta H)$		$\frac{1}{\epsilon_0} \times 10^{-4} \log(\epsilon_0 \times \Delta H)$		$\frac{1}{\epsilon_0} \times 10^{-4} \log(\epsilon_0 \times \Delta H)$		$\frac{1}{\epsilon_0} \times 10^{-4} \log(\epsilon_0 \times \Delta H)$	
2.144	8.6193	2.00	9.9420	1.974	8.0055	2.165	8.660
2.488	8.4817	2.222	9.8293	2.114	9.9051	2.590	8.550
2.870	8.3403	2.500	9.699	2.467	9.7218	3.085	8.393
3.288	8.1869	2.857	9.4983	2.999	9.4261	3.658	8.249
3.764	8.0355	3.334	9.2553	3.626	9.0426	4.650	8.031
4.276	7.8007	4.004	9.0020	4.644	10.8102		

room temperature (curve B after 5 days, though the change in slope of the line is very small (compare curve A and B). The fall of the lines may be attributed to the lowering of the density of freed dislocation brought about by the migration of the vacancies back to the dislocation. However, the change in  $\frac{1}{2}$ , i.e.,  $L_c$  is negligibly small. From relation (3) we may calculate  $L_c$ , the distance between attached vacancies along a dislocation line. Using the volume of vacancy as 77% of that of atoms (Borelius, 1958) and Granato and Lucke value of .02 for  $K$  and  $a = 4.1524 \text{ \AA}$ , we obtain a value of about  $10^{-6} \text{ cm}$  ( $L_c = 2.2 \times 10^{-6} \text{ cm}$ ) for  $L_c$ . Unfortunately no other values of  $L_c$  are available for comparison.

The lines C and D of Fig. 2 correspond to 72 and 120°C respectively. The internal friction at 120°C is influenced by the contribution due to grain boundary slip. The slope of the line D is lower than those of the other lines indicating an increase of  $L_c$ . It has been observed that the slope of the Granato and Lucke plot decreases with the increase of the temperature of measurements (Chambers, 1957) because of the small number of impurity atoms attached to the dislocation at higher temperature (Cottrell, 1953). Thus the lower slope at 120°C is justified. But it is evident from curve C that the slope of the line increased instead of decreasing at 72°C which indicates a decrease in  $L_c$  due to more pinning. This may be due to the migration of excess vacancies, still retained in the lattice, to the dislocation causing further pinning. This anomalous behaviour is due to the non-equilibrium state of vacancy concentration in the lattice at lower temperature.

#### ACKNOWLEDGMENT

The author is indebted to Prof. B. N. Srivastava, D. Sc., F.N.I., for suggesting the work and for helpful discussions.

#### REFERENCE

- Beshers, D. N., 1959, *J. App. Phys.*, **30**, 252.
- Borelius, G., 1958, *Solid State Physics*, **6**, 90.
- Cashwell, H. L., 1958, *J. App. Phys.*, **29**, 1210.
- Chambers, R. H., 1957, Carnegie Inst Tech. Report AT (30-1), 1193.
- Cottrell, A. H., 1953, Dislocation and plastic flow in crystals (Oxford).
- Granato, A. and Lucke, K., 1956, *J. App. Phys.*, **27**, 583, 789.
- Jamison, R. E. and Blewitt, T. H., 1953, *Phys. Rev.* **91**, 237.
- Levy, M., and Motzger, M., 1955, *Phil. Mag.* **46**, 1021.
- Li, C. H., Washburn, J. and Parker, E. R., 1953, *J. Metals*, **5**, 1223.
- Maddin, R. and Cottrell, A. H., 1955, *Phil. Mag.* **46**, 735.
- Mott, P. N., 1952, Imperfection in nearly perfect crystals (John Wiley, N. Y.) Chapter 6.
- Nisbett, D. H. and Wilks, J., 1960, *Advances in Phys.*, **9**, 1.
- Nowick, A. S., 1953, *Prog. Metal Phys.*, **4**, 1.
- Quader, M. A., 1961, *Ind. J. Phys.*, **35**, 446.
- Roswell, A. E. and Nowick, A. S., 1957, *Acta Meta.*, **5**, 228.
- Weertman, J. and Salkovitz, E. I., 1955, *Acta Meta.*, **3**, 1.
- Wert, C. A., 1949, *J. App. Phys.*, **20**, 29.

# THE EMISSION BAND SPECTRA OF SbF AND BiF

T. A. PRASADA RAO AND P. TIRUVENGANNA RAO

SPECTROSCOPIC LABORATORIES, DEPARTMENT OF PHYSICS, ANDURA  
UNIVERSITY, WAITAIN

(Received November 13, 1961)

## Plate II & II A

**ABSTRACT.** The band spectra of SbF and BiF have been excited in emission in high frequency discharge from a 500 Watt oscillator. A new system of bands of SbF in the ultraviolet region  $\lambda 3140\text{--}\lambda 3340 \text{ \AA}$ , designated as B, was obtained and analysed. The analyses shows that the lower state is common to the lower state of  $\lambda_2$ ,  $\lambda_4$ ,  $C_2$  and  $C_4$  systems, and is suggested as the ground state of the SbF molecule. The ultraviolet system of BiF was photographed under high dispersion and shown to consist of three separate systems  $C_1$ ,  $C_2$ , and  $C_3$ . Of these the  $C_1$  and  $C_3$  systems consist of single headed bands while the  $C_2$  system consists of double heads. Vibrational quantum formulae were derived for all the three systems. It is suggested that the ground state of the BiF molecule is a  $O^+$  state and that the visible band system of BiF arises from a  $O^+ \rightarrow O^+$  transition, from the observed rotational structure of some of the bands photographed in the 2nd order of a 21 ft. concave grating spectrograph. The observed electronic states of SbF and BiF are discussed in relation to those expected from electron configuration.

## INTRODUCTION

The characteristic emission spectrum of SbF was obtained independently by Rochester (1937) and by Howell and Rochester (1939). According to these authors, the spectrum of SbF consists of three systems of bands designated as  $A_1$ ,  $A_2$  and  $A_3$  in the visible region  $\lambda 3400\text{--}\lambda 5200 \text{ \AA}$ . These systems were regarded as belonging to a triplet system with unequal splittings of  $3919 \text{ cm}^{-1}$  to  $2105 \text{ cm}^{-1}$ . It could not be definitely established whether these multiplet splittings belong to the upper or lower state or both. In addition to these three systems, Howell and Rochester reported the analysis of another triplet system (System C) with one component lying in the region  $\lambda 2600\text{--}\lambda 2700 \text{ \AA}$  and the other two in the region  $\lambda 2200\text{--}\lambda 2430 \text{ \AA}$ . The final state was suggested as arising from a  $^3I$  state common to both triplet systems. However, the multiplet separations of the states and the nature of their electronic levels are not definitely known.

In the spectrum of BiF, only one band system (System A) in the visible region was reported and analysed by Howell (1936) in emission in high frequency discharge and by Morgan (1936) in absorption. A weaker system on the violet side was reported by Morgan as occurring in absorption, though no analysis was given. Rochester (1937) reported a weak triplet system (System C') in the ultraviolet ( $\lambda 3250\text{--}\lambda 2250 \text{ \AA}$ ) with approximate values of  $\omega_e' = 620 \text{ cm}^{-1}$ ,  $\omega_e'' = 520 \text{ cm}^{-1}$  based on the measurements on low dispersion plates.

The present investigations on the emission spectra of SbF and BiF were started with the object of gaining more information on the nature and properties of the ground state and excited states of these two molecules. The results of a new study of the emission spectra of these molecules are reported in this paper.

#### EXPERIMENTAL

The spectra of SbF and BiF were excited in a high frequency discharge from a 500 Watt oscillator working at a frequency of 30 to 40 Mc/sec. Specpure samples of SbF<sub>3</sub> and BiF<sub>3</sub> were used in the excitation of these spectra. In obtaining the BiF spectrum, external heating of the substance was found necessary to maintain a characteristic bluish discharge. In the visible region, spectra were photographed using a Hilger three prism glass Littrow spectrograph and in the second order of a 21 ft. concave grating spectrograph (1.25 Å/mm). In the ultraviolet region, spectra were taken using a Hilger medium quartz and a Hilger *E*<sub>1</sub> quartz Littrow spectrographs. In both cases, Agfa Isopan super special employed by us, considerably minimised the times of exposure (2 mm to 30 min.) The band heads were measured against iron arc standard lines taken from MIT tables.

#### RESULTS AND ANALYSIS

##### *The Spectrum of SbF*

The spectrum of SbF excited in high frequency discharge from a 500 Watt oscillator, reveals the existence of the three systems in the visible (λ3400–λ5200 Å) *A*<sub>1</sub>, *A*<sub>2</sub>, *A*<sub>3</sub> reported earlier by Rochester and Howell. In the ultraviolet the *C* system in the region λ2200–λ2700 Å is found to consist of three separate systems *C*<sub>1</sub>, *C*<sub>2</sub>, *C*<sub>3</sub>. In addition to the above systems, a new system of bands, here designated as *B*, is obtained in the ultraviolet region λ3140–λ3340 Å. This system, consisting of bands degraded to shorter wavelengths, is reproduced in Fig. 1(a), Plate II. The analysis of the system is simple and straightforward. The most intense band at ν31142.6 is easily identified as the (0,0) band. On the low frequency side the members of the Δ*v* = -1 and Δ*v* = -2 sequences are easily identified. In the weaker Δ*v* = +1 sequence only the (1,0) band is identified. The data and classifications of the some of the strong heads are given in Table 1. The *P* heads could be represented by the following quantum formula

$$\begin{aligned} \nu = & 31096.8 + 707.1(v' - 1/2) - 770(v' + 1/2)^2 \\ & - 612.7(v'' + 1/2) + 2.03(v'' + 1/2)^2 \end{aligned}$$

The vibrational frequency of the lower state of the system ( $\omega_e'' = 612.7 \text{ cm}^{-1}$ ) agrees closely with the lower state of the *A*<sub>2</sub> and *A*<sub>3</sub> systems (612.6  $\text{cm}^{-1}$ ).

##### *The spectrum of BiF*

In the visible region the spectrum of BiF reveals the existence of only one system (system *A*) in the region λ4200–λ5100 Å reported earlier by Howell (1936)

TABLE I  
A new  $B-X_1$  system of SbF

Wavelength Å	Wavenumber $\text{cm}^{-1}$	Intensity	Assignments ( $v'$ , $v''$ )
3339.71	29934.1	4	0,2
3329.45	30026.4	4	1,3
3274.24	30532.7	8	0,1
3264.49	30623.9	6	1,2
3256.11	30702.7	2	2,3
3210.11	31142.6	10	0,0
3201.37	31227.6	6	1,1
3140.50	31832.9	3	1,0

and Morgan (1936) The ultraviolet bands of BiF degraded to shorter wavelengths, were previously attributed to a triplet system (System  $C$ ) by Rochester (1937) with approximate values of  $\omega'_e = 620 \text{ cm}^{-1}$ ,  $\omega''_e = 520 \text{ cm}^{-1}$ . However, the analysis of this triplet system by Rochester was based on plates taken in the low dispersion of Hilger small quartz spectrograph. We have photographed the ultraviolet bands of BiF in the high dispersion of a Hilger  $E_1$  large quartz Littrow spectrograph. According to our analysis based on high dispersion plates, the ultraviolet bands of BiF could be classified as belonging to three separate systems designated as  $C_1$ ,  $C_2$ ,  $C_3$ . The bands of the  $C_1$  system in the region  $\lambda 3045-\lambda 3270 \text{ Å}$  appear single headed and are reproduced in Fig. 1(b), Plate II. The analysis of the system is greatly facilitated by the identification of the strong band at  $\nu 32178.7$  as (0,0). The data and classifications of the  $P$  heads are given in Table 2. The  $P$  heads could be represented by the following quantum formula.

$$\nu = 32139.0 + 614.4(v' + 1/2) - 2.24(v' + 1/2)^2 - 535.0(v'' + 1/2) + 2.20(v'' + 1/2)^2$$

The lower state vibrational frequency  $\omega_r'' = 535.0 \text{ cm}^{-1}$  of this system differs considerably from that of the ground state of the visible system of BiF obtained by Morgan in absorption and by Howell in emission.

The ultraviolet bands of BiF in the region  $\lambda 2660-\lambda 2700 \text{ Å}$  are reproduced in the Fig. 1(c), Plate II. Some of the strong bands appear double headed consisting of  $P$  and  $Q$  heads. The (0, 0), (0, 1), and (0, 2) and (1, 0) bands are easily identified. In the weak (1, 0) band only the  $Q$  head is identified. The data and classifications of the band heads are given in Table 2. The  $Q$  heads could be represented by the following quantum formula.

$$\nu = 36943.4 + 611.8(v' + 1/2) - 542.7(v'' + 1/2) + 2.48(v'' + 1/2)^2$$

TABLE II  
The ultraviolet systems of BiF

Wavelength Å	Wavenumber cm <sup>-1</sup>	Intensity	Assignment (v', v'')
The G <sub>1</sub> —X <sub>2</sub> System			
3267.54	30595.3	2	0,3
3257.49	30689.7	1	1,4
3212.41	31120.2	5	0,2
3203.48	31207.1	3	1,3
3194.42	31295.6	1	2,4
3158.93	31647.2	8	0,1
3150.69	31729.9	6	1,2
3106.75	32178.7	10	0,0
3099.17	32257.4	5	1,1
3049.10	32787.1	3	1,0
3042.09	32862.6	1	2,1
The G <sub>2</sub> —X <sub>3</sub> System			
2827.07	35361.9	1	0,3 P
2825.67	35379.4	3	0,3 Q
2818.64	35467.7	2	1,4 Q
2785.47	35890.0	3	0,2 P
2784.08	35907.9	5	0,2 Q
2777.69	35990.5	4	1,3 Q
2744.76	36422.3	6	0,1 P
2743.39	36440.8	8	0,1 Q
2737.41	36519.9	7	1,2 Q
2704.87	36959.4	8	0,0 P
2703.47	36978.5	10	0,0 Q
2698.05	37052.8	5	1,1 Q
2659.46	37590.5	7	1,0 Q

TABLE II—*contd*

Wavelength Å	Wavenumber cm <sup>-1</sup>	Intensity	Assignment (v', v'')
The C <sub>3</sub> -X <sub>1</sub> System			
2393.06	41775	2	0,5
2385.00	41900	1	1,6
2365.32	42265	4	0,4
2358.69	42383	2	1,5
2337.89	42760	7	0,3
2331.56	42876	5	1,4
2310.92	43260	10	0,2
2304.85	43372	5	1,3
2284.39	43762	8	0,1
2258.19	44269	6	0,0

The ultraviolet bands of BiF in the region  $\lambda 2250$ — $\lambda 2400$  Å shown in the Fig. 1(d), Plate II are assigned to a separate system designated as C<sub>3</sub>. The analysis of this system was easily carried out by the identification of a long  $v''(v' = 0)$  progression. The  $\Delta G''(v)$  intervals of this system agree well with the corresponding  $\Delta G''(v)$  intervals of the ground state of the visible system A. Thus, the lower state is identified as the ground state of the BiF molecule. The data and the classifications of the *P* heads are given in Table 2. The following quantum formula represents the *P* heads.

$$v = 44217 + 612.9(v' + 1/2) - 510.8(v'' + 1/2) + 3.80(v'' + 1/2)^2$$

#### ELECTRONIC STATES AND ELECTRON CONFIGURATIONS OF SbF AND BiF

##### *SbF.*

On the basis of the vibrational analyses of the various band systems of SbF known so far we can identify two low-lying states  $X_1$  and  $X_2$  with vibrational frequencies of  $612.6$  cm<sup>-1</sup> and  $616.9$  cm<sup>-1</sup> respectively. The separation of these two levels is however not experimentally known. Fig. 3 gives the scheme of transitions responsible for the various band systems in SbF. The vibrational frequencies of the various excited states  $A_1, A_2, A_3$  etc. are given on the right hand side. The lower state common to  $A_2, A_3, B, C_2$  and  $C_3$  systems is identified as the ground state ( $X_1$ ) of the SbF molecule. As the separation between  $X_1$  and  $X_2$  is not exactly known, the heights of  $A_1$  and  $C_1$  levels above  $X_1$  are not known. Hence the  $X_2, A_1$  and  $C_1$  levels are represented by broken lines.

The molecule  $\text{SbF}$  is isoelectronic with  $\text{TeO}$ . It was suggested earlier by Haranath, Rao and Sivaramamurty (1959) that the ground state of  $\text{TeO}$  is a  $^3\Sigma^-$  state arising from the configuration

$$\dots(x\sigma)^2(w\pi)^4(v\pi)^2-^1\Sigma^+, ^1\Delta, ^3\Sigma^- \quad \dots (1)$$

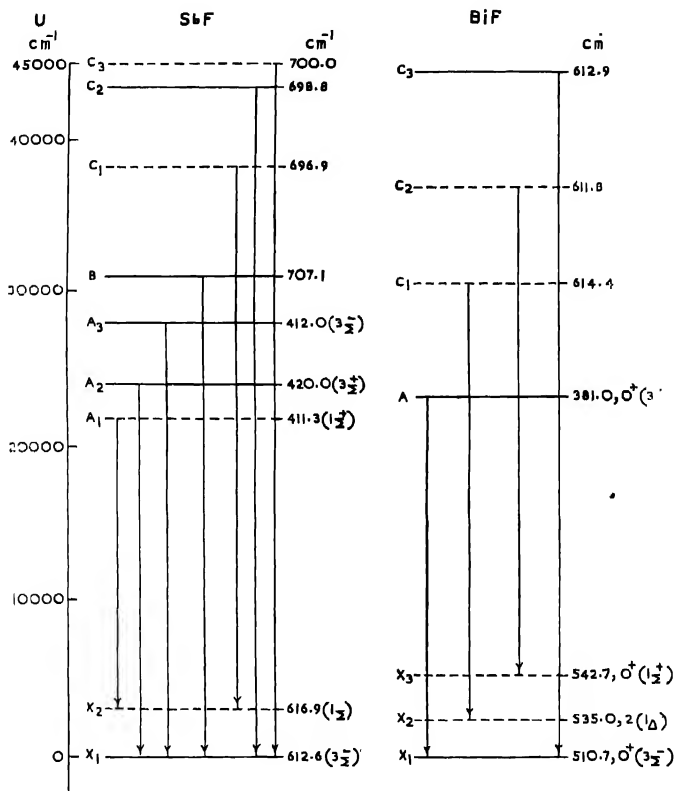


Fig. 3. Energy levels of  $\text{SbF}$  and  $\text{BiF}$ .

By analogy with  $\text{TeO}$  the ground state  $X_1$  of  $\text{SbF}$  may be identified as a  $^3\Sigma^-$  state arising from configuration (1). The state  $X_2$  may be tentatively identified as a  $^1\Sigma$  state arising from the same configuration. As in  $\text{TeO}$ , the first excited electron configuration in  $\text{SbF}$  may be written as

$$\dots(x\sigma)^2(w\pi)^3(v\pi)^2-^1\Sigma^+, ^1\Sigma, ^1\Delta, ^3\Sigma^+, ^3\Sigma^-, ^3\Delta_1 \quad \dots (2)$$



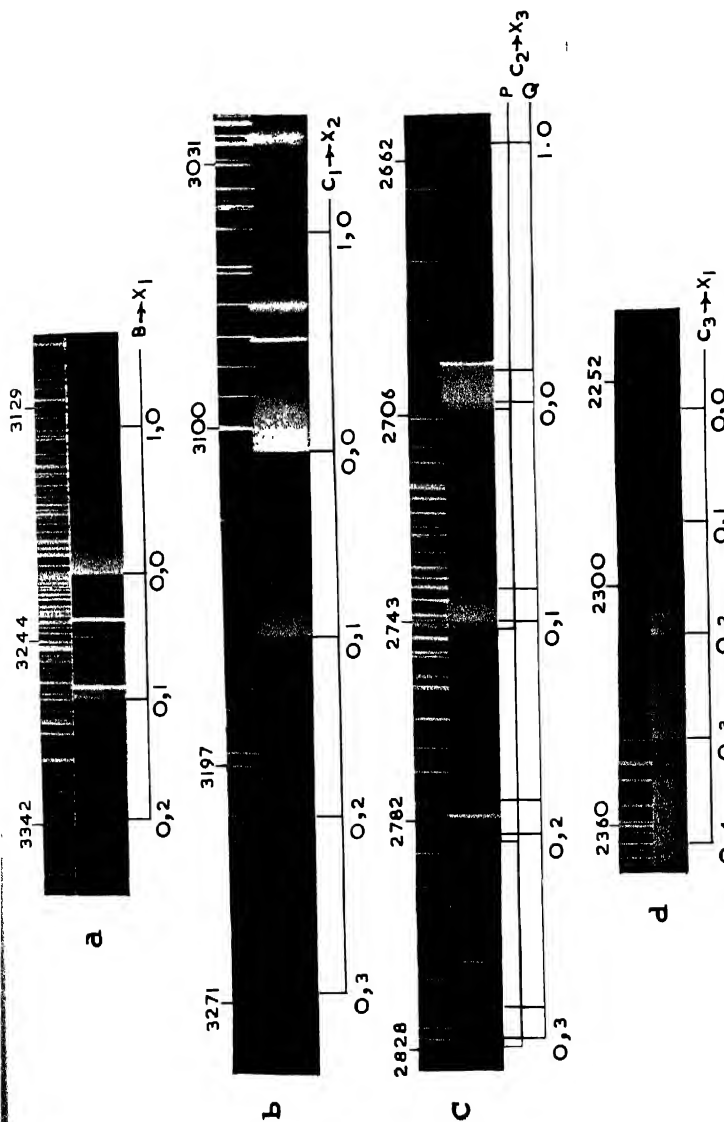


Fig. 1 (a) A new  $B - X_1$  system of SbF medium quartz spectrogram.

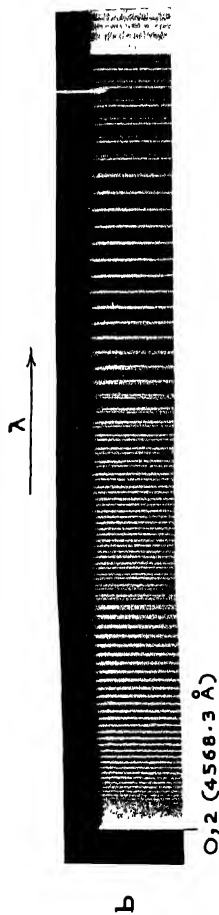
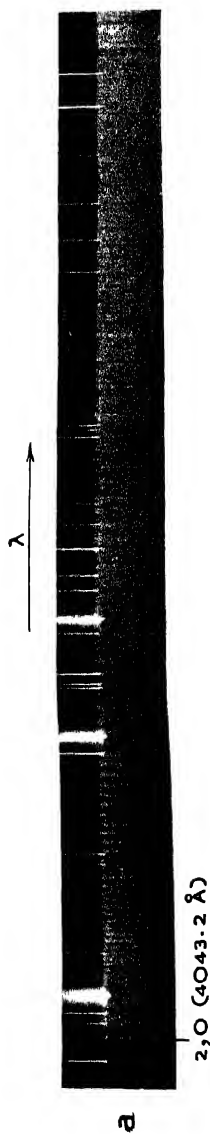


Fig. 2  
Fig. 2 (a) The (2,0) band of  $A_2 - X_1$  system of  $SbF_5$  a 21 ft concave grating spectrogram  
Fig. 2 (b) The (0,2) band of  $A - X_1$  system of  $BiF_3$  21 ft concave grating spectrogram

The levels  $A_1$ ,  $A_2$  and  $A_3$  with vibrational frequencies of  $411.3\text{ cm}^{-1}$ ,  $420.0\text{ cm}^{-1}$  and  $4120\text{ cm}^{-1}$  may all be attributed to this configuration. The reduction in the vibrational frequency of each of these states relative to the ground state  $X_1$  is in harmony with the fact that in this configuration an electron goes from a bonding  $w\pi$  orbital to the corresponding antibonding  $v\pi$  orbital. By analogy with TeO and  $\text{O}_2$ , the  $A_2$  and  $A_3$  levels may be identified with  $^3\Sigma^+$  and  $^3\Sigma^-$  states respectively. The  $A_2-X_1$  system arising from  $^3\Sigma^+-^3\Sigma^-$  is the analogue of the  $A-X$  systems of  $\text{O}_2$  and TeO arising from the forbidden transition  $^3\Sigma^+-^3\Sigma^-$ . The  $A_1$  level may be correlated with the  $^1\Sigma^+$  state belonging to the same configuration.

In Fig. 2(a), Plate II A is shown the rotational structure of the (2, 0) band of the  $A_2-X_1$  system of SbF photographed in the second order of a 21 ft. concave grating spectrograph. Some of the high rotational lines are seen to be split up into three close components due to spin splitting. This confirms the view that the  $A_2-X_1$  system arises really from two  $^3\Sigma$  states. All the excited states  $B$ ,  $C_1$ ,  $C_2$  and  $C_3$  show an increase in the vibrational frequency relative to the ground state. They can be attributed to the configurations of the type

$$\dots(x\sigma)^2(w\pi)^4(v\pi) \begin{cases} n\sigma-^1\Pi, ^3\Pi_r \\ n\rho\sigma-^1\Pi, ^3\Pi_r \end{cases} \quad (3)$$

in which an electron goes from a antibonding  $v\pi$  orbital to a non-bonding  $n\sigma$  or  $n\rho\sigma$  orbital of the Rydberg type resulting in an increase in the vibrational frequency of these states relative to the ground state as observed.

### BiF

Fig. 3 also gives the observed electronic states and the scheme of transitions in BiF. The level  $X_1$  is identified as the ground state of the BiF molecule as the system  $A-X_1$  was obtained by Morgan (1936) in absorption. The levels  $X_1$ ,  $X_2$ ,  $X_3$  may be attributed to  $^3\Sigma^-$ ,  $^1\Delta$ ,  $^1\Sigma^+$  states of the ground state configuration

$$\dots(x\sigma)^2(w\pi)^4(v\pi)^2-^3\Sigma^-, ^1\Delta, ^1\Sigma^+ \quad (4)$$

The  $A-X_1$  system in BiF is thus attributed to  $^3\Sigma^--^3\Sigma^-$ . Since large multiplet splittings are known in the ground and low excited states of the neutral Bi atom, we may expect, as in BiH, a transition from Hund's case *b* to Hund's case *c*. System  $A-X_1$  may then arise from  $0^+(^3\Sigma^-)-0^+(^3\Sigma^-)$  in Hund's case *c*. The rotational structure of the (0, 2) band of the  $A-X_1$  system reproduced in Fig. 2(b), Plate II A actually reveals the existence of only two branches *R* and *P* which do not show any sign of doubling even at high *J* values. Thus the  $A-X_1$  visible band system of BiF appears to arise from a  $0^+-0^+$  case *c* transition which gives rise to a structure similar to a  $^1\Sigma--^1\Sigma$  transition. A detailed rotational analysis of the (1, 0), (0, 0), (0, 1), (0, 2) and (0, 3) bands of this system is now in progress.

The  $C_1$  and  $C_3$  systems consisting of single headed bands may arise from transitions in which  $\Delta\Omega = 0$  in  $H_{\text{ul}}$  case c. The  $C_2$  system consisting of double headed bands arises from a case C transition in which  $\Delta\Omega = \pm 1$ . The complexity of levels  $C_1$ ,  $C_2$  and  $C_3$  are the case C equivalent states of configurations of the type 3.

#### ACKNOWLEDGMENTS

The authors wish to express their thanks to Prof. K. R. Rao for his kind interest in this work. One of the authors (T. A. P. Rao) is grateful to the U.S.I.R. (Delhi) on the award of a Research Fellowship.

#### REFERENCES

- Haranath, P. B. V., Rao, P. T., and Sivaramamurthy, 1959, *Zeit. F. Phys.*, **155**, 507.  
 Howell, H. G., 1936 *Proc. Roy. Soc. London*, **155**, 141.  
 Howell, H. G., and Rochester, G. D., 1939, *Proc. Phys. Soc. London*, **51**, 329.  
 Morgan, F., 1936, *Phys. Rev.*, **49**, 41.  
 Rochester, G. D., 1937, *Phys. Rev.*, **51**, 186.

# A TRIPLE COINCIDENCE PROTON SCINTILLATION SPECTROMETER

R. K. MOHINDRA AND H. S. HANS

DEPARTMENT OF PHYSICS, MUSLIM UNIVERSITY, ALIGARH

(Received June 6, 1961)

**ABSTRACT.** An apparatus is described for studying the energy and angular distribution of protons in  $(n, p)$  reactions produced by 14.8 MeV neutrons. Various coincidence, anticoincidence, and blocking circuits used for defining the particles are described. The background of the spectrometer is very low. The whole instrument has been tested thoroughly with 5.3 MeV alphas from  $\text{Po}^{210}$  and 14.8 MeV recoil protons from a thin polythene radiator. The energy spectrum of protons from aluminum along with the background is also given.

## INTRODUCTION

The direct detection of the products of nuclear reactions by fast neutrons is quite complicated because of the large background. It becomes still more difficult if one has to distinguish between alphas, deuterons and protons emitted from the same reaction. Generally, for such purposes, several detectors are connected in coincidence and anticoincidence to select particles of the required type and energy.

A proton spectrometer has been designed to measure the energy and angular distribution of protons from  $(n, p)$  reactions using 14.8 MeV neutrons as the incident particles (Khurana and Hans, 1958). The spectrometer is similar to the one used by various authors (Colli and Facchini, 1956; Eubank, Peck and Hassler, 1958; Marcazzan, Sona and Pignanelli, 1958) for a similar purpose. The various details of the spectrometer along with its performance are given below.

## DESCRIPTION OF THE SPECTROMETER

The outlines of the Spectrometer are shown in Fig. 1. Essentially it consists of two proportional counters  $C_2$  and  $C_3$  in coincidence with CSI (Tl) scintillation counter. The target under study is kept in front of the proportional counter  $C_2$ . Another proportional counter  $C_1$  is used as an anticoincidence counter to stop any charged particles produced from the top from being counted. Counters  $C_1$ ,  $C_2$  and  $C_3$  only define the particles while CSI(Tl) scintillation counter measures the spectrum of protons from the target T.

### *Proportional Counter Telescope :*

The aim of the proportional counter telescope is to discriminate the protons

from the target and those produced from the walls. The proportional counter telescope along with the photomultiplier is shown in Fig. 1(a). It consists of a common brass chamber which forms the cathodes of the three counters and is filled with a mixture of Argon and  $\text{CO}_2$  at 10 cm. Hg pressure in the ratio 9.1. The walls and the top of the chamber are lined with about 0.013" thick pure gold

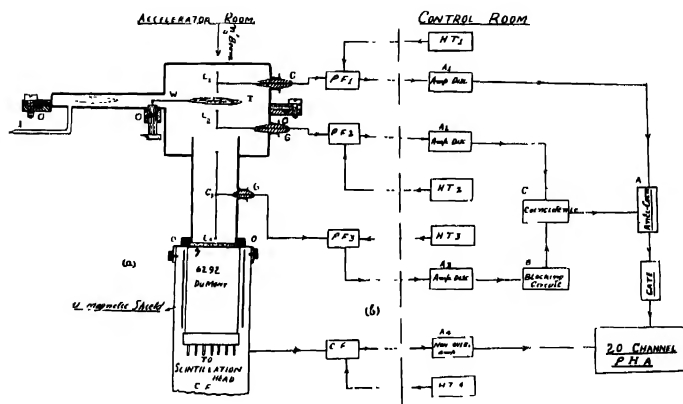


Fig. 1. The block diagram of the spectrometer.

- 1 (a) Proportional counter telescope along with photomultiplier assembly.  
 $C_1$  Anticoincidence counter.  
 $C_2, C_3$  coincidence counters,  $C_4$ —CSI (T1) crystal  
 $O$ —O-ring seals;  $G$ —glass to metal seals,  
 $W$ —wheel for the targets;  $g$ —Dow Corning 200 Silicone grease  
 $T$ —target under study;  $I$ —gas input
- 1 (b) Block-diagram of electronic circuitry

to reduce the background. The counters  $C_1$  and  $C_2$  are of the same dimensions, with their anodes 1.5 cm long made of 6 mil tungsten wire, while the diameter of the cathode is 7 cms. The counter  $C_1$  is an anticoincidence counter to check the protons produced from the top of the chamber, while the counters  $C_2$  and  $C_3$  are put in coincidence. The cathode of  $C_3$  is 6 cm long and 3 cm in diameter, while the anode is 5 cm long made of 6 mil tungsten wire. The central wires in the three proportional counters are fixed to the central tungsten rods of the glass to metal seals, which are in turn soldered to the walls of the chamber. Glass beads are fixed to the two ends of the central wires to avoid sparking.

The wheel  $W$  carries four targets and can be rotated from outside the chamber without disturbing the vacuum. Thus, one can place any one of the four targets between counters  $C_1$  and  $C_2$  for study. The targets are fixed on the thin tungsten

wire loops. One loop is left free to take the background spectrum. The chamber is made vacuum tight from the crystal end by using an O-ring as shown in the diagram. A thin layer of pure Al ( $\sim 0.05$  mg/cm<sup>2</sup>) is deposited on CSI(Tl) crystal by the evaporation process (Strong John). This screens the crystal from the photons produced by Townsend avalanches inside the counters and it also improves the light collection efficiency. A 6292 DuMont photomultiplier is coupled to the crystal in a usual manner using Dow Corning 200 grease. The photomultiplier along with the cathode follower is made mechanically rigid with the proportional counter assembly. This whole system is pivoted on a calibrated scale with the axis of rotation passing through the target.

The working of the three proportional counters was tested with 5.3 Mev alphas from Po<sup>210</sup>.

#### ELECTRONIC CIRCUITRY

The block diagram of the electronic circuitry used is shown in Fig. 1b. Essentially the circuitry consists of an arrangement by which the spectrum of pulses from the scintillation counter  $C_4$  in coincidence with pulses from  $C_2$  and  $C_3$  and in anticoincidence with pulses from  $C_1$ , is displayed on a twenty channel pulse height analyser. The pulses from the proportional counters  $C_2$  and  $C_3$  are amplified by preamplifiers  $PF_2$  and  $PF_3$  (Baird Atomic model 219) and linear amplifier discriminator units  $A_2$  and  $A_3$  (Bell and Jordon, 1947). The discriminator output of  $A_2$  is fed directly to one input of slow coincidence circuit C ( $\tau \approx 1 \mu$  sec.), while the discriminator output of  $A_3$  is fed to second input through the blocking circuit B. The output of this coincidence unit is put in anticoincidence with the pulses from  $C_1$  so that only those coincidence pulses from C, which are not cancelled by pulses from  $C_1$ , are able to pass the anticoincidence unit A. These pulses in turn trigger a gate pulse of  $\sim 2 \mu$  sec. duration, which acts as one of the coincidence pulses in the 20 channel pulse height analyser, the other pulse being provided by the scintillation counter  $C_4$ , whose pulse height spectrum is to be studied. The pulses from scintillation counter  $C_4$  are fed to 20 channel P.H. A. through a cathode follower followed by a Non-overloading Linear Amplifier (Baird-Atomic model 215). The overall resolution of the coincidence circuit in 20 channel P.H.A (Eldorado Electronics) is about  $6 \mu$  sec, though, for each channel, resolution is  $250 \mu$  sec, being limited by the slowness of the scaling units.

The properties and general description of the coincidence, anticoincidence and blocking circuits are given below.

##### 1. Coincidence Unit .

In this unit, the two input pulses are first shaped by the cathode coupled univibrators (using 6J6 tubes). The output of these univibrators, which are of the order of  $0.5 \mu$  sec duration and 6 volts amplitude are fed to the two inputs

## 2. Anticoincidence Unit :

The image contains two hand-drawn circuit diagrams for electronic projects, likely power supplies or signal processors, using vacuum tubes.

**Top Circuit:**

- 6AR5 265 V:** A power tube stage with a 35K resistor on the grid, a 75M resistor on the screen grid, and a 2.00M resistor on the cathode. The input is labeled  $V_{in}$  and the output is labeled  $V_{out}$ .
- 3N34:** A diode tube stage with a 150R resistor on the grid, a 150R resistor on the screen grid, and a 25K resistor on the cathode. The input is labeled  $V_{in}$  and the output is labeled  $V_{out}$ .
- 6J6 150 V:** A pentode stage with a 10K resistor on the grid, a 150R resistor on the screen grid, and a 25K resistor on the cathode. The input is labeled  $V_{in}$  and the output is labeled  $V_{out}$ .
- 6J5N7 150V:** A pentode stage with a 150R resistor on the grid, a 150R resistor on the screen grid, and a 25K resistor on the cathode. The input is labeled  $V_{in}$  and the output is labeled  $V_{out}$ .

**Bottom Circuit:**

- 6AR5 265 V:** A power tube stage with a 35K resistor on the grid, a 75M resistor on the screen grid, and a 2.00M resistor on the cathode. The input is labeled  $V_{in}$  and the output is labeled  $V_{out}$ .
- 6J6 150 V:** A pentode stage with a 10K resistor on the grid, a 150R resistor on the screen grid, and a 25K resistor on the cathode. The input is labeled  $V_{in}$  and the output is labeled  $V_{out}$ .
- 6J5N7 150V:** A pentode stage with a 150R resistor on the grid, a 150R resistor on the screen grid, and a 25K resistor on the cathode. The input is labeled  $V_{in}$  and the output is labeled  $V_{out}$ .

Fig 2. Anticoincidence circuit

### 3. Blocking Circuit :

It essentially consists of two schmitt type discriminators (Elmore and Sands) and an anticoincidence circuit. The pulses from the amplifier are fed to the two discriminators, one with a lower bias and the other with a higher bias. The output of these discriminators is fed to the anticoincidence circuit as shown in Fig. 3. The anticoincidence unit passes the pulses from low bias discriminator only if the



## A Triple Coincidence Proton Scintillation Spectrometer 97

pulses from the other discriminator are not present. The anticoincidence circuit is the same as described above.

### P E R F O R M A N C E

The spectrometer has been tested with 5.3 MeV alphas from  $\text{Po}^{210}$  and 14.8 MeV recoil protons obtained by bombarding a polythene target with neutrons. For alphas, a peak was obtained in the spectrum of pulses from CSI(T1) counter  $C_4$  in coincidence with pulses from  $C_2$  and  $C_3$ . Similarly, when a thin polythene

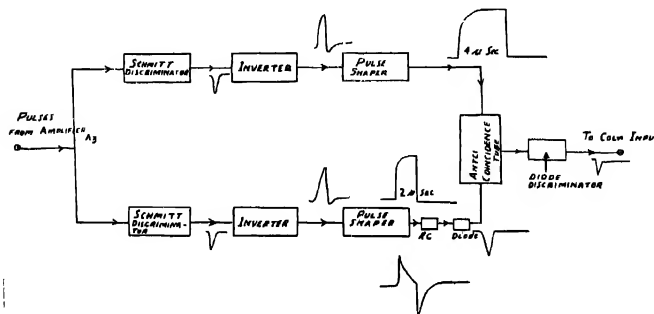


Fig. 3. Block diagram of the blocking circuit

target (13.8 mg/cm<sup>2</sup>) of 1.5 cm diameter was bombarded with 14.8 MeV neutrons, a sharp peak was obtained in the spectrum of pulses from CSI(T1) counter in

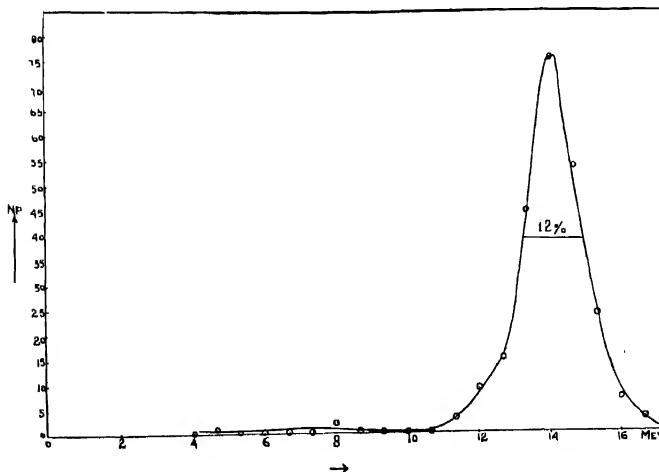
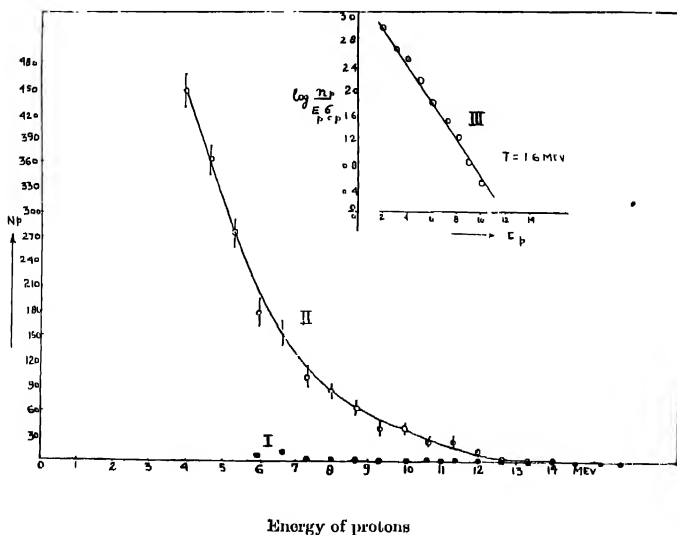


Fig. 4. Energy spectrum of recoil protons from polythene target (13.8 mg/cm<sup>2</sup> and 1.5 cm diameter, distance 10 cm from neutron source) after subtracting the background.

coincidence, with the pulses from  $C_2$  and  $C_3$ , and in anticoincidence with pulses from  $C_1$ . The appropriate biases were used for accepting the pulses from these three proportional counters. The peak obtained under these working conditions is shown in Fig. 4. The distance between the polythene target and neutron source was kept about 10 cms. The resolution of the peak under these conditions is 12%. The protons under this peak are sufficiently mono-energetic for the calibration of the entire energy scale, as CSJ(T1) crystal exhibits linear response up to 18 MeV proton energy (Bashkin, Carlson, Douglas and Jacobs, 1958).

The selection of the biases for the pulses from proportional counters  $C_2$  and  $C_3$  was made carefully so that no pulses were lost because of the high bias. In this connection one should note that the pulse heights due to 14.8 MeV protons in the proportional counters will be the smallest, and the biases allowing these pulses to be registered, are good enough for other lower energy protons. First of all, quite low biases were selected in an ad hoc manner for the two counters so that the



g. 5. Curve I. Background spectrum

II. The energy spectrum of Al target (18.4 mg/cm<sup>2</sup>, 3 cm diameter, distance 10 cm from neutron source) after subtracting background.

III. Curve II is plot of  $\log \frac{N_p}{E_p^2 \sigma_p}$  in the case of Al versus energy. The slope of the experimental points corresponds to a nuclear "temperature" of  $T = 1.6$  MeV, for the residual nucleus  $Mg^{27}$ .

main noise pulses were checked; and the peak in pulses from CSI(T1) was obtained. This was repeated at half the previous gain of the amplifiers of the two counters and  $C_3$ . The shape and the area under the peak remained same for this low gain, showing that in the previous case, biases were well below the required value. However, when the peak was redrawn at 1/4 of the original value of the gain, the area under the peak became less. The experiment was done at the highest gain of the amplifiers.

In the blocking circuit B used for pulses from  $C_3$ , lower bias was selected as discussed above, while the higher bias was adjusted in a manner discussed at the end. The background spectrum, using only a ring of tungsten wire without anything mounted on that, is shown by curve I, Fig. 5. It may be mentioned that before using gold lining, the back-ground was about five times the present back-ground. The contribution of chance coincidences to the background above 4 MeV spectrum is negligible.

Also, a spectrum was obtained by using thin aluminium ( $18.4 \text{ mg/cm}^2$ ) of 3 cm diameter as the target. The spectrum of pulses is shown by curve II, Fig. 5. The nuclear temperature obtained for this case is 1.6 MeV from curve III, Fig. 5, which is in agreement with others. (Storey *et al.*, 1960).

#### CONTRIBUTION OF DEUTERONS AND ALPHAS

A detailed analysis was made of the response curves of protons, deuterons and alphas in CSI(T1) crystal (Bashkin, Carlson, Douglas and Jacobs, 1958) and the behaviour of atomic stopping cross-sections for these particles in argon as a function of energy (Whaling Ward, 1958). This analysis along with our calibration of CSI(T1) crystal and  $C_3$  counter with 5.3 MeV alphas from  $\text{Po}^{210}$ , could be used for determining the values of the higher biases in the blocking circuit for checking the pulses of various energy deuterons and alphas. It was found from such an analysis that a suitable higher bias can be found to block the alphas completely in the range of 0-14 MeV. This bias will also block protons below a certain low energy and will let in deuterons above a certain energy ( $\sim 8 \text{ MeV}$ ). By adjusting the value of this bias, the lower limit of the admissible proton spectrum as well as the deuteron contamination may be changed. The spectrum taken with various higher biases may even allow us to estimate the amount of the deuteron contamination in the proton spectrum and may help us in obtaining the pure proton spectrum.

#### ACKNOWLEDGMENTS

The authors wish to express their sincere gratefulness to Prof. P. S. Gill for his kind interest and continuous encouragement. The cooperation of Mr. Ajit Singh, glass blower, in developing the proportional counter system is acknowledged with thanks.

## REFERENCES

- Bell and Jordon, 1947, *Rev. Sci. Instrs.* **18**, 703.  
Bashkin, Carlson, Douglas and Jacobs, 1958, *Phys. Rev.* **109**, 434.  
Colli, L. and Facchini, U., 1956, *Nuovo Cimento*, **4**, 671.  
Elmore and Sands, *Electronics Experimental Techniques*, Mc-Graw Hill Book Co., 1949  
Eubank, Peck and Hussler; 1958, *Nucl. Phys.*, **9**, 273.  
Fischer and Marshall, 1952, *Rev. Sci. Instrs.*, **23**, 417  
Khutuna, C. S. and Haus, H. S., 1958, *Ind. J. Phys.*, **32**, 468  
Mazzazan, G. Sona, A. and Pignacelli, M., 1958, *Nuovo Cimento*, **10**, 155  
Storey, Ward and Jack 1960, *Proc. Phys. Soc.*, **75**, 526.  
Stuon John. *Modern Laboratory Practice*, Blackie and Sons Ltd, London, Chap IV.  
Whaling Ward, 1958, *Handbuch Der Physik*, Vol XXXIV, P 193.

# ON THE VALIDITY OF THE REVISED ROTATIONAL CONSTANTS OF $\alpha(C \rightarrow X)$ BAND SYSTEM OF $ZrO$

N. SREEDHARA MURTHY\*

DEPARTMENT OF PHYSICS, KARNATAK UNIVERSITY, DHARWAR

(Received December 2, 1961)

**ABSTRACT** Confirmatory test has been made on the validity of the rotational constants of  $\alpha(C \rightarrow X)$  system of  $ZrO$  given by Lagerqvist, Uhler and Barrow, from the theory involving the intensity aspects. The untenability of the old constants of Lowater has been shown.

## INTRODUCTION

Although good amount of work has been stimulated on the band spectrum of  $ZrO$ , on account of its astrophysical status (Babeock, 1934, Bobrovnikoff, 1939, Davis, 1947), all evidence has not been brought to bear on the preference for one or the other of the two sets of values available for the internuclear distances ( $r_e$ ) for the  $C$  and  $X$  states of the molecule. The following values are cited from the earlier literature.

Lowater's data (1935) as given by Herzberg (1950).

$$r_e' = 1.526 \text{ \AA} \quad r_e'' = 1.416 \text{ \AA} \quad \Delta r_e = r_e' - r_e'' = 0.110 \text{ \AA}$$

Tanaka and Horie (1941) have confirmed the above  $r_e''$  value from their own rotational analysis of the  $\gamma(A \rightarrow X)$  system of  $ZrO$ . Herzberg (1950) had, however, expressed doubt about the accuracy of these rotational constants on the ground that one should not expect such low values of  $r_e$  for a heavier molecule like  $ZrO$ . These values are even smaller than the well-established values of  $TiO$ , the preceding molecule in the group, by  $0.2 \text{ \AA}$ . Working on this clue, Lagerqvist, Uhler and Barrow (1954) undertook fresh analysis of the band system and found the values as follows.

$$r_e' = 1.775 \text{ \AA}, r_e'' = 1.728 \text{ \AA} : \Delta r_e = 0.047 \text{ \AA}$$

While justifying these values they state that the ground state value  $r_e''$  obtained by them fits well with that for  $TiO$ , whereas Lowater's value is incompatible with it. They mention that Lowater may have picked out the branches wrongly and express doubts about the correctness of the analysis. With the new values

\* On leave of absence from the Central College, Bangalore.

of  $r_e''$  by Lagerqvist *et al.*, the comparative situation between TiO and ZrO is more in accord with the expected picture as seen from the numerical figures given below.

ZrO	$r_e'' = 1.416 \text{ \AA}$	(Lowater)
	$r_e'' = 1.728 \text{ \AA}$	(Lagerqvist <i>et al.</i> )
TiO	$r_e'' = 1.620 \text{ \AA}$	(Christy, 1929)

Lagerqvist *et al.* have analysed only the (0, 0) band and they have not derived the experimental value of  $\Delta r_e$ . They have estimated it from the expression of Pekeris (1934), and hence their  $B_e$  and  $r_e$  values are not based on experimental data, but are merely approximate figures. In view of this position, a further confirmatory test was thought desirable. It has been undertaken here from the intensity aspects on the lines given by Tawde and Sreedhara Murthy (1957) and Sreedhara Murthy (1961).

#### PROCEDURE

The mathematical technique of Manneback (1951) has been followed for the evaluation of  $\Delta r_e$  with the use of intensity values of the bands. In the nomenclature of Manneback, we have

$$\frac{I(01)}{I(00)} = b = M \left[ \frac{2\omega_e'}{\omega_e' + \omega_e''} \right]^{\frac{1}{2}} \quad \dots (1)$$

where  $M = 0.172205 \mu^{\frac{1}{2}} (r_e' - r_e'') \left[ \frac{\omega_e' \omega_e''}{\omega_e' + \omega_e''} \right]^{\frac{1}{2}}$  and  $\omega_e$  is the vibrational frequency.  $I$  corresponds to the overlap integral and  $I^2$  represents the Franck-Condon factor which is related to the intensity,  $I$  of the band by the relation

$$I/v^4 = K N_v' v^2$$

where  $K$  is a constant,  $N_v'$  is the number of molecules in the upper vibrational level and  $v$  is the wave number of the band head. Hence the expression (1) becomes

$$\left( \frac{I_{01}}{I_{00}} \cdot \frac{v_{00}^4}{v_{01}^4} \right)^{\frac{1}{2}} = 0.172205 \mu^{\frac{1}{2}} (r_e' - r_e'') \left( \frac{\omega_e'}{\omega_e' + \omega_e''} \right) (2\omega_e'')^{\frac{1}{2}} \quad \dots (2)$$

The expression (2) has been used for the computation of  $\Delta r_e$ . The values of  $\mu$  and the vibrational frequencies are taken from Herzberg's treatise (1950) (see also Afaf, 1950). As it is a triplet band system, the estimated intensities of each component are considered for the evaluation of  $\Delta r_e$  from the above expressions. These intensities of the  $R_1$  and  $R_2$  components and  $v$  values are taken from the work of Lowater (1932). They are reproduced below :

	$R_1$	$R_2$
(0, 0)	20	18
(0, 1)	6	5

As the bands considered are (0, 0) and (0, 1) i.e., in the region  $v = 0$  and 1 for which the potential energy curves in the case of both anharmonic and harmonic oscillator may be said almost to coalesce, the increased labour involved in the computation of  $\Delta r_e$  by the application of anharmonic wave function is not called for. Manneback's technique involving the simple harmonic wave function is considered adequate.

#### RESULTS AND DISCUSSION

The computed values of  $\Delta r_e$  are recorded below :

	$\Delta r_e$ in Å	Average $\Delta r_e$ in Å
(0, 1), (0, 0) $R_1$	0.046 <sub>a</sub>	0.046
„ $R_2$	0.044 <sub>b</sub>	

The use of the third component  $R_3$  has not been made as it leads to a somewhat higher value ( $\Delta r_e = 0.060$  Å) probably due to doubtful intensity estimate.

The average value for  $\Delta r_e$  works out to be 0.046 Å which surprisingly comes out almost identical with the value given by Lagerqvist *et al* (0.047 Å). Thus the independent considerations of intensity aspects favour the revised rotational analysis of Lagerqvist *et al*, and bring out the untenability of the earlier data of Lowater (0.110 Å). The present study in conjunction with the work of Tawde and Sreedhara Murthy (1957), and Sreedhara Murthy (1961)\* confirms the efficacy of the method of evaluating  $\Delta r_e$  from intensity aspects. Thus one can rely on reasonably well-estimated intensities to evaluate  $\Delta r_e$  especially in such cases where it is difficult to resolve the spectrum well for structure analysis. The procedure outlined furnishes also a means to check the  $\Delta r_e$  value in the case of doubtful rotational analysis.

\**Note added in proof* : In this investigation  $\Delta r_e$  of LaO ( $B \rightarrow X$ ) system was estimated from intensity aspect to be  $\sim 0.038$  Å. Dr. Lars Åkerlind of the University of Stockholm has informed us in the meantime in a private communication that the rotational analysis of (0,0) band of LaO system is now finished and that  $\Delta r_e$  seems to be 0.030 Å and that  $\Delta r_e$  does not differ very much from this value. According to Dr. Åkerlind's information, the preliminary constants are expected to appear in 'Naturwissenschaften' soon.

#### ACKNOWLEDGMENT

I am deeply grateful to Professor N.R. Tawde, Head of the Department of Physics, Karnatak University for the encouragement and for the help rendered in the preparation of the manuscript of this paper. I am thankful to the National Institute of Sciences of India for the award of a Post-doctoral Senior Research Fellowship.

## R E F E R E N C E S

- Afai, M., *Proc. Phys. Soc.*, 1950, **63**, 1156.  
Babcock, H. D., 1945, *Astrophys. J.*, **102**, 154.  
Bobrovnikoff, N. T., 1939, *Astrophys. J.*, **89**, 301.  
Christy, A., 1929, *Phys. Rev.*, **33**, 701.  
Davis, D. N., 1947, *Astrophys. J.*, **106**, 28.  
Horzberg, G., 1950, *Molecular Spectra and Molecular Structure I*, 2nd Edn (New York Van Nostrand)  
Lagerqvist, A., Uhler, U. and Burrow, R. F., 1954, *Ark. f. Fys.*, **8**, 281.  
Lowater, F., 1932, *Proc. Phys. Soc.*, **44**, 51.  
Mameback, C., 1951, *Physica*, **17**, 1001.  
Pekers, C. L., 1934, *Phys. Rev.*, **45**, 98.  
Sreedhara Murthy, N., 1961, *Nature* **190**, 430.  
Tanaka, T. and Horie, T., 1941, *Proc. Phys. Math. Soc. Japan*, **23**, 404.  
Tawde, N. R. and Sreedhara Murthy, N., 1957, *Ind. J. Phys.*, **31**, 391.



# Letters to the Editor

Contributions must reach the Assistant Editor not later than the 15th of the second month preceding that of the issue in which the letter is to appear. No proof will be sent to the authors.

## 2

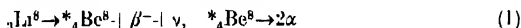
### EJECTION OF A $\text{Li}^9$ -HAMMER' TRACK

G. C. DEKA AND K. M. PATHAK

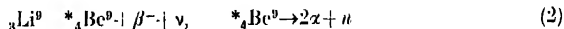
DEPARTMENT OF PHYSICS, COTTON COLLEGE, GAUGHATI

(Received October 13, 1961)

T-shaped nuclear tracks (colloquially known as 'hammer' tracks) are frequently observed in the high energy nuclear disintegrations produced in photographic emulsions. Properties of such 'hammer' tracks have been studied by several authors (Fry, 1953; Munir, 1956; Lock, 1957 and Deka *et al.*, 1961). These 'hammer' tracks are generally interpreted as follows



However, Fry *et al.* (1953) found a 'hammer' track which was interpreted as due to  ${}_3\text{Li}^9$  decay. A similar event was also reported by Munir (1956). Among 798 'hammer' tracks Deka *et al.* (1961) discovered that 4 of them were due to  ${}_3\text{B}^8$ , two were due to  ${}_3\text{Li}^9$ . But no event which is significantly different in appearance from a common 'hammer' track has appeared so far in literatures. The decay scheme of  $\text{Li}^9$  is assumed to be as follows:



Calculations show that the angle of non-collinearity between the two alpha-particles from  $\text{Li}^8$  decay would not exceed  $6^\circ$ , whereas due to the presence of a neutron in the  $\text{Li}^9$  decay would allow much larger angle.

In a scan of some  $9 \times 10^3$  stars of  $N_h \geq 5$ , we found 30 double stars and 112 'hammer' tracks in the 4.6 BeV/c  $\frac{1}{2}$ -meson plates. Among them we discovered one 'hammer' track (Fig. 1) which is significantly different in appearance. The 'hammer' part of it is very flat and it allows an accurate measurements of the angle of non-collinearity and the ranges of the alpha-tracks. The electron track is visible although the back-ground is bad. The relevant data of the event are given in the Table I.

TABLE 1

Parent state	Range of 1 $\alpha$ -track	Range of alpha tracks	Angle of non-collin- earity	Momentum unbalance	Total energy release
$(10 \pm 2)\pi^-$	$358 \pm 4\mu$	(1) $4.17\mu$ (2) $4.58\mu$	$35^\circ \pm 2''$	$58.3 \pm 37$ MeV/c	$4.3 \pm 1$ MeV.



Fig. 1

Careful measurements were also made of  $\delta$ -rays present on this track as well as on the other 'hammer' tracks in the same pellicle. The total numbers of  $\delta$ -rays having grains  $\geq 3$  over the residual range  $360\mu$  were found to be  $17 \pm 4$  on this track and  $20 \pm 4$  on the other 'hammer' tracks. This comparison of  $\delta$ -ray-counts indicates that within experimental errors this track was perhaps due to a nucleus of charge 3.

In the calculation we assume that the  $\text{Li}^9$ -nucleus decayed at rest according to the scheme in Eq. (2). To conserve momentum in the decay,  $58 \pm 37$  MeV/c is assumed to be carried by a neutron which does not produce any observable track in the emulsion. The total energy release in the break up of  ${}^9\text{Be}^9$  indicates that  ${}^9\text{Be}^9$  was probably created in the 6.8 MeV excited state and subsequently decayed with the energy release of  $4.3 \pm 1$  MeV.

## REFERENCES

- Deka, G. C., Evans, D., Prowse, D. J., Baldo-Cecchi, M., 1961, *Nuclear Physics* **23**, 460.,  
 Fry, W. F., 1953, *Phys. Rev.* **89**, 325.  
 Lock, W. O., Goldsack, S. J., and Muir, B. A., 1957, *Phil. Mag.*  
 Muir, B. A., 1956, *Phil. Mag.*, **1**, 355.

# SYMMETRY OF THE CRYSTALLINE ELECTRIC FIELD ON $\text{Yb}^{+++}$ ION IN $\text{Yb}_2(\text{SO}_4)_3 \cdot 8\text{H}_2\text{O}$ CRYSTAL

A. MOOKHERJI AND D. NEOGY

PHYSICAL LABORATORIES, AGRA COLLEGE, AGRA

(Received November 16, 1961)

Penney (1933) attempted to explain the room temperature powder values of the magnetic moment of  $\text{Yb}^{+++}$  ion in  $\text{Yb}_2(\text{SO}_4)_3 \cdot 8\text{H}_2\text{O}$  crystal as obtained by Cabrera (1925), St. Meyer (1925) and Zernike and James (1926) on the assumption of a field of cubic symmetry to which the  $\text{Yb}^{+++}$  ion was subjected. In the absence of low temperature experimental data his calculations were only provisional and no definite conclusion could be drawn.

Elliot and Stevens (1952) rejected the conventional crystal field treatment (i.e. cubic superimposed on it a small tetragonal component) and explained successfully the PRM data of cerium ethyl sulphate using a field of trigonal symmetry and hence suggested that fields of the same symmetry might be effective in other rare earth salts also.

A survey of the magnetic susceptibility anisotropy data (Krishnan and Mookherji, 1938) shows that the magnetic anisotropy in ethyl sulphates and in double nitrates where the paramagnetic units are oriented parallel to each other ranges from 5% to 7% at room temperatures, whereas in halides and in sulphates where the paramagnetic units are not necessarily oriented parallel to each other magnetic anisotropy at room temperature ranges from 11 to 25%. So the probability of a crystal field of the same symmetry as in ethyl sulphate and double nitrates (trigonal) to be effective in halides and in sulphates is very very less. Hence to get an insight as to the nature of the crystal field acting on  $\text{Yb}^{+++}$  ion in  $\text{Yb}_2(\text{SO}_4)_3 \cdot 8\text{H}_2\text{O}$  crystals we have measured its magnetic anisotropy and magnetic moment from room temperature down to liquid oxygen temperature by the method of Krishnan, Mookherji and Bose (1939). The results so obtained were treated theoretically on the same lines as that of Elliot and Stevens (1952), but using a general tetragonal field.

The ground state of free  $\text{Yb}^{+++}$  ion is  $^2F_{7/2}$  which is separated from its next higher level  $^2F_{5/2}$  by  $10,000 \text{ cm}^{-1}$  (Gorherch, 1938) and hence the contribution of  $^2F_{5/2}$  to magnetic susceptibility is zero at room temperature (Van Vleck and Frank, 1929). The crystal field then perturbs this energy state. (We assume that the effect of the crystal field is smaller than that of spin-orbit coupling). The complete Hamiltonian for the perturbed ion is given by

$$H = H_0 + V + \beta H J_g$$

where  $H_0$  stands for the Hamiltonian for the unperturbed state,  $V$  the energy due to the crystal field and  $\beta H J g$  includes the effect of the magnetic field; other symbols have their usual meanings.

The crystal field due to an octahedron of water cluster surrounding the ion is assumed to have general tetragonal symmetry, conforming to a potential given by,

$$V \sim B_2^0(3z^2 - r^2) + B_4^0(35z^2 - 30r^2z^2 - 3r^4) + B_6^0(231z^6 - 315z^4r^2 - 105r^4z^2 - 5r^6) \\ + B_4^4(x^4 - 6x^2y^2 + y^4)$$

where  $B_n^m$  are related to the strength of the crystal field.

The matrix elements due to the crystal field were obtained by changing the potential field operator  $V$  into its equivalent angular momentum operators (Stevens, 1952). The susceptibilities along ( $K_{11}$ ) and normal ( $K_1$ ) to the symmetry axis of the water cluster about  $\text{Yb}^{III}$  ion were calculated by the general expression, as given by Van Vleck (1932), using the energy expressions so obtained. The negative sign of Cotton Mouton constant of cupric sulphate aqueous solution (Chakravorty, 1942) where  $K_{11}$  is greater than  $K_1$  and the findings of Chinchalkar (1931) that the sign of magnetic birefringence is also negative with aqueous solutions of halides of Ce, Pr, and Er, suggest that in  $\text{Yb}_2(\text{SO}_4)_3 \cdot 8\text{H}_2\text{O}$ ,  $K_{11}$  might also be greater than  $K_1$ .

There is no X-ray data nor any PMR data and hence the disposition of the paramagnetic cluster in the unit cell of the crystal is not known. As a result we cannot determine precisely the values of the magnetic anisotropies associated with the individual ionic groups.

It is however fortunate that only a particular set of crystal field parameters give the right nature of the temperature variation of the magnetic anisotropy. With the help of that set of parameters which give the best fit we have calculated  $K_{11}$  and  $K_1$  at different temperatures. It is observed that  $K_{11}$  comes out to be greater than  $K_1$  suggesting the correctness of our earlier arguments. The same set of parameters also give a good fit with the mean moment at different temperatures. Observed and calculated values of  $(K_{11} - K_1)$  and  $\mu^2$  are shown in Table I.

TABLE I

Temperature °K			300	240	200	140	100
$K_{11} - K_1 \times 10^6$	Experimental		1945	3049	4219	7360	10935
	Theoretical		1945	3100	4150	7200	11150
$\mu^2$	Experimental		20.59	20.04	19.05	19.59	18.94
	Theoretical		20.24	19.81	19.78	19.40	18.94

Thus, since the calculated  $(K_{11} - K_1)$  value for the ionic cluster at 300°K is the same as  $(X_1 - X_2)$  for the crystal, we may conclude that all the eight ionic clusters (Zachariasen, 1935) in the unit cell of the crystal are oriented almost parallel to each other making  $X_1 - X_2 = (K_{11} - K_1)$  experimental, as given in Table I.

It may be possible that this close agreement of the temperature variation of  $\Delta K(K_{11} - K_1)$  with that of  $\Delta X(X_1 - X_2)$  may be due to averaging of field parameters in the plane of  $\Delta X$ , but the approximate uniaxial magnetic character about  $X_1 - X_2$  axis ( $X_3/X_2 = 1.04$ ) of the crystal, coupled with high crystal anisotropy (23%) as compared with other sulphates and halides crystals of rare earth ions (10%), does not support this possibility.

The mathematical and other details will be published elsewhere.

## REFERENCES

- Bose, A., 1947, *Ind. J. Phys.*, **21**, 275.  
 Cabrera, B., 1925, *Comp. Rend.* **180**, 669.  
 Chakravorty, D. C., 1942, *Current Science.*, **8**, 110.  
 Choudhalkar, S. W., 1931, *Ind. J. Phys.*, **6**, 581.  
 Elliot, R. J. and Stevens, K. W. Jr., 1952, *Proc. Roy. Soc. A* **215**, 437.  
 Elliot, R. J. and Stevens, K. W. Jr., 1953, *Proc. Roy. Soc. A* **219**, 387.  
 Gorbereht, H., 1938, *Ann. Phys. Lpz.*, **31**, 300.  
 Krishnan, K. S. and Mookherji, A., 1938, *Phil. Trans. A* **237**, 135.  
 Krishnan, K. S., Mookherji, A. and Bose, A., 1939, *Phil. Trans. A* **238**, 125.  
 Krishnan, K. S., Mookherji, A. and Bose, A., 1949, *Ind. J. Phys.*, **23**, 217.  
 Penney, W. G., 1933, *Phys. Rev.*, **43**, 485.  
 Stevens, K. W. Jr., 1952, *Proc. Phys., Soc. A* **65**, 209.  
 St. Meyer, 1925, *Phys. Zeits.*, **26**, 51, 478.  
 Van Vleck, J. H., 1932, *Theory of Electric and Magnetic Susceptibilities*, Oxford Univ. Press, p. 182.  
 Van Vleck, J. H. and Frank, A., 1929, *Phys. Rev.*, **34**, 1454, 1625.  
 Zachariasen, W. Jr., 1935, *J. Chem. Phys.*, **3**, 197.  
 Zenneke, J. and James, C., 1926, *J. Am. Chem. Soc.*, **48**, 2827.



# ASYMMETRIC SHAPE EFFECTS IN DIA- AND PARAMAGNETIC CRYSTALS

MANJU MAJUMDAR

INDIAN ASSOCIATION FOR THE CULTIVATION OF SCIENCE,  
JADAVPUR, CALCUTTA-32.

(Received December 18, 1961)

**ABSTRACT.** The anisotropy of shape of rectangular plates of several isotropic crystals of dia- and paramagnetic materials has been determined. A crystal grinding apparatus was constructed to grind the water or melt-grown crystals into plates of various dimensions. An improved method of anisotropy measurement capable of giving greater accuracy, particularly for crystals of low anisotropy, has been used. The results show that for crystals of a given substance the anisotropy of shape, measured as a fraction of the mean susceptibility, depends not only on the ratio of the dimensions in the horizontal plane, the crystal being vertically suspended, but also on the actual values of the length and breadth, as well as on the dimension in the vertical direction, that is, the height. Methods have been suggested for correlating the shape effects with the dimensions of the crystal by graphical means. The limitations of the method have been discussed.

## INTRODUCTION

The correction for anisotropy of shape presents a difficult problem in the determination of the true magnetic anisotropy of crystals. Although in general for dia- and paramagnetic crystals this is not of as great importance as in the ferromagnetic ones, for crystals of low magnetic anisotropy and high susceptibility the shape effect may become considerable, particularly when they grow in the form of thin plates or long needles.

The asymmetric shape effects may arise from two factors. (1) If the magnetic field,  $H$ , in which the sample is placed is ideally homogeneous (before the body is brought in), the magnetic field inside the body is changed into  $H'$  where  $H - H' = DI$ ,  $I$  being the intensity of magnetisation, assumed homogeneous, inside the body and  $D$  is the 'demagnetising coefficient'. The value of  $D$  can be calculated only for certain simple geometric shapes, where the assumption of uniform magnetisation is more or less valid. Tables and graphs for the general ellipsoid of semi-axes  $a, b, c$  where  $a \geq b \geq c \geq 0$ , for different values of  $c/a$  and  $b/a$  have been presented by Osborne (1945) and Stoner (1945). Snoek (1934) calculated the demagnetising factors for thin circular discs by using the assumption that the cylinder edge may be theoretically replaced by an equivalent ellipsoidal surface. No calculations seem possible for rectangular plates owing to the non-uniformity of the intensity of magnetisation at the edges. However, it is interesting to note that in certain cases the demagnetising energy can be calcu-

lated for *ferromagnetic* bodies in the form of rectangular blocks (Rhodes and Rowlands, 1954). It can be shown that the anisotropy of shape arising from the above cause is proportional to the square of the mean susceptibility and can therefore be neglected for most paramagnetic substances ( $\chi \approx 10^{-3}$ ) except when they approach saturation.

(2) The second factor which gives rise to the observed effects is that the field is not ideally uniform, as is also the induced magnetisation inside the sample placed in the field, which therefore causes a couple to act on the sample. No general theoretical calculation on this effect appears to have been made. It may, however, be shown that this effect is proportional to the mean susceptibility of the crystal and with sufficient initial inhomogeneity of the field it may become considerable. Although with careful shaping of the pole-pieces the effect can be reduced to a negligible minimum, this is not often practicable.

In some of the earlier attempts to eliminate the shape effects at room temperatures (Krishnan and Banerjee, 1936) the crystal was suspended in a mixed liquid bath the susceptibility of which could be adjusted to be the same as the mean susceptibility of the crystal. The method is clearly unsuitable for crystals soluble in the liquids used or for those with very high susceptibilities. The procedure more often followed is to grind the crystal into a cylinder about a chosen axis perpendicular to which the magnetic anisotropy is measured. However, during grinding the sample may become contaminated, and for hygroscopic, efflorescent or chemically unstable crystals further difficulties may be encountered. In such cases it is advisable to use the crystal in its natural form with a suitable protective coating, and the magnetic measurements made immediately after it is prepared. Then, it is necessary to determine and correct for the anisotropy of shape either by direct mathematical calculations from the known shape, which even in the simple case of a rectangular block of the specimen is not easy, as already mentioned, or by comparison with an extensive series of trial experiments on the anisotropy of shape of differently shaped specimens which have no inherent magnetic anisotropy, e.g., crystals belonging to the cubic class of symmetry. As many crystals normally grow in the form of nearly rectangular plates or prisms where shape effects are likely to be large (they are expected to be small for approximately equidimensional crystals), a set of pilot data once obtained on the aforementioned isotropic crystals ground into rectangular plates of various dimensions might give some indications about the appropriate correction terms for the shape anisotropy of the noncubic crystals. The present investigation was undertaken with this object in view.

## EXPERIMENTAL

### (a) *Preparation of single crystals*

Crystals of aluminium potassium, chrome potassium and iron ammonium alums, which belong to the cubic class and are magnetically isotropic, were grown



from solutions at about 5°C and the bigger and more flawless ones (as observed under polarising microscope) selected for the experiments. The first alum is diamagnetic and the other two paramagnetic. Some pure (Harshaw 'optical grade') melt-grown potassium bromide single crystals were also procured and plates of suitable dimensions cleaved out from them. These were ground to suitable shape and size, where necessary.

(b) *Grinding of crystals into rectangular plates*

An apparatus for grinding the crystals into rectangular plates (as well as cylinders, if necessary) with desired crystallographic orientations was designed and constructed in the laboratory. This consisted of a horizontally mounted shaft which could be rotated by means of a fractional H.P. motor through a system of pulleys and belt drive to give speeds ranging from a few hundred to about 3000 r.p.m. At the end of the shaft was fitted a grinding wheel made of finely ground glass disc (it could be replaced with one of alundum, if necessary). A horizontal bed was mounted on a rigid stand below the grinding wheel and could be raised or lowered by means of a knurled nut. A graduated circular rotatable table mounted on a pair of cross-slides fixed to the bed made it possible to rotate the crystal sample and move it to and fro and from side to side. The crystal was fixed on the table by means of 'Durofix' or similar adhesives with a chosen face in contact with it. Pure alcohol (or similar organic solvents) used as a grinding fluid tends to dissolve the adhesive, and pure water tends to dissolve away the crystal more near the edges and also makes the ground surface convex. After a number of trials a mixture of water with ethanol in small quantities was found to be very satisfactory. The upper surface of the crystal was ground by using the edge of the grinding wheel with cross and vertical feeds and the sides were ground by placing the crystal at the edge of the table and using the flat (vertical) surface of the wheel near the rim for grinding with the cross feed of the bed. The orientation of the ground faces to a known crystal face could be made accurately to about 15' by eye estimation, and can be further improved with suitable modifications in design. The dimensions of the plates were measured to 0.001 mm with the help of a Hilger Comparator, by the kind permission of our Department of Optics.

(c) *Measurement of shape anisotropy*

Since the crystals were magnetically isotropic the observed shape effects were assumed to be equivalent to a magnetic anisotropy,  $\Delta\chi$ , and the results expressed as a fraction of the mean magnetic susceptibility,  $\chi$ , both being for gm molar quantities.

The usual method of measuring the anisotropy of a crystal consists in suspending it by means of a torsion fibre in a uniform magnetic field and measuring the 'critical couple' necessary for bringing the crystal from its equilibrium position

(under zero torque of the fibre) to the unstable position in the field. The anisotropy,  $\Delta\chi$ , is then given by (Krishnan and Banerjee, 1936)

$$\Delta\chi = \frac{2MC}{mH^2} \frac{\alpha_c - \pi/4 - \sigma_c}{\cos 2\sigma_c} \quad \dots (1)$$

where  $C$  is the torsion constant of the fibre,  $M$  and  $m$  are the molecular weight and mass of the crystal,  $H$  is the magnetic field,  $\alpha_c$  is the critical torsional angle through which the fibre is twisted and  $\sigma_c$  is a correction term which is small for large values of  $\alpha_c$ . This method is not very satisfactory when  $\alpha_c$  is less than about  $200^\circ$  (which is quite usual for crystals of low anisotropy) as the value of  $\sigma_c$  becomes large and the critical position becomes difficult to determine accurately. Further, it is not possible to observe and control the magnet current near the critical position so that the field may fluctuate, resulting in a premature spinning round of the crystal. An improved method was, therefore, employed as described below, which consisted in measuring the 'maximum couple' acting on the crystal, when the crystal is set at equilibrium at  $45^\circ$  to the field, so that the results are free from uncertainties associated with the earlier method. A somewhat similar method has been described by Stout and Griefel (1950) (see Datta, 1956).

After grinding the crystal into the required shape it was attached to a long thin glass rod using a small quantity of shellac or some other suitable adhesive with a selected plane normal to the rod axis, the orientation being performed with the crystal mounted on a goniometer head. The other end of the rod was fixed to a calibrated quartz fibre suspended from the pointed end of a brass rod passing through the centre of a graduated torsion head provided with a vernier reading to one-tenth of a degree. The assembly was enclosed in a glass tube which opened at the bottom into a rectangular box made of perspex with a sliding front, the chamber being kept dry by using silica gel. The box was situated between a pair of plane and parallel pole-pieces of an electromagnet. The glass tube and the perspex box were properly adjusted and made vertical so that the axis of the suspension system passed through the centre of the pole-gap. The crystal could then be brought to the centre by adjusting the rod carrying the fibre. A diagram of the apparatus used is shown in Fig. 1.

In order to observe the position of the crystal very accurately a hexagonal mirror was constructed by fixing small strips of silvered optically flat microscope cover slips, about  $3 \text{ mm} \times 3 \text{ mm}$ , on the sides of a very light aluminium hexagon,  $5 \text{ mm}$  across and  $1 \text{ mm}$  thick at the edges, the central region being made thinner. The hexagon was mounted near the upper end of the glass rod passing through a bore at its centre, so that it was well outside the pole-gap and at the same time visible through the glass pane when the crystal was placed at the centre of the pole gap. The rotational movement of crystal was observed under high magnification with the help of the reflection of a ground glass scale from a mirror, illuminated

with a fluorescent tube lamp enclosed in a wooden case and the whole mounted on an adjustable stand, seen through with a short focus telescope provided with

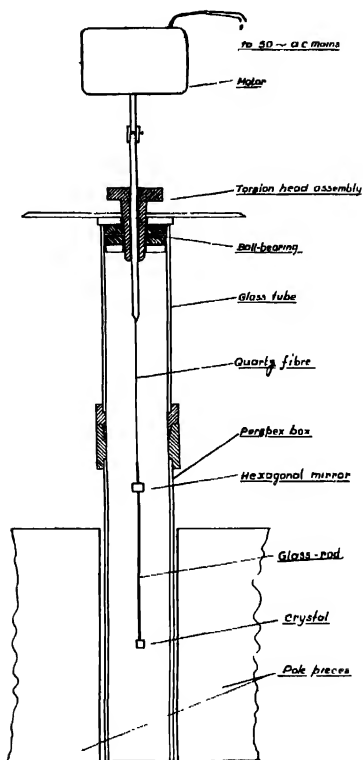


Fig. 1. The torsion apparatus used for the measurement of magnetic anisotropy (diagrammatic).

cross-wires. The advantage of using a hexagonal set of mirrors is that a reflection of the scale was always obtained in the telescope from one mirror or another.

Another important improvement over the previous method consisted in using a small one r.p.m. 4 Watt synchronous motor to rotate the spindle of the torsion head which had consequently to be specially designed and was provided with ball-bearings. The motor was fixed at the top of the spindle and was found to work very smoothly, eliminating all jerks and vibrations which inevitably accompany manual control. Moreover, the torsion head could be rotated by

operating a switch near the observer while looking through the telescope from a distance and was, therefore, very convenient for taking readings.

In the present method the crystal was first brought to its setting position in the field under zero torsion of the fibre using the telescope and scale arrangement to observe even small motions of the crystal when the field is switched on and off. The crystal was then rotated through  $45^\circ$ , keeping the field off, and the position noted on the vernier scale. The field was then switched on when the crystal tended to come back to its setting position. By slowly applying torsion to the fibre with the help of the motor the crystal was brought back smoothly to the  $45^\circ$  position where the maximum magnetic couple acts on the crystal and is balanced by the torsion on the fibre. Under these conditions we have

$$\Delta\chi = \frac{2MC}{mH^2} \cdot \alpha_m \quad \dots (2)$$

where  $\alpha_m$  is the maximum torsional angle of the fibre,  $C$ ,  $M$ ,  $m$  and  $H$  being the same as in (1)  $C$  and  $H$  were determined as described by previous workers in

TABLE I  
Variation of  $\Delta\chi/\chi$  with  $b$

Crystal	length $l$ (cm)	breadth $b$ (cm)	height $h$ (cm)	$l/b$	$\Delta\chi/\chi$ $\times 10^4$
$\text{AlK}(\text{SO}_4)_2 \cdot 12\text{H}_2\text{O}$	.618	.149	.511	4.14	5.02
$\chi = 250 \times 10^{-6}$	.556	.075	.491	7.42	8.94
	.574	.062	.451	9.26	10.81
	.656	.043	.453	15.16	16.01
$\text{KBr}$	1.806	.271	.745	6.68	5.22
$\chi = .491 \times 10^{-6}$	1.734	.136	.740	12.72	11.50
	1.652	.095	.735	17.37	17.89
	1.600	.043	.650	37.04	41.47
$\text{CrK}(\text{SO}_4)_2 \cdot 12\text{H}_2\text{O}$	.654	.113	.496	5.77	2.70
$\chi = 6165 \times 10^{-6}$	.613	.052	.473	12.32	6.57
at $302.5^\circ\text{K}$	.633	.032	.440	20.04	11.43
$\text{FeNH}_4(\text{SO}_4)_2 \cdot 12\text{H}_2\text{O}$	1.185	.239	.716	4.95	4.74
$\chi = 14110 \times 10^{-6}$	1.143	.146	.641	7.85	8.00
at $303^\circ\text{K}$	.957	.047	.501	20.37	20.25

TABLE II  
Variation of  $\Delta\chi/\chi$  with  $h$

Crystal	length $l$ (cm)	breadth $b$ (cm)	height $h$ (cm)	$l/h$	$\Delta\chi/\chi$ $\times 10^3$
$\text{FeNH}_4(\text{SO}_4)_2 \cdot 12\text{H}_2\text{O}$	.602	.104	1.225	.816	.491
	.602	.101	.945	1.058	.637
	.601	.104	.654	1.529	.920
	.601	.104	.313	3.195	1.921

Data on potassium bromide have been included in Table III.

this laboratory (Datta, 1953, 1954; Dutta Roy, 1954). Values of  $\alpha_m$  were taken for clockwise as well as counterclockwise rotations of the crystals.

## RESULTS AND DISCUSSIONS

### (i) Dependence of shape anisotropy on the dimensions of a crystal

It was observed early in course of the experiments that the anisotropy of shape of a rectangular plate depended not only on the ratio of the dimensions in the horizontal plane (for vertical suspensions of the crystal in a horizontal field) but also on their actual values, that is, on the length,  $l$  and breadth,  $b$ , as well as on the height,  $h$ . It was observed that the anisotropy also depends on  $h$ , because of the fact that the couple acting on different sections in the horizontal plane of a crystal of given  $l$  and  $b$  varies with the height and the observed value is an average. Hence, in investigating a particular crystal two of the dimensions were kept as nearly constant as possible (it was almost impossible to keep these dimensions constant due to slight chipping off of the edges during grinding). Results are presented in the following tables which show the effects of varying (1)  $b$ , keeping  $l$  and  $h$

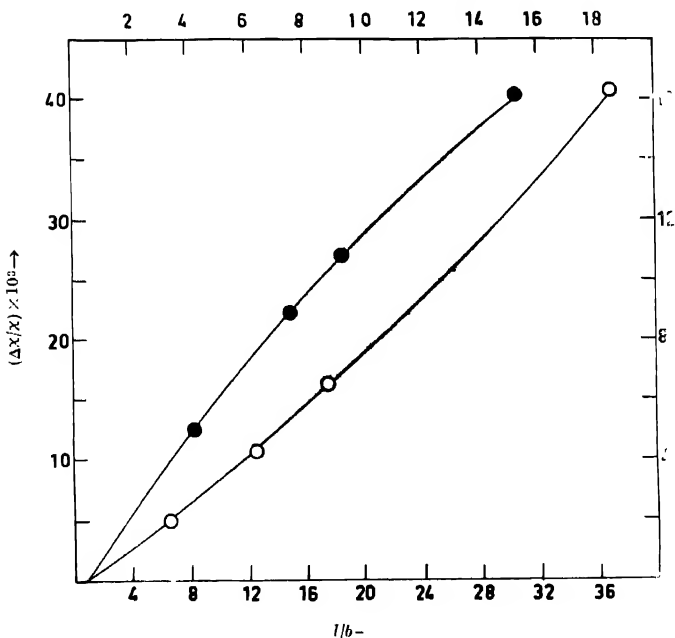


Fig. 2. Variation of  $\Delta\chi/\chi$  with  $l/b$  for diamagnetic crystals. The solid circles denote Al-alum and the hollow circles for KBr.

The co-ordinates for Al-alum are shown at top and right sides of the diagram.

constant, and (2)  $h$ , keeping  $l$  and  $b$  constant. The magnetic field,  $H$ , was 2460 oersteds throughout the experiments. The values of  $\chi$  have been taken from "Tables de constantes et données numériques", Vol. 7, 1957. Positive values of  $\Delta\chi/\chi$  are shown.

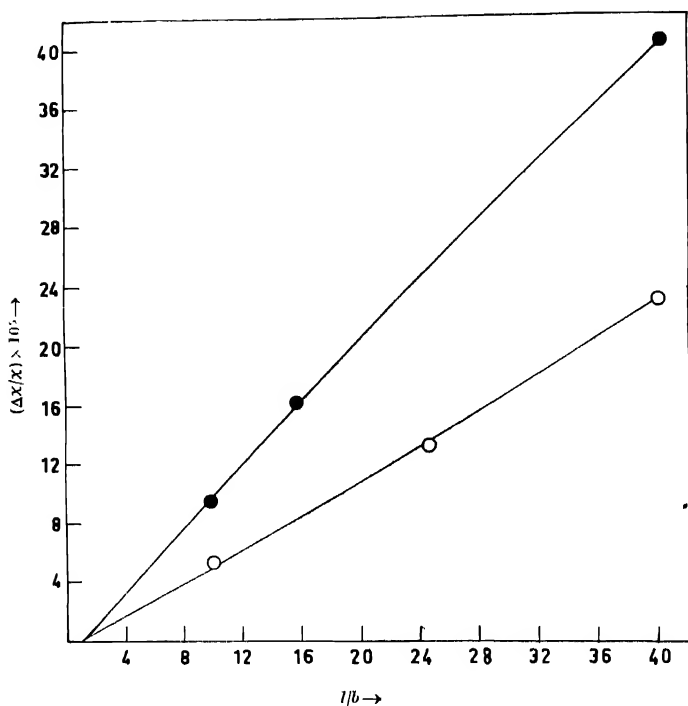


Fig. 3. Variation of  $\Delta\chi/\chi$  with  $l/b$  for paramagnetic crystals. The solid circles represent ferrie alum and the hollow circles chrome alum.

The results are shown graphically in Figs. 2 to 4: in Figs. 2 and 3,  $\Delta\chi/\chi$  has been plotted against  $l/b$  in order to bring out the fact that it tends to become zero for  $l/b = 1$ , i.e., for plates having square sections in the horizontal plane the shape anisotropy vanishes. It may be observed that  $\Delta\chi/\chi$  increases with decreasing breadth, the length and height remaining constant. In Fig. 4,  $\Delta\chi/\chi$  is plotted against  $1/h$  where it is seen to decrease with increasing values of  $h$  and becomes zero when  $h$  tends to infinity. This is not surprising, since in calculating  $\Delta\chi$  the observed values of  $\alpha_m$  are divided by the mass ( $m$ ) of the specimen (refer to Eq. 2) and when  $h \rightarrow \infty$ ,  $m \rightarrow \infty$ , so that  $\Delta\chi$  approaches zero, although  $\alpha_m$  still remains finite.

## Asymmetric Shape Effects in Dia- and Paramagnetic, etc. 119

All these curves have only slight departure from linearity (except for large values of  $l/b$  or  $l/h$ ) which facilitates extrapolation.

(ii) *Determination of shape anisotropy for crystals of any dimensions by interpolation.*

It is clear from above that if we have a set of data for the shape anisotropy of a given crystal with any two of its dimensions fixed but the third varying, then it is possible to determine the shape anisotropy for a similar crystal with any value of the third dimension, provided its other two dimensions are the same. However, as this condition cannot be realized always in practice the following method of interpolation for any given dimensions has been evolved.

Let us suppose we have several large rectangular blocks of a given crystal with their length, breadth and height denoted by  $l, b$  and  $h$  respectively. We first take one of them, cut or grind it to change one of the dimensions, say,  $l$ , into  $l_1$ . We then cut or cleave out several sections along the breadth, say, with  $b$  as  $b_1, b_2, \dots$ , each having the length as  $l_1$  and height as  $h$ . Now, taking each section we study the variation of the shape anisotropy with  $h$ , as before. Next, we choose another block, change the length into  $l_2$ , cut it into sections of breadth  $b'_1, b'_2, \dots$

TABLE III  
Variation of  $\Delta\chi/\chi$  with  $h, b$  and  $l$  for KBr crystals

Length (cm)	Breadth (cm)	Height (cm)	$l/h$	$\Delta\chi/\chi \times 10^3$	$\Delta\chi/\chi \times 10^3$ for $h =$ 0.7 cm      0.5 cm	
	$b_1 =$ 0.52	1.442 1.003 0.752	603 997 1.330	9.73 12.70 17.82	18.7	26.85
$l_1 =$ .3765	$b_2 =$ 0.75	1.041 1.119 0.598	.609 .894 1.460	5.38 7.83 13.95	13.1	19.05
	$b'_1 =$ .051	2.022 1.231 0.598	.495 .813 1.672	6.88 12.22 25.81	21.9	31.9
$l_2 =$ .781	$b'_2 =$ 118	2.251 1.458 0.725 0.351	.444 .685 1.379 2.849	2.68 4.42 10.10 20.81	9.65	14.1
	$b''_1 =$ 118	.876 .582 0.395	1.141 1.718 2.532	11.90 17.20 27.92	14.6	20.9
$l_3 =$ 1.730	$b''_2 =$ .211	.809 0.617 0.404	1.236 1.621 2.475	7.45 8.65 15.63	7.95	11.65

\*Interpolated from Fig. 3. These values have been plotted against the corresponding  $l/b$  values in Fig. 5.

and again determine the variation of shape anisotropy with height for each section. By repeating this process we get results for  $l_1$  with  $b''_1, b''_2, \dots$ . From a graphical representation of the data and interpolation therefrom it may be possible to estimate the shape anisotropy for a specimen with any value of  $l, b$  and  $h$  within the given limits as will be shown below. We choose potassium bromide crystals for this purpose, as this is available in large rectangular blocks from which parallel sections can be readily cleaved out. Moreover, since no grinding is involved (except for very small values of  $b$ ) two of the dimensions can be kept very nearly constant in any particular series of experiments.

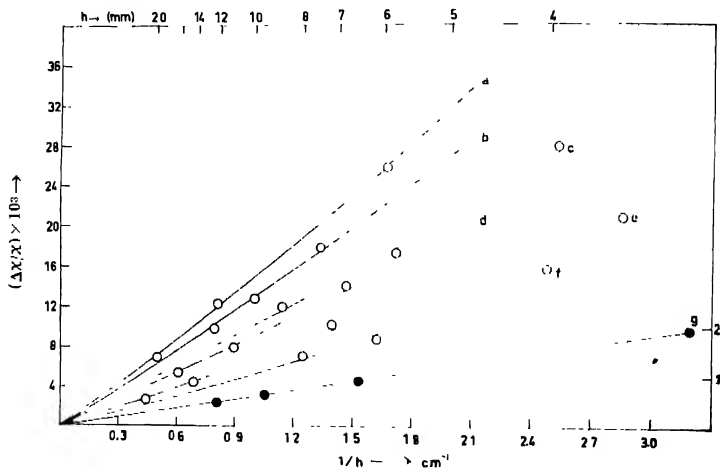


Fig. 4 Variation of  $\Delta\chi/\chi$  with  $1/h$ . The solid circles (curve  $g$ ) represent ferric alum the ordinates for which are shown at right and the rest are for KBr. The  $l$  and  $b$  values for each curve are (in cm) (a) 0.78, 0.051; (b) 0.375, 0.052; (c) 1.73, 0.118; (d) 0.378, 0.075; (e) 0.78, 0.118; (f) 1.73, 0.211.

The above results have been represented graphically in Fig. 4 where the anisotropy values have been plotted against  $1/h$  for the three sets of plates of length  $l_1, l_2, l_3$  and different  $b$  values for each. All of them are almost linear curves passing through the origin.

In estimating the shape anisotropy of any crystal with dimensions  $l, b, h$ , the ordinate at  $1/h_1$  is drawn to intersect the sets of curves in Fig. 4 at points which give the values of  $\Delta\chi/\chi$  for  $h = h_1$  and for different sets of values of  $b$  corresponding to a particular value of  $l$ . From these points a new set of curves is drawn showing the variation of  $\Delta\chi/\chi$  with  $1/b$  for the different values of  $l$ . Each of these curves is made to pass through a point on the abscissa (corresponding to  $\Delta\chi/\chi = 0$ ) at  $1/b = 1/l$ , since it is already seen that the anisotropy vanishes



for  $l = b$  (Figs. 2 and 3). The ordinate at  $1/b_l$  is then drawn to intersect the curves and the value of  $\Delta\chi/\chi$  is obtained by interpolation for the appropriate  $l_i$  value.

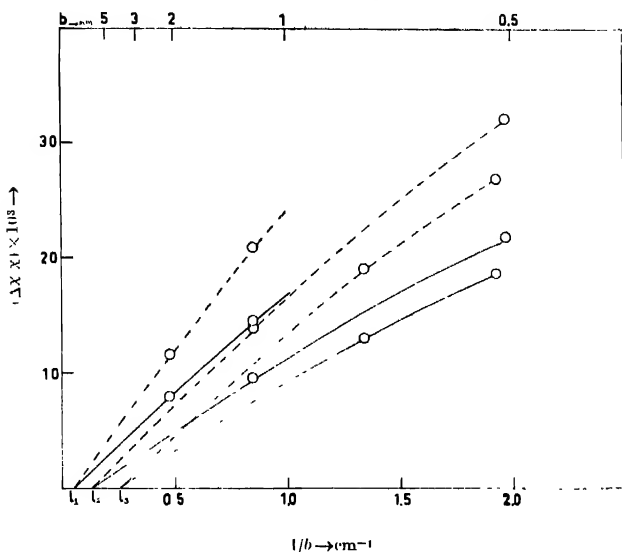


Fig. 5 Variation of  $\Delta\chi/\chi$  with  $1/b$  from interpolated points in Fig. 4 corresponding to  $h = 7$  mm (solid curves) and 5 mm (broken curves) respectively. The values for  $l$  corresponding to each curve shown on the abscissa:  $l_1 = 0.377$  cm,  $l_2 = 0.781$  cm,  $l_3 = 1.73$  cm.

Taking as an illustration  $h$ , to be 7 and 5 mm two sets of curves with solid and broken lines, respectively, have been drawn in Fig. 5 from the points obtained in the above manner from Fig. 4 which are included in Table 3. In order to find the anisotropy of a KBr crystal suspended in a magnetic field and having  $l, b, h$  as 7, 2, 7 mm respectively, which are fairly representative of a comparatively flat experimental crystal, the ordinate at  $1/0.2$  is drawn to meet the solid lines and interpolation of  $l_i = 0.7$  is made between the curves for  $l_2$  and  $l_3$ . The shape anisotropy is seen to be about 0.5%. Similarly, a crystal with  $l = 5$  mm,  $b = 2$  mm and  $h = 5$  mm would have about the same anisotropy, while the corresponding value for  $b = 3$  mm would be 0.2%. The effect of all the three dimensions on the anisotropy is quite evident from these results.

Our previous statement that the anisotropy depends on the actual dimensions of the crystal rather than on their ratios (contrasting with the case of the demagnetising factors for ellipsoids with which our problem bears a formal analogy), can be demonstrated from Fig. 4 directly without taking recourse to interpolation

for  $l$ ,—a method necessarily somewhat approximate in the absence of larger number of closely spaced curves for  $l$ . A crystal with  $l = 0.781$  cm and  $b = 0.200$  cm has  $\Delta\chi/\chi = 0.5\%$ , while another with  $l = 0.377$  cm and  $b = 0.0967$  cm has  $\Delta\chi/\chi = 0.97\%$ , both with  $h = 0.7$  cm and having the same value for  $l/b$ .

It may be noted in conclusion that for most experimental crystals of usual size and shape  $\Delta\chi/\chi$  amounts to a few, say, 2 to 5, parts in a thousand. These remarks apply only to KBr crystals. Our observations on isotropic paramagnetic crystals of different susceptibilities, such as chromium and iron alums show that for crystals of the same dimensions  $\Delta\chi/\chi$  varies almost linearly with  $\chi$ , decreasing with the increasing value of the latter. This is shown in Fig. 6, obtained from the results for a crystal with  $l, b, h$  as 0.620, 0.113, 0.550 cm, respectively, from the data given in Tables I-III. Hence the shape anisotropy for crystals with any intermediate susceptibility can be obtained fairly accurately by interpolation. Further, with a given shape and size of the pole-pieces of the magnet the inhomogeneity decreases slightly with increasing field. For the same crystal the shape anisotropy was found to decrease with increasing value of the field

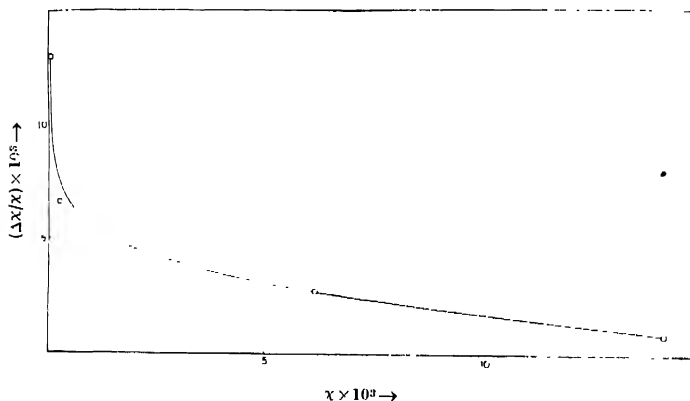


Fig. 6. Variation of  $\Delta\chi/\chi$  with  $\chi$

In order to determine the shape asymmetry of a magnetically anisotropic crystal in the form of a rectangular plate, having a mean susceptibility  $\chi$ , the value of  $\Delta\chi/\chi$  is first obtained for an isotropic crystal having the same  $l, b, h$  and  $\chi$  values. The observed magnetic anisotropy,  $\Delta\chi'$ , say, of the experimental crystal can then be corrected for its shape from a consideration of the location of the magnetic susceptibility axes with respect to  $l, b, h$  and the values of  $\Delta\chi$  and  $\Delta\chi'$ . The application of the method will be different for different cases and will be dealt with in a subsequent publication.

ACKNOWLEDGEMENTS

The author expresses her thanks to Dr. A. Bose, D.Sc., F.N.I., Professor of Physics, Indian Association for the Cultivation of Science, Calcutta-32, for his keen interest in the work and for providing laboratory facilities.

It is a great pleasure to acknowledge my indebtedness to Dr. S. K. Datta for the help I have received from him, both in the theoretical and experimental parts of the work.

REFERENCES

- Datta, S. K. 1953, *Ind. J. Phys.*, **27**, 155.  
Datta, S. K. 1954, *Ind. J. Phys.*, **28**, 239.  
Datta, S. K. 1956, *D. Phil. Thesis* (Calcutta University), p. 39.  
Dutta Roy, S. K. 1954, *Ind. J. Phys.*, **28**, 193.  
Krishnan, K. S. and Banerjee, S., 1936, *Phil. Trans. Roy. Soc. A* **235**, 343.  
Osborne, J. A., 1945, *Phys. Rev.*, **67**, 351.  
Rhodes, P. and Rowlands, G., 1954, *Proc. Leeds. Phil. Soc.*, **6**, 191.  
Snook, J. L., 1934, *Physica*, **1**, 649.  
Stoner, E. O., 1945, *Phil. Mag.*, **36**, 803.  
Stout, J. W. and Griefel, M., 1950, *J. Chem. Phys.*, **18**, 1449.  
Tables de constantes et données numériques, 1957, Edited by G. Foex *et al.*, Vol 7, "Diamagnetisme et Paramagnetisme".

# VERTICAL TRANSPORT OF ELECTRONS DURING PRE-SUNRISE F-LAYER "SPLITTING"

P. BANDYOPADHYAY AND S. K. CHATTERJEE

INSTITUTE OF RADIOPHYSICS AND ELECTRONICS,  
UNIVERSITY OF CALCUTTA

(Received June 17, 1961)

**ABSTRACT.** This note is the extension of an earlier work (Bandyopadhyay, 1959) on the occurrence of a phenomenon observed at Haringhata and called pre-sunrise F-layer "splitting". The phenomenon is examined here as an effect of vertical transport of electrons. On this basis the kind of electron transport that might cause the "splitting" has been studied here by the method of Chandra, Gibbons and Schmerling (1960). The association of the phenomenon with magnetic K-index is also discussed.

## 1. INTRODUCTION

In an earlier work one of us (Bandyopadhyay, 1959) reported the phenomenon of pre-sunrise F-layer "splitting" as observed at Haringhata. The phenomenon is one in which, in the small hours of the morning, the F-layer traces in the ionograms undergo a sequence of changes leading to what appears to be a rapid splitting of the F-layer into two—an upper layer and a lower layer. The phenomenon was sought to be explained in the earlier paper in two different ways. The "splitting" was at first regarded as an apparent one, being due to non-vertical reflections taking place during the passage of travelling ionospheric disturbances of the type studied by Munro and others (Munro, 1949 and 1953; Munro and Heisler, 1956). The difficulties of an explanation of this type were, however, pointed out and it was suggested that the "splitting" might be real. In the latter case, one must seek an explanation of the phenomenon in some kind of vertical transport of electrons taking place in the F-layer during the occurrence of the "splitting". In the present note we have calculated the electron transport profiles at the time of "splitting" following the method of Chandra, Gibbons and Schmerling (1960) to study the kind of drift that might cause the "splitting". Some of these velocity profiles are presented here and discussed.

Another point which we have now re-examined is the question of association of the phenomenon with geomagnetic disturbances. It was pointed out in the earlier paper that the phenomenon is not associated with magnetic storms. A closer examination of this point now shows that the phenomenon is associated with rather low values of the K-index

2. VERTICAL ELECTRON TRANSPORT DURING  
"SPLITTING"2.1. *The method of analysis*

The nature of the electron drift taking place during the pre-sunrise "splitting" of the F-layer has been studied in the following way. A number of good sequence of ionograms depicting the phenomenon are selected. These are first examined carefully for any indication of oblique reflection that may be present. This is done by examining the height of the second order echo. This height, in absence of non-vertical reflections, should, at all frequencies covered by the sweep, be twice that of the first order echo. Any deviation from it, above a certain frequency, would indicate the presence of off angle reflections at those frequencies. Examined in this way, it is found that non-vertical reflections, although sometimes present, cannot be regarded as a predominant feature of the phenomenon. Sequences which do not show any oblique reflections are reduced to true height electron density profiles ( $N-h$  curves) by the method of Schmerling and Ventrice (1959). Vertical drift profiles are then derived from these  $N-h$  curves by the method of Chandra, Gibbons and Schmerling (1960), which is briefly as follows:

The night-time continuity equation may be written as

$$\frac{\partial N}{\partial t} = -\beta N - \frac{\partial}{\partial h}(Nv) \quad (1)$$

where  $\beta$  is the loss-coefficient,  $N$  is the electron density and  $v$  the drift velocity measured positively upwards.

Integration of (1) Eq. yields the amplitude of the vertical drift velocity  $v$  at an height  $h$  as

$$v = \frac{N_0 v_0}{N} - \frac{I_0^h}{N} \quad (2)$$

$$\text{where} \quad I_0^h = \int \left[ \frac{\partial N}{\partial t} + \beta N \right] dh \quad (3)$$

Here  $N_0$  and  $N$  are the electron densities at the height  $h_0$  and  $h$  respectively, and  $v_0$  and  $v$  are the corresponding drift velocities.

It is evident that if the drift velocity  $v_0$  at any height  $h_0$  (which may be the bottom of the layer) is known, that for any other height  $h$  in the layer can be calculated. In our case, however,  $v_0$  is not known. Various values for this quantity have been reported in literature. Under normal conditions the values range from 1 to 15 m/sec. Since the phenomenon under study is not a normal one, we have taken a rather extended range of values for  $v_0$  viz.,  $v_0 = 30, 10, 0, -10, -30$  m/sec. to cover the probable physical situation. Starting with these arbitrarily chosen values of  $v_0$  for the reference height  $h_0$ , values of the drift velocity at other heights are obtained for each ionogram of the sequences selected.

The above calculations require values of the loss-coefficient at different heights. For heights above 260 km Schnerling's (1955) formula has been used, viz.

$$\beta(h) = 2.2 \times 10^{-5} + 0.25e^{-h/37} \quad \dots (4)$$

Below 260 km the loss-coefficient is of the recombination type and effective  $\beta(-\alpha N)$  is calculated as follows

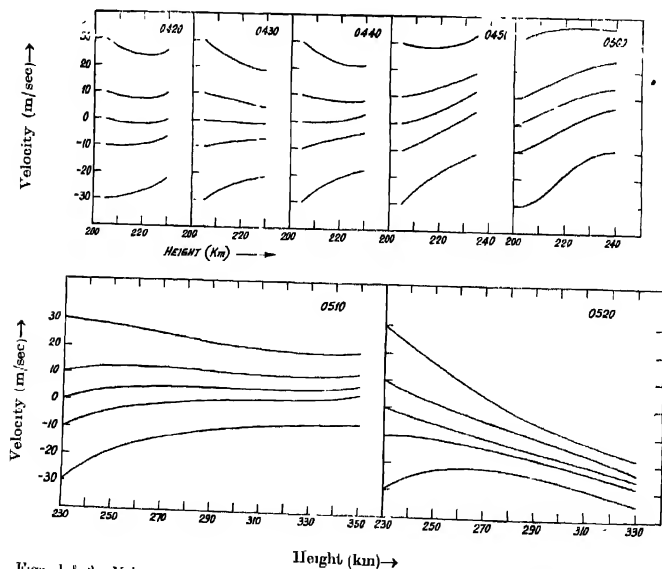
The recombination coefficient  $\alpha$  at the height  $h_0$ , which is near the bottom of the layer, is obtained using Mitra's (1959) formula, viz

$$\alpha = \frac{2 \times 10^{-10} n(O_2)}{2 \times 10^{-11} n(O_2) + 1 \times 10^{-8} N}$$

Multiplying this value of  $\alpha$  by  $N_0$  we get effective  $\beta$  at  $h_0$ . Starting with this value of  $\beta$  at  $h_0$  a smooth monotonic curve is drawn upto 260 km to join it with Schnerling's model (Eq 4). The whole procedure is similar to that followed by Chandra, Gibbons and Schnerling (1960) only that while they used the value  $\alpha = 4 \times 10^{-9}$  cm<sup>3</sup>/sec at 160 km, as given by Bates and Massey (1946), as their starting value, we have found it more convenient to take the value of  $\alpha$  at  $h_0$  from Mitra's formula.

## 2.2 Results and Discussions

Figs. 1 and 2 show typical sets of velocity profiles every 10 minutes for the occurrence of the pre-sunrise F-layer "splitting" on Nov. 13, 1955. The corres-



Figs. 1 & 2. Velocity profiles during pre-sunrise F-layer "splitting" on November 13, 1955.

ponding sequence of ionograms has been published already (Bandyopadhyay, 1959). It will be found from the profiles for 0450, the hour when the "splitting" just begins, that the velocities, particularly at the greater heights, are for most values of  $v_0$  predominantly positive (upwards). This indicates that the "splitting" is associated with a strong upward movement of the upper part of the layer. Although the motion near the bottom of the layer cannot be known by the present method of analysis, the positive gradient of the velocity profiles seems to suggest that whatever the direction, the magnitude of the drift near the bottom must have been small. The succeeding sets of profiles (0500, 0510) show a gradual change in the direction and the gradient of the velocities till at 0520 hr the drift changes sign and becomes predominantly negative (downwards)

### 3. ASSOCIATION OF PRE-SUNRISE "SPLITTING" WITH GEOMAGNETIC DISTURBANCES

The association of pre-sunrise F-layer "splitting" with geomagnetic disturbances has been examined in some detail. The relationship between the frequency of occurrence of the "splitting" as observed during the period 1955-1957 and the K-index as reported by the Kodaikanal observatory is shown in Fig. 3 as a histogram. The figure shows a distinct dependence of frequency of occurrence on K-index with maximum occurring at  $k = 2$ .

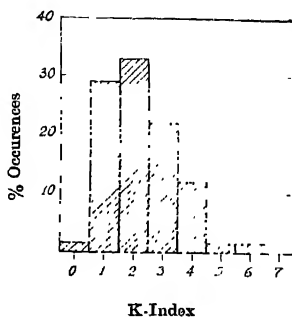


Fig. 3. Percentage occurrences of pre-sunrise F-layer "splitting" against K-index.

### ACKNOWLEDGMENT

The work is supported by a grant from the Council of Scientific and Industrial Research, Government of India and forms part of the programme of the Radio Research Committee. We are indebted to Professor J. N. Bhar for encouragement and advice.

## REFERENCES

- Bandyopadhyay, P., 1959, *J. Atmos. Terr. Phys.*, **16**, 84.  
Chandra, Sushil, Gibbons, J. J. and Schmerling, E. R., 1960, *J. Geophys. Res.*, **65**, 1159.  
Mitra, A. P., 1959, *J. Geophys. Res.*, **64**, 733.  
Munro, G. H., 1949, *Nature*, **163**, 812.  
Munro, G. H., 1953, *Proc. Roy. Soc., A*, **219**, 447.  
Munro, G. H. and Heisler, L. H., 1956, *Aust. J. Phys.*, **9**, 343.  
Schmerling, E. R., 1959, Ph. D. Thesis, Cambridge, Univ.  
Schmerling, E. R. and Ventrice, C. A., 1959, *J. Atmos. Terr. Phys.*, **14**, 249.



# NUMBER OF $N_2^+$ , $N^+$ , $N^{++}$ AND $O_2^+$ , $O^+$ , $O^{++}$ IONS PRODUCED BY SOLAR PROTONS IN THE EARTH'S ATMOSPHERE

S. N. GHOSH AND B. N. SRIVASTAVA

J. K. INSTITUTE OF APPLIED PHYSICS, UNIVERSITY OF ALLAHABAD, ALLAHABAD

(Received May 27, 1961)

**ABSTRACT** In this paper, the total number of nitrogen and oxygen ions ( $N_2^+$ ,  $N^+$ ,  $N^{++}$  and  $O_2^+$ ,  $O^+$ ,  $O^{++}$ ) formed by solar protons of initial energies 57 and 100 KeV between the altitude 130 km and that for complete absorption (112 km for 57 KeV and 106 km for 100 KeV) has been estimated. As these protons penetrate through the atmosphere, they undergo different inelastic collisions with atmospheric gases, e.g. charge exchange, ionization, dissociation followed by ionization etc. For calculating the ion formations, laboratory measurements of cross-sections for different inelastic reaction collision for reactions ( $H^+$ ,  $N_2$ ) and ( $H^+$ ,  $O_2$ ) are utilized. Probability curves for different types of nitrogen and oxygen ion formations at different altitudes between the range 125–105 km by 57 and 100 KeV protons have also been drawn.

## INTRODUCTION

It is well-known that at least a part of auroral spectra is excited by bombardments of upper atmospheric gases by solar protons. As these protons penetrate through the atmosphere, they undergo inelastic collisions with atmospheric gases leading in certain cases to the excitations of atmospheric gases. Il'in, Afrosimov and Fedorenko (1959) obtained separately the cross-sections for the production of  $N_2^+$ ,  $N^+$ ,  $N^{++}$ ,  $O_2^+$ ,  $O^{++}$  and  $O^+$  by 10-180 KeV proton bombardments of air,  $N_2$  and  $O_2$ . From these measurements, the relative importance of different inelastic processes, e.g., charge exchange, ionization, ionization followed by dissociation etc. are obtained and the number of oxygen and nitrogen ions produced by solar protons in the atmosphere has been estimated. The results obtained in this paper can be utilized in elucidating the excitation mechanism of auroral spectra.

## ENERGY OF SOLAR PROTONS AT DIFFERENT ALTITUDES

It has been established from Doppler shift of  $H_\alpha$  lines that solar protons have 57 KeV or more energy (Kuiper, 1954). Recent rocket-borne experiments (McIlwain, 1960) have shown that protons have wide velocity spectrum.

To determine the heights up to which a proton beam of initial energies 57 and 100 KeV can penetrate, one has to know their range in air. Bates and Griffing

(1953) and Vegard (1952) collected data for the range of protons in air at S.T.P., and determined the equivalent path lengths of atmosphere reduced to air at S.T.P. for different altitudes. For the penetration of protons, we have assumed Vegard's value for equivalent path length of the atmosphere at S.T.P. The range of protons of velocity  $v$  cm/sec in air was calculated from the relation given by him namely,

$$R_a = 10^{-27} v^3 \text{ cm} \quad (1)$$

Therefore,

$$v_o^3 - v_x^3 = 10^{27} x \quad (2)$$

where  $v_x$  is the velocity of protons after it has penetrated through a path length (equivalent)  $x$  cm at S.T.P. and  $v_o$  is the original velocity of protons.

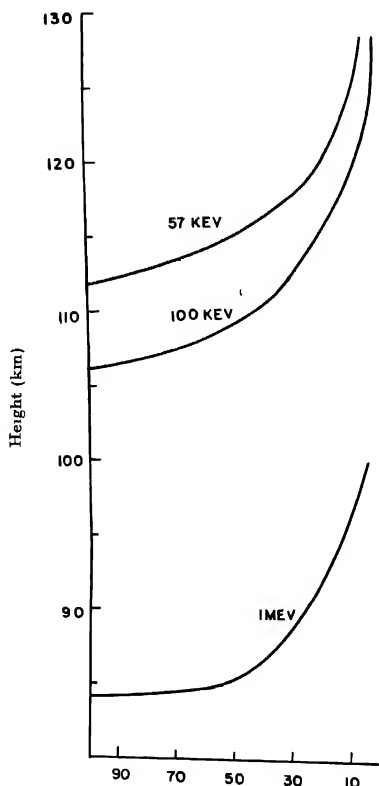


Fig. 1. Percentage reduction of proton energy having energies 57 KeV, 100 KeV and 1 MeV outside the earth's atmosphere, as they penetrate through the atmosphere.

From the relation (2) and the equivalent path lengths of air for different altitudes, curves are drawn for the percentage energy reduction as protons of initial energies of 57 KeV, 100 KeV and 1 MeV penetrate through the atmosphere and are shown in Fig. 1. It is apparent from these curves that protons are heavily attenuated in a small layer of the atmosphere just before they are completely absorbed (112 km for 57 KeV, 106 km for 100 KeV and 84 km for 1 MeV.)

#### ION FORMATIONS AT DIFFERENT ALTITUDES

Recently Il'in *et al.* (1959) obtained the total cross-sections (sum of charge exchange and ionization cross-sections) for the production of  $N_2^+$  and  $O_2^+$  by bombardments of  $N_2$  and  $O_2$  by protons. The difference of these values from the charge exchange cross-sections of reactions ( $H^+$ ,  $N_2$ ) and ( $H^+$ ,  $O_2$ ) obtained by Stier and Barnett, (1956) the ionization cross-sections for reaction ( $H^+$ ,  $N_2$ ) and ( $H^+$ ,  $O_2$ ) are obtained. The energy versus cross-sections for charge exchange, ionization, ionization followed by dissociation for reaction ( $H^+$ ,  $N_2$ ) and ( $H^+$ ,  $O_2$ )

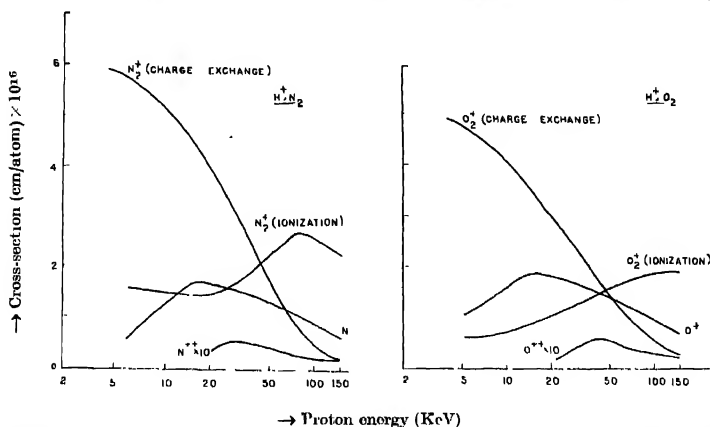


Fig. 2. Illustrating the variations of inelastic collisions for the reactions ( $H^+$ ,  $N_2$ ) and ( $H^+$ ,  $O_2$ ) with energy.

are shown in Fig. 2. From this figure, the probabilities of formation of nitrogen and oxygen ions in the earth's atmosphere between the altitude range 105-125 km by bombardments of protons having initial energies 57 and 100 KeV are calculated. (As ionization cross-sections for reactions ( $H^+$ ,  $N_2$ ) and ( $H^+$ ,  $O_2$ ) are not available, calculations for ion formation by 1 MeV proton bombardments are not undertaken.) In these calculations the distribution of atmospheric constituents given by Miller<sup>7</sup> has been assumed. Applying the relation,

$$\text{Probability} = QN \quad (3)$$

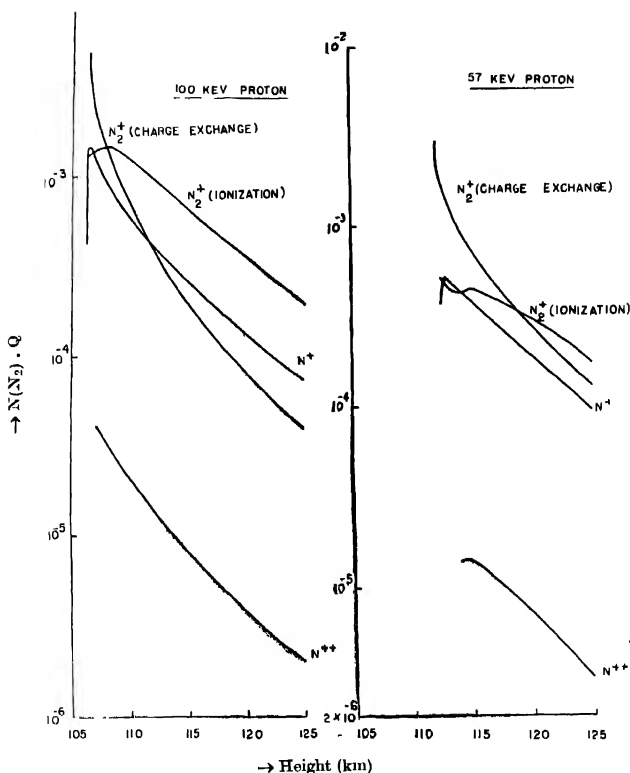


Fig. 3. Probabilities of nitrogen ion formations in the earth's atmosphere between altitude range 105–125 km by bombardments of protons of initial energies 57 and 100 KeV.

where  $Q$  is the cross-sections for the different processes for protons of different energies and  $N$  is the particle density of  $N_2$  or  $O_2$ , the probabilities of formations of  $N_2^+$ ,  $O_2^+$  due to charge exchange and ionization and also of  $N^+$ ,  $N^{4+}$ ,  $O^+$  and  $O^{1+}$  have been calculated for altitude range 105–125 km. These are shown in Figs. 3–4.

#### TOTAL NUMBER OF ION FORMED IN THE EARTH'S ATMOSPHERE

As the energy of protons decreases from  $E_0$  to  $E$ , the number of ions formed is given by (Allison, 1958)

$$N_r = L \int_{\underline{E}}^E Q \left| \frac{dE}{dx} \right| dE \quad \dots (4)$$

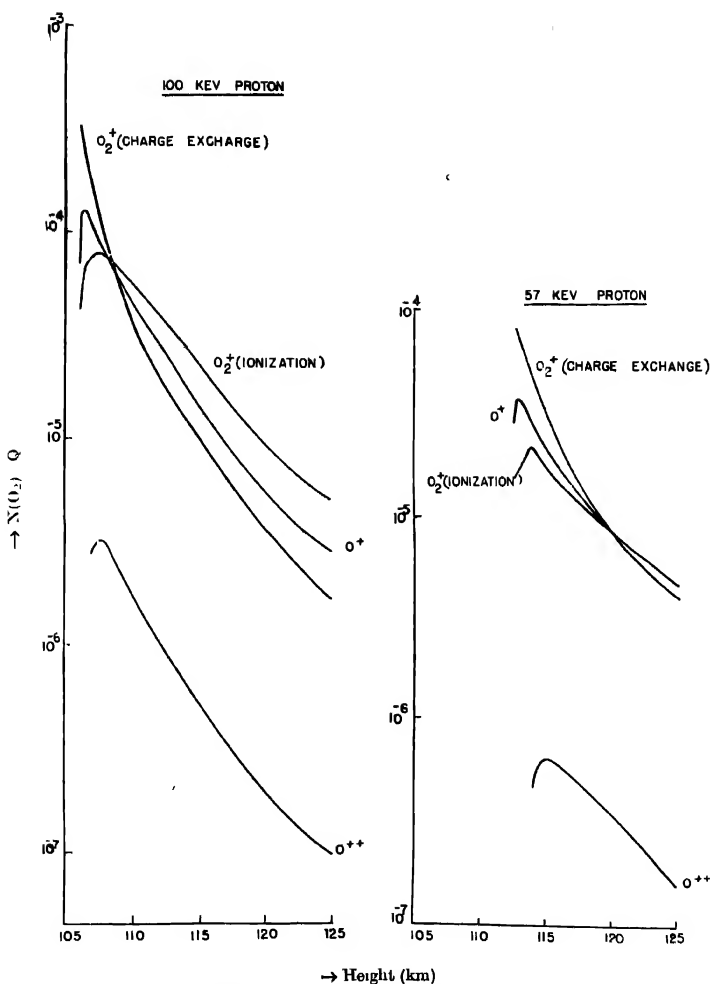


Fig. 4. Probabilities of oxygen ion formations in the earth's atmosphere between altitude range 105–125 km by bombardments of protons of initial energies 57 and 100 KeV.

where,

$N_o$ —number of ions formed

$L$ —Avogadro number

$\xi$ —number of atoms in a molecule

$Q$ —cross-section in  $\text{cm}^2/\text{atom}$  for different processes

$\frac{dE}{dx}$ —stopping power in  $\text{KeV}/\text{cm}$  at N.T.P.

For calculating ion formations, the charge exchange cross section is taken to be  $\frac{\sigma_{01}}{\sigma_{10} + \sigma_{01}}$ , where  $\sigma_{01}$  and  $\sigma_{01}$  are cross-sections for electron capture and electron loss respectively. (A charge exchange process occurs in a close cycle, because the bombarding ion is first neutralized and afterwards on colliding with gas molecule becomes ionized and the process continues.) The values of  $\sigma_{10}$  and  $\sigma_{01}$  for reactions ( $\text{H}^+$ ,  $\text{N}_2$ ) and ( $\text{H}^+$ ,  $\text{O}_2$ ) are taken from data collected by Allison (1958). For the formation of molecular ions due to ionization, and singly and doubly ionized atomic ions due to dissociation followed by ionization, the cross-sections for different processes given by H'in *et al.* (1959) were used. The values of stopping power ( $dE/dx$ ) of  $\text{N}_2$  and  $\text{O}_2$  gases for protons are obtained from the work of Phil-

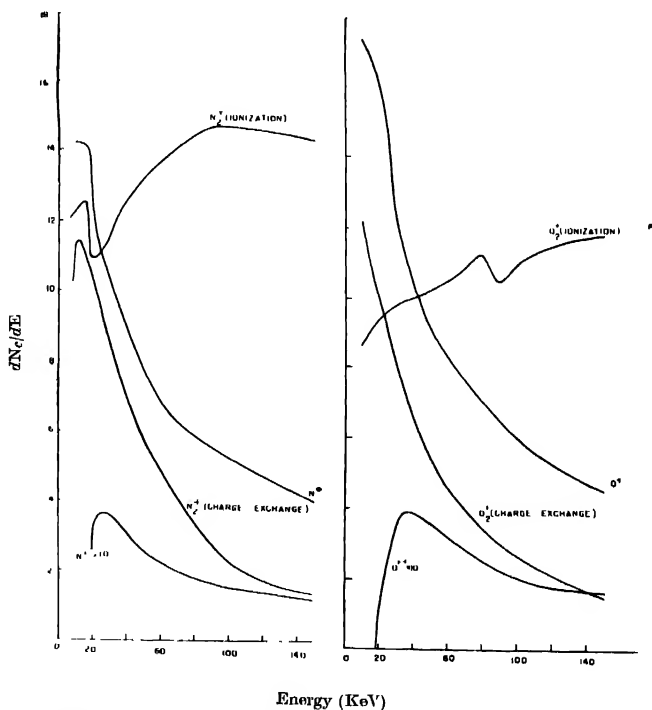


Fig. 5. Total number of different ions formed per KeV energy loss, as protons pass through  $\text{N}_2$  and  $\text{O}_2$  gases.

lips (1953) and the data collected by Allison and Warshaw (1953). Curves are drawn relating to the energy and the number of ions formed per Kev energy loss and are shown in Fig. 5. From the integration of these curves, the total number of ion formations can be obtained. Table I shows the number of ions formed by various processes as protons of initial energies 57 and 100 Kev are slowed down to 10 KeV in nitrogen and oxygen gases separately.

Miller's (1957) table for atmospheric constituents shows that the number of  $N_2$  molecules is 2/3 of the total number of particles at altitudes between 100–130 km, while for  $O_2$  the proportions are 2.6%, 3%, 4%, and 9% at altitudes 130, 120, 110, and 100 km respectively. Therefore, if solar protons of initial energies 57 and 100 Kev are slowed down to 10 KeV while passing through the earth's atmosphere, the total number of ion formations of  $N_2^+$ ,  $N^+$ ,  $N^{++}$  can be taken as 2/3 of the value given in Table I for protons passing through  $N_2$  gas. The formations of  $O_2^+$ ,  $O^+$ ,  $O^{++}$  ions by 100 KeV proton can be assumed approximately 8% and for 57 KeV about 3% of the values given in Table I for protons in  $O_2$  gas.

TABLE I  
Number of nitrogen and oxygen ions in  $N_2$  and  $O_2$  gases

Proton energy (KeV)	Bombarded gas	Number of ions formed by charge exchange	Number of ions formed by ionization	Number of ions formed by dissociation followed by ionization*	
100	$N_2$	540 ( $N_2^+$ )	1186 ( $N^+$ )	942 ( $N^+$ )	19 ( $N^{++}$ )
57	$N_2$	384 ( $N_2^+$ )	576 ( $N^+$ )	485 ( $N^+$ )	11 ( $N^{++}$ )
100	$O_2$	532 ( $O_2^+$ )	917 ( $O^+$ )	895 ( $O^+$ )	24 ( $O^{++}$ )
57	$O_2$	375 ( $O_2^+$ )	455 ( $O^+$ )	589 ( $O^+$ )	13 ( $O^{++}$ )

\*The formation of doubly-ionized ions is not observed when proton energy is below 20 KeV.

TABLE II  
Number of nitrogen and oxygen ions in the earth's atmosphere

Proton energy (KeV)	Number of ions formed by charge exchange		Number of ions formed by ionization		Number of ions formed by dissociation followed by ionization			
	$N_2^+$	$O_2^+$	$N^+$	$O^+$	$N^+$	$O^+$	$N^{++}$	$O^{++}$
100	360	43	796	73	628	72	13	2
57	256	11	384	14	323	18	7	1

Assuming that the atmosphere is a mixture of  $N_2$  and  $O_2$  molecules, (Miller, 1957) the number of ions formed by solar protons of initial energies 57 and 100 Kev between the altitude ranges 130 Km to the altitudes for complete absorption is given in Table 2.

## R E F E R E N C E S

- Allison, S. K. and Warshaw, S. D., 1953, *Rev. Mod. Phys.* **25**, 779.  
 Allison, S. K., 1958, *Rev. Mod. Phys.*, **30**, 1137.  
 Bates, D. R. and Griffing, G., 1953, *J. Atmos. Terr. Phys.*, **3**, 212.  
 G. P. Kuiper, The Earth as a Planet Edited by University of Chicago press, Chicago, 1954), p. 529.  
 Il'm, R. N., Afrosimov, V. V. and Fedorenko, N. V., 1959, *Soviet Physics JETP*, **36**, 29.  
 McIlwain, C. E., 1960, *J. Geophys. Res.*, **65**, 2727.  
 Miller, L. E., 1957, *J. Geophys. Res.*, **62**, 351.  
 Phillips, J. A., 1953, *Phys. Rev.*, **90**, 532.  
 Sten, P. M. and Barnett, C. F., 1956, *Phys. Rev.*, **103**, 896.  
 Vegard, J., 1952 Geo. Phys. Publications, (Oslo) **18**, No. 5.



# FLUXMETER STUDIES OF SLOW ELECTRIC FIELD-CHANGES DUE TO MOVING THUNDER CLOUDS

S. R. KHASTGIR

UNIVERSITY OF CALCUTTA

AND

R. S. SRIVASTAVA

BANARAS HINDU UNIVERSITY

(Received September 5, 1961)

**ABSTRACT.** An electrostatic fluxmeter similar to the one developed by Malan and Schonland (1950) was constructed and used for the study of slow electric field-changes due to nearby thunderclouds. The principle and the constructional details of the instrument are given. The fluxmeter experiments gave the following results:

- (i) The initial electric field due to thundercloud was more often negative than positive.
- (ii) There was a steady decrease of the negative field with time. Sometimes the decrease was slow and showed minor variations.
- (iii) The negative field was sometimes found to increase to an optimum value which was followed by a continuous decrease.
- (iv) The positive field, in many cases, was found to increase attaining an optimum value, after which it was found to decrease passing through zero to a negative value which after attaining an optimum value was found to decrease steadily with time.

In many observations the electric field-changes are shown to be due to the movement of a *negative* cloud or of a *bi-polar* cloud. The effect of the negative charge extending over a very wide region in the cloud has been evident in a number of observations. The minor abrupt changes have been attributed to changes in the charge distribution and to occasional local discharges within the thundercloud.

## INTRODUCTION

An electrostatic fluxmeter similar to the one designed by Malan and Schonland (1950) was constructed and used for measuring the electric field and its slow changes due to the moving thunder clouds. The fluxmeter consisted of a conducting system of small capacity connected to earth through a resistance and was alternatively exposed to and screened from the electric field due to a thundercloud by the movement of a rapidly rotating earthed metal plate. The conditions under which the rotation was performed produced an alternating potential difference across the resistance, the amplitude of the potential difference being proportional to the thundercloud field. This potential difference was suitably amplified and applied to the Y-deflector plates of a cathode-ray tube. The wave-pattern on the fluorescent screen was recorded photographically in a drum-

film-camera rotating about a vertical axis. The amplitude of the envelope of the crests and troughs on this record was proportional to the field strength due to the thundercloud. There was a device in the instrument similar to that in the fluxmeter of Malan and Schonland to indicate the *sense* of the field.

#### WORKING PRINCIPLE OF THE FLUXMETER

The underlying principle of the fluxmeter may be understood by considering Fig. 1. In this circuit the capacity  $C_1$  represents a fixed capacity of the system

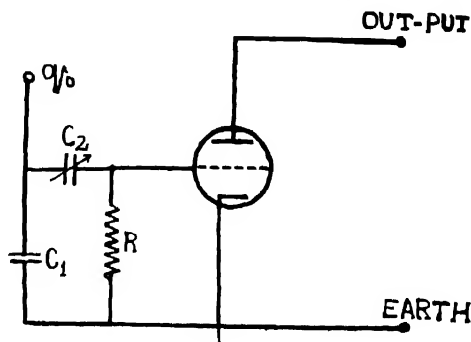


Fig. 1. The circuit adopted for determining the static charge by measuring the amplitude of the alternating potential across the resistance  $R$ .

upon which is placed initially an unknown charge  $q_0$ . The capacity of the condenser  $C_2$  is made periodic by a mechanical device and takes on values between 0 and  $C_2$  varying in a periodic manner. If at time  $t = 0$ , we take  $C_2 = 0$  and the instantaneous charge  $q_1$  on  $C_1$  is taken as equal to the initial charge  $q_0$  on  $C_1$ , then the equation giving the potential difference across different elements at any instant can be written as

$$\frac{q_0}{C_1} - Ri - \frac{C_1 + C_2}{C_1 C_2} \int i dt = 0$$

where  $i$  is the current through the circuit. The potential  $E$  applied to the grid of the vacuum tube is then given by

$$E = Ri = \frac{q_0}{C_1} - \frac{C_1 + C_2}{C_1 C_2} \int i dt \quad \dots (1)$$

Since the instantaneous charge on  $C_1$  is given by

$$q_1 = q_0 - \int i dt$$

we can write

$$E = \frac{q_0}{C_2} \left[ \frac{C_1 + C_2}{C_1} - 1 \right] \quad (2)$$

It is evident from Eq. (2) that in the steady state  $E$  is zero but as  $C_2$  changes periodically as the result of the mechanical arrangement,  $E$  becomes finite and periodic with  $C_2$ . We can however see without analysis that the potential  $E$  across  $R$  increases as  $i \left( = \frac{dq}{dt} \right)$  increases and therefore at low frequencies  $E$  is approximately proportional to the frequency of the variation of  $C_2$ . Thus the net result of interchange of charge between the two condensers,  $C_1$  and  $C_2$ , of which  $C_2$  varies periodically, is an alternating potential across  $R$  of frequency equal to that of the variation of  $C_2$  and of amplitude proportional to the original static charge.

The circuit shown in Fig. 1 can therefore be adopted for the measurement of static charge by simply measuring the amplitude of the alternating potential-difference across the resistance. Since the generated potential is alternating, it can be readily amplified by a vacuum-tube amplifier and thus the sensitivity can be controlled to any desired level.

When the frequency of variation of the capacity of the condenser  $C_2$  approaches the relaxation frequency of the circuit, the condenser systems have insufficient time to completely charge and discharge and therefore  $E$  drops. In general, the maximum  $E$ , for a given applied charge  $q_0$ , occurs when the frequency of the changes in  $C_2$  is slightly less than the effective relaxation frequency of the circuit given by

$$f_r = \frac{1}{2 \sqrt{C_1 C_2}} \dots \quad (2a)$$

where  $C_2$  is the mean value of the periodically varying capacity of the condenser  $C_2$ . This requirement with regard to the driving frequency is not of much importance and needs only to be considered when maximum sensitivity is required.

#### CONSTRUCTIONAL DETAILS

The constructional details of the instrument is shown in Fig. 2. The conducting system was formed by 18 metal studs mounted on an ebonite disc  $B$ . These studs, two of which are visible in the diagram, were constructed from a brass rod of diameter 8 mm and were set in a circle of diameter 30 cm. They were connected together underneath the ebonite disc and were joined to the control grid of a low-capacity triode valve. This disc was mounted inside cylindrical aluminium box  $C$ . The output of the valve was taken from the cathode by

shielded cable to the cathode-ray oscillograph in the recording room for further amplification and display.

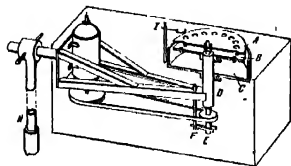


Fig. 2. The constructional details of the fluxmeter. (Reproduced from Malan and Schonland).

The capacity of the stud-grid system was 80pF. The screening disc *A* was made of a brass sheet of 2mm thickness and 33 cm in diameter. It had 18 equally spaced holes of diameter 2.0 cm whose centres lay immediately above the centres of the studs. The spacing between the screening disc and the studs could be adjusted by moving the screening disc up or down after loosening its clamping screws and was usually 2 mm. The screening disc was rotated at the rate of 3000 rpm by a shaft mounted on ball bearings and carrying a pulley which was driven by a suitable A.C. motor.

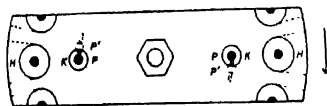


Fig. 3. The plan-view of a portion of the rotating disc *A* above and the ebonite disc *B* below. (Reproduced from Malan and Schonland).

The aluminium box was mounted on the cylindrical ball-bearing container by means of a collar and clamping screws. It was possible to reach the valve without dismantling the two discs by loosening the screws and moving it downward. The framework supporting the device was built of angle-iron with welded joints and carried on a horizontal pipe which was fixed on the boundary wall of the roof of the observation room.

The whole frame work was enclosed in a rectangular earthed aluminium case with the top side open. When it was necessary to run the instrument in rain, it was inverted and in this case the screening disc was below the ebonite disc. However, in the inverted position the sensitivity of the instrument was much less than in the upward position and so it was very seldom used in this position.

An essential part of the equipment was the earthing brush which consisted of a phosphor-bronze springy fork pressing the rotating shaft between them.

The surface of contact of the shaft was periodically cleaned and slightly oiled to ensure a good contact.

The purpose of this brush was to transfer the frictional charges which collected in an irregular manner on the screening disc as a result of its rotation and of the belt drive. The brush and the whole frame work were connected to earth. Unless this earthing was very good, the noise level due to these frictional charges was too high.

In order to obtain a low grid-capacity and low microphonic effects, a Mullard valve EF37A pentode (connected as triode) was used as an amplifier. As an extra precaution, it was suspended on rubber gromets. The valve was used as a cathode-follower and the output was taken from the cathode through a shielded cable and passed to the recording room for further amplification. The H/T and the heater supplies for the valve were also provided through shielded wires from the recording room and thus the whole apparatus could be operated from a distance. Further amplification was obtained by the Y-deflector plate amplifiers of the Cossor Model 1035 oscillograph unit which was used to display the final output.

#### METHOD OF RECORDING

For recording the field-changes due to moving thunderclouds and lightning flashes, a square-wave trigger unit similar to the one used in the Automatic Atmospherics Recorder of Tantry (1958) was used. For recording the photographs, a drum-camera was used with a peripheral velocity of 52 cm/sec. The time-base of the oscillograph was not used and the output on the tube screen was seen as a vertical line which was screened off by a thin strip of black paper. The trigger unit was expected to be operated by the initial slow field-change of a lightning discharge and would thus produce a square-wave of *quasi*-period of about 1 sec. The output of this trigger unit was connected directly to the X-deflector plate of the oscillograph which moved the whole vertical line from behind the screening paper strip and kept on in this position for one second allowing the vertical line to be photographed by the moving drum-camera. Thus the field-changes taking place during this one second due to the flush could be recorded.

#### SENSE-INDICATING DEVICE

In order to show the polarity of the electric field, the strength of which was measured by the envelope of the amplitudes of the sinuous pattern, the device in the fluxmeter of Malan and Schonland was incorporated in the instrument. This automatically increased the height of the crest of the pattern every ninth cycle, if the field was negative and the depth of the trough every ninth cycle, if it was positive. An inspection of the record thus immediately gave the required polarity of the field.

The principle of the polarity-indicator can be understood with the help of Fig. 3 which is the plan-view of a portion of the rotating disc *A* above and the ebonite disc *B* below (as shown in Fig. 2). The plan-view shows the stud-hole combination of the fixed ebonite and the rotating brass discs. *HH* represent the exposure holes in the rotating disc *A* with the studs of the disc *B* momentarily below their centres. Two more holes *KK* of diameter 1.8 cm were placed in the positions shown. Below each of these two holes were two extra studs *PP'* fitted in the two slots in the ebonite disc *B*. These four studs were joined by wire to the main studs. The phase of their contribution to the output could be adjusted by moving them in their slots.

When the disc was rotated in the direction of the arrow, a position would come when the leading edges of the holes *K* and *H* would uncover the peripheral studs and the studs *P* simultaneously, thus increasing the output by the amount contributed by *P*. In the absence of studs *P*, both the crests and troughs would increase in amplitude in this position. However, immediately after this position, the studs *P'* would get exposed, while all the other studs would be screened off, so that the contribution by the studs *P'* would be opposite in sense to that of the other studs *P*. By the adjustment of the position of the *P'* studs, it was possible to neutralize the contribution of the *P* studs during the half-cycle when they were exposed.

#### CALIBRATION OF THE INSTRUMENT

The instrument was calibrated with the help of a circular disc of galvanized iron of diameter 45 cm and maintaining it at a constant potential-difference with respect to the earth over the screening disc, such that the centres of the two were in the same vertical line. The distance between the ebonite and the galvanized discs was varied and the resulting variation in the amplitude of the wave-pattern was measured. A curve showing the distance of the galvanized sheet from the ebonite disc and the amplitude was drawn. This curve was used for measuring any unknown field produced by the thunderclouds. The calibration graph is shown in Fig. 4.

#### SENSITIVITY AND PERFORMANCE

The instrument used by us gave a peak amplitude of 1 cm. in a field of 50 V/m at the maximum amplification and thus could easily indicate the electric field of fine weather which was of the order of 80 V/m. The noise level in the laboratory was about 2 mm. at the maximum amplification. The trigger circuit could easily be operated by lightning flashes at distances of 10 km or less. During the rain when the arrangement was inverted, it gave 1/5th of the above sensitivity, when the rotating disc was one metre from the boundary wall in the horizontal direction and one meter above the ground.

Sometimes, the electric fields of nearby thunderstorms were so large as to require reduction of the amplification, so that the deflection in the oscillograph

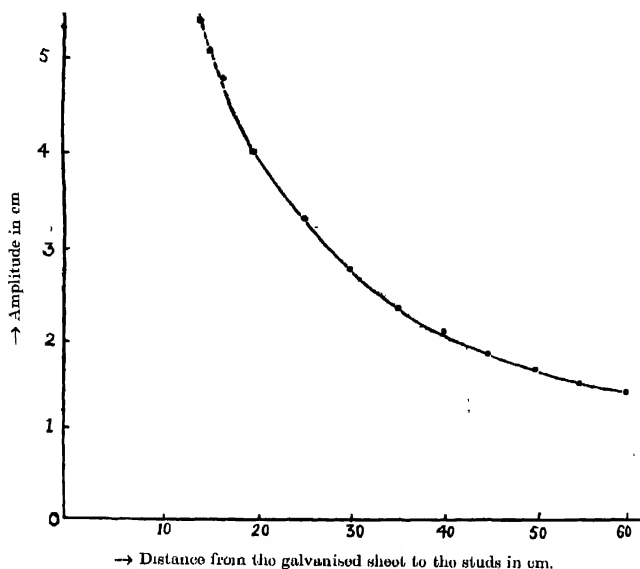


Fig. 4. The calibration graph showing the electric field for various distances between the ebonite disc and the galvanised disc.

was not to go "off-scale". This was easily done by the adjustment of the stepped attenuator of the oscillograph unit.

#### THE RESPONSE TIME OF THE INSTRUMENT

Consider a charge  $+Q$  induced on the upper surface of condenser system by the electric field  $E$ . Since  $E = \frac{4\pi\sigma}{K}$ , where  $\sigma$  is the surface density of charge on the condenser surface and is equal to  $Q/A$  ( $A$  being the effective area of the system, and  $K$  the site-correcting factor), we have

$$E = \frac{4\pi}{K} \cdot \frac{Q}{A} \quad \dots (3)$$

Any sudden change  $\Delta E$  in the electric field-strength must produce a change  $-\Delta Q$  in the charge on the upper surface of the system, so that

$$-\Delta Q = -\frac{KA}{4\pi} \cdot \Delta E \quad \dots (4)$$

A corresponding opposite charge  $-dQ$  must appear on the lower surface. If the field-change occurred during an exposure interval, the response of a device of this kind would be instantaneous. However, it was possible to show that the final steady value of the amplitude was less than the initial response and that a certain time-interval was needed to reach this steady value.

#### EXPERIMENTAL RESULTS

The sense-indicating device showed the polarity of the electric field due to thunderclouds. In the case of negative field, the height of the crest of the sinuous pattern was found to increase after every ninth cycle, while in the case of positive field the depth of the trough was found to increase every ninth cycle. A typical fluxmeter record showing positive electric field is shown in Fig. 5. The magnitude of the electric field was obtained by measuring the amplitude of the envelope of the sinuous wave pattern.



Fig. 5. A typical fluxmeter record

The following experimental results were obtained from the fluxmeter records.

- (i) The initial electric field due to thunderclouds was more often negative than positive.
- (ii) There was a steady decrease of the negative field with time. Sometimes the decrease was slow and indicated minor variations.
- (iii) The negative field was sometimes found to increase to an optimum value which was followed by a continuous decrease.
- (iv) The positive field in many cases was found to increase attaining an optimum value, after which it was found to decrease passing through zero to a negative value which after attaining an optimum value was found to decrease steadily with time.

A steady decrease of the negative field with time is shown in Fig. 6. A slow decrease of the negative field with minor variations is shown in Figs. 7(a) and (b). A gradual increase of the negative field to an optimum value, followed by a continuous decrease is illustrated in Fig. 8. Figs 9-10 illustrate electric field-variations, where the positive field was found to increase to an optimum value after which it was found to decrease passing through zero to a negative value



which after attaining an optimum value was found to decrease steadily with time.

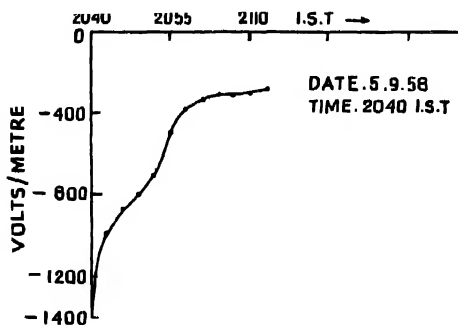


Fig. 6. Steady decrease of the negative field with time.

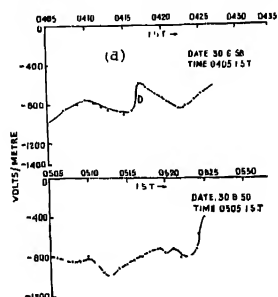


Fig. 7. Slow decrease of the negative field with minor variations

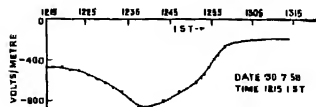


Fig. 8. Gradual increase of the negative field to an optimum value followed by a continuous decrease.

#### INTERPRETATIONS OF THE OBSERVED SLOW FIELD-VARIATIONS WITH TIME

We shall consider here the possible types of charge-distribution in a thunder-cloud :

- (i) The thunder cloud may be negatively charged.

- (ii) The thundercloud may be bipolar with a positive charge at the top and negative charge below.
- (iii) There may be a pocket of positive charge at the base of the cloud just below a doublet with positive charge at the top and with negative charge below.

The pocket of positive charge at the base of the cloud was first observed by Simpson (1926) and by Simpson and Scrase (1937). The subsequent photographic and electrical observations by Malan (1952, 1954) in South Africa confirmed the frequent existence of a pocket of positive charge at the base of a thundercloud. His statistical studies of the electric fields showed that the average value of the lower positive charge was about +10 Coulombs, the charges higher up in the cloud being respectively -40 and +40 Coulombs. The average heights of the lower positive charge, the negative charge and the higher positive charge were taken as 2.5 km, 5.0 km. and 10 km. respectively. Accepting the numerical values given by Malan, we have calculated the values of the electric field at different distances measured from the point of projection on the ground of the cloud charge or charges.

For the sake of calculation, we have used the following expressions for the electric field due to thundercloud at a distance  $r$  on the ground from the point of projection of the cloud charge or charges.

$$(i) \quad E = - \frac{2q_2 h_2}{(h_2^2 + r^2)^{3/2}} \quad \dots (5)$$

in the case of a simple negative cloud of charge  $-q_2$  at a height  $h_2$  from the ground.

$$(ii) \quad E = \frac{2q_1 h_1}{(h_1^2 + r^2)^{3/2}} - \frac{2q_2 h_2}{(h_2^2 + r^2)^{3/2}} \quad \dots (6)$$

in the case of a bipolar cloud where the positive and the negative charges are  $+q_1$  and  $-q_2$  at heights  $h_1$  and  $h_2$  from the ground respectively. Here the magnitude of the positive charge  $q_1$  is taken equal to that of the negative charge  $-q_2$ .

$$(iii) \quad E = \frac{2q_1 h_1}{(h_1^2 + r^2)^{3/2}} - \frac{2q_2 h_2}{(h_2^2 + r^2)^{3/2}} + \frac{2q_3 h_3}{(h_3^2 + r^2)^{3/2}} \quad \dots (7)$$

in the case of a system of charges  $+q_1$ ,  $-q_2$  and  $+q_3$  on the cloud at heights of  $h_1$ ,  $h_2$  and  $h_3$  respectively in the same vertical line.

The variations of the electric field  $E$  with distance  $r$  with the three possible charge-distributions on the cloud are shown in Figs. 11(a), (b) and (c). It can be seen from Fig. 11(a) that in the case of a simple negative cloud, the field at the point immediately under the cloud is negative and the negative field decreases with the increase of  $r$  tending to a zero value. In the case of a bipolar cloud, as is evident from Fig. 11(b), the field underneath the bipolar cloud is negative

and the negative field decreases with the increase of  $r$  to the zero value at some critical distance  $r_c$  and becomes positive and remains positive as the distance

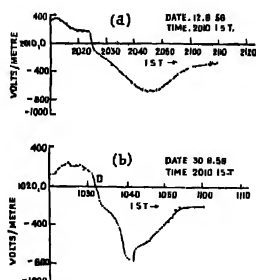


Fig. 9.

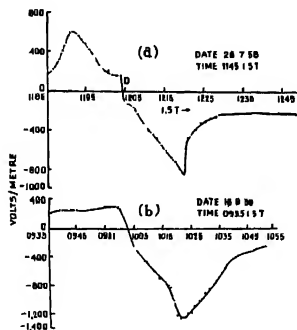


Fig. 10.

Figs. 9. & 10 The electric field variations where the positive field was found to increase to an optimum value after which it was found to decrease passing through zero to a negative value which after attaining an optimum value was found to decrease steadily with time

increases. In the case of a lower positive charge under the doublet, it can be seen from Fig. 11(c) that the electric field just under the system of charges in the cloud, situated one above another in a vertical line, has a positive value which decreases steadily with distance to zero, becomes increasingly negative and attains an optimum value, the negative field decreasing once again to zero and attaining positive values with further increase of the distance.

The steady decrease of the negative field with time, shown in Fig. 6 can be explained as due to the drift of a simple negative cloud from above the observa-

tion centre, as is evident from the curve shown in Fig. 11(a). The gradual decrease of the negative field to an optimum value followed by a continuous decrease can also be attributed to the drift of a simple negative cloud. If we assume that a negative cloud approaches the observation centre, it is expected that the negative electric field will increase steadily and attain an optimum value when the cloud comes just above the observation centre. As the cloud recedes further and further, it is also expected that the negative field will decrease steadily tending to the zero value. Such expected variation of the electric field with distance is similar to the observed variation of electric field with time shown in Fig. 8.

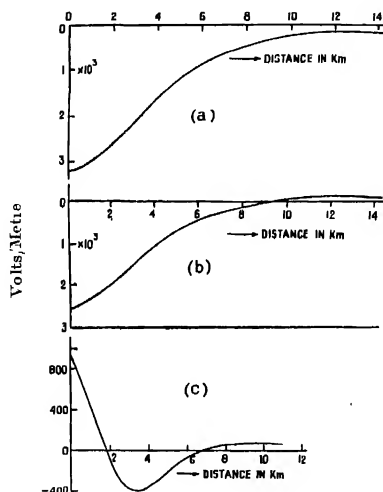


Fig. 11. The expected variations of the electric field with distance with the three possible charge-distributions on the cloud.

The electric field variations shown in Figs. 9 (a, b) and 10 (a, b) can be explained as due to the movement of a cloud, where there is a system of charges,  $+q_1$ ,  $-q_2$  and  $+q_3$ , one above another in a vertical line. If such a cloud approaches the observation centre, it is evident that the positive field will increase and attain a maximum value when the cloud comes just above the fluxmeter. As the cloud recedes further and further, the field variation with distance will be as shown in Fig. 11(c). The observed variations of the electric field with time, illustrated in Figs. 9-10 can therefore be explained with reference to the computed curves shown in Fig. 11(c). There is however a significant difference between the expected and the observed electric field variations. The expected variation shown in Fig. 11(c)

indicates that when the cloud moves away to a great distance, the field should attain once again a positive field. It can be seen from the observed field-variations shown in Figs. 9 and 10, that the final value of the electric field never reached a zero value and was always negative. This significant feature in the observed field-variations was most likely due to the effect of negative charge  $-q_2$ , distributed over an extended region in the cloud. In the theoretical formula (7) the charges  $+q_1$ ,  $-q_2$  and  $+q_3$  were considered as localised and situated one above another in a vertical line. Actually however, the charge  $-q_2$  is not localised in a particular region but extends over a wide expanse in a thundercloud. The pocket of positive charge,  $+q_3$ , at the base of the cloud is more or less localised. The higher positive charge,  $+q_1$  is also not as extensive as the charge  $-q_2$ .

The decrease of the negative field with time (attended at times with minor variations) shown in Figs. 7(a) and (b) was often observed. The decrease of the negative field with time could also be due to the movement of a bipolar cloud away from the observation centre. It is to be noted that final value of the observed electric field was always negative, and the positive field for the larger values of  $r$ , as expected from the formula (6) in the case of a bipolar cloud was never observed. This cannot be taken to mean that there were no bipolar clouds during our observations. We are however inclined to the view that the expected positive field at large distances in the case of a bipolar cloud is masked by the effect of the negative charge,  $-q_2$ , which is not localised but is distributed over an extended region in the cloud.

The minor changes in the observed electric field due to a moving thundercloud are likely to be due to changes in the charge distribution in the cloud and occasionally due to the local discharges within the cloud. The sudden drops in the electric field due to local discharges are marked 'D' in the curves showing the observed electric field-variations with time.

## CONCLUSIONS

The fluxmeter observations of the electric field due to thundercloud have been explained as due to the movement of thunderclouds. The observed field-variations have confirmed the frequent existence of a pocket of positive charge at the base in addition to the usual doublet in a thundercloud. In many cases, the field-variation with time was due to the movement of a simple negative cloud or to a bipolar cloud. The effect of the negative charge  $-q_2$ , extending over a very wide region was clearly evident in many of the observed field-variations. The minor field changes observed were attributed to changes in the charge-distribution and to occasional local discharges in the cloud which were distinctly visible.

## REFERENCES

- Mulan, D. J. 1952, *Ann. des Geophysique*, **8**, 1.  
Mulan, D. J. 1954, *Ann. des Geophysique*, **10**, 1.  
Mulan, D. J. and Schonland, B. F. J. 1950, *Proc. Phys. Soc. (London)* **63-B**, 402.  
Simpson, G. C. 1926, *Proc. Roy. Soc. A* **111**, 56.  
Simpson, G. C. and Searso, F. J. 1937, *Proc. Roy. Soc. A* **161**, 309.  
Tantry, B. A. P. 1958, *Ind. J. Phys.*, **32**, 267.

# INFLUENCE OF ULTRAVIOLET ABSORPTION FREQUENCIES ON THE INTENSITIES OF RAMAN LINES\*

A. K. CHAKRABORTY

OPTICS DEPARTMENT,

INDIAN ASSOCIATION FOR THE CULTIVATION OF SCIENCE,

CALCUTTA-32.

(Received January, 25, 1962)

## Plate I

**ABSTRACT.** The intensities of the Raman line  $1348\text{ cm}^{-1}$  of the  $\text{NO}_2$  group in the solutions of four aromatic nitro compounds in chloroform have been compared quantitatively with the intensity of the line  $1215\text{ cm}^{-1}$  of chloroform from the Raman spectra of dilute solutions of the compounds of known strengths in chloroform. The observed relative intensities of the line due to the  $\text{NO}_2$  group in the different compounds have been compared with those indicated by the theories put forward by Placzek (1934) and Shorygin (1952). For this purpose the effective ultraviolet absorption frequencies have been determined by photographing the ultraviolet absorption spectra of the solutions.

It has been concluded that the results observed agree more with those indicated by Placzek's theory than with those calculated on Shorygin's theory. The cause for this discrepancy has been discussed.

## INTRODUCTION

It was first pointed out by Placzek (1934) that when the frequency  $\nu$  of the incident light is not much smaller than an absorption frequency  $\nu_{rk}$  of the irradiated molecule the intensity of the scattered radiation of frequency  $\nu - \nu_{rk}$  is given by the equation

$$I_R = C(\nu | \nu_{rk})^4 / (\nu_{rk} - \nu)^2 \quad (1)$$

where  $C$  is a constant for the excitation of a particular Raman frequency by a particular incident frequency  $\nu$ . When  $\nu$  is very nearly equal to  $\nu_{rk}$  a damping term  $\gamma_r = 1/4\pi\tau_r$  is introduced in the parenthesis in the denominator,  $\tau_r$  being the life time of the stationary state  $r$ . More recently, Shorygin (1952) put forward a theory of the resonance Raman effect under the simplifying conditions that (1) the molecules are in a non-degenerate electronic state, (2) they are oriented identically in space and (3) the interaction of spin with the incident magnetic

\*Communicated by Prof. S. C. Sarkar

field is absent. According to this theory, when a single absorption frequency  $\nu_{rk}$  is effective the intensity  $I_R$  of the Raman line is given by

$$I_R = C' \frac{4}{h^2} \frac{(\nu_{rk}^2 + \nu^2)^2}{(\nu_{rk}^2 - \nu^2)^4} \quad \dots (2)$$

Later, Rea (1960) discussed the implications of Shorygin's theory and pointed out that according to this theory the limiting value of  $\rho$ , the factor of depolarisation of the resonance Raman line should be 0.50 and he observed that the values of  $\rho$  for the line due to symmetric stretching vibration of the  $\text{NO}_2$  group in solutions of *p*-nitrophenol, *p*-nitroaniline and sodium *p*-nitrophenolate in certain solvents are 0.52, 0.54, 0.60 respectively. He concluded that these results supported Shorygin's theory.

It can be seen from equations (1) and (2) that the results expected from the two theories are quite different from each other and the correctness of the expressions for the intensities can be tested only by comparing quantitatively the intensities of the Raman lines of different compounds the frequencies of the nearest absorption bands of which are definitely known. For this purpose it is necessary to compare the intensity of the Raman line due to the compound in solution with a particular Raman line of the solvent which lies very close to the Raman line of the solute chosen for the purpose. Shorygin (1953) reported the results of investigation of the relative intensities of the Raman line due to the symmetric stretching vibration of the  $\text{NO}_2$  group in a few aromatic nitro compounds, but instead of measuring the relative intensities by choosing a reference Raman line of the solvent, he determined the strength of absorption of the exciting line in the different solutions. Also, the expected theoretical values of the intensities were not given by him. It is, therefore, difficult to judge whether the results reported by him agreed more with his theory than with the theory given by Placzek (1934).

The present investigation was undertaken to compare the relative intensities of the line  $1348 \text{ cm}^{-1}$  due to  $\text{NO}_2$  group in a few aromatic nitro compounds with respect to the intensity of the  $1215 \text{ cm}^{-1}$  line of chloroform and to find out which of the two theories mentioned above could explain the results more accurately. The ultraviolet absorption spectra of the solutions were also studied in order to find out the lowest absorption frequencies.

#### EXPERIMENTAL

The compounds chosen were *p*-chloronitrobenzene, *p*-nitrophenol, 1-chloro, 2, 4-dinitrobenzene and *p*-nitroaniline, and chloroform was used as the solvent. The strengths of the solutions used were 0.025, 0.029, 0.02 and 0.003 mole/litre respectively. In the cases of the first and the third compounds solutions of strengths 0.25 and 0.2 mole/litre were also used. The liquids were distilled under reduced pressure in order to get rid of the coloured impurities. A Fuess spectrograph having a dispersion of about 11.5 Å/mm was used to photograph the spectra.



Microphotometric records of the spectra were taken with a Kipp and Zonen recording spectrophotometer. Ilford Zenith plates were used to photograph the spectra and a blackening-log intensity curve for the region 4600 Å was used to measure the relative intensities of the 1215  $\text{cm}^{-1}$  line of chloroform and the 1348  $\text{cm}^{-1}$  line due to the  $\text{NO}_2$  group in each of the compounds. In the cases of *p*-chloronitrobenzene and 1-chloro 2, 4-dinitrobenzene the relative intensities of the two lines were measured from the spectrograms due to the two different solutions of each of the two compounds in order to find out whether the relative intensities were proportional to the concentrations.

The ultraviolet absorption spectra of the solutions were recorded with an Adam Hilger E 1 quartz spectrograph, iron arc spectrum being used as comparison in each case.

#### RESULTS AND DISCUSSION

The Raman spectra of some of the solutions excited by the Hg line 4358 Å are reproduced in Figs. 1-4, Plate I, in order to show approximately the relative intensities of the 1215  $\text{cm}^{-1}$  of chloroform and the line 1348  $\text{cm}^{-1}$  of the  $\text{NO}_2$  group in each case. The ultraviolet absorption spectra of *p*-nitrophenol and *p*-nitroaniline are also reproduced in figures 5 and 6, Plate I, in order to show the long wavelength limit of the region of absorption. In the case of *p*-nitroaniline a strong continuous luminescence band appeared in the region 4500 Å-4800 Å, but the line due to the  $\text{NO}_2$  group being slightly less intense than the line 1215  $\text{cm}^{-1}$ , it was not very difficult to measure the relative intensities of the lines within a limit of error of about 15%.

The Raman frequencies of the line due to the  $\text{NO}_2$  group in the solutions of the different compounds and the ratio of the intensity of the line to that of the line 1215  $\text{cm}^{-1}$  reduced to the value for a particular molar concentration of the solutions are given in Table I. The wave numbers of the nearest ultraviolet absorption bands of the solutions of the compounds in chloroform are also included in the table. The wave number of the exciting line is given in the last column of the table.

TABLE I

Compound	$\Delta\nu(\text{NO}_2)$ in $\text{cm}^{-1}$	Conc. Mole/litre	$I_R/I_{1215}$	$\nu_{\text{pk}}$ in $\text{cm}^{-1}$	$\nu$ in $\text{cm}^{-1}$
(a) <i>p</i> -Chloro-nitrobenzene	1350	.03	1 : 2	35400	23000
(b) 1-Chloro-2, 4-dinitrobenzene	1350	.03	0.9 : 2	35000	23000
(c) <i>p</i> -Nitrophenol	1346	.03	3.5 : 2	30200	23000
(d) <i>p</i> -Nitroaniline	1340	.003	1.4 : 2	26600	23000

The absorption frequencies for *p*-nitroaniline and *p*-nitrophenol correspond to about 3759Å and 3310Å and these wavelengths are slightly larger than the wavelengths at the centres of the absorption bands. As the absorption at these longer wavelengths is quite strong its influence on the intensity of the Raman line cannot be neglected, and therefore, these frequencies have been taken into consideration in the calculations.

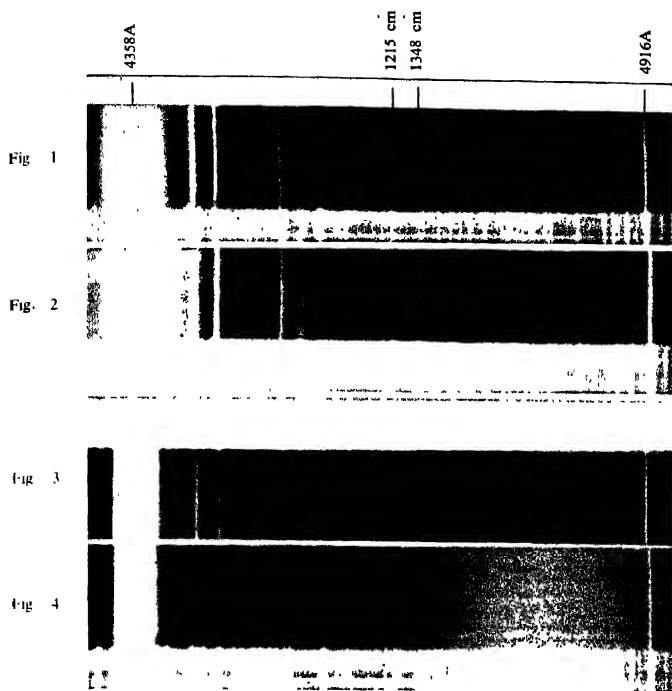
The ratios of the intensities of the line due to the NO<sub>2</sub> group in the different compounds are shown in Table II along with the values expected from Eqs. (1) and (2). In calculating these theoretical values the absorption frequencies given in column 5 of Table I have been used.

TABLE II

Ratio	Observed	Theor. Eq. (1)	Theor. Eq. (2)
I(b) : I(a)	0.9 : 1	0.96 : 1	0.94 : 1
I(c) : I(a)	3.5 : 1	3.0 : 1	8.3 : 1
I(d) : I(a)	14.0 : 1	11.9 : 1	151.8 : 1
I(d) : I(c)	4.0 : 1	4.0 : 1	18.3 : 1

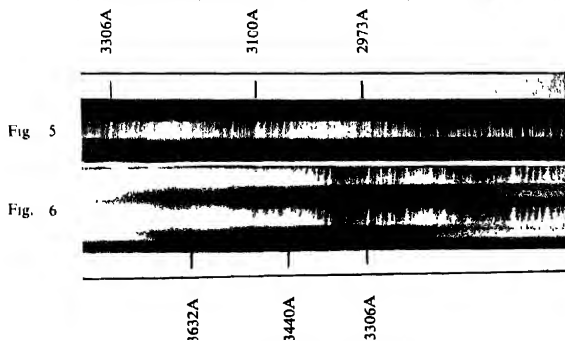
It is evident from Table II that the observed values of the ratio of the intensities of the Raman line due to the solutions of the different compounds agree with those calculated on Placzek's theory, but they differ very widely from the values given by Shorygin's theory. The results also show that when the absorption frequency is very much larger than the exciting frequency as in the cases of *p*-chloronitrobenzene and 1-chloro 2, 4-dinitrobenzene, the influence of the absorption frequency on the intensity of the Raman line indicated by the two theories is almost the same and it is very little, so that the intensity is not altered appreciably by a change of about 200 cm<sup>-1</sup> in the absorption frequency.

The results discussed above are quite different from those reported by Shorygin (1953). The cause for this discrepancy is probably the difference between the method of measuring the relative intensities of the Raman lines adopted by him and that used in the present investigation. In Shorygin's method the relative intensities were estimated by finding out to what extent the incident line was absorbed by the solution, but it is difficult to calculate such loss of intensity of the incident line while traversing the solution, because the Raman line is excited by all the molecules at different points in the path of the incident line and the intensity is different at the different points. Such a source of error does not occur when the intensity of the Raman line is compared with that of a neighbouring line of the solvent.



Raman spectra

- Fig 1. Solution of *p*-chloro-nitro-benzene in chloroform (0.025 mole/litre)  
 Fig 2. Solution of 1-chloro-2,4 dinitro benzene in " (0.2 " )  
 Fig 3. Solution of *p*-nitrophenol " " (0.029 " )  
 Fig 4. Solution of *p*-nitroaniline " " (0.003 " )



Ultra-violet absorption spectra

- Fig 5. Solution of *p*-nitrophenol in chloroform  
 Fig 6. Solution of *p*-nitroaniline in chloroform



#### CONCLUSIONS

The results given in Table II and the above discussions lead to the conclusion that when the absorption frequency of a compound in the ultraviolet region is not much larger than the exciting frequency the enhancement of the intensity of the Raman line due to the influence of the absorption frequency is satisfactorily explained by Placzek's theory. The assumption made in Shorygin's theory that all the molecules are similarly oriented in the liquid has no justification and this assumption may be responsible for the wide discrepancy between the results observed in the present investigation and those deduced from Shorygin's theory.

#### ACKNOWLEDGMENT

The author's thanks are due to Professor S. C. Sirkar, D.Sc., F.N.I., for his guidance throughout the investigation and for valuable discussions.

#### REFERENCES

- Placzek, G., 1934, *Handbuch der Radiologie*, Vol. 6, Part II, p 227.  
Rea, D. G., 1960, *J. Mol. Spectroscopy*, 4, 499.  
Shorygin, P. P., 1952, *Doklady Akad. Nauk, S.S.S.R.*, 87, 201.  
Shorygin, P. P., 1953, *J. Chim. physique Physico-Chim. biol.*, 50, D. 31.

# ON THE INFLUENCE OF DIFFERENT SOLVENTS ON THE SINGLET→TRIPLET ABSORPTION IN SOME HALOGENATED TOLUENES\*

J. K. ROY

OPTICS DEPARTMENT,

INDIAN ASSOCIATION FOR THE CULTIVATION OF SCIENCE,

CALCUTTA-32.

(Received January 25, 1962)

**ABSTRACT.** The continuous absorption in the absorption spectra in the near ultra-violet region of orthobromotoluene, parachlorotoluene and metafluorotoluene in the liquid state with path lengths of 7 mm., 6.5 mm and 7.4 mm has been compared with that due to solutions of the compounds in pyridine, chloroform and ethyl bromide with equivalent path lengths at the room temperature.

It is observed that when the *o*-bromotoluene is dissolved in chloroform the continuous absorption due to the singlet→triplet transition in the region 25000—28000  $\text{cm}^{-1}$  becomes weaker but the solution in pyridine does not show any change in the absorption while that in ethyl bromide shows a little stronger absorption in the region mentioned above. In the case of *p*-chlorotoluene the solvents pyridine and chloroform show no change in the absorption spectra, but ethyl bromide increases the strength of the absorption. The influence of the solvents in the case of *m*-fluorotoluene is similar to that observed in the case of *p*-chlorotoluene.

It has been concluded that the weakening of the absorption in solutions in some of the solvents is partly due to breaking up of the association of the molecules.

## INTRODUCTION

The influence of heavy atoms in the neighbouring molecules on the strength of the singlet→triplet absorption exhibited by some organic molecules was first studied by Kasha (1952) and later, such influence has been studied by many workers including McGlynn and Kasha (1954), McGlynn (1956), Padhye and Patel (1956) and Robertson and Reynolds (1958).

The influence of neighbouring molecules of the same kind on the singlet→triplet absorption in some halogen substituted toluenes and benzenes in the liquid and vapour states was studied recently (Sirkar and Roy, 1960; Roy, 1961 a, b) and it was observed from a comparison of absorption in the equivalent path lengths of each of the compounds in the liquid and vapour states that the region of absorption shifts towards longer wavelengths with the liquefaction of the vapour,

---

\* Communicated by Prof. S. C. Sirkar

the magnitude of the shift being dependent on the atomic weight of the substituent atom.

Forster (1957) on the other hand studied the singlet→triplet absorption in solutions of biacetyl in different solvents and observed that the absorption in solution in heptane is much stronger than that in the solution in pyridine. He attributed this diminution in the strength of absorption in the solution in pyridine to increase in the separation of the vibrational levels due to interaction of the nitrogen atom with the biacetyl molecule. It was not known, however, whether such an influence on the singlet→triplet absorption in other molecules takes place when pyridine is used as the solvent.

For this reason it was thought worthwhile to make a comparative study of the influence of solvents such as ethyl bromide and chloroform with that of pyridine on singlet→triplet absorptions in some halogenated toluenes and the results have been discussed in the present paper.

#### EXPERIMENTAL

For studying the influence of solvents on the absorption spectra the substances chosen in the present investigation are orthobromotoluene, parachlorotoluene and metafluorotoluene. Chemically pure varieties of *o*-bromotoluene *p*-chlorotoluene obtained from the British Drug House, England and *m*-fluorotoluene from Eastman Kodak Co., U.S.A. were distilled several times before use. The liquids ethylbromide, chloroform and pyridine supplied by E. Merck were also fractionally distilled several times under reduced pressure before being used as solvents in the present investigation.

The experimental arrangement for recording the ultraviolet absorption spectra of the substances at the room temperature was the same as that employed in the previous investigations (Sirkar and Roy, 1960, Roy 1961a). The absorption spectra of the substances in the vapour state were photographed first by filling the 18.90 metre long absorption cell with the vapour of the compounds at the saturation pressures at about 24°C. The pressures measured carefully with a differential manometer were found to be about 55 mm, 50 mm and 60 mm of Hg in the cases of orthobromotoluene, parachlorotoluene and meta-fluorotoluene respectively. The equivalent path lengths were 7 mm., 6.5 mm and 7.4 mm respectively for the liquids and 7 cm., 6.5 cm and 7.4 cm respectively for the solutions of the three liquids mentioned above. In each case two empty cells of lengths equal to equivalent path length for the liquid and the solutions were first placed in the path of the beam while the absorption spectrum due to the vapour was recorded with a cell of length 1890 cm. The long cell was then evacuated and the short cell for the liquid was filled with the pure liquid and the absorption spectrum of the liquid was photographed by the side of the spectrum due to the vapour. Next, the liquid was poured out from the cell and the short empty cell for the solution

was filled with the solution of the liquid and its absorption spectrum was photographed by the side of the spectrum due to the liquid. An Adam Hilger medium quartz spectrograph giving a dispersion of about 22Å/mm in the 3500Å region was used for this purpose. Agfa Isopan films backed by metal plates were used for photographing the spectra. Iron arc spectrum was photographed on each spectrogram as comparison. Microphotometric records of the spectrograms were obtained with a self-recording microphotometer made by Kipp and Zonen. The wavelengths in the continuous absorption spectra were measured by drawing a sharp line across the spectrogram in the position of a known iron line in the adjacent iron arc spectrum and comparing the microphotometric record of the iron arc spectrum with that of the absorption spectrum.

#### RESULTS AND DISCUSSION

The microphotometric records of the absorption spectra due to solutions of orthobromotoluene, parachlorotoluene and metafluorotoluene in pyridine, chloroform and ethyl bromide are reproduced in Figs. 1-3, respectively. The microphotometric record of the spectrum due to the pure liquid photographed on the spectrogram due to each of the solutions is also reproduced along with the record of the spectrum due to the corresponding solution because the spectra photographed on different films and developed separately may not have the same contrast and blackening. The wave numbers determined with the help of the record of the iron arc spectrum on which the reference line 4045Å was marked are also given in these figures.

A comparison of the curves due to the solution of *o*-bromotoluene in pyridine with those for the pure liquid photographed under identical conditions on the spectrogram due to the solution and reproduced in Figs. 1(a) and 1(b) show that the nature of absorption in the solution in pyridine in the region 25,000–28,000  $\text{cm}^{-1}$  is almost the same. The apparent smaller height of the curve in Fig. 1(a) than that of the curve in Fig. 1(b) is due to the superposition of a continuous background on the former spectrum. Figs. 1(c) and 1(d), on the other hand show that the absorption in the region 27,000–29,000  $\text{cm}^{-1}$  in the solution in chloroform is weaker than that in the pure liquid. Figs. 1(e) and 1(f) also show that the absorption in solution in ethyl bromide in the region mentioned above is slightly stronger than that in the pure liquid. The curves due to solutions of *p*-chlorotoluene reproduced in Figs. 2(a), 2(c) and 2(e) and the corresponding curves due to the pure liquid in Figs. 2(b), 2(d) and 2(f) respectively show that the absorption in the region 24,700–28,000  $\text{cm}^{-1}$  remains almost unchanged when the pure liquid is dissolved in pyridine and chloroform, but it becomes stronger in the solution in ethyl bromide. The curves due to solutions in *m*-fluorotoluene reproduced in Figs. 3(a), 3(c) and 3(e) show the same effects as observed in the case of *p*-chlorotoluene. The increase in the strength of the absorption in the solution



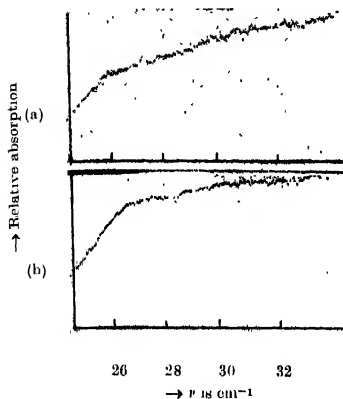


Fig. 1(a). *o*-Bromotoluene in pyridine

(10% solution)

Fig. 1(b). *o*-Bromotoluene (pure liquid)

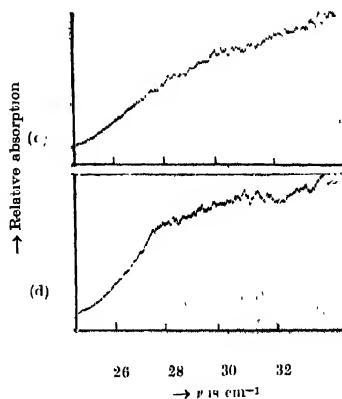


Fig. 1(c). *o*-Bromotoluene in chloroform

(10% solution)

Fig. 1(d). *o*-Bromotoluene (pure liquid)

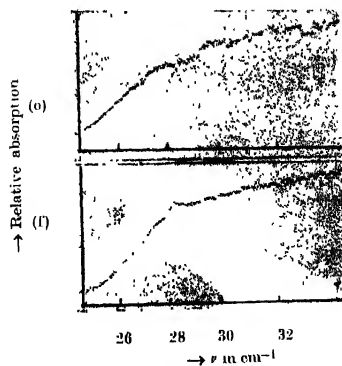


Fig. 1(e). *o*-Bromotoluene in ethyl bromide (10% solution)

Fig. 1(f). *o*-Bromotoluene (pure liquid)

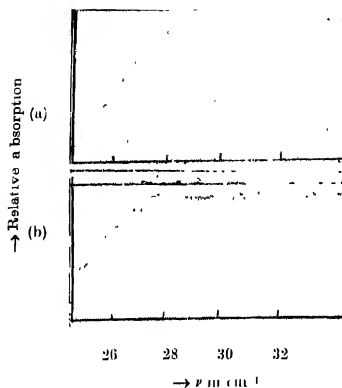


Fig. 2(a) *p*-Chlorotoluene in pyridine  
(10% solution)  
Fig. 2(b) *p*-Chlorotoluene (pure liquid)

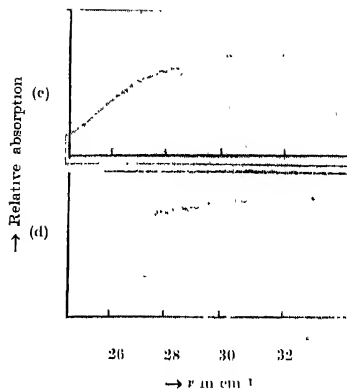


Fig. 2(c) *p*-Chlorotoluene in chloroform  
(10% solution)  
Fig. 2(d) *p*-Chlorotoluene (pure liquid)

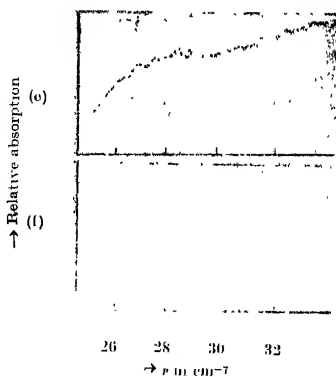


Fig. 2(e) *p*-Chlorotoluene in ethyl bromide (10% solution)  
Fig. 2(f) *p*-Chlorotoluene (pure liquid)

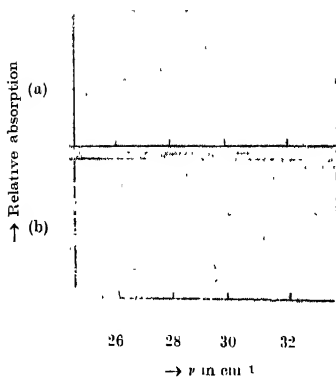


Fig. 3(a) *m*-Fluorotoluene in pyridine  
(10% solution)

Fig. 3(b) *m*-Fluorotoluene (pure liquid)

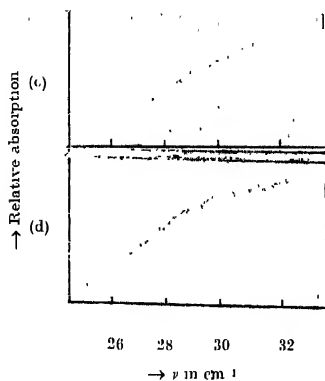


Fig. 3(c) *m*-Fluorotoluene in chloroform  
(10% solution)

Fig. 3(d) *m*-Fluorotoluene (pure liquid)

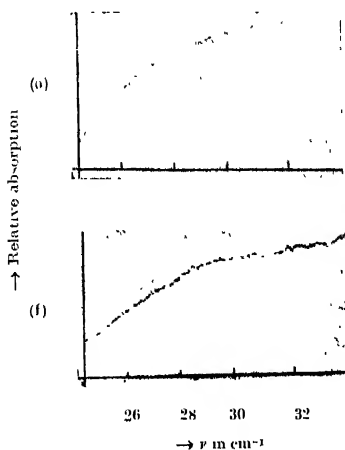


Fig. 3(e) *m*-Fluorotoluene in ethyl bromide (10% solution)

g. 3(f) *m*-Fluorotoluene (pure liquid)

in ethyl bromide in comparison with that in the pure liquid is more conspicuous in this case.

It was formerly observed (Roy, 1961) that the strength of absorption in the region mentioned above increases when the vapours of these compounds are liquefied, the increase being more in the case of the *o*-bromotoluene than in the other two cases. This was attributed to the influence of the heavy bromine atom in the neighbouring molecules in the liquid on the singlet→triplet transition. The results in the present investigation discussed above on the otherhand show that the influence of pyridine molecules in the solution is larger than that of the chlorine molecules in the solutions in chloroform. Hence it appears that there is a second cause for the enhancement of the continuous singlet→triplet absorption besides the influence of surrounding heavy atoms. It appears that the association of the molecules in the pure liquid and in solution in aromatic solvents is also responsible for the enhancement of the absorption. In solution in chloroform probably this association breaks up resulting in partial reduction in the strength of the absorption. This supports a similar conclusion drawn by Biswas (1956, 1957) from the results of investigations on the luminescence spectra of the solutions of these compounds.

The investigations are being extended to solutions in other suitable solvents in order to find out whether the above conclusion is generally applicable.

#### ACKNOWLEDGMENT

The author is highly indebted to Professor S. C. Sirkar, D.Sc., F.N.I., for his kind interest and for guidance throughout the progress of the work.

#### REFERENCES

- Biswas, D. C., 1956, *Ind. J. Phys.*, **30**, 143, 255.  
Biswas, D. C., 1957, D. Sc. Thesis, Calcutta University.  
Kasha, M., 1952, *J. Chem. Phys.*, **20**, 71.  
McGlynn, S. P. and Kasha, M., *Symposium on Molecular Structure and Spectroscopy* (Ohio State Univ., June, 1954).  
McGlynn, S. P., 1956, *Dissertation* (Florida State University, Tallahassee, Florida, January, 1956).  
Padhye, M. R. and Patel, J. C., 1956, *J. Sci. Ind. Res.*, **14B**, 206.  
Robertson, W. W. and Reynolds, R. E., 1958, *J. Chem. Phys.*, **29**, 138.  
Roy, J. K., 1961a, *Ind. J. Phys.*, **35**, 143.  
Roy, J. K., 1961b, *Ind. J. Phys.*, **35**, 628.  
Sirkar, S. C. and Roy, J. K., 1960, *Ind. J. Phys.*, **34**, 581.

INFLUENCE OF SOLVENTS ON HYDROGEN BONDING  
IN ORTHO- AND PARANITROPHENOL

S. B. BANERJEE AND G. S. KASTHA

OPTICS DEPARTMENT

INDIAN ASSOCIATION FOR THE CULTIVATION OF SCIENCE, CALCUTTA-32

(Received January 27, 1962)

**ABSTRACT.** Influence of different polar and non-polar solvents on the hydrogen bonding exhibited by *o*- and *p*-nitrophenol has been investigated by studying the infrared spectra with a Perkin Elmer Model 21 spectrophotometer. The results confirm the existence of intramolecular chelation in the molecules of the ortho compound and intermolecular hydrogen bridge in the para compound. Evidence of association of the OH group with acetone and other molecules in the solutions of both the compounds in these solvents and with the chloroform molecule in the solution of the para compound in chloroform has also been observed.

## INTRODUCTION

From a study of infrared absorption spectrum of polycrystalline films of *p*-nitrophenol, Ginetti (1954) suggested that the molecules of this compound in the solid state are intermolecularly bonded in a chain-like polymer through the hydroxyl group and  $\text{NO}_2$  group of neighbouring molecules. From similar studies with *o*-nitrophenol in the solid state and in solutions it was concluded by Keussler and Rossmi (1956) and by Shigorin (1959) that the internal chelation of OH and  $\text{NO}_2$  groups of the same molecule increases the conjugation of the system and is responsible for the large change in the OH stretching vibrational frequency. Thus the two types of hydrogen bonding in *o*- and *p*-nitrophenol are quite different and it would be interesting to study the effect of polar and non-polar solvents on the two types of hydrogen bonding. Infrared spectra of these compounds in the crystalline state as well as in a number of solvents were, therefore, investigated and the results are reported in the present communication.

## EXPERIMENTAL

The samples of *o*- and *p*-nitrophenol were of chemically pure quality obtained from E. Merck and were further purified by repeated crystallisation from dry chloroform and ether. The solvents used in this investigation were carefully dried and were individually tested to find out if they showed any absorption in the region  $2800\text{--}3800\text{ cm}^{-1}$ . A Perkin Elmer Model 21 spectrophotometer provided with NaCl optics was used to record the absorption spectra. A small amount of molten mass of *o*-nitrophenol was pressed between two NaCl plates to obtain a thin film of crystals. In the case of *p*-nitrophenol thin crystalline films were

obtained by slow evaporation of dilute solutions of the compound in ether and in chloroform spread over one of the NaCl plates. Suitable compensation cells were used in the reference beam in studying the spectra of the solutions.

TABLE I

*o*-Nitrophenol, OH vibrational frequency in  $\text{cm}^{-1}$

Crystal	Solution in				
	$\text{CCl}_4$	$\text{C}_6\text{H}_6$	$\text{HCCl}_3$	$(\text{C}_2\text{H}_5)_2\text{O}$	$(\text{CH}_3)_2\text{CO}$
3268 s	3250 s	3242 s	3262 vs	3240 s 3290 sh	3238 s 3296 s

TABLE II

*p*-Nitrophenol: OH vibrational frequency in  $\text{cm}^{-1}$

Crystal	Solution in		
	$\text{HCCl}_3$	$(\text{C}_2\text{H}_5)_2\text{O}$	$(\text{CH}_3)_2\text{CO}$
Very broad band extending from 3100 - 3500 $\text{cm}^{-1}$ with a maximum at about 3360 $\text{cm}^{-1}$	3210 sh 3382 s, h 3585 ms	3196 s 3390 ms, h	3200 s 3370 ms, h

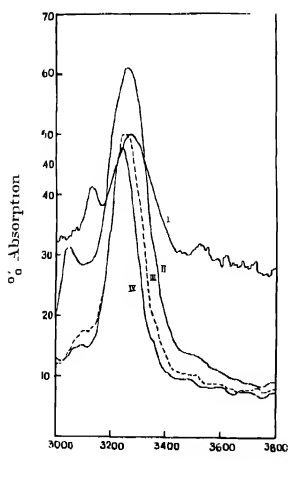


Fig. 1(a) Infrared absorption curves of *o*-nitrophenol

- Curve I Pure solid (thin film)  
 Curve II 5% Solution in chloroform  
 Curve III 4% Solution in carbon tetrachloride  
 Curve IV 4% Solution in cyclohexane

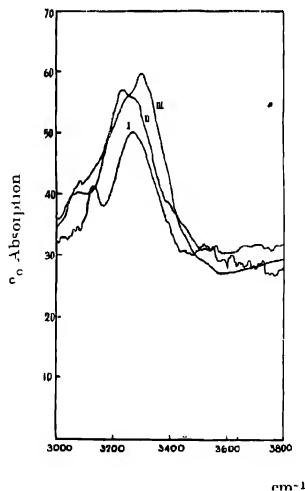


Fig. 1(b) Infrared absorption curves of *o*-nitrophenol

- Curve I Pure solid (thin film)  
 Curve II 4% Solution in ether  
 Curve III 4% Solution in acetone

## RESULTS AND DISCUSSION

The infrared absorption curves are shown in Figs. 1 and 2 and the frequencies of the absorption bands are given in Tables I and II. In the case of broad absorption bands the approximate wave number at the maximum of absorption was noted.

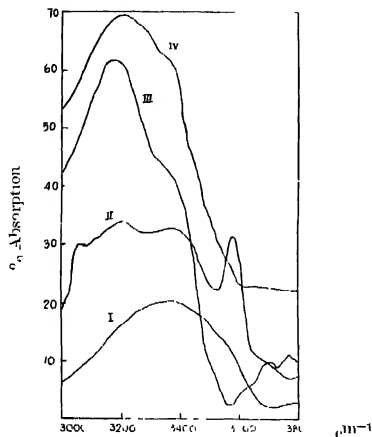


Fig. 2. Infrared absorption curves of *p*-nitrophenol.  
 Curve I Pure solid (thin film).  
 Curve II 5% Solution in chloroform.  
 Curve III 5% Solution in ether.  
 Curve IV 5% Solution in acetone.

*o*-Nitrophenol

In the spectrum of thin polycrystalline film of *o*-nitrophenol the OH stretching frequency appears as a sharp band at  $3268\text{ cm}^{-1}$ . Keussler and Rossmi (1954) have previously reported the intramolecularly bonded OH frequency at  $3264\text{ cm}^{-1}$  in the infrared spectrum of crystals of this compound and proposed that the possibility of resonance between the structures shown in Fig. 3(a) and 3(b) may be

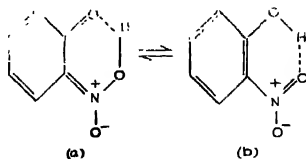


Fig. 3.

responsible for the large lowering of the OH vibrational frequency. In the spectra of dilute solutions of the substance in  $\text{CCl}_4$ ,  $\text{C}_6\text{H}_{12}$  and  $\text{HCCl}_3$  only one sharp and strong band corresponding to the bonded OH stretching vibration is obtained. As can be seen from Table I this frequency is not appreciably different from that observed in the spectrum of the crystals. This shows that the intramolecular hydrogen bond is too strong to be affected by the non-polar as well as polar molecules of the solvents. This would be expected in view of the greater stability of the chelated OH bond arising from the extra conjugation in the ring provided by the  $\text{NO}_2$  group according to the resonance structures mentioned above.

However, striking change in the absorption band of the *o*-nitrophenol molecule is observed when the substance is dissolved in acetone and in ether. In the case of dilute solutions in these solvents, instead of one sharp band, two absorption maxima at about  $3240$  and  $3290\text{ cm}^{-1}$  are observed, the relative intensity of these being nearly the same. It is suggested that the frequency  $3240\text{ cm}^{-1}$  corresponds intramolecularly bonded OH vibrational frequency and the other at  $3290\text{ cm}^{-1}$  represents the vibration of OH group bonded to the oxygen atom of the solvent molecules as indicated in Figs. 4(a) and 4(b).

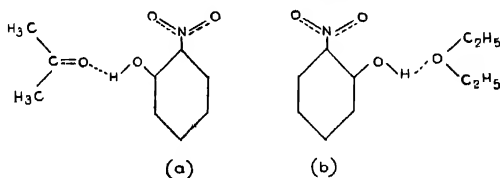


Fig. 4.

### *p*-Nitrophenol

The spectrum of a thin polycrystalline film of *p*-nitrophenol shows a very broad band with a maximum at about  $3360\text{ cm}^{-1}$ . This probably corresponds to the broad band at  $3330\text{ cm}^{-1}$  reported by Gmnetti (1954) who attributed this to the vibration of the OH group associated with the  $\text{NO}_2$  group of a neighbouring molecule and forming a polymer. In the spectrum of *p*-nitrophenol in solution in chloroform three bands with maxima at  $3585$ ,  $3382$  and  $3210\text{ cm}^{-1}$  are observed. Of these, the first band which is quite sharp and intense obviously corresponds to the band at  $3594.5\text{ cm}^{-1}$  observed in very dilute solution in  $\text{CCl}_4$  (Ingraham *et al.*, 1952) and represents the stretching vibrational frequency of free OH group. The appearance of the band at  $3382\text{ cm}^{-1}$  indicates that all the OH groups in *p*-nitrophenol molecule are not free, but a good number of them remain intermolecularly associated in chloroform solution. With increase in dilution, the intensity of this band is found to diminish greatly. In the very dilute solution in  $\text{CCl}_4$  almost all of the polymeric groups are broken up, as is evident from



the results of Ingraham *et al.* (1952) who did not observe any band corresponding to the frequency  $3360\text{ cm}^{-1}$ . The third band at  $3210\text{ cm}^{-1}$  may arise from an association of OH group of *p*-nitrophenol molecule with the polar molecules of chloroform. It may be pointed out that in the case of ethylene chlorohydrin such an association was shown to lower the OH vibrational frequency to about  $3200\text{ cm}^{-1}$  (Mazumder, 1959). In the case of the *o*-nitrophenol molecule, the strong intramolecular chelation obviously does not allow such association with the chloroform molecule.

In the spectra of solutions of *p*-nitrophenol in acetone and in ether, the free OH vibrational frequency is totally absent and only two bands at about  $3370$  and  $3196\text{ cm}^{-1}$  in solution in acetone and at about  $3390$  and  $3200\text{ cm}^{-1}$  in solution in ether, are observed. The frequencies  $3370$  and  $3390\text{ cm}^{-1}$  observed in the two solutions correspond to the vibrational frequency of the intermolecularly bonded OH group observed in the case of the crystals. The frequency at about  $3200\text{ cm}^{-1}$  observed in both the solutions may be due to the vibration of OH group associated with the oxygen atom of the acetone and ether molecules as proposed in the case of *o*-nitrophenol. The complete absence of the free OH vibrational frequency also demonstrates the occurrence of such association with the molecules of the solvents.

Investigations with other phenolic compounds are in progress.

#### ACKNOWLEDGMENT

The authors are grateful to Professor S. C. Sirkar, D.Sc., F.N.I., for his kind interest in the work.

#### REFERENCES

- Ginnetti, Y., 1954, *Naturwiss.*, **41**, 333.  
 Ingraham, L. L., Corse, J., Bailey, G. F., and Still, F., 1952, *J. Am. Chem. Soc.*, **74**, 2297.  
 Kouslov, V. and Rossmi, G., 1956, *Z. Elektrochem.*, **60**, 136.  
 Mazumder, M. M., 1959, *Ind. J. Phys.*, **33**, 346.  
 Shigorin, D. N., 1959, *Hydrogen Bonding* (Pergamon Press), p. 191.



# CHARACTERISTICS OF THE ION-SOURCE OF THE CALCUTTA 37-INCH CYCLOTRON

P. K. DUTT, A. P. PATRO, B. BASU AND A. CHATTERJEE,

SAHA INSTITUTE OF NUCLEAR PHYSICS, CALCUTTA

(Received April 27, 1961)

(Resubmitted January 4, 1962)

**ABSTRACT.** Probe studies have been made for the electron and total ion current output from the hot cathode capillary are type ion-source of the Calcutta 37" cyclotron. The gas used in the ion-source was hydrogen, and the kind of ion of interest for cyclotron acceleration was proton ( $H^+$ ). These studies were made with arc current, arc voltage, gas pressure and magnetic field as variable parameters.

For the high intensity cyclotron ion-sources the following criteria are of great importance, namely (Bakker and Kistemaker, 1949).

1. The production of the ions should be very high in the discharge.
2. The positive ions should be effectively transported to the edge of the plasma or out of the discharge in the direction of the exit opening for extraction.
3. The ions should be extracted from the source without disturbing the discharge.

For the cyclotron ion-source, some other conditions should also be fulfilled.

4. The yield of atomic ions and  $\alpha$ -particles should be very high when hydrogen, deuterium and helium gases are used respectively.
5. The ion emission should occur within a very constricted region at the centre between the dees (Atterling, 1948). For if the ions are spread out horizontally at the start there is inhomogeneity in the final energy (Wilson, 1940) and if the ions are spread out too much vertically at the start the dees will be loaded with off-focus ions resulting in poor-efficiency in cyclotron operation (Livingston, 1946).

Any device which increases the ratio of the atomic to molecular ions causes a better efficiency in cyclotron operation, because the molecular ions from the source which form the main bulk of the space charge (the density of the molecular ions being approximately ten times that of the atomic ions) (Livingston, 1946) are accelerated for a few revolutions before getting out of phase and cause an undesirable loading on the dees.

In early cyclotrons, the electrons emitted from the cathode (an exposed filament) used to produce the ions from the gas introduced in the dee gap region at

the chamber centre. The electrons would spiral tightly about the magnetic lines of force, and be effectively collimated, the radius of the electron-spirals being a fraction of a millimeter. The ion production depending on gas pressure could not be increased much, as the gas pressure was limited by the electrical breakdown in the chamber, which was about  $1 \times 10^{-4}$  mm Hg. The ions were formed in a strip extending across the whole width of the chamber resulting in large intensities of off-focus and nonresonant ions, and so in a very poor efficiency in cyclotron operation. In the production of ions the question of mean free path for ionization is fundamental. Let us designate it by  $\lambda_i$ . The probability of ionization for a single electron emitted from the cathode is approximately  $d/\lambda_i$ , when  $d < \lambda_i$ ,  $d$  being the mean distance of the cathode from the walls (Hoyaux and Onjardin, 1949). The pressure in the ion-source and that in the chamber being equal, if we take  $d = 10$  cm and  $\lambda = 3000$  cm, say, (for a working pressure region of  $1 \times 10^{-6}$  mm Hg), then approximately one ion pair will be created for 300 electrons, and the number of useful ions will be naturally much too low. So to get higher rates of ion-production it is necessary to (1) maintain a sufficiently high pressure-differential between the ion-source and the cyclotron chamber, (2) force the electrons to describe complicated paths before reaching the walls, or (3) a combination of these two principles. From all these considerations, the capillary arc-type ion-sources are now used in almost all the modern cyclotrons, which have definite advantages over the filament type source both from the stand point of production efficiency, as well as the operation efficiency of the cyclotron. These types of sources can operate at a much higher pressure than the cyclotron chamber.

The Calcutta cyclotron used, until very recently a conventional hot filament low-voltage capillary arc-type ion-source, though at present that is being modified to a point cathode, hooded-arc type source following the suggestion of Livingston, Cowie and Ksanda. The present paper reports about the characteristics of the conventional hot-filament capillary arc-type source used in the Calcutta cyclotron upto a discharge current value of 1 ampere, though much larger currents were occasionally drawn.

The processes involved in this type of ion-source can be summarised as follows:

The gas in the ion-source is usually ionized by electron impact.

The number of new ions produced per cm of path by an accelerated electron is given by (Engel and Stoenbeck)

$$\alpha = \frac{600a}{\sqrt{2}} \cdot \frac{V_i p}{\sqrt{\pi}} \cdot \frac{1}{\sqrt{f}} \cdot \frac{2\sqrt{2}}{\sqrt{\pi}} \left( \frac{E}{P} \right) L_{e0} \cdot \left( 1 + \frac{eV_i}{2kT_e} \right)$$

where  $E =$  strength of the electric fields

$V_i =$  ionization potential of the gas

$T_e =$  absolute temp. of the electrons

$f$  = fractional loss of energy on electron collision

$L_{eo}$  = electron mean free path at a pressure of 1 mm Hg.

For high values of  $E/p$ , which condition is roughly valid for low pressure arc sources the above expression for  $\alpha = f(EL)/L$  where  $E$  = field strength, and  $L$  = electron mean free path] can be written in a simpler manner, as

$$\alpha = pAe^{-B/E/P}$$

where  $A$  and  $B$  are constants for a particular gas. Their values are shown below in case of some gases for a range of  $E/P$ .

Gas	A	B	Range of E/P
			Volts/cm/mm Hg
Air	14.6	365	150-600
H	5.0	130	150-40
He	2.8	34	20-150

Thus there is an optimum relation of  $\alpha$  with  $p$ .

Among the other processes photo-ionization will have a share in the production of ions although very small in comparison to the electron-collision process, which can account for most of the arc current in a low pressure hot filament discharge in the ion source (Bakker and Kistemaker, 1949). It can be mentioned in this connection that in a low pressure arc column most of the current is carried by electrons, the positive ions serve to neutralize space charge (Cobino, 1941).

Among the loss processes of electrons and ions from this type of discharge the contribution of recombination of electrons and positive ions is small; the coefficient of recombination is (Kenty, 1928) of the order of  $10^{-10}$ . It is easy to infer that the loss of electrons by recombination is much smaller than the number of electrons present. The electrons are lost mostly to the anode and the walls (Bakker and Kistemaker, 1949). The most important mechanism by which this happens is the dynamical 'drain diffusion' (Bohm *et al.*, 1949) in the strong magnetic field among the other magnetic diffusion processes present, namely, the collision diffusion and the diffusion by motion transverse to electric and magnetic field.

Regarding the transportation of the positive ions from the production zone in the source to the emitting equipotential surface near the exit opening without loosing them to all directions the capillary arc source is not satisfactory. This has been pointed out by Bakker and Kistemaker (1949). A good source is self-focussing. The potential distribution forces the positive ions to the emitting surface. In that case, there will be a potential trough. A bad source has a

potential mountain in the production zone, which gives a diverging ion beam in the plasma itself. This can happen in a capillary arc source.

There is also a possibility of deformation of the equipotential surface (also called the "virtual cathode" of the ion-source) due to the penetrating field of the strongly negative extraction potential which displaces and curves this ion-emitting surface. This may also result in an increase in the value of  $d$ , the distance of the equipotential surface from the extraction electrode. Thus an increasing high tension field partially eliminates its favourable action by increase of  $d$ , as the ion-current extracted is proportional to  $V^{3/2}/d^2$ , where  $V$  is the potential giving rise to the extraction field.

A sketch of the ion-source is shown in Fig. 1 and the experimental arrangement is given in Fig. 2. The jacket and the discharge chamber (also called the cavity) of the ion-source are made of copper provided with an elktonite tip screwed

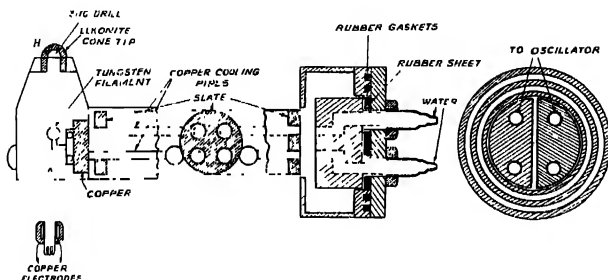


Fig. 1. A sketch of the capillary arc type ion-source.

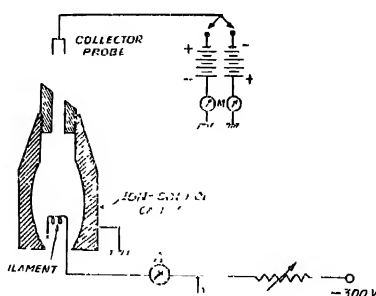


Fig. 2. A sketch of the experimental arrangement.

on the cavity above the filament housing. The elkonite tip has a 3/16 inch through bore *H* for exit of ions in the cyclotron chamber. Several drill sizes were used for the bore but the 3/16 inch one was found most suitable. The filament, a two-and-a-half turn helix of 40 mil. tungsten wire, is heated by a high radio-frequency current to avoid warping in the magnetic field. An arc is produced between the filament kept at -ve potential (emission voltage) and the discharge chamber which is grounded. A molybdenum baffle *M*, kept at filament potential, prevents the arc from striking below. The filament assembly can be introduced into the arc chamber through a lock-gate provided with Wilson seals, which permits the installation of a new filament any number of times without disturbing the cyclotron chamber vacuum. Both the filament-holder electrodes and the jacket are provided with water cooling arrangements. The average filament life was approximately 12 hours.

The gas used for the ion-production is let into the arc discharge chamber from an electrolysis unit by means of a flow-control device. Ions and electrons come out from the arc chamber into the cyclotron tank through the exit hole *H* in tight spirals, strongly focussed by the cyclotron magnetic field. These ions are available for acceleration between the dees. The gas used for the present investigation is hydrogen.

In this paper the characteristics of the ion-source with arc voltage drop between 50-200 volts and total discharge current up to 1 amp., have been described.

To get an idea of the dependence of the ion and electron output of the source on the gas pressure, the arc current, the arc voltage and the magnetic field, we have used a test electrode or probe (Fig. 2) insulated from the chamber which is inserted through a Wilson seal so that the position of the probe can be accurately adjusted above the exit hole *H* of the source.

For the information about the ion output the probe was maintained at a voltage of -340 volts and to collect electron through the outlet hole the probe was kept at a voltage of +220V (positive). The currents through the test probe were directly measured by means of meter.

The results obtained are shown in Figs 3, 4, 5 and 6.

The problem of measuring the true ion beam current in a cyclotron is a difficult one, due to radio-frequency pick-up and secondary emission. These effects were eliminated by Richardson (1948) and others when they performed experiments with the synchro-cyclotron by using a pulsed ions source. The same procedure of using a pulsed ions source may be used with a fixed frequency cyclotron, which we have adopted for measuring the ion beam current. The method adopted for pulsing the ion source is somewhat similar to that developed by Fryer (1946). The repetition frequency of the pulser is 50 cycles/sec., and the tubes employed are FG 67 mercury vapour thyratrons. Fig. 7 shows the circuit for emission supply, consisting of 250 volt D.C. supply and the pulser. The D.C.

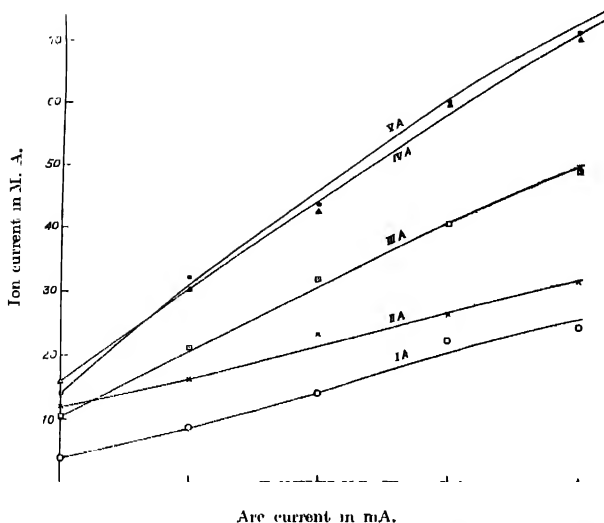


Fig. 3 Shows dependence of the output ion-current on the arc current. Gas used—Hydrogen; Arc voltage—100v; Magnetic field—4.5 kilogauss; Gas-flow rate—IA—2.69 mgm./min., IIA—1.07 mgm./min., IIIA—0.67 mgm./min., IVA—0.29 mgm./min., VA—0.18 mgm./min.

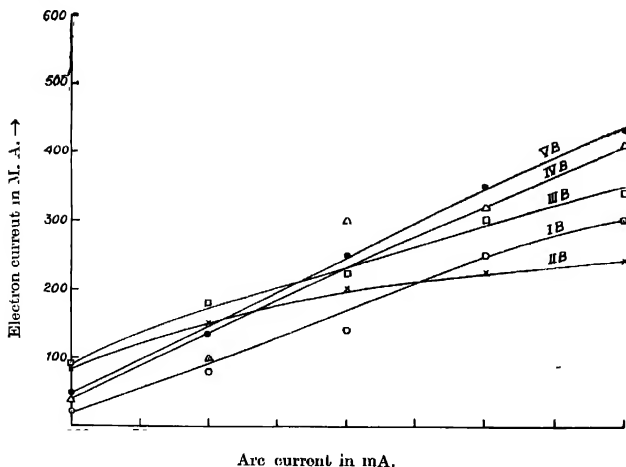


Fig. 4. Shows dependence of the electron-output current on the arc current. Gas used—hydrogen, Arc voltage—100 v; Magnetic field—4.5 kilogauss; Gas-flow rate—IB—2.69 mgm./min., IIB—1.07 mgm./min.; IIIB—0.67 mgm./min.; IVB—0.29 mgm./min., VB—0.18 mgm./min.



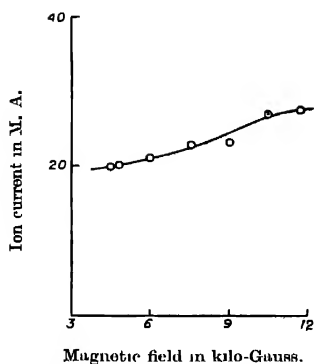


Fig. 5. (a) Shows variation of the output ion-current with magnetic field.

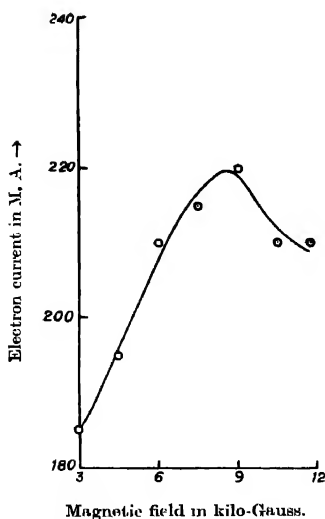


Fig. 5(b) Shows variation of the output electron-current with magnetic field.

Gas used—hydrogen. Gas-flow rate —1.07 mgm./min Arc voltage —100V.  
Arc current —600 mA.

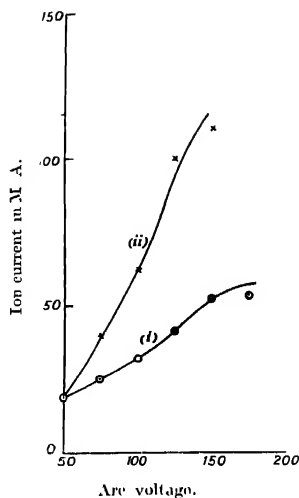


Fig. 6 Dependence of the output ion-current on the arc voltage. Gas used --hydrogen. Arc current —800 mA. Magnetic field —4.5 kilogauss. Gas-flow rate —(i) 1.10 mgm./mm., (ii) 0.18 mgm./mm.

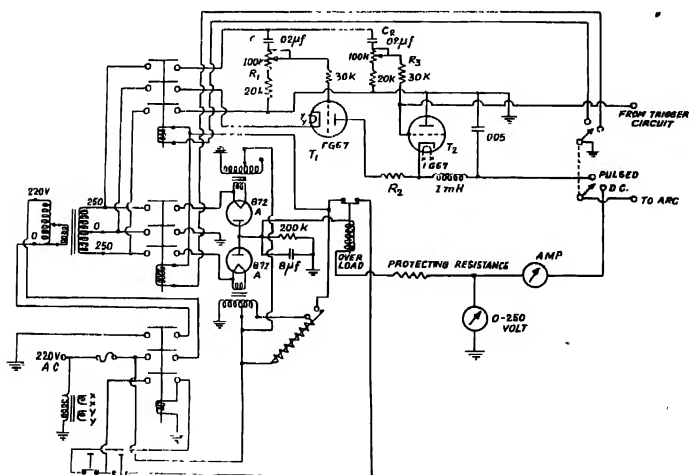


Fig. 7. Power supply for D.C. and pulsed operations

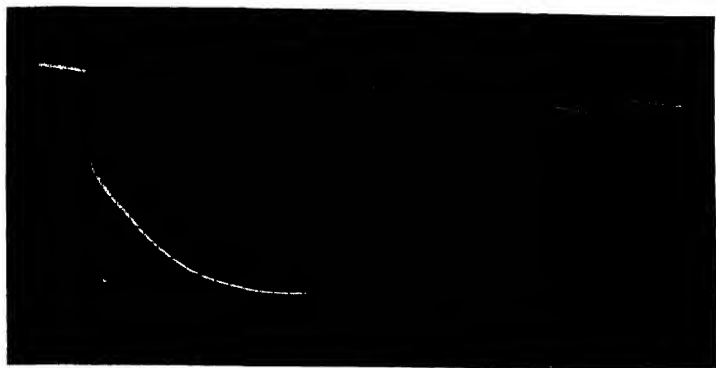


Fig. 8 (a)

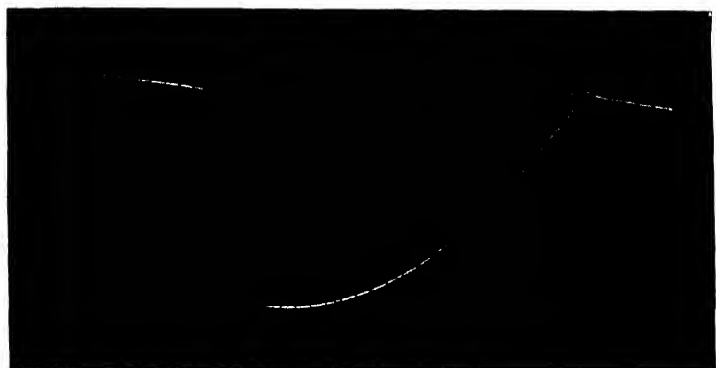


Fig. 8 (b)



Fig. 8 (c)

Figs. 8 a, b & c. Show width and position of the pulse with respect to an A.C. half-cycle chosen for different settings of the two phase-shifting circuits.

supply is a conventional full wave rectifier. The pulser consists of two thyratrons  $T_1$  and  $T_2$  which act as switches. The thyatron  $T_1$  is in series with the arc and  $T_2$  is in parallel to the arc. The modulating pulse starts when the grid of the thyatron  $T_1$  reaches the firing voltage. This voltage is controlled by the phase-shifting circuit  $C_1R_1$  and can be made to lag the plate voltage in time. The second thyatron  $T_2$  is parallel to the arc, so that as it fires, the arc is essentially short-circuited terminating the modulating pulse. The ignition of  $T_2$  is controlled by the phase-shifting circuit  $C_2R_2$  adjusted so that the grid voltage lags that of  $T_1$ . Thus with the help of the two resistances  $R_1$  and  $R_2$  it is possible to vary the position and width of the pulse with respect to the A.C. half cycle. Fig. 8 shows the width and position of the pulse with respect to the A.C. half cycle chosen for different settings of the two phase-shifting circuits. As the ion source is modulated the ion output current on the probe is also modulated. By using this pulsed ion source ion beam currents could be measured in the high radio-frequency field without trouble. Secondary emission is also suppressed as found by the fact that on giving +ve and -ve D.C. voltages on the probe the ion beam current remained unaltered. This method has the added advantage of measuring large beam currents without melting the probe. This method is useful for measuring the characteristics of the ion-source, as the variation of the ion output with variation of arc voltage, arc current can be obtained simultaneously. Fig. 9 shows the variation of ion output with arc voltage.

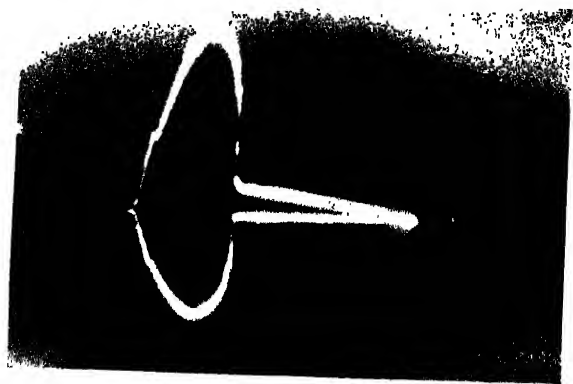


Fig. 9. Shows the variation of ion-output with arc voltage on an oscilloscope screen, the upper curve being the ion-output profile.

The characteristics of the ion-source as studied in this experiment can be summarised as follows:

For a particular supply of primary electrons from the filament, there is a pressure-optimum, above which the ion-current output decreases.

The ion output increases with arc current, arc voltage, and also with magnetic field.

The ratio of  $\frac{\text{ion-current}}{\text{electron current}}$  output in the range of our experiment varies between 0.1 to 0.22. For a particular gas-flow setting if the arc current is not varied too much, the ratio is roughly constant for different values of current. It is also found to be nearly constant for the same value of current for different gas-flows if they do not differ too much.

The electron and ion output are very sensitive to the alignment of the filament with respect to the outlet hole. The optimum condition is obtained when the central portion of the helix is under the outlet hole. With aging of the filament the ion output has been found to increase. This is probably due to the fact that the central portion of the filament from which maximum electron emission occurs gets thinner than the other portions due to ion-bombardment, and the magnetically constrained arc is better focussed under the exit hole, yielding more ion output.

These observations led us to the development of a point-cathode, hooded arc type ion-source which we expect will yield more ions than the conventional capillary arc type one.

#### ACKNOWLEDGMENT

The authors wish to thank Prof. B. D. Nag for his keen interest in the work and valuable suggestions and Prof. D. N. Kundu for helpful discussions.

#### REFERENCES

- Attorling, H., 1948, *Arkiv for Matematik, Astronomi Och. Fysik* Band 35A, No. 32.  
Bakker C. J. and Kistemaker, J., 1949, *Internationaler Kongress Ueber-Kernphysik und Quantenelektrodynamik*, 5, 9.  
Bohm, D., Burhop, E. M. S., Massey, H. S. W. and Williams, R. M., 1949, Guthrie and Wakerling, "The Characteristics of electrical discharge in magnetic fields" p. 68.  
Cobine, J. D., 1941, *Gaseous conductors*, McGraw-Hill Book Co., Inc. p. 317.  
Engel, A. V., and Stenbeck, M., *Elektrische gasentladungen*, Vol. 1, p. 88.  
Fryer, E. M., 1946, *Phys. Rev.*, **70**, 231.  
Hoyaux, Max and Dujardin, Ignace, 1949, *Nuclonics*, May.  
Kenty, C., 1928, *Phys. Rev.*, **32**, 624.  
Livingston, M. Stanley, 1946, *Rev. Mod. Phys.*, **18**, 293.  
Richardson, J. R., 1948, *Phys. Rev.*, **73**, 428.  
Wilson, R. R., 1940, *J. Appl. Phys.*, **11**, 781.

# ON THE EVALUATION OF $\alpha_e$ AND $\omega_e x_e$ FROM THREE CONSTANT POTENTIAL ENERGY FUNCTIONS

M. R. KATTI\*

FACULTY OF APPLIED PHYSICS AND MECH. ENGINEERING  
INSTITUTE OF ARMAMENT STUDIES, KIRKEE

(Received October 13, 1961)

**ABSTRACT.** Following the recent technique of Varshni and Shukla for evaluating the anharmonicity constant  $\omega_e x_e$ , an alternative procedure is suggested for estimating the rotation constant  $\alpha_e$ . It is shown in the case of a large number of molecules, that the present method (called method II) yields percentage errors significantly lower than the previous method I.

An empirical relation for  $\omega_e x_e$ , evolved as a result of this study, is also examined. The results obtained by using this expression are comparable with those of Varshni and Shukla. This study also confirms that the experimental value of  $\omega_e x_e$  for the ground state of  $\text{Cl}_2$  may be in error.

## INTRODUCTION

In a recent paper (Varshni and Shukla, 1961) the anharmonicity constant  $\omega_e x_e$  in the case of 23 neutral diatomic molecules has been evaluated by a procedure which is a modification of the earlier techniques (Varshni, 1957; Tawde and Katti, 1959), based on interconnecting the various molecular constants by relations resulting from the fundamental properties of potential energy functions. Varshni and Shukla (1961) have shown that this procedure (denoted by method II) leads to values of % errors in  $\omega_e x_e$  higher than those given by the previous method I (Varshni 1957, denoted by method I). Further, from the behaviour of the predicted values of  $\omega_e x_e$  with the experimental value they have proposed an empirical relation which has been found to be satisfactory. In this paper, it is proposed to present a parallel technique for evaluating the rotation constant  $\alpha_e$  and also another empirical relation for  $\omega_e x_e$  emerging as a consequence of this study.

The closed analytical function for the potential energy  $U(r)$  of a diatomic molecule has been expressed (Varshni, 1957) as

$$U(r) = \frac{1}{2} U''(r_e)(r-r_e)^2 + \frac{1}{3} U'''(r_e)(r-r_e)^3 + \frac{1}{4} U^{IV}(r_e)(r-r_e)^4 + \dots \quad (1)$$

\* Now at Defence Science Laboratory, Delhi.

Where  $r$  is the internuclear distance and  $r_e$  its equilibrium value

$$\text{Putting } U'''(r_\theta)/U''(r_\theta) = X \quad \dots \quad (2)$$

$$\text{and} \quad U(r_e)/U''(r_e) = Y \quad \dots (3)$$

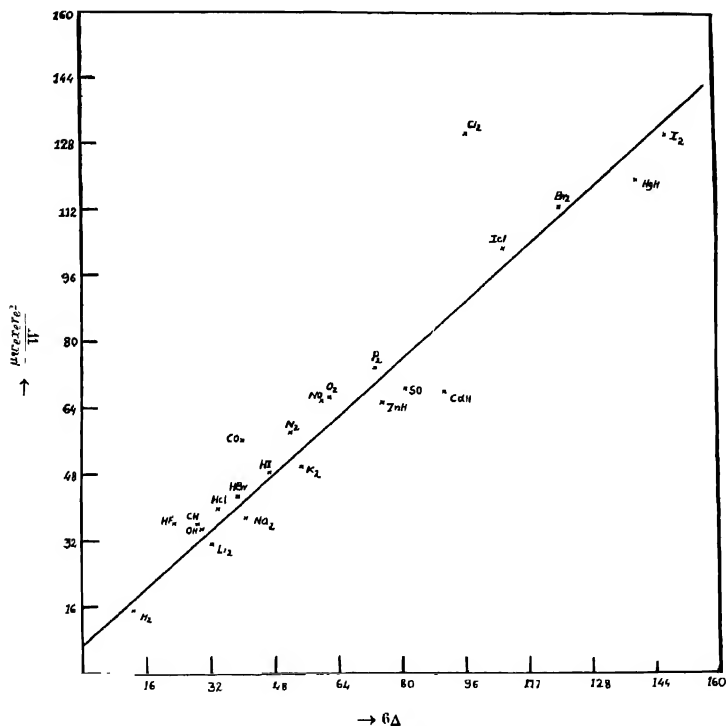


Fig. 1 Values of  $\mu_{\text{eff}}^2/W$  plotted against  $6\Delta$

the rotation constant,

$$\alpha_e = - \left[ \frac{X r_e}{3} + 1 \right] \frac{6 B_e^2}{\omega_e} \quad \dots \quad (4)$$

and 
$$\omega_{\theta} v_{\theta} = \left[ \frac{5}{3} X^2 - Y \right] \frac{W}{\mu_A} \quad \dots \quad (5)$$

where  $W = 2.1078 \times 10^{-16}$  and the other constants have their conventional meaning, Herzberg (1950).

Several different forms have been proposed for  $U(r)$  but in the above Eqs. (4) and (5) it is only the quantities  $\left[ \frac{Xr_e}{3} + 1 \right]$  and  $\left[ \frac{5}{3} X^2 - Y \right]$  which will be different for different functions and in each case they can be expressed as functions of Sutherland's parameter  $\Delta$

where

$$\Delta = K_e r_e^2 / 2D_e$$

$K_e$  and  $D_e$  being the force constant and the Dissociation energy respectively. Thus from a knowledge of  $K_e$ ,  $r_e$  and  $D_e$  one can evaluate  $X$  and  $Y$  and hence  $\alpha_e$  and  $\omega_e x_e$ .

The following scheme enumerates the different methods of estimating  $\alpha_e$  or  $\omega_e x_e$

$\alpha_e$  -

Method (I) Calculate theoretically  $X$  from Eq. (2) with any assumed p.c. function and hence  $\alpha_e$  from Eq. (4)

Method (II) Calculate theoretically  $Y$  from eqn (3) and combining this with the knowledge of the exptl. value of  $\omega_e x_e$ ,  $X$  can be obtained from Eq (5) and then  $\alpha_e$  from Eq. (4).

$\omega_e x_e$  -

Method (I) Calculate theoretically  $X$  and  $Y$  from Eqs. (2) and (3) and hence  $\omega_e x_e$  from Eq. (5).

Method (II) Obtain the value of  $X$  from a knowledge of the exptl. value of  $\alpha_e$  using Eq. (4) and combining this with the theoretically calculated value of  $Y$  from Eq. (3) estimate the value of  $\omega_e x_e$  from Eq. (5)

The value of  $\alpha_e$  or  $\omega_e x_e$  obtained by either of the above methods can then be compared with the experimental value. It will be seen in method (II), in each case, the estimated value of one of the two constants is dependent on a knowledge of the exptl. value of the other.

Varshni and Shukla (1961) have evaluated  $\omega_e x_e$ . Employing six potential energy expressions viz. Morse, Rydberg, Poschl-Teller and three more proposed by Varshni (1957), they found that in each case the average % error in the estimation of  $\omega_e x_e$  obtained by using method (II) was higher than that obtained by using method (I). They have shown that for

Morse fn. the % error increased from 31.2 to 40

for Rydberg fn. it increased from 22.7 to 35

and for Poschl-Teller it increased from 31.2 to 37

In the present paper, this study has been extended to the evaluation of  $\alpha_e$  by method (II), and it is shown that in this case, method (II) leads to % errors



significantly lower than that obtained with method (I). Reasons are also given why one should expect a higher % error for  $\omega_e x_e$  in the method (II) adopted by Varshni and Shukla than one obtains in method (I).

# RESULTS AND DISCUSSION

Some clarification is necessary about the method (II) for evaluating  $\omega_e x_e$ . For Morse function, the two relations employed by them for  $\omega_e x_e$  with methods (I) and (II) are

$$(I) \quad \omega_e x_e = 8\Delta W / \mu r_e^2 \quad \dots (6)$$

$$(II) \quad \omega_e x_e = \left[ 15\Gamma - 7\Delta \right] \frac{W}{\mu r_e^2} \quad \dots (7)$$

Where 
$$\Gamma = \left( 1 + \frac{\alpha_e \omega_e}{6B_e^2} \right)^2$$

From method (I) it is also known that

$$\alpha_e = (\Delta - 1) \frac{6B_e^3}{\omega_e} \quad \dots (8)$$

which gives 
$$\Delta = \left( 1 + \frac{\alpha_e \text{ theo } \omega_e}{6B_e^2} \right)^2 \quad \dots (9)$$

and according to Varshni and Shukla's notation

$$\Gamma = \left( 1 + \frac{\alpha_e \text{ expt } \omega_e}{6B_e^2} \right)^2 \quad \dots (10)$$

Thus it may be noted from Eqs. (9) and (10) that  $\Delta$  and  $\Gamma$  depend on  $\alpha_{e \text{ theo}}$  and  $\alpha_{e \text{ expt}}$ , respectively. It is the disparity between  $\alpha_{e \text{ theo}}$  and  $\alpha_{e \text{ expt}}$ , hence  $\Delta$  and  $\Gamma$  (vide Table I, Varshni and Shukla (1961)) which shows up in the method II for  $\omega_e x_e$ .

Varshni (1957) employing method (I) showed that with most of the p.c. expressions,  $\omega_e x_e$  can be estimated to a greater degree of accuracy than  $\alpha_e$ . This may be attributed to the approximate nature of the relation for  $\alpha_e$  compared to that of  $\omega_e x_e$ . It is apparent that because of these approximations in the relation for  $\alpha_e$ , the value of  $X$  calculated from the same with experimental  $\alpha_e$  inherits these defects. This on substitution in the relation for  $\omega_e x_e$  brings down its efficiency further as  $X$  appears in the second power. Hence, it occurred to the author that

a reverse procedure of the same viz. method (II) for  $\alpha_e$  might lead to some interesting results.

For calculating  $\alpha_e$  the value of  $X$  is found from Eq. (5) with the exptl. value of  $\omega_e x_e$  and is then substituted in Eq. (4). Thus Eq. (5) gives

$$X = \left\{ \frac{3}{5} \left( \frac{\mu \omega_e x_e}{W} + Y \right) \right\}^{\frac{1}{2}} \quad \dots \quad (11)$$

on putting this in Eq (4) we get

$$\alpha_e = \left\{ \left[ \frac{1}{15} \left( \frac{\mu \omega_e x_e r_e^2}{W} + Y r_e^2 \right) \right]^{\frac{1}{2}} - 1 \right\} \frac{6B_e^2}{\omega_e} \quad \dots \quad (12)$$

with this relation (12) denoted as method II the calculated values and errors have been recorded here for Morse and Rydberg functions in the following Tables I and II. The same molecules studied by Varshni and Shukla have been examined here. The values of all the relevant molecular constants have been taken from Varshni (1957) and Varshni and Shukla (1961).

#### MORSE FUNCTION

The Morse (1929) curve is represented by

$$U(r) = D_e [1 - e^{-a(r-r_e)}]^2 \quad \dots \quad (13)$$

$$\text{with } X = -3a \quad \text{and} \quad Y = 7a^2 \quad \text{where} \quad a^2 = \frac{K_e}{2D_e} = \frac{\Delta}{r_e^2}$$

This gives

$$(I) \quad \alpha_e = (\Delta^{\frac{1}{2}} - 1) \frac{6B_e^2}{\omega_e} \quad \dots \quad (14)$$

$$(II) \quad \alpha_e = \left\{ \left[ \frac{1}{15} \left( \frac{\mu \omega_e x_e r_e^2}{W} + 7\Delta \right) \right]^{\frac{1}{2}} - 1 \right\} \frac{6B_e^2}{\omega_e} \quad \dots \quad (15)$$

Estimated results and % errors by the two relations (I) and (II) are shown in Table I. Values of  $\Delta$  used here are the same as those quoted in Varshni and Shukla (1961).

#### RYDBERG FUNCTION

Rydberg (1931) proposed

$$U(r) = -D_e [1 + b\rho]^{-bp} \quad \dots \quad (16)$$

where  $\rho = r - r_e$

one gets

$$(I) \quad \alpha_e = \left[ \frac{2\sqrt{2}\Delta^{\frac{1}{2}}}{3} - 1 \right] \frac{6B_e^2}{\omega_e} \quad (17)$$

$$(II) \quad \alpha_e = \left\{ \left[ \frac{1}{15} \left( \frac{\mu \omega_e x_e r_e^2}{W} + 6\Delta \right) \right]^{\frac{1}{2}} - 1 \right\} \frac{6B_e^2}{\omega_e} \quad (18)$$

Results for this function are recorded in Table II

TABLE I  
(Morse function)

Molecule	$\alpha_e$ (exptl)	$\alpha_e$ Cal. (I)	% error	$\alpha_e$ cal (II)	% error
H <sub>2</sub>	2.993	2.222	-25.8	2.095	-37.8
ZnH	0.2500	0.4248	+69.9	0.3673	+46.8
CdH	0.2180	0.3599	+65.1	0.3507	+60.9
HgH	0.3120	0.5090	+63.1	0.4448	+42.3
CH	0.5340	0.5238	-1.9	0.5035	-5.7
OH	0.7140	0.7076	-0.9	0.6838	-4.2
HF	0.7705	0.6055	-22.2	0.6481	-16.9
HCl	0.3019	0.3109	+3.3	0.2916	-3.5
HBr	0.2260	0.2540	+12.4	0.2325	+2.9
HI	0.1830	0.2583	+41.1	0.1817	-0.7
Li <sub>2</sub>	0.00704	0.0103	+46.3	0.00889	+26.3
Na <sub>2</sub>	0.00079	0.00146	+84.8	0.00125	+58.2
K <sub>2</sub>	0.000219	0.00412	+1881	0.000360	+64.4
N <sub>2</sub>	0.0187	0.01969	+5.3	0.01860	-0.5
P <sub>2</sub>	0.00142	0.00177	+24.7	0.00160	+12.7
O <sub>2</sub>	0.01579	0.0175	+10.8	0.0168	+6.5
SO	0.00562	0.00719	+27.9	0.00619	+10.1
Cl <sub>2</sub>	0.0017	0.00190	+11.8	0.001915	+12.9
Br <sub>2</sub>	0.000275	0.000423	+53.8	0.000378	+37.5
I <sub>2</sub>	0.000117	0.000154	+31.6	0.0001365	+17.1
ICl	0.000536	0.000670	+25.0	0.000588	+9.7
CO	0.01748	0.01844	+5.5	0.01637	-6.4
NO	0.0178	0.0198	+11.2	0.01837	+3.2

Average 31.9

Average 20.5

TABLE II  
(Rydberg function)

Molecule	$\alpha_r$ (expd)	$\alpha_r$ Calc (I)	% error	$\alpha_r$ Calc (II)	% error
HF	2.993	1.853	-38.1	1.844	-38.4
ZnH	0.2500	0.3950	+58.0	0.3437	+37.5
CdH	0.2180	0.3355	+54.0	0.2802	+28.5
HgH	0.3120	0.1765	-52.7	0.4204	+34.7
CH	0.5340	0.4744	-11.2	0.4702	-11.4
OH	0.7140	0.6425	-10.1	0.6202	-13.1
HF	0.7705	0.5429	-29.5	0.6065	-21.3
HCl	0.3019	0.2836	-6.0	0.2727	-9.7
HBr	0.2260	0.2326	+3.0	0.2176	-3.7
HJ	0.1830	0.1857	+1.5	0.1703	-6.9
Li <sub>2</sub>	0.00701	0.00938	+30.0	0.00823	+16.9
Na <sub>2</sub>	0.00079	0.001342	+70.0	0.00116	+46.8
K <sub>2</sub>	0.000219	0.0003813	+74.1	0.000337	+53.9
N <sub>2</sub>	0.0187	0.01844	-1.4	0.01748	-5.7
P <sub>2</sub>	0.00112	0.01644	+15.8	0.00127	+10.6
O <sub>2</sub>	0.01579	0.01619	+2.5	0.0153	-3.2
SO	0.00562	0.01026	+82.5	0.00581	+3.4
Cl <sub>2</sub>	0.0017	0.001775	+4.4	0.001829	+7.6
Br <sub>2</sub>	0.000275	0.0003957	+43.8	0.000358	+30.4
I <sub>2</sub>	0.000117	0.0001446	+23.6	0.000132	+12.8
ICl	0.000536	0.000689	+27.6	0.000556	+3.7
CO	0.01748	0.01506	-13.8	0.01300	-25.6
NO	0.0178	0.01832	+3.0	0.01730	-3.0
			Average 28.0	Average 18.6	

It may be noted from Tables I and II that with Morse and Rydberg expressions the average % error by the present method (II) are much lower than those by the earlier method (I). The same behaviour is expected of other functions, viz., Poschl-Teller and Varshni's functions. Thus on the basis of the above results it may be said that the method (II) is favourable only for the evaluation of  $\alpha_e$ .

It was noticed during these computations that the quantity  $\mu\omega_e x_e r_e^2/W$  was closely following the value of  $6\Delta$  for 17 molecules and for the remaining 6 molecules relatively large dispersion was found. Fig. (1) shows the observed values of  $\mu\omega_e x_e r_e^2/W$  against  $6\Delta$  for all the molecules under consideration.

A straight line equation was fitted for the variation of these two quantities by the least squares method. The equation obtained is

$$\frac{\mu\omega_e x_e r_e^2}{W} = 5.2766\Delta + 7.666 \quad (19)$$

$$\text{or } \omega_e x_e = 5.2766 \frac{\Delta W}{\mu r_e^2} + 7.666 \frac{W}{\mu r_e^2} \quad \dots (20)$$

Relation (20) may be compared with a similar empirical relation

$$\omega_e x_e = (5\Delta + 9) \frac{W}{\mu r_e^2} \quad \dots (21)$$

proposed earlier by Varshni (1957) on other considerations. The performance of this new relation (20) has been examined by the estimates of  $\omega_e x_e$  in the case of all the molecules studied here. The results and % errors are recorded in Table III.

TABLE III

Molecule	$\omega_e x_e$ (exptl)	$\omega_e x_e$ (Varshni Emp)	% error	$\omega_e x_e$ Present paper	% error
H <sub>2</sub>	117.09	136.70	+ 15.86	141.51	+ 19.9
ZnH	55.14	57.78	+ 4.79	61.82	+ 12.1
CdH	46.3	56.78	+ 22.42	59.78	(+ 29.1)
HgH	83.01	89.08	+ 7.31	90.71	+ 9.3
CH	64.3	62.31	- 3.09	59.72	- 14.9
OH	82.81	83.54	+ 0.88	80.32	- 3.0
HF	90.069	91.643	+ 1.75	91.56	+ 1.70
HCl	52.05	51.09	- 1.84	48.6	- 6.6
HBr	45.21	43.59	- 3.58		
HI	39.73	11.00			
I <sub>2</sub>	2.592	2.526	- 2.55	2.42	- 6.6
Na <sub>2</sub>	0.726	0.7255	- 0.07	0.719	+ 3.2
K <sub>2</sub>	0.354	0.3547	+ 0.20	0.4190	+ 14.7
N <sub>2</sub>	14.456	14.217	- 1.65	13.00	- 10.1
P <sub>2</sub>	2.804	2.660	- 5.14	2.742	- 2.2
O <sub>2</sub>	12.073	11.650	- 3.50	11.18	- 7.4
SO	6.116	6.764	+ 10.6	7.002	+ 14.5
Cl <sub>2</sub>	4.0	3.025	(- 24.37)	2.826	(- 29.4)
Br <sub>2</sub>	1.145	1.106	- 3.41	1.149	+ 0.35
I <sub>2</sub>	0.6127	0.6318	+ 3.12	0.6416	+ 4.7
ICl	1.465	1.454	- 0.75	0.1443	- 1.5
CO	13.46	12.28	- 8.77	10.42	- 22.6
NO	13.97	13.32	- 4.65	12.86	- 8.0

Average = 4.96

Average = 7.94

The results are found to be satisfactory, the average % error being only 7.94 (with two exceptions CdH and Cl<sub>2</sub>) which is comparable with 4.96 and 11.1

obtained by Varshni and Shukla (1961), Varshni (1957). The present study also confirms the observation of Varshni and Shukla (1961) regarding the high % error found for  $\text{Cl}_2$  which may be due to large error in the constants of the ground state.

It may also be noted that even for those molecules, where  $\frac{\mu\omega_e x_e r_e^2}{W}$  is found to deviate more from  $6\Delta$ , the estimated value of  $\omega_e x_e$  show comparatively less discrepancy.

#### ACKNOWLEDGMENTS

I am indebted to Professor B. Patnaik for suggesting many interesting aspects of the present work and for innumerable helpful discussions. I am thankful to Air Commodore O. P. Mehra, Dean, Institute of Armament Studies, for permission to publish this paper. Thanks are also due to Research and Development Organisation, Ministry of Defence, for the award of a Research Training Fellowship.

#### REFERENCES

- Herzberg, G., 1950, *Spectra of Diatomic Molecules* (D. Van Nostrand Co. Inc, Princeton)  
 Morse, P. M., 1929, *Phys. Rev.*, **34**, 57  
 Rydberg, 1931, *Z. Physik*, **73**, 376.  
 Tawde, N. R. and Katti, M. R., 1959, *Ind. J. Phys.*, **33**, 18, 89.  
 Varshni, Y. P., 1957, *Rev. Mod. Phys.*, **29**, 661.  
 Varshni, Y. P., and Shukla, 1961, *Trans. Farad. Soc.*, **57**, 537

# SCATTERING OF POSITRONS BY SIX-FOLD IONIZED URANIUM ATOM

BHAJAN SINGH

SCIENCE COLLEGE, PATNA

AND

BROJENDRA K. GUHA

B. N. COLLEGE, PATNA

(Received October 14, 1961)

**ABSTRACT.** The *S*-wave scattering cross section for the elastic scattering of low velocity positrons by the six-fold ionized atom of U has been calculated using the modified Coulomb potential. It is found that the Coulomb part is predominantly effective.

The differential cross section for the scattering of electrons by the bare nucleus of uranium was calculated by Yadav (1955). In the present paper the *S*-wave differential cross section for the scattering of positrons by the six-fold ionized atom of uranium has been calculated. The distortion of the electronic cloud has been neglected and the interaction is assumed to be due to the modified Coulomb potential of the ionized atom expressed in terms of the effective charge  $Z_p e$  i.e.,

$$V = \frac{Z_p}{r} e^2$$

$Z_p$  has been tabulated by Ridley (Ridley, 1954) using Hartree method without exchange.

The solution of the appropriate Schroedinger equation can be expressed as

$$u = \sum_{l=0}^{\infty} \frac{\chi_l(r)}{r} P_l(\cos \theta) \quad \dots (1)$$

where the equation satisfied by  $\chi_l(r)$  is

$$\frac{d^2 \chi_l}{d\rho^2} + \left\{ k^2 - \frac{2\alpha k}{\rho} - \frac{l(l+1)}{\rho^2} \right\} \chi_l = 0 \quad \dots (2)$$

where now the distance has been expressed in atomic units with

$$k^2 = \frac{8\pi^2 m}{h^2} a_0^2 E \text{ or } E = 13.6 k^2 \text{ ev, where } a_0 \text{ is the first Bohr radius, and}$$

$$\alpha k = \frac{4\pi^2 m}{h^2} a_0 e^2 Z_p = Z_p.$$

Eq. (2) reduces to

$$\frac{d^2 \chi_l}{d\rho^2} + \left\{ k^2 - \frac{2Z_p}{\rho} - \frac{l(l+1)}{\rho^2} \right\} \chi_l = 0 \quad (3)$$

The asymptotic solution of (3) is

$$\chi_l \xrightarrow{\rho \rightarrow \infty} A \sin \left( k\rho - \frac{1}{2}l\pi - \alpha \ln 2k\rho + \eta_l + \delta_l \right) \quad (4)$$

where  $\eta_l$  and  $\delta_l$  are the Coulomb and the non-Coulomb phase shifts respectively (Schiff, 1949). The differential cross section can be written as

$$\sigma(\theta) = |f_m(\theta)|^2$$

$$\text{where } f_m(\theta) = f_c(\theta) + \sum_{l=0}^{\infty} k^{-1} (2l+1) \cdot e^{i(2\eta_l + \delta_l)} \cdot \sin \delta_l \cdot P_l(\cos \theta)$$

$$= f_c(\theta) + \frac{1}{2ik} \sum_{l=0}^{\infty} (2l+1) \cdot e^{2i\eta_l} (e^{2i\delta_l} - 1) P_l(\cos \theta).$$

$$\text{where } f_c(\theta) = -\frac{\alpha}{2k \sin^2 \frac{\theta}{2}} \cdot e^{i\alpha \ln \sin^2 \frac{\theta}{2}} \quad (\text{Schiff, 1949})$$

Since we are dealing with low energies ( $k = 2$  corresponds to 55 ev approximately) and the potential anomaly is of short range ( $\rho = 3.6$  atomic units), it is reasonable to assume that only the  $S$ -wave will be affected. The same conclusion can be drawn from the consideration of the W.K.B integrals (Mott and Massey, 1949). The lower limits of these integrals fall outside the potential anomaly indicating that there will be no marked deviation from Coulomb scattering. So,

$$f_m(\theta) = f_c(\theta) + \frac{1}{2ik} \cdot e^{2i\eta_0} (e^{2i\delta_0} - 1) \quad \dots (6)$$

$$\text{Let } \sigma(\theta) = \sigma_c(\theta) + \sigma_{n.c.}(\theta) \quad \dots (7)$$

$$\text{where } \sigma_c(\theta) = \frac{\alpha^2}{4k^2} \cdot \operatorname{cosec}^4 \frac{\theta}{2} = \frac{Z_p^2}{4k^4} \operatorname{cosec}^4 \frac{\theta}{2}, \quad (Z_p = 6) \quad \dots (7a)$$

$$\text{and } \sigma_{n.c.}(\theta) = \frac{1}{k^2} \left\{ \begin{array}{c} \alpha \sin \delta_0 \cos \left( \alpha \ln 2 \sin^2 \frac{\theta}{2} \right) \\ \sin^2 \delta_0 - \sin^2 \frac{\theta}{2} \end{array} \right\} \quad \dots (7b)$$

$\delta_0$  was calculated by solving Eq. (3) for  $l = 0$  numerically and matching the solution with the theoretical value given by Eq. (4) with

$$\eta_0 = \alpha \sigma_0 \cdot \Gamma(1+i\alpha)$$



which was taken from Coulomb Wave-function Table of Nat. Bur. of Standard, U.S. The ratio

$$R = 1 + \frac{\sigma_{n,c}}{\sigma_e}$$

has been calculated.

TABLE I  
Variation of phase-shift with energy

$k$	$\delta_0$	$\eta_0$	$(\delta_0 + \eta_0)$
1	0.62	5.52	6.14
2	0.04	1.05	1.09

TABLE II

$k$	$\theta/\pi$	$\sigma_e$	$\sigma_{n,c}$	$R$
1	1.00	9.0	0.113	1.01
	0.75	12.3	3.49	1.28
	0.50	36.0	-5.32	0.85
	0.25	420	-20.8	0.95
	0.10	$150 \times 10^2$	-28.6	1.00
	0.02	$925 \times 10^4$	$-205 \times 10$	1.00
	0.01	$149 \times 10^6$	$-657 \times 10$	1.00
2	1.00	0.563	$1.65 \times 10^{-2}$	1.03
	0.75	0.772	$1.26 \times 10^{-2}$	1.02
	0.50	2.25	$-0.10 \times 10^{-2}$	0.97
	0.25	26.2	2.185	1.01
	0.10	939	1.15	1.00
	0.02	$578 \times 10^2$	-30.5	1.00
	0.01	$924 \times 10^4$	85.0	1.00

#### CONCLUSIONS

In most cases  $R$  is nearly unity indicating that most of the contribution to scattering is from the Coulomb part. The other part is mainly effective in backward scattering. This effect increases with the energy.

The differential cross section for the scattering of more energetic positrons is being calculated by us and will be published in due course.

#### ACKNOWLEDGMENTS

We wish to express our deep sense of gratitude to Prof. H. N. Yadav for his guidance and to Prof. B. N. Singh for his constant encouragement.

#### REFERENCES

- Mott, N. F. and Massey, H. S. W., 1949, *The Theory of Atomic Collisions*, p. 127.  
Ridley, E. G., 1957, *Proc. Roy. Soc. (Lond.)* **243**, 422.  
Schiff, L. I., 1955, *Quantum Mechanics*, p. 120.  
Yadav, H. N., 1955, *Proc. Phys. Soc. (Lond.)*, **A68**, 4, 348.

# MUTUAL DIFFUSION OF BINARY MIXTURES OF AMMONIA WITH He, Ne AND Xe

I. B. SRIVASTAVA

INDIAN ASSOCIATION FOR THE CULTIVATION OF SCIENCE, CALCUTTA-32,

INDIA

(Received December 29, 1961)

**ABSTRACT.** Experimental measurements of the binary diffusion coefficients for  $\text{NH}_3$ -He,  $\text{NH}_3$ -Ne and  $\text{NH}_3$ -Xe systems over the temperature range 0–60°C are reported. The measurements were made by the two bulb technique by allowing the diffusion to take place between the two bulbs through a precision capillary tube. A differential thermal conductivity analyzer was employed for analysing the samples of the gas withdrawn from one of the bulbs at different times. The data have been used for determining the force parameters for the unlike molecular interaction of the Lennard-Jones (12-6) potential model. These parameters have been utilised, in conjunction with the semiempirical combination rules to obtain the force constants of  $\text{NH}_3$  for the Stockmayer potential model. It has been concluded that the combination rules give a fairly good approximation and the force constants of  $\text{NH}_3$  determined from viscosity by Monchick and Mason are sufficiently reliable.

## INTRODUCTION

Experimental determinations of the forces between unlike molecules have aroused considerable interest from the point of view of understanding many properties of gaseous mixtures. The mutual diffusion coefficient,  $D_{12}$ , is one of the most suitable transport properties for providing information about the unlike molecular interactions, since it depends, in the first approximation, only on the forces between unlike molecules. Very recently, a number of workers have measured  $D_{12}$  for certain gas mixtures at different temperatures and used their data for calculating the unlike interaction parameters for different potential models. A full summary of the  $D_{12}$  data upto date have been given by Westenberg (1957) and by Paul and Srivastava (1961a). However, the measurements of  $D_{12}$  for mixtures of a polar and a nonpolar gas are very few and no data are available for  $D_{12}$  of mixtures of polar gases. Detailed references to the available data for the  $D_{12}$  of polar-nonpolar binary mixtures have been given by Srivastava and Srivastava (1962).

In the absence of suitable experimental data for determining the forces between unlike molecules, it is necessary to calculate these forces from the corresponding forces between like molecules, using some semi-empirical combination rules. The combination rules for calculating theoretically the forces between unlike spherical nonpolar molecules for the Lennard-Jones (12-6) and (exp-6) potential models,

have been shown to be quite satisfactory by many workers but probably no investigation has yielded any definite conclusion about the adequacy of the combining laws for obtaining the polar-non polar interaction parameters for the Lennard-Jones (12.6) potential model. The early investigators, however, had used the force constants for the polar molecules obtained from the second virial coefficient,  $B(T)$ , for the Stockmayer potential model. These values of the force constants may be inappropriate for calculating the transport properties, as the assumption of the point-dipole model is likely to cause greater error in the second virial coefficient than in the transport properties.

Kreiger (1951) evaluated the collision integrals for a modified Stockmayer potential model for calculating viscosity and thermal conductivity of polar gases and used them for calculating the force constants of several molecules from viscosity. But, Ilean *et al* (1960) have detected some error in his calculations and showed that the force constants obtained from experimental data by using the corrected calculations were physically unrealistic. Very recently Monchick and Mason (1960) have reported values of the collision integrals for the Stockmayer (12 : 6 : 3) potential model which are required for calculating the transport properties of polar gases and have determined the force constants of several polar molecules from viscosity. It is therefore of considerable interest to measure the different transport properties of polar gases and their mixtures and see how far the calculations of Monchick and Mason which are based on certain simplifying assumptions, are successful in explaining the observed transport properties.

A number of workers in this laboratory have measured the diffusion coefficients of binary mixtures of non-polar gases. The references to these works are given by Srivastava and Srivastava (1962), where they have reported the measurements of the diffusion coefficient for the binary mixtures of ammonia with argon and krypton and have concluded that the combination rules for polar-nonpolar systems can give good approximations and the force constants of ammonia obtained by Monchick and Mason are not in very good agreement with those obtained from diffusion data. In the present work, the diffusion coefficients of  $\text{NH}_3\text{-He}$ ,  $\text{NH}_3\text{-Ne}$  and  $\text{NH}_3\text{-Xe}$  have been measured in the temperature range 0–60°C and the conclusions obtained by Srivastava and Srivastava (1962) are further tested.

#### APPARATUS AND THEORY

The two bulb technique of Ney and Armistead (1947) was employed for measuring the diffusion coefficients. The details of the apparatus and the experimental procedure have been discussed fully by Srivastava and Srivastava (1959) and Paul and Srivastava (1961b).

The rare gases were supplied by the British Oxygen Company, England and were quoted to be spectroscopically pure except Xe which contained about 1% krypton. Pure and dry ammonia was prepared by heating a mixture of pure ammonium chloride and calcium oxide and passing the issuing gas through three

large U-tubes containing sodium hydroxide pellets. The gas was further purified by liquefying it in a cooling trap containing metallic sodium and then in two more cooling traps and finally distilling in evacuated gas cylinder.

It has been shown by Ney and Arnistead that the relaxation time  $1/\alpha$  of the system, as defined by the relation

$$(\bar{C}_1 - C_1^t)/(C_1^0 - C_1^t) = \exp(-\alpha t) \quad \dots (1)$$

is given

$$\alpha = (D_p A/l) \times (V_0/V_1 V_2) \quad \dots (2)$$

where  $C_1^0$ ,  $C_1^t$  and  $\bar{C}_1$  are respectively the concentrations of the heavier gas initially, at time  $t$  sec. and after complete mixing. The quantities  $V_1$  and  $V_2$  are the volumes of two bulbs,  $V_0$  being equal to  $(V_1 + V_2)$ . The quantity  $D_p$  is the coefficient of diffusion in  $\text{cm}^2/\text{sec.}$  at a pressure  $p$  cm. of Hg,  $A$ ,  $l$  being the effective cross sectional area and the effective length of the diffusion path respectively.

The quantity,  $\alpha$ , is obtained from the slope of the plot of  $\log (\bar{C}_1 - C_1^t)$  against  $t$  and  $D_p$  can be calculated from Eq. (2). The diffusion coefficient at atmospheric pressure,  $D_{atm.}$  is related to  $D_p$  by the equation

$$D_{atm.} = D_p \times p/76 \quad \dots (3)$$

#### EXPERIMENTAL RESULTS

The quantity  $\bar{C}_1 = .373$  was calculated from the initial concentrations in the two bulbs, which was further checked for some runs by determining the concentration at an interval of seven times the relaxation time.

Fig. (1) gives the calibration curves for the three gas pairs and Fig. (2) shows the plot of  $\log_{10} (\bar{C}_1 - C_1^t)$  versus  $t$  for  $\text{NH}_3\text{-Ne}$  pair.

The experimental values of the diffusion coefficients obtained in the present work are given in Table I. No other data for the systems considered here are available for comparison.

#### DETERMINATION OF POTENTIAL PARAMETERS

Since the effective total energy of interaction between a polar and a nonpolar molecule has the same form as that between two non-polar molecules which are spherically symmetric (Hirschfelder *et al.* 1954), the force constants for the unlike interactions have been determined from  $D_{12}$  data on the Lennard-Jones (12:6) potential model, by the intersection method of Buckingham (1938) followed by a least square fitting. The details of the method have been discussed by Paul and Srivastava (1961b). The values of the force parameter, thus obtained are given in column 3 of Table II.

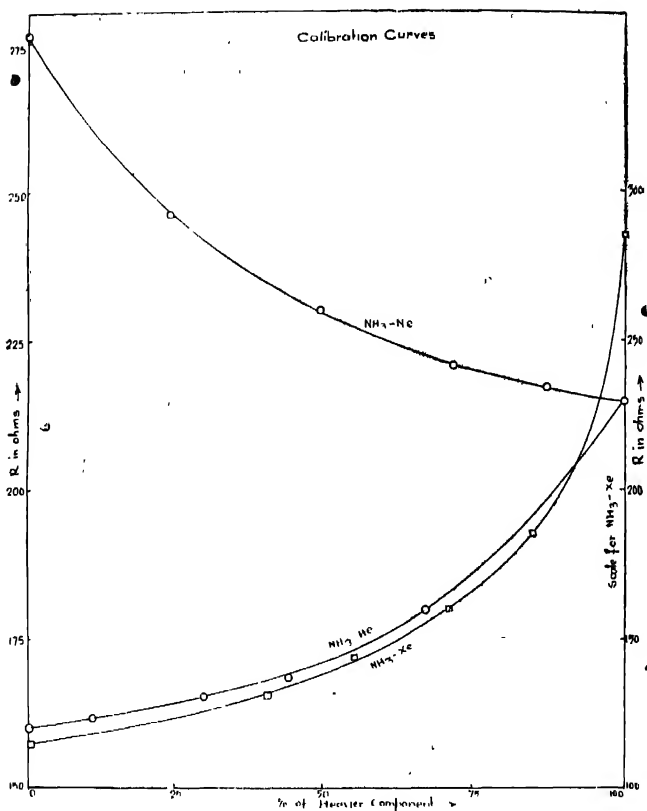


Fig. 1

A set of parameters has also been obtained, for each system, from the semi-empirical combination rules for the polar-nonpolar systems (Hirschfelder, Curtiss and Bird, 1954) by making use of the force constants of nonpolar gases derived from viscosity and those for ammonia from  $B(T)$  and also from viscosity. These are recorded in column 4 and 5 of Table II.

A comparison of the force constants obtained by different methods shows that the  $\epsilon/k$  values for a given system obtained by the different methods are in fairly good agreement. The values of  $\sigma$  for these systems, obtained from the diffusion data, are also in reasonable agreement with those obtained from the combination rules when force constants of ammonia obtained from viscosity are used. But when force constants for ammonia are taken from  $B(T)$  the combi-

TABLE I  
Mutual diffusion coefficients in cm<sup>2</sup>/sec.

Gas Mixtures	Temp. 'K	Pressure in mm. Hg	$D_p$	$D_{atm}$			
				Expt.	a	b	c
NH <sub>3</sub> -He	274.2	57.50	8.83	0.668	0.650	0.815	0.659
	308.2	55.54	10.71	0.783	0.802	1.002	0.810
	333.1	62.05	10.79	0.881	0.903	1.131	0.924
NH <sub>3</sub> -Ne	274.2	55.10	4.11	0.298	0.303	0.379	0.308
	308.4	52.91	5.43	0.378	0.374	0.471	0.383
	333.1	60.91	5.23	0.419	0.423	0.542	0.440
NH <sub>3</sub> -Xe	274.2	56.09	1.54	0.114	0.116	0.132	0.114
	308.4	59.81	1.84	0.145	0.146	0.167	0.144
	333.1	58.70	2.24	0.173	0.171	0.195	0.169

a. Calculated from force constants fitted to  $D_{12}$  data.

b. Calculated from combination rules and force constants for NH<sub>3</sub> from  $B(T)$ .

c. Calculated from combination rules and force constants for NH<sub>3</sub> from viscosity.

nation rules give  $\sigma$  values much smaller than those from the  $D_{12}$  data. This is due to the very low value of  $\sigma$  for NH<sub>3</sub> obtained from second virial coefficient. It has been pointed out by Rowlinson (1949) that the low value of  $\sigma$  for ammonia may be due to the hydrogen bonding.

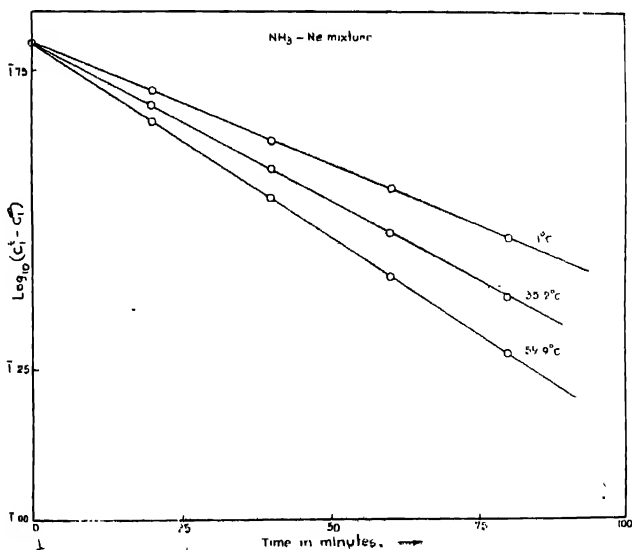


Fig. 2

TABLE II

Potential parameters on the Lennard-Jones (12:6) model

Gas pair	Force parameters	Present work from $D_{12}$ data	Combination rules	
			a	b
$\text{NH}_3\text{--He}$	$\epsilon_{12}/k$ °K	62.15	62.63	63.46
	$\sigma_{12}$ Å	2.872	2.569	2.852
	$\epsilon_{12}/k$ °K	109.10	115.19	117.60
$\text{NH}_3\text{--Ne}$	$\sigma_{12}$ Å	3.029	2.678	2.961
	$\epsilon_{12}/k$ °K	291.35	298.47	301.6
	$\sigma_{12}$ Å	3.558	3.301	3.546

a. Using force constants for  $\text{NH}_3$  from  $B(T)$ b. Using force constants for  $\text{NH}_3$  from viscosity

## COMPARISON WITH EXPERIMENTS

The experimental  $D_{12}$  values have been compared in Table I with those calculated by using the three sets of parameters given in Table II. The force parameters obtained from the observed diffusion data reproduce the  $D_{12}$  values quite satisfactorily for all the systems. It appears, therefore, that the Lennard-Jones (12:6) model is sufficiently adequate for explaining the transport properties for these systems. No further test for the reliability of the force constants obtained here is possible as no other data for these systems are available.

The force constants for unlike interaction obtained with the help of the combination rules and the second virial data for ammonia give  $D_{12}$  values much higher than the experimental values for all the systems. This is due to the low value of  $\sigma$  for ammonia due to hydrogen bonding as remarked earlier. When the force constants from viscosity are used, the agreement is fairly satisfactory but some discrepancies are observed in the cases of  $\text{NH}_3\text{--He}$  and  $\text{NH}_3\text{--Ne}$  systems, which may be due to either the inadequacy of the combining laws or possible errors in the force constants of pure components.

## FORCE PARAMETERS FOR AMMONIA FROM DIFFUSION COEFFICIENTS OF BINARY MIXTURES

The force parameters for unlike interactions obtained from the experimental values of  $D_{12}$  can be utilized to calculate the force constants of ammonia by making use of the combining laws and the available data for the dipole moment of  $\text{NH}_3$  and the polarizability and the force constants of the nonpolar molecules. In this way, a set of values for the force constants is obtained from the  $D_{12}$  data of each pair, and these are recorded in Table III, along with those obtained earlier from the diffusion data of  $\text{NH}_3\text{--A}$  and  $\text{NH}_3\text{--Kr}$ , by Srivastava and Srivastava (1962) and also from other sources. It will be seen that the different sets of values obtained from  $D_{12}$  data do not agree very well among themselves and



further, the  $\sigma$  values are generally somewhat higher and the  $\epsilon/k$  values lower than the values given by Monchick and Mason. Also the  $\sigma$ -value obtained from  $B(T)$  is too low but the  $\epsilon/k$  value is fairly reliable.

TABLE III  
Force constants of  $\text{NH}_3$  for Stockmayer potential model.

Force constants	gas pair	From $D_{12}$ (expt.) and combination rules					Mean value	From viscosity (Monchick and Mason)	From $B(T)$
		$\text{NH}_3\text{-He}$	$\text{NH}_3\text{-Ne}$	$\text{NH}_3\text{-Ar}$	$\text{NH}_3\text{-Kr}$	$\text{NH}_3\text{-Xe}$			
$\epsilon/k$	K	343.8	308.8	369.7	333.0	331.0	337.3	358	320
	Å	3.240	3.280	3.215	3.165	3.130	3.206	3.15	2.80

\*Srivastava and Srivastava (1962)

Our experiments give for ammonia the mean value  $\epsilon/k = 337$ ,  $\sigma = 3.21$  as compared to Monchick and Mason's value of  $\epsilon/k = 358$ ,  $\sigma = 3.15$  which were calculated from viscosity data by using an approximate theory. Further, from the lack of good agreement between the different sets of values, it appears that the combining laws for polar-nonpolar interaction give good approximation but are not quite adequate for accurate work.

#### ACKNOWLEDGMENTS

The author is grateful to Professor B. N. Srivastava, D.Sc., F.N.I., for his guidance and valuable discussions throughout the progress of the work. He is also thankful to Mr. R. Paul for some help in the experiment.

#### REFERENCES

- Buckingham, R. A., 1938, *Proc. Roy. Soc. (London)*, **A 168**, 264.
- Hirschfelder, J. O., Curtiss, C. F., and Bird, R. B., 1954, *Molecular Theory of Gases and Liquids* (John Wiley & Sons Inc., N. Y.)
- Itou, E. C., Glueck, A. R. and Svehla, R. A. 1960, NASA Tech. Note D-481
- Krieger, F. J., July, 1951, The viscosity of Polar Gases, Project Rand Research Memorandum, No. RM-646.
- Monchick, L. and Mason, E. A., 1961, *J. Chem. Phys.*, **35**, 1676.
- Nev, E., and Armistead, F. C., 1947, *Phys. Rev.*, **71**, 14.
- Paul, R. and Srivastava, I. B., 1961a, *J. Chem. Phys.*, **35**, 1621.
- Paul, R. and Srivastava, I. B., 1961b, *Ind. J. Phys.*, **35**, 465.
- Rowlinson, J. S., 1949, *Trans. Farad. Soc.*, **45**, 974.
- Srivastava, B. N. and Srivastava, K. P., 1959, *J. Chem. Phys.*, **30**, 984.
- Srivastava, B. N. and Srivastava, I. B., 1962, *J. Chem. Phys.* (In Press)
- Westenberg, A. A., 1957, *Combustion and Flame*, **1**, 346.

# NONLINEARITY OF THERMAL EXPANSION OF SOLIDS WITH TEMPERATURE

G. B. MITRA AND S. K. MITRA\*

DEPARTMENT OF PHYSICS, INDIAN INSTITUTE OF TECHNOLOGY, KANPUR

(Received January 18, 1962)

**ABSTRACT.** An extremely precise X-ray diffraction technique has been utilised for determining the lattice constants of copper, gold, aluminium, germanium and four alloys consisting of copper and aluminium at various temperatures between 30°C to 500°C. Coefficients of thermal expansion at different temperatures for each substance were observed to be different. The difference between the lattice constant actually observed at a given temperature and that which would be obtained if the coefficient of thermal expansion were constant at its room temperature value has been termed the 'anomalous thermal expansion at that temperature'. Plots of logarithms of the 'anomalous thermal expansions at various temperatures with the reciprocals of the corresponding temperatures in °K for all the substances studied have been found to be straight lines, slopes of which have been observed to be of the order of the vacant lattice site activation energy of the corresponding solids.

## INTRODUCTION

The thermal expansion of solids has been attributed to the anharmonic vibration of atoms about their mean position. The average position of atoms at temperature  $T^{\circ}\text{K}$  has been shown to be

$$r = 3kTp/4q^2$$

where  $k$  is the Boltzmann constant and  $p$  and  $q$  are constants occurring in the expression for the interatomic potential function. Thus the coefficient of thermal

expansion  $\frac{1}{x_0} \cdot \frac{dx}{dT}$  where  $x_0$  is the position coordinate of the atom at  $0^{\circ}\text{K}$ , is expected

to be independent of temperature. In other words, the length vs temperature ( $a-T$ ) curve should be linear. However, experimental ( $a-T$ ) curves are found to be nonlinear showing that the coefficient of thermal expansion is dependent on temperature. Lawson (1950) studied the nonlinearity of the thermal expansion curves in the case of silver halides. He defined a new quantity

$$\delta = \frac{a_T - a_r}{a_r} - \alpha_r(T - T_r)\delta$$

where  $a_r$  was the lattice constant at temperature  $T^{\circ}\text{K}$

$a_r$  was the lattice constant at room temperature  $T_r^{\circ}\text{K}$

and  $\alpha_r$  was the coefficient of thermal expansion at  $T_r^{\circ}\text{K}$ .

\*Present address:—Physical Metallurgy Section, University of California, Berkeley, California, U.S.A.

Lawson (1950) named the quantity ' $\delta$ ' as the 'anomalous thermal expansion' because it indicated departure of the  $\alpha_T$  value at  $T^\circ\text{K}$  from the value predicted if the coefficient of thermal expansion ( $\alpha_T$ ) at  $T_r^\circ\text{K}$  were constant even upto the temperature  $T^\circ\text{K}$ . Lawson (1950) plotted  $\log \delta$  against  $1/T$  for silver halide crystals. He obtained a linear relation between the two quantities. This led to the equation

$$\delta = A \exp(-U/RT) \quad \dots (1)$$

where  $A$  and  $U$  are arbitrary constants. The similarity of this equation with the relation representing the concentration of defects with temperature led him to attribute the 'anomalous expansion' to defects in the crystals. Lawson (1950), therefore, attempted to identify  $U$  with the activation energy of silver in silver halides. The value of the activation energy calculated from the thermal expansion data was found to agree more or less with that from other data and Lawson (1950) even claimed that the defects could be distinguished as the Schottky type or the Frenkel type. Uno (1952) obtained the same results for sodium chloride. Fischmeister (1956) found that the plot of  $\log \delta$  against  $1/T$  in the case of alkali halides was not strictly linear. The values of the activation energies calculated from the mean straight line curves were found to differ quite considerably from those calculated from electrical conductivity data.

Fletcher (1957) and Eastabrook (1957) have shown theoretically that non-linearity of the thermal expansion curve follows from Gruneisen equation itself. They have, however, not been able to explain the experimental results of Lawson (1950) and Uno (1952) as embodied in Eq. (1). Since, as yet, no theoretical proof of Eq. (1) has been provided, it has been considered worth while to investigate how far it is valid experimentally and under what circumstances. Since all the previous work has been carried out with ionic solids only, it was decided to extend the investigations to metals, alloys and semiconductors. With this in view, in course of the present work, thermal expansion of copper, gold, aluminium, germanium and four alloys comprising copper and aluminium has been studied.

## EXPERIMENTAL

The thermal expansion curves have been obtained with the help of the X-ray diffraction method. For this purpose, an Unicam 19 cm high temperature camera was used in conjunction with nickel filtered copper radiations from a Norelco X-ray diffraction unit. The temperature of the sample was controlled within a range of  $\pm 1^\circ\text{C}$ . No temperature gradient was allowed to be formed along the length of the sample by maintaining the temperature of the two heater coils equal and stable with the help of two independent controlling devices. The samples were spectroscopically pure. The lattice constants were determined with the help of the extrapolation technique due to Taylor and Sinclair (1945). The accuracy of measurements was  $\pm 0.0001 \text{ \AA.U.}$

## RESULTS AND DISCUSSIONS

## (i) Copper

In Figs. 1 and 2 the values of  $\log \delta$  for copper described in the previous section have been plotted against  $1/T$  for five different values of  $T_r$  viz. 200°, 250°, 300°, 350° and 400°K respectively, from the data of Nix and MacNair (1941) and 300°K, 400°K and 500°K from the data obtained in course of the present investigation. The mean curves are found to be straight lines in all the cases. From the slopes of these straight lines, the values of  $U$  for various values of  $T_r$  have been calculated and collected in the Table I. It is observed that the value of  $U$  lies approximately in the range 0.1 ev. to 0.5 ev. It is interesting to compare it with the value of the activation energy of copper for vacant lattice sites as determined by Seeger (1955) and Maninveld (1952). Their value lies in the range of 0.2 ev. to 0.5 ev. Thus, one is tempted to identify  $U$  with the vacant lattice site activation energy of copper.

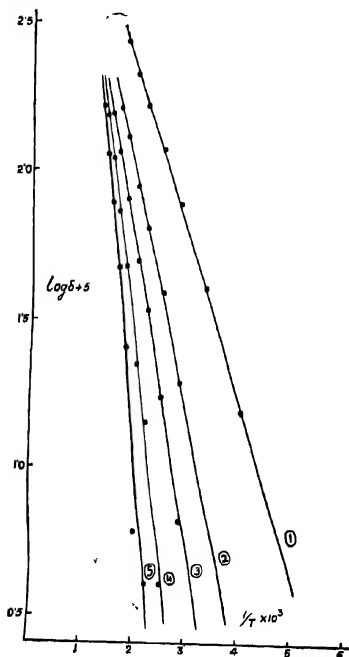


Fig. 1. The plot of  $\log \delta$  for copper against  $1/T$  for different values of  $T_r$  (1) 200°K (2) 250°K (3) 300°K (4) 350°K (5) 400°K as obtained from the data due to Nix and Mac Nair (1941).

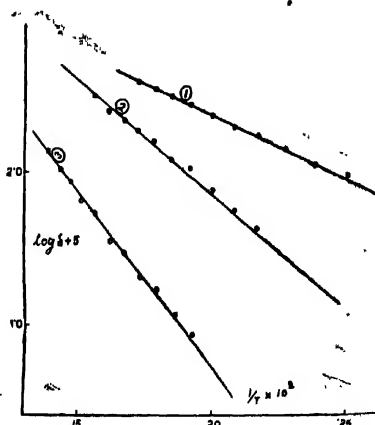


Fig. 2. The plot of  $\log \delta$  for copper against  $1/T$  at three different values of  $T_r$  (1) 300°K (2) 400°K (3) 500°K as obtained from the present measurement.

TABLE I

Temp. $T_r$ °K	U in ev.	
	Values obtained from data due to Nix and MacNair	Values obtained from the present investigation
200	.12	--
250	.10	-
300	.20	20
350	.28	-
400	.38	32
500	-	.47

(ii) *Gold*

For gold, the experimental data have been taken from the work of Nix and MacNair (1941). Although their investigations have been carried on massive samples by the interferometric method, the thermal expansions measured by them have been taken to be the same as determined by the X-ray diffraction method. This is because of the overwhelming experimental evidence in support of the conclusion that macroscopic and microscopic measurements of thermal expansion lead to the same results provided, of course, that the specimen under test does not have any macroscopic impurity or blowhole etc. The data due to Nix and MacNair (1941) on the thermal expansion of gold have been converted into the data on the variation of lattice spacings of gold with temperature on the basis of the value being 4.0781 A.U. at 18°C. This value has been taken from the table collected by Mason and Wood (1957).

The ( $a_T$ -- $T$ ) curve is a nonlinear one whose behaviour can be summarised by the equation

$$a_T = 4.06322 + 4.28 \times 10^{-5}T + 3 \times 10^{-8}T^2$$

where  $a_T$  is the lattice spacing of gold at  $T$ °K. Fig. 3 shows the variation of  $\log \delta$  with  $1/T$  where  $T$  is in °K for values of  $T_r = 100, 200$  and  $300$ °K respectively. Fig. 3 shows that the plots of  $\log \delta$  against  $1/T$  are all straight lines. From the slopes of these lines, the values of  $U$  for three values of  $T_r$  have been calculated and collected in Table II.

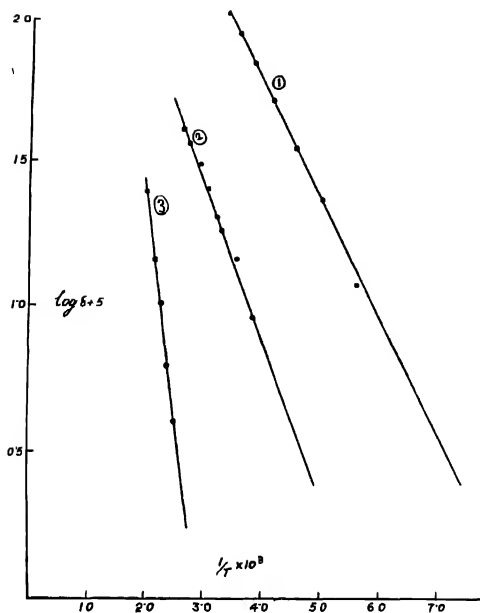


Fig. 3. The values of  $\log \delta$  for gold calculated from the data due to Nix and Mac Nair plotted against  $1/T$  at three different values of  $T_r$  (1)  $300^\circ\text{K}$  (2)  $400^\circ\text{K}$  (3)  $500^\circ\text{K}$

TABLE II

Temp. $T_r^\circ\text{K}$	U in ev.
	Obtained from the data due to Nix and MacNair
100	.081
200	.107
300	.320

Marx, Cooper and Henderson (1952) have shown that the activation energies of copper and gold as measured by the change in electrical resistivity of these metals due to irradiation by deuterons are the same and equal to .15 ev. Manintveld (1952) has also shown that the defect lattice activation energy of gold, like

that of copper, lies in the range of .2 to .55 ev. Thus  $U$  may be identified with the defect lattice activation energy of gold.

### (iii) Aluminium

As in the case of copper, the 'anomalous thermal expansion' as observed in course of these investigations as well as from the data of Nix and MacNair (1941) has been studied. The logarithm of the anomalous thermal expansion has been plotted against  $1/T$  for both these sets of data. The data of Nix and MacNair (1941) have been converted into lattice distances of aluminium at various temperatures on the basis of the value 4.0495 A.U. at 25°C as given by Mason and Wood (1957). Figs. 4 and 5 show the values of  $\log \delta$  against  $1/T$  for  $T_r = 300^\circ$ ,

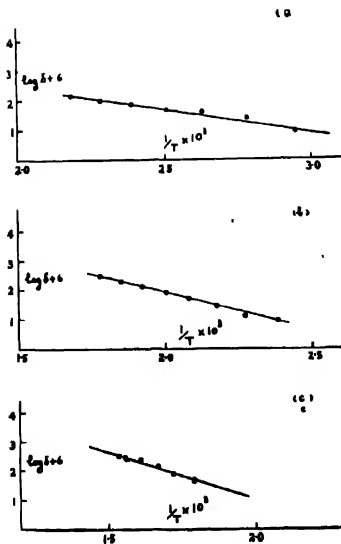


Fig. 4. The plot of  $\log \delta$  for aluminium calculated from the data of Nix and Mac Nair against  $1/T$  at three different values of  $T_r$  (a)  $300^\circ\text{K}$  (b)  $400^\circ\text{K}$  (c)  $500^\circ\text{K}$ .

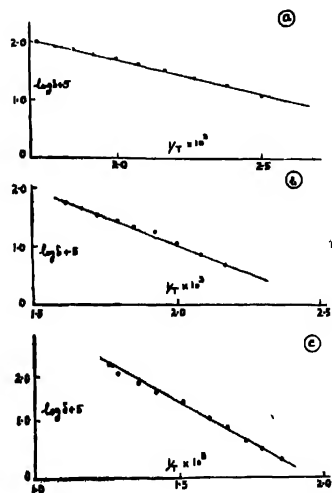


Fig. 5. The plot of  $\log \delta$  for aluminium as obtained from the present measurement against  $1/T$  for three different values of  $T_r$  (a)  $300^\circ\text{K}$  (b)  $400^\circ\text{K}$  (c)  $500^\circ\text{K}$ .

$400^\circ$  and  $500^\circ\text{K}$ . It is observed that for all these sets of values the plots of  $\log \delta$  against  $1/T$  are linear. The values of  $U$  as measured from the slopes of these lines have been determined and shown in Table III.

TABLE III

Temp. $T_r$ °K	U in ev.	
	Obtained from the data due to Nix and Mac-Nan	Obtained from present investigation
300	0.27	0.24
400	0.50	0.42
500	0.65	0.60

In this connection, it is interesting to note that Schoeck and Seeger (1954) have found the activation energy of aluminium for screw dislocations to be nearly 0.11 ev. which is of the same order as that obtained in course of this study. Thus  $U$  can again be interpreted to be the activation energy of aluminium in this present case.

(iv) *Germanium*

For germanium the values of  $\log \delta$  vs.  $1/T$  have been shown in Fig. 6. The plots have been made for  $T_r = 300^\circ\text{K}$ ,  $400^\circ\text{K}$  and  $500^\circ\text{K}$  with the data

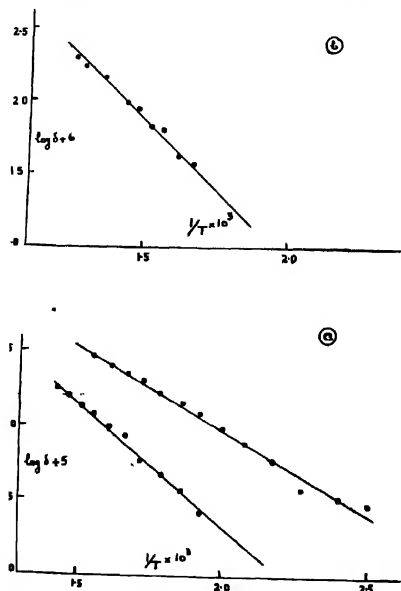


Fig. 6 The plot of  $\log \delta$  for germanium as obtained from the present measurement against  $1/T$  for three different values of  $T_r$  (a)  $300^\circ\text{K}$  and  $400^\circ\text{K}$  (b)  $500^\circ\text{K}$ .



collected in course of present studies. It is observed that all the plots are straight lines. From the inclinations of these plots with the  $1/T$ -axis, the values of  $U$  have been determined and shown in Table IV.

TABLE IV

Temp. $T_r$ °K	U in ev.
	Obtained from the present investigation
300	23
400	33
500	41

Here it may be mentioned that Letaw *et al* (1954) obtained the value of activation energy of mobility as 23.5 kcal/mole (1.0 ev).

(v) *Four alloys containing copper and aluminium*

The logarithms of the anomalous thermal expansion of .08% copper in aluminium, 5.87% aluminium in copper, 5% copper in aluminium and 10% copper in aluminium alloys for various values of the reciprocal of temperature in °K have been shown graphically in Figs 7 to 10. It is to be noted in this connec-

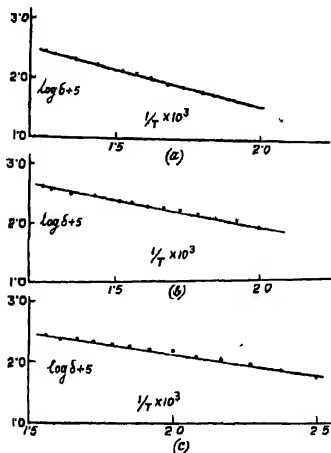


Fig. 7. The plot of  $\log \delta$  for the alloy containing 0.08% by weight of copper in aluminium as obtained from the present measurements against  $1/T$  at different values of  $T_r$  (a) 500°K (b) 40°K (c) 300°K.

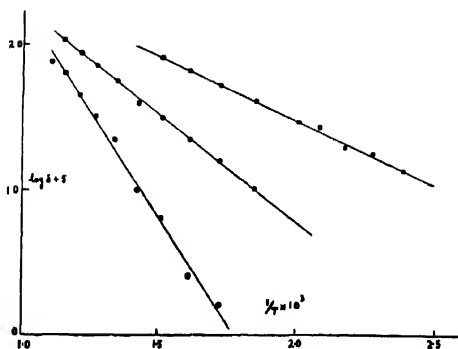


Fig. 8 The plot of  $\log \delta$  for the alloy containing 5.8% by weight of aluminum in copper as obtained from the present measurements against  $1/T$  at different values of  $T_r$  (1) 300°K (2) 400°K (3) 500°K.

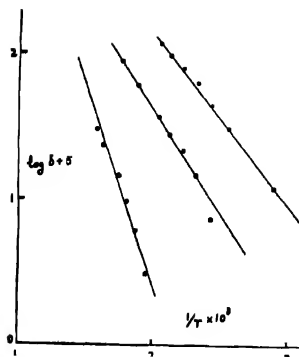


Fig. 9 The plot of  $\log \delta$  for the alloy containing 10% by weight of copper in aluminum as obtained from the present measurements against  $1/T$  at different values of  $T_r$  (1) 300°K (2) 400°K (3) 500°K.

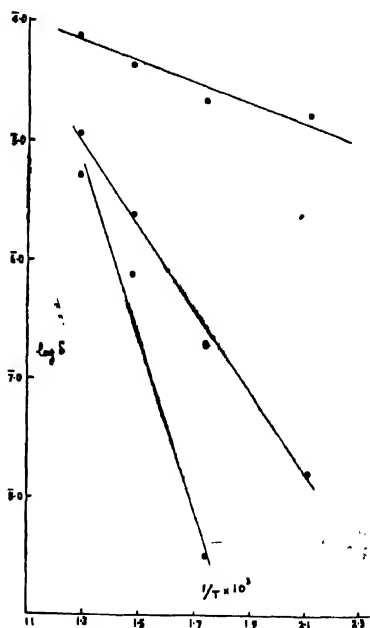


Fig. 10. The plot of  $\log \delta$  for the alloy containing 4% by weight of copper in aluminum as obtained from the present measurements against  $1/T$  at different values of  $T_r$  (1) 303°K (2) 373°K (3) 473°K.

tion that the last two alloys mentioned above are two phase alloys and our studies are restricted only to the solid solution phase. Strictly speaking, the term "thermal expansion" should not be used even, in these two cases. However, it has been observed that the lattice dimensions of the solid solution phases for both these alloys change with temperature in a regular way. The plots of the lattice dimensions of the solid solution phase against temperature have been found to be regular curves almost of the same nature as thermal expansion curves of single phase substances. The "anomalous thermal expansions" in these two cases have been defined in analogy with that for single phase substances. The  $(da/dT)$  in these cases being the rate of change of direction of these two  $(a-T)$  curves. It is interesting to note that for all these four alloys, the  $(\log \delta - 1/T)$  curves are linear. It is also to be noted that the values of  $U$ , calculated from the slope of these straight lines and collected in Table V, range between the values .07 ev to .621 ev., thus approximately covering the range for the vacant lattice site activation energy of copper. For the last two alloys, this is understandable. For, if the 'anomalous thermal expansion' is to be attributed to concentration of defects at various temperatures, it can be very well done in these two cases. In both these cases, the lattice strain increases with the precipitation of the "theta" phase which is due to the segregation of copper atoms. Thus a corre-

TABLE V

Values of  $U$  calculated from the slope of the plot of  $\log \delta$  vs.  $1/T$  for some aluminium-copper alloys obtained during the present investigation (see Figs.7 to 10).

Composition	Temperature °K	U e.v
		Obtained from the present investigation
4% Cu, 96% Al by Wt. %	303	.074
	373	.297
	473	.621
10% Cu 90% Al	293	.234
	373	.280
	473	.540
.08% Cu 99.9% Al	300	.151
	400	.227
	500	.312
5.87% Al 94.13% Cu	300	.180
	400	.290
	500	.530

lation can be established between the precipitation of the "theta" phase and the fact that the value of  $U$  corresponds to the vacant lattice site activation energy of copper. In the 5.87% aluminium in copper alloy which consists of a single phase the overwhelming majority of atoms being copper, the thermal expansion is due mainly to the anisotropic vibration of copper atoms. But it is very difficult to understand why in the .08% copper in aluminium single phase alloy the value of  $U$  corresponds to the vacant lattice site activation energy of copper. The thermal expansion being mostly due to aluminium atoms, it was expected that the value of  $U$  would correspond to that for aluminium. It appears that more theoretical as well as experimental work has to be carried out to understand this phenomenon.

#### (vi) Conclusion

The identification of  $U$  with the activation energy of atoms is purely empirical having no theoretical basis as yet. However, the experimental results go to prove that this may have some basis of truth at least in the case of metals and alloys. What is interesting in this connection is that in all these cases studied, the activation energy is due to the vacant lattice site. Lawson (1950) and Uno (1952) had also observed that the activation energy of sodium in sodium chloride crystals was due to Schottky defects. This may mean that thermal expansion of solids is associated with the creation of such defects. Thus, a more detailed study of this phenomenon may lead to a better understanding of the thermal expansion of solids.

#### REFERENCES

- Mastabrook, J. N. 1957, *Phil. Mag. Ser.*, **8**, 2, 1421.  
 Fischmeister, H. F., 1956, *Acta Cryst.*, **9**, 416.  
 Fletcher, G. C., 1957, *Phil. Mag. Ser.* **8**, 2, 639.  
 Lawson, A. W., 1950, *Phys. Rev.* **78**, 185.  
 Lotaw, H., Shifkin, J. M. and Portnoy, W. M., 1954, *Phys. Rev.*, **93**, 892.  
 Manntvold, J. A., 1952, *Nature*, **169**, 623.  
 Marx, J. W., Cooper, H. G. and Henderson, J. W., 1952, *Phys. Rev.*, **88**, 106.  
 Mason, W. P. and Wood, E. A., 1957, *Hand book Amer. Inst. Physics.*, 2-48.  
 Nix, P. C. and MacNair, D., 1941, *Phys. Rev.* **60**, 597.  
 Schoeck, G. and Soeger, A., 1954, *Proc. Bristol Conf. on defects of solids*, 340.  
 Soeger, A., 1955, *Hand buch der Physik*, **7**, 392.  
 Taylor, A. and Sinclair, H., 1945, *Proc. Phys. Soc.*, **57**, 108.  
 Uno, R., 1952, *Chem. Abst.*, **46**, 6890.

## Letters to the Editor

The Board of Editors will not hold itself responsible for opinions expressed in the letters published in this section. The notes containing reports of new work communicated for this section should not contain many figures and should not exceed 500 words in length. The contributions must reach the Assistant Editor not later than the 15th of the second month preceding that of the issue in which the letter is to appear. No proof will be sent to the authors.

### 4

## ULTRAVIOLET ABSORPTION OF $\text{NO}_3^-$ ION

A. MOOKHERJI AND S. P. TANDON\*

PHYSICAL LABORATORIES, AGRA COLLEGE, AGRA.

(Received December 12, 1961)

Nitrates are well known for their heavy absorption in the ultraviolet. In the absence of any knowledge of vibrational and electronic energy of  $\text{NO}_3^-$  ion, Krishnan and Guha (1934) suggested photodissociation of  $\text{NO}_3^-$  ion into  $\text{NO}_2^-$  and O as the cause of the two simple structureless bands as observed at about 200  $\text{m}\mu$  and at 300  $\text{m}\mu$  by Halban *et al.* (International Critical Tables). The present authors, however, could not detect the presence of nitrite ion due to photodissociation by colourimetric method. Pure alkali nitrate melts, when tested for nitrite ion by Smith and Boston (1961), gave negative results, it must be remembered that in melts the concentration of nitrite ions formed as a result of dissociation should be more detectable.

Previous workers failed to explore the exact position and the structure of these bands due to large band width and due to non-elimination of the container and solvent effect. Hence, the present authors eliminated the solvent and container effect by using a UVISPEK and reduced the band width to a few angstroms by improved technique of reducing the band width. Eleven salts containing  $\text{NO}_3^-$  ion studied in this way showed that the band at 200  $\text{m}\mu$  consists of five peaks.

Following Heath and Linnett (1948), Vankateswarlu and Sundaram (1955), Lindeman and Wilson (1956) and Janz and Mikawa (1960), the vibrational energy of these peaks have been calculated. The electronic transitions were calculated by the method of Pariser and Parr (1953, 1955), Pople (1953, 1955), Mc Ewen (1960, 1961). All these calculations reveal that the band at 300  $\text{m}\mu$  could be attributed to  $n \rightarrow \pi^*$  transition and that at 200  $\text{m}\mu$  to  $\pi \rightarrow \pi^*$  transition.

Oscillator strength of these bands were calculated following Jorgensen (1954), Tanabe and Sugano (1954) and Smith and Boston (1961) from which the transition

---

\* Physics Department, Government College, Ajmir.

probabilities were deduced. It seems that electric dipole coupled with vibration is responsible for these bands.

Utilising the observed ultraviolet and infrared bands (Ram Das, 1953) to the problem of optical birefringence (Bragg, 1924; Ramchandran, 1947) the ratio of the ultraviolet dispersing electrons contributing to the two indices of refraction in the case of  $\text{KNO}_3$  and  $\text{NaNO}_3$  crystals came out as 1:2.

These absorption frequencies go to show that the diamagnetic susceptibility in the plane of the nitrate ion should be numerically greater than that normal to the plane, in complete agreement with the findings of Krishnan, Guha and Banerji (1933)

#### REFERENCES

- Bragg, W. L., 1924, *Proc. Roy. Soc.*, **105**, 370  
 Bragg, W. L., 1924, *Proc. Roy. Soc.*, **106**, 346.  
 Halban *et al.*, International Critical Tables, **5**, 329.  
 Hoath, D. F. and Lunett, J. W., 1948, *Trans. Faraday Soc.*, **44**, 873, 884.  
 Janz, G. J. and Mikawa, Y., 1960, *J. Mol. Spectroscopy*, **5**, 92.  
 Jorgensen, C.H.R. Klixbull, 1954, *Acta. Chem. Scand.*, **8**, 1502.  
 Krishnan, K. S. and Guha, A. C., 1934, *Proc. Ind. Acad. Sci.*, **1(4)**, 212.  
 Krishnan, K. S., Guha, A. C. and Banerji, S., 1933, *Phil. Trans.*, A **231**, 241.  
 Landoman, P. and Wilson, M. K., 1956, *J. Chem. Phys.*, **24**, 242.  
 McEwen, K. L., 1960, *J. Chem. Phys.*, **32**, 1801.  
 McEwen, K. L., 1961, *J. Chem. Phys.*, **34**, 547.  
 Pariser, R. and Parr, R. G., 1953, *J. Chem. Phys.*, **21**, 466, 767.  
 Pariser, R. and Parr, R. G., 1955, *J. Chem. Phys.*, **23**, 711.  
 Pople, J. A., 1953, *Trans. Faraday Soc.*, **49**, 1375.  
 Pople, J. A., 1955, *Proc. Roy. Soc., A* **68**, 81.  
 Ramchandran, G. N., 1947, *Proc. Ind. Acad. Sci.*, **26A**, 114.  
 Ram Das, A. K., 1953, *Proc. Ind. Acad. Sci.*, **37-38**, 441.  
 Smith, G. P. and Boston, C. R., 1961, *J. Chem. Phys.*, **34**, 1396.  
 Tanabe, Y. and Sugano, S., 1954, *J. Phys. Soc., Japan*, **9**, 766.  
 Venkateswarlu, K. and Sunderam, S., 1955, *J. Chem. Phys.*, **23**, 2368.

# THE NEAR ULTRAVIOLET ABSORPTION SPECTRUM OF PARA-FLUORO-NITROBENZENE

ACHYUTA RAO, IYYANKI

DEPARTMENT OF PHYSICS, GAUHATI UNIVERSITY.

(Received January 20, 1962)

The near ultraviolet absorption spectrum of para fluoro-nitrobenzene has been studied in the vapour phase using 'burning magnesium ribbon' as a source of continuum in the ultraviolet. Earlier workers, (Gruber 1953, Ungnade 1954, and Schubert *et al.*, 1957, 1958) studied mainly the absorption spectra of its solutions in various solvents. The band data and vibrational analysis were not presented earlier for the vapour spectrum.

In the present work a path length of 90 cm. was used and the spectra were taken at various saturation pressures as the container was kept at temperatures ranging from  $-15^{\circ}$  to  $120^{\circ}\text{C}$ . About thirty bands were measured in the region 2900-2630 Å. The bands on the short wavelength end were found to be diffuse probably due to predissociation. The 0, 0 band was identified at 2876.6 Å. ( $34754\text{ cm}^{-1}$ ). Most of the observed bands could be interpreted on the basis of two ground state ( $150$  and  $230\text{ cm}^{-1}$ ) and seven excited state ( $149$ ,  $202$ ,  $389$ ,  $436$ ,  $732$ ,  $946$  and  $1529\text{ cm}^{-1}$ ) fundamentals.

Definite conclusions can not be drawn until the ortho and meta isomers are also studied in detail in the vapour phase. Secondly, Raman and infrared absorption data for these compounds were not available in literature to make any correlation of the observed fundamentals with those data. A complete investigation of both the electronic and vibrational spectra of these three isomers is undertaken in this laboratory.

The detailed paper will be published shortly.

## ACKNOWLEDGMENTS

The author expresses his grateful thanks to Prof P. C. Mahanta for his kind interest in the work.

## REFERENCES

- Gruber, W., 1953, *Can. J. Chem.* **31**, 1020.  
Schubert, W. M., Craven, J. M., Steadly, H. and Robins, J., 1957, *J. Org. Chem.*, **22**, 1285.  
Schubert, W. M. Craven, J. M. and Steadly, H., 1958, *J. Am. Chem. Soc.*, **81**, 269.  
Ungnade, H. E., 1954, *J. Am. Chem. Soc.* **76** 160.





# MAGNETIC STUDIES ON $\text{Co}^{++}$ ION IN PINK AND BLUE SOLUTION OF $\text{CoCl}_2$

T. MOOKHERJI

PHYSICS LABORATORIES, AGRA COLLEGE, AGRA

(Received August 17, 1961)

**ABSTRACT.** The striking contrast in the magnetic behaviour of six-coordinated (pink) and tetra-coordinated (blue)  $\text{Co}^{++}$  ion in aqueous solution of cobalt chloride, predicted by the theory is verified experimentally. The moment of hexa-coordinated salt deviates more from the spin-only value than that of the tetra-coordinated salts. The moment of the blue salt is almost independent of temperature between 307°K and 345°K while that of the pink salt varies slightly. The moment of  $\text{Co}^{++}$  ion in hexa-coordinated cobalt chloride aqueous solution was found to increase slightly with dilution which may be attributed to distant atom effect.

## INTRODUCTION

The change of pink colour of aqueous solution of  $\text{Co}^{++}$  ion salts, to blue on the addition of an alkaline salt has attracted much attention and many theories have been advanced to account for the observed change in colour.

Hill and Howell (1924) by comparing the absorption spectra of solution of  $\text{Co}^{++}$  ion salts, with those of solids of known crystalline structure came to the conclusion that the solid blue compound is associated with four other atoms, the same arrangement accounts for the blue solution and that in the pink solid and pink solution the  $\text{Co}^{++}$  ion is associated with six other atoms.

Krishnan and Mookherji (1937 and 1938) as a result of magnetic measurements on single crystals of blue  $\text{Cs}_2\text{CoCl}_4$  and also the pink variety observed that in pink salts  $\text{Co}^{++}$  ion has an octahedral distribution of negative charges while for blue salts the negative charges have tetrahedral symmetry. This is also supported by X-ray fine structure studies on these salts (Hofmann, 1931; Powel and Wells, 1935). Therefore a single crystal of blue  $\text{Co}^{++}$  ion salt behaves like a single crystal of  $\text{Ni}^{++}$  ion or  $\text{Cr}^{++}$  ion salts magnetically according to crystal field theory (Van Vleck, 1932).

In state of solution the lattice structure breaks down completely but the individual units retain their identity (Krishnan, 1939; Chakravarty, 1942; Mookherji and Chhonkar, 1959). Hence magnetic properties of blue solution of cobaltous ion must show the same characteristics as  $\text{Ni}^{++}$  ion or  $\text{Cr}^{++}$  ion salts.

Thus a study of magnetic properties of blue and pink cobaltous salts in state of solution and viewed in the light of crystalline field theory of Van Vleck would be interesting.

## EXPERIMENTAL

For the measurement of susceptibility of solution a very sensitive and accurate microbalance as developed by Neogy and Lal (1962) was used. The balance consists of a light pyrex glass beam, which is supported at its centre by a thin quartz fibre running at right angles to the glass beam. This quartz fibre is stretched between a chuck and the torsion pin of a torsion head. The chuck end of the quartz fibre is first fused to a small quartz rod which is then fixed to the chuck, to ensure nonslipping of the fibre from the chuck. The whole arrangement is enclosed in a wooden box with sliding glass cover and windows. The two ends of the pyrex glass beam projects out of the glass windows.

A coil made of thin copper wire is fixed to the centre of the glass beam with its plane horizontal. The two terminals of the coil are taken out of the balance box along the length of the fibre to ensure minimum resistance to the rotation of the beam. A light and small plane mirror is attached to the beam at its centre which in coordination with lamp and scale arrangement allows to note the position of the beam. To reduce mechanical vibration and oscillation of the beam a paper damping vane is attached to one end of the beam. The coil is connected in series with an accumulator key, 1 ohm standard resistance and rheostat (for coarse and fine adjustment of current). The terminals of 1 ohm coil is connected to the test terminals of a portable PYE potentiometer capable of measuring 0.01 mV.

The solution is filled in an ampule and suspended from one end of the balance beam with a fine nylon fibre, passing through a hole at the bottom of the window cover and protected on its way to constant gradient position of the field by a glass tube. Constant gradient was obtained by using special pole pieces (Dutta Roy, 1955). The push or pull on the solution is measured in terms of the current sent through the coil which in turn is measured as a voltage developed across the standard resistance by the potentiometer.

The susceptibility of the solution (unknown) is determined by comparing the push on it with that on purest variety carbon tetrachloride; and the pull on it with that on nickel chloride (as solution at a concentration of about 30%), taken as standard.

Thus, if the force on  $\text{CCl}_4$  or  $\text{NiCl}_2$  solution is  $F_s$  for volume  $V_s$  with volume susceptibility  $k_s$ ; and the force on unknown solution is  $F$  for volume  $V$  with volume susceptibility  $k$ , then we have

$$\frac{F_s}{F} = \frac{I_s'}{I'} = \frac{(k_s - k_a)V_s}{(k - k_a)V}$$

where  $I_s'$  and  $I'$  are the currents required to balance the force on standard and the unknown solution respectively, corrected for the amount of current required to balance the force on empty ampule, and  $k_a$  is the volume susceptibility of air.

From this we have

$$x_{sol} = \frac{m_s}{m} \cdot \frac{I'}{I_s'} \cdot \left( x_s - \frac{k_a}{\rho_s} \right) + \frac{k_a}{\rho}$$

$\rho_s$  and  $\rho$  are the densities for standard and unknown solution respectively.

Temperature variation of moment was measured by a modified Gouy balance (Bose, 1935).

pH value was measured by a Cambridge compact type pH-meter.

## RESULTS

The results are collected in Tables I to V. Mass susceptibility was calculated by assuming Wiedemann's additive law i.e.,  $X_{sol} = X_1C_1 + X_2C_2 + \dots + X_nC_n$ , where  $C$  = weight of substance dissolved/total weight of solution.

The effective Bohr Magneton number is given by the expression  $\mu_B = 2.827 \times \sqrt{X'_M \cdot T}$ , where  $X'_M$  is the gram-mol. susceptibility corrected for diamagnetism and  $T$  is the absolute temperature.

The pH value of the solution was found to be fairly constant up to 4%.

TABLE I

Temperature 307°K

Concentration of $\text{CoCl}_2$	$\mu_B$
0.4493	4.848
0.4193	4.856
0.3845	4.868
0.3219	4.893
0.2679	4.913
0.2520	4.919
0.2339	4.929
0.2220	4.936
0.1860	4.951
0.1674	4.962
0.1508	4.973
0.1329	4.979
0.1120	4.987
0.0866	4.989
0.0680	5.019
0.0496	5.094
0.00978	5.154

TABLE II

Temperature 307°K

Concentration of $\text{CaCl}_2$	$\mu_B$
0.2743	4.433
0.3009	4.323
0.3223	4.291
0.3434	4.232
0.3723	4.154
0.3973	4.076
0.4327	3.934

TABLE III

Concentration of  $\text{CoCl}_2 = 0.2916$ 

Temperature °K	$\mu$
305	4.905
315	4.905
320	4.903
325	4.896
330	4.886
335	4.871
340	4.857
345	4.844

TABLE IV

Concentration of  $\text{CoCl}_2 = 0.2248$ Concentration of  $\text{CaCl}_2 = 0.4140$ 

Temperature °K	$\mu_B$
307	4.010
315	4.016
320	4.008
325	4.012
330	4.010
335	4.002
340	4.015
345	4.000

TABLE V

Concentration of  $\text{CoCl}_2 = 0.2120$ 

Temperature 305°K

Solution of $\text{CoCl}_2$ in	$\mu_B$
Methyl alcohol	3.925
Ethyl alcohol	3.930
Amyl alcohol	3.941

## DISCUSSION

a. *Mutual inversion of Stark-levels for tetra- and hexa-coordinated  $\text{Co}^{++}$  ion salts.*

Following Van Vleck (1932) the Stark patterns of octahedral  $\text{Co}^{++}$  and  $\text{Ni}^{++}$  ions whose ground states are  $d^7\ ^4F$  and  $d^8\ ^3F$  respectively are very similar, except for the important difference that the pattern for  $^4F$  is inverted with respect to  $^3F$ . Since in the Stark pattern the triplet is the lowest for cobalt there will be a large orbital contribution whereas if the singlet is lowest then there will be a less orbital contribution to the magnetic moment. Thus, in ordinary cobalt salt one expects more orbital contribution than ordinary nickel salts. This is what is observed experimentally (Krishnan and Mookherji, 1938; Bose, 1948).

According to Gorter (1932) an octahedral arrangement of negative charges about the paramagnetic ion will give rise to a cubic field of positive sign while if the paramagnetic ion is surrounded by four equal negative charges lying at the corners of a tetrahedron the cubic field will be negative. Thus, for a negative cubic field

the Stark pattern will be reverse of that obtaining with the octahedral distribution for the same ion.

### b. Pink and blue cobalt salts

From X-ray fine structure studies (Hofmann, 1931) on pink cobalt salts it was found that  $\text{Co}^{++}$  ion is surrounded by six water dipoles forming an approximate octahedron. In state of solution these octahedrons retain their identity as has been mentioned already, and hence in a pink cobalt salt hexa-coordination results.

Powel and Wells (1935) by X-ray analysis of blue chlorides of cobalt with alkali metals found that the  $\text{Co}^{++}$  ion is closely associated with four chlorine atoms which form a tetrahedron about the  $\text{Co}^{++}$  ion at the centre. Thus tetrahedral coordination may be expected in blue cobalt salts.

### c. Crystal field in blue cobalt salts

From what has been said so far it is clear that the pink cobalt salt will be acted upon by a field of predominantly positive cubic symmetry on which a small tetragonal component is superimposed, while in the blue salt a predominantly negative cubic field with a small trigonal component will result. As a result the Stark pattern will be as shown in Fig. 1. It must be mentioned here that

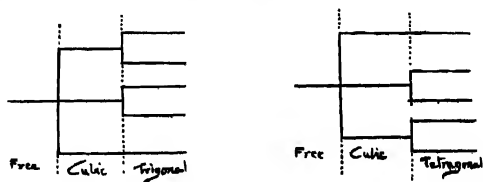


Fig. 1. Blue  $\text{Co}^{++}$  ion

Pink  $\text{Co}^{++}$  ion.

for the blue as well as pink salts the spin quadruplet is split into two Kramer's doublets by fields of lower symmetry than cubic, combined with the spin-orbit coupling.

Thus the results obtained with blue cobalt salts can be discussed in relation to the splitting of the energy levels in the crystalline electric field in the same manner as in octahedrally coordinated chromium ion, to which the blue cobalt salts are analogous.

Following Schlapp and Penney (1932) the mean magnetic moment  $\mu_B$  is connected with the crystal field constant  $\alpha$  by the following equation

$$\alpha = \frac{\mu_B^2 - 15}{15(8\lambda - 3kT)}$$

where  $\lambda = -180 \text{ cm}^{-1}$  and others have usual meaning. Now substituting  $\mu_B$

from Table II.  $\alpha$  comes out to be equal to  $-151 \times 10^{-6}$ . This compares very favourably with the value of  $\text{Cs}_2\text{CoCl}_4$  crystal as obtained by Bose (loc. cit.) namely,  $-159 \times 10^{-6}$ .

It is significant that the value of  $\mu_B$  equal to 3.934 as obtained by us for the blue cobalt salts is much less than that of pink  $\text{CoCl}_2$  solution and is correspondingly nearer to the spin-only value (3.87) as predicted by Van Vleck's theory.

d. *Calculation of  $g$ —the splitting factor.*

According to Owen (1955) the splitting factor  $g$  is given by the relation

$$g = 2 - \frac{4\xi f^2}{\Delta E}$$

where  $\xi = 2S\lambda$ ,  $S$  being the spin quantum number and  $\lambda$  spin-orbit coupling coefficient, and  $f^2$  is the covalency factor. Now for  $\text{Co}^{++}$  ion,  $S = 3/2$  and  $\lambda = -180 \text{ cm}^{-1}$ , so

$$g = 2.12 \times 180 \cdot \frac{f^2}{\Delta E}$$

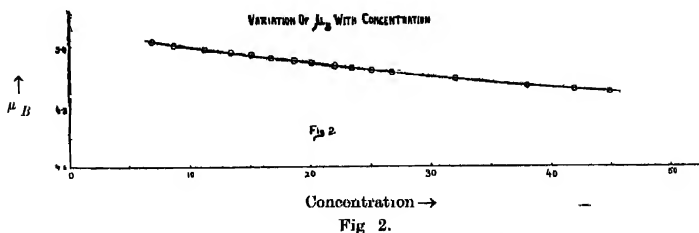
Now  $f^2/\Delta E = -\alpha$  and hence suppling  $\alpha$  we have

$$g = 2.32$$

There is no experimental data for  $\text{CaCl}_2$ — $\text{CoCl}_2$  system. But a comparison with the  $g$ -value (2.29) for the blue crystal  $\text{Cs}_2\text{CoCl}_5$  shows that we are in the right line.

c. *Variation of moment with concentration*

We have measured the moment of pink  $\text{CoCl}_2$  solution at different concentration within a range in which the pH value remains fairly steady. It is observed (Fig. 2) that  $\mu$ -values increase slightly with decrease of concentration. The



electric field acting on the paramagnetic ion can be taken as made up from primary water cluster and that due to the effect of distant atoms. As a result of dilution the distant atom effects may change making the electrostatic field on the  $\text{Co}^{++}$  ion weaker and hence there is an increase of the magnetic moment. On the other hand it is very probable that in the state of solution a certain percen-

tage of tetrahedral coordination is present which decreases with decreasing concentration, tending to increase the average moment.

The observed variation of moment with concentration in the range of .45 to .07 can be expressed by a formula of the type

$$\mu_B = A + B.C_n + C.C_n^2$$

By elaborate least square method the value of  $A$ ,  $B$  and  $C$  have been evaluated.

The calculated values of  $\mu_B$  with these constants are compared with the observed values as shown in the table.

TABLE VI

$$A = 5.064, \quad B = 0.007141, \quad C = 0.00006308$$

Concentration	$\mu_B$ (obs.)	$\mu_B$ (calc.)
0.4491	4.848	4.847
0.4193	4.856	4.856
0.3845	4.868	4.868
0.3219	4.893	4.893
0.2679	4.913	4.914
0.2220	4.936	4.936
0.1860	4.951	4.953
0.1508	4.973	4.972
0.1120	4.987	4.989
0.0680	5.019	5.018

The variation of  $\mu_B$  in case of the blue salt with variation of concentration of  $\text{CaCl}_2$  is shown in Fig. 3. The moment falls from 4.936 to 3.934, nearer to the

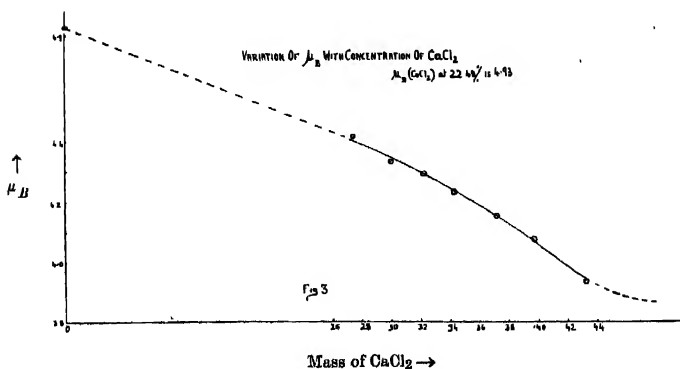


Fig. 3.

spin-only value. It is evident that only at a concentration of 0.4327 of  $\text{CaCl}_2$  almost all pink salt is converted into blue.

In state of solution the blue salt approaches more near to the spin-only value (3.934) than in the crystalline state where it is 4.46 (Bose, 1948) at 297°K and behaves like an *S*-state ion, but in these two cases the ligand atoms are probably somewhat different. Fahlenbrach (1932) obtained with  $\text{CoCl}_2$  in pyridine and ethyl alcohol solution a value of 3.83. Our values for nonaqueous solvents are closer to the spin-only value (Table V).

#### f. Temperature variation of moment

We have already seen that the Stark pattern of the *F*-state ion under a field with positive cubic field coefficient the singlet may either correspond to the highest or lowest value of the energy in the pattern (Fig. 1).

If the singlet lies lowest, since the triplet will be far removed from it at all ordinary temperatures practically the singlet level will be only occupied. Hence the total magnetic moment will be the contribution from this level and the contribution from the upper levels, which will be independent of temperature. Thus there will be small deviation from simple Curie law.

On the other hand, if the triplet lies lowest the separation between its components will be comparable to  $kT$  and the population of upper components of the lowest level will be quite appreciable. The temperature variation will therefore naturally be complicated.

The singlet in the Stark pattern for  $\text{Co}^{++}$  ion in the blue cobalt salt lies lowest as cubic field coefficient is negative in it and hence its moment will be almost independent of temperature. This is what is observed within the range studied as shown in Fig. 4.

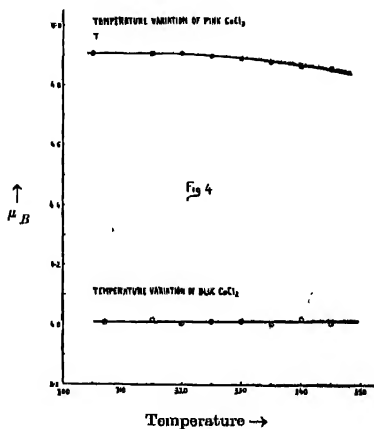


Fig. 4.



For the pink cobalt salts, the triplet lies lowest as cubic field coefficient is positive and hence, should vary with temperature. The variation of  $\mu_B$  with temp. is shown in Fig. 4. With 0.29 concentration of cobalt in the solution we find that  $\mu_B$  decreases slightly with the rise of temperature. Fahlenbrach (1932) has also observed such a change with a solution of concentration of about 0.07.

#### ACKNOWLEDGMENT

The author takes this opportunity of thanking Prof. A. Mookherji, D.Sc. for suggesting the problem, Sri S. C. Mathur, M.Sc., for the kind help and Prof. A. Bose, D.Sc., F.N.I., for helpful criticisms.

#### REFERENCES

- Bose, A., 1948, *Ind. J. Phys.*, **22**, 376.  
Bose, A., 1935, *Proc. Ind. Acad. Sci.*, **A1**, 605.  
Chakravarty, D. C., 1942, *Sci. Cult.*, **7**, 140.  
Datta Roy, S. K., 1955, *Ind. J. Phys.*, **29**, 429.  
Fahlenbrach, H., 1932, *Ann. de Phys.*, **13**, 265.  
Gorter, C. J., 1932, *Phys. Rev.*, **42**, 437.  
Hill, R. and Howell, C. R., 1924, *Phil. Mag.*, **48**, 933.  
Hofmann, 1931, *Z. Kristallo.*, **78**, 279.  
Krishnan, K. S. and Mookherji, A., 1937, *Phys. Rev.*, **51**, 588 and 774.  
Krishnan, K. S. and Mookherji, A., 1938, *Phys. Trans. A*, **237**, 135.  
Krishnan, K. S., (1939), *Nature*, **143**, 600.  
Mookherji, A. and Chhonkar, N. S. (1959), *Ind. J. Phys.*, **33**, 74.  
Neogy, D. and Lal, R. B., 1962, *J. Sci. Industrial Res.*, **21B**, 103.  
Owen, J., 1955, *Proc. Roy. Soc.*, **227**, 183.  
Powell, H. and Wells, A. F., 1935, *J. Chem. Soc.*, 359.  
Van Vleck, J. H., 1932, *Phys. Rev.*, **41**, 208.

# CERTAIN OPERATIONAL CHARACTERISTICS FOR C.E.C. 21-103C MASS SPECTROMETER USING BORON TRIFLUORIDE

K. N. BHIDE AND S. C. SAXENA\*

ATOMIC ENERGY ESTABLISHMENT TROMBAY, BOMBAY

(Received March 21, 1961)

**ABSTRACT.** Several very useful characteristics, essential for an adequate performance of the C.E.C. 21-103C type mass spectrometer, have been recorded by using boron trifluoride gas samples. Dependences of ion current on the energy of the ionizing electrons, ionizing current, sample pressure, repeller settings and magnet current have been discussed. Consideration has also been given to the cracking pattern of boron trifluoride gas, memory effects and the percentage efficiency of the filament. All these individual characteristics are extremely useful in selecting the proper operating conditions.

## INTRODUCTION

Since the first spectrometer of Aston (1919) considerable advance has been made on this subject and is adequately described by Barnard (1953), Duckworth (1958) and Weldron (1956). Several very precise spectrometers are now commercially available with either a semicircular, Dempster (1918), or a sector type, Duckworth (1958), magnetic field to focus the ion beam. Various designs for the ion source have also been developed, Duckworth (1958), and in fact, the variety of spectrometers now commercially available differ only in some such details. Positive ions, after acceleration through a potential difference,  $V$ , acquire kinetic energy,  $Ve - (1/2)mv^2$ , where  $m$ ,  $v$  and  $e$  represent the mass, velocity and charge of the ion respectively. A fraction of this beam after collimation is deflected by a magnetic field of strength  $H$  in a circle of radius  $R$  so that

$$\frac{mv^2}{R} = Hev,$$

we have finally

$$\frac{m}{e} = \frac{H^2 R^2}{2V} \quad \dots \quad (1)$$

The different ion groups then in turn, can be brought to focus on the ion collector for detection by appropriately varying the accelerating potential,  $V$ , (electros-

\*Physics Department, Rajasthan University, Jaipur.

tatic focusing) or by varying the magnetic field,  $H$ , (magnetic focusing). Advantages of both these types of focusing as well as the use of either sector or semi-circular magnetic field are well known and the criterion for a particular choice depends upon the purpose and precision to which it is aimed at.

The Consolidated Electrodynamics Corporation, type 21-103C, mass spectrometer uses the Dempster type, also called as  $\pi$ -type magnetic focusing, and has an ion source which is a modification of the Nier's pattern (1940, 1947). The filament assembly (filament, heater and the shield), anode, repellers and the three accelerating and collimating slits are referred as the Isatron, as shown in figure 1. In this instrument the magnet current can be varied from 0.070 to 0.750

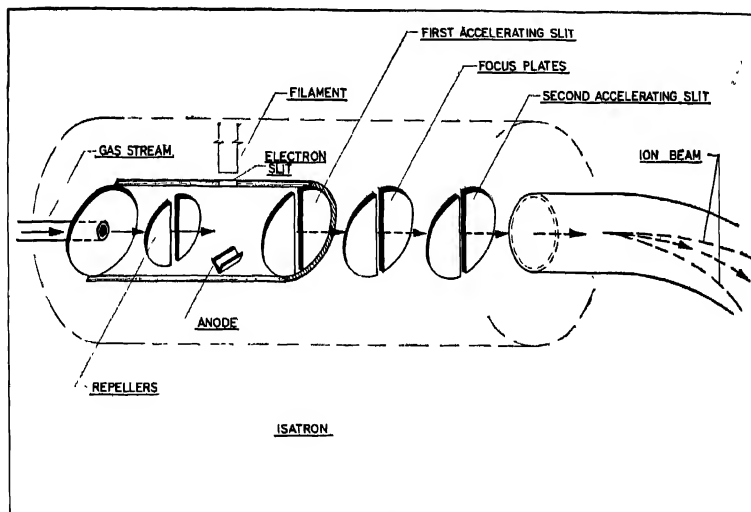


Fig. 1. Schematic diagram of the Isatron.

amp in three steps and the accelerating potential from 400 to 4000 V, again in three steps. With the Spectro-SADIC data processing system model 34-104, in the circuit the maximum voltage drops to 3400 V. The instrument provides for electrostatic scanning and covers  $m/e$  values upto 700 by appropriately choosing the magnet current and the collector slit. The instrument also provides controls to vary the energy of the ionizing electrons, the ionizing current, and the repeller plates potentials. In this paper we have investigated the effect of varying these controls by running boron trifluoride samples. A detailed description of the instrument is given in the operation and maintenance manual provided by the manufacturers (1955). The ion current, which is usually of the order of  $10^{-18}$

amp or more, is fed to a preamplifier through a resistor of  $5 \times 10^{10}$  ohm, and the output after further amplification is fed to the recording system, consisting of an ordinary meter, or a photographic device or a digital automatic computer. This instrument is also fitted with an electronic device to mark the mass index, and an automatic controlled heating at  $250^\circ\text{C}$  for the ionization chamber. The instrument has a very efficient gas inlet system and all the gaseous or liquid samples, which have enough vapour pressure ( $> 20\mu$ ) upto  $150^\circ\text{C}$ , can be efficiently analysed. The gas inlet pressure can be measured by a micro-manometer from  $0.1\mu$  to approximately  $500\mu$ . The gas enters into the Isatron through a molecular leak, comprising of two tiny holes in a gold foil, imbedded in a glass tube.

## EXPERIMENTAL

### (a) *Cracking pattern*

When boron trifluoride is ionized by electron bombardment in the Isatron, it breaks down to give the principal peaks  $\text{BF}_3^+$ ,  $\text{BF}_2^+$ ,  $\text{BF}^+$  and  $\text{B}^+$ , as shown in Table I. In principle, it is possible to calculate the isotopic abundance of boron by making measurements on any of these peaks. In actual practice, it gets complicated because of the mass discrimination effect in the Isatron and interference peaks. Bentley (1957) found that if the ratios  $R(48/49)$  and  $R(10/11)$  are measured the value of the quantity,  $\alpha = R(10/11)/R(48/49)$ , is approximately constant varying from 1.00 to 0.91 and having a mean value of 0.94. In most of our measurements this ratio was close to unity with an average departure of 3% and a maximum of 6%. All the fragments causing interference peaks can be prevented from entering into the Isatron by cooling the  $\text{BF}_3$  sample to about  $-80^\circ\text{C}$ , say with solid carbon dioxide. We, however, had a few undesirable backgrounds because of organic compounds like ether etc. and pump oil. This background was fairly constant and we do not anticipate any material error because of this. It is further interesting to note that the relative magnitudes of the principal peaks, found in the present work, are in disagreement with Bentley (1957). He found  $\text{BF}^+$ , peak bigger than  $\text{B}^+$  peak. On the other hand our results are in qualitative agreement with those of Palmer *et al.* (1956). We took this cracking pattern with widely different samples of  $\text{B}^{10}$  concentration and after long gaps but always found a similar trend. In the present work all the isotopic abundances have been computed from elemental  $\text{B}^+$  peaks which have no interference effects.

### (b) *Memory effect*

The memory effect is caused by the adsorbed  $\text{BF}_3$  gas on the walls of the gas inlet system, Isatron, analyser tube, and also because boron of the gaseous samples exchanges with that present in the pyrex glass. To reduce this effect the system should be baked in between two samples so that the adsorbed  $\text{BF}_3$  gas gets desorbed as much as possible, and also the system should be flushed several times

with the fresh sample. Bentley (1957) and Palmer *et al.* (1956) have discussed in detail the various ways to reduce the memory effect.

TABLE I

Cracking pattern of boron trifluoride gas enriched 44.3% in B<sup>10</sup>.  
 Filament current = 3.6 amp, Ionizing voltage = 70V,  
 Ionizing current = 15 $\mu$ a, Magnet current = 227mA  
 Repeller settings = 26 and 60, Sample pressure = 50 $\mu$ .

$m$ $e$	Principal peaks	Percentage	Interference peaks
10	B <sup>10</sup>	6.8	
11	B <sup>11</sup>		
28			Si <sup>28</sup>
29	B <sup>10</sup> F	1.2	Si <sup>29</sup>
30	B <sup>11</sup> F		HB <sup>10</sup> F, Si <sup>30</sup>
31			HB <sup>11</sup> F
47			HB <sup>10</sup> F(OH), Si <sup>28</sup> F
48	B <sup>10</sup> F <sub>2</sub>	89.9	HB <sup>11</sup> F(OH), Si <sup>29</sup> F
49	B <sup>11</sup> F <sub>2</sub>		HB <sup>10</sup> F <sub>2</sub> , Si <sup>28</sup> F
50			HB <sup>11</sup> F <sub>2</sub>
67	B <sup>10</sup> F <sub>3</sub>	2.1	Si <sup>28</sup> F <sub>2</sub>
68	B <sup>11</sup> F <sub>3</sub>		Si <sup>29</sup> F <sub>2</sub>
85			Si <sup>28</sup> F <sub>3</sub>

Table II shows the effect of nine flushings with a sample of BF<sub>3</sub> enriched upto 83% in B<sup>10</sup> in the spectrometer which previously analysed a sample of 44.3% enriched in B<sup>10</sup>. The B<sup>10</sup> and B<sup>11</sup> peaks were recorded for each flushing after first and fifth minute of introducing the sample in the Isatron. No attempt was made to keep the pressure constant during this time. Both the peak heights for masses 10 and 11 went down with time. The one minute readings correspond almost to the situation when the sample has been introduced into the Isatron and probably the diffusive mixing of the sample with the adsorbed layer on the wall has started. As the time passes an equilibrium is attained and the previous adsorbed layer dilutes the introduced sample and hence the percentage of B<sup>10</sup> decreases consistently in each flushing with time. This difference levels off with the increase in the number of flushings as the adsorbed layer gets more and more into equilibrium with the sample. The boron of the glass exchanges only with the immediate adsorbed layer on the glass and therefore, this process will involve longer time as well as the larger number of flushings. This mechanism is fully confirmed by the records of Table II.

Data for the memory effect in the mass spectrometer.

Filament current = 3.6 amp, Ionizing voltage = 70V,

**Ionizing current =  $15\mu A$ , Magnet current = 227 mA,**

Repeller settings = 26 and 60, Sample pressure = 50  $\mu$ .[illegible]

In another attempt records were taken of the percentage of  $B^{10}$  as the system is flushed a number of times with an enriched sample. The results of flushing the spectrometer with an enriched sample of approximately 44%  $B^{10}$ , which analysed previously a 10%  $B^{10}$  sample are; twentytwo flushings increased the percentage of  $B^{10}$  from 25.2 to 31.0. The removable parts of the gas inlet system were then cleaned by  $(NH_4)_2F$  and a fresh sample introduced. Ten flushings then raised the percentage of  $B^{10}$  from 35.0 to 37.3. The system was then again cleaned and eight flushings boosted the value from 41% to 42.5%. These cleanings and flushings were repeated for three times more before fairly steady results were attained.

(c) *Dependence of the ionization probability on the energy of the ionizing electrons*

The phenomenon of the ionization of gases by the electrons of different energy has been discussed by Francis (1960) and others. We have measured the ion current as a function of the energy of the ionizing electrons for a fixed value of the ionizing current, magnet current, gas pressure and repeller settings. The results for masses 10, 11, 48 and 49 for the energy of the ionizing electrons varying from 51 to 78 *ev* are listed in Table III. The ion current continuously increases as the energy of the ionizing electrons is increased; the rate of increase considerably decreases around 75 *ev* and we have used this value for all our subsequent work.

TABLE III

Ion current for several masses as a function of the energy of the ionizing electrons.

Filament current = 3.4 amp, Ionizing current =  $30\mu A$ ,  
Magnet current = 230 mA, Repeller settings = 4 and 17,  
Sample pressure =  $100\mu$ .

Ionizing voltage, V	51	60	65	70	74	78
Peak height $B^{10}$	15.1	16.8	17.4	18.2	18.5	18.5
Peak height $B^{11}$	47.0	52.8	54.5	56.3	57.3	58
Peak height $B^{10}F_2$	273.3	292.0	299.0	304.0	308.0	307.0
Peak height $B^{11}F_2$	878.0	934.0	957.0	975.0	990.0	993.0
Ratio $B^{10}/B^{11}$	0.321	0.319	0.310	0.323	0.323	0.319
Ratio $B^{10}F_2/B^{11}F_2$	0.311	0.313	0.312	0.312	0.311	0.309
$\alpha$	1.03	1.02	1.02	1.04	1.04	1.03

It is also interesting to note in Table III that the ratio  $R(10/11)$  or  $R(48/49)$  remains constant within about one percent. This shows the independence of the computed isotopic abundance ratio on the energy of the ionizing electrons. The value of  $\alpha$  is also close to unity within the uncertainty of the individual ratio

values showing the absence of memory and mass discrimination effects. This ratio has been calculated in some of the later tables also with similar result.

(d) *Dependence of the ion current on the ionizing current*

For the same filament emission and energy of the ionizing electrons, the ionizing current can be increased by increasing the anode potential in the Isatron. The values of the ion current as a function of the ionizing current for masses 11, 48 and 49 for a fixed value of the gas pressure, ionizing voltage, magnet current and repeller settings were taken. The ion currents for masses 11 and 49 are plotted as a function of the ionizing current in Fig. 2. From this figure, it follows that ion current increases almost linearly with the ionizing current. It can,

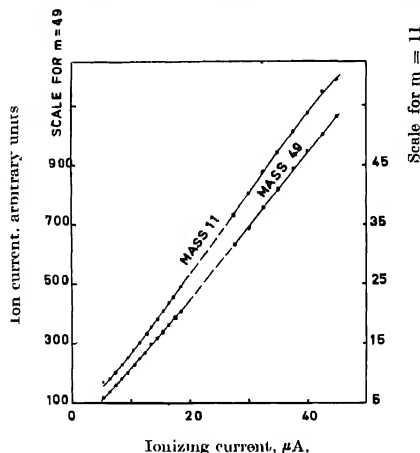


Fig. 2. Dependence of the ion current on the ionizing current. Filament current = 3.4 amp, ionizing voltage = 70V, magnet current = 230ma, repeller setting 4 and 7

therefore, be readily concluded that the spectrometer should be operated with as high a value for the ionizing current as possible. Practical considerations, regarding the life of the filament etc., however, require to keep it at a moderately low value. The ratio of mass peaks 48 to 49 was also computed as a function of the ionizing current and was found to be constant within the limits of experimental uncertainty. Thus, as expected, the isotopic analysis is independent of the ionizing current.

(e) *Dependence of filament efficiency on the ionizing current*

As the anode potential is increased, keeping constant potential difference between the filament and the block, more and more electrons emitted from the filament get into the ionization chamber and consequently both the ionizing and the ion currents increase. On the other hand the block current increases



relatively slowly. The total emission from the filament is equal to the sum of the ionizing current and the block current. As the block current does not serve any useful purpose, it would be preferable to operate the spectrometer under conditions where it is relatively small and hence the filament is being used most efficiently. Let the efficiency of the filament be defined as the ratio of the ionizing current to the total emission current from the filament, for fixed values of the block potential and the filament current. It would then be interesting to investigate the dependence of the filament efficiency on the ionizing current.

Fig. 3 gives two such plots for a fixed value of the block potential, magnet current, and repeller settings. Curve *a* is for a filament which had been in use for about a year and was about to burn off while curve *b* is for an almost new filament. It can be concluded from the shape of these curves that for a new filament the filament efficiency is almost independent of the ionizing current in the range 5 to 20  $\mu A$ , while for an old wire the efficiency increases rapidly till it reaches an optimum where it levels off. It is also seen that the efficiency for a new wire is much higher than that for an old wire even for a much smaller value of the ionizing current. We feel that a part of this difference should be attributed to the orientation of the filament with respect to the slit in the ionization chamber and to the condition of the filament which becomes thinner at the central part of the filament with usage. With the new filament the spectrometer was operated for a much smaller value of the ionizing current.

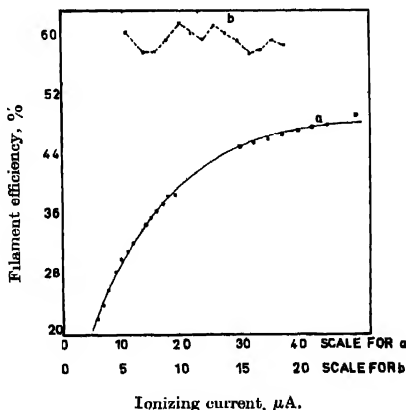


Fig. 3. Filament efficiency as a function of the ionizing current. Ionizing voltage = 70V.

(f) *Dependence of the ion current on the repeller settings*

As shown in Fig. 1, there is a set of two plates in the ionization chamber which can be given varying potentials with respect to the chamber and thus help in collimating the ion beam towards the accelerating plates. It is inter-

esting to investigate the variation of the ion current as the potentials on these plates are varied. One of these plates is called as the inner repeller while the other as the outer repeller. Tables IV(a) and IV(b) respectively tabulate the maximum ion current for several masses as the outer repeller potential is adjusted to a specific value and the inner repeller potential is varied to get the maximum ion current or vice versa. It may be noted that readings in Table IV(b) were taken after the Isatron was dismantled for filament replacement, while those of Table IV(a) were taken with the older filament. All the other controls were given specific values and kept constant in taking the readings in either case, and are listed in respective Tables. It will be seen that in both the cases the ion current increases in the beginning as the fixed potential of the plate is increased, till an optimum value is reached, when ion current does not show any appreciable increase even when the constant potential is doubled. It is, therefore, advisable to keep the potential of one of these plates fixed and close to some such value and adjust the potential of the other plate so that the ion current is maximum.

Tables IV(a) and IV(b) also list the ratios for mass peaks 10 and 11, and 48 and 49. Within the limits of our precision these ratios are fairly, constant, establishing thereby that the isotopic analysis of  $\text{BF}_3$  samples is independent of the repeller settings.  $\alpha$  values are also listed in these tables.

TABLE IV(a)

Ion current for several masses as a function of repeller settings.

Filament current = 3.4 amp, Ionizing current =  $30\mu\text{A}$ ,

Ionizing voltage = 70V, Magnet current = 230 mA,

Sample pressure =  $100\mu$ .

Outer repeller	10.0	20.0	40.0	60.0	80.0	95.0
Inner repeller	47.0	53.0	60.0	94.0	95.0	95.0
Peak height $\text{B}^{10}$	35.1	35.7	37.1	38.0	37.7	37.0
Peak height $\text{B}^{11}$	18.4	18.9	19.6	20.3	20.0	19.7
Peak height $\text{B}^{10}\text{F}_2$	515.0	527.0	—	543.0	556.0	550.0
Peak height $\text{B}^{11}\text{F}_2$	282.0	291.0	—	297.0	305.0	303.0
Ratio $\text{B}^{10}/\text{B}^{11}$	1.91	1.89	1.00	1.87	1.89	1.88
Ratio $\text{B}^{10}\text{F}_2/\text{B}^{11}\text{F}_2$	1.83	1.81	—	1.83	1.82	1.82
$\alpha$	1.04	1.04	—	1.02	1.04	1.04

(g) *Dependence of ion current on sample pressure*

As the sample pressure in the Isatron is increased, one would expect an increase in the ion current and it is, therefore, always preferable to operate the Isatron for safe maximum pressure to get the best precision. Even for a very sensitive instrument and for all the controls at the optimum setting this character-

TABLE IV(b)

Ion current for several masses as a function of repeller settings  
 Filament current = 3.8 amp, Ionizing current =  $15.0\mu\text{A}$ ,  
 Ionizing voltage = 70V, Magnet current 227 mA,  
 Sample pressure =  $50\mu$

Inner repeller	10.0	20.0	30.0	50.0	60.0	70.0	80.0	90.0	95.0
Outer repeller	27.0	42.0	42.0	41.0	42.0	46.0	52.0	53.0	55.0
Peak height $B^{10}$	23.9	24.7	26.6	30.5	31.5	32.1	32.1	32.2	32.0
Peak height $B^{11}$	29.6	30.9	33.5	38.3	39.8	40.3	40.3	40.5	40.2
Peak height $B^{10}F_2$	272.0	271.0	307.0	362.0	376.0	383.0	391.0	395.0	397.0
Peak height $B^{11}F_2$	360.0	360.0	404.0	477.0	497.0	507.0	515.0	521.0	521.0
Ratio $B^{10}/B^{11}$	0.796	0.799	0.794	0.796	0.792	0.793	0.795	0.795	0.796
Ratio $B^{10}F_2/B^{11}F_2$	0.755	0.753	0.760	0.759	0.757	0.755	0.759	0.758	0.762
	1.05	1.06	1.04	1.05	1.05	1.05	1.05	1.05	1.04

istic is extremely useful and important. The pressure can not be indefinitely increased, for then the memory effect, because of increased adsorption on the walls, becomes a troublesome affair. As already discussed this memory effect is quite pronounced in the case of  $BF_3$  and hence this characteristic is of special importance.

In Fig. 4 and 5 are plotted the peak heights for several masses as a function of gas pressure in the Isatron and for fixed settings of the other controls. In Fig 5 the data were taken with the new filament while in the former with the old one. The sensitivity of the instrument is very much higher with the new filament. This should be partly attributed to the change of the molecular leak assembly. In the older peak we found that the pin holes were plugged with use. The sensitivity of the instrument is now in agreement with the specifications of the manufacturers. The peak heights continuously increase, almost linearly, in this pressure range. For  $BF_3$  we have selected sample pressure of  $50\mu$ , almost double than one should choose normally, in view of the fact that  $B^{10}$  peak is only about seven percent of the total. Operation at still higher pressures with  $BF_3$  gas causes considerable memory effect. The ratios of the peak heights for masses 10 and 11, and 48 and 49 remain constant with sample pressure. The value of  $\alpha$  also clusters around 1.05.

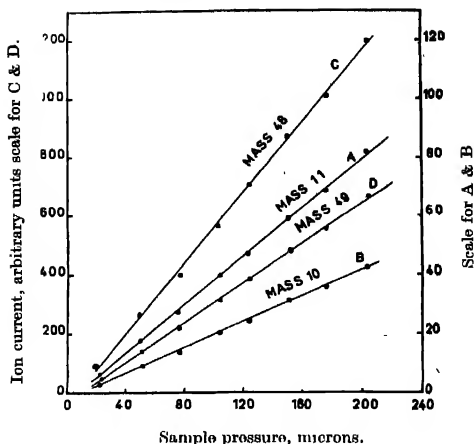


Fig. 4. Dependence of the ion current on the sample pressure. Filament current = 3.4 amp, ionizing voltage = 70V, Ionizing current =  $30 \mu\text{A}$ , Magnet current = 230 mA, Repeller settings = 4 and 17.

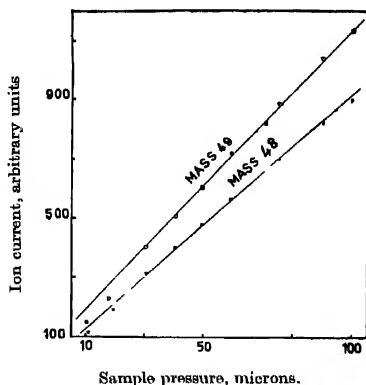


Fig. 5. Dependence of the ion current on the sample pressure. Filament current = 3.6 amp, ionizing current =  $15 \mu\text{A}$ , ionizing voltage = 70V, magnet current = 225 mA, repeller settings = 26 and 60.

#### (h) Voltage effect in the Isatron

It is known that the efficiency of the Isatron increases as the accelerating voltage is increased. The nature of this dependence is a characteristic of the particular instrument. We have also investigated this effect in terms of the bending magnetic field or more precisely the magnet current. As the magnet current is increased a higher accelerating voltage is needed, (Eq. 1), to focus the ions. In Fig. 6, these data have been plotted for masses 10 and 11. It is seen that the

ion current continuously increases as the potential of the focusing plates is increased. For mass 10 the range shown in Fig. 6 corresponds to a variation in the accelerating voltage from about 800V to 3100V. Thus, we see that the efficiency of focusing increases as the scanning potential is increased. It is for this reason we have consistently kept the magnet current at 225ma.

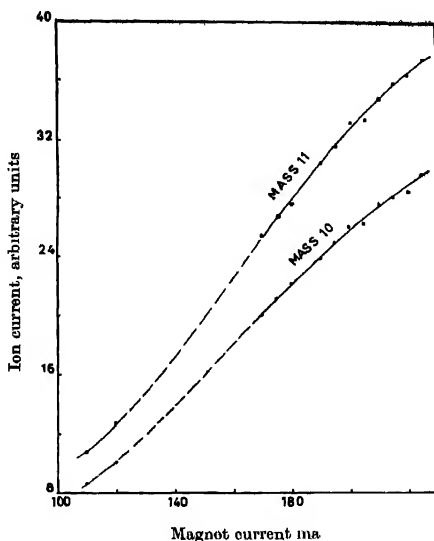


Fig. 6. Dependence of the current on the accelerating voltage. The latter being plotted in terms of the magnet current. Filament current = 3.6 amp, ionizing voltage = 70V, ionizing current = 15  $\mu$ A., repeller settings = 26 and 60, sample pressure = 50 $\mu$

Thus, it is possible to select proper operating conditions from the individual characteristics of this type. It may be of interest to mention here that the instruction manual provided by the manufacturers does not give such plots of the dependence of the ion current on these variables. Chemical and Petroleum Research Laboratory (1959) has published mass spectral data using this type of spectrometer. These data also deal only with the cracking patterns of a number of hydrocarbons but do not discuss anything about the effects of varying these parameters.

#### ACKNOWLEDGMENT

The authors are grateful to Dr. J. Shankar for his interest and encouragement, and making available to us all the facilities.

## REFERENCES

- Aston, F. W., 1919, *Phil. Mag.*, **38**, 709.
- Barnard, G. P., 1953, *Modern Mass Spectrometry*, The Institute of Physics, London.
- Bentley, P. G., 1957, *United Kingdom Atomic Energy Authority, Industrial Group*, Report No IGR-R/C A-253,
- Bentley, P. G., 1960, *I. Sci. Instr.*, **37**, 332.
- Consolidated Electrodynamics Corporation, 1955, *Operation and Maintenance manual*, 300, North Sierra Madre Villa, Pasadena, California.
- Dompster, A. J., 1918, *Phys. Rev.*, **11**, 316.
- Duckworth, H. E., 1958, *Mass Spectroscopy*, Cambridge, University Press.
- Francis, G., 1960, *Ionization Phenomena in Gases*, Butterworths Scientific Publications, London.
- Mass Spectral Data, 1959, American Petroleum Institute Research Project, 44, Chemical and Petroleum Research Laboratory, Carnegie Institute of Technology, Pittsburgh 13, Pennsylvania.
- Nier, A. O., 1940, *Rev. Sci. Instr.*, **11**, 212.
- Nier, A. O., 1947, *Rev. Sci. Instr.*, **18**, 308.
- Palmer, G. H., Dance, D. F., and Atken, K. L., 1956, *AERE, GP/R*, 1994.
- Waldron, J. D., 1956, *Research*, **9**, 306.

# SOLAR AND TERRESTRIAL RELATIONSHIPS OF DAILY VARIATION OF COSMIC RAYS DURING THE I. G. Y\*.

R. P. KANE

PHYSICAL RESEARCH LABORATORY, AHMEDABAD

(Received September 5, 1961)

**ABSTRACT.** Solar and geomagnetic relationship of the daily variation of cosmic ray nucleonic component observed at Climax, Lincoln, Gottingen, Yakutsk, Huancayo, Makerere and Lae have been studied with particular attention to possible "distortion effects" due to isotropic changes observed world-wide in the mean level of cosmic ray intensity and also to the actual scatter of values in individual groups. No significant relationship is indicated for several solar and geomagnetic criteria except for a slight association with geomagnetic storms. Comparison of amplitudes of the first harmonic at various stations shows that on many days, amplitudes are large, moderate or low simultaneously at all stations and the hours of maxima are mostly in the afternoon, but sometimes at night hours also, at all stations. On many other days, amplitudes are high only at one or two stations, indicating short lived anisotropies, though instrumental troubles are also indicated to some extent. The second harmonic is smaller than the first harmonic for high latitudes; but at low latitudes the two are comparable. Many other details are discussed

## I INTRODUCTION

In an earlier communication (Kane, 1961) it was shown that the isotropic changes observed world-wide in the mean level of cosmic ray intensity could produce considerable distortions in the true form of the daily variation of cosmic rays. In the present paper, solar and terrestrial relationships of daily variation will be studied with special emphasis on detecting such distortions, if any.

Table 1 gives details of the neutron monitor stations chosen in such a way that one gets triplets of stations with roughly equal longitudinal spacing.

From these, three factors  $W$ ,  $W'$  and  $W''$  are calculated by adding values for the same U.T. as follows:

$$\begin{aligned} W &= \frac{1}{3} (C+G+Y) \\ W' &= \frac{1}{3} (L+G+Y) \\ W'' &= \frac{1}{3} (H+M+La) \end{aligned} \quad \dots (1)$$

As discussed in detail in the earlier communication, the quantities  $W$ ,  $W'$  or  $W''$  represent the world-wide, isotropic changes of mean level of cosmic ray intensity. Hence, if these are subtracted from the original data, one could study the genuine

---

\* Communicated by Prof. V. Sarabhai

daily variation. Since Climax and Huancayo are high altitude stations, the factors  $W$  and  $W''$  are less valid than  $W'$ .

TABLE 1

Station	Symbol	Quenby & Webber's Geomagnetic lati- tude	Geographic longitude	Altitude (meters)	Poisson standard error	
					Bi-hourly value	Daily har- monics
Climax	C	49° 0	106°W	3400	0.12%	0.05%
Lincoln	L	52° 8	97°W	350	0.53%	0.21%
Gottingen	G	50° 8	10°E	273	0.41%	0.17%
Yakutsk	Y	57° 8	130°E	105	0.50%	0.23%
Huancayo	H	— 0° 1	75°W	3400	0.18%	0.07%
Makerere	M	— 7° 1	33°E	1196	0.28%	0.11%
Lao	La	— 14° 7	147°E	S.L	0.78%	0.31%

Bi-hourly values of  $(C-W)$ ,  $(L-W')$ ,  $(G-W')$ ,  $(Y-W')$ ,  $(H-W'')$ ,  $(M-W'')$  and  $(La-W'')$  were evaluated and the daily variation studied by harmonically analysing 12 successive bi-hourly values starting from midnight *local time* for each station. Thus, for every day for which data were available, the amplitudes ( $r_1, r_2$ ) and hours of maxima ( $\phi_1, \phi_2$ ) of the first and second harmonics were evaluated for Climax, Lincoln, Gottingen, Yakutsk, Huancayo, Makerere, Lao,  $(C-W)$ ,  $(L-W')$ ,  $(G-W')$ ,  $(Y-W')$ ,  $(H-W'')$ ,  $(M-W'')$  and  $(La-W'')$ . Averages of  $r_1, r_2, \phi_1$  and  $\phi_2$  for groups of days selected on specific geomagnetic or solar epochs were studied.

## II STANDARD ERRORS FOR AVERAGES OVER GROUPS OF DAYS

For comparison of group characteristics of the amplitudes and phases of daily variation, one should know the standard errors of the various quantities involved. Generally the bi-hourly cosmic ray intensity is assumed to obey Poisson distribution. The % Poisson standard error can be calculated as  $\sigma = \frac{100}{\sqrt{N \cdot x}}$  where  $N$  = observed counting rate and  $x$  = scaling factor. For the amplitude of the various daily harmonics (1st, 2nd etc.), the standard error is  $\frac{\sigma}{\sqrt{6}}$ . While comparing average amplitudes of two sets of days, the usual practice is to calculate standard errors as  $\frac{\sigma}{\sqrt{6K}}$  where  $K$  = number of days in a particular set and to see whether the difference  $(r' - r'')$  of the amplitudes  $r'$  and  $r''$  of the two sets is outside the Poisson twice standard error limit given by  $2 \cdot \sqrt{\frac{\sigma_1^2}{6K_1} + \frac{\sigma_2^2}{6K_2}}$ .



In the above procedure, it is assumed that all statistical characteristics of cosmic rays are guided by Poisson distribution and nothing else. However, cosmic rays are known to undergo systematic variations such as 27-day recurrences, Forbush decreases, etc. Therefore, for a group of days, cosmic ray intensity, whether considered on a bi-hourly basis or a daily mean basis, will show a range of values which is guided not only by Poisson fluctuations but genuine changes due to physical causes. Both these can be taken into account simultaneously if the standard errors are calculated not from standard Poisson formulae as given above but from the actual deviations from mean for a given sample. This is illustrated by the following example:

Consider the dependence of daily mean intensity of neutron component at Climax on geomagnetic index  $C_p$ . Table II gives the average mean intensity for various  $C_p$  values.

TABLE II

$C_p$	0-0.3	0.4-0.7	0.8-1.1	1.2-1.5	>1.5
Days	60	54	40	14	13
Relative C.R. Int. (%)	$\pm 0.41$	$\pm 0.15$	$-0.26$	$-0.54$	$-1.44$
Poisson std. error (%)	$\pm 0.005$	$\pm 0.005$	$\pm 0.006$	$\pm 0.010$	$\pm 0.010$
Actual std. error (%)	$\pm 0.15$	$\pm 0.16$	$\pm 0.18$	$\pm 0.40$	$\pm 0.60$

Since the Poisson standard error of the daily mean intensity at Climax is very small ( $\sim .04\%$ ), even differences of the order of a tenth of a percent are statistically significant. But, in each of the above indicated groups, the % daily mean intensity fluctuates in a wide range of  $\pm 5.0\%$ . Therefore, one should calculate the *actual* standard error for each of the 5 groups by the formula

$$\sigma = \sqrt{\frac{1}{n} \cdot \sum_k (I_k - I)^2} \quad (2)$$

where  $I_k$  = intensity on individual days,  $I$  = average value for the group and  $n$  = number of days in the group. The standard error of the mean will then be given by  $\sigma/\sqrt{n}$ . These *actual* standard errors are indicated in the last row of Table II. It will be seen that broadly speaking, high  $C_p$  values are still associated with low mean intensities, but the finer details are now not as significant as one would have thought they would be from purely Poisson error considerations.

The same consideration should apply for the standard errors of the amplitudes of the daily variation. Since the harmonic component of the daily

variation is a vector, one would need to find the standard errors of its 0 hour and 6 hour components. Thus if the first harmonic  $(r_1, \psi_1)$  is given by

$$r_1 \cos(\theta + \psi_1) = a_1 \cos \theta + b_1 \sin \theta \quad \dots (3)$$

$$\text{then} \quad r_1^2 \cdot \sigma_{r_1}^2 = a_1^2 \cdot \sigma_{a_1}^2 + b_1^2 \cdot \sigma_{b_1}^2 \quad \dots (4)$$

where  $\sigma_{a_1}$  and  $\sigma_{b_1}$  are the standard errors of the  $a_1$  and  $b_1$  distributions and should be calculated by formula similar to Eq. (2) to be applied to the *actual* set of  $(a_1, b_1)$  values in any particular group. For the average value  $\bar{r}_1$  of a group,

$$\text{standard error } \sigma_{\bar{r}_1} = \frac{\sigma_{r_1}}{\sqrt{n}}.$$

It may be noted that the  $\sigma$  value so calculated is an "estimated" value and hence will have a standard error given by  $\sigma/\sqrt{2n}$ . For a small group of days, this could be appreciable. Thus, for a group of 12 days, the error in standard error could be 1/5th of the value of the standard error itself. In such cases, it would be difficult to fix the  $2\sigma$  limit precisely. Perhaps, evaluation of standard errors from such small samples may not even be justified. Hence, in what follows, we shall first examine which effects stand out as statistically significant on a  $2\sigma$  level by using the actual standard errors; and when the samples are small, we will further check whether the group averages are not dominated by a few abnormally large values on individual days.

### III GEOMAGNETIC RELATIONSHIPS OF DAILY VARIATION

Geomagnetic disturbances indicated by the following indices will be considered.

- (1)  $C_p$ , the daily geomagnetic planetary index.
- (2) Horizontal component of earth's magnetic field at the equator.
- (3) Occurrence of sudden commencement and gradual magnetic storms.

(1)  $C_p$  Values.  $C_p$  is an index of daily geomagnetic disturbance ranging from 0 to about 2.0. Table III gives the average amplitudes and hours of maxima of the first and second harmonics of daily variation for various  $C_p$  groups.

The following remarks may be made:

(a) The amplitude of the first harmonic is about the same for  $C_p$  values up to 1.5 but increases for higher  $C_p$  values at high latitudes. From Poisson considerations, the increase is far beyond a  $3\sigma$  limit and hence one would conclude that the amplitude of the first harmonic is significantly higher for  $C_p$  values  $> 1.5$ .

(b) However, if the standard errors are calculated from the *actual* scatter of points in each group, an altogether different picture emerges. Thus, for Climax (C), the amplitudes given in Table III would be associated with standard errors as shown in Table IV.

TABLE III

$C_p$ (days)	Station	$r_1$	$\phi_1$	$r_2$	$\phi_2$	Station	$r_1$	$\phi_1$	$r_2$	$\phi_2$
0 - .3 (~120 days)	C	0.31	$\pi - 42$	0.09	39	C-W	0.31	$\pi + 59$	0.03	45
	L	0.30	$\pi + 57$	0.05	$\pi - 53$	L-W'	0.31	$\pi + 57$	0.01	$\pi$
	G	0.28	$\pi + 17$	0.05	-37	G-W'	0.27	$\pi + 17$	0.03	45
	Y	0.18	$\pi + 45$	0.10	$\pi + 6$	Y-W'	0.25	$\pi + 53$	0.09	$\pi - 21$
.4 - .7 (~140 days)	C	0.38	$\pi + 42$	0.08	30	C-W	0.37	$\pi + 52$	0.01	$\pi - 45$
	L	0.36	$\pi + 48$	0.03	0	L-W'	0.38	$\pi + 45$	0.02	-90
	G	0.37	$\pi + 6$	0.02	-90	G-W'	0.37	$\pi + 9$	0.03	18
	Y	0.30	$\pi + 66$	0.06	$\pi - 39$	Y-W'	0.33	$\pi + 50$	0.03	$\pi - 45$
.8 - 1.1 (~130 days)	C	0.28	$\pi + 36$	0.01	60	C-W	0.25	$\pi + 53$	0.02	$\pi - 27$
	L	0.29	$\pi + 25$	0.06	$\pi - 39$	L-W'	0.26	$\pi + 32$	0.05	$\pi - 37$
	G	0.26	$\pi + 13$	0.07	$\pi - 45$	G-W'	0.23	$\pi + 2$	0.06	$\pi - 51$
	Y	0.12	$\pi + 35$	0.04	$\pi + 14$	Y-W'	0.22	$\pi + 30$	0.02	$\pi - 27$
1.2 - 1.5 (~80 days)	C	0.29	$\pi + 50$	0.03	78	C-W'	0.26	$\pi + 74$	0.04	$\pi + 45$
	L	0.37	$\pi + 46$	0.04	76	L-W'	0.29	$\pi + 59$	0.02	$\pi + 27$
	G	0.35	$\pi + 24$	0.06	$\pi + 45$	G-W'	0.30	$\pi + 6$	0.02	90
	Y	0.15	$\pi - 37$	0.14	$\pi + 17$	Y-W'	0.27	$\pi + 34$	0.06	$\pi + 51$
1.5 (~40 days)	C	0.47	$\pi + 54$	0.04	$\pi + 4$	C-W'	0.43	$\pi + 25$	0.04	-76
	L	0.47	$\pi - 4$	0.13	$\pi + 23$	L-W'	0.52	$\pi + 8$	2.14	$\pi - 54$
	G	0.50	$\pi - 22$	0.08	-7	G-W'	0.46	$\pi - 14$	0.02	-90
	Y	0.46	$\pi + 20$	0.08	$\pi + 23$	Y-W'	0.50	$\pi + 25$	0.13	$\pi - 29$

TABLE III (contd.)

$C_p$ (days)	Station	$r_1$	$\phi_1$	$r_2$	$\phi_2$	Station	$r_1$	$\phi_1$	$r_2$	$\phi_2$
0 -0.3 (~120 days)	H	0.20	$\pi + 6$	0.10	-6	H-W''	0.25	$\pi + 18$	0.12	24
	M	0.47	$\pi - 23$	0.38	-16	M-W''	0.38	$\pi - 23$	0.28	-23
	La	0.25	$\pi + 12$	0.19	$\pi - 43$	La-W''	0.35	$\pi - 12$	0.23	72
.4-0.7 (~140 days)	H	0.27	$\pi + 17$	0.05	0	H-W''	0.26	$\pi + 28$	0.08	60
	M	0.47	$\pi - 18$	0.24	-5	M-W''	0.43	$\pi - 23$	0.28	-15
	La	0.13	$\pi - 27$	0.12	$\pi - 70$	La-W''	0.28	$\pi - 21$	0.24	81
0.8-1.1 (~130 days)	H	0.24	$\pi + 5$	0.06	-18	H-W''	0.24	$\pi + 19$	0.07	56
	M	0.41	$\pi - 19$	0.19	-5	M-W''	0.35	$\pi - 25$	0.25	-23
	La	0.14	$\pi - 21$	0.19	$\pi - 74$	La-W''	0.28	$\pi - 17$	0.27	77
1.2-1.5 (~80 days)	H	0.23	$\pi + 29$	0.04	-14	H-W''	0.19	$\pi + 36$	0.08	83
	M	0.36	$\pi - 11$	0.19	-17	M-W''	0.40	$\pi - 19$	0.22	-32
	La	0.08	$\pi - 40$	0.17	73	La-W''	0.22	$\pi - 16$	0.28	73
> 1.5 (~40 days)	H	0.24	$\pi - 12$	0.05	$\pi + 79$	H-W''	0.26	$\pi + 18$	0.10	11
	M	0.56	$\pi - 27$	0.35	-7	M-W''	0.44	$\pi - 28$	0.29	-29
	La	0.22	$\pi + 5$	0.33	$\pi - 25$	La-W''	0.30	$\pi - 26$	0.25	-83

TABLE IV

$C_p$ value	Days	Amp. $r_1$ with actual Std. error
0-0.3	126	$0.31 \pm 0.03$
0.4-0.7	145	$0.38 \pm 0.03$
0.8-1.1	130	$0.28 \pm 0.04$
1.2-1.5	80	$0.29 \pm 0.05$
> 1.5	38	$0.47 \pm 0.11$

The amplitudes in the various groups are now not significantly different from each other. This applies to all other stations as well.

(c) From Table IV, it seems that the amplitude is in no way related to  $C_p$  values. The higher value for  $C_p > 1.5$  is probably due to the fact that the number of days in this group is the smallest. This could be checked by subdividing one of the larger groups. The first group corresponding to  $C_p = 0-0.3$  was subdivided into 4 groups of about 30 successive days. The average amplitude with the actual standard errors are as shown in Table V for Climax.

TABLE V

$C_p$	Days	Amp. $r_1$ with actual std. error
0-0.3	33	$0.40 \pm 0.06$
"	33	$0.34 \pm 0.10$
"	33	$0.25 \pm 0.06$
"	27	$0.28 \pm 0.06$
> 1.5	38	$0.47 \pm 0.11$

It is clear from Table V that the amplitudes vary largely within the same group and hence differences between the various  $C_p$  groups in Table III may not be meaningful.

(d) For high latitude stations, the second harmonic is negligible. For equatorial stations, it is almost comparable to the first harmonic. But no relationship between  $C_p$  and the amplitude of the second harmonic is indicated.

(e) Since the standard errors of the amplitudes are large, differences in their hours of maxima are not significant.

(f) Regarding slope, curvature and short-term effects, it seems that the amplitudes of the various groups are not altered by more than about 0.1% due to such effects. (Compare  $C$  with  $C-W$ ,  $L$  with  $L-W'$  etc.). This is understandable, because for averages over groups of large number of days, such effects tend to average out.

The broad conclusion would, therefore, be that the first and second harmonics of the daily variation have no relation with  $C_p$  values in general. This conclusion is not affected by slope, curvature and short-term effects. (These will henceforth be termed as "distortion effects" for brevity).

There is a possibility that days of  $C_p$  maxima may be related to the diurnal variation with a time lag. To study this, Chree analysis was carried out with days of  $C_p$  maxima as epoch days. A finer classification of  $C_p$  maxima was also made as follows :

$+C_p^+ - C_p$  maxima preceded and followed by maxima at  $27 \pm 1$  days.

$+C_p^0 - C_p$  maxima preceded but not followed by maxima at  $27 \pm 1$  days.

$^0C_p^+ - C_p$  maxima followed but not preceded by maxima at  $27 \pm 1$  days.

$^0C_p^0 - C_p$  maxima neither followed nor preceded by maxima at  $27 \pm 1$  days

For each type of  $C_p$  maxima, the vectorial average amplitudes and hours of maxima of the first and second harmonics were evaluated for the epoch day as also for  $-7$  to  $+7$  days for all stations. The results are shown in Fig. 1, where amplitudes of the first harmonic are plotted. Epoch dates are given in Appendix. Full curves refer to  $C$ ,  $L$ ,  $G$ ,  $Y$ ,  $H$ ,  $M$ ,  $La$  and dotted curves to  $C-W$ ,  $L-W'$  etc.

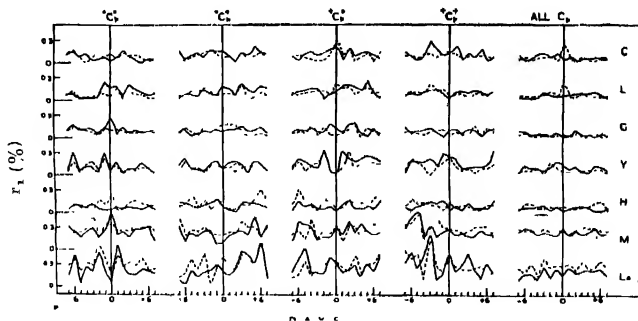


Fig. 1. Chree diagrams for the amplitudes of the first harmonic ( $r_1$ ) for  $C_p$  maxima epochs.

The following points may be noted :

(a) For  ${}^0C_p^0$ , there were 18 epoch dates during the I.G.Y. It will be seen from Fig. 1 that for some stations, the amplitudes are higher before the epoch than after the epoch. However, this effect reduces when corrections for "distortion effects" are applied. Thus, for Climax (C), the amplitude is 0.5 % for -3 day while for (C-W) it is only 0.32% and its contrast with the value 0.20% for the +1 or +2 days is no more so striking. Also the *actual* standard errors are quite high. Thus, for Climax,

For -5th day, amplitude $r_1$	$= 0.10 \pm .10 \pm .02$
„ -3rd day, „	$= 0.50 \pm .16 \pm .03$
„ +2nd day „	$= 0.20 \pm .11 \pm .02$
„ +6th day, „	$= 0.50 \pm .03 \pm .01$

The various ups and downs are not statistically significant on a  $2\sigma$  level. It may be concluded, therefore, that  ${}^0C_p^0$  maxima have no relationship with cosmic ray daily variation.

(b) For  ${}^0C_p^+$  maxima, there were 14 epoch days. On examining the various ups and downs with due attention to their actual standard errors, one is led to a conclusion similar to that in (a) above.

(c) For  ${}^+C_p^0$  maxima, for which there are 13 epoch days, Climax and Lincoln show two maxima with high amplitudes near the epoch and two days later. However, the amplitudes are considerably smaller for C-W and L-W' indicating a large "distortion effect". Also, none of the maxima is significantly different from any of the dips. Hence, no relationship is indicated.

(d) For  ${}^+C_p^+$  maxima (14 epochs), there seems to be an indication that the amplitudes are high prior to epoch and low after the epoch. The effect is reduced for (C-W) etc., but is, nevertheless, still there. For high latitude stations (C, L, G, Y), the amplitudes are high upto the -1th day and then drop steadily from -1 to about +3 days and later rise again. For equatorial stations, the effect is less prominent and the fall of amplitude starts earlier, from -3 days to about +3 days. For Climax, the amplitudes with actual standard errors and their standard errors are :

-2nd day, amplitude $r_1$	$= .51 \pm .13 \pm .03$
-1st day, „	$= .45 \pm .16 \pm .03$
0 day, „	$= .64 \pm .13 \pm .03$
+1st day, „	$= .39 \pm .10 \pm .02$
+2nd day, „	$= .11 \pm .08 \pm .02$
+3rd day, „	$= .16 \pm .05 \pm .01$

Thus, the effect seems to be genuine. (This is discussed further below).

(c) In Fig. 1, the last column represents the curves for all  $C_p$  maxima (59 epochs) which show characteristics similar to those for  $+C_p^+$  maxima but to a reduced extent. A point worth noting is that many of the maxima and minima are due to "distortion effects" as is evident by their absence in the dotted curves referring to  $C-W$ ,  $L-W'$  etc.

In conclusion, it seems that amongst the various types of  $C_p$  maxima, only  $+C_p^+$  seems to have some relationship with cosmic ray daily variation. The amplitudes are large immediately before the epochs and small after the epochs.

It must be remembered, however, that there are only 14 events of the  $+C_p^+$  maxima during I.G.Y. The sample is, therefore, very small and the working out of standard errors as shown above in (d) is unreliable. It has to be checked, therefore, whether the set of  $(r_1, \phi_1, r_2, \phi_2)$  values for these 14 events is consistent within itself or whether the mean characteristics are completely dominated by just one or two events. Table VI gives the actual  $r_1, \phi_1, r_2, \phi_2$  values for Climax for the epoch days and the  $+2$  days for  $+C_p^+$  maxima.

TABLE VI

$+C_p^+$ maxima dates (epochs)	For epoch dates				For +2 dates			
	$r_1(\%)$	$\phi_1$	$r_2(\%)$	$\phi_2$	$r_1(\%)$	$\phi_1$	$r_2(\%)$	$\phi_2$
Sep. 2, 1957	1.95	$\pi+31$	0.51	$\pi+63$	0.84	$\pi-65$	0.42	$\pi+61$
Oct. 21, 1957	1.83	$\pi+33$	0.98	60	0.49	$\pi+30$	1.21	$\pi+52$
Nov. 9, 1957	0.18	$\pi+81$	0.44	-14	0.44	$\pi+34$	0.11	38
Nov. 18, 1957	0.29	$\pi-50$	0.10	31	0.34	$\pi+49$	0.16	25
Dec. 5, 1957	0.72	$\pi+71$	0.40	25	0.21	$\pi+75$	0.13	2
Mar. 6, 1958	0.63	-25	0.59	$\pi+50$	0.56	17	0.37	47
Apr. 2, 1958	0.48	$\pi+80$	0.33	$\pi+20$	0.23	$\pi+73$	0.44	29
Apr. 29, 1958	0.76	$\pi+88$	0.36	$\pi+23$	0.57	$\pi+56$	0.07	87
May. 14, 1958	0.67	$\pi+00$	0.25	$\pi+23$	0.37	-3	0.24	$\pi-3$
May. 26, 1958	0.31	$\pi+24$	0.26	$\pi-7$	0.50	$\pi+40$	0.17	88
Jun. 10, 1958	1.07	$\pi+87$	0.27	$\pi-2$	0.30	-33	0.05	23
Jun. 21, 1958	1.15	$\pi+80$	0.51	$\pi+45$	0.27	$\pi+82$	0.04	4
Jun. 29, 1958	0.51	-39	0.23	59	0.34	85	0.18	$\pi-30$
Jul. 27, 1958	0.81	-75	0.64	$\pi+16$	0.39	$\pi-47$	0.21	$\pi-58$
Vectorial average	0.64 $\pm .13$	$\pi+67$	0.13 $\pm .08$	$\pi+15$	0.11 $\pm .08$	$\pi+23$	0.03 $\pm .07$	$\pi+15$



In Table VI, the amplitudes show very large fluctuations within the group. It is obvious that one is dealing here with a very heterogeneous group. Therefore, the conclusion drawn in (d) viz. amplitudes are high before  $+C_p^+$  maxima and low afterwards has to be accepted with great caution. The possibility of this occurring accidentally is not ruled out completely.

It would be interesting to see how the hour of maximum is affected during this transition from high to low amplitudes. Fig. 2 shows the Chree diagrams for the hour of maximum  $\phi_1$ , for  $+C_p^+$  maxima as epochs.

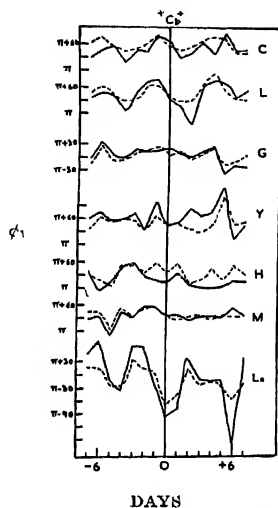


Fig. 2. Chree diagram for the hour of maxima of the first harmonic ( $\phi_1$ ) for  $+C_p^+$  maxima as epochs.

A significant point to note in Fig. 2 is that whereas the original hours of maxima show large fluctuations while passing from  $-3$  to  $+3$ rd day, the fluctuations are small (within  $\pm 2$  hours) in the dotted curves, which indicates that they are only due to "distortion effects". In the absence of  $C-W$ ,  $L-W'$  etc., these would be misinterpreted as advances or recessions of the hour of maxima!

So far we have discussed the amplitudes and phases of the first harmonic only. For the second harmonic, the amplitudes are by no means negligible on individual days as can be seen from Table VI. However, the phase scatter is so large that the vectorial averages for groups yield very low amplitudes in general. Fig. 3 shows the Chree diagrams for the amplitudes of the second harmonic for various types of  $C_p$  maxima as epoch days. Notable points are :

- (a) For high latitudes, the average amplitudes are low ( $\sim 0.2\%$ ) in general.

- (b) For low latitudes, the amplitudes are high for Makerere and Lae but not for Huancayo. This is difficult to understand. Before using for analysis, the data for Makerere were corrected for barometric pressure

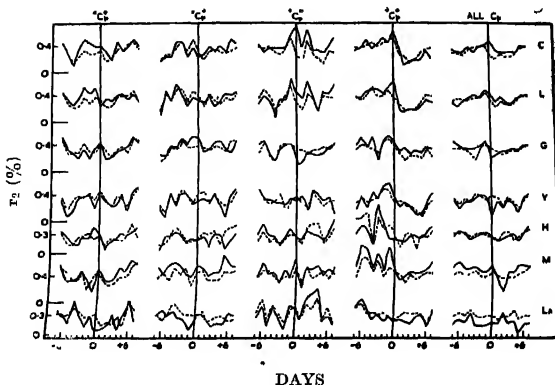


Fig. 3. Chree diagram for the amplitudes of the second harmonic ( $r_2$ ) for  $C_p$  maxima as epochs

by using a coefficient of  $0.72\%/mb.$  Hg., same as for Huancayo and Lae. So the discrepancy could not be due to difference in pressure coefficient. If the second harmonic is due to extra-terrestrial causes, its attenuation due to atmospheric scattering etc. will be more at larger depths (Brunberg, 1955) and its amplitude should be higher at higher altitudes, i.e. at Huancayo, which is contrary to what is observed.

- (c) There are many maxima and minima, but there is no consistent pattern for relationship with any type of  $C_p$  maxima. Fluctuations for Lae are quite erratic.

From the above discussion it seems that neither the first harmonic nor the second harmonic have any relationship with geomagnetic disturbance as represented by  $C_p$  in general, though some relation with  $+C_p$  maxima is indicated for the first harmonic amplitude (but not phase).

## (2) Horizontal component of earth's magnetic field

Apart from the general  $C_p$  index of geomagnetic disturbance, one could also use the intensity of the earth's magnetic field as a criterion. Since the horizontal component represents the bulk of the geomagnetic field at equator, we have used data for the same, recorded at the Solar Physics Observatory, Kodaikanal, India. From the plot of the daily mean values of the horizontal component, days were chosen corresponding to large ( $> 100$  gamma) and small minima. The epoch

dates are given in the Appendix. Fig. 4 shows the Chree diagrams for the amplitudes of the first and second harmonics. Following comments may be made :

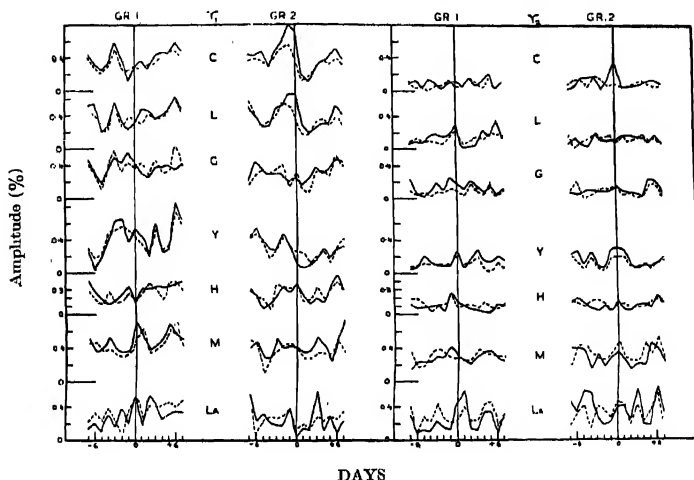


Fig. 4. Chree diagrams for the amplitudes  $r_1$  and  $r_2$  for large (Group 1) and small (Group 2) minima of horizontal component of earth's magnetic field as epochs.

(a) Group 1 corresponding to large minima has 14 epoch days. The first harmonic seems to be maximum on  $-3$  and  $+6$  days for high latitudes. Thus, for Climax

$$\text{Amplitude on } -3 \text{ day} = 0.60 \pm 0.12 \pm .02\%$$

$$\text{Amplitude on } -1 \text{ day} = 0.12 \pm 0.15 \pm .03\%$$

$$\text{Difference} = 0.48 \pm 0.19 \pm .04\%$$

Thus the difference is marginally significant on a  $2\sigma$  level. For low latitudes, no consistent effect is observable.

(b) For Group 2 corresponding to small minima, there are about 12 epochs. Here one finds that the amplitude of the first harmonic is quite large on about  $-1$  day for Climax and Lincoln, but not for other stations. Also the amplitude is considerably reduced in the dotted curves. This is, therefore, a clear case of "distortion effect." However, the main pattern, viz. high amplitudes prior to epoch and low amplitudes after epoch, seems to be shown by all high latitude stations to some extent.

In conclusion, it would seem from (a) and (b) above that for high latitude stations, the amplitudes of the first harmonic are high before epoch and low after epoch, a result similar to the one obtained for  $+C_p^+$  maxima epochs with the ex-

ception that the pattern is not observed for equatorial stations. The amplitudes of the second harmonic do not show any consistent relationship for any group.

Fig. 5 gives the average curves for Group 1 and Group 2 for high latitude and low latitude stations, with the same dates as in Fig. 4, for epochs.

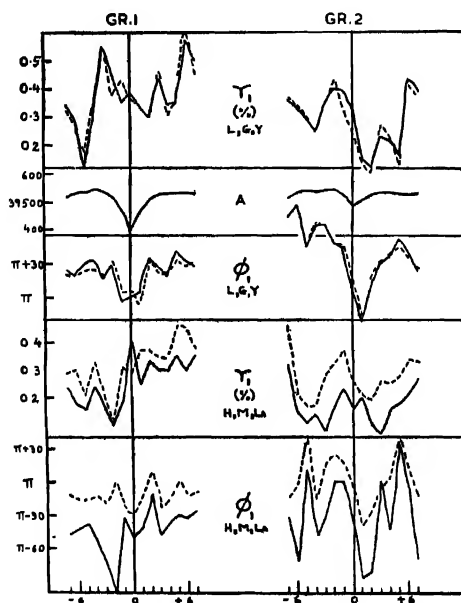


Fig. 5. Three diagrams for average values of  $r_1$ ,  $\phi_1$  for high and low latitude stations with epochs as in Fig. 4. Curve A refers to horizontal component of earth's magnetic field.

It will be seen from Fig. 5 that the amplitude and hour of maximum of the first harmonic follow the following pattern, particularly at high latitudes :

- (i) About 4 to 6 days prior to epoch the amplitudes are low and hour of maximum is in the afternoon.
- (ii) About 2 to 4 days prior to epoch, amplitudes suddenly increase. Hour of maximum is unaltered.
- (iii) From about -2 to +2 days, the amplitudes slowly decrease and the hour of maximum shifts to earlier hours.
- (iv) From about +2 days onwards, amplitudes and hour of maxima start recouping to the state (ii).

This pattern is more evident for Group 2 than for Group 1, which corresponds to large minima. It seems, therefore, that in the highly disturbed state, the diurnal variation patterns are less systematic. Also the high latitude and the low latitude stations do not show similar patterns. It is only during moderate geomagnetic disturbances (Group 2) that the pattern is very striking for both amplitude and phase of diurnal variation at both high and low latitudes. Since moderate geomagnetic disturbances recur after 27 days while large disturbances do not, the resemblance of the pattern shown by Group 2 above with the one of  $+C_p$  maxima is understandable.

Here again, a word of caution is necessary. In Group 2 there are only 11 epochs. So it needs to be checked whether the pattern is largely influenced by single events. Table VII gives the amplitudes and hour of maximum for  $(L-W')$  for the  $-2nd$  and  $+1st$  days, which are days of maximum contrast for Group 2.

TABLE VII

$-2nd$ day		$+1st$ day	
$r_1$	$\phi_1$	$r_1$	$\phi_1$
0.79	$\pi - 41$	0.32	$\pi + 148$
0.23	$\pi - 25$	0.38	$\pi - 83$
0.38	$\pi + 25$	0.48	$\pi - 37$
0.39	$\pi + 61$	0.24	$\pi - 35$
0.14	$\pi + 120$	0.29	$\pi - 35$
1.14	$\pi + 36$	0.09	$\pi - 63$
1.25	$\pi + 67$	0.57	$\pi + 14$
0.88	$\pi + 77$	0.11	$\pi + 10$
1.04	$\pi + 104$	1.09	$\pi - 62$
1.15	$\pi + 76$	0.34	$\pi - 163$
0.63	$\pi - 55$	0.38	$\pi + 58$
Average	0.56 $\pi + 59$	0.18 $\pi - 38$	

It can be seen from Table VII that in both groups the amplitudes range from 0.1% to 1.0% and the hours of maxima have a very large spread. The average of the first group is greatly dominated by 3-4 events. It seems, therefore, that the conclusions drawn above about the group characteristics may be of doubtful validity.

(3) *Geomagnetic storms*

Most of the minima of horizontal component of geomagnetic field referred to above are part of what are known as geomagnetic storms. These can be of the sudden commencement type (with or without initial impulse) or of gradual type. Dates of such storms, reported by about a dozen laboratories, are given in *Journal of Geophysical Research*. Now, it often happens that the same date is reported as associated with a storm of one type by one station, and of some other type by another. Therefore, data from *all* reporting laboratories were scrutinized and dates were considered in the following priority :

S.C.\*S—Sudden commencement storms with initial impulse, (Severe).

S.C.S.—Sudden commencement storms without initial impulse, (Severe).

S.C.\*MS—Sudden commencement storms with initial impulse, (Moderately severe).

S.C. MS—Sudden commencement storms without initial impulse, (Moderately severe).

G.S. —Gradual storms, (Severe).

Storms reported as S.C.\* or S.C. moderate and gradual, moderately severe and moderate have been neglected. The dates of storms selected for analysis are given in Appendix.

With these dates as epochs, Chree analysis was done. Fig. 6 shows the Chree diagrams for the amplitude of the first harmonic. Following conclusions may be drawn :

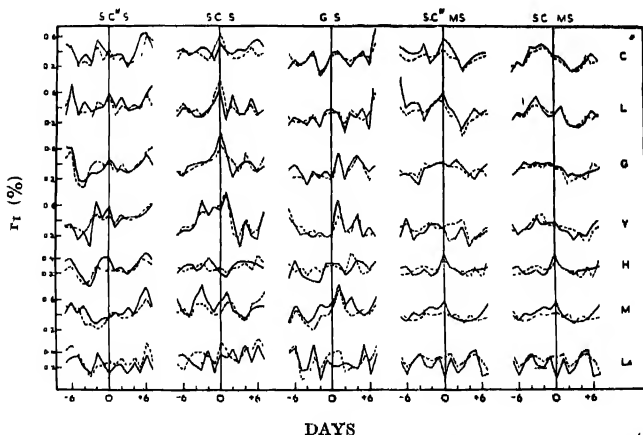


Fig. 6. Chree diagrams for amplitude  $r_1$  for days of S.C.\* S, S.C.S., G.S., S.C.\*MS and S.C.MS storms as epochs.

- (1) For days of severe S.C.\*. storms, there is no relationship, consistent at all stations.

- (2) For severe S.C. storms, amplitudes seem to rise upto the epoch day and then fall rapidly after epoch. The effect is pronounced at high latitudes but not so at low latitudes.
- (3) For severe gradual storms, no consistent relation.
- (4) For moderately severe S. C\*. storms, there is some indication of a pattern like (2) for some stations but not for all.
- (5) For moderately severe S.C. storms, a pattern similar to (2) is visible for high latitudes and to a lesser extent for low latitudes.

Thus, amongst the various types of magnetic storms, the severe S. C. storms and moderately severe S.C. and S.C\*. storms seem to show a pattern similar to what  $+C_p$  maxima and small  $H$  minima showed viz. high amplitudes before epoch and low amplitudes after epochs. However, a scrutiny of amplitudes on individual days shows that the average effects are largely dominated by data of a few days.

In conclusion, one would state that whereas for some types of geomagnetic criteria, large amplitudes before epoch and small amplitudes after epoch are indicated for the first harmonic on the average, these characteristics are not shown consistently for all individual events. The scatter about mean values is very large and the means are greatly influenced by individual values. Therefore, whereas an indirect relationship between some geomagnetic criteria and the daily variation is not completely ruled out, the results could have also been due to the fact that some dates coincide by chance with days of large amplitudes which may owe their existence to some other criteria.

#### IV SOLAR RELATIONSHIP OF DAILY VARIATION

There are several solar phenomena which can be studied to see their relationship with diurnal variation of cosmic ray intensity. We have chosen the following:

- (1) C.M.P. of active sunspot groups.
  - (2) Solar radio emission (200 m c/s).
  - (3) Type IV solar radio outbursts.
  - (4) Leinbach events.
  - (5) Solar flares.
- (1) *C.M.P. of active sunspot groups*
- For these, (a) the very intense and, (b) the pronounced sunspot groups were considered. Epoch dates are given in Appendix.

Fig. 7 shows the Chree diagram for the amplitude of the first harmonic. Following points may be noted :

- (i) For group (a) viz. C.M.P. of very intense sunspot groups, there is indication of a pattern when amplitudes are high a few days ( $\sim 3$ ) before and few days after the epoch but quite low on or near the epoch days.

- (ii) From statistical considerations, the effect is marginally significant on a  $2\sigma$  level. But on inspection of amplitudes on individual days, a very large scatter is observed. Averages are affected greatly by individual values.
- (iii) For group (b), no clear relationship is indicated.

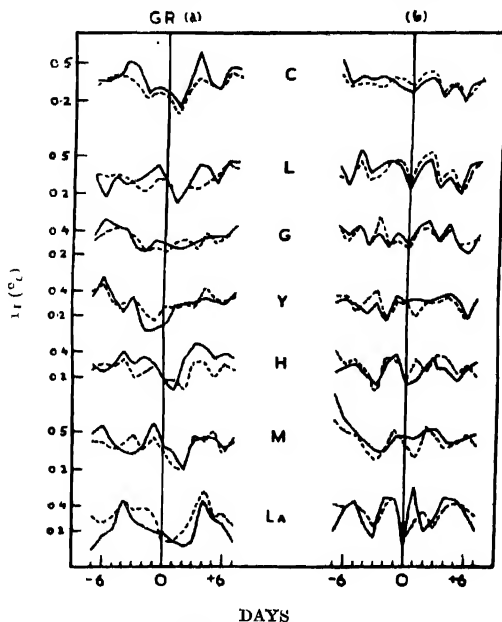


Fig. 7. Chree diagram for  $r_1$  for C.M.P. dates of (a) very intense and (b) pronounced sunspot groups as epochs.

## (2) Solar radio emission

The maxima of the daily index of solar radio emission were classed into 2 groups corresponding to large and small maxima. Fig. 8 shows the Chree diagrams for the amplitude of the first harmonic. It will be seen that no consistent relationship is indicated for either group.

## (3) Type IV solar radio outbursts

These are major radio outbursts in the solar corona and are supposed to be giving out synchrotron radiation by relativistic electrons. They are usually followed by polar cap blackouts i.e. heavy attenuation of radio waves passing through polar regions. During I.G.Y., there were 22 such events. Fig. 9 shows the Chree diagrams for the first harmonics for such events as epoch days. There is a very



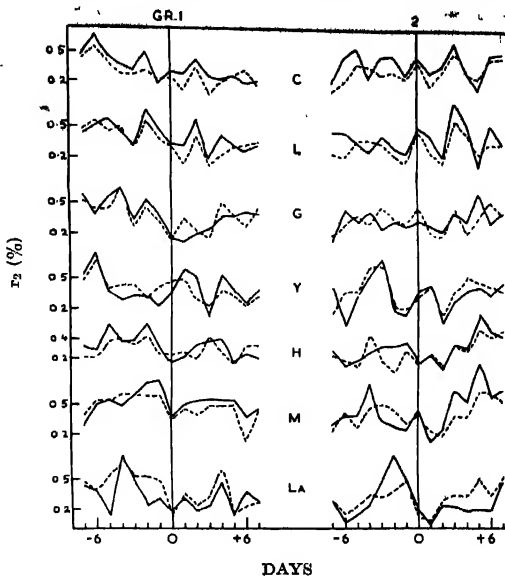


Fig. 8. Chree diagram for  $r_1$  for large (Group 1) and small (Group 2) maxima of 200 mc/s solar radio emission as epoch dates.

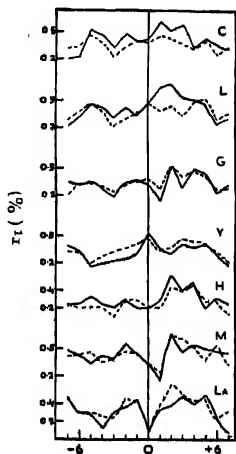


Fig. 9. Chree diagram for  $r_1$  for dates of Type IV solar radio outbursts as epochs.

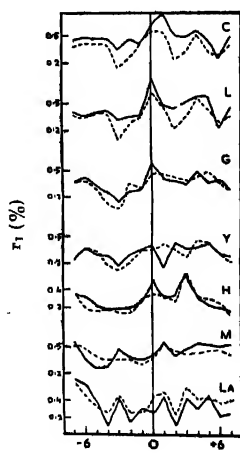


Fig. 10. Chree diagram for  $r_1$  for dates of Leinbach events as epochs.

slight indication of higher amplitudes after epochs. However, the differences are within actual standard errors. Hence, there is no consistent relationship indicated between such events and cosmic ray daily variation.

#### (4) *Leinbach events*

On several occasions, cosmic radio noise shows abnormal attenuations, specially in the polar region. Reid and Leinbach (1959) have reported several such events during the I.G.Y.

Fig. 10 shows the Chree diagrams for the amplitude of the first harmonic for such events as epoch days. It will be seen that there is no definite relation discernible between the two, except that amplitudes are high near epoch day for Climax and Lincoln but not for other stations.

#### (5) *Solar flares*

The I.G.Y. period was conspicuous by the occurrence of several intense solar flares. The days on which flares of intensity  $2^+$ , 3 and  $3^+$  occurred were selected and divided into 12 groups according to their occurrence in the bi-hourly intervals 0–2, 2–4, ..... hrs U.T. For each of these groups, the *average* bihourly values for the day of occurrence of the solar flare and one day prior and later were evaluated. These are plotted in Fig. 11 for Climax for  $2^+$  and 3 and  $3^+$  flares separately as *dotted* lines. Successive curves are for days on which flares occurred in the successive bihourly intervals starting from 0–2 hours U.T., which are indicated by vertical arrows. Now, apart from the effects due to solar flares, there might be an *average diurnal variation* included in all the dotted curves. This can be estimated by finding the average of all the 12 curves. It is shown as the 13th curve at the bottom. Since the flares occur at different hours in different curves, the average is expected to be devoid of any solar flare effect. The average curve was subtracted out from the original curves. The resulting curves are shown as full curves superimposed upon the original dotted curves in Fig. 11.

If there is an effect due to solar flares, it should be visible in the full curves as enhanced intensities near the arrows. It will be seen that at no particular hour is the effect clearly visible for both  $2^+$  and 3 and  $3^+$  flares. In the 12th curve corresponding to solar flares occurring at 22–24 hours U.T. there is actually a *decrease* in the cosmic ray intensity near the arrow. It may be concluded, therefore, that an enhancement of cosmic ray intensity soon after an intense solar flare does not occur invariably. It must be remembered that such effects can be observed only if the station happens to be in the proper impact zones. For Climax, favourable hours are about 9 A.M., 4 A.M., and 8 P.M. which correspond to 16 hours, 11 hours and 3 hours U.T. i.e. the 2nd, 8th and 9th or 10th curves in Fig. 11. As can be seen, no particularly remarkable increase is seen near the arrows even in these curves.

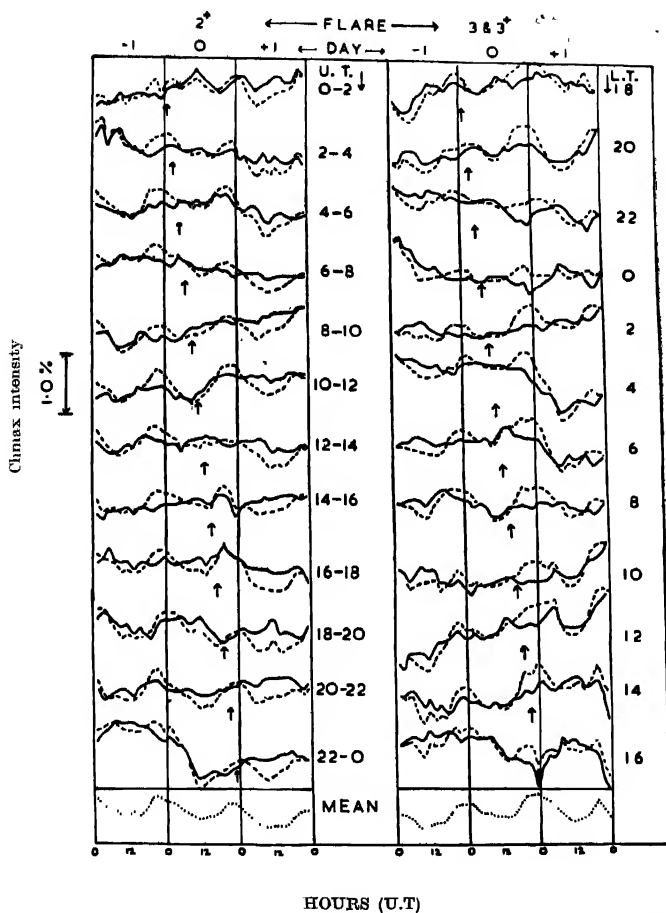


Fig. 11. Plot of average bi-hourly intensity of Climax neutrons for days of occurrence of 2° and 3 & 3° solar flares and for one day earlier and later.

#### V. CORRELATED CHANGES BETWEEN DAILY VARIATION AND DAILY MEAN INTENSITY

During the I.G.Y. several cosmic ray storms occurred. Daily mean intensity suffered large, rapid decreases (known as Forbush decreases), as also moderate and small fluctuations on several occasions. The mean intensity decreases were

classified into three groups as large, moderate and small. Fig. 12 shows the Chree diagrams with the minima of cosmic ray intensity as epochs. The results are :

- (i) For very large minima as epochs (Group 1, 8 events) there is no consistent relationship between daily variation and daily mean intensity.
- (ii) For moderate minima (Group 2, 13 events) the amplitude of the first harmonic attains large values a few days before the minima.
- (iii) For small minima (Group 3, 18 events) no consistent relationship is evident.

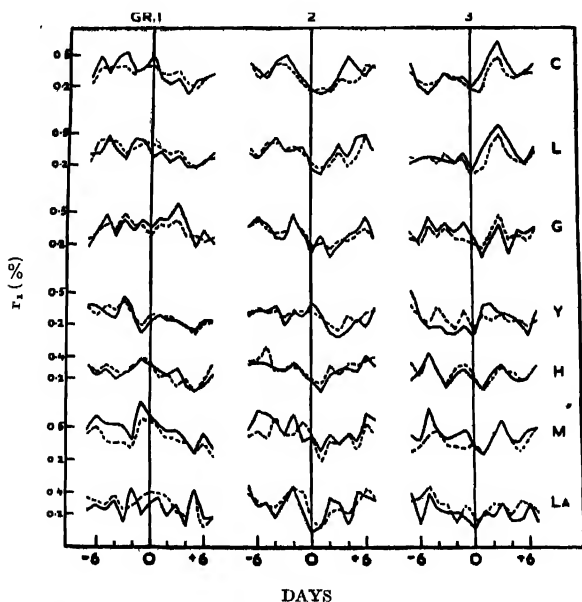


Fig. 12. Chree diagram for  $r_1$  for large (Group 1), moderate (Group 2) and small (Group 3) minima of daily mean intensity of cosmic ray neutrons at Climax as epochs.

Here again, further scrutiny shows that the large amplitudes before epochs are not always so for all events. Amplitudes on individual days have a large influence on the average characteristics.

## VI POSSIBILITY OF CHANCE COINCIDENCES

We saw in the previous sections that some geomagnetic and solar criteria indicate some systematic relationships with daily variation while some others do not. Amongst the former, in some cases the effects are "distortion effects"; in some the actual standard errors make the effects insignificant; in some the results are

significant inspite of these two but are not homogeneously exhibited by all events in a group. It is clear, therefore, that none of the solar or geomagnetic criteria discussed here has a unique relationship with the amplitudes and/or phases of the daily variation. Now, the daily variation has significantly large amplitudes on many days; many more than we have considered so far in any single group. Therefore, the possibility of picking up a few such days in any particular group by pure chance is by no means negligible. To test the effect of pure, reandom selection of epoch dates, three computers of our laboratory were asked to write down in a short time any 20 dates that they could think of. Fig. 13 shows the Chree diagrams for the first harmonic amplitudes for 3 groups of such randomly chosen dates as epochs. It will be seen that in each case the amplitudes show large fluctuations from day to day! Thus, it seems that results obtained in the previous sections for geomagnetic and solar criteria could also possibly be obtained by random chance.

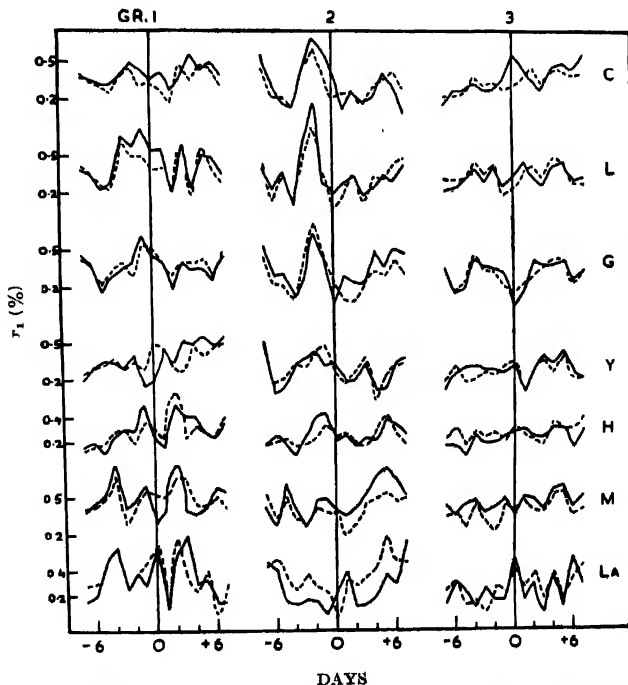


Fig. 13. Chree diagram for  $r_1$  for 3 groups each of randomly chosen 20 days as epochs.

It would be interesting to consider at this stage what would be the estimated standard errors if the data for all days in the I.G.Y. are considered as one sample.

For Climax, the set of 528 daily values of  $a_1$  and  $b_1$  yields standard errors  $\sigma a_1 = 0.45\%$  and  $\sigma b_1 = 0.46\%$  which, according to eq.(4), yield  $\sigma r_1 = 0.45\%$  for a single day. Hence, for a group of, say, 16 days, the standard error of  $r_1$  would be about  $0.11\%$ . For comparing the average amplitudes of two such groups, the standard error of the difference in amplitude would be about  $0.15\%$ , which fixes a  $2\sigma$  level of about  $0.3\%$ . Thus, groups of about 16 days will have to show amplitude differences exceeding  $0.3\%$  to be significant on a  $2\sigma$  level and about  $0.45\%$  for a  $3\sigma$  level. It will thus be seen that most of the cases we discussed in the previous sections are marginally significant on a  $2\sigma$  level.

## VII NATURE OF THE DAILY VARIATION

As seen in the previous sections, no solar and geomagnetic relationships stand out clearly. Also in many cases, results for all stations are not alike. This raises a basic question whether daily variation is really a world-wide phenomenon. In an earlier communication (Kane, 1961), possibilities of a transient nature of daily variation were discussed in detail. A possible approach would be, therefore, to tackle the problem from the other end and see on which days the amplitudes were really high and ask the question, why. In the past such an approach has not been possible because the Poisson standard errors on individual days were too high to warrant any conclusions except for averages over a group of days. During the I.G.Y., several stations have high counting rates with bi-hourly standard errors  $< 0.5\%$  and hence standard errors of harmonic coefficients  $< 0.2\%$ . Thus, amplitudes of the order of  $0.5\%$  are already significant on a  $2\sigma$  level.

In the present case, Climax, Lincoln, Gottingen and Yakutsk—all satisfy this condition adequately. Hence, the first and second harmonic amplitudes for every day were classed as low, medium and high if they were less than  $0.6\%$ , between  $0.6$  and  $1.0\%$  and above  $1.0\%$  respectively. Further, following questions were asked for every day :

- (1) Are the amplitudes high and/or medium for all stations? If so, do they remain so even after correcting for "distortion effects"?
- (2) If the amplitudes are not similar for all stations, are they similar for any three/any two stations? Do they remain so after removing "distortion effects"?
- (3) Are they high just for one station? Do they decrease after removing "distortion effects"?

It is obvious that such a scrutiny could be done only for those days on which data for all stations were simultaneously available. This reduced the number of available days to some extent. Nevertheless, the picture that emerges out is quite revealing. Table VIII gives the number of days on which amplitudes were high or medium at any one, any two, any three or all stations and also the number

of days on which this was due to "distortion effects". The total number of days considered in I. G. Y. was 512.

TABLE VIII

Set	Stations	1st harmonic		2nd harmonic	
		Days genuine	Days having distortion	Days genuine	Days having distortion
1	C	10	15	2	14
	L	18	10	49	29
	G	17	28	29	23
	Y	44	40	66	37
2	C, L	41	20	24	14
	C, G	5	3	4	7
	C, Y	12	7	2	6
	L, G	7	6	18	12
	L, Y	19	7	30	20
	G, Y	23	8	17	15
3	C, L, G	37	5	13	1
	C, L, Y	35	5	7	5
	C, G, Y	9	0	4	1
	L, G, Y	12	3	13	5
4	Very high ( $>1.5\%$ )	6	0	0	0
	World-wide High (1.0-1.5%)	26	0	3	0
	Med. (0.6-1.0%)	87	2	15	2
	Low (0.4-0.6%)	23	0	9	0
	Very low ( $<0.4\%$ )	33	0	0	0

The first set (first four rows) of Table VIII gives the number of days on which *only one* station showed high amplitudes. Such days could occur due to :

- An anisotropy of a very transient nature and so short-lived that its intensity reduces before another station can see it 8 hours later.
- A superfluous effect which creeps in because of isotropic changes of world-wide intensity (distortion effects).
- Instrumental troubles like picking up false pulses or losing pulses due to power failure etc.

Possibility (a) is not ruled out. But it is difficult to see how anything can be seen by Climax and missed completely by Lincoln or, vice versa. From the

columns headed "Days having distortions", it is obvious that on almost half the number of days, amplitudes are large due to "distortion effects". Out of the other half, nonsimultaneity at Climax and Lincoln (which are near each other) indicates that these high amplitudes may be due to instrumental troubles. This could also be true for Gottingen and Yakutsk.

The second set in Table VIII represents the days when *pairs* of stations show high amplitudes, indicating in general a transient anisotropy of life-time more than 8 hours. Here, *C, L* is not on par with other pairs as Climax and Lincoln are in the same region. *C, L* indicates a state of affairs similar to that in set 1 for individual stations, except that this time, it is more likely to be a genuine transient anisotropy rather than instrumental trouble. In this set also, on some days, the amplitudes are large due to "distortion effects". But on many more days, the anisotropy is genuinely transient. Since the sequence in which an anisotropy is seen is, Yakutsk first, Gottingen second and Climax or Lincoln third on the same date, the sequences *C, L*; (*C* or *L*), *G*; *G, Y* are understandable. But it is difficult to see how (*C* or *L, Y*) could occur without Gottingen also seeing the anisotropy. This throws some doubt about the conclusion that the days in set 2 represent a perfectly genuine transient anisotropy.

The third set represents days when three stations see the anisotropy. Here again *C, L, G* or *C, L, Y* deserves to be included in set 2. Also, keeping in mind the sequence in which anisotropy is seen, *C, L, Y* seems to be an impossibility as Gottingen, which is in-between, should have seen the anisotropy. Nevertheless, days in Set 3, except for those which are due to "distortion effects", could be classed as almost world-wide.

Set 4 represents days on which anisotropy was seen by *all* the stations. This has been subdivided into 5 groups depending upon whether the amplitudes were very high ( $> 1.50\%$ ), high (1.01 to 1.50%), medium (0.61 to 1.00%), low (0.41 to 0.60%) and very low ( $< 0.41\%$ ). This set is the most interesting one as it consists of days which will influence the average pattern of any group in which they will be included.

For the first harmonic, there were 6 days on which amplitudes exceeded about 1.5%. For the second harmonic, there were none. On 26 and 3 days, amplitudes were roughly 1.0-1.5% for 1st and 2nd harmonics respectively. A very large number of days (87 for 1st harmonic and 15 for second) had amplitudes between 0.61 and 1.00 %. It will thus be seen that on about 120 days out of a total of about 500 days, the amplitudes of the first harmonic exceeded 0.6%. The probability of encountering such a day by sheer chance is thus almost 25%. If, therefore, a random group of about 20 epoch days is chosen, about 5 days will have amplitudes exceeding 0.6%. In individual cases this number may vary from group to group and would lead to group averages which may



easily show differences in amplitudes of the order of a few tenths of a percent, which may not be physically meaningful.

Table IX below gives the dates of the very high, high and moderate amplitudes of the first and second harmonic.

TABLE IX

	1st harmonic		2nd harmonic	
Very high	Aug. 5, 1957, Jun. 8, 1958 Sep. 2, 1957, Aug. 24, 1958 Dec. 23, 1957, Dec. 8, 1958 (6 days)		Nil (40 days)	
High	Aug. 4, 13, 14, 18, 21, 1957 Sep. 6, 7, 20, 21, 1957 Nov. 26, 30, 1957 Dec. 31, 1957 Mar. 17, 20, 1958 Apr. 28, 1958 May 10, 1958 Jun. 7, 20, 21, 1958 Jul. 26, 1958 Aug. 2, 17, 1958 Sep. 2, 27, 1958 Dec. 11, 18, 1958 (26 days)	Sep. 21, 1957 Oct. 22, 1957 Dec. 23, 1957		
Moderate	Jul. 23, 27, 28, 29, 1957 Aug. 1, 2, 11, 19, 20, 1957 23, 1957 Sep. 3, 4, 5, 11, 12, 1957 13, 15, 16, 18, 1957 Oct. 8, 9, 11, 19, 20, 1957 23, 1957 Nov. 14, 19, 24, 28, 1957 Dec. 3, 4, 5, 14, 18, 1957 19, 1957 Jan. 4, 9, 10, 28, 1958 Feb. 3, 11, 22, 1958 Mar. 5, 13, 18, 27, 29, 1958 Apr. 10, 12, 1958 May 7, 25, 30, 31, 1958 Jun. 4, 10, 11, 27, 29, 1958 Jul. 6, 7, 8, 10, 13, 1958 16, 17, 1958 Aug. 4, 6, 7, 16, 27, 30, 1958 3, 15, 21, 28, 30, 1958 Oct. 23, 28, 1958 Nov. 1, 11, 21, 22, 28, 1958 Dec. 4, 5, 7, 12, 1958 (87 days)	Aug. 5, 6, 19, 21, 1957 Sep. 30, 1957 Oct. 11, 23, 31, 1957 Nov. 29, 1957 Dec. 22, 1957 Mar. 6, 1958 Jun. 7, 8, 1958 Aug. 24, 25, 1958 Oct. 22, 24, 1958		
Low	(23 days)		(0 days)	
Very low	(33 days)		(118 days)	

It will be seen from Table IX that days of large amplitudes of second harmonic are fewer than those of first harmonic at high latitudes. Many of these are common (underlined dates). Since there is no particular reason to believe that the first and second harmonics do necessarily have independent physical interpretations,

this could be interpreted (provided the phases are proper) as indicating that the daily variation at high latitudes is mostly broad-peaked, though on some days it is sharp-peaked (yielding second and higher harmonics).

With the dates corresponding to groups in Table IX, one can re-examine solar and geomagnetic relationships of daily variation.

(1) *Relationship with  $C_p$  values:* Table X below gives the average amplitudes and hours of maxima for the first and second harmonic for the three stations L, G and Y combined, as also the corresponding average  $C_p$  values for the five groups of Table IX.

TABLE X

Group amp (1st harm)	No. of days	For (L, G, Y)				Average $C_p$
		$r_1$	$\phi_1$	$r_2$	$\phi_2$	
Very high	6	0.96	$\pi + 15$	0.24	-35	$0.97 \pm 0.26$
High	26	0.75	$\pi + 42$	0.08	104	$1.00 \pm 0.10$
Moderate	87	0.43	$\pi + 36$	0.10	7	$0.79 \pm 0.06$
Low	23	0.35	$\pi + 40$	0.11	$\pi - 49$	$0.91 \pm 0.11$
Very low	33	0.06	$\pi + 9$	0.08	$\pi + 67$	$0.72 \pm 0.07$

The standard errors for  $C_p$  are calculated from the actual spread of  $C_p$  values in each group. Considering the fact that the general range of  $C_p$  is from 0 to about 2.0, it is obvious that there is no definite relationship between  $C_p$  and cosmic ray daily variation. To study if there is any time lag between the two, the 32 days of very high and high amplitudes of 1st harmonic were considered as epochs and Chree analysis was done for  $C_p$  values. The Chree diagram is shown in Fig. 14 as curve A. As can be seen,  $C_p$  values show a very small range (0.65 to 1.00) from -10 to +10 days in contrast to their usual range from 0.00 to 2.00. However, there exists a small maximum at the epoch day. A scrutiny of the individual days shows that the contrast between this maximum at  $n = 0$  and the low value at  $n = -3$  is caused by the coincidence at  $n = 0$  of the following types of  $C_p$  maxima.

Type	Date	Type	Date	Type
13- 8-57 $^oC_p^o$	26 11-57	$^oC_p^o$		
2- 9-57 $+C_p^+$	31-12-57	$+C_p^+$	17- 8-58	$+C_p^+$
21- 9-57 $^oC_p^o$	7- 6-58	$^oC_p^+$	24- 8-58	$+C_p^+$

Thus, out of 32 days of high amplitudes, 3 coincide with  $C_p$  max. of the (0, 0) type, 1 of (0, +) type, 3 of (+, 0) type and 2 of (+, +) type. It is clear, therefore, that the types of  $C_p$  maxima as classified above do not have any special

significance to cosmic ray daily variation. Also, out of 59  $C_p$  maxima during I.G.Y., only 9 seem to coincide with days of high daily variation as shown above. These days do not seem to have any particular geomagnetic or solar significance in common.

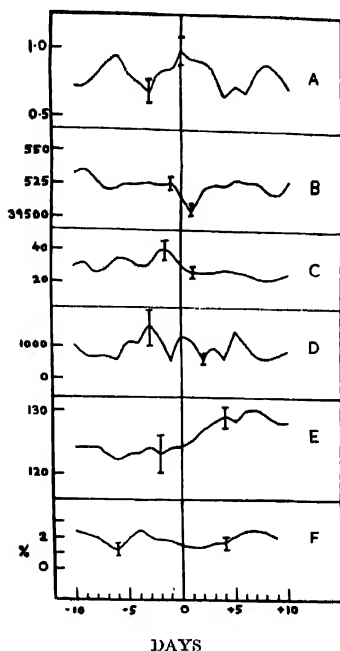


Fig. 14. Chree diagrams for (A)  $C_p$  values, (B) Horizontal component of earth's magnetic field, (C) Solar radio emission flux at 200 mc/s, (D) Solar flare index of Sae. Peak, (E) 5303 Green coronal emission for visible solar disc and (F) Daily mean intensity of cosmic ray neutrons at Chmax w.r.t. very high and high amplitude of daily variation as epoch days

(2) *Relation with horizontal component of geomagnetic field*: Curve B in Fig. 14 is the Chree diagram for the horizontal component of earth's magnetic field with high and very high amplitudes of 1st harmonic as epochs. A lack of any definite relationship is evident. The dip at +1 day is only about 25 gamma in contrast to several hundred gamma usually encountered in individual events.

(3) *Relation with S.C. and gradual storms*: Since there is no *daily* index for such storms, Chree analysis is not possible. However, one can examine the frequency distribution of time delay of occurrence of storms with respect to days of high and very high amplitudes. Curve A in Fig. 15 is a frequency diagram

for S.C. storms of the severe and moderately severe type and Gradual, severe type. There is a slight indication of excess occurrence at or about 0 day. However, a  $\chi^2$  test indicates a probability of 0.30. If the number of days around epoch is reduced, one gets a minimum value of  $p = 0.18$  for  $\pm 4$  days around epoch. Thus, the result is nowhere significant at a 5% level. A possibility of some storms being connected with high daily variation is not ruled out. However, no special characteristic of such *effective* storms is evident as they seem to belong to all the 5 categories viz. S.C.\* S; S.C.S; S.C.\* MS; S.C.MS and G. S. (Black portions in Fig. 15 A refer to severe storms).

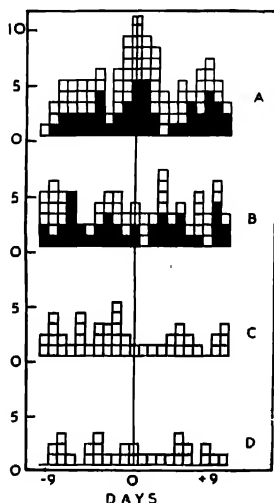


Fig. 15. Frequency distribution of occurrence of (A) S.C.\*, S.C. and B magnetic storms, severe (black) and moderately severe, (B) C.M.P. of very intense (black) and pronounced sunspot groups, (C) Type IV solar radio outbursts and (D) Lombach events with reference to very high and high amplitudes of daily variation as epoch days.

(4) *Relation with C.M.P. of active sunspot groups*: Here again there is no daily index but only certain epoch dates. A frequency diagram for occurrence of these with fixed time delays is given as curve B in Fig. 15. The spread is wide and a  $\chi^2$  test does not indicate any significant relation at a 5% level.

(5) *Relation with solar radio emission*: For this, a daily index is available. Curve C in Fig. 14 is a Chree diagram for the solar radio emission flux at 200 mc/s for dates of Very High and High amplitudes of first harmonic as epoch dates. No relation is discernable.

(6) *Relation with type IV solar radio outbursts*: In the absence of a daily index, frequency diagram of time delays is calculated. This is shown as curve C in Fig. 15. Grouping 3 successive days,  $\chi^2$  test gives  $p = .40$ . Hence no relationship at 5% level is indicated.

(7) *Relation with Leinbach events*: Curve D in Fig. 15 gives the time-delay frequency distribution for such events.  $\chi^2$  test gives  $p = 0.85$ . No relation is, therefore, indicated.

(8) *Relation with solar flares*: For this, one could use the daily solar flare index estimated at Sacramento Peak. Fig. 14, curve D, gives the Chree diagram for this index. Considering the standard deviations of the actual scatter, no relationship is indicated.

(9) *Relation with green coronal emission*: For the Green 5303 line emission from the visible solar disc, a daily index is available. Fig. 14, curve E, is the Chree diagram for the same. No relation is indicated.

(10) *Relation with daily mean intensity of cosmic rays*: For this, the daily mean intensity of Climax neutrons was utilised. Fig. 14, curve F, is the Chree diagram for the same. It will be seen that the range of mean intensity values hardly exceeds 2% and no relation with daily variation is indicated.

It may be concluded, therefore, that whereas the daily variation on many days is world-wide in nature i.e. amplitudes are consistently large or small at stations situated wide apart in longitude, the days of high amplitudes do not have any clear-cut relationship with several geomagnetic and solar criteria. In some cases, e.g. geomagnetic storms, some storms days coincide with days of high amplitudes. Now, the total number of S.C. and S.C.\* type severe and moderately severe and gradual severe storms during I.G.Y. was 81. The number of days on which these would coincide accidentally with days of high amplitude which are 32 in a total of 512, would be about  $(32 \times 81)/512 \approx 5$ . In Fig 15, the top curve (A) shows a frequency of 11 on the epoch day. Thus there is an indication that some storms may occur genuinely simultaneously with high amplitudes. If one considers the epoch day and one more day on either side, the expected frequency would be 16. In Fig. 15, the total frequency for  $-1, 0$  and  $+1$  day for curve A is 29, which is somewhat higher than the expected frequency 16, but much lower than the total number of storms viz. 81. Table XI gives the 32 epoch dates corresponding to very high and high amplitudes of cosmic ray daily variation and indicates the occurrence of several geomagnetic and solar phenomena either on the epoch day or on  $\pm 1$  day of the epoch. The last two rows give the observed frequencies of the various phenomena and the frequencies expected by random chance. As can be seen, only relationship with storm days stands out with some significance; but storms of all types seem to be involved and the relationship is by no means one-to-one.

It would be interesting to study the properties of the daily variation apart from its solar and geomagnetic relationship. One characteristic frequently reported is the 27-day recurrence tendency of the amplitude of the first harmonic. Fig. 16

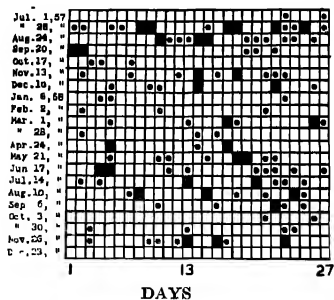


Fig. 16. Bartels diagram for days of very high and high amplitudes (black squares) and moderate amplitudes (black circles).

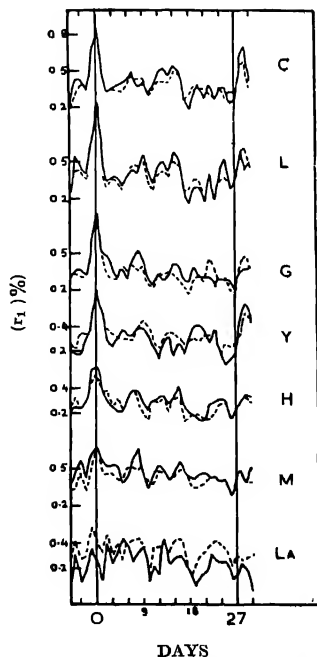


Fig. 17. Chres diagram of  $r_1$  for days of very high and high amplitudes as epochs.

TABLE XI

Epoch dates	C <sub>p</sub> Max. type	H Munna type	Storms type	C.M.P. sunspot type	Solar radio emiss. max. type	Typo IV solar radio out- burst	Lein- bach events	Cosmic ray mun. type
4- 8-57	0, +		S.C.*, MS	b				I
5- 8-57	0, +		S.C.*, MS	b				I
13- 8-57	0, 0		S.C., MS					
14- 8-57			S.C., MS					
18- 8-57								
21- 8-57			G., S	b				
2- 9-57			S.C.*, MS			✓	✓	
6- 9-57		1	S.C.*, MS					
7- 9-57			S.C.*, S					
20- 9-57			S.C.*, S	a	1			
21- 9-57			S.C.*, S S.C., S		1		✓	
26-11-57	0, 0		S.C., S G., S	b	1			I
30-11-57			S.C.*, MS	b	11			
23-12-57					1			
31-12-57			S.C., MS S.C., S					
17- 3-58			S.C.*, MS					
26- 3-58	0, 0		S.C.*, MS				✓	I
28- 4-58	1-, +		S.C.*, MS					
10- 5-58								II
7- 6-58	0, 1		S.C., S S.C., MS			✓		
8- 6-58	0, +		S.C., S S.C.*, MS					II
20- 6-58	1, 1	II	S.C., MS					II
21- 6-58	1, 1	II	S.C., MS					II
26- 7-58	1-, 1-		G., S	a b				
2- 8-58								
17- 8-58	1, 0	II	S.C.*, MS			✓	✓	
24- 8-58	+, 0	II	S.C.*, MS			I		II
27- 9-58								
8-12-58				b				
11-12-58				a		✓		
18-12-58		II	S.C.*, S					
Observed frequency	13	6	29	10	6	4	4	8
Expected frequency	12	5	16	10	4	4	3	4

TABLE XII

Hour of maximum (degrees)	C	L	G	X	G-W	L-W	G-W'	Y-W'
1-60	Dec. 23, 57	Dec. 23, 57	Dec. 23, 57	Aug. 18, 57	Dec. 23, 57	Dec. 23, 57	Dec. 23, 57	X
				Aug. 17, 58			Aug. 17, 58	
61-120	X	X	Dec. 31, 57	Aug. 24, 58	X	X	Dec. 31, 57	Dec. 23, 57
121-180	Aug. 18, 57	Aug. 21, 57	Sep. 2, 20,	Sep. 2, 57	Nov. 26, 57	Aug. 14, 57	Nov. 26, 57	
	Sep. 21, 57	Sep. 21, 57	21, 57	Nov. 26, 57	Dec. 31, 57	Sep. 2, 20,	Mar. 17,	
	Nov. 30, 57	Nov. 30, 57	Nov. 26,	Dec. 23, 57		21, 57	26, 58	
	Dec. 31, 57	Dec. 31, 57	30, 57	Mar. 17,		Nov. 26,	Apr. 28, 58	
	Mar. 26, 58		Mar. 26, 58	26, 58		30, 57		
			Jun. 8,	Apr. 28, 58		Mar. 26, 58		
			21, 58	Dec. 18, 58		Jun. 8,		
			Sep. 2, 58			21, 58		
						Sep. 2, 58		
						Dec. 18, 58		
180-240	Aug. 21, 57	Aug. 5,	Aug. 4, 5,	Sep. 7, 57	Aug. 5	Aug. 5	Aug. 21, 57	
	Sep. 2, 57	14, 21, 57	14, 21, 57	Nov. 2, 57	18, 21, 57	5, 21, 57	Sep. 2,	
	Nov. 2, 57	Sep. 6,	Sep. 6,	Nov. 30, 57	Sep. 2, 6,	Sep. 6,	20, 21,	
	Mar. 20, 58	7, 57	7, 57	May 10, 58	7, 20, 57	7, 57	Nov. 30, 57	
	May 10, 58	Nov. 11, 57	Mar. 17, 58	Jun. 8, 58	Nov. 30, 57	Mar. 17, 58	Dec. 31, 57	
	Jun. 8, 58	Mar. 26, 58	Apr. 28, 58	Dec. 8, 58	Dec. 31, 57	Apr. 28, 58	Jun. 8, 58	
	Aug. 2, 17,	May 10, 58	May 10, 58		May 10, 58	May 10, 58	Dec. 8, 18, 58	
	24, 58	Jun. 7,	Jun. 7,		Jun. 6,	Jun. 7,		
	Sep. 2,	8, 21, 58	20, 58		8, 21, 58	Aug. 2,		
	27, 58	Aug. 2,	Aug. 2, 58		8, 58	Aug. 2,		
	Dec. 8,	17, 24, 58	Sep. 27, 58		17, 24, 58	Sep. 27, 58		
	18, 58	Sep. 2, 27, 58	Dec. 8, 11, 58		Sep. 2, 27, 58	Dec. 8, 11, 58		
		18, 58			Dec. 8, 11, 58			
241-300	Aug. 5,	Sep. 6, 57	Aug. 13,	Aug. 4, 5, 13,	Aug. 13, 14,	Aug. 4, 18,	Aug. 4, 5, 13,	
	13, 14, 57	Apr. 28, 58	18, 57	14, 21, 57	57	57	14, 57	
	Nov. 26, 57	Jun. 20, 58	Aug. 26, 58	Sep. 6, 57	Mar. 17, 58	Sep. 6, 57	Sep. 6, 7, 57	
	Mar. 17, 57	Jul. 26, 58	Aug. 24, 58	Dec. 31, 57	Apr. 28, 58	Apr. 28, 58	May 10, 58	
	Jun. 7, 58			Jun. 17, 58	Jun. 20,	Jun. 20, 58	Jun. 7, 20, 21,	
	20, 21, 58			20, 21, 58	21, 58	Aug. 2,	58	
	Dec. 11, 58			Aug. 2,	Sep. 27, 58		Aug. 2, 17, 24,	
				17, 58	Dec. 11, 58		58	
				Sep. 2,			Sep. 2, 27, 58	
				27, 58			Dec. 11, 58	
				Dec. 11, 58				
301-360	Aug. 4, 57	Aug. 4,	Dec. 18, 58	Jul. 26, 58	Aug. 4, 57	Aug. 13, 57	Aug. 18, 57	
	Jul. 26, 58	Mar. 17, 58		Jul. 26, 58	Jul. 26, 58	Mar. 17, 58	Jul. 26, 58	
		Mar. 17, 58				Jul. 26, 58		



is a Bartels diagram for the I.G.Y. period. There seems to be some tendency for days of high amplitudes to occur in groups and also to recur after 27 days. It would be necessary, however, to check whether the recurrence is not due to "distortion effects". Fig. 17 shows Chree diagrams for the amplitudes of the first harmonic with the 32 days of very high and high amplitudes as epoch days. It seems that the amplitudes recur after about 29 days even after correcting for "distortion effects".

A similar analysis was carried out for huancayo, Makerere and Lae. Due to lack of continuity, there were few common days. Amongst these, one could choose days on which amplitudes were high at all the three stations. It was found that most of these coincided with days of high amplitudes at Climax etc. The reverse was not, however, invariably true. Thus, on days of very high and high amplitudes at Climax etc., Huancayo generally showed high amplitudes, but Makerere and Lae did not always do so. This is reflected in the Chree diagram of Fig. 17, where Huancayo shows a clear maximum on epoch (0 day), but Makerere and specially Lae does not. In conjunction with discrepancies observed earlier, this could be taken as additional evidence of improper working on some days of the instruments at Makerere and Lae.

Another characteristic of daily variation is the frequency distribution of the amplitudes and hours of maxima. In Table XI we have already chosen days according to the magnitude of their amplitudes. Fig. 18 shows the frequency distribution of the hours of maxima for the various groups. (Group 1—Very high and high amplitude, Group 2—Moderate, Group 3—Low and very low). It will be seen that the hours of maxima have a broad distribution in all the groups, though the maximum frequency occurs in the afternoon. Thus, whereas on majority of days the hour of maximum is in the afternoon, there are days when it is at other hours also. Table XII gives the dates of the 32 days of Very high and High amplitudes on which the hour of maximum was at various hours at various stations.

It will be seen from Table XII that on some dates, all stations show a night time hour of maximum.

There are, however, a few disconcerting features. Firstly, the frequency distributions of the hours of maxima are not fully similar for all stations. Thus, Yakutsk shows a larger spread towards evening hours. Also, a scrutiny of individual values of amplitudes of the first harmonic for the 32 days given in Table XII shows that whereas amplitudes are high for all these days, they are not the same at all stations. Thus, for the 6 days of very high amplitudes, values of  $r_1$  are as given in Table XIII.

The differences between values for different stations for the same day sometimes exceed the Poisson  $2\sigma$  limit. This is perhaps indicative of the fact that the

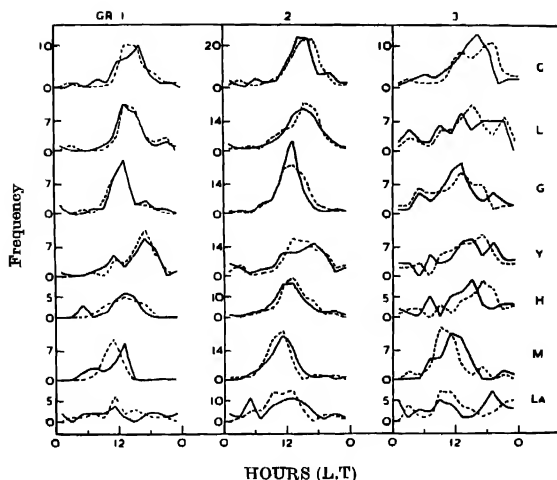


Fig. 18. Frequency distribution of the hour of maximum  $\phi_1$  of the first harmonic for days of very high and high (Group 1), moderate (Group 2) and low and very low (Group 3) amplitudes of the first harmonic.

TABLE XIII

DATE	5-8-57	3-9-57	23-12-57	8-6-58	24-8-58	9-12-58	Poisson std error
C	1.93	1.95	2.18	1.88	3.54	1.20	$\pm 0.05$
L	1.53	2.40	2.11	1.13	2.90	1.67	$\pm 0.21$
G	1.97	0.83	2.08	1.45	1.79	1.03	$\pm 0.17$
Y	1.65	1.39	0.75	2.20	1.04	1.90	$\pm 0.23$
C-W	1.53	1.87	1.89	1.48	1.63	1.02	$\pm 0.18$
L-W'	1.63	2.04	1.96	1.14	1.03	1.56	$\pm 0.20$
G-W'	1.89	1.05	1.55	1.56	1.16	1.28	$\pm 0.26$
Y-W'	1.20	0.72	1.17	1.96	0.77	1.64	$\pm 0.31$

anisotropy is essentially of a transient nature and fluctuates considerably within 24 hours both in strength and in mean energy as reflected in changes of phase.

This raises a question about the meaningfulness of the average amplitudes for groups of days. Table XIV gives the average amplitudes and hours of maxima of the first harmonic for the five groups of days corresponding to very high, high, moderate, low and very low amplitudes.

It will be seen from Table XIV that for the same group of days, amplitudes at different places differ outside Poisson  $2\sigma$  limits. The differences are sometimes

TABLE XIV

Station	Very High		High		Moderate		Low		Very low	
	$r_1$	$\phi_1$	$r_1$	$\phi_1$	$r_1$	$\phi_1$	$r_1$	$\phi_1$	$r_1$	$\phi_1$
C	1.30 $\pm .02$	$\pi+21$	.86 $\pm .01$	$\pi-37$	.42 $\pm .005$	$\pi+47$	.31 $\pm .01$	$\pi+46$	.11 $\pm .01$	$\pi+30$
L	1.22 $\pm .08$	$\pi+13$	.98 $\pm .03$	$\pi-48$	.53 $\pm .02$	$\pi-53$	.30 $\pm .04$	$\pi+53$	.07 $\pm .04$	$\pi+45$
G	0.67 $\pm .07$	$\pi+19$	.87 $\pm .03$	$\pi+10$	.53 $\pm .02$	$\pi-4$	.39 $\pm .03$	$\pi+35$	.09 $\pm .03$	$\pi-32$
Y	.98 $\pm .09$	$\pi+17$	.72 $\pm .04$	$\pi+62$	.37 $\pm .02$	$\pi-57$	.41 $\pm .05$	$\pi+62$	.06 $\pm .04$	$\pi+45$
C-W	.94	$\pi+18$	.78	$\pi-58$	.45	$\pi+50$	.37	$\pi+77$	.13	$\pi+57$
L-W'	.90	$\pi+12$	1.00	$\pi+50$	.55	$\pi-44$	.27	$\pi+54$	.11	$\pi-22$
G-W'	.85	$\pi-5$	.55	$\pi+15$	.51	$\pi-8$	.32	$\pi+34$	.07	$\pi-43$
Y-W'	.86	$\pi+37$	.77	$\pi+51$	.38	$\pi-51$	.36	$\pi+58$	.07	$\pi+16$
Days	6		26		87		23		33	

due to "distortion effects" as they disappear after correction for these (see *C-W* etc.). But this is not invariably so. It is very difficult to say whether these differences are due to non-averaging out of effects due to transient nature of the daily variation or whether they are due to any instrumental troubles.

We have concentrated so far only on the last (world-wide) set of days from Table VIII which represents only about 1/3rd of the total number of days. There are still about 300 days in the other sets which represent days of daily variation of transient, short-lived type. On this basis, one could prepare a complete description of the daily variation for almost every day during I.G.Y. Such a venture would, however, be unreliable because of the following reasons:

- (1) On many days, the amplitudes are high at individual or pairs of stations due to "distortion effects". These cannot be justifiably used for description of daily variation
- (2) On days on which amplitudes are high even after correcting for distortion effects, one is not sure that instrumental troubles are not causing these.

A possible method of minimising instrumental troubles is to combine data from stations at roughly similar latitude, longitude and altitude. From the I.G.Y. grid, one can get many stations in the European and North American longitudes but not so in other regions. Thus, there is no station for which data are comparable to those at Yakutsk. Nevertheless, one can adopt this procedure wherever possible. Work in this direction is in progress.

A few general observations can be made. From Table IX, it seems that the days of high amplitude are proportionately more in the early part of I.G.Y. In Fig. 19 are plotted the monthly average amplitudes of the first harmonic for the 18 months of I.G.Y. Similar plots for some solar and geomagnetic phenomena are also given. There does not seem to be any consistent relationship between the various geomagnetic and solar phenomena and cosmic ray daily variation even on a monthly basis.

Fig. 20 gives the frequency distribution of  $r_1$ ,  $\phi_1$ ,  $r_2$ ,  $\phi_2$  for the whole I.G.Y. period for each station. It will be noticed that the range of the first harmonic is from 0 to  $>1.5\%$  for all stations. For the second harmonic, the range is lesser (about 0 to  $1\%$ ) at all stations. For the hour of maximum  $\phi_1$  of the first harmonic, there is a preponderance at noon or afternoon hours. But for  $\phi_2$ , the hour of maximum of the second harmonic, the spread is almost all round the clock, more so for high latitudes. Thus, on individual days, the second harmonic is not negligible. At high latitudes, the phase scatter is so large that average amplitudes of  $r_2$  for groups of days turn out to be negligible. For low latitudes, phase scatter is comparatively small and hence average amplitudes are still substantial. It must be

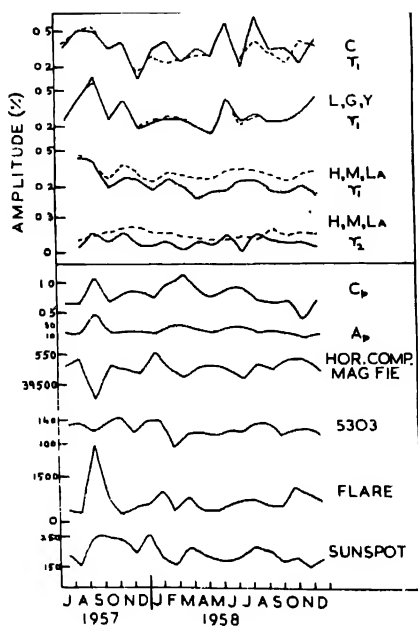


Fig. 19. Monthly averages of amplitudes  $r_1$  and  $r_2$  and various solar and geomagnetic indices.

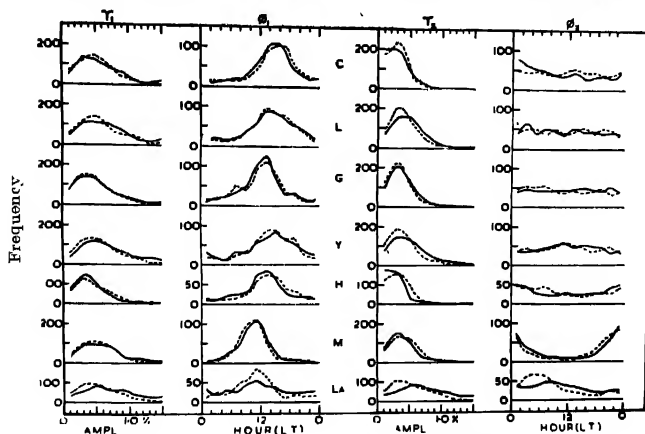


Fig. 20. Frequency distribution of  $r_1$ ,  $\phi_1$ ,  $r_2$ ,  $\phi_2$ , at various stations during I.G.Y.

noted, however, that there is lot of dissimilarity between the low latitude stations of Huancayo, Lae and Makerere. In many aspects Huancayo compares better with high latitude stations than with Lae and Makerere. This could be partly due to the lower energy response of Huancayo neutrons due to its high altitude. But indications are that the data for Lae and Makerere are subject to large instrumental errors. Preponderance of  $\phi_2$  values only at certain hours may also be indicative of some errors in barometric pressure correction.

### VIII DISCUSSION

The results of the present investigation can be summarised as follows :

(1) The relationships of daily variation of cosmic ray nucleonic component recorded at Climax, Lincoln, Gottingen, Yakutsk, Huancayo, Makerere and Lae with several geomagnetic and solar phenomena were studied by Chree analysis. From Poisson error considerations some criteria like  $+C_p$  maxima, moderate minima of horizontal component of geomagnetic field, some types of magnetic storms etc. seem to be associated with large amplitudes (about 0.5%) of first harmonic before epoch and small amplitudes (about 0.2%) after epoch. The hour of maximum is in afternoon before epoch and in forenoon after epoch.

(2) On considering "distortion effects" due to world-wide isotropic changes of cosmic ray intensity as also after due consideration of the *actual* standard errors, it was found that

- (i) Many of the amplitude and phase fluctuations are due to "distortion effects".
- (ii) The amplitude differences before and after epochs are many times within the *actual*  $2\sigma$  limit.
- (iii) A scrutiny of individual days in the various groups shows that the average amplitudes for the group are largely dominated by a very few number of days having abnormally high amplitudes ( $> 1.0\%$ ). Thus, while comparing two groups of say, 15 days each, the possibility remains that amplitude differences of about 0.3% could occur just because 3-4 days of amplitudes  $> 1.0\%$  occurred accidentally in one group out not in the other.
- (iv) To check this possibility, three random groups each of some *arbitrarily* chosen 20 days, were used as epochs. The resulting Chree diagrams show fluctuations in amplitudes of the same order ( $\sim 0.3\%$ ) as encountered in all the previous Chree diagrams. This confirms the suspicion that the various relationships indicated in (1) above could have occurred accidentally.

(3) The amplitudes of the first and second harmonic on individual days at Climax, Lincoln, Gottingen and Yakutsk were compared. The following was observed :

- (i) On some days, only a single station showed high amplitudes. Parts of these were due to "distortion effects". The rest could be due to an "impact zone" type effect and/or due to instrumental troubles.
- (ii) On some days, more than one station (2 or 3) showed high amplitudes. These probably represent days of a genuine, transient, short-lived anisotropy.
- (iii) On some days (about 175 in a total of 512 days in I.G.Y.), the amplitudes were similar at all stations. This set was further divided into days of very high ( $>1.5\%$ ), high ( $1.0-1.5\%$ ), moderate ( $0.6-1.0\%$ ), low ( $0.4-0.6\%$ ) and very low ( $<0.4\%$ ) amplitudes. There were 6 days in the very high and 26 in the high amplitude category for the first harmonic. Similar days for the second harmonic were very few and were mostly coincident with those for first harmonic.
- (iv) The 32 days of very high and high amplitudes of first harmonic at Climax, Lincoln, Gottingen and Yakutsk, were chosen as epochs and three analysis done for various geomagnetic and solar phenomena. No significant relation was indicated with (a)  $C_p$  values, (b) Various types of  $C_p$  maxima, (c) Horizontal component of geomagnetic field, (d) Various types of magnetic storms (S.C.\*, S.C., Gradual), (e) C.M.P. of active sunspot groups, (f) Solar radio emission at 200 Mc/s, (g) Type IV solar radio outbursts, (h) Leimbach events, (i) Green coronal emission of the 5303 line from visible solar disc, (j) Solar flares and (k) Daily mean intensity of cosmic rays.

There is a slight indication that *some* storm days coincide with days of high amplitudes. No particular characteristics for such storms are clearly distinguishable. It is likely that 27-day recurrence tendency is a common factor.

- (v) Three analysis with the above 32 dates as epochs shows that there is a  $29 \pm 1$  day recurrence tendency of high amplitudes of the first harmonics.
- (vi) The hour of maximum of the first harmonic for the above 32 days is mostly in the afternoon. However, some days show night time maxima at *all* stations.
- (vii) Even though the 32 days do represent world-wide high amplitudes, the amplitudes are not the same even within  $2\sigma$  Poisson limits at *all* stations. After correcting for "distortion effects" this difference is reduced on some days but not on all. Also the phase-scatter is not

exactly alike for all stations. This indicates an essentially transient nature of daily variation, though a part of the discrepancies could be due to instrumental troubles also.

- (viii) Similar analysis and comparison was done for the equatorial stations of Huancayo, Makerere and Lae. Due to lack of continuous data, the number of common days for this triplet was far less than the days for the high latitude quartet. Days of high amplitude at *all* the three stations were very few but they did coincide with the days of very high, and moderate amplitudes at high latitudes. Amongst these, Huancayo seems to show daily variation characteristics similar to those at high latitudes, but Lae and Makerere do not. Instrumental trouble and/or errors in barometric pressure correction at Lae and Makerere are suspected.

(4) Since the amplitudes on individual days vary in a wide range (0 to 3%), average amplitudes over groups of days are subject to large actual standard errors, much larger than the Poisson standard errors. Monthly or yearly averages do not have, therefore, an unambiguous interpretation. Also, there is no particular reason to believe that the first and second harmonics are necessarily related to independent physical processes. They could be indicative of the sharpness or broadness of the main anisotropy coupled with its diffusion in the earth's atmosphere. On the other hand, separate mechanisms for the first and second harmonic cannot be ruled out. If so, data from equatorial stations seem to be very useful for its study. Unfortunately, I.G.Y. data do not seem to be as fault-free as one would like them to be for such a study.

In the past, several workers have reported geomagnetic relationships of cosmic ray daily variation. Thus, Sekido and Kodama (1952) and Sandstrom (1956) report increase of diurnal amplitudes and shifting of its hour of maximum to earlier hours for geomagnetically disturbed days. Kane (1955) has reported enhanced amplitudes associated with some  $K_p$  maxima, though not all. Sekido and Yoshida (1951) report reduction of second harmonic amplitudes on magnetically disturbed days. The present investigation does not support these findings.

Firor *et al.* (1954), Remy and Sittkus (1955), Sittkus (1955), Kane (1955), Yoshida and Kondo (1954), Sarabhai and Nerurkar (1955), Sarabhai and Bhavsar (1958) report occurrence of high amplitude days in groups of days and a 27-day recurrence tendency for high amplitudes. This seems to be true for the I.G.Y. period also.

It is difficult to say whether the disagreement between results of some aspects of the present investigation with results reported earlier is due to a different period of observation or due to a different statistical approach adopted in the present investigation.



APPENDIX  
(Epoch dates)

Month	$C_p$ flux				H minima				Magnetic storms			
	$oC_p^0$	$oC_p^+$	$+C_p^0$	$+C_p^+$	Large ( $\geq 100\%$ )	Small	S. C* sev.	S. C. sev.	G sev.	S. C* Mod. sev.	S. C. Mod.	
Jul. 57							5	2			4, 22	
Aug. 57	13	3, 6	30						22	3, 6, 29	13	
Sep. 57	13	23	29	2	5, 13, 23, 30		2, 4, 13, 21, 29	12, 22		6	23	
Oct. 57		14		21		14			14	21	9, 26	
Nov. 57	26	7, 14		9, 18	27	7		26	9, 14, 25	6	5, 6	
Dec. 57	1		11, 15	5				31		1, 19	5, 30	
Jan. 58	18	21	1		1						20	
Feb. 58	11	6, 21	17		11	18	11		10	16	4, 13, 20	
Mar. 58	12, 23, 30		19	6		13	11		13	3, 14, 25	5, 9, 24, 30	
Apr. 58	4	17		2, 29		17				26, 27		
May 58	29			14, 26		14	31		25	12		
Jun. 58		1, 7		10, 21, 29	1, 29	10, 21		7, 28		8, 14	21, 23	
Jul. 58		21		4, 8, 18	27	9	8		27	21	4	
Aug. 58	27		17, 22, 24			18, 24				17, 22, 24, 27		
Sep. 58	4, 9, 16	25			5, 25	17		3, 25			4, 30	
Oct. 58	24, 28		22		24		22	24		27, 28		
Nov. 58												
Dec. 58	4				5	13, 18	4, 17			13	2	
Total events	18	14	14	14	14	13	13	10	9	25	24	

APPENDIX  
(Epoch adtes *contd.*)

Month	C.M.P. sunspot		Solar radio emission 200 mc/s		Type IV Solar radio out-burst	Leunbach events	C. R. Minima			Random		
	Very int.	Pro-nounced	Large	Small			Large	Mode-rate	Small	Gr. 1	Gr. 2	Gr. 3z
Jul. 75	21	26			3, 16, 24	3, 24			31			
Aug. 57	30, 31	1, 4, 22	31		28, 31	29	5, 30	16	26	15	30	
Sep. 57	11, 19, 27	9	11, 19, 22		2, 11, 12	2, 12, 26, 21		14, 23, 29	8	19	9, 29	9
Oct. 37	17		13		20	21	23	7, 15	25	23	8	
Nov. 37	26, 29	25	4, 29		24		27	4, 10	29		25	
Dec. 57	20, 25	3, 18	20, 22		14, 17		21	9, 29	31	31	22, 30	
Jan. 58		15					18	6	8	1, 15	4	
Feb. 58	7	7, 26			9	10	12		12	5, 27	8	
Mar. 58	13, 22, 29	7	30		23	25	26	13	1, 17	3, 6	30	
Apr. 58	4	4, 8			10			6, 13	25, 30	7	4, 7	
May 58	3	1, 15, 30					9, 30		1, 13	9, 18	8, 22	
Jun. 58	10	18, 28			4, 5, 6		9, 22		11, 25	14	18, 29	
Jul. 58	26	5, 7, 8, 18			7, 29	7, 29	9	2, 22, 28	18	23	22	
Aug. 58	12, 21	3, 31	23		16, 22, 26	16, 21, 22, 26	24	17	8	20	14	
Sep. 58	19	8			22		17		12		28	
Oct. 58	21		21, 29		21		23	1		22	22	
Nov. 58	3	24, 30					12			30		
Dec. 58	11, 20, 23	9	5		12			18	2	14	25	
Total Events	24	27	12	9	24	18	8	13	18	20	20	20

ACKNOWLEDGMENTS

The author is grateful to Professor V. A. Sarabhai for helpful discussions and to Miss Kundbala, Mr. Bhavsar and others for computational assistance. Thanks are due to Atomic Energy Commission of India for financial support.

REFERENCES

- Brunberg, E. A., 1959, *Arkiv for Fysik.*, **14**, 195.  
Firor, J. W., Fonger, W. M., and Simpson, J. A., 1954., *Phys. Rev.* **94**, 1031.  
Kane, R. P., 1955, *Phys. Rev.*, **98**, 130.  
Kane, R. P., 1961, *Ind. J. Phys.*, **35**, 213.  
Reid, G. C., and Leinbach, H., 1950, *J. Geophys Res.*, **64**, 1801.  
Remy, E., and Sittkus, A., 1955, *Z. Naturforsch.*, **10a**, 172.  
Sandstrom, A. E., 1956, *Tellus.*, **8**, 18.  
Sarabhai, V., and Bhavsar, P. D., 1958, *Nuovo Cim. Suppl.*, **8**, 209.  
Sarabhai, V., and Norurkar, N. W., 1955, *Proc I.U.P.A.P. Cosmic Ray Congress (Mexico)*.  
Sekido, Y., and Kodama, M., 1952, *Rept. Ionosphere Res Japan*, **6**, 111.  
Sokido, Y., and Kodama, M., 1952, *Rkpt Ionosphere Res. Japan*, **5**, 111.  
Sittkus, A., 1955, *J Atmos. Terr. Phys.*, **7**, 80.  
Yoshida, S., and Kondo, I., 1954, *J. Geomagn. Geoelect.*, **6**, 15.



# LOW ENERGY SCATTERING OF ELECTRON BY VARIATIONAL METHOD

S. C. MUKHERJEE AND N. C. SIL

DEPARTMENT OF THEORETICAL PHYSICS,  
INDIAN ASSOCIATION FOR THE CULTIVATION OF SCIENCE,  
JADAVPUR, CALCUTTA-32.

(Received March 31, 1962)

**ABSTRACT.** In this paper the cross section of elastic scattering of slow electron by helium atom is calculated with allowance for exchange effect. We have taken wave functions of the form of Taylor and Parr (1952) with two sets of parameters for the ground state of helium atom. The phases are calculated by the variational method of Hulthén (1944) from the differential equation. At very low energy the result of our theoretical calculation agrees closely with the theoretical findings of Moiseiwitsch (1961) who used the wave function of Green, *et al.* (1954) for the ground state of helium atom and solved the resulting differential equation numerically. Further our theoretical results are in good agreement with the experimental results of Pack, Phelps and Frost (1960).

## INTRODUCTION

Recently a large number of experiments on collision of slow electrons by helium atom have been performed by using micro-wave technique. The values of momentum transfer cross section which at very low energies is practically the same as the elastic scattering cross section, have been experimentally found by Anderson and Goldstein (1956) and Pack, Phelps and Frost (1960) and Phelps, Fundingsland and Brown (1951).

The scattering of electron at low energy involves the effect of exchange because of the indistinguishability of the incident electron from the atomic electron. There is a possibility of the incident electron being captured and the atomic electron being ejected, in the process of slow collision. The first theoretical investigation of the elastic scattering of electrons by helium atom in which the exchange effects were taken into account was carried out by Morse and Allis (1933). For a range of electron energies up to 120 e.V., they chose for the ground state of helium atom a Hartree wave function. The appropriate integro-differential equation was solved by them by numerical method. Moiseiwitsch (1953) adopting a simple wave function of Hylleraas calculated the same elastic cross section by using the variational method of Hulthén (1944). Very recently Moiseiwitsch (1961) by taking the wave function of Green *et al.* (1954), calculated the scattering length of electron-helium collision by numerical method.

In this paper we propose to take the open-shell type of wave function as

$$\psi_0(r_1, r_2) = \frac{N}{\sqrt{2}} \left\{ \phi \left( \frac{\zeta}{r_1} \right) \phi \left( \frac{\zeta'}{r_2} \right) + \phi \left( \frac{\zeta'}{r_1} \right) \phi \left( \frac{\zeta}{r_2} \right) \right\}$$

where  $\exp \left( \frac{\zeta}{r_i} \right) = \left( \frac{\zeta^3}{\pi a_0^3} \right)^{1/2} \exp \left\{ - \left( \frac{\zeta}{a_0} \right) r_i \right\}$  and  $N = \left[ 1 + \frac{64(\zeta\zeta')^3}{(\zeta + \zeta')^6} \right]^{-1/2}$

is the normalization factor. We choose two sets of values for the parameters  $\zeta$  and  $\zeta'$ . The first choice is

- 1)  $\zeta = 1.19$ ,  $\zeta' = 2.184$  and the other choice is
- 2)  $\zeta = 1$ ,  $\zeta' = 2.1$

According to Taylor and Parr (1952) the first choice gives better value for the ground state energy, viz.  $E_0 = -2.8756 \frac{e^2}{a_0}$  and by the second choice the ground state energy becomes  $E_0 = -2.8554 \frac{e^2}{a_0}$ , which also is better than the value found by the wave function of Hylleraas. It should be noted that the wave function of Hylleraas is a special case of Taylor and Parr wave function with  $\zeta = \zeta' = 1.6875$ . The energy value found by using the Hylleraas wave function is  $E_0 = -2.8477 \frac{e^2}{a_0}$ , the experimental value being  $-2.904 \frac{e^2}{a_0}$ . Huzinaga (1960) by taking the open shell wave function with the two sets of parameters mentioned above calculated the elastic scattering of fast electron by helium atom by the Born approximation method.

In this paper we have deduced the expression for the scattering cross section for slow electrons which takes into account the exchange effect, by applying a simple variational method of Hulthén (1944). Since we are interested at very low energies the phase values for  $l = 0$  only have been considered, the effects of higher values of  $l$  have been neglected as their effects are very small.

## RESULTS AND DISCUSSIONS

The wave equation for the system of helium atom and the incident electron is

$$\left[ \Delta_1^2 + \Delta_2^2 + \Delta_3^2 + \frac{4}{r_1} + \frac{4}{r_2} + \frac{4}{r_3} - \frac{2}{r_{12}} - \frac{2}{r_{13}} - \frac{2}{r_{23}} + E \right] \psi = 0 \quad \dots (1)$$

where  $r_1, r_2, r_3$  are the distances of the three electrons from the nucleus of the helium atom,  $r_{12}, r_{13}, r_{23}$  are the distances between the electron and  $E$  is the total energy of the system and units are expressed in Bohr radius ( $m = 1, e = 1, \hbar = 1$ ).

Expanding  $\psi$  in terms of the orthogonal set of helium atom wave function  $\psi_n$  we have

$$\psi = \sum \psi_n(r_1, r_2) F_n(r_3) \quad \dots \quad (2)$$

where  $F_n$  have the asymptotic forms

$$F_0 \sim e^{ik_0 z} + r^{-1} e^{ik_0 r} g_0(\theta)$$

and

$$F_n \sim r^{-1} e^{ik_n r} g_n(\theta) \quad (n \neq 0)$$

where the total energy of the system,  $E = K_0^2 + E$   
 $= K_n^2 + E_n$

$K_0$  being the wave number of the incident electron in atomic units.

The ground state wave function we have used for helium atom, as

$$\psi_0(r_1, r_2) = \frac{N}{\sqrt{2}} \left\{ \frac{\xi^3}{\pi a_0^3} \left[ e^{-(\xi r_1 + \xi' r_2)/a_0} + e^{-(\xi' r_1 + \xi r_2)/a_0} \right] \right\} \quad \dots \quad (3)$$

where  $N$  is the normalization factor.

The potential function as shown by Huzinaga (1960) is

$$V(r) = -e^2 \left[ 1 + \frac{64(\xi\xi')^3}{(\xi + \xi')^6} \right]^{-1} \left\{ \left( \frac{1}{r} + \frac{\xi}{a_0} \right) e^{-\frac{2\xi}{a_0} r} + \left( \frac{1}{r} + \frac{\xi'}{a_0} \right) e^{-\frac{2\xi'}{a_0} r} \right. \\ \left. + \frac{128(\xi\xi')^3}{(\xi + \xi')^6} \left( \frac{1}{r} + \frac{\xi + \xi'}{2a_0} \right) e^{-\left( \frac{\xi + \xi'}{a_0} \right) r} \right\} \quad \dots \quad (4)$$

After making allowance for exchange, the wave function becomes

$$\psi = \psi_0(r_1, r_2) F_0(r_3) \frac{1}{\sqrt{2}} (\alpha_1 \beta_2 - \alpha_2 \beta_1) + \psi_0(r_2, r_3) F_0(r_1) \frac{1}{\sqrt{2}} (\alpha_2 \beta_3 - \alpha_3 \beta_2) \alpha_1 \\ + \psi_0(r_3, r_1) F_0(r_2) (\alpha_3 \beta_1 - \alpha_1 \beta_3) \alpha_2 \quad \dots \quad (5)$$

where  $\alpha$ 's,  $\beta$ 's are the spin wave function and the spin function  $\frac{1}{\sqrt{2}} (\alpha_1 \beta_2 - \alpha_2 \beta_1)$  is antisymmetric w.r. to electrons (1) and (2). Substituting (5) in (1) and multiplying by  $\frac{1}{\sqrt{2}} (\alpha_1 \beta_2 - \alpha_2 \beta_1) \alpha_3 \psi_0(r_1, r_2)$  and summing over the spin coordinates and integrating w.r. to  $r_1$  and  $r_2$  we obtain

$$[\Delta_3^2 + K_0^2 - V_0(r_3)] F_0(r_3) = \iint F_0(r_1) P_0(r_1, r_2, r_3) d\vec{r}_1 d\vec{r}_2 \quad \dots \quad (6)$$

where  $P_0(r_1, r_2, r_3) = \psi_0(r_2, r_3) \Delta_1^2 \psi_0(r_1, r_2) + \psi_0(r_1, r_2) \Delta_2^2 \psi_0(r_2, r_3) \\ + \psi_0(r_1, r_2) \Delta_3^2 \psi_0(r_2, r_3) + \psi_0(r_1, r_2) \psi_0(r_2, r_3)$

$$\left\{ \frac{4}{r_1} + \frac{4}{r_2} + \frac{4}{r_3} - \frac{2}{r_{12}} - \frac{2}{r_{13}} - \frac{2}{r_{23}} + E \right\}$$

$$\begin{aligned}
\text{i.e. } P_0(r_1, r_2, r_3) &\sim 2\xi^2 [e^{-(\zeta r_1 + \zeta' r_2) - (\zeta r_2 + \zeta' r_3)} + e^{-(\zeta r_1 + \zeta' r_2) - (\zeta' r_2 + \zeta r_3)}] \\
&+ 2\xi'^2 [e^{-(\zeta' r_1 + \zeta r_2) - (\zeta r_2 + \zeta' r_3)} + e^{-(\zeta' r_1 + \zeta r_2) - (\zeta' r_2 + \zeta r_3)}] \\
&- \frac{2}{r_1} [\xi e^{-(\zeta r_1 + \zeta' r_2) - (\zeta r_2 + \zeta' r_3)} + \xi' e^{-(\zeta' r_1 + \zeta r_2) - (\zeta r_2 + \zeta' r_3)} + \xi e^{-(\zeta r_1 + \zeta' r_2) - (\zeta' r_2 + \zeta r_3)} \\
&\quad + \xi' e^{-(\zeta' r_1 + \zeta r_2) - (\zeta' r_2 + \zeta r_3)}] \\
&- \frac{2}{r_2} [\xi e^{-(\zeta r_1 + \zeta' r_2) - (\zeta r_2 + \zeta' r_3)} + \xi' e^{-(\zeta r_1 + \zeta' r_2) - (\zeta' r_2 + \zeta r_3)} + \xi e^{-(\zeta' r_1 + \zeta r_2) - (\zeta r_2 + \zeta' r_3)} \\
&\quad + \xi' e^{-(\zeta' r_1 + \zeta r_2) - (\zeta' r_2 + \zeta r_3)}] \\
&- \frac{2}{r_3} [\xi' e^{-(\zeta r_1 + \zeta' r_2) - (\zeta r_2 + \zeta' r_3)} + \xi e^{-(\zeta r_1 + \zeta' r_2) - (\zeta' r_2 + \zeta r_3)} \\
&\quad + \xi' e^{-(\zeta' r_1 + \zeta r_2) - (\zeta r_2 + \zeta' r_3)} + \xi e^{-(\zeta' r_1 + \zeta r_2) - (\zeta' r_2 + \zeta r_3)}] + [\xi'^2 e^{-(\zeta r_1 + \zeta' r_2) - (\zeta' r_2 + \zeta r_3)} \\
&\quad + \xi^2 e^{-(\zeta' r_1 + \zeta r_2) - (\zeta r_2 + \zeta' r_3)} + \xi'^2 e^{-(\zeta r_1 + \zeta' r_2) - (\zeta' r_2 + \zeta r_3)} \\
&\quad + \xi^2 e^{-(\zeta' r_1 + \zeta r_2) - (\zeta' r_2 + \zeta r_3)}] + [e^{-(\zeta r_1 + \zeta' r_2) - (\zeta r_2 + \zeta' r_3)} + e^{-(\zeta r_1 + \zeta' r_2) - (\zeta' r_2 + \zeta r_3)} \\
&\quad + e^{-(\zeta' r_1 + \zeta r_2) - (\zeta r_2 + \zeta' r_3)}] \left[ \frac{4}{r_1} + \frac{4}{r_2} + \frac{4}{r_3} - \frac{2}{r_{12}} - \frac{2}{r_{13}} - \frac{2}{r_{23}} + E \right]
\end{aligned}$$

Expanding  $F_0(r) = \frac{1}{r} \sum_{l=0}^{\infty} f_l(r) P_l(\cos \theta) - \dots (7)$  in Legendre Polynomial

where

$$f_l \sim \sin(K_0 r - \frac{1}{2} l \pi + \eta_l)$$

$\eta_l$  being the phase shifts.

The total scattering cross section

$$Q = \frac{4\pi}{K_0^2} \sum_{l=0}^{\infty} (2l+1) \sin^2 \eta_l \quad \dots (8)$$

Substituting the value of  $F_0(r)$  from Eq. (7) into Eq. (6) and multiplying both sides by  $P_l(\cos \theta_3) \sin \theta_3 d\theta_3$  and integrating over the space we get finally

$$\left[ \frac{d^3}{dr_3^2} + K_0^2 - V_0(r_3) - \frac{l(l+1)}{r_3^2} \right] f_l(r_3) = \int \int f_l(r_1) Q_l(r_1, r_2, r_3) d\bar{r}_1 d\bar{r}_2 \quad (9)$$

where

$$\begin{aligned}
Q_l(r_1, r_2, r_3) &= \frac{16\pi^2 r_1^2 r_2^2 r_3}{2l+1} \left\{ 2\xi^2 [e^{-(\zeta r_1 + \zeta' r_2) - (\zeta r_2 + \zeta' r_3)} + e^{-(\zeta r_1 + \zeta' r_2) - (\zeta' r_2 + \zeta r_3)}] \right. \\
&\quad \left. + 2\xi'^2 [e^{-(\zeta' r_1 + \zeta r_2) - (\zeta r_2 + \zeta' r_3)} + e^{-(\zeta' r_1 + \zeta r_2) - (\zeta' r_2 + \zeta r_3)}] \right.
\end{aligned}$$



$$\begin{aligned}
 & + e - (\xi' r_1 + \xi r_2) - (\xi' r_2 + \xi r_3) ] \delta_{0l} - \frac{2}{r_1} [ \xi e - (\xi r_1 + \xi' r_2) - (\xi r_2 + \xi' r_3) + \xi' e - (\xi' r_1 + \xi r_2) - (\xi r_2 + \xi' r_3) \\
 & + \xi e - (\xi r_1 + \xi' r_2) - (\xi' r_2 + \xi r_3) + \xi' e - (\xi' r_1 + \xi r_2) - (\xi r_2 + \xi' r_3) ] \delta_{0l} - \frac{2}{r_2} \\
 & \quad [ \xi e - (\xi r_1 + \xi' r_2) - (\xi r_2 + \xi' r_3) + \xi' e - (\xi' r_1 + \xi r_2) - (\xi r_2 + \xi' r_3) ] \\
 & + \xi' e - (\xi r_1 + \xi' r_2) - (\xi' r_2 + \xi r_3) + \xi e - (\xi r_1 + \xi' r_2) - (\xi r_2 + \xi' r_3) + \xi' e - (\xi' r_1 + \xi r_2) - (\xi r_2 + \xi' r_3) ] \\
 & + \delta_{0l} - \frac{2}{r_3} [ \xi' e - (\xi r_1 + \xi' r_2) - (\xi r_2 + \xi' r_3) + \xi e - (\xi r_1 + \xi' r_2) - (\xi r_2 + \xi' r_3) \\
 & + \xi' e - (\xi' r_1 + \xi r_2) - (\xi r_2 + \xi' r_3) + \xi e - (\xi r_1 + \xi' r_2) - (\xi r_2 + \xi' r_3) ] \delta_{0l} \\
 & \quad + [ \xi'^2 e - (\xi r_1 + \xi' r_2) - (\xi r_2 + \xi' r_3) - (\xi' r_2 + \xi r_3) ] \delta_{0l} \\
 & + \xi^2 e - (\xi' r_1 + \xi r_2) - (\xi r_2 + \xi' r_3) + \xi'^2 e - (\xi r_1 + \xi' r_2) - (\xi r_2 + \xi' r_3) + \xi^2 e - (\xi' r_1 + \xi r_2) - (\xi r_2 + \xi' r_3) ] \delta_{0l} \\
 & + [ e - (\xi r_1 + \xi' r_2) - (\xi r_2 + \xi' r_3) + e - (\xi r_1 + \xi' r_2) - (\xi r_2 + \xi' r_3) + e - (\xi r_1 + \xi' r_2) - (\xi r_2 + \xi' r_3) \\
 & + e - (\xi' r_1 + \xi r_2) - (\xi r_2 + \xi' r_3) ] \left[ \left( \frac{4}{r_1} + \frac{4}{r_2} + \frac{4}{r_3} - 2\gamma_l(r_1, r_2) - 2\gamma_l(r_2, r_3) + E \right) \delta_{0l} \right. \\
 & \quad \left. - 2\gamma_l(r_1, r_3) \right] \}
 \end{aligned}$$

$$\begin{aligned}
 \text{where} \quad \gamma_l(r_1, r_2) &= r_1^l / r_2^{l+1} \quad (r_1 < r_2) \\
 &= r_2^l / r_1^{l+1} \quad (r_2 < r_1)
 \end{aligned}$$

$$\begin{aligned}
 \text{and} \quad \delta_{0l} &= 0, \quad l \neq 0 \\
 \delta_{0l} &= 1, \quad l = 0
 \end{aligned}$$

$$\text{since} \quad \int_{-1}^{+1} |P_n(Z)|^2 dz = \frac{2}{2n+1}$$

$$\text{and} \quad \int \dot{P}_l(\cos \theta) \sin \theta d\theta = 2\delta_{0l} \quad [\text{vide Magnus oberhettinger (1954)}]$$

when  $l = 0$  Eqn. (9) becomes

$$\left[ \frac{d^2}{dr_3^2} + K_0^2 - V_0(r_3) \right] f_0(r_3) = \int \int f_0(r_1) Q_0(r_1, r_2, r_3) dr_1 dr_2 \quad \dots \quad (10)$$

We solve the Eq. (10) by the variational method of Hulthen (1944). The trial wave function we have used is of the same form as that of Moiseiwitsch (1953) i.e.

$$f_e(r) = \sin K_0 r + (a + b e^{-Zr})(1 - e^{-Zr}) \cos K_0 r, \text{ where } Z = \frac{27}{16}$$

The phase is given by  $\eta_0 = \tan^{-1} a$

The values of the parameters  $a$ ,  $b$ , are found from the simultaneous Equation

$$L = 0, \quad \frac{\partial L}{\partial a} = 0, \quad \text{and} \quad \frac{\partial L}{\partial b} = 0$$

$$\text{where } L = \int_0^\infty f_1(r_3) \left[ \left\{ \frac{d^2}{dr_3^2} + K_0^2 - V_0(r_3) \right\} f_1(r_3) - \int_0^\infty \int_0^\infty f_1(r_1) Q_0(r_1, r_2, r_3) dr_1 dr_2 \right] dr_3$$

TABLE I

The total scattering cross section for the low energy range is tabulated below.

A comparison has been made for three types of helium atom wave forms.

Electron wave No. $K_0$ in atomic units	Value of the Parameter $a$			Value of Total Cross Section in $\pi a_0^2$		
	(I) $\zeta = \zeta' = 1.6875$ $\zeta = 2.184$	(II) $\zeta = 1.19$ $\zeta' = 2.1$	(III) $\zeta = 1.0$ $\zeta' = 2.1$	(I) $\zeta = \zeta' = 1.6875$ $\zeta' = 2.184$	(II) $\zeta = 1.19$ $\zeta' = 2.1$	(III) $\zeta = 1.0$ $\zeta' = 2.1$
.136	— .200	— .175	— .216	8.30	7.436	9.61
.608	— 1.10	— 1.06	— 1.18	5.93	5.911	6.25
1.053	— 3.62	— 3.358	— 3.73	3.35	3.30	3.39
1.922	3.51	2.76	3.45	1.00	9566	998

Pack, Phelps and Frost (1960) have reported the value  $19a_0^2$  for  $Q_m$  (momentum transfer cross section) at mean electron energies in the range .003 eV to .05 eV, which they have derived from the drift velocity measurement. At the energy .04 eV, Phelps, Fundingsland and Brown (1951) have observed the cross section as  $19.16a_0^2$ . At the same energy the cross section calculated by Moiseiwitsch (1953) with Hylleraas wave function is  $28.906a_0^2$  by the variational method and  $27.02a_0^2$  by numerical integration when the effect of exchange is taken into account; whereas the cross section on ignoring exchange effect becomes  $349.01a_0^2$  as calculated by variational method and  $248.2a_0^2$  by numerical integration. In a recent paper Moiseiwitsch (1961) has numerically calculated the integro-differential equation using a wave function of Green *et al.* (1954) and has found the value for the total cross section as  $26.1a_0^2$  in the limit of zero energy. On solving the integro differential equation by the variational method of Hulthen we have found the total cross section at .04 eV as  $27.21a_0^2$  and  $28.10a_0^2$  for the two choices of wave functions mentioned earlier. These values of the cross section agree closely with the values found by Moiseiwitsch (1961). Further the first choice of the wave function gives better agreement than the second. The variational method of

Hulthen in a very low energy region gives the value of the cross section close to that obtained by the numerical method, but deviates from the numerical method with the increase of energy. The discrepancy between the theoretical and observed value is considerably removed by a suitable choice of wave function and by including the effect of exchange in calculation. The discrepancy still left may be due to the neglect of polarization.

## ACKNOWLEDGMENT

The authors are indebted to Prof. D. Basu for his sustained interest in the preparation of this paper.

## REFERENCES

- Anderson, J. M., and Goldstein, L., 1956, *Phys. Rev.*, **102**, 933.  
 Groom, L. C., Mulder, M. M., Lewis, M. N., 1954, *Phys. Rev.* **93**, 757.  
 Hulthen, L., 1944, *K. fysicgr Sällsk Lund Forh* **14**, No. 21.  
 Huzinaga, S., 1960, *Prog. Th. Phys.*, **23**, 562.  
 Magnus, W., Oberhettinger, F., 1954, *Formulas and Theorems for the Mathematical Physics*, Chelsea Publishing Company, New York.  
 Moisewitsch, B. L., 1953, *Proc. Roy. Soc.*, **219**, 102.  
 Moisewitsch, B. L., 1961, *Proc. Phys. Soc.* **77**, 722.  
 Morse, P. M., and Allis, W. P., 1933, *Phys. Rev.*, **44**, 269.  
 Phelps, A. V., Pack, J. L., and Frost, L. S., 1960, *Phys. Rev. Letter*, **5**, 532.  
 Phelps, A. V., Rundingsland, O. T., and Brown, S. C., 1951, *Phys. Rev.* **84**, 559.  
 Taylor, G. R., and Parr, R. G., 1952, *Proc. Nat. Acad. Sci.* **38**, 154.

# ON THE RAMAN AND INFRARED SPECTRA OF 1,4-DICHLOROBUTANE AND PROPIONYL CHLORIDE IN DIFFERENT STATES\*

K. K. DEB

OPTICS DEPARTMENT,

INDIAN ASSOCIATION FOR THE CULTIVATION OF SCIENCE,  
CALCUTTA-32.

(Received March 12, 1962)

**ABSTRACT.** The Raman spectra of 1,4-dichlorobutane and propionyl chloride in the liquid and solid states at  $-180^{\circ}\text{C}$  and also the infrared spectra of the pure liquids and of their solutions in suitable aliphatic solvents in the region  $600\text{ cm}^{-1}$  to  $3200\text{ cm}^{-1}$  have been investigated. It has been observed that in both the cases the liquid consists of two types of molecules, but the form which persists in the solid state is other than centro-symmetrical. In the solid state at  $-180^{\circ}\text{C}$ , 1, 4-dichlorobutane exhibits no new line in the low frequency region while propionyl chloride exhibits three such lines of shifts 43, 53 and  $97\text{ cm}^{-1}$  respectively. These lines have been assigned to intermolecular coupling.

Besides these changes some changes in the vibrational modes of the compounds are also observed in the infrared spectra of the solutions. The significance of all these changes have been discussed.

## INTRODUCTION

The infra-red spectra of tetramethylene bromide in the liquid and solid states were studied by Brown *et al* (1950a). It was concluded from a comparison of the results for the liquid and solid states of the molecule that the liquid consists of molecules of two isomeric forms while in the solid state only a single isomer with centro-symmetrical configuration is present. They further compared the spectra with those for *n*-propyl chloride and *n*-propyl bromide and concluded that in the solid state the bromine atoms of the tetramethyl bromide lie on the opposite sides of the plane through the carbon chain. As the Raman spectra of tetramethylene chloride had not been investigated in the liquid and solid states by any previous worker, it was thought worthwhile to study the Raman spectra of the compound in the two different states in order to find out how they support the above conclusions.

Propionyl chloride is another molecule in which one  $\text{CH}_2\text{Cl}$  group of trimethylene chloride is replaced by the  $\text{COCl}$  group. In order to find out the changes in the spectrum with the solidification of the liquid, the Raman spectra of the compound in the liquid and solid states have also been investigated.

\*Communicated by Prof. S. C. Sirkar.

The infrared spectra of both the compounds in the liquid state and of their solutions in some chosen aliphatic solvents have also been investigated in the region from  $600\text{ cm}^{-1}$  to  $3200\text{ cm}^{-1}$  in order to find out the influence of the surrounding molecules on the intramolecular vibrational modes.

The results for the Raman and infrared spectra have been discussed in the present paper.

#### EXPERIMENTAL

The liquids studied in the present investigation were obtained from the Eastman Kodak Co. Ltd. and were of chemically pure quality. They were further purified by distillation under reduced pressure. The technique used for recording the Raman spectra in the solid state at  $-180^{\circ}\text{C}$  and in the liquid state at the room temperature was the same as that used by Biswas (1954). The polarisation of the Raman lines of the liquids was studied in the usual way (Deb, 1960). All the spectra were photographed on Ilford Zenith plates with the help of a Fuess glass spectrograph having a dispersion of about  $11\text{ \AA/mm}$  in the region  $4047\text{ \AA}$ .

The infrared absorption spectra of the liquids and of their solutions in  $\text{CCl}_4$ ,  $\text{CHCl}_3$ ,  $\text{CS}_2$  and *n*-hexane were recorded in the region  $607\text{--}3200\text{ cm}^{-1}$  with the help of a Perkin-Elmer model 21 spectrophotometer with NaCl optics. An absorption cell  $0.05\text{ mm}$  thick was used in recording the spectra of the solutions while a thin film of the liquid contained between two NaCl discs was used in the case of the pure liquids. Suitable compensation cells were used in recording the absorption spectra of the solutions.

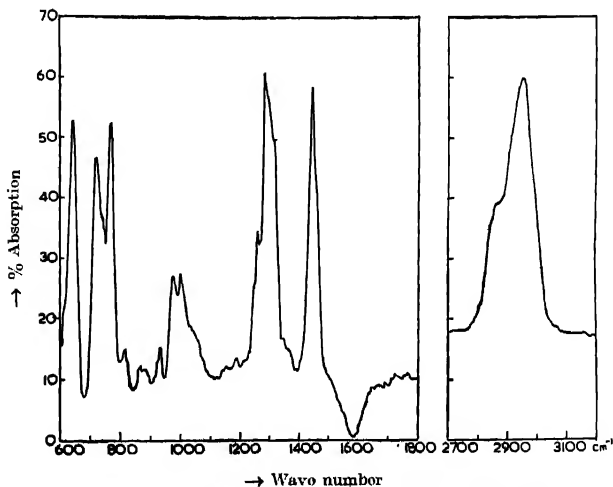


Fig. 3(a) Infrared spectrum of pure 1,4-dichlorobutane.

## RESULTS

The Raman spectra for the liquid and solid states of the two substances are reproduced in Figs. 1 and 2, Plate IV. The frequency-shifts are given in Tables I and III. The state of polarisation of the Raman lines is indicated in the table by the letters *P* and *D*, the letter *D* indicating the totally depolarised nature of the line.

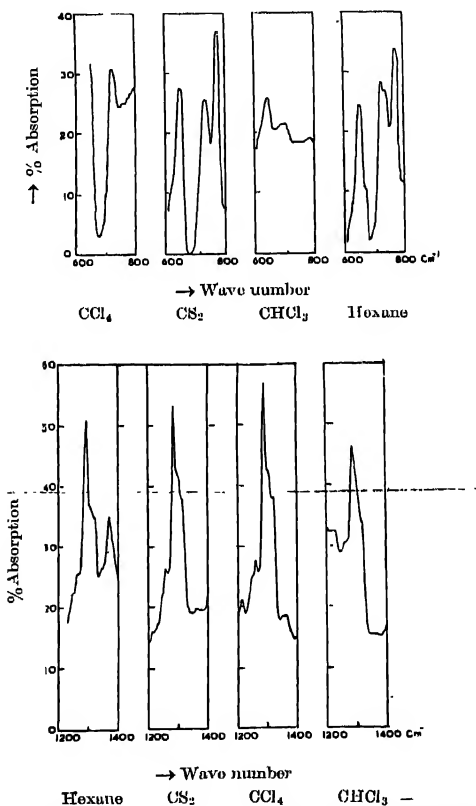


Fig. 3(b). Infrared spectra of solutions of 1, 4-dichlorobutane in the solvents shown.

The infrared spectra of the compounds in the liquid state and of their solutions in CCl<sub>4</sub>, CHCl<sub>3</sub>, CS<sub>2</sub> and *n*-hexane and also the infrared spectrum of pure 1 : 2 dibromo ethane are shown in Figs. 3, 4 and 5. The infrared bands are tabulated in Tables II and IV. The visually estimated strengths of the bands are indicated by the usual symbols in the parentheses.

## 1, 4-Dichlorobutane :

*Changes in the Raman spectra with the solidification of the liquid.*

It can be seen from Table I that the Raman lines 361, 724 and  $2876\text{ cm}^{-1}$  in the spectrum of pure 1, 4-dichlorobutane disappear when the liquid is solidified. Brown *et al.* (1955) observed similar changes in the infrared spectra and concluded that in the solid state there is only one type of molecule with a centre of symmetry. It is to be pointed out, however, that the existence of a centre of symmetry should have made some of the Raman and infrared active fundamentals

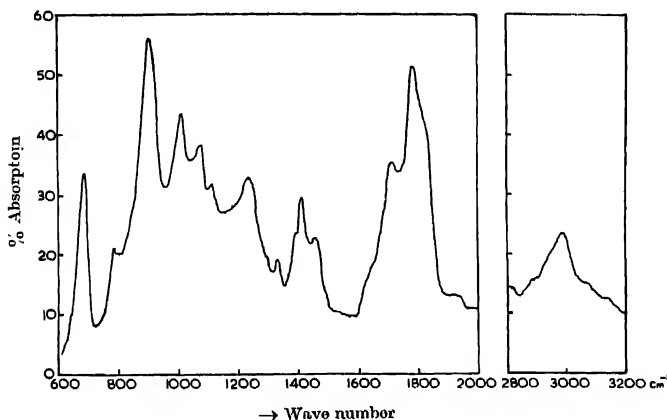


Fig. 4(a). Infrared spectrum of pure propionyl chloride.

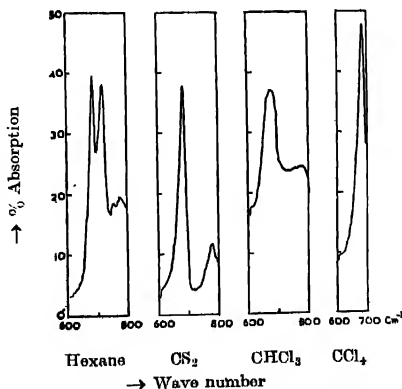


Fig. 4(b). Infrared spectra of solutions of propionyl chloride in the solvents shown.

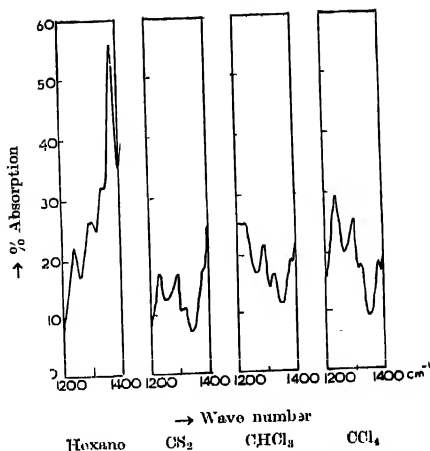


Fig. 4(c). Infrared spectra of solutions of propionyl chloride in the solvents shown.

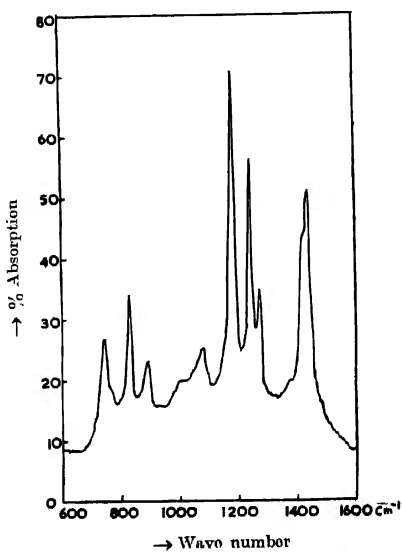


Fig. 5. Infrared spectrum of 1, 2-dibromoethane.

mutually exclusive. For instance, the line  $667\text{ cm}^{-1}$  in the Raman spectrum of 1, 2-dibromoethane persists and the lines  $551$  and  $583\text{ cm}^{-1}$  disappear when the liquid is solidified (Mizushima, 1938). The infrared spectra of 1, 2-dibromoethane



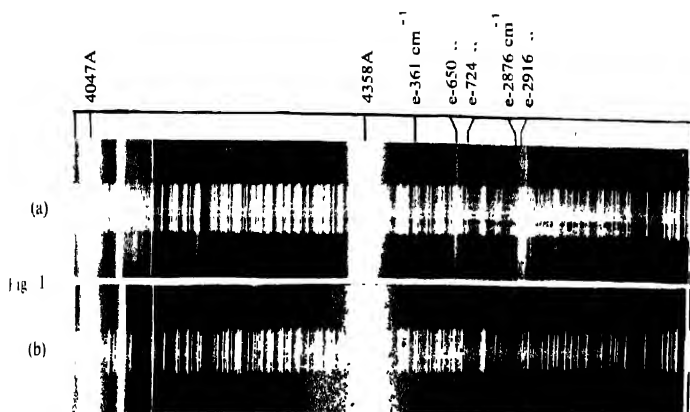


Fig. 1 (a) Raman spectrum of 1,4-dichlorobutane liquid at 30°C  
(b) " " " " " solid at -180°C

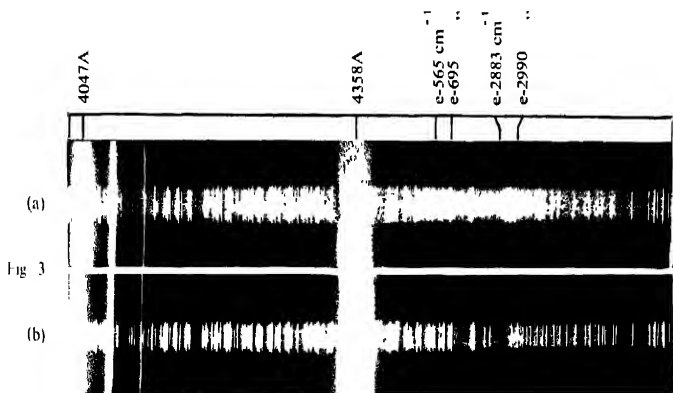


Fig 3 (a) Raman spectrum of propionyl chloride, liquid at 30°C  
(b) " " " " " solid at -180°C



TABLE 1

Raman and infrared spectra of 1, 4-dichlorobutane  $\nu$  in  $\text{cm}^{-1}$ 

Raman shifts (Present author)		Infrared bands (Brown <i>et al.</i> , 1955)	
Pure liquid	Solid at $-180^{\circ}\text{C}$	Pure liquid	Solid
232 (2) P	233 (1)		
	246 (1)		
274 (4b) P	272 (2)		
311 (2) P	311 (1)		
361 (4) P			
496 (1) P			
650 (12b) P	642 (10)	650 (s)	650 (s)
724 (6) P		728 (w)	
738 (2) P		745 (s)	
774 (3) P	774 (1)	775 (s)	775 (s)
811 (1) P	811 (1)		
824 (0)	824 (0)	824 (m)	
870 (ob)	870 (ob)	872 (m)	871 (m)
		887 (m)	
		940 (m)	900 (m)
980 (2) P	977 (2)	988 (s)	
		1008 (s)	1008 (s)
		1017 (m)	
1034 (0)		1041 (m)	1040 (w)
1053 (0)		1062 (m)	
		1135 (w)	1126 (w)
		1166 (w)	
1194 (1)		1189 (w)	1193 (m)
		1215 (w)	
1262 (1)	1264 (1)	1262 (s)	
1297 (1b)		1297 (s)	1295 (s)
			1317 (m)
1432 (4) D?		1446 (s)	
1445 (5) P			1451 (s)
2844 (1)	2844 (0)		
2876 (4) P			
2916 (10) P	2914 (8)		
	2926 (5)		
2960 (10) P	2962 (8)		
3003 (4) P	3004 (4)		

TABLE II

Infrared spectra of 1,4-dichlorobutane  $\nu$  in  $\text{cm}^{-1}$ 

Pure liquid Present author	Infrared bands of solutions in (Present author)			
	in $\text{CCl}_4$	in $\text{CHCl}_3$	in $\text{CS}_2$	in <i>n</i> -hexane
646 (s)		640 (m)		615 (m)
722 (s)	722 (s)	700 (m)		670 (w)
			650 (m)	720 (s)
			735 (s)	740 (s)
745 (s)			778 (vs)	770 (s)
			812 (vw)	818 (vw)
772 (s)			860 (w)	860 (w)
820 (w)	810 (s)		885 (vw)	880 (w)
865 (w)	865 (vw)			
890 (w)	890 (vw)		905 (vw)	905 (vw)
905 (vw)	905 (vw)		935 (w)	935 (w)
935 (w)	932 (w)	922 (w)		
982 (m)	980 (m)	978 (m)	980 (m)	982 (m)
1005 (m)	1002 (m)	1002 (m)	1002 (m)	1002 (m)
1040 (w)	1040 (w)	1040 (w)	1040 (w)	1040 (w)
1062 (w)	1068 (w)		1065 (w)	1062 (w)
1140 (w)	1145 (w)	1140 (w)	1140 (w)	1138 (w)
1160 (w)	1160 (w)		1165 (w)	1160 (w)
1189 (w)	1190 (w)		1190 (w)	1170 (w)
1220 (w)	1220 (w)	1230 (s)	1220 (w)	1220 (w)
1250 (m)	1250 (m)		1250 (m)	1250 (m)
1260 (s)	1260 (m)	1260 (s)	1260 (m)	1260 (m)
1290 (vs)	1290 (vs)	1290 (vs)	1290 (vs)	1290 (vs)
1300 (vs)	1305 (s)		1305 (vs)	1302 (s)
1318 (s)	1320 (s)	1320 (s)	1320 (vs)	1320 (s)
1350 (w)	1350 (w)			1342 (m)
1365 (w)	1370 (w)		1362 (m)	1370 (s)
1445 (vs)	1450 (vs)	1450 (vs)	1435 (s)	1440 (s)
1460 (s)	1465 (s)	1465 (s)	—	1480 (m)
2842 (m)				
2865 (s)	2865 (s)			
2952 (vs)	2970 (s)	2962 (vs)	2958 (vs)	
3000 (s)	3005 (s)	3005 (s)	3000 (s)	

TABLE III

*Raman spectra of propionyl chloride.  $\Delta\nu$  in  $\text{cm}^{-1}$*

Pure liquid		Solid at $-180^\circ\text{C}$
Landolt-Bornstein Table (1951)	Present author	Present author
		43 (2)
		53 (0)
		97 (0)
232 (2)	192 (3) P	192 (1)
	261 (2) P	261 (1)
354 (7) P	354 (6) P	358 (3)
432 (10sb) P	433 (10b) P	433 (0)
	488 (2) P	485 (0)
	503 (3) P	494 (2)
565 (4sb) P	567 (4) P	
689 (6b) P	695 (4) P	690 (4)
789 (0)		
890 (0)	898 (0)	—
1016 (2) P	1010 (1) P	
1080 (5) P	1082 (5) P	1081 (2)
1252 (0)	1253 (1) P	
1406 (2) D	1406 (4) D	1407 (4)
1454 (2sb) P	1454 (3) P	1458 (2)
1787 (3b) P	1794 (2) P ?	1788 (2)
1833 (1)		
2748 (1)		
2884 (3b)	2883 (3) P	
2905 (1)	2917 (3b) P	2917 (3)
2921 (2)		
2945 (8)	2945 (10) P	2943 (8)
2989 (4sb)	2990 (5) P	2988 (2)
		3006 (4)

TABLE IV

Infrared spectra of propionyl chloride.  $\nu$  in  $\text{cm}^{-1}$ 

Pure liquid Present author	Infrared bands of solutions (Present author)			
	m $\text{CCl}_4$	m $\text{CHCl}_3$	in $\text{CS}_2$	in $n\text{-hexane}$
670 (m)	670 (vw)	665 (m)	670 (m)	670 (vw)
690 (vs)	685 (vs)	680 (vs)	685 (vs)	690 (vs)
				760 (w)
788 (m)			780 (w)	780 (w)
808 (vs)	910 (vs)	910 (vs)	910 (vs)	910 (vs)
				915 (w)
1012 (s)	1010 (s)	1010 (s)	1010 (s)	1010 (s)
				1060 (m)
1078 (m)	1080 (s)	1080 (s)	1080 (m)	1080 (m)
1118 (m)	1110 (m)	1110 (m)	1110 (w)	1125 (s)
1240 (s)	1240 (s)	1234 (m)	1235 (m)	1240 (m)
1300 (vw)	1300 (m)	1292 (m)	1300 (m)	1300 (m)
1330 (w)	1325 (m)	1330 (w)	1325 (w)	1340 (s)
1390 (m)	1380 (m)	1385 (m)	1380 (m)	1380 (s)
1410 (s)	1410 (s)	1410 (s)	1405 (s)	
1430 (m)	1430 (s)			1430 (vw)
1460 (w)	1460 (m)	1460 (s)		1460 (vs)
1650 (w)	1645 (w)			
1718 (s)	1710 (vs)	1710 (s)	1710 (s)	1718 (m)
1788 (vs)	1785 (vs)	1782 (vs)	1784 (vs)	1788 (vs)
1838 (vs)	1838 (vs)	1840 (s)	1835 (s)	1840 (s)
2882 (w)	2882 (w)	2885 (m)	2880 (w)	
2900 (w)	2905 (m)	2905 (m)		
2990 (m)	2990 (s)	2990 (s)	2980 (s)	
3020 (m)	3020 (w)	3025 (s)		

in the liquid and solid states were investigated by Brown *et al.* (1950) and they observed the disappearances of the strong bands  $834$  and  $1248\text{ cm}^{-1}$  with solidification of the liquid. They however, did not record the spectrum below  $700\text{ cm}^{-1}$ . In order to verify whether there is any band in the  $600\text{--}700\text{ cm}^{-1}$  region the infrared spectrum of the liquid was recorded with a Perkin-Elmer infrared spectrophotometer with NaCl optics and the record so obtained does not show any band in the region mentioned above. So, in this case the band  $650\text{ cm}^{-1}$  is forbidden in the infrared. The appearance of the frequency  $650\text{ cm}^{-1}$  both in the Raman spectrum and in the infrared spectrum of 1, 4-dichlorobutane on the otherhand suggests that the molecule giving this frequency has no centre of symmetry. The disappearance of the strong line  $724\text{ cm}^{-1}$  and of the infrared band of the same frequency along with other lines with the solidification of the liquid indicates that the liquid consists of two types of molecules as suggested by Brown *et al.* (1955), but the configuration of the molecule which persists in the solid states is other than centro-symmetrical. It may be of the form GTG in which the chlorine atoms are on the same side of the plane through the carbon chain.

In addition to the above changes mentioned above some other changes also take place with the solidification of the liquid. Each of the Raman lines  $274$  and  $2916\text{ cm}^{-1}$  splits up into two lines when the compound is solidified and cooled to  $-180^{\circ}\text{C}$ . The line  $274\text{ cm}^{-1}$  splits up into the components  $246\text{ cm}^{-1}$ ,  $272\text{ cm}^{-1}$  and the line  $2916\text{ cm}^{-1}$  into the components  $2914\text{ cm}^{-1}$  and  $2926\text{ cm}^{-1}$ . The line  $274\text{ cm}^{-1}$  may be due to the bending oscillation of the C-Cl group and the line  $2916\text{ cm}^{-1}$  due to C-H valence oscillation. Also the line  $650\text{ cm}^{-1}$  due to C-Cl valence oscillation shifts to  $642\text{ cm}^{-1}$  under similar conditions. Hence, these changes might be due to the formation of associated groups of molecules through H atoms in the frozen state of the substance at  $-180^{\circ}\text{C}$ .

#### *Infrared spectra of solutions*

It is seen from Table II that all the infrared bands of the liquid recorded in the present investigation closely agree with those observed in the previous workers, excepting the bands  $1300$ ,  $1318$  and  $1460\text{ cm}^{-1}$  which were not resolved from the neighbouring bands in the previous investigation.

It can be seen from Table I and II that there are four infrared bands in the region  $600\text{--}800\text{ cm}^{-1}$  in the absorption spectrum of 1, 4-dichlorobutane and some of these undergo changes when the liquid is dissolved in the solvents mentioned earlier. Of these the band  $646\text{ cm}^{-1}$  becomes weaker with respect to the band  $772\text{ cm}^{-1}$  and the band  $745\text{ cm}^{-1}$  becomes stronger when the liquid is dissolved in either *n*-hexane or  $\text{CS}_2$ . In the other two solutions due to the presence of absorption bands of the solvents and also for want of accurate compensation the changes are not reliable. The band  $772\text{ cm}^{-1}$  is most probably due to C-H mode because it is present in the spectrum of ethane. The band  $650\text{ cm}^{-1}$  is due

to the GTG configuration of the molecule. Hence the number of molecules of this configuration diminishes in solutions mentioned and that of the molecules of some other configuration giving the band  $745\text{ cm}^{-1}$  increases. In the case of solution in *n*-hexane the band  $646\text{ cm}^{-1}$  splits up into two components at  $645\text{ cm}^{-1}$  and  $670\text{ cm}^{-1}$  respectively while in solution in  $\text{CS}_2$  no such influence is observed. The width of the band  $1290\text{ cm}^{-1}$  due to C-H oscillation diminishes considerably but the integrated absorption remains almost unchanged when the liquid is dissolved in either *n*-hexane or  $\text{CCl}_4$ , but such change is smaller in the solution in  $\text{CS}_2$  and absent in the solution in  $\text{CHCl}_3$ .

### *Propionyl chloride*

#### *A. Changes in the Raman spectra with the solidification of the liquid*

It can be seen from Table III that most of the Raman lines of the liquid observed in the present investigation agree closely with those reported by previous workers, excepting the lines  $231$  and  $2921\text{ cm}^{-1}$  which are not visible in the present spectrogram. The line  $2921\text{ cm}^{-1}$  together with the line  $2905\text{ cm}^{-1}$  reported by previous workers appears as a broad line at  $2917\text{ cm}^{-1}$  and four more lines of Raman shifts  $192$ ,  $261$ ,  $433$  and  $503\text{ cm}^{-1}$  are clearly visible in the spectrogram obtained in the present investigation.

It can be seen from Table III that the Raman lines  $567$  and  $2883\text{ cm}^{-1}$  due to pure propionyl chloride disappear with the solidification of the liquid. It is evident from these results that the liquid consists of two types of molecules one of which disappears with the solidification of the liquid. From a comparison with the results obtained in the infrared spectra of *n*-propyl halides in different states (Brown *et al.*, 1954b) the lines  $567$  and  $695\text{ cm}^{-1}$  may represent the C-Cl frequency of gauche and trans types of molecules respectively. The disappearance of the line  $567\text{ cm}^{-1}$  thus suggest the presence of only the trans isomer in the solid state. The infrared data of the compound in the solid state are not available, but similar changes are also expected in the case of the infrared spectra with solidification, because there is no centre of symmetry in the molecule.

Some significant changes take place also in some other Raman lines with the solidification of the liquid. The line  $2990\text{ cm}^{-1}$  splits up into two lines  $3006$  and  $2988\text{ cm}^{-1}$  and the lines  $695\text{ cm}^{-1}$  and  $1794\text{ cm}^{-1}$  shift to  $690\text{ cm}^{-1}$  and  $1788\text{ cm}^{-1}$  respectively. Also, three low-frequency Raman lines  $43$ ,  $53$  and  $97\text{ cm}^{-1}$  appear in the spectrum due to the solid. The changes are evidently due to weak intermolecular coupling in the solid state and the above results show that such coupling takes place through the chlorine and oxygen atoms of any molecule with the hydrogen atoms of the neighbouring molecules. The low-frequency lines also may be due to oscillations between weakly coupled molecules in the crystal. As pointed out by Mazumder (1959) the persence of only one form of molecule in the solid is also due to the consequence of such weak intermolecular coupling.



## B. Infrared spectra of solutions

The changes observed in the infrared bands of propionyl chloride on dissolving the liquid in  $\text{CCl}_4$ ,  $\text{CHCl}_3$ ,  $\text{CS}_2$  and *n*-hexane are indicated in Table IV by the underlined figures. The strength of the band  $670\text{ cm}^{-1}$  diminishes in comparison with that of the band  $690\text{ cm}^{-1}$  when the liquid is dissolved in the solvents mentioned above, but this change is more conspicuous in solutions in  $\text{CCl}_4$  and *n*-hexane than in the other two cases. The band  $690\text{ cm}^{-1}$  appears also in the Raman spectrum but the line  $670\text{ cm}^{-1}$  is absent in the Raman spectrum. The latter mode may be that of the associated molecule as pointed out by Mazumder (1958) and in that case the band  $690\text{ cm}^{-1}$  is due to the single molecule. It appears from the strength of the band  $690\text{ cm}^{-1}$  due to solutions that the solvents break up some of the associated molecules into single molecules. Table IV shows that the ratio of the strengths of the bands  $1300\text{ cm}^{-1}$  and  $1240\text{ cm}^{-1}$  also increases when the liquid is dissolved in the solvents. The band  $1300\text{ cm}^{-1}$  may therefore be assigned to a single molecule. The decrease in this frequency with association of the molecules indicates that hydrogen bonding with chlorine atom is responsible for the association.

## ACKNOWLEDGMENT

The author acknowledges his ever grateful indebtedness to Professor S. C. Sirkar, D.Sc., F.N.I., for his kind help and inspiring guidance throughout the progress of this work.

## REFERENCES

- Biswas, D. C., 1954, *Ind. J. Phys.*, **28**, 303.  
Brown, J. K. and Shoffard, N., 1950a, *Disc. Faraday Soc.*, **9**, 144.  
Brown, J. K. and Shoffard, N., 1955, *Proc. Roy. Soc., London*, **231A**, 555.  
Brown, J. K. and Shoffard, N., 1954, *Trans. Faraday Soc.*, **50**, 116A.  
Dob, K. K., 1960, *Ind. J. Phys.*, **34**, 247.  
Mazumder, M., 1959, *Ind. J. Phys.*, **33**, 92.  
Mazumder, M., 1958, *Ind. J. Phys.*, **32**, 451.  
Mizushima, S. and Morino, Y., 1938, *Proc. Ind. Acad. Sci.*, **8A**, 315.

# ELECTRONIC SPECTRA OF $\beta$ -CHLORONAPHTHALENE IN DIFFERENT STATES\*

T. N. MISRA

OPTICS DEPARTMENT,

INDIAN ASSOCIATION FOR THE CULTIVATION OF SCIENCE,  
CALCUTTA-32.

(Received April 19, 1962)

**ABSTRACT.** The near ultraviolet absorption spectra of  $\beta$ -chloro-naphthalene have been studied in the vapour and liquid phases and in the solid state at 32°C and -180°C. The substance yields two systems of bands in the near ultraviolet region, one due to  $A_{1g} - B_{3u}$  and the other due to  $A_{1g} - B_{2u}$  transition. It has been observed that the substitution of chlorine atom in the  $\beta$ -position in the naphthalene ring shifts the weak first system by 700  $\text{cm}^{-1}$  towards the red and the strong second system only by 340  $\text{cm}^{-1}$ . Further, on liquefaction of the vapour of  $\beta$ -chloronaphthalene, the 0,0 band of the first system is shifted by only 351  $\text{cm}^{-1}$  towards red, whereas in the case of the second system the shift is 1343  $\text{cm}^{-1}$ . When the liquid is solidified, the 0,0 band of either of the systems appears to be split up into three components by the crystal fields at the room temperature and the split components become sharper when the crystals are cooled to -180°C. It has been suggested that the interaction between transition moment and the permanent dipoles of neighbouring molecules might be responsible for the large splitting observed in this case, because the Davydov-splitting is expected to be too small to account for such a large splitting.

## INTRODUCTION

The near ultraviolet absorption spectrum of naphthalene in the vapour state shows two distinct systems of bands in the regions 3200Å--2900Å and 2750Å--2500Å, and a third system extending from 2250Å to shorter wave lengths. The first system is weak and is now established to be due to  $A_{1g} - B_{3u}$  transition with the transition moment along the long axis of the molecule. The stronger second system on the short wavelength side is due to  $A_{1g} - B_{2u}$  transition, the transition moment being along the short axis of the molecule, and the third system is due to  $A_{1g} - B_{3u}^+$  transition (McClure, 1954, '59, McClure and Schnepf, 1955; Baba and Suzuki, 1961). The energies calculated theoretically by Praiser (1956) seem to agree with the observed values.

In the case of monosubstituted naphthalenes the substitution reduces the symmetry  $D_{2h}$  of naphthalene to  $C_2$ . However, the energy levels of the derivatives may be denoted by the analogy of the notation for the corresponding quantities of the parent hydrocarbon. Thus Baba and Suzuki (1961) designated the lowest excited state of the derivatives as  $B_{3u}$ . It was observed by many

\*Communicated by Prof. S. C. Sirkar.

previous workers that the substitution shifts the band systems towards longer wavelengths.

Data furnishing the information about the influence of intermolecular field of the crystal lattice on the electronic states of molecule of monosubstituted naphthalenes are meagre. Deb (1954) and Banerjee (1956) studied the ultraviolet absorption spectra of a few monosubstituted naphthalenes in different states in order to find out the influence of intermolecular field on the spectra.

The ultraviolet absorption spectra of  $\beta$ -chloronaphthalene in hexane solution was first studied by de Lazlo (1926). Recently, Ferguson (1954) studied the ultraviolet absorption spectrum of  $\beta$ -chloronaphthalene dispersed in rigid glass medium at  $-180^{\circ}\text{C}$ . The influence of intermolecular field on the absorption spectrum of  $\beta$ -chloronaphthalene had not been investigated earlier. The present work was, therefore, undertaken to study the absorption spectra of this substance in the liquid state and in the solid state at room temperature and at low temperature and to compare the results with those for the vapour in order to find out the influence of intermolecular field in the lattice.

#### EXPERIMENTAL

The experimental set-up was the same as described in an earlier paper (Misra, 1960). Chemically pure  $\beta$ -chloronaphthalene was repeatedly crystallised from solution in alcohol and the crystals were further purified by vacuum sublimation before use. For studying the absorption spectrum of the vapour, a 50 cm long absorption tube was used. The temperature of the bulb containing the substance was kept at  $120^{\circ}\text{C}$  to record the first system and at  $40^{\circ}\text{C}$  to record the second system, the temperature of the absorption tube being always kept at about  $10^{\circ}\text{C}$  above that of the bulb.

Thin films of substance of thickness of the order of a few microns were required to produce bands in the liquid and solid states. The spectrograms were taken on Agfa Isopan films with a Hilger E1 spectrograph giving a dispersion of about  $3\text{\AA}$  per mm in the  $2600\text{\AA}$  region. Microphotometric records were taken with a Kipp and Zonen Moll microphotometer and the absorption spectra were calibrated with the help of microphotometric records of iron arc spectrum photographed on each spectrogram as explained in an earlier paper (Sirkar and Misra, 1959).

#### RESULTS AND DISCUSSIONS

The microphotometric records of the absorption spectra are reproduced in Figs. 1, 2 and 3. The wave numbers of the bands with their approximate visual intensities and probable assignments are given in Tables I and II.

It can be seen from the figures as well as from Tables I and II that the absorption spectrum of  $\beta$ -chloronaphthalene consists of two groups of bands. The relative intensities of the bands in the two groups clearly indicate that they

constitute two separate systems. The feeble group of bands on the long wavelength side was called Part I by de Lazlo (1926) while the other group was called Part II. In this paper, they are designated as the first system and the second system of bands respectively. The results obtained are discussed in the following paragraphs.

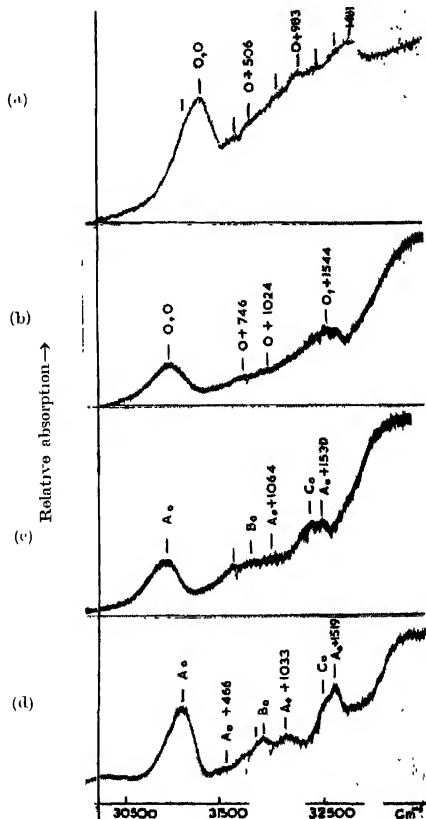


Fig. 1. Microphotometric records of ultraviolet absorption bands of  $\beta$ -chloronaphthalene (First system)

- (a) vapour phase. (b) liquid at  $70^{\circ}\text{C}$  (c) solid at  $32^{\circ}\text{C}$ . (d) solid at  $-180^{\circ}\text{C}$ .  
(a) Spectrum due to the vapour phase.

When a 50 cm long absorption tube is used the strong system (second system) appears in the region  $35000\text{ cm}^{-1}$  –  $37500\text{ cm}^{-1}$  at the saturation vapour

pressure of the substance at 40°C. When the temperature of the substance is raised to 120°C the weak system (first system) makes its appearance at the saturation vapour pressure of the substance at this temperature in the region from 31000  $\text{cm}^{-1}$  to 33000  $\text{cm}^{-1}$ .

In the first system, eight prominent bands have been observed, the strong 0,0 band is at 31311  $\text{cm}^{-1}$ . The other bands can be analysed in terms of excited state vibrational frequencies 365, 506, 745, 983, 1150 and 1481  $\text{cm}^{-1}$  respectively. There is a weak band at 32641  $\text{cm}^{-1}$  which is at a distance of 1330  $\text{cm}^{-1}$  from the 0,0 band. Though there is a strong Raman frequency 1386  $\text{cm}^{-1}$  to which this frequency may correspond in the excited state, no such frequency was observed in the rigid glass solution at -180°C. Thus it is probable that this is a  $\nu-\nu'$  transition represented as 0+1481-150. The occurrence of the hump at 31161  $\text{cm}^{-1}$  (0-150) on the long wavelength side of the 0,0 band supports this assignment. Recently, Craig *et al.* (1959) studied the first system in the spectrum due to naphthalene vapour and observed that the system has three interpenetrating sets of bands, with the 0,0 band at 32020  $\text{cm}^{-1}$ . Thus the 0,0 band of this system is shifted by 709  $\text{cm}^{-1}$  towards longer wavelength by the substitution of chlorine atom in the  $\beta$ -position.

In the second system about twenty prominent bands are observed. The transition being allowed, a strong 0,0 band is expected in this case and the very strong band at 35497  $\text{cm}^{-1}$  was taken as the 0,0 band of this system. Craig did not study the second system of naphthalene vapour. Hourri and de Lazlo (1924) studied the spectrum of naphthalene vapour and from the spectrum reproduced by them it appears that the 0,0 band of the second system of naphthalene in the vapour phase is at 35844  $\text{cm}^{-1}$ . Thus this system is shifted by only 347  $\text{cm}^{-1}$  towards red due to the substitution.

The other bands of the system may then be explained in terms of frequencies 190 and 417  $\text{cm}^{-1}$  in the ground state and 117, 409, 528, 858, 1149, 1324, 1419 and 1556  $\text{cm}^{-1}$  in the excited state as shown in Table 1. The Raman frequencies of the substance as reported in Landolt and Bornstein's Tables

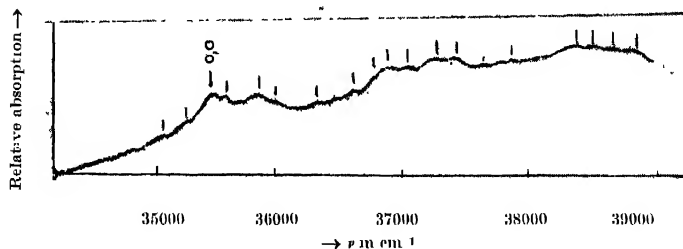


Fig. 2. Microphotometric record of absorption spectra of  $\beta$ -chloronaphthalene in the vapour phase. (Second system)

(1952) are 282(1), 355(3), 415(2), 516(4), 533(4), 769(5), 863(3), 949(2), 1017(2), 1086(2), 1153(1), 1248(2), 1386(10), 1433(4), 1458(3), 1570(7), 1624(2), 2927(2) and 3052(3)  $\text{cm}^{-1}$ , the intensities being given in the parentheses. It can be seen that the frequencies observed in the present investigation agree fairly well with the reported Raman frequencies.

TABLE I

Ultraviolet absorption bands of  $\beta$ -chloronaphthalene in the vapour phase

Wave Number and Intensity	Assignment	Wave Number and Intensity	Assignment
First system		Second system	
31161 (vw)	0 $\rightarrow$ 365 - 516	35080 (m)	0 - 417
31311 (vs)	0,0	35307 (m)	0 - 190
31676 (m)	0 $\rightarrow$ 365	35497 (vs)	0,0
31817 (w)	0 $\rightarrow$ 506	35614 (m)	0 $\rightarrow$ 117
32056 (w)	0 $\rightarrow$ 745	35906 (vs)	0 $\rightarrow$ 409
32234 (m)	0 $\rightarrow$ 983	36025 (m)	0 $\rightarrow$ 528
32461 (m)	0 $\rightarrow$ 1150	36355 (m)	0 $\rightarrow$ 858
32641 (w)	0 $\rightarrow$ 1330	36646 (m)	0 $\rightarrow$ 1149
	0 $\rightarrow$ 1481 + 365 - 516	36821 (m)	0 $\rightarrow$ 1324
32792 (vs)	0 $\rightarrow$ 1181	36916 (vs)	0 $\rightarrow$ 1419
		37053 (m)	0 $\rightarrow$ 1556
		37316 (vs)	0 $\rightarrow$ 409 $\rightarrow$ 1419
		37464 (s)	0 $\rightarrow$ 409 + 1556
		38349 (vs)	0 $\rightarrow$ 2 $\times$ 1419
		38460 (m)	0 $\rightarrow$ 2 $\times$ 1419 $\rightarrow$ 117
		38757 (s)	0 $\rightarrow$ 2 $\times$ 1419 $\rightarrow$ 409

The excited state frequencies 365, 506, 745, 983, 1150 and 1481  $\text{cm}^{-1}$  observed in the first system probably correspond to the Raman frequencies 415, 533, 769, 1017, 1153 and 1570  $\text{cm}^{-1}$  respectively.

The excited state frequencies 409, 528, 858, 1149, 1324 and 1556  $\text{cm}^{-1}$  observed in the second system probably correspond to the Raman frequencies 415, 533, 863, 1153, 1386 and 1570  $\text{cm}^{-1}$  respectively in the ground state. The Raman frequency 415  $\text{cm}^{-1}$  agrees well with the ground state frequency 417  $\text{cm}^{-1}$  observed in the present investigation as  $v \rightarrow 0$  transition. No Raman frequency corresponding to the upper state fundamental 117  $\text{cm}^{-1}$  was reported; this, however, may correspond to the ground state frequency 190  $\text{cm}^{-1}$  observed in the present

investigation as  $v \rightarrow 0$  transition. There are two moderately strong Raman lines  $1433 \text{ cm}^{-1}$  and  $1458 \text{ cm}^{-1}$ , but only one upper state fundamental  $1419 \text{ cm}^{-1}$  is observed in the second system.

(b) *Spectra due to the liquid and solid states.*

(i) *Bands of the first system*

In the liquid state at  $70^\circ\text{C}$ , the 0, 0 band is at  $30960 \text{ cm}^{-1}$  and its position is shifted towards red by  $351 \text{ cm}^{-1}$  from that in the case of the vapour. Though the band with excited state vibrational frequency  $1544 \text{ cm}^{-1}$  is still prominent, the bands with other vibrational frequencies seem to merge into a broad envelope. This is evidently due to the fluctuation of intermolecular field and consequent broadening of the bands caused by thermal motion of molecules in the liquid state.

When the liquid is frozen at room temperature, the 0,0 band shifts further to  $30941 \text{ cm}^{-1}$ . The bands become sharper and those bands at distances  $696 \text{ cm}^{-1}$ ,  $866 \text{ cm}^{-1}$ ,  $1064 \text{ cm}^{-1}$ ,  $1446 \text{ cm}^{-1}$  and  $1530 \text{ cm}^{-1}$  from the 0, 0 band are well resolved.

When the crystals are cooled to  $-180^\circ\text{C}$ , the bands become still sharper. The strong band at  $31085 \text{ cm}^{-1}$  can be easily recognised as the 0, 0 band of the system. The other bands are at distances  $466 \text{ cm}^{-1}$ ,  $740 \text{ cm}^{-1}$ ,  $831 \text{ cm}^{-1}$ ,  $1033 \text{ cm}^{-1}$ ,  $1407 \text{ cm}^{-1}$  and  $1519 \text{ cm}^{-1}$  respectively from the 0,0 band.

On comparing the spectrum due to the crystals with that due to the substance in the vapour state some differences are observed. In the latter spectrum there is no sharp rise in the strength of absorption beyond  $32792 \text{ cm}^{-1}$  while in the former spectrum the absorption curve rises sharply beyond  $32604 \text{ cm}^{-1}$ . Moreover, the wave number difference between the bands in the vapour phase do not agree with the corresponding differences in the spectrum due to crystals. A band at a distance of  $839 \text{ cm}^{-1}$  from the 0, 0 band was observed in the spectrum due to crystals at  $-180^\circ\text{C}$ , but no such frequency was observed in the vapour phase or in the rigid glass solution (Ferguson, 1954). Thus it seems that this may be one of the components of the 0, 0 band which is split up in the crystal field. The bands on the shorter wavelength side of the 0, 0 band in the case of the vapour are stronger than those due to the crystal at  $-180^\circ\text{C}$ . In the spectrum due to crystals at  $-180^\circ\text{C}$ , there is a band at  $32492 \text{ cm}^{-1}$ , which is at a distance of  $1407 \text{ cm}^{-1}$  from 0, 0 band. There is no corresponding band in the spectrum due to the vapour. Hence this band may be another component of the 0, 0 band. The analysis is made on this assumption. It may be pointed out here that in the spectrum of the crystal at  $32^\circ\text{C}$  similar splitting is observed and therefore the phenomenon is not due to any strain in the crystal.

(ii) *Bands of the second system.*

In the liquid state only five broad envelopes are observed in this system. On comparing this spectrum with that due to the substance in the gaseous state,

TABLE II

Ultraviolet absorption bands of  $\beta$ -chloronaphthalene

	Liquid at 70°C		Solid at 32°C		Solid at -180°C	
	Wave Number and Intensity	Assignment	Wave Number and Intensity	Assignment	Wave Number and Intensity	Assignment
First system	30960 (s)	0,0	30941 (s)	A <sub>0</sub>	31085 (vs)	A <sub>0</sub>
	31706 (vw)	0 + 746	31637 (niw)	A <sub>0</sub> + 696	31551 (vw)	A <sub>0</sub> + 406
	31984 (vw)	0 + 1024	31807 (m)	B <sub>0</sub>	31825 (m)	A <sub>0</sub> + 740
	32504 (s)	0 + 1544	32005 (m)	A <sub>0</sub> + 1064	31924 (s)	B <sub>0</sub>
			32387 (mw)	C <sub>0</sub>	32118 (s)	A <sub>0</sub> + 1033
			32471 (s)	A <sub>0</sub> + 1530	32492 (mw)	C <sub>0</sub>
					32604 (s)	A <sub>0</sub> + 1519
Second system	34154 (m)	0,0	33624 (m)	A <sub>0</sub>	33578 (s)	A <sub>0</sub>
	34556 (m)	0 + 402	34034 (s)	A <sub>0</sub> + 410	33988 (s)	A <sub>0</sub> + 410
	35003 (m)	0 + 849	34108 (s)	B <sub>0</sub>	34002 (s)	B <sub>0</sub>
	35639 (s)	0 + 1485	34518 (m)	B <sub>0</sub> + 410	34472 (m)	B <sub>0</sub> + 410
	36478 (s)	0 + 849	34979 (bs)	C <sub>0</sub>	34881 (vs)	C <sub>0</sub>
		+ 1485	35034 (s)	A <sub>0</sub> + 1410	34991 (vs)	A <sub>0</sub> + 1410
			35389 (s)	C <sub>0</sub> + 110	35295 (s)	C <sub>0</sub> + 410
	37108 (s)	0 + 2 × 1485	35518 (s)	B <sub>0</sub> + 1410	35472 (ms)	B <sub>0</sub> + 1410
			36389 (m)	C <sub>0</sub> + 1410	36291 (s)	C <sub>0</sub> + 1410

it seems that the first envelope in the spectrum of the substance in the liquid state is due to the broadening of the 0, 0 band and the overlapping of this band on the band with excited state frequency 409  $\text{cm}^{-1}$  in the vapour phase. Thus the edge of the first envelope at 34154  $\text{cm}^{-1}$  seems to be the position of the 0, 0 band. Then the prominent excited state frequency 409  $\text{cm}^{-1}$  in the vapour phase is in the first envelope. The excited frequency 825  $\text{cm}^{-1}$  in the vapour phase may be traced in the second envelope. The third strong band is at a distance of 1485  $\text{cm}^{-1}$  from the position of the 0, 0 band and this evidently is the mean of the two excited state frequencies 1419  $\text{cm}^{-1}$  and 1556  $\text{cm}^{-1}$  in the gaseous state. The fourth envelope is a combination of the bands with upper state fundamentals 849  $\text{cm}^{-1}$  and 1485  $\text{cm}^{-1}$ , whereas the higher harmonic of 1485  $\text{cm}^{-1}$  may be identified with the fifth envelope. Thus the structure of the band system in the spectrum of the liquid may be attributed to the broadening of the bands due to the fluctuation of the intermolecular field and their consequent overlapping as discussed in the case of the first system.



When the substance is solidified at room temperature, not only the bands in the spectrum of the solid become stronger and some of the bands are resolved but also the structure of the spectrum appears to differ considerably from that due to the substance in the vapour phase. The 0, 0 band in the spectrum of the vapour seems to have been replaced by three bands at  $33624\text{ cm}^{-1}$ ,  $34108\text{ cm}^{-1}$  and  $34979\text{ cm}^{-1}$  in the spectrum due to the crystal at the room temperature. The other bands can then be explained in terms of excited state frequencies  $410$  and  $1410\text{ cm}^{-1}$  as shown in Table II. It may be assumed that the 0, 0 band due to free molecules in the vapour phase has been split up by the influence of the crystal field and the three components of the 0, 0 band are shifted by  $518\text{ cm}^{-1}$ ,  $1389\text{ cm}^{-1}$  and  $1873\text{ cm}^{-1}$  respectively towards red from the position

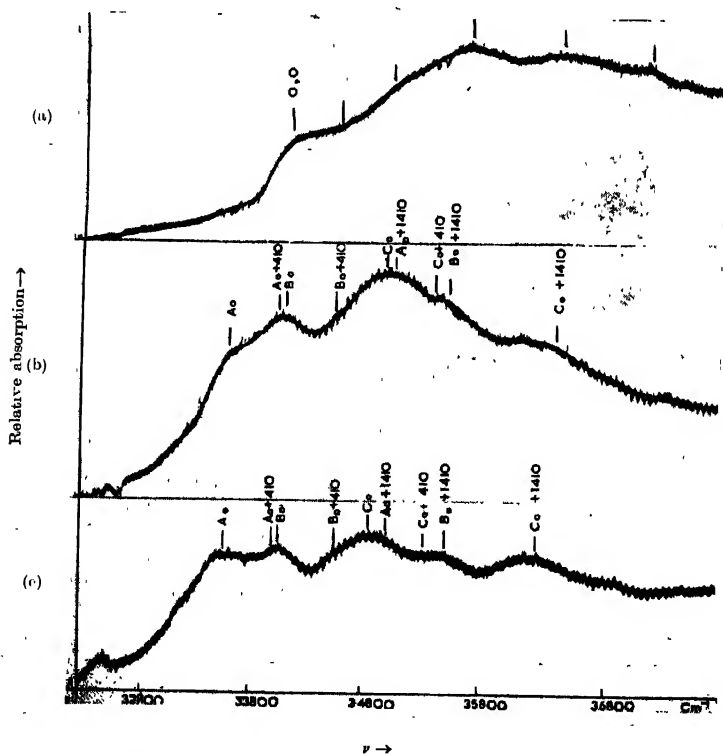


Fig. 3. Microphotometric records of ultraviolet absorption bands of  $\beta$ -chloronaphthalene. (Second system)

(a) liquid at  $70^\circ\text{C}$ . (b) solid at  $32^\circ\text{C}$ . (c) solid at  $-180^\circ\text{C}$ .

of the 0, 0 band due to the substance in the gaseous state. The split components are denoted by  $A_0$ ,  $B_0$  and  $C_0$  in Table II.

On further lowering the temperature of the crystals to  $-180^\circ\text{C}$  only some minor changes in the structure of the spectrum are observed. The bands become stronger and particularly  $A_0$  component of the 0, 0 band becomes sharper appreciably and the bands are slightly shifted towards red. The three components of the 0, 0 band are now at  $33578\text{ cm}^{-1}$ ,  $34062\text{ cm}^{-1}$  and  $34881\text{ cm}^{-1}$  respectively. The other bands can then be explained in terms of excited state frequencies  $410\text{ cm}^{-1}$  and  $1410\text{ cm}^{-1}$  as in the case of the crystals at the room temperature. In the spectra due to the crystals at room temperature and also at  $-180^\circ\text{C}$ , the  $B_0$  component of the 0,0 band and the band  $A_0+410\text{ cm}^{-1}$  coalesce to form a broad band, the  $C_0$  component of the 0, 0 band and the bands  $B_0+410$  and  $A_0+1410$  merge into one another to form a strong broad band. Similarly, the bands  $C_0+410$  and  $B_0+1410$  form a band of medium strength. It is also seen that on cooling the crystals to  $-180^\circ\text{C}$ , a further red shift of the components of the 0, 0 band by about  $46\text{ cm}^{-1}$  takes place.

It can be seen from the tables that the two systems of bands due to the crystals behave differently with change of temperature of the crystals. In the spectrum of the crystals at room temperature, the shift of the  $A_0$  component of the 0, 0 band of the first system towards red is  $370\text{ cm}^{-1}$  from the 0, 0 band of free molecules whereas in the case of the crystal at  $-180^\circ\text{C}$ , the shift is only  $226\text{ cm}^{-1}$  in the same direction. Thus, with the lowering of temperature of the crystals, the  $A_0$  component of the 0, 0 band in the latter case shows a blue shift of about  $144\text{ cm}^{-1}$ . In the case of the second system of bands, the red shift of the  $A_0$  component in the spectrum of the crystals at room temperature with respect to the 0, 0 band of the vapour phase is as large as  $1873\text{ cm}^{-1}$  but the effect of cooling the crystals to  $-180^\circ\text{C}$  produces a very small red shift of about  $46\text{ cm}^{-1}$ . Incidentally, it may be pointed out that in the rigid glass solution at  $-180^\circ\text{C}$ , the red shift of the 0, 0 band of the second system with respect to the band of the vapour is only about  $240\text{ cm}^{-1}$  (Ferguson, 1954) whereas in the case of the crystals at  $-180^\circ\text{C}$  the shift is  $1919\text{ cm}^{-1}$  for the  $A_0$  component. This shows that the interaction between molecules in the lattice plays a dominant role in determining the energy levels of molecules in the crystals.

The crystals of  $\beta$ -chloronaphthalene contains four molecules per unit cell (Neuhaus, 1939) and it belongs to the monoclinic system. Winston (1951) has put forward a theory of the splitting of electronic energy level in molecular crystals with nonpolar molecules. Fox and Schnepf (1955) applied the theory to find out the energy level in the crystals of benzene in which there are four molecules per unit cell. They found that each of the  $B_{1u}$  and  $B_{2u}$  states of the free molecule gives three allowed transitions polarised along the three axes of the crystal. The molecules of benzene are centrosymmetrical while those of  $\beta$ -chloronaphthalene

are not so and it has also a permanent dipole. Hence the theory mentioned above cannot be applied direct in the present case.

In the case of naphthalene, the short axis transition should exhibit a Davydov splitting less than  $15\text{ cm}^{-1}$  (Craig and Walsh, 1956) and the long axis transition exhibits a splitting of  $160\text{ cm}^{-1}$  (McClure, 1959). The calculated Davydov splitting for this transition due to dipole-dipole interaction is less than  $20\text{ cm}^{-1}$  (McClure, 1959). This discrepancy has been explained by McClure by suggesting that the interaction may be of octupole-octupole type in this case. However, the work of Broude *et al.* (1957) shows that the splitting is absent in strain free crystals. Hence it appears that in the case of absorption bands of the crystals with low oscillator strength Davydov's theory cannot be applied as pointed out by Sirkar (1961). The large splitting in the case of  $\beta$ -chloronaphthalene probably indicates that the interaction between the transition moment and the permanent dipole of the neighbouring molecules plays a dominant role in producing the splitting of molecular energy levels in the crystal field (Sirkar, 1961). As the exact orientation of molecules of  $\beta$ -chloronaphthalene in the crystal lattice is not known, it was not possible to calculate the magnitude of Davydov splitting in the present case.

#### ACKNOWLEDGMENT

The author is grateful to Professor S. C. Sirkar, D.Sc., F.N.I., for his kind interest and guidance in the work. Thanks are also due to Dr. G. S. Kastha, D.Sc., for many helpful discussions.

#### REFERENCES

- Babu, H. and Suzuki, S., 1961, *Bull. Chem. Soc. Japan.*, **34**, 82.  
 Banerjee, S. B., 1956, *Ind. J. Phys.*, **30**, 106.  
 Broude, V. L., Pakhomov, O. S. and Prikhodjko, A. F., 1957, *Optika i Spektroskopiya*, **2**, 323.  
 Craig, D. P. and Walsh, J. R., 1956, *J. Chem. Phys.*, **24**, 471.  
 Craig, D. P., Hollas, J. M., Redies, M. F. and Wail, S. C., 1959, *Proc. Chem. Soc. London.*, 362.  
 Deb, A. R., 1954, *Ind. J. Phys.*, **28**, 21.  
 De Lazlo, H. G., 1926, *Proc. Roy. Soc., A* **111**, 355.  
 Ferguson, J., 1954, *J. Chem. Soc.*, 304.  
 Fox, D. and Schnepf, O., 1955, *J. Chem. Phys.*, **23**, 767.  
 Henri, and de Lazlo, H. G., 1924, *Proc. Roy. Soc., A* **105**, 662.  
 Landolt and Bornstein Table, 1951, Vol. 2, 525.  
 McClure, D. S., 1954, *J. Chem. Phys.*, **22**, 1668.  
 McClure, D. S. and Schnepf, O. P., 1955, *J. Chem. Phys.*, **23**, 1575.  
 McClure, D. S., 1959, *Solid State Physics*, Vol. 8, 1.  
 Misra, T. N., 1960, *Ind. J. Phys.*, **34**, 381.  
 Neuhaus, A., 1939, *Z. Krist.*, **101**, 177.  
 Praiser, R., 1956, *J. Chem. Phys.*, **24**, 250.  
 Sirkar, S. C., 1961, *Proc. Natl. Inst. Sc. of India*, **27A**, 568.  
 Sirkar, S. C. and Misra, T. N., 1959, *Ind. J. Phys.*, **33**, 45.  
 Winston, H., 1951, *J. Chem. Phys.*, **19**, 156.

# MAXIMUM SUPERHEAT OF BINARY LIQUID MIXTURES

A. K. JALALUDDIN AND D. B. SINHA

DEPARTMENT OF APPLIED PHYSICS, CALCUTTA UNIVERSITY COLLEGE OF  
TECHNOLOGY, CALCUTTA-9, INDIA

(Received April 2, 1962)

**ABSTRACT.** Maximum superheat temperature attainable by binary liquid mixtures at different concentrations of the components has been experimentally determined. The mixtures studied were chloroform-ethanol, methanol-carbon tetrachloride, benzene-*n*-propanol, benzene-isopropanol, carbon disulphide-chloroform, acetone-chloroform, methanol-benzene and carbon tetrachloride-benzene. The change in maximum superheat with concentration of the mixture has been shown graphically and the difficulties of theoretically calculating the results have been discussed.

## INTRODUCTION

The maximum temperature to which a liquid can be raised at atmospheric pressure without giving rise to ebullition may be calculated to a good degree of approximation from the Van der Waals equation of state. The equations for the rate of homogeneous nucleation in liquids deduced by Volmer (1939), Döring (1937), Frenkel (1946) and others on the basis of statistical mechanics are, however, more appropriate to the liquid state. The values of the limit of superheat for pure liquids obtained experimentally agree reasonably well with the predictions made from these equations. But no theoretical equation is available for calculating the limit of superheat of mixtures. This is mainly due to the complexities of the intermolecular forces involved in such cases, as also due to the effect of solvation and association. van Laar's (1910) method of calculating the critical constants of mixtures from the corresponding values of the pure components is of no avail, for the critical temperature of a mixture is experimentally found to differ strongly from the value obtained for that concentration from the straight line joining the critical temperatures of the two components. A relation of the type of van Laar may, however, be roughly applicable for simple mixtures having the critical temperature of the two components near each other. Theoretical determination of the superheat limits for mixtures is also not possible from the application of Volmer's equation because of the deviation of the values of surface tension and heat of vaporisation for such mixtures from those obtainable from the theoretical additivity rule. In the case of the simple binary mixture, benzene-carbon tetrachloride, the surface tension-concentration curve is practically a straight line (Belton, 1935) so is the mean curve for the maximum superheat as found from the experimental results reported here. This seems to be in conformity with the

Volmer's theory of nucleation according to which the work function for the formation of a vapour bubble is to be largely influenced by the surface tension of the liquid.

#### EXPERIMENTAL METHOD

Experiments on the direct determination of superheat always involve either a solid-liquid interface (Wismer *et al.*, (1922), or a liquid-liquid interface (Wakeshima and Takata, 1958) which introduces a heterogeneity in the system. But it appears that such heterogeneity has but little effect on the results when the angle of contact at the interface is nearer to zero. Recently we devised a method (Saha and Jalaluddin, 1961) of measuring the superheat of stagnant liquid films at a degassed glass-liquid interface in the steady state of heat transfer. The bulk of the liquid was maintained at the boiling point. The steady heat input to the heater was gradually raised by steps and the temperature of the liquid layer at the outer surface of the bulb was calculated from the steady temperature of mercury with which the bulb was filled.

Since a system consisting of two miscible liquids in equilibrium with the vapour has two degrees of freedom the composition of the mixture has to be kept constant by suitable control device so as to maintain the vapour pressure and consequently the boiling point of the mixture constant.

In this method the bulk temperature of the mixture at different compositions was kept very near to the boiling point with the help of a jacketing liquid. For this purpose auxiliary heating or cooling circuits were used according to necessity.

The container was sealed with a rubber cork provided with holes for admission of the heater tube, thermometer and condenser. Ice-cold water was circulated through the jacket of the condenser for recovery of the vapour issuing from the mixture. The liquid level in the container remained almost constant during any set of experiments. All measurements with any particular binary mixture were carried out keeping the same heating glass surface always immersed in the mixture in order to avoid the possibility of any change in the surface condition of the heater. The composition of the mixture was gradually changed after each set of experiments by slowly pouring either liquid through the reflex condenser during the nucleate boiling of the mixture. This helped a thorough mixing of the components and degassing of the liquid drops.

The maximum superheat temperature was generally found to be reproducible within 2 to 3°C. In the steep portions of the curves a small variation in the composition of the mixture, however, gave a larger change in the maximum superheat temperature and this range was found to increase slightly. On the whole it was an improvement over the earlier results (Sinha and Jalaluddin, 1961) and it was achieved through greater refinements introduced in the stabilisation

of the current supply to the heater, and in the temperature control device. The maximum superheat temperature at different concentrations were obtained from a set of about ten runs for each. It should be noted, since a very thin interfacial layer of the liquid is superheated (bulk liquid remaining at the boiling point) in the present method, dust particles are not likely to become active centres of nucleation.

## RESULTS

Maximum superheat temperature,  $T_m$ , of eight binary liquid mixtures were measured at different concentrations,  $x$ , of the components. These mixtures include cases of both positive and negative deviations from Raoult's law (azeotropes of both kinds) and of polar-polar, polar-nonpolar and nonpolar-nonpolar components. These are respectively ethanol-chloroform, benzene-isopropanol, acetone-chloroform, methanol-carbon tetrachloride, benzene-*n*-propanol, carbon disulphide-chloroform, and carbon tetrachloride-benzene and methanol-benzene. Of these mixtures the familiar negative mixture of acetone-chloroform and also methanol-benzene were found not to withstand superheat by more than 30°–50°C at higher concentration of the components. The other results have been shown graphically in the figure. The values of the maximum superheat of pure liquids used here are those obtained by us experimentally and reported partially before (Sinha and Jalaluddin, 1961). They are, excepting the case of carbon tetrachloride for which no other experimental value seems to have been reported in the literature, comparable to those of Wismer *et al.* and of Wakeshima and Takata.

## DISCUSSION

It is evident from the results that the superheat limit of a component A does not change appreciably at low concentrations of the other component B until the concentration of the latter reaches a value of about 20-50 mole%. For carbon tetrachloride-benzene which is a non polar-nonpolar mixture, the superheat vs concentration curve follows almost a linear relationship, i.e. the maximum superheat steadily approaches the limiting value of either of the pure components with the increase of the corresponding concentration. All the other curves deviate from this behaviour. The polar-nonpolar mixtures of methanol-carbon tetrachloride and isopropanol-benzene for which the superheat limits of the components are widely different, show sharp changes in maximum superheat values in the concentration range of 25-50 mole % of either of the components. A similar pattern of behaviour is obtained in the case of the polar-polar mixture, ethanol-chloroform, the components having widely different superheat limits. The curves for the mixtures chloroform-carbon disulphide and benzene-*n*-propanol (polar-nonpolar) for which the maximum superheats of the components are almost equal are concave upwards. The pattern of behaviour remained unchanged in

the case of the azeotropic mixtures also (86 mole% chloroform+14 mole % ethanol, and 39.3 mole % isopropanol+60.7 mole % benzene).

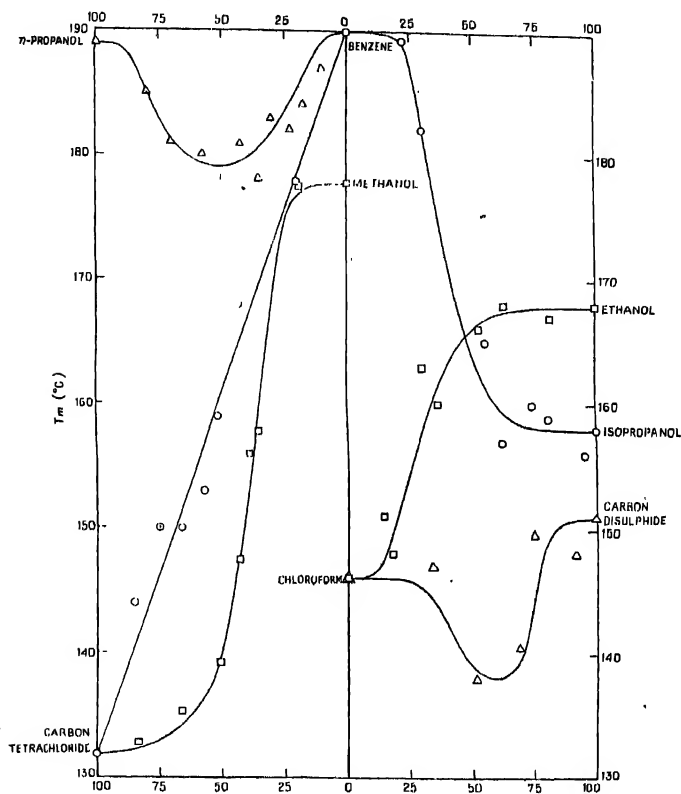


Fig. 1. Maximum superheat temperature ( $T_m$ ) as function and composition ( $x$  in mole %) of six binary liquid mixtures.

The acetone-chloroform and methanol-benzene mixtures differ from the others investigated in not being able to withstand any appreciable superheat. It may be noted in this connection that the excess free-energy, excess-heat and excess entropy for the former combination of components are all negative and the excess volume is also negative except for mixtures weak in chloroform (Rowlinson, 1959).

From the experimental results it seems possible to distinguish a few mixtures which are able to withstand high superheat from those which did not. It was

also possible in most of the cases to ascertain qualitatively the nature of  $T_m-x$  curves. These curves resemble  $T_c-x$  curves of some of the binary liquid systems (Rowlinson, 1959). Much lower values of  $T_m$  at higher  $x$  of the additives in the case of chloroform-acetone and methanol-benzene, though could not be confirmed to be due to any known thermodynamic function, might be supposed to be an indication of phase separation of the mixtures; the possibility of such behaviour in the case of methanol-benzene has been discussed by Starobinets *et al.* (1951).

The above study seems to have importance in connection with the heat transfer properties of binary mixtures, and the characteristics of bubble chambers using binary mixtures, and also for elucidation of the nature of the intermolecular forces and other physical properties of binary liquid mixtures.

#### ACKNOWLEDGMENT

The authors would like to thank Sri Mihir Sengupta, Department of Physical Chemistry, University of Calcutta, for helpful discussions.

#### REFERENCES

- Belton, J. W., 1935, *Trans. Faraday Soc.*, **31**, 1642.
- Doring, W., 1937, *Z. Phys. Chem.*, **36**, 37.
- Frenkel, J., 1946, "Kinetic Theory of Liquids", Oxford U.P.
- Kerrick, F. B., Gilbert, C. S. and Wismer, K. L., 1924, *J. Phys. Chem.*, **28**, 1297.
- Rowlinson, J. S., "Liquids and Liquid Mixtures", p. 182, Butterworths Scientific Publications, 1959.
- Sinha, D. B., and Jalaluddin, A. K., 1961, *Ind. J. Phys.*, **35**, 311.
- Starobinets, G. L., Starobinets, K. S., and Ryzhukova, L. A., 1951, *Zhur. fiz. Khim.*, **25**, 1186.
- van Laar, J. J., 1910, *Z. Physik. Chem.*, **72**, 723.
- Volmer, M., 1939, "Kinetik der Phasenbildung", Steinfelt, Dresden and Leipzig.
- Wisner, K. L., 1922, *J. Phys. Chem.*, **26**, 301.
- Wakeshima, H. and Takata, K., 1958, *J. Phys. Soc., Japan*, **13**, 1398.



# ON CLASSIFICATION OF SWITCHING FUNCTIONS

## Part I

A. K. CHOUDHURY AND M. S. BASU

INSTITUTE OF RADIO PHYSICS AND ELECTRONICS,  
UNIVERSITY OF CALCUTTA

(Received December 20, 1961)

**ABSTRACT.** The geometrical concept of representation of switching functions as nodes of unit  $n$ -dimensional cube has been utilised for developing the necessary and sufficient conditions for two functions to belong to the same equivalence class. A systematic procedure for testing the equivalence between two given functions has been presented. A method of finding out the operations required for transforming one function into another of the same equivalence class has been suggested.

### 1. INTRODUCTION

It is a well-known idea that the terms (i.e., minterms) of any switching function of  $n$ -variables can be represented by the nodes of a unit  $n$ -cube (Hamming, 1950; Lee, 1954; Svoboda, 1957; Urbano and Mueller, 1956). The unit  $n$ -cube is made up of cells of different dimensions. A switching function may be interpreted as a collection of nodes of the unit  $n$ -cube. Any function and its complement has a certain geometrical structure depending on the nodes that go to form the function. The cell structure of any function and also its complementary function remain invariant under all permutation and priming of the variables. The above operations are simply equivalent to re-numbering of the nodes. After identical permutation and priming operations on the function and its complementary function, the sum of the two functions must again be the same unit  $n$ -cube. The permutation and priming of the variables in general convert one function into other functions, keeping the structure (i.e., the geometrical disposition of the different nodes that form the function) unchanged and this is true for the complementary function also. It follows therefore that switching functions of  $n$ -variables can be classified into different classes—each class being composed of a number of functions out of the total number of  $2^{2^n}$  functions of  $n$ -variables. A function in any class can be transformed into any other member of the same class by suitable permutation and priming of the variables. Each class is called an equivalence class. Various authors (Golomb, 1959; Slepian, 1954; Troye, 1959) have suggested different methods for classification of switching functions. In this paper we shall derive the necessary and sufficient conditions for two given functions to belong to the same equivalence class. A method

for testing the equivalence between two given functions utilizing the above conditions will be presented. In the Part II of the paper we shall present a method of classification of functions of  $n$ -variables and methods of finding representative functions of each class will also be suggested.

## 2. THE CELL STRUCTURE OF A SWITCHING FUNCTION

In an  $n$ -variable function, there can be  $2^n$  different minterms, corresponding to the  $2^n$  nodes of a unit  $n$ -cube. In the collection of  $2^n$  minterms, any minterm is related by one change of variable to  $n$  other minterms. This means that corresponding to any node in the unit  $n$ -cube model there are " $n$ " nodes which are separated by unit distance. A unit  $n$ -cube or any function containing a number of nodes thereof, is made up of cells. The cells may be of different dimensions such as :

- (a) 0-cell or a node—a point.
- (b) 1-cell or a line segment composed to two nodes related by one change of variable
- (c) 2-cell or a quadrilateral composed of 4 nodes and 4 lines segments. There will be two lines segments incident with each node.
- (d) 3-cell or a unit cube, composed of 8 nodes and 12 lines segments. There will be three lines segments incident with each node.
- (e)  $k$ -cell, composed of  $2^k$  nodes,  $k \times 2^{k-1}$  line segments and  $k$  line segments incident with each node.

It can be shown that the total number of  $k$ -cells in a unit  $n$ -cube is  $n C_k 2^{n-k}$  i.e.  $n C_k 2^{n-k}$ . The different cells are composed of certain number of nodes and a certain number of 1-cells, incident with each node. We define the "Weight" of any node as the total number of 1-cells incident with that node. In other words, the weight of any term of a switching function is the number of other terms of the function which are related by one change of variable with that particular term.

For our purpose of classification of switching functions, the knowledge about the cell structure of a function is important. By this we mean the arrangement of the different nodes that represent the different terms of the function and their interconnection among themselves. If in any function two terms differ by two changes of variables, then in the unit  $n$ -cube model, the corresponding nodes will be separated by distance  $\sqrt{2}$ . Similarly if two terms differ by " $a$ " changes of variables, then the corresponding nodes in their geometrical representation will be  $\sqrt{a}$  distance apart. We can call the total number of terms of any function which differ by 2, 3, 4 etc. variables from one particular term as the weights of the order 2, 3, 4, etc. respectively of that term. For the purpose of gaining insight into the geometrical structure of any function, these weights are of very great

significance because they give an idea as to the relative distances between the different nodes of the unit  $n$ -cube which represent the terms of the function. As an illustration, we can consider the following 4-variable function

$$T = \Sigma(0, 1, 2, 4, 5, 6)$$

The terms 0, 1, 2, 4, 5, 6 have weights 3, 2, 2, 3, 2, 2 respectively. If we rearrange the terms according to non-ascending weights, the weights become 3, 3, 2, 2, 2, 2. This array of number is called the "weight distribution" of the function. We shall write down the binary equivalents of the decimal numbers corresponding to each term of the function. The array of numbers representing the binary equivalent of the decimal numbers is the transmission matrix of the function. The transmission matrix of the function along with weights of the different orders of each terms is shown in Table I.

TABLE I

	$w_1$	$w_2$	$w_3$	$w_4$		$w_1$	$w_2$	$w_3$	$w_4$	$w_5$
0	0	0	0	0		3	2	0	0	1
4	0	1	0	0		3	2	0	0	1
1	0	0	0	1		2	2	1	0	1
2	0	0	1	0		2	2	1	0	1
5	0	1	0	1		2	2	1	0	1
6	0	1	1	0		2	2	1	0	1

It will be seen that the terms are so arranged that the weights come in non-ascending order. The horizontal line is drawn to divide the terms into groups. All the terms of any group have the same weight. Certain system is followed in arranging the terms of the lower group. The first term of it (i.e., the term 1) differs by one variable from the first term of the previous group. The next term is also similarly related to the first term of the previous group. Then comes term 5, which is related by one change of variable with the second term of the previous group and so on.

Then for each term, the weights of the order 2, 3, 4 are found out and entered in the columns marked  $w_2$ ,  $w_3$ ,  $w_4$ . The array of number 3 2 0 0 is called the "distance vector" of the term 0. Similarly, the distance vector of the term 4 is 3 2 0 0, that of the term 1 is 2 2 1 0 and so on.

In the last column named  $w_5$ , the weight distribution when the members of each group are considered among themselves, is entered.

A look at the transmission matrix of the function will reveal that there are only 0's in one column. This means that though it is a four variable function,

the nodes of the unit-4-cube which represent the terms of the function are embedded in a three dimensional space. The dimension of the function is thus 3. We would have made the same conclusion if there were only 1's in any column.

For a description of the geometrical structure of a function, we should know the number of 1-cells incident with each node of the function, the interconnection between the 1-cells and the relative distances between the different nodes of the function and also the dimension of the function. Therefore, the structure of a function is described by the following :

- (1) The weight distribution of the function,
- (2) The distance vector of each term of the function,
- (3) Dimension of the function,
- (4) The interconnection amongst the one cells and consequent formation of  $k$  cells in the body of the function.

When these are known, we can have a full picture of the function in our  $n$ -dimensional unit cube model. The geometrical structure of the function  $f = \Sigma(0, 1, 2, 4, 5, 6)$  is shown in Fig. 1. Each of the above mentioned four parameters

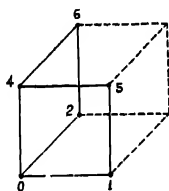


Fig 1 The function  $f = \Sigma(0, 1, 2, 4, 5, 6)$ .

of any function will remain invariant under all permutation and priming operations of the variables

### 3. NECESSARY AND SUFFICIENT CONDITION FOR TWO GIVEN FUNCTIONS TO BELONG TO SAME EQUIVALENCE CLASS

The distance vectors of the terms of a function give information regarding the total number of terms in the function related by certain changes of variables with respect to that particular term. If the distance vector of a term in four variable function is '3 2 1 1' this means that the total number of true states is eight and in the body of the function there are three other terms related by one change of variable, two other terms related by two changes of variables, one term related by three changes of variables and one term related by four changes of variables with respect to that particular term. If we compare the distance vectors of the terms of two given functions and find that corresponding to one

or more of the distance vectors of the terms in one function there is no such terms with corresponding distance vector in the other function, then it means that the relative separations of one or more of the terms in one function is different from those of the terms in the other function. Hence the necessary condition :

(1) If two functions belong to the same equivalence class, then distance vectors of the terms in one function must have one to one correspondence with the distance vectors of the terms in the other function.

If there are two functions which satisfy the above necessary condition, we choose two rows, one from each of the transmission matrices of the functions, such that the distance vectors of these rows are identical. If the two matrices have rows with distinct distance vectors then these rows should be chosen. It may so happen that there is no row with a distinct distance vector but there are groups of terms having identical distance vectors. Then any term from these groups can be chosen provided that the matrices exhibit group invariances such that any reordering between these terms having identical distance vectors is possible without affecting the transmission matrix (Choudhury and Basu, 1962 ; McCluskey, 1956). We prime the columns of the transmission matrices where "1" occurs in those rows. After priming we shall find that the two matrices will contain equal number of rows having  $K_i$  1's in the rows, where  $K_i$  can have any value 0 to  $n$  inclusive. In order that the two functions may belong to the same equivalence class, it is necessary that if the distance vectors of the rows related by  $K_1, K_2, K_3 \dots$ , changes of variables with respect to the row having zero at all column positions in one matrix have values  $A, B, C, \dots$  respectively, then in the other matrix the distance vectors of the terms having  $K_1, K_2, K_3 \dots$  1's in the rows of the transmission matrix must have values  $A, B, C, \dots$  respectively. Hence the necessary condition :

(2) If two functions belong to the same equivalence class and if we choose two terms, one from each transmission matrix such that the distance vectors of those terms are identical and the terms correspond to each other, then we shall find that the terms identically separated from those terms in the two matrices will have identical distance vectors. The correspondence of the two terms can be found as explained previously.

(3) If we now observe the two matrices columnwise and find that there are "Z" columns having 0's at all positions in one of the matrices then the other matrix must have identical number of columns with 0's at all positions i.e., the dimensions of the body of the two functions must be identical.

In order to understand the other necessary condition, some discussions on the properties of distance vectors will be helpful.

Square of the distance between two terms having  $K_1$  and  $K_2$  1's in the binary representation of the terms, can have values  $(K_1 + K_2 - 2d)$  where " $d$ " can have

any value between  $d_{min}$  to  $K_2$  inclusive when  $K_1 > K_2$  and  $d_{min} = K_1 + K_2 - n$  where  $n$  is the total number of variables of the function. It is to be noted that in computing the possible relative distances of the terms we shall only take the positive values of " $d$ ". If  $K_1 = K_2$ ,  $d$  can have values,  $d_{min}$  to  $(K_2 - 1)$ . It follows therefore that the distance between two terms can have different values depending on the number of positions in which 1's coincide in the binary representation of the terms i.e., on the value of " $d$ ".

If both  $K_1$  and  $K_2$  for the terms of a function with only two terms are even then the value of odd order weights of the two must be zero and value of any of the even order weight will be "one" depending on the value of " $d$ ". If  $K_1 + K_2$  is odd the value of even order weights must be zero and value of any of the odd order weight will be "one" depending on the value of " $d$ ".

It follows therefore that in a function consisting of more than two true states there must be terms having distance vectors in which value of any of the even order weight is other than zero. If the distance vectors of the terms of a function have zeroes at its odd order weight positions, then the maximum number of true states in the function can be  $2^{n-1}$ . If we break up a function into two groups by collecting terms having even number of 1's in their binary representation in one group and terms having odd number of 1's, in the other group, the distance vector of the terms in the two groups will have zero at the odd order weight positions.

In a function having odd number of true states the distance vectors of two terms, one having even number of 1's and the other having odd number of 1's in its binary representation cannot be identical. Because if we prime the columns of the transmission matrix odd number of times, rows with even number of 1's in the original matrix contain odd number of 1's after priming. Therefore, if the distance vector of the two rows, one having odd and the other having even number of 1's are to be identical, then ratio between rows containing even number of 1's to rows containing odd number of 1's in their binary representation must be unity. But the distance vectors of two rows, one having odd and the other even number of 1's can be identical provided the number of true states is even and ratio between rows with even number of 1's to odd number 1's is unity. It is to be observed that in any function if there are  $N_e$  terms having even number of 1's and  $N_o$  terms having odd number of 1's, then the ratio  $N_e/N_o$  remains invariant under all permutation operation and becomes  $N_o/N_e$  for odd number of priming operations.

From the above discussion it is obvious that a term of a matrix can derive its weight of the order  $K$  by combining with rows having different number of 1's.

While examining the two transmission matrices, which are found to satisfy the necessary conditions (1), (2) and (3), it may be observed that the weights of

the different orders of one or more rows of one matrix are derived by combining with rows having different number of 1's when compared with corresponding row or rows of the other matrix. If they differ in this manner, it will be impossible to find a permutation operation which will convert one matrix to other; hence the two functions cannot belong to the same equivalence class.

(4) Hence another necessary condition for the equivalence of the two functions is that the different order weights in the distance vectors of the terms containing identical number of 1's in the two matrices, obtained after testing the second necessary condition, must be derived by combining with rows having identical number of 1's. This, in other words means that the total number of one cells present in the body of the two functions must be identical and the interconnection of the one cells must be identical i.e., the total number  $k$  cells present in the body of the two functions must be same. The weight distribution among members of the subgroups must also be identical.

#### 4. SYSTEMATIC PROCEDURE FOR TESTING WHETHER TWO FUNCTIONS BELONG TO THE SAME EQUIVALENCE CLASS

As a consequence of our previous statements, we can formulate a procedure for testing the equivalence between two given functions. The testing may be done according to the following steps.

(1) For the two functions to belong to the same equivalence class, the number of true states in the functions must be identical. Hence, check if the number of terms in the two given functions are identical. If not, they cannot belong to the same equivalence class.

(2) Find out the ratio  $N_e/N_o$  for each of the two functions.  $N_e$  denotes the number of terms containing even number of 1's and  $N_o$  denotes the number of terms containing odd number of 1's in the binary representations. The ratio should be either same for the two functions or one should be the inverse of the other. If this condition is not satisfied, the functions cannot belong to the same equivalence class.

(3) The dimensions of the body of the two functions must be identical for the equivalence of the two functions. Hence test whether the dimensions of the body of the two functions are identical or not. If the dimensions are different, the two functions cannot belong to the same equivalence class.

(4) For the two functions to belong to the same equivalence class, weight distributions of the two functions must be identical. Hence test whether the weight distributions of the two functions are identical or not.

(5) If the two functions satisfy all the conditions up to the step (4), then, arrange the terms in order of non-ascending weights. Draw horizontal lines to divide the functions into groups of terms having equal weights. Find out

the weight distribution of the terms of each group considered amongst themselves. For the two functions to belong to the same equivalence class the weight distribution of the corresponding groups must be identical.

(6) If all the conditions up to step (5) are satisfied then find out the distance vector of each term in the two matrices. If corresponding to the distance vectors of one or more terms in one matrix there is no term having identical distance vector in the other matrix, then the two functions must belong to different equivalence classes.

(7) If all the conditions up to steps (6) are satisfied, then we must test to see if the weights of different orders in the distance vector of each term have been properly derived. For this we choose one term from each of the two matrices which satisfy the conditions stated in section 3 regarding the correspondence of the terms and prime the columns where 1 occurs in those rows. If now we find that the different order weights of all the terms have been derived from rows having identical number of 1's in the two matrices, then the two functions must belong to the same equivalence class. We can draw the same conclusion if we find that the two functions satisfy the conditions up to (6) and the functions contain identical  $k$ -cells incident with corresponding terms in the body of the two functions.

*Example:*

To test whether the following two given functions belong to the same equivalence class or not.

$$T_1 = \Sigma (0, 1, 2, 5, 14, 15)$$

$$T_2 = \Sigma (0, 1, 2, 12, 13, 15)$$

In Table II(a) and (b) the transmission matrices of the functions along with the distance vectors are given.

TABLE II

(a)										(b)									
$x_4$	$x_3$	$x_2$	$x_1$	$w_1$	$w_2$	$w_3$	$w_4$	$w_5$		$x_4$	$x_3$	$x_2$	$x_1$	$w_1$	$w_2$	$w_3$	$w_4$	$w_5$	
0	0	0	0	0	2	1	1	1	1	0	0	0	0	0	2	1	1	1	0
1	0	0	0	1	2	1	1	1	1	13	1	1	0	1	2	1	1	1	0
2	0	0	1	0	1	2	2	0	0	1	0	0	0	1	1	2	2	0	0
5	0	1	0	1	1	2	2	0	0	2	0	0	1	0	1	1	2	1	0
14	1	1	1	0	1	1	2	1	1	12	1	1	0	0	1	2	2	0	0
15	1	1	1	1	1	1	2	1	1	15	1	1	1	1	1	1	2	1	0

An inspection of the above tables will reveal that the two functions satisfy the conditions mentioned under steps (1) to (4) but they differ in the weight distribution among the members of the groups. So they cannot belong to the same



equivalence class. Another interesting example is presented in Table III in which (a) and (b) give the transmission matrices of the functions

$$T_1 = \Sigma (0, 1, 2, 3, 12, 13, 14, 15) \text{ and}$$

$$T_2 = \Sigma (0, 1, 2, 5, 10, 13, 14, 15).$$

TABLE III

(a)									(b)								
	$x_4$	$x_3$	$x_2$	$x_1$	$w_1$	$w_2$	$w_3$	$w_4$		$x_4$	$x_3$	$x_2$	$x_1$	$w_1$	$w_2$	$w_3$	$w_4$
0	0	0	0	0	2	2	2	1	0	0	0	0	0	2	2	2	1
1	0	0	0	1	2	2	2	1	1	0	0	0	1	2	2	2	1
2	0	0	1	0	2	2	2	1	2	0	0	1	0	2	2	2	1
3	0	0	1	1	2	2	2	1	5	0	1	0	1	2	2	2	1
12	1	1	0	0	2	2	2	1	10	1	0	1	0	2	2	2	1
13	1	1	0	1	2	2	2	1	13	1	1	0	1	2	2	2	1
14	1	1	1	0	2	2	2	1	14	1	1	1	0	2	2	2	1
15	1	1	1	1	2	2	2	1	15	1	1	1	1	2	2	2	1

It is found that the weight distribution and the distance vectors are identical for the two functions and as the weights of all the terms are identical, apparently there is no indication that the functions can be broken up into groups of terms. If we attempt to arrange the terms in such a way so that any term is related by one change of variable to a term previous to it, it is found that this can be done in the case of function  $T_2$  but not for the function  $T_1$ . In the latter case the terms 0, 1, 2, 3 form a distinct group in the sense that none of the other terms coming after them is related by one change of variable with any one of the group. The two functions thus differ in their cell structures and as such cannot belong to the same equivalence class. The same conclusion can be drawn if we try to find out how the different order weights of the terms in two matrices have been obtained. It will be seen that in the matrix (a), a row with two 1's has derived its weight of the order one by combining with two rows having one 1's in their binary representation, whereas in the transmission Matrix (b), a row having two 1's has derived its weight of the order one by combining with one row having one 1 and another row having three 1's.

##### 5. METHOD FOR FINDING OPERATIONS REQUIRED TO TRANSFORM ONE FUNCTION INTO OTHER BELONGING TO THE SAME EQUIVALENCE CLASS

The distance vectors of the terms remain invariant under all priming and permutation operations. This fact can be utilised for finding operations required

to transform one function into any other function belonging to the same equivalence class. It is obvious that the solution in majority of cases is not unique. There may be many different ways of transforming one function into the other function depending on the nature of group invariance exhibited by the function.

When the transmission matrices of the two functions are arranged in non-ascending weights and distance vectors are all written and terms are properly divided into groups and arranged as explained in Section 2, it becomes comparatively simple matter to find out the specific operations which will transform one function into the other. The arrangement of the two matrices more or less reveals the correspondence between the terms, i.e., which term of the function in one matrix has been converted to a term in the other matrix. The simplest case occurs when only one term in each of the two functions has a distance vector distinct from those of the remaining terms. In such a case it is at once obvious that the particular term in one matrix has been transformed to the other term in the other matrix. If we compare the distance vectors of the terms in one matrix with those of the terms in the other matrix and find that the terms having identical distance vectors in the two matrices have identical number of 1's in their rows, then one matrix can be transformed into the other by permutation operation. The required permutation operations will be those which will transform the term with distinct distance vector of one matrix to the similar term in the other matrix. If the functions do not satisfy the above conditions then as a first step we must find certain pruning operations which make the number of 1's in different rows of the two transmission matrices having corresponding distance vectors identical. If the ratio  $N_e/N_0$  for the two matrices are respectively  $N_1/N_2$  and  $N_2/N_1$  then total number of pruning operations for making the number of 1's in the rows of the two matrices identical will be odd. If ratio  $N_e/N_0$  ( $N_e \neq N_0$ ) is same for the two matrices it will require even number of pruning operations. The particular columns that have to be pruned can be chosen relatively easily by observing one fact that when one matrix is to be transformed to the other matrix, then after pruning the two matrices must have columns such that ratio of 0's and 1's of the columns have one to one correspondence. In the next step the columns are to be suitably permuted to convert one function into the other. Required permutation can be very easily found by locating the particular term to which we have to transform the chosen term.

If there happens to be no term having a distinct distance vector but there are groups of terms having identical distance vectors then any one term of one function in a group may be converted to any term of the second function in the same group provided the functions exhibit such group invariance that any reordering between those terms is possible without affecting the transmission matrix. Rest of the procedure will be same as stated in connection with the functions having terms with distinct distance vector. We will illustrate the method by the following example.

Example :

Find the operations which will transform the function

$$T_1 = \Sigma(4, 6, 7, 8, 9, 11, 12, 15) \text{ in the function}$$

$$T_2 = \Sigma(1, 2, 3, 5, 6, 12, 13, 14).$$

The transmission matrices along with the distance vectors of the two functions are given in the Table IV(a) and (b).

TABLE IV

(a) $T = \Sigma(4, 6, 7, 8, 9, 11, 12, 15)$										(b) $T = \Sigma(1, 2, 3, 5, 6, 12, 13, 14)$									
$x_4$	$x_3$	$w_2$	$w_1$	$w_1$	$w_2$	$w_3$	$w_4$			$x_4$	$x_3$	$x_2$	$x_1$	$w_1$	$w_2$	$w_3$	$w_4$		
4	0	1	0	0	2	2	2	1	1	1	0	0	0	1	2	2	2	1	1
6	0	1	1	0	2	2	2	1	2	3	0	0	1	1	2	2	2	1	2
12	1	1	0	0	2	3	2	0	2	5	0	1	0	1	2	3	2	0	2
7	0	1	1	1	2	2	2	1	3	2	0	0	1	0	2	2	2	1	1
8	1	0	0	0	2	2	2	2	1	13	1	1	0	1	2	2	2	1	3
15	1	1	1	1	2	3	2	0	4	6	0	1	1	0	2	3	2	0	2
9	1	0	0	1	2	2	2	1	2	12	1	1	0	0	2	2	2	1	2
11	1	0	1	1	2	2	2	1	3	14	1	1	1	0	2	2	2	1	3
5	5	4	4							3	5	4	4						
3	3	4	4							5	3	4	1						

In the last columns are written the number of 1's in the different rows and the last rows give the ratio of 1's and 0's of different columns. All terms of the matrices have weight 2. The terms have been arranged according to the procedure suggested in Section 2. It will be observed that in the matrix for the function  $T_1$  there is no column having ratios of 1's and 0's 3/5, hence in transforming matrix  $T_1$  to  $T_2$  one of those columns having ratio 5/3 must be primed. It will be observed that in the two matrices there are six terms having distance vector (2 2 2 1) and two terms having distance vector (2 3 2 0). Since the group of terms having distance vector (2 3 2 0) is smaller we will concentrate our attention to this particular group. It will be seen that in the two matrices it is possible to reorder between the terms having distance vector (2 3 2 0) without affecting the transmission matrix. Hence in transforming  $T_1$  to  $T_2$  we can transform either of the terms 12 or 15 in  $T_1$  to 5 or 6 in  $T_2$ . Since the number of 1's in the rows having distance vector (2 3 2 0) is 2 in one matrix, and 2 and 4 in the other matrix, hence the minimum number of priming operations required is two. In priming the columns, we must choose one column from the group ( $x_4, x_3$ ) and another column from

group  $(x_2, x_1)$ . If we choose column  $x_3$  of the transmission matrix  $T_1$  then the other column that can be primed keeping the number of 1's in the rows having distance vector  $(2\ 2\ 2\ 1)$  identical to that of the rows in matrix  $T_2$  is  $x_1$ . The Table V shows the matrix  $T_1$  after the columns  $x_3$  and  $x_1$  have been primed.

TABLE V

$x_4$	$x_3$	$x_2$	$x_1$
0	0	0	1
0	0	1	1
1	0	0	1
0	0	1	0
1	1	0	1
1	0	1	0
1	1	0	0
1	1	1	0

The columns  $x_3$  and  $x_4$  are permuted after priming to transform matrix  $T_1$  to  $T_2$ . This operation will transform 12 in the matrix  $T_1$  to 5 in matrix  $T_2$ . Alternatively we can transform 12 to 6 by a simultaneously permuting columns  $x_3, x_4$  and  $x_1, x_2$  after above priming operation.

The matrix  $T_1$  can be transformed to the matrix  $T_2$  by priming the columns  $x_4$  and  $x_2$ . It may be noted that this operation transforms 15 to 5 and 12 to 6.

## 6. CONCLUSION

The geometrical concept of a switching function is utilised for developing the necessary and sufficient conditions for two functions to belong to the same equivalence class. The procedure suggested for testing the equivalence between two functions is valid for any number of variables and presents no difficulty when the number of variables is large. The task of finding the distance vectors of the terms can be simplified by the use of suitable charts which can also be mechanised. The distance vectors, which remain invariant for all permutation and priming operations give an unmistakable stamp to each term of a function so that they can be recognised under all transformed conditions of the function.

## 7. ACKNOWLEDGMENT

The authors wish to express their indebtedness to Professor J. N. Bhar, D.Sc., F.N.I., for guidance and keen interest in the work.

## 8. REFERENCES

- Caldwell, S. H., 1958, *Switching Circuits and Logical Design*, John Wiley and Sons, New York.

- Choudhury, A. K. and Basu, M. S., "On Detection of Group Invariance or Total Symmetry of a Boolean Function", 1962, *Ind. J. Phys.* **36**, 31.
- Golomb, S. W., 1959, *I.R.E. Transactions on Circuit Theory*, Vol. CT-6, Special Supplement, May 1959, 176-186.
- Hanuning, R. W., 1950, *Bell System Tech. Jour.*, **29**, 146-160.
- Hohn, F. E., 1960, *Applied Boolean Algebra—An Elementary Introduction*, The Macmillan & Company, New York.
- Humphrey, W. S., Jr., 1958, *Switching Circuits with Computer Applications*, McGraw-Hill Book Company.
- Joe, C. Y., 1954, *Trans. A.I.E.E.*, Part 1, 289-291.
- McCluskey, C. J., Jr., 1956, *Bell System. Jour.*, **35**, 1445.
- Slepian, D., 1954, *Canadian Journal of Mathematics*, **5**, No. 2, p. 185-193.
- Svoboda, A., 1957, *Proceedings of an International Symposium on the Theory of Switching*, 2-5 April, 1957. Part 1, Harvard University Press, Cambridge, Massachusetts, 1959.
- "Synthesis of Electronic Computing and Control Circuits" by staff of the Computation Laboratory, Harvard University, Press, Cambridge, Massachusetts, 1951.
- Troyo, N. C. de, 1959, *Phillips Research Report* 14.
- Urbano, R. H. and Mueller, R. K., 1956, *I.R.E. Trans. on Electronic Computer* **15C**-5, September.

## INTERNAL FRICTION IN AU-NI ALLOY

M. A. QUADER\*

INDIAN ASSOCIATION FOR THE CULTIVATION OF SCIENCE, CALCUTTA-32

(Received February 24, Resubmitted March 24, 1962)

**ABSTRACT.** The internal friction in Au-74 at. % Ni alloy is studied by the torsional pendulum. A transient internal friction peak is obtained at 120°C which moves towards lower temperatures at successive measurements until it disappears. Also the peak is not reproducible by giving identical heat treatment. The origin of the internal friction peak is not known from the present measurements.

## INTRODUCTION

Recent studies of the precipitation phenomena in the gold-nickel alloys have added some complexities in the early stage of precipitation. The first of these is the internal friction study of these alloys by Ang *et al* (1955). Two unstable internal friction peaks were observed in alloys quenched from solution treated temperatures, such as for the 30 at. % Ni alloy the peaks occurred at 250°C and 400°C at 1 cps. The 400°C peak was identified as the Zener peak and was found to disappear slowly on ageing with the kinetics of the phase separation. But the 250°C peak was found to be dependent on the quenching temperature and absent in specimens quenched from just below the solubility temperature. Also this peak annealed out much more rapidly than the 400°C peak and disappeared completely before resistivity measurements and microscopic examination could reveal the start of precipitation. No explanation for the origin of this transient internal friction peak was advanced.

More recently Sivertsen and Wert (1959) have studied the changes of resistivity, volume and Young's modulus during low temperature annealing of the quenched 30 at. % Ni alloy. They observed a transient resistivity changes in the early parts of ageing which was supposed to be due to either rearrangement of vacancies retained upon quenching or some clustering of atoms. They also indicated that the observed effects might be due to the formation of at least one metastable phase which is unstable above 225°C.

The studies of the low angle scattering of X-rays in Au-Ni alloys by Flin *et al* (1953) have shown an unusual short range ordering in the alloys quenched from temperatures above the miscibility gap. Also the thermodynamic studies by Siegle *et al* (1952) have revealed positive enthalpies of mixing for the Au-Ni alloys. These results show that the gold-nickel solid solutions do not fit the

---

\*Present address: National Metallurgical Laboratory, Jamshedpur-7, India.

usual quasi-chemical theories in which the entire heat of mixing is an electro-chemical bonding between nearest neighbours.

The present paper is concerned with an experimental investigation of the internal friction in the gold-74 at. % nickel alloy. According to Ang *et al* (1955) the low temperature transient internal friction peak is absent in alloys of compositions around 75 at. % Ni. The diffusion measurements of Raynolds *et al* (1957), have shown that the interdiffusion coefficient and the thermodynamic factor are minimum for the 80 at. % Ni alloy and also the activation energy for diffusion is abnormally high.

#### EXPERIMENTAL PROCEDURE AND RESULTS

The 74 at. % Ni alloy was obtained from Baker & Co., Inc., U.S.A., in the form of a wire of 1 mm. diameter. The alloy specimen was sealed in evacuated pyrex tube and annealed at 650°C (a temperature within the miscibility gap) for 2 hours and water quenched. Internal friction measurements were obtained in the torsional pendulum (Quader, 1961) at a frequency of 1 cps. during heating and cooling. Also several runs of measurements were obtained during successive heatings without giving any further heat treatments except the heatings during measurements. The results are shown in Fig. 1 (a and b). At the first heating the internal friction went through a very weak and flat maximum at about 120°C, and above 300°C it increased rapidly without reaching to any other maximum at least up to 500°C. These are shown by curve A in Fig. 1a.

However, during cooling from 500°C (curve B, Fig. 1a) the internal friction was lower and also the 120°C peak did not appear. The curve A in Fig. 1b is a replot of curve A of Fig. 1a and shows clearly the 120°C peak while curves B, C and D represent the internal friction obtained at successive runs. It is clear from the curves that the internal friction was reduced to a large extent and also the peak appeared at 62°C and 57°C at the second and third runs respectively. However, in the fourth run (curve D) the peak was eliminated completely while the background increased slightly.

The alloy specimen was again quenched from 650°C and measurements were obtained at a frequency of 3.1 cps. The results for two successive runs are shown by curves E and F in Fig. 1b. At the first heating the room temperature internal friction was high and decreased slowly with temperature, but in the 2nd run the room temperature internal friction was low and also the weak maximum appeared at 55°C (curve F). In the third run (not shown in the figure) again the maximum disappeared while the background increased slightly. These results showed that the internal friction in this alloy was not reproducible by quenching from the same temperature and it may have some relations with the previous cold workings done to the specimen.

The specimen was then annealed at 900°C (which is above the solid solubility temperature) for 30 min and quenched in cold water. The internal frictions

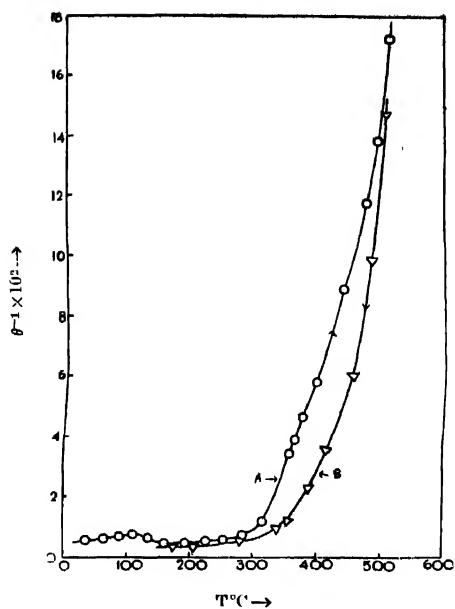


Fig. 1a. Internal friction in the Au-74 at.% Ni alloy.

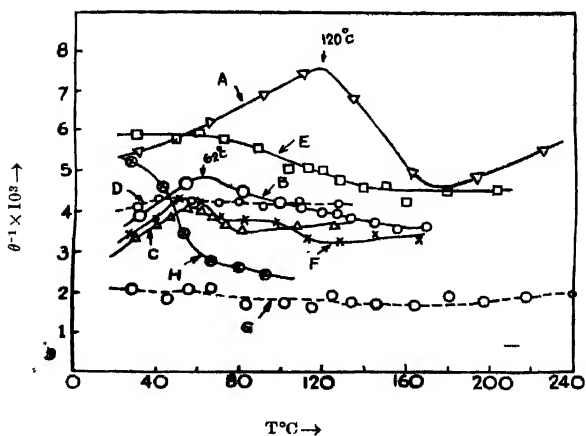


Fig. 1b Effect of successive measurements and heat treatments on the internal friction of the Au-74 at. % Ni alloy



measured at a frequency of 1.7 cps during heating are shown in curves G and H in Fig. 1b. In the freshly quenched specimen the internal friction was very low (see curve G) and practically remained constant up to 300°C. In the second heating the internal friction was again high at room temperature and decreased rapidly with the rise of temperature (Curve H) showing the probability of a peak at about the room temperature. No further measurement could be made as the specimen was damaged in the subsequent heat treatment operation.

Since the internal friction peak is not reproducible and also apparently it does not shift with the frequency of measurements, the activation energy for the relaxation process could not be calculated. Also from the present results the origin of the internal friction peak could not be ascertained definitely. However, it may be either due to the rearrangement of vacancies upon quenching or due to the clustering of atoms forming a metastable phase as concluded by Sivertsen and Wert (1959) from the resistivity measurements. Although no calculations could be made from the present measurements yet they provide a striking example of great sensitivity of the internal friction effects accompanying atomic movements in the early stages of precipitation in precipitating alloys.

#### ACKNOWLEDGMENT

I wish to express my sincere thanks to Prof. B. N. Srivastava, D. Sc., F.N.I., for his valuable guidance during the progress of the above investigation.

#### REFERENCES

- Ang, C. V., Sivertsen, J. and Wert, C., 1955, *Acta Meta*, **3**, 558.
- Flin, P. A., Averbach, B. L., and Cohen, M., 1953, *Acta Meta*, **1**, 664.
- Quader, M. A., 1961, *Ind. J. Phys.*, **35**, 446.
- Reynolds, J. E., Averbach, B. L., and Cohen, M., 1957, *Acta Meta*, **5**, 29.
- Seigle, L., Cohen, M., and Averbach, B. L., 1952, *Trans AIME* **194**, 1320.
- Sivertsen, J. and Wert, C., 1959, *Acta Meta*, **7**, 275.



# CONSTRUCTION AND WORKING PRINCIPLES OF THE BANERJEE CAMERA FOR STUDYING SMALL ANGLE SCATTERING OF X-RAYS

G. B. MITRA AND J. C. MAITRA

DEPARTMENT OF PHYSICS, INDIAN INSTITUTE OF TECHNOLOGY, KHARAGPUR

(Received January 22, 1962)

**ABSTRACT.** Actual construction of a camera for studying scattering of X-rays at extremely small angles utilising the principles due to Banerjee and Maitra (1951) has been described. An expression for the intensity of X-rays scattered at low angles in terms of observable has been derived. Corrections to be applied for obtaining the intensity of scattered radiations have been discussed. Distribution of intensity of X-rays scattered at low angles with angle for cold worked copper and aluminium as obtained by this apparatus has been compared with that obtained by conventional methods.

## INTRODUCTION

It is well known that recording of small angle scattering of X-rays is fraught with severe technical difficulties. On the other hand, ever since the pioneering work of Guinier (1939), small angle scattering of X-rays has been acquiring increasing importance in various fields of study in Physics, Metallurgy, Chemistry, Biology and Biochemistry. Hence any attempt at simplifying the technique and at rendering recording of X-ray scattering at low angles practicable is worth the while. A novel method of studying extremely low angle scattering of X-rays has been described by Banerjee and Maitra (1951) which, while using an single crystal monochromator, has got the advantages of a double crystal device and is capable of measuring scattering of X-rays at angles as small as one minute of arc. So far, however, no work has been done with this arrangement. The purpose of the present paper is to explore the possibilities of undertaking investigations on scattering of X-rays at low angles with the help of an apparatus of the above type. An actual apparatus has been described and an expression for the intensity of the scattered radiation in terms of the observables obtained. Finally corrections for the observed intensities have been discussed and intensity of X-rays scattered at extremely low angles by cold worked copper and aluminium has been studied.

## GENERAL DESCRIPTION OF THE APPARATUS

A general description of the arrangements is shown in Fig. 1. The (100) plane of a calcite crystal ( $A_1$ ) is used for the Bragg reflection. The crystal holder

---

\*Present address: Defence Research and Development Laboratory, Metcalfe House, Delhi-6.

( $A_2$ ) is so designed that the crystal is capable of being moved bodily in a lateral direction with a screw arrangement ( $A_3$ ). This crystal holder is fixed on a gonio-

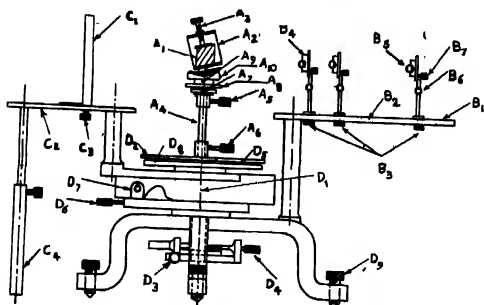


Fig. 1.

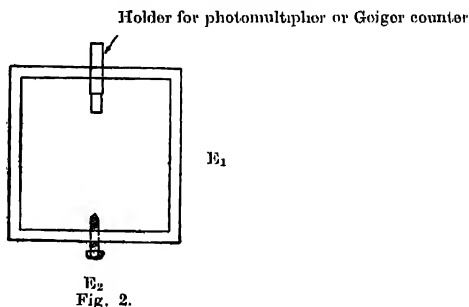
meter head which is fixed axially in the spectrometer by means of a rod ( $A_1$ ). As this rod is fixed to the goniometer head by a screw ( $A_5$ ), the goniometer head is capable of being bodily removed. The height of the crystal system can also be adjusted by the screw ( $A_6$ ). This crystal holding system is capable of translational and lateral movements to a uniform extent by rack and pinion arrangement by operating with a hexagonal head for which suitable pins are provided ( $A_7$ ,  $A_8$ ). The inclination of crystal face can also be adjusted about vertical and horizontal axes to an order of  $30^\circ$  by a similar rack and pinion arrangement which can be operated by the same hexagonal head at suitable pins ( $A_9$ ,  $A_{10}$ ).

The slit system consists of three identical slits. All the three slits are capable of translational movement on the lever arrangement ( $B_1$ ). This lever has a groove ( $B_2$ ) through its length for facilitation of fixing the slits at any desired distances the slit is capable of adjustment by a screw arrangement ( $B_3$ ). The slit is also capable of being adjusted at any desired height by means of the screw ( $B_4$ ). The slit can be rotated about a vertical axis and fixed at any angle by the fixing screw ( $B_7$ ). In order to provide freedom of fine adjustment in a lateral direction, a small horizontal slot is provided through which the fixing screw ( $B_7$ ) is provided. Thus it will be seen that all freedoms of movement have been provided in the design of each slit.

The film holder ( $C_1$ ) is set at right angles to the lever ( $C_2$ ) on which it is fixed. The film holder can be moved through suitable distances along the groove of the lever and can be fixed at any distance by means of the stud and the fixing screw ( $C_3$ ). By means of fixing arrangement at the back of the film holder, it is capable of being unloaded and loaded with film without disturbing its fixed position on the lever. This also allows a small amount of freedom of angular movement of the film about a horizontal and with respect to the film holder. A sup-

port ( $C_4$ ) to the lever ( $C_1$ ) is also provided. The crystal holding system, the lever arrangement ( $B_1$ ) on which the slit system is fixed, and the lever ( $C_2$ ) on which the film holder is fixed is capable of rotation about the central axis of rotation ( $D_1$ ). The crystal holding system can be fixed to the disc ( $D_2$ ) by the fixing screw ( $A_6$ ). This disc and consequently the angular orientation of the crystal with respect to the incident beam can be fixed at any angular position by means of the screw ( $D_3$ ). Once fixed, fine angular adjustments can be done by the screw ( $D_4$ ). The lever ( $C_2$ ) on which the film holder is fixed can be clamped to the disc ( $D_5$ ) by means of the screw ( $D_6$ ). After clamping, fine angular adjustments of the film holder, if necessary, can be done by the screw ( $D_7$ ). The disc ( $D_8$ ) is graduated from which the angular positions of the crystals and film holder can be found by means of the verniers ( $D_9$ ). The entire system can be bodily adjusted at suitable inclination by means of the three levelling screws ( $D_9$ ). To eliminate air scattering, the whole apparatus is fitted in an evacuated enclosure.

A suitable arrangement for the use of a photomultiplier or a geiger counter in place of the film holder is shown in Fig. 2. The photomultiplier tube can be



fixed on the base ( $E_1$ ). The height of the base is however adjustable by up and down movement through a system of slots and can be fixed by the screw ( $E_2$ ). The distance from the reflecting crystal can be adjusted as in the case of the photographic filmholder on the lever ( $C_2$ ) and can be fixed by means of a stud. The photomultiplier tube will of course require a suitable material for excitation of fluorescence by the X-rays and application of the requisite voltage on its dynodes. The region from which the scattered X-rays enter the photomultiplier tube can be limited to the desired minimum extent by means of a suitable window in front of the tube. The same arrangement will be of use when a Geiger counter is used.

#### DERIVATION OF AN EXPRESSION FOR THE INTENSITY

The polychromatic beam of X-rays from the X-ray tube is incident on the slit  $S$  (Fig. 3). The calcite crystal  $PQ$  is so oriented that the direct beam  $SC$  and

the scattered characteristic beam  $SB$  satisfy the relations  $2d \sin \theta_L = \lambda_L$ ,  $2d \sin \theta_B = \lambda_B$  where  $\lambda_L$ ,  $\lambda_B$  are their respective wavelengths and  $\theta_L$ ,  $\theta_B$  are their angles of reflection.

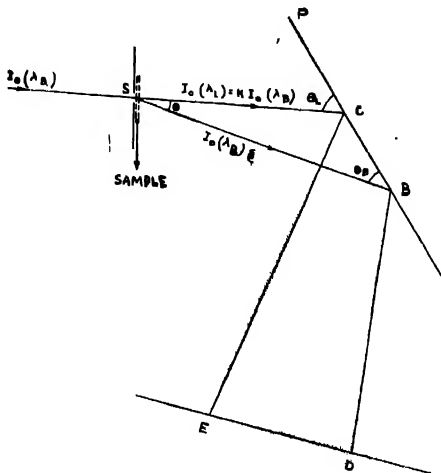


Fig. 3.

If, in the absence of the sample, there is any characteristic radiation in the direction  $BD$ , then there will be a reflection in the direction  $BD$ . Similarly, components of the incident radiation of wavelength  $\lambda_L$  will be reflected along  $CE$ . On a film  $ED$  two images of the slit for the two wavelengths ( $\lambda_B$  and  $\lambda_L$ ) will be recorded.

By changing the inclination ( $\psi_L$ ) of the crystal face  $PQ$  with respect to the direct beam  $SC$ , the angle of scattering for the characteristic radiation is changed since

$$\psi_L - \psi_B = 0$$

Various wavelengths  $\lambda_L$  are, however, brought into play by this process. The relative intensities of these radiations are determined by the intensity distribution of the spectra emitted by the target of the X-ray tube and by its voltage-current characteristics.

Let  $I_0(\lambda_B)$  be the intensity of the characteristic radiation and  $I_0(\lambda_L) = KI_0(\lambda_B)$  be that of the general radiation of wavelength  $\lambda_L$  satisfying Bragg reflection condition for the angle  $\psi_L$ ,  $K$  being a constant for this. Let  $\alpha$  be the fraction of the intensity of the instrumental scattering of the characteristic radiation in the

direction  $SB$  i.e., a direction making an angle  $\theta$  with the direct beam  $SC$ ,  $\alpha$  will clearly be a function of  $\theta$ . The intensity of the characteristic radiation along  $SB$  will then be  $I_0(\lambda_B)\alpha$  in the absence of the sample. Distances  $SB$  and  $SC$  can be taken for all purpose to be same.

The intensities received at  $E$  and  $D$  will then be given respectively by

$$I_{L0} = KI_0(\lambda_B)\mu(\psi_L) j F_L^2 \quad \dots (1)$$

and

$$I_{B0} = I_0(\lambda_B)\alpha\mu(\psi_B)j F_B^2 \quad \dots (2)$$

where  $\mu(\psi_L)$ ,  $\mu(\psi_B)$  are angle factors including absorption, Lorentz and polarisation factors for the general radiation  $\lambda_L$  and  $\lambda_B$  respectively.

$j$  is multiplicity factor for the crystal face

$F_L, F_B$  are structure factors for the given planes of the crystal including Debye temperature factor for  $\lambda_L, \lambda_B$  respectively.

Suppose that the sample scatters the characteristic radiation in the small angle direction  $\theta$  and let  $\sigma$  be the fraction of the incident intensity scattered in that direction. Then intensity scattered in the direction  $\theta$  by the sample is

$$I_\sigma = \sigma I_0(\lambda_B) \quad \dots (3)$$

when the sample is put before the slit  $S$ , all components of the incident beam are absorbed by factors characteristic of the radiation involved. The absorption factor of the wavelength  $\lambda_L$  will be  $A_L$  whereas that for  $\lambda_B$  will be  $A_B$ . The absorption factor, strictly speaking, should vary with  $\theta$ .

Thus, with the sample in position, the intensities recorded at  $E$  and  $D$  will be given respectively by

$$I_{L1} = KI_0(\lambda_B)A_L\mu(\psi_L) j F_L^2 \quad \dots (4)$$

$$I_{B1} = A_B(\theta) I_0(\lambda_B)[\alpha + \sigma] \mu(\psi_B) j F_B^2 \quad \dots (5)$$

From Eqs. (2) and (5)

$$\frac{I_{B1}}{I_{B0}} = A_B(\theta)(\alpha + \sigma) \quad \dots (6)$$

or

$$\sigma = \left( \frac{I_{B1}}{I_{B0} A_B(\theta)} - 1 \right) \alpha \quad \dots (7)$$

For another angle of scattering  $\theta'$ , the equation is

$$\sigma' = \left( \frac{I_{B1}'}{I_{B0}' A_B(\theta')} - 1 \right) \alpha' \quad \dots (8)$$

where the primed quantities mean the quantities in Eq. (7) for the new setting at  $\theta'$ . For determining  $\alpha$  and  $\alpha'$ ,  $I_{\theta 0}$  is plotted against  $\theta$  and the resulting curve is extrapolated to  $\theta = 0$ .

From Eq. (2), we have

$$\frac{(I_{\theta 0})_{\theta=\theta'}}{(I_{\theta 0})_{\theta=0}} = \alpha \quad \dots (9)$$

The values of  $\alpha$ ,  $\alpha'$  can be determined from this equation with the help of this graph.

#### CORRECTIONS FOR SLIT DIMENSIONS

The intensity expression derived in Eq. (7) assumes a point source of X-rays and a perfectly parallel and infinitesimally narrow beam. In the experimental arrangement, however, a collimating system consisting of three slits were used. In all the three slits, the height was very much greater than the width so that they could be taken as fair approximations to a slit of infinite height. The calcite crystal can also be taken as a slit of infinite height. Thus the observed intensity is due to a very large number of point X-ray sources distributed according to the slit geometry, which will modify the actual scattered intensity. It has been shown by authors like Spencer (1931), Jones (1938), etc. that the observed angular intensity distribution is the convolution of the actual diffracted intensity distribution and an instrumental weight functions. Various authors like Guinier and Fournet (1947), Kratky, Porod and Kahovec (1951), Shull and Roess (1947), Kranjc (1954) etc. have described methods of recovering the actual diffracted intensity distribution from the observed intensity distribution. The method followed in course of this experiment is essentially that due to Guinier and Fournet (1947).

For each setting of the crystal, the image of the slit for the characteristic radiation ( $\lambda_B$ ) without the sample in position is scanned microphotometrically parallel to its width as well as height. It is observed that although there is a distinct intensity distribution along the width, that along the height is approximately constant. Let us denote the mean intensity distribution along the width by  $I(x)$  and that along height by  $I(y)$  where

$$x = \frac{2\pi}{\lambda} \times \frac{\text{distance along width from origin}}{\text{overall sample to plate distance}}$$

and 
$$y = \frac{2\pi}{\lambda} \times \frac{\text{distance along height from origin}}{\text{overall sample to plate distance}}$$

Let, 
$$h = \frac{2\pi\theta}{\lambda}$$



Since for every value of  $y_1$ ,  $I(x)$  is constant, we may write

$$G(h) = \iint I(x) I(y) F[h(x, y)] dx dy \quad \dots (9)$$

where  $G(h)$  is the observed intensity for a given value of  $h$  and  $F(h)$  the actually diffracted intensity.

Let  $\int I(y) \cdot F(h) dy$  be denoted by  $K(h)$

Then  $\int I(x) K(h) dx = G(h) \quad \dots (10)$

Let us express  $G(h)$ ,  $K(h)$  and  $I(x)$  in terms of their Fourier expansions

$$G(h) = \int_{-\infty}^{\infty} G^*(u) \cos 2\pi hu du \quad \dots (11)$$

$$K(h) = \int_{-\infty}^{\infty} K^*(u) \cos 2\pi hu du \quad \dots (12)$$

$$I(x) = \int_{-\infty}^{\infty} I^*(u) \cos 2\pi xu du \quad \dots (13)$$

Only the cosine terms have been used in the expansions because the functions are symmetrical. The Fourier transforms of the functions are given by

$$G^*(u) = \int_{-\infty}^{\infty} G(h) \cos 2\pi hu dh \quad \dots (14)$$

$$K^*(u) = \int_{-\infty}^{\infty} K(h) \cos 2\pi hu dh \quad \dots (15)$$

$$I^*(u) = \int_{-\infty}^{\infty} I(x) \cos 2\pi xu dx \quad \dots (16)$$

Now,  $G^*(u) = K^*(u) I^*(u) \quad \dots (17)$

or,  $K^*(u) = \frac{G^*(u)}{I^*(u)} \quad \dots (18)$

For a given sample,  $\sigma$  vs  $\theta$  graph is the same as the  $G(h)$  vs  $h$  curve. Both  $G(h)$  vs  $h$  and  $I(x)$  vs  $x$  curves were drawn by adjusting the scales so that bases of both the curves had the same linear dimension. The bases were divided into 60 equal parts and for each point of division along the abscissa, the value of the ordinate

for both the curves were determined. The integrations in Eqs. (14) and (16) were thus replaced by the summations

$$G^*(u) = \frac{1}{60} \sum_{-30}^{+30} G(h) \cos 2\pi h \frac{u}{60} \quad \dots (19)$$

$$I^*(u) = \frac{1}{60} \sum_{-30}^{+30} I(x) \cos 2\pi x \frac{u}{60} \quad \dots (20)$$

Eqs. (19) and (20) were easily evaluated knowing the experimental values  $G(h)$  and  $I(x)$ . Then from Eqs. (18)  $K^*(u)$  was evaluated. Eqn. (12) was then replaced by the summation

$$K(h) = \frac{1}{60} \sum_{-30}^{+30} K^*(u) \cos 2\pi h \frac{u}{60} \quad \dots (21)$$

Determining (21) from various values of  $h$ , the graph of  $K(h)$  vs  $h$  was drawn. The graph of  $K(h)$  vs  $h$  represented in terms of another set of variables the graph of  $K(\sqrt{h^2+u^2})$  vs  $\sqrt{h^2+u^2}$ ,  $u$  being any arbitrary variable of no physical significance.

From this graph the values of the derivatives  $K'(\sqrt{h^2+u^2}) = \frac{dK(\sqrt{h^2+u^2})}{d(\sqrt{h^2+u^2})}$

were determined and from them the functions  $\frac{K'(\sqrt{h^2+u^2})}{\sqrt{h^2+u^2}}$  were formed. Next,

for each value of  $h$  and  $u = 0$  to  $u = v$  so that  $\frac{K'(\sqrt{h^2+v^2})}{\sqrt{h^2+v^2}} = 0$ , graphs of

$\frac{K'(\sqrt{h^2+u^2})}{\sqrt{h^2+u^2}}$  were plotted against  $u$ . The area of this curve gave the value of

$$\int_0^v \frac{K'(\sqrt{h^2+u^2})}{\sqrt{h^2+u^2}} du$$

From these integrals, the values of  $F(h)$  were calculated from

$$F(h) = - \frac{1}{\pi\lambda} \int_0^v \frac{K'(\sqrt{h^2+u^2})}{\sqrt{h^2+u^2}} du \quad \dots (22)$$

where  $\lambda = I(y) = \text{a constant}$ . The plot of  $F(h)$  against  $h$  was then drawn from

these data. This gave the distribution of the actual intensity of scattering with the angle of scattering.

### RESULTS AND DISCUSSIONS

In Figs. 4 and 5, the distributions of intensity of X-rays scattered by cold worked aluminium and copper at extremely small angles with the angle of scat-

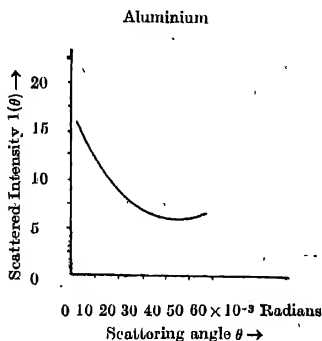


Fig. 4.

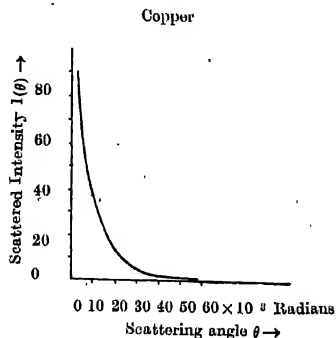


Fig. 5.

tering have been shown. The intensities in both cases are observed to decrease monotonously, almost exponentially. This is in agreement with the results obtained by Blin and Guinier (1953).

### ACKNOWLEDGMENTS

The authors wish to express their thanks of gratitude to Prof. K. Banerjee and Prof. S. Gupta for encouragement. J. C. Maitra expresses his thanks to the authorities of the Indian Institute of Technology for permitting him to work in the laboratory of the Physics Department. Thanks are also due to Shri J. Ray and Shri J. C. Mitra for helping in the actual construction of the camera.

### REFERENCES

- Banerjee, K. and Maitra, J. C., 1951, *Ind. J. Phys.* **25**, 141.  
 Blin, J. and Guinier, A., 1953, *Compt. Rendu.* **236**, 2150.  
 Guinier, A., 1939, *Ann. Phys.*, **12**, 161.  
 Guinier, A. and Fournet, G., 1947, *J. Phys. Radium*, **8**, 395.  
 Jones, P. W., 1938, *Proc. Phys. Soc.*, **A116**, 16.  
 Kranjc, K., 1954, *Acta Cryst.*, **7**, 709.  
 Kratky, O., Porod, G. and Kahovec, L., 1951, *Z. Electrochem.*, **55**, 53.  
 Shull, C. G. and Roess, L. C., 1947, *J. App. Phys.*, **18**, 295.  
 Spencer, R. C., 1932, *Phys. Rev.*, **38**.

# LIGHT ABSORPTION IN $\text{NO}_3^-$ ION IN STATE OF SOLUTION

## PART I—300m $\mu$ BAND

A. MOOKHERJI AND S. P. TANDON\*

PHYSICAL LABORATORIES, AGRA COLLEGE, AGRA (INDIA)

(Received March 14, 1962)

**ABSTRACT.** The ultra-violet absorption in ten nitrates having mono, di, and trivalent cations, were studied by a "UVISPEK" spectrophotometer. The observed molar extinction coefficient, oscillator strength, and polarisation go to show that the 300m $\mu$  band is a  $D_{3h}$  symmetry forbidden  $n \rightarrow \pi^*$  transition buried under the symmetry allowed  $\pi \rightarrow \pi^*$  transition.

### INTRODUCTION

The study of the absorption spectra of nitrate ions in different physical states (Schaeffer, 1910, 1916; Smakula 1927; Rhodes and Ubbelohde, 1959; Halban *et al.*, International Critical Tables; Krishnan and Guha, 1934) revealed two structureless bands; one of them in the near ultra-violet extending from 350 to 260 m $\mu$  which is weak, and the other at about 200 m $\mu$ .

Due to the large band width and the nonelimination of container and solvent effect, the previous workers failed to study these bands in detail. The present authors eliminated the solvent and container effect by using a "UVISPEK" and by improved technique reduced the band width to a few angstroms.

A systematic change in energy of the absorption spectra of nitrate ion, as we pass from  $\text{LiNO}_3$  to  $\text{CsNO}_3$  due to ion-ion interaction was observed by Sydnan (1950), and Smith and Boston (1961). This change in energy was avoided in the present work by using only aqueous solution so as to get the spectral character of the  $\text{NO}_3^-$  ion only.

The present communication reports a systematic study of the 300m $\mu$  band of  $\text{NO}_3^-$  ion in ten nitrates having mono, di, and trivalent cations in aqueous solutions and viewed in the light of the work of Van Vleck (1937), Jorgensen (1954), Sugano and Tanabe (1954), Smith and Boston (1961), and Friend and Lyon (1959).

### EXPERIMENTAL

Chemicals used were of Merck's A. R. quality. The measurement on Light absorption in aqueous solutions in the ultraviolet region were carried out by

---

\*Physics Laboratory, Government College, Ajmer (India).

a "UVISPEK" Hilger Photoelectric Spectrophotometer following Mookherji and Chhonkar (1959) and the technique of reducing band-width (Tandon, 1962). Temperature of measurements centred round about  $25^\circ\text{C}$ . Slight variations in the room temperature did not effect the band maximum noticeably.

## RESULTS

Results of measurement are collected in Table I. In order to get prominent absorption peaks for the salts studied, the solutions had to be diluted. Progressive dilution from that concentration at which prominent peak is obtained does not change the position of the peak. The nature of the variation of absorption is shown graphically in Fig. 1.

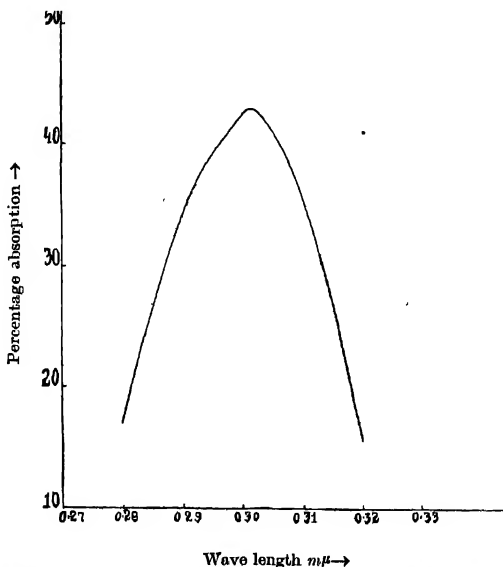


Fig. 1. Absorption curve between percentage absorption and wavelength showing general nature of the  $300\text{ m}\mu$  band of  $\text{No}_3^-$  ion in state of aqueous solution.

## DISCUSSION

### (a) Oscillator Strength

The oscillator strength  $P$  is given approximately by the relation (Jorgensen, 1954).

$$P = 4.60 \times 10^{-9} E [\delta(-) + \delta(+)] \quad \dots (1)$$

where  $E$  is the molar extinction coefficient,  $\delta(-)$  and  $\delta(+)$  are the half band-widths towards smaller and larger wave numbers respectively.

$E$  for solutions is defined by the relation,

$$Ect = \log_{10} (I/I_0) = 2.303 \times \text{absorption density};$$

$t$  is the thickness of solution in cms.;  $c$  is the concentration in mol. per litre.

For the band maximum we have observed the absorption density directly from potentiometer scales (vide Manual H 700.308 Sec.3d) which are converted to the molar extinction coefficient  $E$  and are given in Table I.

A Gaussian analysis of the curves gave  $\delta(-)$  and  $\delta(+)$ . These are included in Table I. Putting all these values in Eq. (1), we have calculated the  $P$  values which are also included in Table I. It is seen that in state of aqueous solution there is no striking dependence of  $P$  values on the cation.

TABLE I

Salt	Concen- tration%	Absorption cm <sup>-1</sup>	Max. $\lambda$	$E$	$\delta(+)+\delta(-)$ Cm <sup>-1</sup>	$P \times 10^5$
LiNO <sub>3</sub>	0.25	33,167	3015	18.60	37,973	23.29
NaNO <sub>3</sub>	0.50	33,223	3010	18.01	37,910	22.23
KNO <sub>3</sub>	0.50	33,223	3010	18.38	37,966	22.98
NH <sub>4</sub> NO <sub>3</sub>	0.25	33,223	3010	23.95	38,470	33.69
AgNO <sub>3</sub>	0.50	33,167	3015	23.47	38,745	35.13
Ba(NO <sub>3</sub> ) <sub>2</sub>	0.40	33,167	3015	24.46	37,803	29.47
Sr(NO <sub>3</sub> ) <sub>2</sub>	0.40	33,167	3015	23.27	36,964	23.10
Mg(NO <sub>3</sub> ) <sub>2</sub>	0.40	33,112	3020	21.67	37,226	22.45
Cd(NO <sub>3</sub> ) <sub>2</sub>	0.50	33,223	3010	19.73	38,235	26.25
Al(NO <sub>3</sub> ) <sub>3</sub>	0.50	33,223	3010	19.57	38,035	24.67

Smith and Boston (1961) with Lowry-Hudson and Kuhn-Brown models calculated  $P$  values, and observed some dependence on cation in case of pure alkali nitrate melts. A comparison with our values is shown in Table II.  $P$  values of melts show ion-ion interaction effect, while our solution  $P$  values show no such variation as is expected.

(b) *Nature of Transition* :

It is seen from Table I that the values of  $E$  are very low and the oscillator strength has values only of the order of  $10^{-6}$ . These experimental findings suggest that the NO<sub>3</sub> ion absorption band is due to forbidden transitions (Mookherji and Tandon, 1962).

Among the forbidden transitions, according to Van Vleck (1937) the following can have non-vanishing intensity :—

- (A) The electric quadrupole
- (B) The magnetic quadrupole, and
- (C) The electric dipole coupled with vibration

TABLE II

Salt	Our values	$P \times 10^5$	
		Smith & Bostons' values on models	
		Lowry-Hudson	Kuhn-Brown
$\text{LiNO}_3$	23.29	39.8—40.5	37.3
$\text{NaNO}_3$	22.23	47.1—17.4	10.3
$\text{KNO}_3$	22.98	9.5—9.3	9.0

It would be interesting to estimate transition probabilities for these kinds of transitions following Van Vleck (1937). Let  $\sigma_1$ ,  $\sigma_2$  and  $\sigma_3$  represent the transition probabilities for these three types (A), (B) and (C) respectively. Then,

$$\sigma_1 = 32\pi^6 \nu^5 e^2 Q^2 / 5hC^6 \quad \dots (2)$$

$$\sigma_2 = 64\pi^4 \nu^3 M^2 / 3hC^3 \quad \dots (3)$$

and,

where, 
$$\sigma_3 = \sigma_{allowed} \left( \frac{V_{hem}}{h\nu'} \right)^2 \quad \dots (4)$$

$$\sigma_{allowed} = 64\pi^4 e^2 \nu^3 Q^2 / 3hC^3 \quad \dots (5)$$

$Q$  is comparable dimensionally with mean square radius of the orbit and hence can be estimated from the relation  $Q \approx r^2$  and  $M$  is of the order of Bohr magneton and  $\nu' \approx 10^5 \text{ cm}^{-1}$ . The other symbols have the usual meanings.

$V_{hem}$  can be estimated using the relation

$$V_{hem} \approx \left( \frac{\partial R}{\bar{r}} \right) V_0$$

where,  $\partial R$  is given by

$$\frac{1}{2} h \nu_0 = 2\pi \mu \nu_0^2 (\partial R)^2$$

$\nu_0$  is fundamental frequency of vibration  $\approx 1000 \text{ cm}^{-1}$  (Herzberg, 1946; Janz and James, 1961) and  $\mu$  is the effective mass for the ion  $\approx 14 \times 1.64 \times 10^{-24}$ .

Now,

$$V_0 \approx 3 \times 10^4 \text{ cm}^{-1}$$

and

$$\bar{r} \approx 10^{-8} \text{ cm.}$$

and hence

$$V_{hem} \approx 0.6 \times 10^3 \text{ cm}^{-1}.$$

Thus estimating the values of  $\sigma_1$ ,  $\sigma_2$  and  $\sigma_3$ , we have calculated the oscillator strengths  $P_1$ ,  $P_2$ , and  $P_3$  for these types (A), (B) and (C) respectively. They are related by the expression

$$P_i = \frac{\sigma_i}{\sigma_{allowed}} \quad \text{where } i = 1, 2, 3.$$

$P_i$ 's are calculated by utilising our observational data. Thus, we obtain,

$$P_1 \approx 10^{-1}$$

$$P_2 \approx 4 \times 10^{-8}$$

$$P_3 \approx 10^{-4}$$

Thus it is evident that probably electric dipole coupled with vibration predominates in these transitions. According to Smith and Boston (1961) the transition  $n \rightarrow \pi^*$  shifts charge density from the neighbourhood of oxygens to the neighbourhood of nitrogen with a conservation of total charge. This might be responsible for coupling vibration with electric dipole transition. The possibility of a magnetic dipole transition cannot be altogether ruled out, as our estimates are only approximate.

(C) *Assignments of band :*

Smith and Boston (1961) and McEwen (1960, 61) by LCAO method have calculated the energy levels of  $\text{NO}_3^-$  ion, using the experimentally observed (Inkinen, 1960) N—O distance 1.22 Å and  $D_{3h}$  symmetry properties of ion. These are shown in Fig. 2.

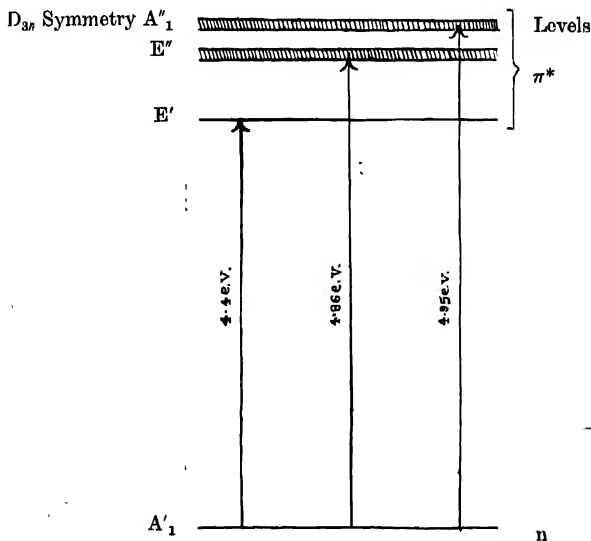


Fig. 2. Energy level diagram showing probable transitions giving rise to 300  $m\mu$  band.



The 24 electrons (Walsh, 1953) of the ion may be divided into

- (1)  $\pi$ -electrons, bonding and antibonding
- (2)  $\sigma$ -electrons, bonding and antibonding.

According to McEwens (1961), and Smith and Boston (1961) the 300  $\mu$ . band is due to excitation of the lone pair nonbonding electron ( $n$ -orbital) on oxygen into an antibonding  $\pi$  orbital ( $\pi^*$  orbital) of the  $\text{NO}_3^-$  ion that is,  $n \rightarrow \pi^*$  transition. The ground state ' $n$ ' has the symmetry  $A_1'$  of  $D_{3h}$  group (Friend and Lyons, 1959). The upper state may be either of the five states with symmetry  $A_1''$ ,  $E''$ ,  ${}^2A_1''$ ,  ${}^3E''$  and  ${}^3E'$ ;  $A_1'$  and  ${}^2A_1''$ ,  $E''$  and  ${}^3E''$  have almost the same energy and hence only the three transitions shown in Fig. 2 are possible. Among these  $A_1' \rightarrow A_1''$  and  $A_1' \rightarrow E''$  are symmetry forbidden while  $A_1' \rightarrow E'$  is symmetry allowed transition. Now our observed values of absorption maximum in  $\text{NO}_3^-$  ion correspond to 4.1 e.v. This is near to  $A_1' \rightarrow E'$ , the symmetry allowed transition. But experimentally observed oscillator strengths ( $P \approx 10^{-5}$ ) and molar extinction coefficients ( $E \approx 20$ ) coupled with the result of measurement on  $\text{KNO}_3$  and  $\text{NaNO}_3$  with polarised light (Krishnan and Dasgupta, 1933) go to support the symmetry forbidden  $A_1' \rightarrow E''$  and  $A_1' \rightarrow A_1''$ ,  $n \rightarrow \pi^*$  transitions.

We have suggested in the previous section that the oscillator strength as estimated from our observed values suggest an electric dipole transition coupled with vibration. So following Smith and Roston (1961) it may be suggested that  $A_1' \rightarrow E''$  might receive some allowed character due to this vibration perturbation. Consequently, the 300  $\mu$  band may be assigned to the forbidden  $n \rightarrow \pi^*$  transition perturbed by vibration buried under the symmetry allowed  $A_1' \rightarrow E'$ ,  $\pi \rightarrow \pi^*$  transition.

We could not observe any vibrational structure for this band in state of solution. It may be due to the low intensity and the superposition of  $A_1' \rightarrow E'$ ,  $A_1' \rightarrow E''$ ,  $A_1' \rightarrow A_1''$ ,  $n \rightarrow \pi^*$  transitions. The tail of the strong symmetry allowed  $\pi \rightarrow \pi^*$  transition will also mask it.

#### ACKNOWLEDGMENTS

This work was started in the Physical Laboratories, Agra College, Agra and completed in the Physics Laboratory, Government College, Ajmer. One of us (S.P.T.) is grateful to Prof. G. L. Gupta, Ph.D., Head of the Physics Department and Principal Bhim Sen, Government College, Ajmer, for providing facilities to complete the work.

#### REFERENCES

- Friend, J. A. and Lyons, L. E., 1959, *J. Chem. Soc.*, 1572.  
 Halban *et al.*, *Handbuch der Physik*, 21, 329.  
 ———— *International Critical Tables*, 5, 329-31.  
 Herzberg, G., 1946, *Molecular Spectra and Molecular Structure*, Part II, D. Van Nostrand Company, Inc., New York, 178.

- Inkinen, O., 1960, *Ann. Acad. Sci. Fennica (Finland)*, **55**, 43.
- Janz, G. J. and James, D. W., 1961, *J. Chem. Phys.*, **35**, 739.
- Jorgenson, C. K., 1954, *Acta. Chem. Scand.*, **8**, 1495, 1502.
- Krishnan, K. S. and Guha, A. C., 1934, *Proc. Ind. Acad. Sci.*, **1**(4), 242.
- Krishnan, K. S. and Dasgupta, A. C., 1933, *Ind. J. Phys.*, **8**, 49.
- McEwens, K. L., 1960, *J. Chem. Phys.*, **32**, 1801.
- 1961, *J. Chem. Phys.*, **34**, 547.
- Mookherji, A. and Chhonkar, N. S., 1959, *Ind. J. Phys.*, **33**, 74.
- Mookherji, A. and Tandon, S. P., 1962, *Ind. J. Phys.*, **36**, 211.
- Rhodes, E. and Ubbelohde, A. R., 1959, *Proc. Roy. Soc. (London)*, **A251**, 156.
- Schlaefli, 1910, *Zeits. f. Wiss. photogr.*, **8**, 260.
- 1916, *Zeits. Anorg. Chem.*, **97**, 285.
- Sidman, J. W., 1950, *Chem. Rev.*, **58**, 689.
- Smalcula, 1927, *Zeits. f. physik*, **45**, 1.
- Smith, G. P. and Boston, C. R., 1961, *J. Chem. Phys.*, **34**, 1396.
- Tanabe, Y. and Sugano, S., 1954, *J. Phys. Soc. Japan*, **9**, 766.
- Tandon, S. P., 1962, *Raj. Univ. Studies*, (Under publication).
- Van Vleck, J. H., 1937, *J. Chem. Phys.*, **41**, 67.
- Walsh, A. D., 1953, *J. Chem. Soc.*, 2301.

## HELMHOLTZ INSTABILITY IN HYDROMAGNETICS

S. P. TALWAR

DEPARTMENT OF PHYSICS, DELHI UNIVERSITY, DELHI

(Received August 9, 1961)

**ABSTRACT.** The Helmholtz instability for two inviscid, incompressible, perfectly conducting superposed fluids is investigated under the joint influence of a horizontal magnetic field and Coriolis force. After establishing the general equations of the problem three special cases are discussed: (i) Rotating configuration with field but no tangential motion, (ii) Rotating configuration with tangential motion but no field, (iii) Single fluid subject to rotation and magnetic field. Both magnetic field and rotation have a stabilizing influence on the configuration, the former for disturbances of short wavelength and the latter for long wave disturbances.

## INTRODUCTION

In ordinary hydrodynamics Helmholtz instability arises when two fluids are in relative tangential motion at a plane boundary. A disturbance of the plane boundary is unstable and leads to a mixing of the two fluids. Another kind of instability (Rayleigh instability) occurs when the density gradient of fluid in the vertical direction is anywhere positive in a gravitational field. A study of the analog of these two types of instabilities in hydromagnetics is of considerable importance in astrophysics (e.g. sunspots, stellar atmospheres, solar ion-beam, streamers, cosmic jets). Talwar in a series of two papers (1959, 1960) investigated the Rayleigh problem in hydromagnetics for two density distributions—two superposed fluids and a stratified layer of fluid—with and without Coriolis force.

In this paper we shall investigate the magneto-hydrodynamical stability of two superposed fluids in relative tangential motion at the horizontal interface when the whole system is partaking in a uniform rotation about the vertical axis. Particular cases for *non-rotating* configuration have been obtained by Michael (1955), Axford (1960), Talwar (1961). In section (2) we shall develop the equations of the problem assuming the fluid to be incompressible, infinitely conducting, inviscid and stratified in the vertical direction.

## EQUATIONS OF THE PROBLEM

Consider axes  $OXYZ$  such that  $OZ$  is vertical. Suppose that a plane surface of discontinuity of tangential velocity (vortex sheet) and of magnetic field (current sheet) exist in the configuration of the two superposed fluids at the common horizontal interface  $Z = 0$ . Let the velocities and the uniform magnetic fields

(both in the  $X$ -direction) be  $U_1, U_2$  and  $H_1, H_2$  respectively for  $Z < 0$  and  $Z > 0$ . Let  $\rho_1, \rho_2$  denote the uniform densities of the lower and the upper fluids respectively. Further suppose that the configuration is uniformly rotating with an angular velocity  $\Omega$  about the  $Z$ -axis.

The equation of motion, with respect to a set of rotating axes with fixed origin, for the problem under consideration is.

$$\rho \frac{\partial V}{\partial t} + \rho(V \cdot \nabla)V = -\nabla p + g\rho + \frac{\mu}{4\pi} [(\nabla \times H) \times H] + 2\rho(V \times \Omega) \quad \dots (1)$$

where  $V, H$  denote the velocity vector and the magnetic field vector, with respect to the rotating axes, and  $p, \rho, g$  respectively denote the pressure, density at a point and the acceleration due to gravity with component  $-g$  in the  $Z$ -direction ( $g$  may even denote the net acceleration downward if there is an additional imposed acceleration).  $\mu$  is the permeability of the medium.

The incompressibility of the medium requires

$$\frac{D\rho}{Dt} = \frac{\partial \rho}{\partial t} + (V \cdot \nabla)\rho = 0 \quad \dots (2)$$

which ensures that the density of every element remains unchanged during motion.

The equation of continuity of matter is then

$$\nabla \cdot V = 0 \quad \dots (3)$$

In addition we have for a perfectly conducting fluid,

$$\frac{\partial H}{\partial t} + (V \cdot \nabla)H = (H \cdot \nabla)V \quad \dots (4)$$

and finally we have

$$\nabla \cdot H = 0 \quad \dots (5)$$

The initial state is characterized by a uniform field  $H_0$  and uniform velocity  $U_0$  both in the  $X$ -direction, and a density gradient in the  $Z$ -direction. In the perturbed state we have

$$\begin{aligned} V &= (U_0, 0, 0) + u \\ H &= (H_0, 0, 0) + h \\ p &= p_0 + \delta p \\ \rho &= \rho_0 + \delta \rho \end{aligned} \quad \dots (6)$$

Here  $u$ ,  $h$ ,  $\delta p$  and  $\delta \rho$  denote perturbations of the first order of smallness in velocity, magnetic field, pressure and density respectively, and vary with  $x$ ,  $y$ ,  $z$ ,  $t$  as (some function of  $z$ )  $\exp. (ik_x x + ik_y y + nt)$  where  $k_x$  and  $k_y$  are the horizontal wave numbers of the harmonic disturbance. On substituting in the above equations (1)-(5) we get the following equations for perturbation components,

$$\rho_0(n + ik_x U_0)u - 2\rho_0 v \Omega = -ik_x \delta p \quad \dots (7)$$

$$\rho_0(n + ik_x U_0)v + 2\rho_0 u \Omega = -ik_y \delta p + \frac{\mu H_0}{4\pi} (ik_x h_y - ik_y h_x) \quad \dots (8)$$

$$\rho_0(n + ik_x U_0)w = -D\delta p - g\delta \rho - \frac{\mu H_0}{4\pi} (Dh_x - ik_x h_z) \quad \dots (9)$$

$$(n + ik_x U_0)\delta \rho + wD\rho_0 = 0 \quad \dots (10)$$

$$ik_x u + ik_y v + Dw = 0 \quad \dots (11)$$

$$(n + ik_x U_0)h = H_0 ik_x u \quad \dots (12)$$

and

$$ik_x h_x + ik_y h_y + Dh_z = 0 \quad \dots (13)$$

where  $D$  stands for  $d/dz$ .

Let us now eliminate some of the variables and derive an equation for, say, the component  $w$  of velocity perturbation vector. Multiply (7), (8) by  $ik_x$  and  $ik_y$  respectively and add, we get, on making use of (11),

$$-(n + ik_x U_0)\rho_0 Dw - 2\rho_0 \Omega \zeta - \frac{\mu}{4\pi} (ik_x h_y - ik_y h_x) ik_y H_0 = \quad \dots (14)$$

where  $k^2 = k_x^2 + k_y^2$  and  $\zeta$  stands for  $(ik_x v - ik_y u)$ .

Eliminate  $\delta p$  from Eq. (9) and (14) after having eliminated  $\delta \rho$  by using Eq. (10). We get

$$\begin{aligned} & -(n + ik_x U_0)D(\rho_0 Dw) + \rho_0(n + ik_x U_0)k^2 w - 2\Omega D(\rho_0 \zeta) - \frac{gk^2 w D\rho_0}{(n + ik_x U_0)} \\ & + \frac{\mu H_0}{4\pi} [k^2(Dh_z - ik_x h_z) - ik_y(ik_x Dh_y - ik_y Dh_x)] = 0 \quad \dots (15) \end{aligned}$$

Making use of Eq. (12) and (13), the above equation reduces to,

$$\begin{aligned} & \left[ \rho_0(n + ik_x U_0) - \frac{gD\rho_0}{(n + ik_x U_0)} \right] k^2 w - (n + ik_x U_0)D(\rho_0 Dw) \\ & - \frac{\mu H_0^2}{4\pi} \frac{k_x^2}{(n + ik_x U_0)} (D^2 - k^2)w = 2\Omega D(\rho_0 \zeta) \quad \dots (16) \end{aligned}$$

The expression for  $\zeta (= ik_x v - ik_y u)$  can be got from Eqs. (7), and (8) by eliminating  $\delta p$  and employing Eqs. (12) and (13). After some simplifications we get

$$\zeta = \frac{2\Omega D w}{(n + ik_x U_0)} \left[ 1 + \frac{\mu H_0^2}{4\pi\rho_0} \frac{k_x^2}{(n + ik_x U_0)^2} \right]^{-1} \quad \dots (17)$$

Eliminating  $\zeta$  in Eqs. (16) and (17) and putting  $D\rho_0 = 0$  (uniform fluid), we get the equation for  $w$  as,

$$D^2 w \left[ 1 + \frac{4\Omega^2(n + ik_x U_0)^2}{\{(n + ik_x U_0)^2 + k_x^2 V^2\}^2} \right] - k^2 w = 0 \quad \dots (18)$$

where  $V^2 = \frac{\mu H_0^2}{4\pi\rho_0}$  ( $V$  = hydromagnetic velocity).

#### DISPERSION RELATION

For a configuration of two superposed uniform fluids extending indefinitely on either side of the horizontal interface  $z = 0$ , the solution of the above Eq. (18) is

$$w_1(z) = A_1 e^{m_1 z} \quad (z < 0)$$

and

$$w_2(z) = A_2 e^{-m_2 z} \quad (z > 0) \quad \dots (19)$$

where

$$m_1 = k \left[ 1 + \frac{A\Omega^2}{(n + ik_x U_1)^2 \left\{ 1 + \frac{k_x^2 U_1^2}{(n + ik_x U_1)^2} \right\}^2} \right]^{-\frac{1}{2}}$$

and

$$m_2 = k \left[ 1 + \frac{4\Omega^2(n + ik_x U_2)^2}{\{(n + ik_x U_2)^2 + k_x^2 V_2^2\}^2} \right]^{-\frac{1}{2}} \quad \dots (20)$$

where  $V_1^2 = \frac{\mu H_1^2}{4\pi\rho_1}$ , and  $V_2^2 = \frac{\mu H_2^2}{4\pi\rho_2}$ . The constants  $A_1, A_2$  are to be determined by appropriate boundary conditions.

#### Boundary Conditions

(i) At the common interface the normal component of velocity is continuous. Thus

$$w_1 - U_1 \frac{\partial \xi}{\partial x} = w_2 - U_2 \frac{\partial \xi}{\partial x} = \frac{\partial \xi}{\partial t} \quad \dots (21)$$

where  $\xi$  denotes the small displacement of the interface.

Hence

$$w_1(n + ik_x U_2) = w_2(n + ik_x U_1) \text{ at } z = 0 \quad \dots (22)$$

Using Eq. (19) we get

$$A_2 = A_1 \cdot \frac{n + ik_x U_2}{n + ik_x U_1} \quad \dots (23)$$

(ii) The normal component of magnetic field is continuous at the interface.

It can be easily verified that this condition of continuity of normal field automatically follows from Eqs. (12) and (22).

(iii) The pressure should be continuous across the interface which means that,

$$\delta p_1 - \delta p_2 + g(\rho_2 - \rho_1)\xi + \frac{\mu}{4\pi} \left[ H_1^2(h_x)_1 - H_2^2(h_x)_2 \right] = 0$$

Making use of Eqs. (12), (13), (14), (17), (19) and (23) and simplifying, the above Eq. (24) gives

$$\begin{aligned} k^2 g(\rho_2 - \rho_1) = m_1 \rho_1 \left\{ (n + ik_x U_1)^2 + k_x^2 V_1^2 \right\} \left\{ 1 + \frac{4\Omega^2(n + ik_x U_1)^2}{[(n + ik_x U_1)^2 + k_x^2 V_1^2]^2} \right\} \\ + m_2 \rho_2 \left\{ (n + ik_x U_2)^2 + k_x^2 V_2^2 \right\} \left\{ 1 + \frac{4\Omega^2(n + ik_x U_2)^2}{[(n + ik_x U_2)^2 + k_x^2 V_2^2]^2} \right\} \quad \dots (25) \end{aligned}$$

With the help of Eq. (20) the Eq. (25) can be rewritten as

$$\begin{aligned} gk(\rho_2 - \rho_1) = \rho_1 \left\{ (n + ik_x U_1)^2 + k_x^2 V_1^2 \right\} \left\{ 1 + \frac{4\Omega^2(n + ik_x U_1)^2}{[(n + ik_x U_1)^2 + k_x^2 V_1^2]^2} \right\}^{\frac{1}{2}} \\ + \rho_2 \left\{ (n + ik_x U_2)^2 + k_x^2 V_2^2 \right\} \left\{ 1 + \frac{4\Omega^2(n + ik_x U_2)^2}{[(n + ik_x U_2)^2 + k_x^2 V_2^2]^2} \right\}^{\frac{1}{2}} \quad \dots (26) \end{aligned}$$

The Eq. (26) is the characteristic equation for  $n$ , the parameter determining the stability of the configuration. The configuration shall be stable or unstable depending on whether  $n^2$  is negative or positive. If  $n$  is complex with a positive real part, it corresponds to an 'overstable' situation. The above equation is rather cumbersome for discussion in the general case. We shall therefore investigate some simple special cases.

(1) *Rotating Superposed Fluids, with magnetic field but with no tangential motion :*

The configuration characterised by a constant magnetic field was discussed in earlier paper (Talwar 1960). However, if we assume that two fluids carry different uniform fields so that they are characterised by the same Alfvén speeds

$V$  (i.e.  $H_1^2/\rho_1 = H_2^2/\rho_2$ ) then the equation is rather simpler to interpret. The characteristic equation is then, written as

$$n^4 + n^2(4\Omega^2 + 2k_x^2 V^2) + (k_x^4 V^4 - g^2 k^2 \alpha^2) = 0 \quad \dots (27)$$

where  $\alpha = \frac{\rho_2 - \rho_1}{\rho_2 + \rho_1}$ . If the upper fluid is less dense than the lower fluid, the con-

figuration is thoroughly stable and the phase velocity  $U_{p,x}$  in the  $X$ -direction of horizontally propagated waves is given by

$$\left(\frac{U_{p,x}}{V}\right)^2 = (1 + 2x^2) \pm 2x(1 + x^2 + y^2/4x^2)^{1/2} \quad \dots (28)$$

where 
$$x = \frac{\Omega}{k_x V}, \quad \text{and} \quad y = \frac{gk\alpha}{k_x^2 V^2}.$$

When the upper fluid is heavier than the lower, the situation will be unstable only when (vide Eq. (27)),  $k < k_*$  where  $k_*$  is given by

$$k_* = \frac{g\alpha}{V_k^2} \quad \dots (29)$$

Here  $V_k$  denotes the component of the hydromagnetic velocity in direction of  $k$ . Thus it follows that rotation does not change the range of stability in superposed fluids with horizontal field.

Again when  $\alpha > 0$  it follows from Eq. (27) that there exists a mode of maximum instability. If  $k_m$  and  $n_m$  denote the wave number and the growth rate of the mode of maximum instability, they can be easily shown to be given by,

$$k_m^2 = \frac{g^2 \alpha^2 (g^2 \alpha^2 + 8\Omega^2 V^2)}{4V^4 (g^2 \alpha^2 + 4\Omega^2 V^2)} \quad \dots (30)$$

$$n_m^2 = \frac{g^2 \alpha^2}{2V^2} - k_m^2 V^2$$

The Eq. (30) clearly shows that the presence of slow rotation in superposed fluids with horizontal field decreases the growth rate of the mode of maximum instability and increases the wave number of this mode.

(ii) *Rotating superposed fluids in tangential motion (no magnetic field)*

This is purely a hydrodynamic case, and the equation for  $n$  is

$$gk(\rho_2 - \rho_1) = \rho_1(n + ik_x U_1)^2 \left[ 1 + \frac{4\Omega^2}{(n + ik_x U_1)^2} \right]^{1/2}$$

$$+ \rho_2(n + ik_x U_2)^2 \left[ 1 + \frac{4\Omega^2}{(n + ik_x U_2)^2} \right]^{1/2} \quad \dots (31)$$



The equation (31) for small wavelengths simplifies to

$$n(\rho_1 + \rho_2) = -ik_x(\rho_1 U_1 + \rho_2 U_2) \pm [\rho_1 \rho_2 k_x^2 (U_1 - U_2)^2 - gk(\rho_1^2 - \rho_2^2) - 2\Omega^2(\rho_1 + \rho_2)^2]^{\frac{1}{2}} \quad \dots (32)$$

The system shall be unstable if the term under the radical sign is positive and stable if it be negative. Thus the condition of stability is written as

$$(U_1 - U_2)^2 < \frac{g(\rho_1^2 - \rho_2^2)}{k\rho_1\rho_2} + \frac{2\Omega^2(\rho_1 + \rho_2)^2}{k^2\rho_1\rho_2} \quad \dots (33)$$

if  $k_y$  is zero. This result (when  $\Omega = 0$ ) is identical to that obtained earlier (Talwar 1961) with no interfacial tension.

For disturbances characterised by long wavelengths (or high rotation) the equation (31) gives

$$n = \frac{gk\alpha}{2\Omega} - \frac{ik_x(\rho_1 U_1 + \rho_2 U_2)}{\rho_1 + \rho_2} \quad \dots (34)$$

When  $\alpha > 0$  (top fluid heavier), it follows from equation (34) that the configuration is 'Overstable'. If the fluid be less dense ( $\alpha < 0$ ), the disturbances are periodically damped with phase velocity  $U_{px}$  given by

$$U_{px} = \frac{I(n)}{k_x} = \frac{\rho_1 U_1 + \rho_2 U_2}{\rho_1 + \rho_2} \quad \dots (35)$$

(iii) *Homogenous single Fluid with tangential motion, subject to rotation and uniform horizontal field.*

For  $\rho_1 = \rho_2$  and  $V_1 = V_2$  the Eq. (26) gives

$$n^2 + nik_x(U_1 + U_2) + \left[ 2\Omega^2 + k_x^2 \left( V^2 - \frac{U_1^2 + U_2^2}{2} \right) \right] = 0 \quad (36)$$

as the characteristic equation for  $n$ . Thus

$$in = \frac{k_x(U_1 + U_2)}{2} \pm \left[ 2\Omega^2 + k_x^2 \left\{ V^2 - \left( \frac{U_1 - U_2}{2} \right)^2 \right\} \right]^{\frac{1}{2}} \quad (37)$$

which gives the condition of instability as,

$$(U_1 - U_2)^2 > \frac{8\Omega^2}{k_x^2} + 4V^2 \quad (38)$$

Therefore, if two parts of a single medium move with a relative tangential velocity less than twice the hydromagnetic velocity, the system is thoroughly stable

for all  $k$ . Rotation has stabilising influence for long wave lengths as is evidenced by Eq. (38). However, if relative velocity is more than twice the hydromagnetic velocity, we can define from Eq. (38) a critical wavelength  $\lambda_x^* (= 2\pi/k_x^*)$  such that the system is stable for perturbations with wave lengths in the  $X$ -direction larger than  $\lambda_x^*$  and unstable for  $\lambda_x < \lambda_x^*$  only. Rotation and magnetic field for a given tangential velocity decrease  $\lambda_x^*$  and thus have a stabilising influence.

The phase velocity  $U_p$  in the  $x$ -direction for stable configuration is written as

$$U_{p1,2} = \frac{U_1 + U_2}{2} \pm \left[ \left( V^2 + \frac{2\Omega^2}{k_x^2} \right) - \left( \frac{U_1 - U_2}{2} \right)^2 \right]^{1/2} \quad \dots (39)$$

and the group velocity  $U_g$  in the  $x$ -direction is

$$U_{g1,2} = \frac{U_1 + U_2}{2} \pm \left[ V^2 - \left( \frac{U_1 - U_2}{2} \right)^2 \right]^{1/2} \left[ \frac{2\Omega^2}{k_x^2} + \left\{ V^2 - \left( \frac{U_1 - U_2}{2} \right)^2 \right\} \right]^{-1/2} \quad \dots (40)$$

The following properties of  $U_p$  and  $U_g$  are implicit in equations (39) and (40).

When  $k_x \rightarrow 0$ ,  $|U_p| \rightarrow \infty$  and  $U_g \rightarrow \frac{U_1 + U_2}{2}$  as  $k_x \rightarrow \infty$  [when  $(U_1 - U_2) < 2V$ ] and

at  $k_x = k_x^*$  [when  $(U_1 - U_2) > 2V$ ]. Again  $U_g = \frac{U_1 + U_2}{2}$  when  $k_x \rightarrow 0$  and

$U_g \rightarrow \infty$  when  $k_x = k_x^*$  [when  $(U_1 - U_2) > 2V$ ] and at  $k_x \rightarrow \infty$  [when  $(U_1 - U_2) < 2V$ ].

#### REFERENCES

- Axford, W. I., 1960, *Q. Journal mech. and App. math.*, **13**, Part 3, 314.  
 Michael, D. H., 1955, *Proc. Camb. Phil. Soc.*, **51**, 528.  
 Talwar, S. P., 1959, *Zeits Für Astrophysik*, **47**, 1616.  
 Talwar, S. P., 1960, *Journal Fluid Mechanics*, **9**, 581.  
 Talwar, S. P., 1961, *Proc. Nat. Inst. Sci. (India)* **27**, 263.

# ON THE DETERMINATION OF ACTIVATION ENERGY OF DIFFUSION THROUGH DISLOCATIONS

A. L. LASKAR

PHYSICS DEPARTMENT,

INDIAN INSTITUTE OF TECHNOLOGY, KHARAGPUR

(Received May 19, 1961)

**ABSTRACT.** A method has been developed to determine the activation energy of diffusion through dislocations based on the model of straight dislocation pipes running through the crystals. The activation energy for the pipe diffusion of NaCl through LiF crystals has been determined to be nearly 0.2 e.v. The low value of the activation energy has been explained in terms of the short-circuit path provided by the dislocations.

## INTRODUCTION

The phenomenon of "pipe-diffusion" necessitates the re-appraisal of the bulk diffusion data in many cases. It is well-known that there is considerable scatter in the diffusion data for the same element obtained from different sources, and by different workers. It may be noted that a re-analysis by several authors, of earlier experimental results on diffusion showed the prominent role played by the dislocations. Williams and Slifkin (1958) concluded from their study of rare earth traces of silver and lead that the tail which was more prominent at low temperature in their diffusion curves, could be explained by the presence of foreign atoms in one atomic site in a thousand along a dislocation line. The role of dislocations on diffusion through solids has been discussed by a number of authors, a review of which is given by Amelinckx and Dekeyser (1959). The dislocations are recognised as microscopic pipes through the solid body. In the atomistic theory of diffusion these dislocation pipes would provide short circuit paths for diffusion and this again will have a great effect on the electrical conductivity in case of polar and homopolar crystals. In recent years Tucker and Gibbs (1958), Ibuki and Yamashita (1959) have reported enhanced diffusion and increase of conductivity current in the order of 1000 times in some cases, in presence of dislocations.

It is believed that the concentration of pipes in a sample will determine the effect of dislocations on the bulk properties. If the diffusion phenomenon for dislocation channels is studied independently and the activation energy for the process is estimated, then a comparison with bulk diffusion data for the same sample will clearly indicate the role played by the dislocations. If we now have another sample of the same elements with a different concentration of dislocations,

it would be probable to estimate the change in diffusion properties. This will lead to a better understanding of the role played by dislocations on other structure-sensitive properties. Experimental results of the study of enhanced diffusion and conductivity through individual dislocations have been reported by Laskar and Tucker (1960, 1961). In the present paper a method has been developed to determine the activation energy needed for the diffusive flow through a dislocation pipe. This method has been used to determine the activation energy of pipe diffusion of NaCl in LiF crystals.

## RESULTS AND CONCLUSIONS

The theory was worked out in case of diffusion of single ionized Na atoms through a LiF chloride crystal when D.C. voltage is applied through a microprobe sitting on a dislocation while the lower surface was plated with radioactive NaCl. The microprobe was made negative with respect to the lower surface. In order to correlate the diffusive current with the usual parameters the following relationships were established for an ideal dislocation pipe through a crystal :

(a) Considering the field effect alone

$$J = n_0 v_0 \frac{e a^2}{K T} E_{ext} \exp \{ -(E_1 + E_m)/K T \} \quad (1)$$

where  $J$  = current flux.

$n_0$  = probability of an atom site being occupied.

$v_0$  = jump frequency.

$a$  = interatomic distance.

$E_{ext}$  = externally applied electric field.

$E_1$  = injection energy, i.e. the energy needed for the ions to penetrate the barrier layer at the bottom.

$E_m$  = motion energy of the particles through the pipe.

$e, K, T$  have the usual significance.

(b) Time independent one dimensional diffusion equation in presence of an electric field has the form :

$$J = \mu n E_{ext} + \mu n E_{int} - D \frac{dn}{dx} + \gamma$$

where  $\mu$  = mobility.

$E_{int}$  = internal field due to the distributions of charged particles along the dislocation lines.

$D$  = diffusivity.

$\gamma$  = the sum total effect of the jogs and Cottrell atmosphere along the pipes.

Neglecting  $\gamma$  which is, after, all a small effect, the following expression of current through the dislocation was obtained.

$$J_x = \mu(n_0 + \eta_x)E_{ext} - 2\mu en_0 \eta'_x \log N - D\eta'_x \quad \dots (2)$$

where  $\eta_x$  = the perturbation on the distribution through the channel.

$N$  = total particles in the dislocation channel.

$N$  is given by

$$N = n_0 + \beta/\alpha \left[ \frac{1}{\alpha} (e^{aL} - 1) \right] - L \quad (3)$$

Expressions for  $\alpha$  and  $\beta$  are

$$\left. \begin{aligned} \alpha &= \frac{\mu E_x}{D + 2\mu en_0 \log N} \\ \beta &= \frac{\mu n_0 E_x - J}{D + 2\mu en_0 \log N} \end{aligned} \right\} \quad (4)$$

Estimate is made with the following typical data

$$\left. \begin{aligned} I &= \text{conductivity current} \dots 10^{-8} \text{ amps.} \\ V &= \text{applied D.C. voltage} \dots 300 \text{ volts.} \\ T &= \text{temperature of the sample under study} \dots 700^\circ \text{K} \\ d &= \text{thickness of sample} \\ (E_1 + E_m) &= \text{total activation energy for the process} \dots 0.74 \text{ ev.} \\ \nu_0 &= \text{frequency} \dots 10^{13}. \end{aligned} \right\} \dots (5)$$

With the help of above data one obtains

$$E_{ext} = \frac{V}{Kd^2}$$

$$\therefore E_{ext} = 2.7 \times 10^{-2} \frac{\text{volt}}{\text{meter}} \text{ using M.K.S. system of units.}$$

The dielectric constant for LiF is taken as  $K = \epsilon \epsilon_0$

$$\text{where} \quad c = 5$$

From equations (1) and (4) one gets

$$n_0 = 10^{-2}/\text{cm} = 1/\text{meter} \quad (6)$$

$$\alpha = \frac{1.6 \times 2.7 \times 10^{-}}{1 + 3.2 \times 1.6 (\log N \cdot n_0) \times 10^{-}}$$

$$= 0.432 \quad (7)$$

$$\beta = \alpha n_0 - \frac{J}{D + (2\mu e n_0 \log N)}$$

$$= \alpha n_0 - \frac{10^{-31}}{(F)[1 + 5(\log N \cdot n_0) \times 10^{-8}]} \quad \dots (8)$$

where  $F = a^2 e^{-E_m/KT}$  ... (9)

From equation (2) one obtains

$$J_x = (F \cdot n_0)(4.32 \times 10^{12} e^{-4322})[1 - (n_0 \log N)5.12 \times 10^{-6} - 1] \quad \dots (10)$$

The three quantities within the double bracket should be identified with the external field term, the internal field term and the diffusion term respectively. Expression (10) shows order of magnitude calculation only for the square bracket. The internal field term is of the order of  $10^{-3}$  or  $10^{-4}$  and one can write that the current flowing through the central region is given by

$$J \simeq (1.7 \times 10^{-7}) e^{-E_m/KT} [1 - 10^{-4} - 1] \quad \dots (11)$$

where  $x = L/2 = 2.5 \times 10^{-4}$  meters.

This estimate shows that the internal field has got negligible effect on the diffusive current flow, whereas the external field term and diffusion term are of the same order of magnitude.

In order of magnitude calculation then equation (11) may be rewritten as

$$J \simeq (1.7) \times 10^{-7} e^{-E_m/KT} \quad \dots (12)$$

The following is the order of current calculated by assuming different values of  $E_m$ .

$E_m$ in e.v.	$J$ in amps
0.1	$\sim 3 \times 10^{-8}$
0.2	$\sim 6 \times 10^{-9}$
0.4	$\sim 2 \times 10^{-10}$
0.5	$\sim 2 \times 10^{-11}$
0.7	$\sim 1 \times 10^{-12}$

Experimentally obtained current is of the order of  $10^{-8}$  amperes. Hence it may be estimated that the motion energy for the diffusive current is .2 e.v. or less. The activation energy estimated from bulk diffusion data is more than 1 e.v. It is thus seen that the activation energy for diffusion through dislocation pipes in presence of externally applied electric field is very much smaller. This conclusion is also supported by the microscopic observations (which has been

reported by author (1960)) of massive deposit near the microprobe at a temperature where bulk diffusion in LiF crystals is extremely small. It is to be noted, however, that this calculations are based on a simple model which assumes a uniform dislocation pipe running from the bottom to the top of the crystals. Even if the dislocation pipe is of mixed type, the broad aspects of theory still can be applied, so long there is a continuity of the pipe through the crystal. Calculations along these lines, with other experimental data, are in progress. Similar experiments with homopolar crystals would be interesting in understanding the basic atomic mechanism for diffusion process.

#### ACKNOWLEDGMENT

The author is indebted to Prof. Robb. Thomson and Dr. Ross. N. Tucker for their interest and guidance during the progress of work and to Prof. J. S. Kochler for some helpful criticism.

#### REFERENCES

- Amelinckx, S. and Dekeyser, W., 1959, *Solid State Physics* (Academic Press), Vol. 8, 407.  
Hubner, K. and Shockley, W., 1959, *Structure and Properties of Thin Films* (Wiley), 302. A paper to be published in *Phys. Rev.*  
Ibuki and Yamashita, 1959, *J. of Phys. Soc. Japan*, **14**, 1827.  
Laskar, A. L. and Tucker, R. N., 1960, Rept. of Solid State Sciences, Air Force Office of Scientific Research. (U.S.A.), A paper is to be published in *Phys. Rev.*  
Laskar, A. L., 1962, *Proc. Nat. Inst. of Sciences, India*, **28A**.  
Tucker, R. N. and Gibbs, P., 1958, *J. Appl. Phys.*, **9**, 1375.  
Williams, G. P., and Shifkin, L., *Phys. Rev. Letters* **1**, 243.

## GRID CONTROL OF GAS-TUBE NOISE

K. K. BOSE AND P. L. DASGUPTA

INDIAN INSTITUTE OF TECHNOLOGY, Kharagpur

(Received August 2, 1961)

**ABSTRACT.** Gas tubes are the most common sources of electrical noise voltage. In the thyatron it has been observed that the control grid, which has no influence on the main anode current after the discharge has started, possesses considerable control on the noise output of the valve. No reference of this fact has been found anywhere by the authors, but it confirms the suggestion made by Labrun and Bigg (1952) that the noise from a discharge tube is not of thermal origin. It has been shown in the following how the noise amplitude (as measured in oscilloscope) varies with the negative grid bias, and the experimental results have been presented.

## INTRODUCTION

Normally, the grid of a gas triode loses all its control on the flow of current once the discharge between the cathode and anode is initiated. The grid of a thyatron is able only to initiate the discharge between the cathode and anode, but loses all its control on the flow of current once the tube starts to conduct. This is because the positive ions produced by the ionisation by collisions are attracted towards the negative grid and surround it with a sheath of positive ions and neutralise the electrostatic effect of the grid, destroying its control action. The positive ions are also attracted towards the cathode and neutralise the space charge.

It has been found, however, that even after the discharge has started the noise voltage produced in the tube can be very smoothly controlled by the negative grid voltage, anode current remaining unaffected. The noise voltage has a peak or maximum value for particular values of the anode current; and it is also found that the point where the noise amplitude becomes maximum, shifts with the variation of negative grid voltage. No attempt has been made to measure the noise spectra, which has already been done by many workers (Martin and 400 *sd*, 1952 and Teong saw yak, 1955). The purpose of the experiment was only to study the effect of negative grid bias on the integrated and over all noise produced in the gas discharge tube, which, according to authors' information, has not been investigated as yet.

The experiment was carried out with the RCA 884 thyatron. A current limiting non-inductive resistance of 500 ohms was connected in the anode circuit. The noise output from the anode of the thyatron was fed to a cathode follower and the output of the cathode follower was connected to the vertical amplifier of the oscilloscope through a calibrated attenuator and a low-pass filter (cut off



frequency about 200Kc/s). The low-pass filter was provided to avoid the high frequency discrete oscillations which were observed at particular values of plate current. The frequency of discrete oscillations was found to increase with the anode current, in confirmation with the results obtained by Martin and Woods (1952). Just like noise, the amplitude of these discrete oscillations could be controlled by the negative bias of the thyatron grid.

## EXPERIMENTAL RESULTS

The grid bias of the thyatron was set to different negative voltages, and for each setting of the bias the d.c. discharge current was varied by varying the anode

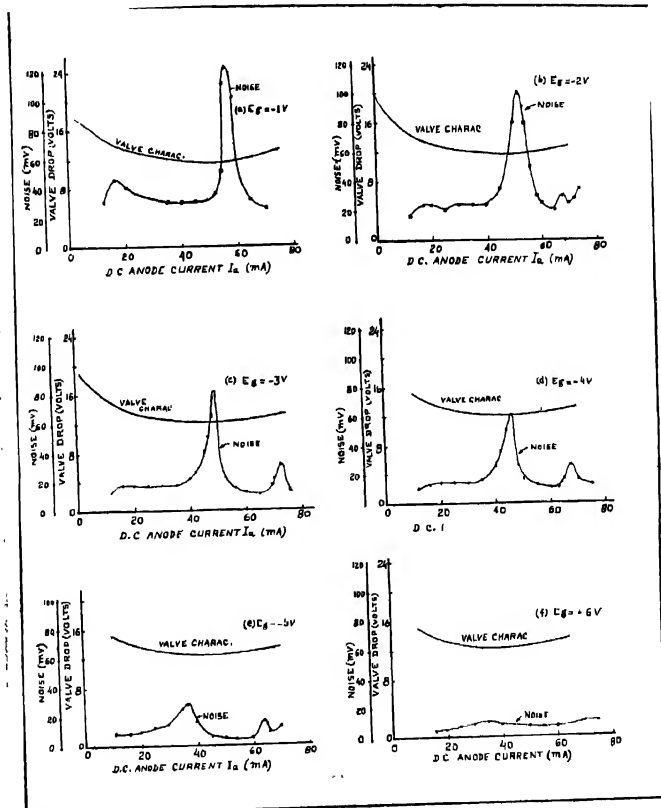
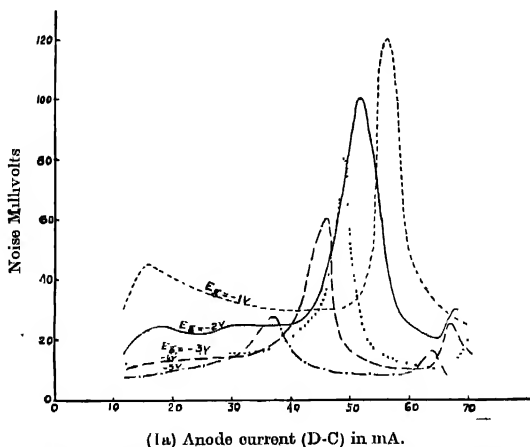


Fig. 1. Showing the relationship between noise output and grid bias ( $E_g$ .)

voltage and the corresponding values of tube drop and noise output measured. Fig. 1 shows the results. Here the tube drop and noise voltage are plotted against the tube current for six values of grid voltage from  $-1$  Volt to  $-6$  Volts. The noise voltage is not the absolute r.m.s. voltage, but as measured from peak to peak in the oscilloscope. The object was only to compare the relative magnitudes of the noise voltage under different conditions, and hence, only the total height of the noise voltage was measured in the oscilloscope.

In Fig. 3, the five curves of Fig. 1 (corresponding to grid voltage  $-1$  V,  $-2$  V,  $-3$  V,  $-4$  V and  $-5$  V) are shown together, under same scale and same axes, for better orientation. The results concerning the relationship between the thyatron noise and thyatron characteristic confirmed in general the observations made by Martin and Wood (1952). Martin and Wood pointed out that on the nearly horizontal part of the tube characteristic the noise went through various maxima, and ultimately falling to low values as saturation was approached. But with the thyatron and in the region of our present investigation only one or two maxima were observed, and one maximum was very large. This maximum noise was found to appear at the point where the tube drop was apparently minimum, as shown in Fig. 1. The discharge current at which the maximum noise voltage was produced was found to vary with the negative grid voltage. An increase in the negative grid voltage causes the maximum to occur at lower value of discharge current (Fig. 2). Amplitude of the maximum values of the noise voltage



(1a) Anode current (D-C) in mA.  
Fig. 2. Effect of grid bias on noise amplitude. Noise becomes maximum (peak) at particular values of  $I_a$ .

decreased, practically linearly with increasing negative grid bias. This has been shown in Fig. 3, where the vertical axis shows the amplitude of the noise

maxima, which occur at different values of the plate current when the grid bias is varied. When the grid voltage was more than  $-6$  volts, no distinguishable maximum of the noise voltage was observed for this particular thyatron.

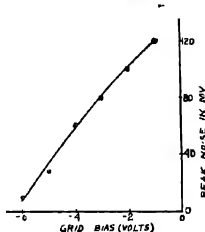


Fig. 3. Shows the effect of grid bias on peak noise.  $I_a$  variable.

In Fig. 4, the noise voltage is plotted against negative grid bias in the region of the tube characteristic where there were no sharp maxima. The noise voltage has been shown for two values of the discharge currents, 15 mA and 25 mA.

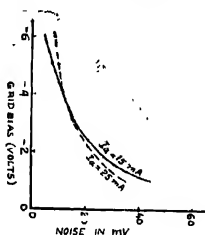


Fig. 4. Shows the effect of grid bias on noise amplitude.  $I_a$  constant.

Here one can see that the noise output from the thyatron can be smoothly controlled by the grid voltage.

#### DISCUSSION

It is not very clearly understood how the noise output of the thyatron is controlled by the grid, but a possible explanation is given here, which is very tentative. The fact that the noise is controlled by negative grid bias, suggests that the noise of the discharge tube could not be of thermal origin. This has also been corroborated by Labrum and Bigg (1952); for, to generate a noise output of about one micro-microwatt per cycle per second, the thermal source should have a temperature of about  $10^{11}$  deg.  $K$ , whereas the electron temperature in the discharges was known to be less than a million degree absolute. Labrum and Bigg, who had worked with the two electrode discharge tube, suggested that the noise was due to electron and ion oscillation, analogous to those in the Barkhausen-Kurz oscillator, in a region where the potential on the axis of the discharge passes

through a maximum value. In fact noise was only generated in discharges in which such a reversal of potential gradient do occur. To our observations the noise output from the thyatron, after the conduction has started, originate primarily from the random oscillation of the positive ions only. Although electrons and ions are simultaneously produced in the discharge, electrons being lighter move at higher velocity than the positive ions and their density in the space near cathode is low. Because of the lower mobility of the ions they leave the space more slowly than the electrons, as a result of which the space charge becomes positive and the space charge distribution curve assumes the well known upward curvature. The negative grid holds the positive ions bound around it and the thickness of the ion-sheath surrounding the grid depends on the grid potential. The contribution of these bound ions to the noise output is thereby lost, but the discharge current remains unaffected, since in the thyatron the discharge current is almost equal to the total electron current emitted from the cathode, the positive ions only help to neutralise the space charge. It is interesting to note here that the vacuum tube retarding field oscillators usually operate also at negligible space charge.

The experiment, however, shows that it is possible to construct a variable-output noise-generator whose output can be smoothly controlled by grid bias. Another important application of this effect could be the construction of a d.c. power-supply with minimum noise. Gas tube rectifiers are generally not used in radio receiver sets inspite of their large current output because of the high noise level inherent to such tubes which interfere the reception considerably. If thyatrons with negative grid bias are used as rectifiers the noise level in d.c. output could be minimised and even reduced to negligible value, if the bias is made sufficiently negative. If thyatrons in place of gas-diodes are used in big d.c. power supplies, the output can be thus made practically noise-free, and such power supplies may be used for sensitive electronic apparatus.

#### ACKNOWLEDGMENT

The authors wish to express their thanks to Prof. H. Rakshit, Head of the Department of Electronics and Electrical Communication Engineering, for his kind help and interest in the work.

#### REFERENCES

- Labrum and Bigg, 1952, *Proc. Phys. Soc.* **65**, Pt. 5
- Martin, H. and Woods, H. A., 1952, *Proc. Phys. Soc.*, **B65**, 281.
- Thong Saw Pak, 1955, *Proc. Phys. Soc.*, **B68**, 292.

# A TWIN-TUNED R-C NETWORK

S. C. DUTTA ROY\*

ELECTRONICS SECTION, RIVER RESEARCH INSTITUTE, WEST BENGAL

(Received August 22, 1961, Resubmitted March 26, 1962)

**ABSTRACT.** A resistance capacitance network having two resonance frequencies of adjustable separation has been described. A special feature of the network is that the attenuation is infinite at the frequency of the dip, whatever be the separation or the magnitude of the peaks

## INTRODUCTION

At radio frequencies, a response characteristic with two pronounced peaks can be obtained by inductive coupling of two  $L-C$  resonant circuits. In the low frequency range, however, such a method is not practical because even moderate coupling requires an iron core and tuning demands impracticably large values of inductance and capacitance. Even if two resonant circuits can be made and coupled satisfactorily, the value of  $Q$  obtainable for either circuit and the overall transfer characteristic will be very low. Also, because of the use of a solid core, the coupling cannot be changed easily and as such the separation of the peaks will not be easily adjustable. Capacitance coupling can be used, but since the largest practical value of a variable capacitance is about 500  $pF$ , the coefficient of coupling will be very small for even the maximum setting of the capacitor. A large value of the coupling capacitance will be required for obtaining a reasonable amount of coupling, and as in the inductive case, the selectivity will be very poor.

In this paper is described a resistance capacitance network which gives a twin tuning effect with reasonable values of  $Q$  for either resonance. As in the coupled circuit, the magnitude of the peaks can be made equal and the separation between them can be conveniently adjusted. A special feature of the  $R-C$  network is that the dip frequency is completely suppressed, whatever be the separation or the amplitude of the peaks. This cannot ordinarily be obtained in a coupled circuit in which the magnitude of the dip changes with change in the coupling and an infinite coefficient of coupling is required to suppress the dip frequency completely.

## THE NETWORK CONFIGURATION

The network having two resonance frequencies is realised by a cascade connection of a twin- $T$   $R-C$  network and a selective  $R-C$  network similar to that

\*Present address: Department of Physics, University of Kalyani, Harinaghat, P.O. Mohanpur, Dist. Nadia, West Bengal.

used in a Wien bridge oscillator, and is shown in Fig. 1. The latter will henceforward be referred to as the Wien network for convenience. The components of the two networks are so chosen that the rejection frequency of the former is the same as the frequency of maximum response of the latter. The transfer characteristic of the Wien network resembles a resonance curve while that of the twin- $T$  network is an inverted resonance curve with zero transmission at a particular frequency. If these two curves can be multiplied then the overall characteristic will show the rejection property of the latter and two peaks on either side of this null frequency. A true multiplication effect can be obtained by cascading the two networks, provided that the output impedance of the twin- $T$  is small compared with the input impedance of the Wien network. It will be shown that this condition can be satisfied by a proper design of the latter.

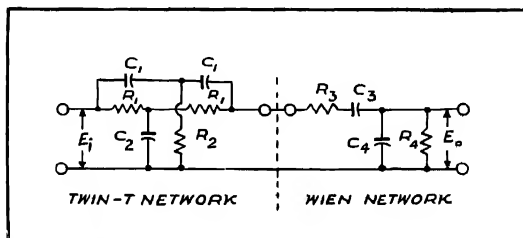


Fig. 1. Showing the network configuration for obtaining a twin tuning effect.

#### THE TWIN-T NETWORK

The transfer function of the twin- $T$  network of Fig. 1 under the conditions of zero source and infinite load impedances is given by

$$A_T = \frac{1}{1 - j \frac{2(k^3 + k^{-1})}{(x - 1/x)}}$$

where  $x = \omega/\omega_0$  is the normalised frequency,  $\omega_0 = (2R_1R_2C_1^2)^{-1/2} = (C_1C_2R_1^2/2)^{-1/2}$  is the null frequency in radians/sec, and  $k = R_1/(2R_2) = 2C_1/C_2$  is a design parameter controlling the selectivity of the transfer characteristic. Maximising  $A_T$  with respect to  $k$  gives a value  $k = 1$ . Since it is desired to obtain the highest possible selectivity for the individual resonances in the response of the twin tuned circuit, we shall assume a maximum selective twin- $T$  configuration for which  $R_1 = 2R_2 = R$  (say),  $C_1 = C_2/2 = C$  (say),  $\omega_0 = 1/(RC)$  and

$$A_T = \frac{1}{1 - j \frac{4}{(x - 1/x)}} \quad \dots (1)$$

THE WIEN NETWORK

The resonance frequency of the Wien network is given by  $\omega_0' = (R_3 R_4 C_3 C_4)^{-1/2}$ . It was shown in an earlier work (Dutta Roy, 1962) that instead of using the conventional configuration with  $R_3 = R_4$  and  $C_3 = C_4$ , the selectivity of the network can be increased by using unequal elements. A design parameter,  $n$  was defined as  $n = (R_4/R_3)^{1/2} = (C_3/C_4)^{1/2}$  and it was shown that  $Q$  of the circuit increases with decreasing  $n$ .

In terms of  $n$ ,  $nR_3 = R_4/n = R'$  (say) and  $nC_4 = C_3/n = C'$  (say) so that  $\omega_0' = 1/(R'C')$ . Since it is desired that  $\omega_0 = \omega_0'$ , we choose  $R = R'$  and  $C = C'$ . Then the transfer function of the Wien network is given by

$$A_W = \frac{n^2/(n^2+2)}{1+j(x-1/x)/(n^2+2)} \quad \dots (2)$$

With such choice of components, the network of Fig. 1 now takes the form shown in Fig. 2.

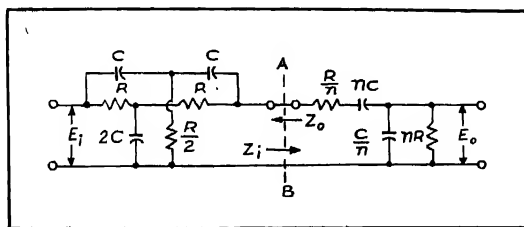


Fig. 2. The network of Fig. 1 redrawn with chosen values of components.

CHARACTERISTICS OF THE TWIN TUNED CIRCUIT

It is shown in Appendix 1 that if the source impedance is negligible, the transfer function of the network of Fig. 2 is given by

$$A = \frac{1}{\frac{n^2+2n+6}{n^2} + j \left\{ \frac{y}{n^2} \left( 1 + \frac{4n}{16+y^2} \right) - \frac{4}{y} \left( 1 + \frac{2}{n^2} + \frac{2}{n} \frac{8+y^2}{16+y^2} \right) \right\}} \quad \dots (3)$$

where  $y = x - 1/x$ . At  $x = 1$ , i.e.  $\omega = \omega_0$ , the denominator of (3) is infinite and therefore the transmission is nil. The frequencies of maximum response can be obtained by equating the imaginary part of the denominator of (3) to zero. This gives on simplification

$$y^4 - 4(n^2 + n - 2)y^2 - 64(n^2 + n + 2) = 0$$

Under the restriction that  $y^2$  must be positive for real frequencies the above equation has the solution

$$y^2 = 4(n^2 + n + 2) \quad \dots (4)$$

It can be shown that positive frequencies ( $x_{02}, x_{01}$ ) satisfying equation (4) have a separation given by the square root of the right hand side, i.e.

$$S = x_{02} - x_{01} = 2(n^2 + n + 2)^{1/2} \quad \dots (5)$$

Fig. 3 shows the variation of  $S$  with  $n$ . Minimum separation occurs when  $n$  tends to zero, the value being given by  $S_{min} = 2.83$ . The response at either resonance is given by

$$A_0 = n^2 / (n^2 + 2n + 6) \quad \dots (6)$$

The variation of  $A_0$  (in decibels) with  $n$  is also shown in Fig. 3.

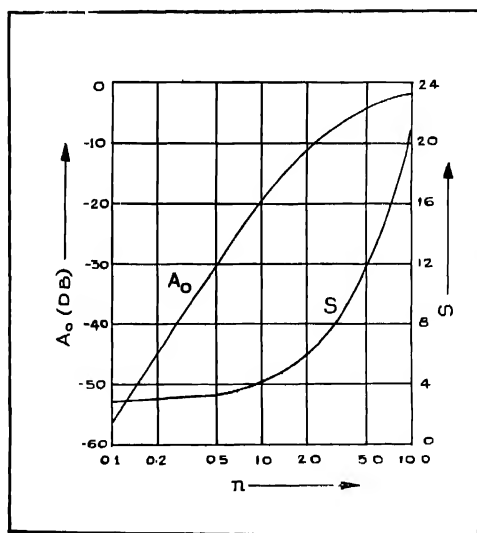


Fig. 3. Showing the variation of the response at resonance ( $A_0$ ) and the separation between the peaks ( $S$ ) with the design parameter of the Wien network ( $n$ ).

The separation between the peaks can be adjusted by varying  $n$ . This requires two potentiometers for  $R_3$  and  $R_4$  and two decade capacitors together with two trimmer capacitors for  $C_3$  and  $C_4$  (Fig. 1).  $C_3$  and  $C_4$  are first set to the nearest decade value; the trimmers are then adjusted to get exact values.



Expression (3) is too much complicated to be manipulated for finding out an expression for the selectivity of the twin tuned circuit at either resonance; for it gives an eighth degree equation in  $y$  (in which all the powers of  $y$  are present) to be solved for finding the frequencies at which  $|A| = 0.707 A_0$ . An approximate analysis is given in Appendix 2 on the assumption that the input impedance of the Wien network ( $Z_i$ ) is far greater than the output impedance of the twin-T network ( $Z_0$ ). The range of values of  $n$  for which this assumption is valid is discussed in Appendix 3. The results of the approximate analysis are shown in Fig. 4 where the subscripts  $l$  and  $h$  refer to the lower and the higher frequency resonances respectively. It is noted that  $Q_l > Q_h$  and that  $Q$  for either resonance, especially  $Q_l$ , is appreciably greater than that obtainable with the Wien network alone. For example, at  $n = 1$ ,  $Q_l = 0.67$  and  $Q_h = 0.56$ , while the Wien network gives a  $Q = 0.33$  only.

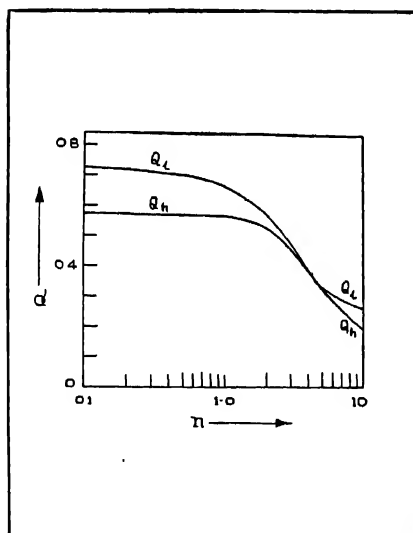


Fig. 4. Showing the variation of  $Q_l$  and  $Q_h$  with  $n$ .

#### EXPERIMENTAL RESULTS AND INTERPRETATION

The experimentally obtained transmission curves for a rejection frequency of 1500 c/s and  $n = 0.5, 1.0, 2.0$  and  $4.0$  are shown in Fig. 5. It is observed that :

(i) Each curve has two peaks and a dip. The magnitude of the dip is very small compared with those of the peaks. It is approximately the same for all the curves.

- (ii) The separation between the peaks increases with increasing  $n$  approximately in accordance with (5).
- (iii) The magnitude of the peak response increases with increasing  $n$  approximately in accordance with (6).
- (iv) The lower frequency resonance is sharper than the higher frequency one.

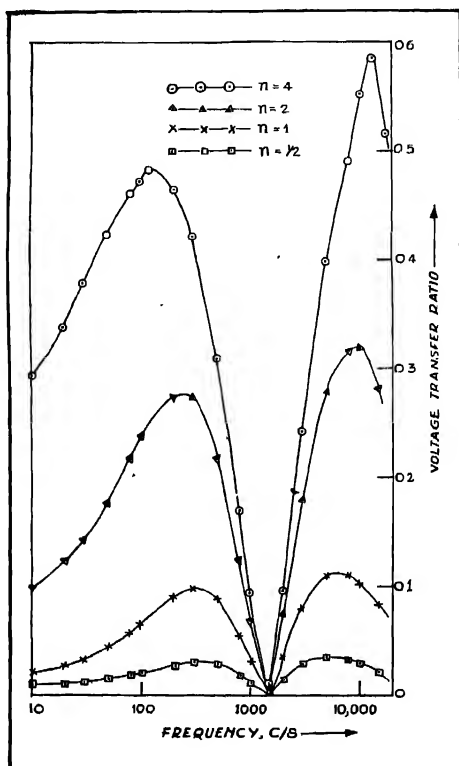


Fig 5. Experimentally obtained transmission curves of the twin-tuned circuit for a rejection frequency of 1500 c/s and  $n = 0.5, 1.0, 2.0$  and  $4.0$ .

The magnitude of the dip is not perfectly zero; the discrepancy is caused by two factors, viz., (i) harmonics in the output of the oscillator used to measure the curves and (ii) stray capacitances.

The unequal peaks observed in the experimental curves may be due to one or more of the following reasons : (i) slight difference between  $\omega_0$  and  $\omega_0'$  resulting

from use of components correct to not more than two significant figures, and (ii) asymmetry in the response of one or both the networks resulting from (a) stray capacitances and /or (b) unequal harmonic generation by the oscillator in the low and high frequency bands. The word 'asymmetry' of course refers to the plot of amplitude transfer function versus  $\log_{10}$  (frequency)

### CONCLUSIONS

In what has been discussed so far, the twin- $T$  network has been assumed to be fixed and the effect of a variation in  $n$  has been considered. This is convenient from practical point of view, because changing  $k$  will not only change the separation but also the rejection frequency; to have a symmetrical response curve with equal peaks, one has to change simultaneously all the components of the twin- $T$  as well as the Wien network.

Nevertheless, when a fixed separation and null frequency are desired, a value of  $k \neq 1$  may be used. The relevant equations may be obtained from an approximate analysis (assuming  $Z_0 \ll Z_i$ ) as

$$S = \{2(n^2 + 2)(k^{\frac{1}{2}} + k^{-\frac{1}{2}})\}^{\frac{1}{2}}$$

$$A_0 = \frac{n^2}{n^2 + 2 + 2(k^{\frac{1}{2}} + k^{-\frac{1}{2}})}$$

For getting equal peaks, the Wien network resistance and capacitance parameters  $R'$  and  $C'$  are to be so chosen that

$$\omega_0 = k^{\frac{1}{2}}/(RC') = 1/(R'C')$$

The salient characteristics of the twin tuned R-C network can now be summarised as follows :

- (i) It has two resonance frequencies and a frequency of very high (theoretically infinite) attenuation in between them.
- (ii) The magnitude of the peaks are equal when the null frequency of the twin- $T$  network is the same as the resonance frequency of the Wien network and when the individual response curves are perfectly symmetrical, any deviation from these two conditions will result in unequal peaks.
- (iii) The frequency separation of the two peaks can be conveniently adjusted by keeping the twin- $T$  network fixed and by varying  $n$ , the design parameter of the Wien network.
- (iv) The separation cannot be decreased indefinitely, a minimum value of 2.83 (normalised with respect to the rejection frequency) being reached when  $n$  tends to zero.
- (v) The magnitude of the dip and the frequency at which it occurs are independent of the separation or the height of the peaks.

- (vi) The lower frequency resonance is sharper than the higher frequency one.
- (vii)  $Q$  for either resonance is appreciably greater than that obtainable with the Wien network alone.

## ACKNOWLEDGMENT

The author is deeply indebted to Professor J. N. Bhar., D.Sc., F.N.I., for his kind help and guidance and to Dr. A. K. Chowdhury, M.Sc., D.Phil., for valuable discussions. The work is published with the kind permission of the Director, River Research Institute.

## REFERENCE

Dutta Roy, S. C., 1962, Communicated to the Indian Journal of Physics.

## APPENDIX 1

Looking back from the junction  $A B$  (Fig. 2), the source (assumed to have zero internal impedance) and the twin- $T$  network can be replaced by an equivalent Thevenin generator having an open circuit voltage given by

$$E = E_i A_T = \frac{E_i}{1-j \frac{4}{4/(x-1/x)}}$$

and an internal impedance  $Z_0$  equal to the output impedance of the twin- $T$  network with the input terminals short circuited i.e.,

$$Z_0 = \frac{2R(u+1)}{(u+1)^2 + 2u} \quad \dots (7)$$

where  $u = j\omega CR = jx$ . The impedance of the series ( $Z_1$ ) and the shunt ( $Z_2$ ) arms of the Wien network can be written as

$$Z_1 = R(u+1)/(nu) \quad \text{and} \quad Z_2 = Rn/(u+1)$$

Therefore, ~

$$A = E_0/E_i = (E_0/E_i) \cdot (E/E_i)$$

$$= \frac{Z_2}{Z_0 + Z_1 + Z_2} \cdot \frac{1}{1-j4/y}$$

Substituting for the various impedances, simplifying and separating into real and imaginary parts leads to the expression (3) of the paper.

## APPENDIX 2

Referring to Fig. 2, if  $Z_0 < Z_i$ , then  $A = A_T A_W$ , where  $A_T$  and  $A_W$  are given by (1) and (2). The resultant expression is normalised with respect to the resonant response given by  $A_0 = n^2/(n^2+6)$ , and simplified. The result is

$$A_n = \frac{1}{1+j \frac{n^2+2}{n^2+6} \left( \frac{y}{n^2+2} - \frac{4}{y} \right)}$$

The frequencies at which  $|A_n| = 0.707$  can be found from the above as given by the following equation

$$y^4 - y^2(n^4 + 20n^2 + 52) + 16(n^4 + 4n^2 + 4) = 0$$

This gives four values of  $y$  of which two are positive and two negative, corresponding respectively to the higher and the lower frequency resonances. Each value of  $y$  gives a positive value of  $x$ ; let these be denoted by  $x_{i1}$  and  $x_{i2}$  for the negative values of  $y$  and  $x_{h1}$  and  $x_{h2}$  for the positive values of  $y$ . The resonance frequencies in this case are given by

$$y_0^2 = 4(n^2+2)$$

The positive values of  $x$ , satisfying this equation are

$$x_{0l} = (n^2+3)^{\frac{1}{2}} - (n^2+2)^{\frac{1}{2}}$$

$$x_{0h} = (n^2+3)^{\frac{1}{2}} + (n^2+2)^{\frac{1}{2}}$$

Finally,  $Q_l$  and  $Q_h$  are computed as

$$Q_l = \frac{x_{0l}}{x_{i1} \sim x_{i2}} \quad \text{and} \quad Q_h = \frac{x_{0h}}{x_{h1} \sim x_{h2}}$$

## APPENDIX 3

Referring to Fig. 2 and Appendix 1,

$$Z_i = Z_1 + Z_2 = R \frac{(u+1)^2 + n^2 u}{nu(u+1)}$$

$Z_0$  is given by expression (7) in Appendix 1. The ratio

$$r = \frac{Z_0}{Z_i} = \frac{2nu(u+1)^2}{\{(u+1)^2 + 2u\}\{(u+1)^2 + n^2 u\}}$$

is a measure of the loading of the twin- $T$  by the Wien network at the junction  $AB$ . The loading will be negligible when  $r \ll 1$ . Simplification of the above expression gives

$$r = \frac{2n}{\left(4 + n^2 + \frac{4n^2}{4+y^2}\right) + jy \left(1 - \frac{2n^2}{4+y^2}\right)}$$

The expression is similar to the response of a tuned circuit; as the frequency is varied,  $r$  will be a maximum when

$$y^2 = 2(n^2 - 2)$$

The maximum value of  $r$  is  $r_{max} = 2n/(6+n^2)$ . Fig. 6 shows a plot of  $r_{max}$  versus  $n$ . The curve has a maximum at  $dr_{max}/dn = 0$ , i.e., at  $n = 6^{\frac{1}{2}}$ . The absolute maximum value of  $r$  is 0.408. Since the resonance frequencies of the twin tuned

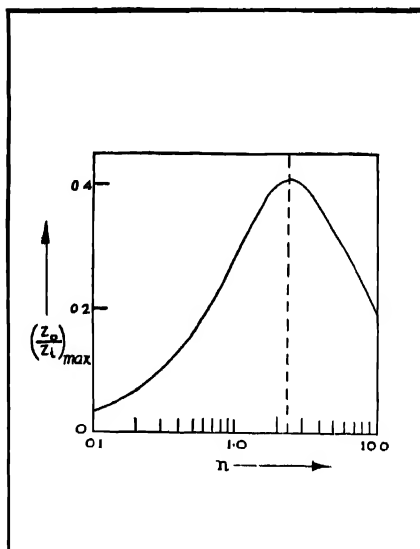


Fig. 6. Showing the variation of  $(Z_0/Z_1)_{max}$  with  $n$ .

circuit given by (4) are away from those at which  $r$  is maximum, the actual loading in two small bands of frequencies centred around the former will be less than that given by the curve. If  $r_{max} = 0.2$  is taken as the tolerable limit, then the analysis of Appendix 2 will be valid for  $8 < n < 0.8$ .

## BOOK REVIEWS

**PERMANENT MAGNETS AND THEIR APPLICATIONS;** By R. J. Parker and R. J. Studders. Published by J. Wiley and Sons, N.Y. and London. Pp. 406. Price \$ 16.00

The book consists of nine chapters, dealing with the basic concepts of magnetism, the theory of magnetization and the vast differences in the ferromagnetic behaviours of magnetic materials in practice depending upon impurities, admixtures, thermal and mechanical histories of the materials etc. with specific reference to permanent magnetization. The authors have attempted to explain various difficulty understood practical problems so that magnetic performances of specific materials used for permanent magnets may become to a great extent predictable and reproducible.

This is a book particularly valuable to permanent magnet designers as well as persons interested in the application of permanent magnets in a variety of techniques ranging from motors and generators, measuring instruments to various electromagnetic control devices and recorders.

Beginning with a historical outline of permanent magnets the authors carry us through successive chapters on some basic principles and theory, the properties and manufacture of magnetic materials, calculations on design of permanent magnets, their magnetic performance data, applications in various electromagnetic and magnetic instruments, the process of magnetizing and demagnetizing of magnets, stability characteristics of magnets and measurements of permanent magnet characteristics.

A glossary of terms and their definitions and an index as usual completes the book. The 20 pages of the historical chapter are *informative but might* have been more profitably replaced by giving greater details of manufacturing processes and specific applications. For the size the book appears to be too highly priced.

A. Bose

**RESEARCHES ON METEORITES;** Edited by C. B. Moore. Published by M/s J. Wiley and Sons, New York and London. Pp. 277. Price not mentioned.

This book is a collection of twelve research papers by different authors and is based upon the proceedings of a symposium on meteorites held at the Arizona State University in 1961. The papers represent variety of subjects of meteorite

research, such as importance of meteorite investigations and problems of specimen recovery and use, mineralogical and petrological aspects, nuclear studies, metallurgical studies, relationship of meteorite studies to the Earth and the origin of meteorites. The papers included generally contain a review on the respective subjects as well as the author's own contribution and a useful bibliography.

In view of the very recent interest in problems in connection with interplanetary space and also in view of the fact that meteorites are the only major source of extra-terrestrial matter available for investigation, any work on properties and behaviours of meteorites will naturally be of great importance. A collection (first of its kind) of such works as are included in the present volume will therefore be of much help to all workers in this line. The publishers have certainly done a good work in timely bringing out such a volume.

A. Bose

#### PROGRESS IN ELEMENTARY PARTICLE AND COSMIC RAY PHYSICS

VOLUME IV—Edited by J. G. Wilson and S. A. Wouthuysen, Pp. 470 + xii. North Holland Publishing Company, Amsterdam, 1958. Price 45 guilders.

This is the fourth volume of the series of reviews published earlier under the title 'Progress in Cosmic Ray Physics'. The elementary particle has been included in the title of the present volume in view of the fact that much experimental work on 'strange particle' is now being done in the laboratory with the help of large accelerating machines. There are altogether five chapters written by different authors and each chapter has an introduction.

The first chapter written by B. D'espagnat and J. Prentki deals with some theoretical aspects of the strong interactions of the new particles. A table giving the nomenclature of these particles along with their properties and brief discussions on observed reactions are included in the Introduction to this chapter. In Section 1 of this Chapter the role of the isotopic spin and the new quantum number  $S$ , the strangeness, in different kinds of interactions is discussed and the selection rules for the interaction processes are deduced. Section 2 deals with a theory different from the phenomenological one and involving rotations and symmetries in a three dimensional spin-space and the theories in four dimensional spin-space are discussed and compared with the former theory in Section 3. The next section deals with compound models suggested for hyperons and mesons. Some other features of strong interactions, such as parity doublet theory and the interaction Lagrangian are discussed in Section 5. The last section gives the summary and conclusions. There is an Appendix dealing with some properties of spinors.

Chapter II contributed by W. D. Walker deals with the properties and production of K-mesons. The properties discussed include decay modes, masses,



lifetimes, spin and parity of the K-mesons. Section 6 of this chapter is devoted to interaction of K-mesons and in the last section the possibility of mixing up of two different particles to produce an anomalous particle has been discussed briefly.

Chapter III contributed by G. N. Fowler and A. W. Wolfendale deals with the interaction of  $\mu$ -mesons with matter. Starting with discussions on classical electromagnetic interaction of  $\mu$ -mesons including collisions with free electrons, bremsstrahlung, pair production, etc., various other interactions, such as scattering of  $\mu$ -mesons by nuclei, non-classical electromagnetic interactions and the universal Fermi interaction involving weak interaction between half-spin particles have been discussed in great detail in this chapter. Beautiful photographs of cloud chamber tracks of  $V$ -particles secondaries,  $S$ -particle secondary and penetrating particles constituting a shower have been reproduced as illustrations.

The fourth chapter dealing with the primary cosmic radiation and its time variations has been contributed by S. F. Singer. In Section 1 of this chapter the geomagnetic theory first put forward by Stormer and expanded by Lemaitre and Vallarta has been discussed in detail and twentyfive graphs showing the two coordinates of the asymmetric velocity vector of the particle, north latitude and longitude angle, for different latitudes of the observer have been reproduced. Section 2 deals with composition of primary cosmic radiation. The abundance of the light elements and the fragmentation theory have been discussed in this section. The next sections deal respectively with the primary proton spectrum, the primary alpha-particle spectrum and the latitude cut off 'knee'. The methods for studying primary variations have been discussed in Section 6 and solar flare increases and possible mechanism for such increase has been discussed in Section 7. The next two sections deal with magnetic storm effects and secular variations of primary cosmic rays. In the last section some conclusions have been drawn and some outstanding problems have been enumerated.

The work on the origin of cosmic radiation has been reviewed by V. L. Ginzburg in Chapter V. In section 1 of this chapter, the composition and energy spectrum of the primary cosmic radiation just outside the boundary of earth's atmosphere have been discussed. The next section deals with magnetic bremsstrahlung nature of cosmic radio emission and the distribution of cosmic rays in the galaxy. Section 3 deals with movement of cosmic particles in the interstellar medium and in the next section the possibility of Supernovae and Novae as source of cosmic radiation has been discussed in great detail.

There is an author index at the end of the volume and at the end of each chapter a list of references has been included.

This brief review will show that this volume will serve as a very valuable reference book which is extremely useful to research workers interested in cosmic rays and nuclear physics. Probably by this time many of the scientific libraries have already acquired this volume and those which have not done so may find

it worthwhile adding this volume to their lists in order to possess the complete series, the next volume of which has already been published. The get up of the volume is excellent.

*S. C. S.*

**NUCLEAR REACTOR PHYSICS**—By Raymond L. Murray, Pp. 315+xi.  
Macmillan and Co. Ltd., London. 1959, Price 30s.

As mentioned in the preface the material presented in the book is based on a series of undergraduate and graduate courses given by the author during 1950-54 in the Nuclear Engineering Curriculum at the North Carolina State College. The first chapter starts with nuclear reactions which take place in reactors and then different types of reactors are briefly described. The second chapter deals with different moderators and the expressions for flux of neutrons of different velocity ranges are deduced. The methods of calculating the critical size and fuel content of simple reactors have been discussed in Chapter 3. The properties of heterogeneous reactors and theoretical methods of determining these properties have been discussed in Chapter 4. The two-group theory, taking into account the thermal and fast neutron groups, has been fully discussed in the fifth chapter. The variation of power of a reactor with time has been investigated theoretically in Chapter 6 and the next chapter deals with temperature effect on the multiplication factor. Chapter 8 deals in detail with the means by which safe operation of a reactor can be guaranteed and describes various methods controlling the reactor. The transport theory for neutrons of one speed is discussed in Chapter 9. The various methods of solving the energy-dependent transport equation on different simplified assumptions have been correlated and a particular multi-group method has been discussed in the last chapter. There are three appendices dealing with Bessel functions, physical constants and Laplace transforms respectively.

The special feature of this volume is the inclusion of a large number of numerical problems in each chapter and also solutions of some of them. This requires intimate knowledge about the theories and their applications in actual reactors, and evidently, the author not only possesses such practical experience but has also made valuable contribution to such theories. Any serious student going through the book will be able to grasp the fundamentals of the various theories involved in the working of a reactor and if he cares to work out the examples he will soon become a reactor engineer. Probably by this time many students have read the book and found it very useful. The book is useful not only to those who want to take up the course of Nuclear Engineering but also to nuclear physicists who want to acquaint themselves with the principles of working of nuclear reactors. It will, of course, serve as an ideal text book.

*S. C. S.*

## ON CLASSIFICATION OF SWITCHING FUNCTIONS

## Part II

A. K. CHOUDHURY AND M. S. BASU

INSTITUTE OF RADIO PHYSICS AND ELECTRONICS,  
UNIVERSITY OF CALCUTTA

(Received December 20, 1961)

**ABSTRACT.** Methods of classifying  $n$ -variable switching functions and finding out the representative functions of the different equivalence classes have been presented in this paper. The geometrical concept of switching functions has been utilised for this purpose. Representatives of all the equivalence classes of 4-variable functions have been found out and presented in a table which can be conveniently used for finding out the equivalence class to which any given function belongs.

## INTRODUCTION

In the Part I of this paper the geometrical concept of representing switching functions as nodes of unit  $n$ -dimensional cube has been utilised for establishing the necessary and sufficient conditions for two functions to belong to the same equivalence class. The geometrical structures of two functions belonging to the same equivalence class must be identical. This concept will be utilised for broadly classifying the functions of  $n$ -variables and for ultimately recognising the representatives of the different equivalence classes. If we write down the decimal numbers corresponding to the terms of any function in ascending order, then that function for which this represents the smallest number with a sufficiently high radix is branded as the representative of the equivalence class to which it belongs. It follows therefore that all such representative functions will begin with the term 0.

By methods developed in this paper, representatives of all the equivalence class of 4-variable switching functions will be found out.

## SOME PROPERTIES OF THE WEIGHTS OF TERMS

In our method of classification, the sum of the weights of the terms of a function will play a significant part. So it will be helpful to investigate at this stage some properties of the weights of the terms of a function.

I. If we find the sum of the weights of the terms of any function, we count each 1-cell twice. Hence.

*The sum of the weights of the terms of any function must be even.*

II. If we remove any term with weight  $K$  from any function, we take away  $K$  1-cells incident with that term. The sum of the weights in the function is therefore reduced by  $2K$ . If we remove  $b$  nodes from a unit  $n$ -cube to form a function and if the sum of the weights of those  $b$  nodes of the function be  $S$  then it follows that the sum of the weights in the complementary function is

$$S_c = n \times 2^n - (b \times 2n - S) \quad \dots (1)$$

III. In a function with  $b$  terms, the sum of the weights will be maximum if the  $b$  terms can form a  $K$ -cell, so that  $b = 2^K$ . The weight of each term then becomes equal to  $K$  and sum of the weights becomes  $b \times K = K \times 2^K$ . The total number of 1-cells in the function becomes  $= K \times 2^{K-1}$ . In the Table I is shown the maximum value of the sum of the weight ( $S_{max}$ ) when  $b$  has different values corresponding to  $K = 0, 1, 2, 3, 4$ .

TABLE I

$K$	$b = 2^K$	$S_{max}$
0	1	0
1	2	2
2	4	8
3	8	24
4	16	64

IV. The above idea can be extended for finding out  $S_{max}$  for a function having any number of terms. It should be understood that the actual number of variables in any function may be quite large, but the sum of the weights of the terms will tend to a maximum value when the different nodes representing the terms are situated in a close formation in the unit cube model, that means, the dimension of the body of the function becomes minimum compatible with the number of terms. Hence for finding out the maximum value of the sum of the weights when the number of terms of the function is three, we can consider it to be the complementary function of a function with only one term in two variables. So using equation (1) and Table I,

$$S_3_{max} = 2 \times 2^2 - (1.2.2 - 0) = 4.$$

Similarly,

$$S_5_{max} = 3 \times 2^3 - (3 \times 2 \times 3 - 4) = 10.$$

if we assume the function with five terms as the complementary function of a function with three terms in three variables.

Table II gives the values of  $S_{max}$  for different values of number of terms in a function up to  $b = 16$ .

TABLE II

$b$	$S_{max}$	$b$	$S_{max}$	$b$	$S_{max}$
1	0	7	18	13	44
2	2	8	24	14	50
3	4	9	26	15	56
4	8	10	30	16	64
5	10	11	34		
6	14	12	40		

CLASSIFICATION OF FUNCTIONS OF  $N$ -VARIABLES

We shall now consider how the different functions of  $n$ -variables can be subdivided into different classes or groups. The first and obvious group will be the one in which all the members are functions composed of only one true state or term. The total number of members belonging to this group will be  $2^n C_1$ . The next group will be formed by functions each of which has only two terms. The total number of members of this group will be  $2^n C_2$ . In general, the  $K$ -th group will be composed of functions having  $K$  terms each. The total number of members belonging to the  $K$ -th group will be  $2^n C_K$ . This method of subdivision will be continued up to  $2^{n-1}$  groups, because functions with larger number of terms will be merely complements of functions included in the lower order groups.

Now, if we consider any one of such groups, the members of it can further be subdivided into sub-groups on the basis of the number of 1-cells present in the function. Thus in a 4-variable function composed of six terms, we have seen that the maximum value of the sum of the weights is 14 which corresponds to 7 1-cells present in the function. The six terms of the function can present other structures corresponding to the presence of 6, 5, 4, 3, 2, 1, or 0 1-cells. Thus the group which is composed of functions having six terms can further be subdivided into eight subgroups, the total number of 1-cells present in the members of each subgroup being same. The Table III gives the sub-classes of each group on the basis of the number of 1-cells present in the functions of 3 and 4 variables.

It will be observed that in the 4-variable functions all possible values of the total number of 1-cells from maximum to zero do not occur in some of the groups.

If we consider the subgroups of any group, these subgroups can be further subdivided on the basis of interconnection of the 1 cells and the relative separation between terms. Two functions having different interconnections of the 1-cells or different relative separations between the terms (with identical number of 1-cells) will belong to different equivalence classes. As an example we consider the subgroup with zero 1-cell in the group 2 of 4-variable functions. Functions

TABLE III

number of variables	Group number	Total number of true states	Total number of ono colls	Sum of the weights.
3	1	1	0	0
	2	2 2	1 0	2 0
	3	3 3 3	2 1 0	4 2 0
	4	4 4 4 4	4 3 2 0	8 6 4 0
	1	1	0	0
	2	2 2	1 0	2 0
	3	3 3 3	2 1 0	4 2 0
	4	4 4 4 4 4	4 3 2 1 0	8 6 4 2 0
	5	5 5 5 5 5 5	5 4 3 2 1 0	10 8 6 4 2 0
	6	6 6 6 6 6 6 6 6	7 6 5 4 3 2 1 0	14 12 10 8 6 4 2 0
	7	7 7 7 7 7 7 7 7	9 8 7 6 5 4 3 2 0	18 16 14 12 10 8 6 4 0

TABLE III (contd.)

number of variables	Group number	Total number of true states	Total number of one cells	Sum of the weights.
		8	12	24
		8	10	20
		8	9	18
		8	8	16
		8	7	14
		8	6	12
		8	5	10
		8	4	8
		8	3	6
		8	0	0

(0, 3), (0, 7), (0, 15) all belong to this group. But the mutual separation between the terms in each of the above functions are different. Hence though they are included in the same subgroup, they must belong to different equivalence classes.

METHOD FOR FINDING REPRESENTATIVES OF THE  
DIFFERENT EQUIVALENCE CLASSES OF 3 AND 4  
VARIABLE FUNCTIONS

For finding out the representative functions of different equivalence classes we shall utilise one chart which can be called "distance chart." The chart is constructed in the following manner. A squared paper is taken. Numbers 0, 1, 2, 3, 4 ... 15, which represent different terms of 4 variable functions are written at the top as column headings. Similarly, the rows are also marked by the same numbers 0, 1, 2, ... 15. Any square on the graph is designated by its row and column numbers. Now let us take up the row 0. We know that the term 0 differs by one variable from the terms 1, 2, 4, 8. The squares 0-1, 0-2, 0-4, 0-8 are marked by dots at the centre. Again the terms 0 differs by two variables from the terms 3, 5, 6, 9, 10, 12. So the squares 0-3, 0-5, 0-6, 0-9, 0-10 and 0-12 are marked by writing the number 2 inside each of them. Similarly, the squares 0-7, 0-11, 0-13 and 0-14 are marked by the number 3 and the square 0-15 is marked by the number 4. In this way all the different rows are considered. Then an oblique line is drawn wherever there is a dot in the centre of a square and the consecutive oblique lines are joined. There will be one continuous diagonal line and other off-diagonal oblique lines in shorter or longer sections. The squares through which oblique lines do not pass are marked 2, 3 or 4 depending on the relative separation between the terms which designate those squares. A distance chart for 4 variables is shown in Fig. 1.

Now first of all we shall consider functions composed of a single true state. We shall call the terms "0" as the representative of this equivalence class, as this is the smallest number. Next we consider functions composed of two true states. We shall add one more term to the term "0". The number of 1-cells present in the functions formed in this manner can either be 1 or 0, depending on the





Thus when the term 2 is added to the function  $\Sigma(0, 1)$ , the square of the distances of the term 2 with 0 and 1 respectively will be 1 and 2. Similarly, the term 3 has the square of distances from 0 and 1 as 2 and 1 respectively. For the term 14 these values are 3 and 4 respectively and so on. With the addition of one more term to the function  $\Sigma(0, 1)$  there may or may not be the addition of one more 1-cell. Thus in the functions  $\Sigma(0, 1, 2)$ ,  $\Sigma(0, 1, 3)$ ,  $\Sigma(0, 1, 4)$ ,  $\Sigma(0, 1, 5)$ ,  $\Sigma(0, 1, 8)$ , etc. there is addition of one more 1-cell and the value of  $n_1$  becomes 2 for these functions, whereas in case of the functions  $\Sigma(0, 1, 6)$ ,  $\Sigma(0, 1, 7)$ ,  $\Sigma(0, 1, 10)$ , etc. the number of 1-cells remains unchanged, i.e., 1. The value of  $n_1$  of each new function is indicated in the last but one row of the chart.

From the chart it is observed that the relative distances of the terms 2, 4 and 8 with respect to the terms 0 and 1 respectively are all same. It is also observed that for the terms 3, 5 and 9, the relative distances with respect to 0 and 1 are again identical and in these cases the same distances are coming in the reverse order when compared to the case of the terms 2, 4 and 8. With this information it becomes easy to test that the functions  $\Sigma(0, 1, 2)$ ,  $\Sigma(0, 1, 3)$ ,  $\Sigma(0, 1, 4)$ ,  $\Sigma(0, 1, 5)$ ,  $\Sigma(0, 1, 8)$ ,  $\Sigma(0, 1, 9)$ , all belong to the same equivalence class and the function  $\Sigma(0, 1, 2)$  is the representative of this class. Similarly, observing the relative distances of the terms 6, 7, 10, 11, 12 and 13 with respect to the terms 0 and 1 respectively, it is concluded that the function  $\Sigma(0, 1, 6)$ ,  $\Sigma(0, 1, 7)$ ,  $\Sigma(0, 1, 10)$ ,  $\Sigma(0, 1, 11)$ ,  $\Sigma(0, 1, 12)$  and  $\Sigma(0, 1, 13)$  belong to same equivalence class which is distinct from the previous one and the function  $\Sigma(0, 1, 6)$  is their representative. Similarly,  $\Sigma(0, 1, 14)$  represent still another equivalence class which includes the function  $\Sigma(0, 1, 15)$ . These representative functions together with their  $n_1$  values are noted on the left side. The functions are cross marked at the bottom row as shown to indicate that they have been represented.

Similarly, we take up the function  $\Sigma(0, 3)$  and proceed in the same manner and tabulate as shown below :

$n_1=0$	$n_1=0$	1	2	4	5	6	7	8	9	10	11	12	13	14	15
0, 3	5	0	1	1	1	2	2	3	1	2	2	3	2	3	4
	12	3	1	1	3	2	2	1	3	2	2	1	4	3	2
	13	2	2	1	0	0	1	1	0	0	1	0	0	0	0
		×	×	×		×	×	×	×	×	×			×	×

The function  $\Sigma(0, 3, 1)$  has already been considered and belongs to an equivalence class which is represented by  $\Sigma(0, 1, 2)$ . The function  $\Sigma(0, 3, 2)$  belongs to this same equivalence class. The functions  $\Sigma(0, 3, 5)$ ,  $\Sigma(0, 3, 6)$ ,  $\Sigma(0, 3, 9)$ ,  $\Sigma(0, 3, 10)$  belong to the same equivalence class as they present identical structures regarding number of 1-cells and relative distances. The representative function is  $\Sigma(0, 3, 5)$ . Similarly  $\Sigma(0, 3, 12)$  and  $\Sigma(0, 3, 13)$  represent two other equivalence

We are now left with the functions  $\Sigma(0, 3, 4)$ ,  $\Sigma(0, 3, 7)$ ,  $\Sigma(0, 3, 8)$ ,

$\Sigma(0, 3, 11)$ . They are found to present identical structure regarding the number of 1-cells and relative distances. So they are within the same equivalence class. But we shall have to see whether this is any new equivalence class or one of the equivalence classes already found out when the number of 1-cells is one. It is seen that the function  $\Sigma(0, 1, 6)$  and  $\Sigma(0, 3, 4)$  belong to the same equivalence class. So  $\Sigma(0, 1, 6)$  is representative of this equivalence class also.

In this way we can find out the other equivalence classes for functions having three true states. Then we can add one more term to each of the representative functions having three terms and can obtain the representatives of the equivalence class with 4 true states. For this we tabulate the number of 1-cells, contained in each function obtained by addition of one term and relative distances as explained previously by consulting the distance chart. Then we can pick up the functions which belong to the same equivalence class and mark their representative functions. Thus we see that this method enables us to find out all the equivalence classes, the procedure being very systematic and applicable to any number of variables. If we are given any function having  $K$  terms, we can always say what new equivalence classes are formed if we add one more term to the function to make the number of terms equal to  $K+1$ .

The concept of the unit  $n$ -dimensional cube, the vertices of which represent the terms of  $n$ -variable switching functions can be utilised in a still different way for finding out all the equivalence classes. The method can be called method of analysis as distinguished from the method just presented which may be called a method of synthesis. The procedure for doing this can be briefly outlined as follows. Let us consider four variable functions. The complete unit 4-cube will consist of 16 vertices. Four 1-cells are incident with each vertex so that the weight of each vertex is four and in the complete 4-cube the sum of the weights of all the vertices is 64. Now if we take out one single term out of it, there will be 15 vertices left in the 4-cube. Four terms will have their weights reduced by one, i.e., their weights become 3 and other 11 terms will be unaffected and their weights will still be equal to 4. This same picture will be presented whatever single vertex we take out. The term that is taken out may be called a function having a single true state and "0" may be called as the representative of this equivalence class. The unit 4-cube with 15 vertices left is its complementary function. So it is evident that the sum of the weights in the complementary function will be  $4 \times 3 + 11 \times 4 = 56$ .

The function in the present case has only one term having a weight 0 and terms having weight 4, 3, 2 or 1 are absent. This is represented by writing the number (0, 0, 0, 1) and is called the weight distribution vector of the function. It follows that the weight distribution vector of the complementary function is (11, 4, 0, 0) which means that in the complementary function there are 11 terms with weight 4 and four terms having weight 3. Terms having weight 2, 1 or 0 are absent.

Weight distribution vectors of a function and its complement remain invariant under all permutation and priming operations and these can be found very easily by means of mechanised grouping chart (Choudhury and Basu, 1962).

In order to find out the representative functions with two true states we shall take one more vertex out of the  $n$ -cube. This will make the number of terms in the complementary function equal to 14. The term that we take out may be one having a weight three or one having weight four. In the former case the sum of the weights in the complementary function will be reduced by six and it will become 50. In the latter case it will become 48. Thus if we take away the terms (0, 1) or (0, 2) or (0, 4) or (0, 8), the sum of the weights of the function in all cases is 2 and sum of the weights of the complementary function is 50, and weight distribution vectors of all the above functions and their complementary function are identical and on testing they are found to belong to the same equivalence class. Function  $\Sigma(0, 1)$  is taken as the representative of the class. For finding the representative of the function with three states by adding one more term to the function  $\Sigma(0, 1)$ , we keep a record of the complementary function of the function  $\Sigma(0, 1)$  along with weights of the individual terms of the complementary function. Thus after we have taken out the terms (0 and 1), the complementary function has the terms, 2, 3, 4 ... 15 and weights of the terms respectively are (3, 3, 3, 3, 4, 4, 3, 3, 4, 4, 4, 4, 4). Similarly, if we take out the term 0 and any one of the terms 3, 5, 6, 7, 9, 10, 11, 12, 13, 14 or 15, the sum of weights of the complementary function is in each case equal to 48. But all these functions obviously cannot belong to the same equivalence class because neither the ratios of terms with odd number of 1's to those having even number of 1's are all same nor are the distance vectoris of the terms are same in the different functions. Also the weight distribution of the complementary functions are not all identical. On testing we find that the functions  $\Sigma(0, 3)$ ,  $\Sigma(0, 5)$ ,  $\Sigma(0, 6)$ ,  $\Sigma(0, 9)$ ,  $\Sigma(0, 10)$  and  $\Sigma(0, 12)$  belong to the same equivalence class, and  $\Sigma(0, 3)$  is taken as representative of the class. Similarly  $\Sigma(0, 7)$ ,  $\Sigma(0, 11)$ ,  $\Sigma(0, 13)$  and  $\Sigma(0, 14)$  are found to belong to the same equivalence class and  $\Sigma(0, 7)$  is taken as the representative of the class.  $\Sigma(0, 15)$  represents another equivalence class. This completes the list of all the representatives of the 4 variable function with two true states. In this way we can proceed step by step, taking one term out at each step from the unit 4-cube. We examine the weight distribution and sum of the weights for the functions so formed and also for the complementary functions. In forming functions with  $K+1$  true states, we first take the function having the largest sum of the weights with  $K$  true states and associate with the  $K$ -terms different terms of its complementary function one at a time. We collect all these functions with  $K+1$  terms so formed into groups. Those functions for which weight distribution as well as the weight distribution of their complementary functions are identical are collected into one group. From the list we

TABLE IV

$G$	$N$	$f$	$4$	$3$	$\frac{w_d}{2}$	$1$	$0$	$S$	$4$	$3$	$\frac{w_d}{2}$	$1$	$0$	$\bar{S}$	Remark
1	1	0	0	0	0	0	1	0	11	4	0	0	0	56	
2	2	0 1	0	0	0	2	0	2	8	6	0	0	0	50	
3	3	0 3	0	0	0	0	2	0	8	4	2	0	0	48	
4	4	0 7	0	0	0	0	2	0	6	8	0	0	0	48	$N_e/N_o = 1/1$
5	5	0 15	0	0	0	0	2	0	6	8	0	0	0	48	$N_d/N_o = 2/0$
3	6	0 1 2	0	0	1	2	0	4	6	6	1	0	0	44	
7	7	0 1 6	0	0	0	2	1	2	5	6	2	0	0	42	
8	8	0 1 14	0	0	0	2	1	2	3	10	0	0	0	42	
9	9	0 3 5	0	0	0	0	3	0	6	3	3	1	0	40	
10	10	0 3 12	0	0	0	0	3	0	5	4	4	0	0	40	
11	11	0 3 13	0	0	0	0	3	0	3	8	2	0	0	40	
4	12	0 1 2 3	0	0	4	0	0	8	4	8	0	0	0	40	
13	13	0 1 2 4	0	1	0	3	0	6	5	4	3	0	0	38	
14	14	0 1 2 5	0	0	2	2	0	6	4	6	2	0	0	38	
15	15	0 1 2 7	0	0	1	2	1	4	4	5	2	1	0	36	
16	16	0 1 2 12	0	0, 1	2	1	4	4	3	6	3	0	0	36	$N_e/N_o = 2/2$
17	17	0 1 2 13	0	0	1	2	1	4	3	6	3	0	0	36	$N_e/N_o = 1/3$

TABLE IV (contd.)

$G$	$N$	$f$	$w_d$			$S$			$\overline{w_d}$			$\overline{S}$			Remark
			4	3	2	1	0		4	3	2	1	0		
4	18	0 1 2 15	0	0	1	2	1	4	1	10	1	0	0	36	
	19	0 1 6 7	0	0	0	4	0	4	4	4	4	0	0	36	
	20	0 1 6 14	0	0	0	4	0	4	2	8	2	0	0	36	
	21	0 1 14 15	0	0	0	4	0	4	0	12	0	0	0	36	
	22	0 1 6 10	0	0	0	2	2	2	3	5	3	1	0	34	
5	23	0 1 6 11	0	0	0	2	2	2	2	6	4	0	0	34	$N_e/N_o = 2/2$
	24	0 1 6 15	0	0	0	2	2	2	2	6	4	0	0	34	$N_e/N_o = 3/1$
	25	0 3 5 6	0	0	0	0	4	0	4	4	0	4	0	32	
	26	0 3 5 9	0	0	0	0	4	0	5	0	6	0	1	32	
	27	0 3 5 10	0	0	0	0	4	0	4	2	4	2	0	32	
	28	0 3 5 14	0	0	0	0	4	0	1	7	3	1	0	32	
	29	0 3 12 15	0	0	0	0	4	0	4	0	8	0	0	32	
	30	0 3 13 14	0	0	0	0	4	0	0	8	4	0	0	32	
	31	0 1 2 3 4	0	1	3	1	0	10	3	6	2	0	0	34	
	32	0 1 2 4 8	1	0	0	4	0	8	5	0	6	0	0	32	
	33	0 1 2 4 9	0	1	1	3	0	8	3	4	4	0	0	32	
	34	0 1 2 3 12	0	0	4	0	1	8	1	8	2	0	0	32	

TABLE IV (contd.)

$G$	$N$	$f$						$w_d$						$S$	$\overline{w_d}$					$\overline{S}$	Remark
		0	1	2	5	6		0	0	3	2	0	8		3	5	2	1	0		
5	35	0	1	2	5	6		0	0	3	2	0	8		3	5	2	1	0	32	
	36	0	1	2	5	10		0	0	3	2	0	8		2	6	3	0	0	32	
	37	0	1	2	4	7		0	1	0	3	1	6		3	5	0	3	0	30	
	38	0	1	2	4	11		0	1	0	3	1	6		3	3	4	1	0	30	
	39	0	1	2	4	15		0	1	0	3	1	6		0	8	3	0	0	30	
	40	0	1	2	5	11		0	0	2	2	1	6		2	5	3	1	0	30	
	41	0	1	2	5	14		0	0	2	2	1	6		1	6	4	0	0	30	
	42	0	1	2	7	15		0	0	1	4	0	6		1	7	2	1	0	30	
	43	0	1	2	12	13		0	0	1	4	0	6		2	4	5	0	0	30	
	44	0	1	2	13	15		0	0	1	4	0	6		0	8	3	0	0	30	
	45	0	1	2	7	11		0	0	1	2	2	4		3	2	5	0	1	28	
	46	0	1	2	7	12		0	0	1	2	2	4		1	5	4	1	0	28	
	47	0	1	2	7	13		0	0	1	2	2	4		2	4	3	2	0	28	
	48	0	1	2	12	15		0	0	1	2	2	4		0	6	5	0	0	28	
	49	0	1	2	13	14		0	0	1	2	2	4		2	2	7	0	0	28	
	50	0	1	6	7	10		0	0	0	4	1	4		2	3	5	1	0	28	
	51	0	1	6	11	14		0	0	0	4	1	4		1	4	6	0	0	28	
	52	0	1	6	10	12		0	0	0	2	3	2		1	6	0	4	0	26	
	53	0	1	6	10	13		0	0	0	2	3	2		0	7	1	3	0	26	

TABLE IV (contd.)

$G$	$N$	$f$										$w_d$				$S$	$\bar{w}_d$				$\bar{S}$	Remarks
		4	3	2	1	0	4	3	2	1	0	4	3	2	1	0						
5	54	0	1	6	10	15	0	0	0	2	3	2	1	4	4	2	0	26				
	55	0	3	5	6	9	0	0	0	0	5	0	3	1	3	3	1	24				
	56	0	3	5	9	14	0	0	0	0	5	0	0	4	6	0	1	24				
	57	0	3	5	10	12	0	0	0	0	5	0	3	0	4	4	0	24				
	58	0	1	2	3	4	5	0	2	4	0	0	14	2	6	2	0	30				
6	59	0	1	2	3	4	8	1	0	3	2	0	12	3	2	5	0	28				
	60	0	1	2	3	4	7	0	2	2	2	0	12	3	2	5	0	28				
	61	0	1	2	3	4	9	0	2	2	2	0	12	2	4	4	0	28	$N_e/N_o = 3/3$			
	62	0	1	2	3	4	11	0	2	2	2	0	12	2	4	4	0	28	$N_e/N_o = 2/4$			
	63	0	1	2	3	4	12	0	1	4	1	0	12	1	6	3	0	28				
	64	0	1	2	5	6	7	0	0	6	0	0	12	2	6	0	2	28				
	65	0	1	2	3	4	13	0	1	3	1	1	10	1	5	3	1	26				
	66	0	1	2	3	4	15	0	1	3	1	1	10	0	6	4	0	26				
	67	0	1	2	4	9	10	0	1	2	3	0	10	2	3	4	1	0	26	$N_e/N_o = 3/3$		
	68	0	1	2	4	9	11	0	1	2	3	0	10	2	3	4	1	0	26	$N_e/N_o = 2/4$		
	69	0	1	2	3	12	13	0	0	4	2	0	10	0	6	4	0	0	26	There is a 2-cell in the body of the function		
	70	0	1	2	5	10	13	0	0	4	2	0	10	0	6	4	0	0	26	No 2-cell present in the function		
71	0	1	2	5	6	13	0	0	4	2	0	10	1	5	3	1	0	26				
72	0	1	2	4	7	8	1	0	0	4	1	8	3	1	3	3	0	24				

TABLE IV (contd.)

$G$	$N$	$f$	$w_d$	$S$	$w_d$	$S$	$w_d$	$S$	Remarks				
			4	3	2	1	0	4	3	2	1	0	
6	73	0 1 2 4 8 15	1	0	0	4	1	8	0	4	6	0	24
	74	0 1 2 4 7 9	0	1	1	3	1	8	1	5	1	3	0
	75	0 1 2 4 9 14	0	1	1	3	1	8	1	3	5	1	0
	76	0 1 2 4 9 15	0	1	1	3	1	8	0	4	6	0	24
	77	0 1 2 4 7 15	0	1	0	5	0	8	0	7	0	3	0
	78	0 1 2 4 11 15	0	1	0	5	0	8	0	5	4	1	0
	79	0 1 2 3 12 15	0	0	4	0	2	8	0	4	6	0	0
	80	0 1 2 5 6 11	0	0	3	2	1	8	1	4	3	2	0
	81	0 1 2 5 6 15	0	0	3	2	1	8	1	4	3	2	0
	82	0 1 2 5 10 12	0	0	3	2	1	8	1	4	3	2	0
	83	0 1 2 5 6 12	0	0	3	2	1	8	2	2	5	0	1
	84	0 1 2 5 10 15	0	0	3	2	1	8	1	2	7	0	0
	85	0 1 2 5 11 15	0	0	2	4	0	8	1	3	5	1	0
	86	0 1 2 5 14 15	0	0	2	4	0	8	0	4	6	0	0
	87	0 1 2 12 13 15	0	0	2	4	0	8	0	4	6	0	0
	88	0 1 2 13 14 15	0	0	2	4	0	8	0	4	6	0	0
	89	0 1 2 7 11 15	0	0	2	4	0	8	1	4	4	0	1



TABLE IV (contd.)

G	N	f	$w_d$			S			$w_d$			S			Remarks
			4	3	2	1	0		4	3	2	1	0		
6	90	0 1 2 7 13 15	0	0	2	4	0	8	0	6	2	2	0	24	
	91	0 1 2 12 13 14	0	0	2	4	0	8	2	0	8	0	0	24	
	92	0 1 2 4 7 11	0	1	0	3	2	6	2	2	3	2	1	22	
	93	0 1 2 4 11 13	0	1	0	3	2	6	2	1	4	3	0	22	
94	0 1 2 5 11 12	0	0	2	2	2	2	7	0	4	4	2	0	22	$N_0/N_6 = 3/3$
95	0 1 2 5 11 14	0	0	2	2	2	2	6	0	4	4	2	0	22	$N_0/N_6 = 2/4$
96	0 1 2 7 12 13	0	0	1	4	1	6	1	2	5	2	0	22		
97	0 1 2 7 12 15	0	0	1	4	1	6	0	3	6	1	0	22		
98	0 1 6 7 10 11	0	0	0	6	0	6	2	0	6	2	0	22		
99	0 1 2 7 11 12	0	0	1	2	3	4	0	2	7	0	1	20		
100	0 1 2 7 11 13	0	0	1	2	3	4	1	3	2	3	1	20		
101	0 1 2 7 13 14	0	0	1	2	3	4	1	2	3	4	0	20		
102	0 1 6 7 10 12	0	0	0	4	2	4	0	4	2	4	0	20		weight of the order 4 is 0 for all the terms,
103	0 1 6 10 13 15	0	0	0	4	2	4	0	4	2	4	0	20		weight of the order 4 is 1 for two terms.
104	0 1 6 7 10 13	0	0	0	4	2	4	0	2	6	2	0	20		
105	0 1 6 10 12 15	0	0	0	2	4	2	0	3	3	3	1	18		
106	0 3 5 6 9 10	0	0	0	0	6	0	2	0	2	4	2	16		
107	0 3 5 10 12 15	0	0	0	0	6	0	2	0	0	8	0	16		

TABLE IV (contd.)

$G$	$N$	$f$										$w_d$	$S$	$w_d$	$\bar{S}$
		0	1	2	3	4	5	6		4	3	2	1	0	0
7	108	0	1	2	3	4	5	6		0	4	3	0	0	18
	109	0	1	2	3	4	5	8		1	1	4	1	0	16
	110	0	1	2	3	4	8	12		1	0	6	0	0	16
	111	0	1	2	3	4	5	10		0	3	3	1	0	16
	112	0	1	2	3	4	7	8		1	1	2	3	0	14
	113	0	1	2	3	4	7	9		0	3	1	3	0	14
	114	0	1	2	3	4	5	14		0	2	4	0	1	14
	115	0	1	2	3	4	7	12		0	2	3	2	0	14
	116	0	1	2	3	4	9	12		0	2	3	2	0	14
	117	0	1	2	3	4	11	12		0	2	3	2	0	14
	118	0	1	2	3	4	12	13		0	1	5	1	0	14
	119	0	1	2	4	9	10	11		0	1	5	1	0	14
	120	0	1	2	3	4	8	13		1	0	3	2	1	12
	121	0	1	2	3	4	8	15		1	0	3	2	1	12
7	122	0	1	2	3	4	7	13		0	2	2	2	1	12
	123	0	1	2	3	4	9	14		0	2	2	2	1	12
	124	0	1	2	3	4	11	13		0	2	2	2	1	12
	125	0	1	2	3	4	12	15		0	1	4	1	1	12

TABLE IV (contd.)

$G$	$N$	$f$										$w_d$				$S$	$w_d$				$\bar{S}$	Remark
		0	1	2	3	4	13	15	0	1	3	3	0	12	0	4	3	2	1	0		
	126	0	1	2	3	4	13	15	0	1	3	3	0	12	0	3	5	1	0	20	There is a 2-cell in the body of the function.	
	127	0	1	2	4	9	11	15	1	0	3	3	0	12	0	3	5	1	0	20	No 2-cell is present in the function.	
	128	0	1	2	4	9	10	12	0	1	3	3	0	12	2	0	6	0	1	20		
	129	0	1	2	4	9	10	13	0	1	3	3	0	12	1	2	4	2	0	20		
	130	0	1	2	3	12	13	14	0	0	5	2	0	12	0	2	7	0	0	20	A 2-cell is present in the function.	
	131	0	1	2	5	10	13	14	0	0	5	2	0	12	0	2	7	0	0	20	No 2-cell is present in the function.	
	132	0	1	2	5	6	12	13	0	0	5	2	0	12	1	2	5	0	1	20		
	133	0	1	2	5	6	13	14	0	0	5	2	0	12	0	4	3	2	0	20		
	134	0	1	2	5	6	13	15	0	0	5	2	0	12	1	1	6	1	0	20		
	135	0	1	2	4	9	11	13	0	2	1	4	0	12	2	0	5	2	0	20		
	136	0	1	2	5	6	7	11	0	0	6	0	1	12	1	3	3	1	1	20		
7	137	0	1	2	4	7	8	15	1	0	0	6	0	10	0	3	3	3	0	18		
	138	0	1	2	3	4	13	14	0	1	3	1	2	10	0	3	3	3	0	18		
	139	0	1	2	4	7	9	10	0	1	2	3	1	10	0	4	1	4	0	18		
	140	0	1	2	4	7	9	11	0	1	2	3	1	10	1	2	3	2	1	18		
	141	0	1	2	4	9	10	15	0	1	2	3	1	10	0	2	5	2	0	18		
	142	0	1	2	4	9	11	14	0	1	2	3	1	10	1	1	4	3	0	18		
	143	0	1	2	4	7	9	15	0	1	1	5	0	10	0	3	3	3	0	18	$N_e/N_o = 3/4$	



TABLE IV (contd.)

G	N	f												S	$w_d$				S	Remark
		0	1	2	3	4	5	6	7	8	9	10	11	12	4	3	2	1	0	
8	163	0	3	5	6	9	10	12	0	0	0	0	7	0	1	0	0	4	4	8
	164	0	1	2	3	4	5	6	7	0	8	0	0	0	24	0	8	0	0	24
	165	0	1	2	3	4	5	8	9	2	0	6	0	0	20	2	0	6	0	20
	166	0	1	2	3	4	5	6	8	1	3	3	1	0	20	1	3	3	1	20
	167	0	1	2	3	4	5	6	9	1	3	3	1	0	20	1	3	3	1	20
168	0	1	2	3	4	5	8	10	1	2	5	0	0	0	20	1	2	5	0	20
169	0	1	2	3	4	5	6	11	0	5	2	1	0	0	20	0	5	2	1	20
170	0	1	2	3	4	5	10	11	0	4	4	0	0	0	20	0	4	4	0	20
171	0	1	2	3	4	5	8	11	1	2	3	2	0	18	1	2	3	2	0	18
172	0	1	2	3	4	7	8	12	1	1	3	1	0	18	0	4	2	2	0	18
173	0	1	2	3	4	5	6	15	0	4	3	0	1	18	0	4	3	0	1	18
174	0	1	2	3	4	5	10	12	0	4	2	2	0	18	1	1	5	1	0	18
175	0	1	2	3	4	5	10	13	0	4	2	2	0	18	0	2	6	0	0	18
176	0	1	2	3	4	5	10	14	0	3	4	1	0	18	0	3	4	1	0	18
177	0	1	2	3	4	9	12	13	0	2	6	0	0	18	0	4	2	2	0	18
178	0	1	2	3	4	7	8	11	2	0	2	4	0	16	2	0	2	4	0	16
179	0	1	2	3	4	5	8	14	1	1	4	1	1	16	0	3	2	3	0	16
180	0	1	2	3	4	5	8	15	1	1	4	1	1	16	0	1	6	1	0	16
181	0	1	2	3	4	7	8	15	1	1	3	3	0	16	0	2	4	2	0	16

 $N_e/N_o = 4/4$  $N_e/N_o = 5/3$

TABLE IV (contd.)

$g$	$N$	$f$										$w_d$					$S$	$w_d$					$\bar{S}$	Remark
		0	1	2	3	4	8	12	15	1	0	6	0	1	16	0	0	8	0	0	16			
8	182	0	1	2	3	4	8	12	15	1	0	6	0	1	16	0	0	8	0	0	16		$N_e/N_o = 3/5$ . One 2-cell in the body of the function. $N_e/N_o = 35$ No 2-cell in the body of the function. $N_e/N_o = 3/5$ Weight distribution of group with weight 2 = 0011. $N_e/N_o = 3/5$ Weight distribution of the group with weight 2 = 1102. $N_e/N_o = 4/4$ Weight distribution of all the groups has '1' at each position. $N_e/N_o = 4/4$ Weight distribution of all the groups is zero. $N_e/N_o = 4/4$ Weight distribution in one group is different from that in other two groups. $N_e/N_o = 4/4$ No 2-cell in the body of the function.	
	183	0	1	2	3	4	7	9	10	0	4	0	4	0	16	0	4	0	4	0	16			
	184	0	1	2	3	4	5	10	15	0	3	3	1	1	16	0	2	4	2	0	16			
	185	0	1	2	3	4	7	9	12	0	3	2	3	0	16	0	3	2	3	0	16			
	186	0	1	2	3	4	7	9	13	0	3	2	3	0	16	1	1	4	1	1	16			
	187	0	1	2	3	4	7	12	13	0	2	4	2	0	16	0	3	3	1	1	16			
	188	0	1	2	4	9	10	11	13	0	2	4	2	0	16	0	3	3	1	1	16			
	189	0	1	2	3	4	11	12	13	0	2	4	2	0	16	0	2	4	2	0	16			
	190	0	1	2	3	4	12	13	14	0	2	4	2	0	16	0	2	4	2	0	16			
	191	0	1	2	3	4	5	14	15	0	2	4	2	0	16	0	2	4	2	0	16			
8	192	0	1	2	3	4	7	12	15	0	2	4	2	0	16	0	2	4	2	0	16			
	193	0	1	2	3	4	9	12	14	0	2	4	2	0	16	0	2	4	2	0	16			
	194	0	1	2	4	9	10	11	15	0	2	4	2	0	16	0	2	4	2	0	16			
8	195	0	1	2	3	4	11	12	15	0	2	4	2	0	16	0	0	8	0	0	16			

TABLE IV (contd.)

$G$	$N$	$f$										$w_d$					$S$	$\overline{w_d}$					$\overline{S}$	Remark				
		0	1	2	3	4	12	13	15	0	1	6	1	0	16	0	1	6	1	0	16	0	1	6	1	0	16	
	196	0	1	2	3	4	12	13	15	0	1	6	1	0	16	0	1	6	1	0	16	0	1	6	1	0	16	
	197	0	1	2	4	9	10	11	12	0	1	6	1	0	16	1	1	4	1	1	16						16	
	198	0	1	2	3	12	13	14	15	0	0	8	0	0	16	0	0	8	0	0	16						16	There are two 2-cells.
	199	0	1	2	5	10	13	14	15	0	0	8	0	0	16	0	0	8	0	0	16						16	There is no 2-cell.
	200	0	1	2	5	6	12	13	14	0	0	8	0	0	16	1	0	6	0	1	16						16	
	201	0	1	2	5	6	13	14	15	0	0	8	0	0	16	0	2	4	2	0	16						16	
	202	0	1	2	3	4	7	8	13	1	1	2	3	1	14	1	1	2	3	1	14						14	
	203	0	1	2	3	4	8	13	15	1	0	3	4	0	14	0	1	4	3	0	14						14	
	204	0	1	2	3	4	7	9	14	0	3	1	3	1	14	0	1	5	1	1	14						14	
	205	0	1	2	3	4	9	12	15	0	2	3	2	1	14	0	1	4	3	0	14						14	
	206	0	1	2	3	4	9	14	15	0	2	2	4	0	14	0	0	6	2	0	14						14	
	207	0	1	2	4	7	9	10	11	0	1	5	1	1	14	0	3	1	3	1	14						14	
	208	0	1	2	3	4	13	14	15	0	1	4	3	0	14	0	1	4	3	0	14						14	$N_e/N_o = 3/5$ There is a 2-cell
8	209	0	1	2	4	9	10	13	15	0	1	4	3	0	14	0	1	4	3	0	14						14	$N_e/N_o = 4/4$
	210	0	1	2	4	9	11	14	15	0	1	4	3	0	14	0	1	4	3	0	14						14	$N_e/N_o = 3/5$ There is no 2-cell.
	211	0	1	2	4	7	9	11	15	0	1	4	3	0	14	0	2	3	2	1	14						14	
	212	0	1	2	4	9	10	13	14	0	1	4	3	0	14	1	0	3	4	0	14						14	
	213	0	1	2	5	6	11	13	15	0	0	6	2	0	14	0	2	2	4	0	14						14	

TABLE IV (contd.)

$G$	$N$	$f$															$w_d$					$S$	$w_d$					$S$	Remark		
		0	1	2	3	4	5	6	7	8	9	10	11	12	13	14	15	16	17	18	19	20	21	22	23	24	25	26	27	28	29
	214	0	1	2	3	4	5	6	7	8	9	10	11	12	13	14	15	16	17	18	19	20	21	22	23	24	25	26	27	28	29
	215	0	1	2	3	4	5	6	7	8	9	10	11	12	13	14	15	16	17	18	19	20	21	22	23	24	25	26	27	28	29
	216	0	1	2	3	4	5	6	7	8	9	10	11	12	13	14	15	16	17	18	19	20	21	22	23	24	25	26	27	28	29
	217	0	1	2	3	4	5	6	7	8	9	10	11	12	13	14	15	16	17	18	19	20	21	22	23	24	25	26	27	28	29
	218	0	1	2	3	4	5	6	7	8	9	10	11	12	13	14	15	16	17	18	19	20	21	22	23	24	25	26	27	28	29
	219	0	1	2	3	4	5	6	7	8	9	10	11	12	13	14	15	16	17	18	19	20	21	22	23	24	25	26	27	28	29
	220	0	1	2	3	4	5	6	7	8	9	10	11	12	13	14	15	16	17	18	19	20	21	22	23	24	25	26	27	28	29
	221	0	1	2	3	4	5	6	7	8	9	10	11	12	13	14	15	16	17	18	19	20	21	22	23	24	25	26	27	28	29
	222	0	1	2	3	4	5	6	7	8	9	10	11	12	13	14	15	16	17	18	19	20	21	22	23	24	25	26	27	28	29
	223	0	1	2	3	4	5	6	7	8	9	10	11	12	13	14	15	16	17	18	19	20	21	22	23	24	25	26	27	28	29
	224	0	1	2	3	4	5	6	7	8	9	10	11	12	13	14	15	16	17	18	19	20	21	22	23	24	25	26	27	28	29
	225	0	1	2	3	4	5	6	7	8	9	10	11	12	13	14	15	16	17	18	19	20	21	22	23	24	25	26	27	28	29
	226	0	1	2	3	4	5	6	7	8	9	10	11	12	13	14	15	16	17	18	19	20	21	22	23	24	25	26	27	28	29
	227	0	1	2	3	4	5	6	7	8	9	10	11	12	13	14	15	16	17	18	19	20	21	22	23	24	25	26	27	28	29
	228	0	1	2	3	4	5	6	7	8	9	10	11	12	13	14	15	16	17	18	19	20	21	22	23	24	25	26	27	28	29
	229	0	1	2	3	4	5	6	7	8	9	10	11	12	13	14	15	16	17	18	19	20	21	22	23	24	25	26	27	28	29

$N_e/N_o = 4/4$

$N_e/N_o = 3/5$  Distance vector of the term sixth weight 3 is 3220.

$N_e/N_o = 5/3$  Distance vector of the term with weight 3 is 3301.

 $N_e/N_o = 4/4$  $N_e/N_o = 3/5$  Distance vector of the term with weight 3 is 3220. $N_e/N_o = 5/3$  Distance vector of the term with weight 3 is 3301.



TABLE IV (contd.)

$G$	$N$	$f$															$v_d$						$S$	$w_d$					$\bar{S}$	Remark
		0	1	2	5	11	12	14	15	0	0	4	4	0	12	0	0	4	4	0	4	0	12	0	0	4	4	0	12	
230		0	1	2	5	11	12	14	15	0	0	4	4	0	12	0	0	4	4	0	4	0	12	0	0	4	4	0	12	
231		0	1	2	4	7	9	11	14	0	1	2	3	2	10	0	1	2	3	2	10	0	10	0	1	2	3	2	10	
232		0	1	2	5	6	11	12	15	0	0	3	4	1	10	0	0	3	4	1	10	0	10	0	0	3	4	1	10	
233		0	1	2	4	7	8	11	13	1	0	0	4	3	8	1	0	0	4	3	8	1	8	1	0	0	4	3	8	
234		0	1	2	7	11	12	13	14	0	0	2	4	2	8	0	0	2	4	2	8	0	8	0	0	2	4	2	8	
235		0	1	6	7	10	11	12	13	0	0	0	8	0	8	0	0	0	8	0	8	0	8	0	0	0	8	0	8	
236		0	1	2	4	7	11	13	14	0	1	0	3	4	6	0	1	0	3	4	6	0	6	0	1	0	3	4	6	
237		0	3	5	6	9	10	12	15	0	0	0	0	8	0	0	0	0	8	0	0	0	0	0	0	0	8	0	0	

select the representative functions of the equivalence class by testing the functions. We try in a similar manner with all the functions with  $K$  true states. The procedure can be easily systemised. In Table IV are given the representatives of the equivalence classes of 4 variable functions. The table contains all the representative function with upto 8 true states. In the columns with heading  $w_d$  and  $\bar{w}_d$  in the table are given the weight distribution vectors of the representative functions of the equivalence classes and their complementary functions respectively. A study of the table will reveal that majority of the functions differ in having different weight distribution vectors of the complementary function. However, there are certain functions which have identical weight distribution vectors and the weight distribution vectors of their complementary functions are also same. In the remark column is entered the easiest possible test that has to be applied for distinguishing between the representative functions. Hence, the table can be used for finding the class to which a given four-variable function belongs.

EXPLANATION AND METHOD OF USING THE TABLE  
FOR FINDING THE EQUIVALENCE CLASS OF A  
GIVEN 4-VARIABLE FUNCTION

The first column headed by  $U$  gives the total number of true states for the function. The column " $N$ " gives the serial number of the function. The column " $f$ " gives the representative function. Symbols  $w_d$  and  $\bar{w}_d$  have already been explained. In the columns  $S$  and  $\bar{S}$  are sum of the weights of the function and their complements respectively. In the remark column is entered the procedure for distinguishing between the different representative classes when they cannot be distinguished on the basis of the weight distribution vector alone.

For finding the equivalence class of a given 4-variable function, we first find out the weight distribution vector of the given function. This can be done very easily with the help of a mechanised grouping chart. Next we compute the sum of the weights of the function. We search in the table amongst the functions having same sum of the weights for a function which have  $w_d$  identical to the given function. If there happen to be more than one function having the same  $w_d$ , we compute  $\bar{w}_d$  for the given function and again search in the table. If  $w_d$  and  $\bar{w}_d$  are not distinct for the function, we finally apply the test procedure suggested in the remark column to find out the class.

CONCLUSION

The methods presented in this paper are quite straightforward and applicable to any number of variables. The tables furnished which contain a list of all the equivalence classes of 4-variable functions can be very conveniently used for searching out the equivalence class to which any given function belongs. It is

observed that in most cases the weight distribution vector of the function and its complement are sufficient indications for recognising the equivalence class and ambiguity arises in very few cases. These vectors can be easily computed with the help of mechanised grouping chart.

#### ACKNOWLEDGMENT

The authors wish to express their indebtedness to Professor J. N. Bhar for guidance and keen interest in the work.

#### REFERENCES

- "Synthesis of Electronic Computing and Control Circuits"—by staff of the Computation Laboratory, Harvard University Press, Cambridge, Massachusetts, 1951.  
Troye, N. C. De, 1959, *Phillips Research Report*, 14.  
Urbano, R. H. and Mueller, R. K., 1956, *I.R.E. Trans. on Electric Computer* EC-5, September.  
Chaudhuri, A. K. and Basu, M. S., 1962 *Ind. J. Phys.* 36, 1.

# ELASTIC SCATTERING OF FAST PROTONS BY DEFORMED NUCLEUS

S. K. DUTTA AND N. C. SIL

DEPARTMENT OF THEORETICAL PHYSICS,  
INDIAN ASSOCIATION FOR THE CULTIVATION OF SCIENCE,  
JADAVPUR CALCUTTA-32.

(Received March 31, 1962)

**ABSTRACT.** In this paper the authors have calculated by the method of Born approximation the elastic scattering cross-section of fast protons by a prolate spheroidal nucleus; the nuclear potential is represented by a complex rectangular well of constant depth and sharp cut-off and the Coulomb potential is taken to be that due to a uniform distribution of the protons within the nucleus. Numerical results for tantalum nucleus ( $A = 171$ ,  $Z = 73$ ) are in fair agreement with the experimental data.

## INTRODUCTION

The nuclear shell model predicts that the heavy nuclei which are away from the closed shells possess non-spherical deformation and as a result, the average potential fields associated with these nuclei also possess large equilibrium deformation. This deformation of shape is supported by experimental facts such as, the energy levels in rotational spectra and the electric quadrupole moments of the nuclei which show that those nuclei cannot be perfect spheres but must have some non-spherical deformations. These deformations are of spheroidal type and the sign of the quadrupole moments shows that in most of the cases these nuclei are of prolate spheroidal shape. It is hoped that this consideration of the deformation of shape will have significant consequences for the scattering of nuclear particles. This suggests that it might be more realistic to calculate nuclear scattering cross-sections on the basis of a model which employs a complex potential well as in the optical model but with appropriately nonspherical shape. In particular, in this paper we have investigated the elastic scattering of fast protons by a semi-transparent prolate spheroidal nucleus. The nuclear interaction between the proton and the nucleus is represented by a complex rectangular well of constant depth and sharp cut-off at the nuclear boundary. The spin of the proton and hence the spin-orbit coupling terms are omitted. As for the electrostatic field generated by the nucleus, it is assumed that the protons within the nucleus are uniformly distributed.

The scattering amplitude is calculated by the Born's approximation method. The differential scattering cross section is calculated for the case of a nucleus

oriented in a particular direction which is then averaged over all possible orientations.

This problem of nuclear scattering by the deformed nuclei has been attempted by various authors during the past few years. The case of fast neutron scattering by even-even, semi-transparent and non-spherical nucleus has been investigated by Inopin (1956) using Born's approximation method. He has taken the nuclear potential to be of constant depth with a sharp cut-off at the boundary. Schey (1959) has investigated the scattering of neutrons by non-spherical nuclei, where the deformation is represented by  $P_2(\cos \gamma)$ ,  $\gamma$  being the angle between the assumed nuclear symmetry axis and the radius vector to the scattered neutron. This non-central potential is assumed small relative to the spin-dependent central potential and thus the added term is treated as a perturbation and the calculation is carried to second order approximation. The calculation was done for neutron and the Schrödinger equation was solved numerically. Margolis and Troubetzkoy (1957) have investigated low energy neutron scattering by a complex square well potential of non-spherical shape, where the deformation is considered as a deviation from the spherical shape of a quadrupole character, and the calculations have been made by expanding the neutron wave function in terms of appropriate spherical Bessel and Neumann functions multiplied by spherical harmonics.

Our calculation makes use of the adiabatic approximation, which is the assumption that the target nucleus does not rotate during the time it interacts with the incident proton. The validity of this approximation has been demonstrated by direct calculation by Chase, Wilets and Edmonds, (1958) and Margolis and Troubetzkoy (1957). The deformed nucleus is assumed to have the same volume as that of the conventional sphere with the same mass. The values of the parameters,  $R$ -the nuclear radius of equivalent sphere,  $V_1$  and  $V_2$  the depth of the real and imaginary part respectively, of the complex nuclear potential are taken from the paper on Proton Scattering by Chase and Rohrich (1954) with appropriate modification for the variation of  $V_2$  with the incident energy of the proton. The value of the semi-major axis  $a$  and semi-minor axis  $b$  of the prolate spheroid are calculated from the constant volume consideration and the value of the electric quadrupole moment of the nucleus concerned. The case has been numerically investigated for the tantalum nucleus which possesses a large value of electric quadrupole moment, and hence appreciable prolate spheroidal deformation.

## RESULTS AND DISCUSSIONS

The nuclear potential is given by

$$\begin{aligned} V(r) &= -(V_1 + iV_2), & \text{within the spheroid,} \\ &= 0, & \text{outside the spheroid,} \end{aligned}$$

and the coulomb potential is given by

$$U(r) = \int \frac{\rho_1 d\mathbf{r}'}{|\mathbf{r} - \mathbf{r}'|}$$

where  $\rho_1$  is the charge density due to the uniform distribution of the protons.

The scattering amplitude, by Born's approximation method, is given by

$$f(\theta, \phi) = \frac{1}{4\pi} \cdot \frac{2\mu}{\hbar^2} \int W(\mathbf{r}) e^{i\mathbf{k} \cdot \mathbf{r}} d^3\mathbf{r},$$

where

$$W(\mathbf{r}) = V(\mathbf{r}) + U(\mathbf{r})$$

and

$$\mathbf{K} = \mathbf{K}_i - \mathbf{K}_f, |\mathbf{K}| = 2k \sin \frac{\theta}{2}, |\mathbf{K}_i| = |\mathbf{K}_f| = k,$$

where

$$k^2 = \frac{2\mu E}{\hbar^2}$$

and  $\mu$  is the reduced mass and  $E$  is the energy of the incident proton. Thus,

$$f(\theta, \phi) = -\frac{\mu(V_1 + iV_2)}{2\pi\hbar^2} \int_{\text{spheroid}} e^{i\mathbf{k} \cdot \mathbf{r}'} d^3\mathbf{r}' + \frac{\mu\rho_1}{2\pi\hbar^2} \int \int \frac{e^{i\mathbf{k} \cdot \mathbf{r}} d^3\mathbf{r}' d^3\mathbf{r}}{|\mathbf{r} - \mathbf{r}'|}$$

Now, making use of the identity

$$\frac{e^{-\lambda R}}{R} = \frac{1}{2\pi^2} \int \frac{e^{-i\mathbf{p} \cdot \mathbf{R}}}{p^2 + \lambda^2} d^3\mathbf{p}$$

we get

$$\begin{aligned} \int \int \frac{e^{i\mathbf{k} \cdot \mathbf{r}} d^3\mathbf{r} d^3\mathbf{r}'}{|\mathbf{r} - \mathbf{r}'|} &= \frac{1}{2\pi^2} \int \int \int \frac{e^{i\mathbf{k} \cdot \mathbf{r}} e^{-i\mathbf{p} \cdot (\mathbf{r} - \mathbf{r}')}}{p^2} d^3\mathbf{p} d^3\mathbf{r} d^3\mathbf{r}' \\ &= \frac{1}{2\pi^2} \int \int \frac{e^{i\mathbf{p} \cdot \mathbf{r}'}}{p^2} d^3\mathbf{p} d^3\mathbf{r}' \int e^{i(\mathbf{k} - \mathbf{p}) \cdot \mathbf{r}} d^3\mathbf{r} \\ &= \frac{4\pi}{K^2} \int_{\text{spheroid}} e^{i\mathbf{k} \cdot \mathbf{r}'} d^3\mathbf{r}' \end{aligned}$$

Thus

$$f(\theta, \phi) = \frac{\mu}{\hbar^2} \left[ \frac{-(V_1 + iV_2)}{2\pi} + \frac{2\rho_1}{K^2} \right] \int_{\text{spheroid}} e^{i\mathbf{k} \cdot \mathbf{r}'} d^3\mathbf{r}'.$$

Let

$$I = \int_{\text{spheroid}} e^{i\mathbf{k} \cdot \mathbf{r}'} d^3\mathbf{r}'.$$

for the convenience in calculation it is assumed that the axis of symmetry of the prolate spheroid is the  $Z$ -axis, and the vector  $\mathbf{K} = \mathbf{K}_i - \mathbf{K}_f$  lies in the  $XZ$  plane. Let  $\alpha$  be the angle of orientation, the angle between the vector  $\mathbf{K}$  and the  $Z$ -axis. Now, choosing the  $\rho, Z, \phi$  coordinate system, we write,

$$I = \int_0^b \int_0^{2\pi} \exp\{iK\rho \sin \alpha \cos \phi + iKZ \cos \alpha\} \rho d\rho dZ d\phi.$$

where  $a$  and  $b$  are the semi-major and semi-minor axis respectively of the prolate spheroid.

Now, using the relation (Watson, pp-20)

$$J_n(Z) = \frac{1}{2\pi} \int_{-\pi}^{\pi} e^{i(n\theta - Z \sin \theta)} d\theta.$$

we get,

$$I = 2\pi \int_0^b \int_0^{2\pi} \exp(iKZ \cos \alpha) J_0(K\rho \sin \alpha) dZ \rho d\phi.$$

Integrating further with respect to  $Z$ , we have

$$I = \frac{4\pi}{K \cos \alpha} \int_0^b \sin(aK \cos \alpha \sqrt{1 - \rho^2/b^2}) J_0(K\rho \sin \alpha) \rho d\rho.$$

Now, putting

$$\rho = b \sin \psi, \quad aK \cos \alpha = \lambda, \quad \text{and} \quad bK \sin \alpha = \mu$$

we get

$$I = \frac{4\pi b^2}{K \cos \alpha} \int_0^{\pi/2} \sin(\lambda \cos \psi) J_0(\mu \sin \psi) \sin \psi \cos \psi d\psi$$

Further, we make use of the relation (Watson, Pp-379)

$$\begin{aligned} & \int_0^\pi \sin(z \cos \theta \cos \psi) J_{\nu-1}(z \sin \theta \sin \psi) C_\nu^r(\cos \theta) \sin \theta^{\nu+1} d\theta \\ &= (-1)^{\frac{1}{2}(r-1)} \left( \frac{2\pi}{Z} \right)^{\frac{1}{2}} \sin \psi^{r-\frac{1}{2}} C_r^r(\cos \psi) J_{\nu+r}(Z), \text{ when } r \text{ is odd.} \end{aligned}$$

Hence

$$I = \frac{(2\pi)^{3/2} b^2 a}{(\lambda^2 + \mu^2)^{3/4}} \cdot J_{3/2}(\sqrt{\lambda^2 + \mu^2}).$$

Thus the differential scattering cross-section is given by

$$\sigma(\theta, \phi) = |f(\theta, \phi)|^2 = (2\pi)^3 \left[ \frac{\mu b^2 a}{\hbar^2} \right]^2 \left[ \frac{-(V_1 + iV_2)}{2\pi} + \frac{2\rho_1}{K^2} \right]^2 \left[ \frac{J_{3/2}(\sqrt{\lambda^2 + \mu^2})}{(\lambda^2 + \mu^2)^{3/4}} \right]^2$$

This is the expression for the differential scattering cross-section when the nucleus is oriented at an angle  $\alpha$  with respect to the  $K$  vector. The averaging over-all orientations of the nucleus is carried out by integrating the above expression with

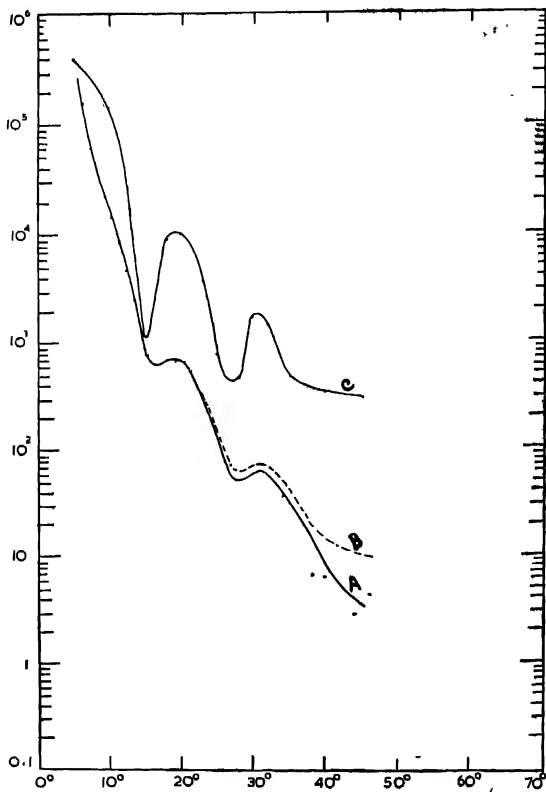


Fig. 1. Tantalum elastic scattering differential cross-section.

The dashed curve B represents an "upper limit" to the elastic scattering cross-section. The solid curve A represents the "extrapolated" elastic scattering cross-section. The solid curve C represents the theoretical value of the elastic scattering cross-section as calculated in this paper.



respect to the angle  $\alpha$  and dividing by 2. Thus the average differential scattering cross-section is given by

$$\sigma_{avg}(\theta, \phi) = (2\pi)^3 \left( \frac{\mu b^2 a}{\hbar^2} \right)^2 \left[ -\frac{(V_1 + iV_2)}{2\pi} + \frac{2\rho_1}{K^2} \right]^2 \int_0^1 \left[ \frac{J_{3/2}(K\sqrt{b^2 + (a^2 - b^2)y^2})}{(K\sqrt{b^2 + (a^2 - b^2)y^2})^{3/2}} \right]^2 dy$$

where  $y = \cos \alpha$

The integral is numerically evaluated by the Simpson's summation rule. The values of the parameters are taken from Chase and Rohlich (1954). The value of  $V_2$ , the imaginary part of the nuclear potential, is determined by using the formula given by above authors.

$$V_2 = \frac{4.5(E + V_1)}{\Lambda}$$

where  $\Lambda$  is the mean free path of the proton in the nucleus at the energy  $E$ .

The values of the parameters are

$$V_1 = 45 \text{ Mev}, \quad V_2 = 13.36 \text{ Mev}, \quad E = 96 \text{ Mev}.$$

$\Lambda(90 \text{ Mev}) \sim 4 \times 10^{-13} \text{ cm}$ , which we have used for 96 Mev also and  $R = 1.42A^{1/3} \times 10^{-13} \text{ cm}$ .

where  $R$  is the radius of the sphere of volume equal to that of the prolate spheroid.

The calculated results for the elastic scattering of 96 Mev protons by tantalum nucleus ( $A = 171$ ,  $Z = 73$ ) are compared with the experimental results given by Gerstein, Niederer and Strauch (1957). The calculations show that at very small angles of scattering  $\theta < 3^\circ$  the influence of the coulomb potential is greater than that of the nuclear potential on the scattering cross-section while at about  $\theta = 3^\circ$  the effects of the coulomb potential and the real part of the nuclear potential on the scattering cross-section are more or less equal in magnitude and therefore nearly cancel each other and the scattering cross section is given by the imaginary part of the nuclear potential. When  $\theta > 3^\circ$  the contribution of the coulomb potential to the scattering cross-section decreases sharply and that of the nuclear potential increases. The pronounced minima in the theoretical differential cross-section for a nucleus with spherical shape become less pronounced now due to the spheroidal deformation of the nuclear shape. The theory predicts correct angular distribution of the maxima and minima of the scattering cross-section. In spite of an overall agreement the theoretical result is, however, in marked disagreement with the experimental finding specially for large angles of scattering; the theoretical cross-section is too large at large angles.

#### ACKNOWLEDGMENT

The authors wish to record their deep sense of gratitude to Prof. D. Basu, for his kind interest in the problem and many valuable discussions during the progress of the work.

## REFERENCES

- Chase, D. M., and Rohrlich, F., 1954, *Phys. Rev.*, **94**, 81.  
Chase, D. M., Wilets, L. and Edmonds, A. R., 1958, *Phys. Rev.*, **110**, 1080.  
Gerstein, G., Niederer, J., and Strauch, K., 1957, *Phys. Rev.* **108**, 427.  
Inopin, E. V., Soviet Physics JETP, 1956, Vol. 3, 134.  
Margolis, B., and Troubetzkoy, E. S., 1957, *Phys. Rev.*, **106**, 105.  
Schey, H. M., 1959, *Phys. Rev.*, **113**, 900.  
Watson, G. N., A Treatise on the theory of Bessel function, Cambridge University Press—1944.

# INTENSITY OF FLUORESCENCE OF DYESTUFFS IN SOLUTION

JUGAL KISHORE, M. K. MACHWE, K. GOPALA KRISHNAN  
AND K. D. CHAUDHURI

DEPARTMENT OF PHYSICS, DELHI UNIVERSITY, DELHI.

(Received February 6, 1962)

**ABSTRACT** The intensity of fluorescence of dyestuffs in solution has been measured for concentrations varying from  $2 \times 10^{-7}$  g/cc to  $2 \times 10^{-3}$  g/cc. The results, along with the polarisation measurements reported earlier, have been used to explain the concentration quenching of fluorescence of dyes in solution.

## INTRODUCTION

Two different theories are generally put forward to explain concentration quenching of fluorescence in solution :—(1) quenching due to collisions of the second kind (Wawilow, 1929) and (2) decrease in fluorescence yield with increasing concentration due to the formation of associated molecules (Levshin, 1927, 1934 and Rabinowitch, 1941). We have here attempted to correlate the results on concentration quenching obtained from intensity measurements with those from polarisation measurements (Chaudhuri, 1959) and examine these results in the light of the above theories.

## EXPERIMENTAL ARRANGEMENT

The intensity of fluorescence in the transverse direction for different concentrations in glycerine is measured in terms of the intensity of the incident light, using a sensitive potentiometer balancing arrangement and photovoltaic cells. The exciting radiations are the unpolarised Hg lines : 4358 Å and 5461 Å. Three dyestuffs Eosin, Acriflavine and Rose Bengal are investigated for concentrations varying from  $2 \times 10^{-7}$  g/c.c. to  $2 \times 10^{-3}$  g/cc. The results of intensity measurements are shown graphically in Fig. 1. The intensity curves and polarisation curves have been drawn together for comparison.

## DISCUSSION OF THE RESULTS

The close parallelism between the two sets of curves shows that the mechanism responsible for the change of intensity and polarisation with concentration may be the same. For a detailed examination, the two sets of curves are divided into three regions :—(1) the region where the intensity increases with

concentration, (2) where it remains constant and (3) where it decreases with further increase in concentration. It should be noted that in the first region, a part of the incident light is transmitted through the fluorescence cell while for

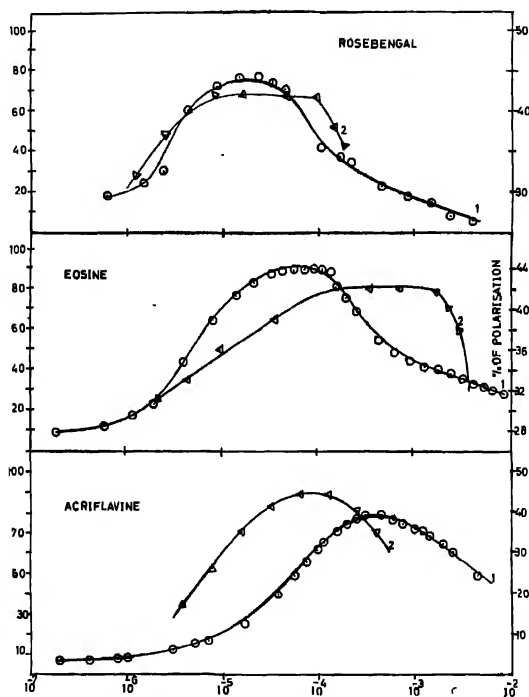


Fig. 1. The variation of (a) the intensity (curve no. 1) and (b) the polarisation (curve no. 2), of fluorescence with concentration in the case of Rose Bengal, Eosin and Acriflavine.

the second and third regions, the total incident light is absorbed in the cell. Therefore in the second and third regions the measured intensity also gives a measure of the fluorescence yield. For discussion the following relations are useful :—

$$A_s = n_s(\alpha_0 + \alpha_s) = n_s/T_s$$

$$I_s = n_s\alpha_0 = n_s/T_0$$

$$Q_s = T_s/T_0$$

]

( $A$ ,—Energy absorbed;  $n$ ,—number of excited molecules;  $\alpha_0$  and  $\alpha$ ,—spontaneous transition probabilities without and with collisions respectively;  $T_s$  and  $T_0$ ,—life times with and without collisions respectively;  $Q$ ,—Fluorescence yield.)

In the first range, the increase in intensity can be due to (1) the increased number of excited molecules and (2) the diminished life period due to collisions. According to Perrin (1931), the life period is connected with the degree of polarisation and the decrease of the life period follows from the polarisation curves as well. For the second and third regions, according to the relations I,  $T_s$  should go on decreasing with increase in concentration. From polarisation experiments it has been found that  $T_s$  decreases with concentration, reaches a minimum value and then increases again. Since  $T_s$  increases after the optimum concentration it follows that the fluorescence yield should also increase with increase in  $T_s$ . But experiments show that the fluorescence yield decreases. These changes in  $T_s$  and the yield can be explained in the following way. Since  $T_s$  increases after the minimum has been reached, it follows that the mechanism is not a pure collision process. Since the micelle formation starts at this concentration approximately it is not unreasonable to connect the increase in  $T_s$  with the formation of associated molecules.  $T_s$  increases, because, the actual concentration of the fluorescence molecules decreases with increase in concentration, due to the formation of nonfluorescent associated molecules. Since concentration is directly dependent on polarisation and inversely on the life period, the increase of the life period can be easily explained. The decrease in the fluorescence yield in this region cannot be explained so easily. If it were simply a case of the formation of the associated molecules, the life period  $T_0$  would have remained unaffected. This is because the formation of associated molecules would have reduced the number of fluorescent molecules without affecting the natural life period. The fluorescence yield would have been given by

$$Q = \frac{n_s \alpha_0}{n_s \alpha_0 + W}$$

where  $W$  is the energy absorbed by the associated molecules which does not affect the life period. Since, however,  $T_s$  goes on increasing after the minimum has been reached and since the actual concentration of the fluorescent molecules decreases with increase in concentration in this region, the behaviour of  $T_s$  can be explained by the theory of the collision of the second kind. It might be reasonably argued why the excited molecules are not deactivated in a collision of the second kind with an associated molecule. It has been suggested that these collisions can be conceived as a quantum mechanical resonance phenomenon and if the colliding molecules are alike the proximity of the energy levels facilitates the transfer in a collision. In other words, the excited molecules will be

easily deactivated in a collision of the second kind with the unexcited molecules of the same kind. As for the fluorescence yield, we will have

$$Q = \frac{n_s \alpha_0}{n_s(\alpha_0 + \alpha_s) + W} = \frac{n_s \alpha_0}{A_s + W}$$

So long as  $W = 0$ , i.e., so long as associated molecules are not formed,  $Q$  decreases with concentration and the life period also decreases. When the formation of associated molecules starts, the life period is still solely determined by  $(\alpha_0 + \alpha_s)$ . As the effective concentration of the fluorescent molecule decreases,  $\alpha_s$  which is a function of concentration also decreases. This means that  $(\alpha_0 + \alpha_s)$  decreases, i.e., the life period increases. Now, as  $n_s$  and  $\alpha_s$  decrease in this region with concentration while  $W$  increases, it follows that the yield may decrease, because the increase in  $W$  may be greater than the decrease in  $n_s(\alpha_0 + \alpha_s)$ . In other words, the increase in the energy absorbed by the associated molecules may be greater than the decrease in the energy absorbed by the fluorescent molecules. We have, therefore, a satisfactory explanation of the decrease in the fluorescence yield in this region. It is therefore, concluded that the theory of the collision of the second kind explains the concentrations, quenching in a satisfactory way.

#### REFERENCES

- Chaudhuri, K. D., 1959, *Z. Physik*, **154**, 34.  
 Levshin, W. L., 1927, *Z. Physik*, **43**, 230.  
 Levshin, W. L., 1934, *Acta. Phys. Chim. U.S.S.R.*, **1**, 685.  
 Perrin, F., 1931, *C. R. Acad. Sci., Paris*, **192**, 1727.  
 Perrin, F., 1931, Fluorescence decroce elementaire d'émision lum Paris, Hermann.  
 Rabmowitch, E., and Epstein, J. F., 1941, *J. Am. Chem. Soc.*, **63**, 69.  
 Wawilow, S. T., 1929, *Z. Physik*, **53**, 665.

# MÖSSBAUER SCATTERING OF LOW ENERGY GAMMA-RAYS

B. S. SOOD

PHYSICS DEPARTMENT,  
PUNJAB UNIVERSITY, CHANDIGARH-3.

(Received April 6, 1962)

**ABSTRACT.** Mössbauer scattering cross-section of 14.4 Kev. gamma rays in iron-57 is found to be  $142 \pm 30$  barns; this agrees with theory if the levels involved in the scattering are assumed to be split. This type of scattering may be used to investigate problems regarding the coherence between resonance and Rayleigh scattering processes.

## INTRODUCTION

Mössbauer scattering of low energy gamma rays though more difficult to measure than the absorption, because of the large internal conversion of low-energy gamma transitions, should be useful for investigating problems related to coherence of resonance and Rayleigh processes. It should, under favourable circumstances also show the lattice interference pattern which will yield important information regarding the positions of the resonantly scattering nuclei and phase of scattering. With this in view, an effort has been made to measure Mössbauer scattering of the well known 14.4 Kev. gamma rays in iron-57, its absorption has already been studied by several workers (Pound and Rebka, 1959), Sciffer and Marshal, 1959).

## EXPERIMENTAL PROCEDURE

The angular distribution of Mössbauer scattering being known, its average cross-section has been calculated from the measurement of the differential cross-section at a mean angle of  $120^\circ$ . At this scattering angle the conditions regarding the relative amplitudes and polarizations of Mössbauer and Rayleigh processes for the interference between them to be experimentally observable, are very unfavourable. Therefore, this angle was chosen in the present investigations in order to be able to examine only Mössbauer scattering without any complications arising from its interference with Rayleigh scattering. The experimental arrangement is shown in Fig. 1.

The determination of the differential cross-section consisted of measuring Mössbauer scattering intensity, the strength of the source, the solid angles subtended by the scatterer at the source and the detector and the effective thickness of the scatterer.

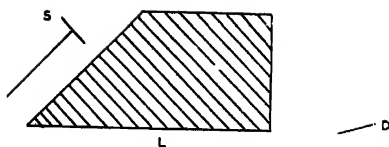


Fig. 1. Experimental arrangement for the measurement of Mossbauer scattering cross section. S, Sc D and L are source, scatterer, window of the detector and lead shield respectively.

The intensity of Mossbauer scattering was determined from the difference of counts recorded by the proportional counter spectrometer due to elastically scattered gamma rays from a thin foil of pure iron with stationary and moving cobalt-57 source. The relevant decay scheme of cobalt-57 is shown in Fig. 2. With the stationary source the scattering consisted mainly of Mossbauer radiation (85%), the Rayleigh component was small (15%) and its contribution was determined by moving the source with the help of a vibrator driven sinusoidally at 33.3 c/sec. so that the source-scatterer relative velocity was sufficient to destroy the resonance condition completely.

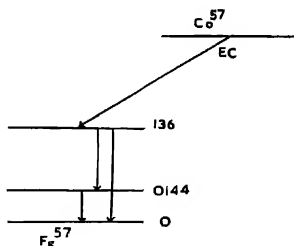


Fig. 2. Decay scheme of  $^{57}\text{Co}$ .

The strength of the source used was determined in terms of the counting rate in the channels corresponding to the energies accepted in the main experiment, the absolute strength being not needed.

The solid angle subtended by the scatterer at source was calculated from the known geometry while the scatterer-detector solid angle was determined experimentally. For this purpose the scatterer was divided into sixteen equal parts, a small source was moved across the various segments and the corresponding



counting rates in the accepted channels were measured. The small source was then compared with the actual source used in the experiment.

The effective thickness of the scatterer was calculated by taking the self-absorption in the scatterer into account.

#### RESULTS AND DISCUSSION

By comparing the number of gamma rays undergoing Mössbauer scattering through  $120^\circ$  to the number incident on the scatterer and taking into account the angular distribution of Mössbauer radiation, a mean value of  $4.45 \times 10^{-4}$  was obtained for the probability of interaction. The value of cross-section was calculated from the probability of interaction from the relation

$$P = \sigma nt$$

where  $p$  is the probability of interaction,  $\sigma$  the cross-section,  $n$  the number of resonant type nuclei per c.c. and  $t$  the effective thickness of the scatterer. Substituting for  $n = 1.82 \times 10^{21}$  nuclei/c.c. and the effective thickness  $= 1.72 \times 10^{-3}$  cm Mössbauer cross section  $\sigma = 142 \times 10^{-24}$  cm<sup>2</sup> was obtained. A probable error of about 20 per cent is estimated in the value of the cross-section.

The magnitude of Mössbauer scattering cross-section would depend upon the conditions whether or not the ground and 14.4 Kev. state in  $^{57}\text{Fe}$  were degenerate; the intrinsic internal magnetic field in the source and scatterer might split either or both the states depending upon their magnetic moments.

The experimental value is compared in Table I with theoretical values calculated for four possible different conditions of the states assuming that 60% of the gamma rays are emitted and absorbed without recoil.

TABLE I

Ground State	Upper state	Theoretical cross-section	Experimental cross-section
(i) degenerate	degenerate	610 Barns	$142 \pm 30$ Barns
(ii) degenerate	split	153 Barns	
(iii) split	degenerate	305 Barns	
(iv) split	split	119 Barns	

The experimental value lies between (ii) and (iv); this suggests that the states are split which is in agreement with absorption experiments.

The success of the scattering experiments suggests the possibility of exploiting the problems related to coherence of Resonance and Rayleigh scattering processes.

#### ACKNOWLEDGMENTS

It is a great pleasure to thank Prof. B. M. Anand for providing excellent facilities to complete this work.

#### REFERENCES

- Pound, R. V. and Rebka, G. A., 1959. *Phys. Rev. Letters*, **3**, 551.  
 Seiffer, J. P. and Marshall, W., 1959. *Phys. Rev. Letters*, **3**, 556.

## SECOND VIRIAL AND ZERO PRESSURE JOULE-THOMSON COEFFICIENTS OF NON-POLAR QUASI-SPHERICAL MOLECULES

S. C. SAXENA AND K. M. JOSHI

PHYSICS DEPARTMENT, RAJASTHAN UNIVERSITY,  
JAIPUR, INDIA.

(Received February 26, 1962)

**ABSTRACT.** A new potential, which considers the repulsive and attractive energies varying as 18 and 6 power of the intermolecular separation respectively, is proposed for the calculation of properties of non-polar quasi-spherical molecules. The reduced virial and zero pressure Joule-Thomson coefficients are evaluated according to this potential, and the values are tabulated as a function of the reduced temperature in the range 0.5 to 400. Treatment of the experimental data shows some preference for this potential over the conventional Lennard-Jones (12-6) potential and is probably more appropriate and accurate for computation of gaseous properties at high temperatures.

### INTRODUCTION

Second virial and zero pressure Joule-Thomson coefficients like other properties of gases require a precise knowledge of intermolecular forces for their complete description on an entirely theoretical basis. Bird and Spotz (1950) have tabulated the second virial coefficient for the familiar Lennard-Jones (12-6) potential :

$$\phi(r) = \epsilon[(\sigma/r)^{12} - 2(\sigma/r)^6], \quad \dots (1)$$

and Rice and Hirschfelder (1954) for the modified Buckingham exp-six potential :

$$\phi(r) = \frac{\epsilon}{1-6|\alpha|} \left[ \frac{6}{\alpha} e^{\frac{\alpha}{6} \left(1 - \frac{r}{\sigma}\right)} - \left(\frac{\sigma}{r}\right)^6 \right]. \quad \dots (2)$$

Here  $\phi(r)$  is the potential energy of interaction between two molecules at a separation distance  $r$ ,  $\epsilon$  is the depth of the potential energy minimum,  $\sigma$  its position, and  $\alpha$  is a parameter which determines the steepness of potential energy. Both these potentials are reasonably successful, probably with a slight preference for the exp-six potential, in accounting the observed properties of non-polar monoatomic spherically symmetric molecules. For those polyatomic molecules which exhibit spherical symmetry i.e. quasi-spherical Hamann and Lambert (1954) have shown that the repulsion is much steeper than given by the potential of

Eq. (1). They suggest instead the following (28-7) type of Lennard-Jones potential :

$$\psi(r) = c/3[(\sigma/r)^{23} - 4(\sigma/r)^7]. \quad (3)$$

Wohl (1931) and Rowlinson (1954) also suggested the need of choosing a higher index than 12 for the repulsive part of the interaction energy. Work of Tanczos (1956) and Amme and Legvold (1959, 1960) on the temperature dependence of collision life-times in complex molecules also support the view of a steeper repulsion than given by the exponent 12 in Eq. (1). One objection against the potential of Eq.(3) is that it departs from the theoretically understood  $1/r^6$  attraction. In fact Pollara and Funke (1959) have suggested an alternative potential which retains the theoretically predicted form for the attraction energy, and also possesses a hard repulsion and an adjustable bowl. This particular potential thus becomes not only complicated but also somewhat unrealistic for small  $r$  values in as much as the repulsion energy is more of an exponential nature than that of a rigid spherical model as assumed by Pollara and Funke (1959). The flexibility of having three disposable parameters is definitely liable to give a better reproduction of the experimental data over a limited temperature range. This indeed is demonstrated by Pollara and Funke (1959) for neo-pentane. However, much more elaborate comparison of this potential with the experimental data is essential before a reliable assessment may be possible. Work of McCoubrey and Singh (1957, 1959, 1960) throw some light on the potential of Eq. (3).

In view of this we, therefore, propose the following (18-6) type of Lennard-Jones potential :

$$\phi(r) = c/2[(\sigma/r)^{18} - 3(\sigma/r)^6], \quad (4)$$

or in an alternative form

$$\psi(r) = 4c_0[(\sigma_0/r)^{18} - (\sigma_0/r)^6]. \quad (4a)$$

The potential parameters of Eqs. (4) and (4a) are interrelated, so that

$$c = 8c_0/3\sqrt{3}, \text{ and } \sigma = (3)^{1/2}\sigma_0. \quad \dots (4b)$$

The potential of Eq. (4) is simpler and the calculation of equilibrium and non-equilibrium properties is much easier than that proposed by Pollara and Funke (1959). This new potential retains the theoretically predicted  $1/r^6$  variation of attraction energy with  $r$  and provides a steeper repulsion than the conventional (12-6) potential. We have calculated in this paper the second virial and zero pressure Joule-Thomson coefficients and the results discussed later reveal that potential (4) yields result which are as accurate as those obtained on the basis

of Pollara and Funke potential. Second virial coefficient data as a function of temperature have been interpreted and the two potential parameters,  $\epsilon$  and  $\sigma$ , Eq. (4) are determined. These parameters are also used to compute the zero pressure Joule-Thomson coefficient of methane and ethane at temperatures where the experimental data are available.

#### THEORETICAL FORMULAE

The classical second virial coefficient,  $B(T)$ , is given by

$$B(T) = 2\pi N \int_0^{\infty} (1 - e^{-\phi(r)/kT}) r^2 dr, \quad \dots (5)$$

where  $N$  is Avogadro's constant,  $k$  is Boltzmann's constant, and  $T$  is the temperature of the gas. Lennard-Jones evaluated  $B(T)$  by substituting for  $\phi(r)$  the following bireciprocal potential :

$$\phi(r) = c \left[ \frac{m}{n-m} \left( \frac{\sigma}{r} \right)^n - \frac{n}{m-n} \left( \frac{\sigma}{r} \right)^m \right], \quad \dots (6)$$

where  $n > m$ . However, if the potential of Eq. (4a) is inserted in Eq. (5) and the integration is performed we finally get

$$B(T) = (2/3)\pi N \sigma_0^3 F(T^*), \quad \dots (7)$$

where

$$F(T^*) = y^{-2} \{ H_{18}(y) - (1/3) H_6(y) \}, \quad \dots (8)$$

$$y = 2(\epsilon_0/kT)^{1/2} = 2(1/T^*)^{1/2}, \quad \dots (9)$$

and

$$H_k(y) = y^{\frac{39-k}{9}} \sum_{l=0}^{\infty} \frac{1}{l!} y^{\frac{4l}{3}} \Gamma\left(\frac{K+6l-3}{18}\right). \quad \dots (10)$$

The zero pressure Joule-Thomson coefficient,  $\mu^0$ , of a pure gas is given by

$$\mu^0 = (b_0/C_p)[F_1(T^*) - F'(T^*)]. \quad \dots (11)$$

Here  $C_p$  is the zero pressure molar specific heat,  $F_1(T^*)$  is the product of the reduced temperature,  $T^*$ , and the first derivatives of  $F(T^*)$  with respect to  $T^*$ .

Computed values of  $H_k(y)$  as a function of  $T^*$  in the range 0.50 to 400 and for values of  $K$  equal to 6, 12, 18 and 24 are given by Saxena and Joshi (1962) in connection with the calculation of  $B(T)$  for polar gases. Utilising these  $H_k(y)$  values, the function  $F(T^*)$  has been calculated according to Eqs. (7), (8) and (9) as a function of  $T^*$  and are reported in Table 1. Values of  $F_1(T^*)$  and  $F'_1(T^*)$

TABLE I

Functions for calculating the second virial and zero pressure Joule-Thomson coefficients as a function of temperature

T*	F(T*)	F <sub>1</sub> (T*)	F <sub>1</sub> (T*)—F(T*)
0.50	—17.1578 1	—	—
0.55	—13.5311 1	32.672	46.203
0.60	—11.0415	24.976	36.017
0.65	—9.24776	20.448	29.696
0.70	—7.85000	16.176	24.026
0.75	—6.80356	13.054	20.518
0.80	—6.03505	11.883	17.018
0.85	—5.36227	10.378	15.739
0.90	—4.80488	9.1585	13.963
0.95	—4.33720	8.1499	12.487
1.00	—3.93846	7.3949	11.333
1.05	—3.59108	6.7044	10.296
1.10	—3.29321	6.0919	9.3851
1.15	—3.03634	5.6902	8.7266
1.20	—2.80381	5.1919	7.9957
1.25	—2.59983	4.7869	7.3867
1.30	—2.41592	4.5543	6.9702
1.35	—2.24975	4.2600	6.5097
1.40	—2.09971	3.9951	6.0948
1.45	—1.96352	3.7969	5.7604
1.50	—1.83827	3.5803	5.4186
1.55	—1.72417	3.3820	5.1062
1.60	—1.61936	3.2281	4.8475
1.65	—1.52225	3.1121	4.6343
1.70	—1.43236	2.9360	4.3683
1.75	—1.34912	2.8035	4.1526
1.80	—1.27198	2.6844	3.9564
1.85	—1.19922	2.5705	3.7697
1.90	—1.13212	2.4689	3.6010
1.95	—1.06895	2.3896	3.4585
2.0	—1.01002	2.3075	3.3175
2.1	—0.901217	2.1503	3.0516
2.2	—0.804778	1.9904	2.7951
2.3	—0.718851	1.8755	2.5943
2.4	—0.640571	1.7854	2.4260
2.5	—0.569891	1.6775	2.2518
2.6	—0.506005	1.5924	2.0984
2.7	—0.447536	1.5099	1.9574
2.8	—0.394298	1.4370	1.8313
2.9	—0.344906	1.3766	1.7215
3.0	—0.299401	1.3057	1.6051
3.1	—0.257624	1.24202	1.4996
3.2	—0.218871	1.20026	1.4251
3.3	—0.182437	1.15579	1.3382
3.4	—0.148048	1.1127	1.2613
3.5	—0.116992	1.0673	1.1843
3.6	—0.087435	1.0343	1.1217
3.7	—0.059578	0.99216	1.0517

TABLE I (contd.)

T*	F(T*)	F <sub>1</sub> (T*)	F <sub>1</sub> (T*)—F(T*)
3.8	— 0 033500	0 95756	0 99100
3.9	— 0 009146	0 92152	0 93067
4	0 014037	0 88258	0 88258
5	0 183543	0 69873	0 51519
6	0 297407	0 56083	0 37708
7	0 370579	0 44063	0 07005
8	0 424649	0 36741	—0 05724
9	0 464102	0 30473	—0 15937
10	0 494302	0 26779	—0 22652
12	0 536819	0 20233	—0 33440
14	0 564421	0 15898	—0 40545
16	0 583434	0 12783	—0 45561
18	0 596788	0 10058	—0 46896
20	0 606112	0 096875	—0 50924
30	0 626061	0 024014	—0 00204
40	0 627895	—0 0065143	—0 63441
50	0 624343	—0 024027	—0 64837
60	0 618948	—0 033420	—0 65237
70	0 613104	—0 041437	—0 65454
80	0 606942	—0 049303	—0 65624
90	0 601051	—0 051562	—0 65261
100	0 595445	—0 054926	—0 65037
200	0 552018	—0 067997	—0 62002
300	0 523979	—0 069673	—0 59365
400	0 503756	—0 071091	—0 57485

— $F(T^*)$  are also recorded in this Table. The first derivative of  $F(T^*)$  is calculated according to the expressions given by Margenau and Murphy (1956).

#### DETERMINATION OF POTENTIAL PARAMETERS

Experimental data of  $B(T)$  as a function of temperature of neo-C<sub>5</sub>H<sub>12</sub>, SiF<sub>4</sub>, SF<sub>6</sub>, C<sub>2</sub>N<sub>2</sub>, C<sub>3</sub>H<sub>4</sub>, C<sub>2</sub>H<sub>6</sub> and CH<sub>4</sub> are used to determine the potential parameters of Eq. (4a). The procedure used for neo-C<sub>5</sub>H<sub>12</sub> is the well known graphical method of the translation along the two axes given by Keesom (1912). For the remaining gases we have used the following numerical method :

The experimental  $B(T)$  values at two temperatures are chosen and the experimental values of  $F(T^*)$  are tabulated at each temperature for a series of arbitrarily chosen  $\sigma_0$  values. A comparison of these experimental values of  $F(T^*)$  with the tabulated values will give directly  $T^*$  and hence  $\epsilon_0/k$  for each value of  $\sigma_0$ . Thus, two sets of coupled values of  $\epsilon_0/k$  and  $\sigma_0$  are obtained corresponding to the initially chosen temperatures. Each set characterized by a temperature will yield a curve on plotting  $\epsilon_0/k$  and  $\sigma_0$ , and the intersection of the curves will give the unique values for  $\epsilon_0/k$  and  $\sigma_0$ . Values of the potential parameters so determined are listed in Table II,

TABLE II  
Potential parameters according to the modified Lennard-Jones (18-6)  
potential

Gas	$\epsilon_0/k$ °K	$\sigma_0$ Å	$b_0 = (2/3)\pi N\sigma_0^3$ cc/mole	Reference
Neo-pentane	219	6.68	376	a
Silicon tetrafluoride	128	5.39	197.4	b
Sulphur hexafluoride	158	5.80	246.0	b
Cynogen	154	5.50	210.0	b
Propadine	174	6.02	272.5	b
Ethane	189	4.40	107.5	c
Methane	129	3.64	60.8	d

(a) Hamann, *et al.* (1954).(b) Hamann, *et al.* (1953).(c) Rowner, *et al.* (1944).(d) Schamp, *et al.* (1958).

## RESULTS AND DISCUSSION

The  $c/k$  and  $\sigma$  values for the three potentials, viz., Lennard-Jones (18-6), (12-6), and (28-7) are listed in Table III for a number of gases. We find that the

TABLE III  
Potential parameters for (18-6), (12-6) and (28-7) potentials and (28-7)  
potentials

Gas	(18-6) potential <sup>a</sup>		(12-6) potential		(28-7) potential	
	$\epsilon_0/k^\circ\text{K}$	$\sigma^\text{Å}$	$\epsilon/k^\circ\text{K}$	$\sigma^\text{Å}$	$\epsilon/k^\circ\text{K}$	$\sigma^\text{Å}$
Neo-pentane	337	7.08	236 <sup>b</sup>	8.25 <sup>b</sup>	581	6.09 <sup>b</sup>
Silicon tetrafluoride	197	5.91	149 <sup>b</sup>	6.28	331 <sup>b</sup>	5.03 <sup>b</sup>
Sulphur hexafluoride	243	6.35	189 <sup>b</sup>	6.63 <sup>b</sup>	414 <sup>b</sup>	5.27 <sup>b</sup>
Cynogen	237	6.03	—	—	—	—
Propadine	268	6.60	—	—	—	—
Ethane	201	4.63	243.0 <sup>c</sup>	4.44 <sup>c</sup>	—	—
Methane	199	3.90	148.2 <sup>b</sup>	4.28	310 <sup>b</sup>	3.63

(a) Present work.

(b) Hamann, *et al.* (1954).(c) Hirschfelder, *et al.* (1954).

position of the potential energy minimum is always at a smaller intermolecular separation distance for the (28-7) potential than the (12-6), while for the (18-6) the values are usually intermediate. On the other hand, the depth of the potential well,  $\epsilon$  values, follow a different trend, (28-7) values are the greatest, (18-6) values are the smallest, while the (12-6) values lie usually in between. The dispersion energy according to these three potentials, is  $4\epsilon_0\sigma^6$ , or  $(3/2)\epsilon\sigma^6$  for the (18-6),  $2\epsilon\sigma^6$  for the (12-6) and  $(4/3)\epsilon\sigma^7$  for the (28-7). Actual calculations in the case of neo-C<sub>5</sub>H<sub>12</sub>, SiF<sub>4</sub>, SF<sub>6</sub> and CH<sub>4</sub> revealed that the dispersion energy in the case of (28-7) potential is the greatest being approximately double than that of the (12-6) potential, except in the case of CH<sub>4</sub> it is three times. The dispersion energy for the (18-6) potential is the minimum and is approximately two-third of the (12-6) potential except the case of neo-C<sub>5</sub>H<sub>12</sub> it is one-twentieth and in C<sub>2</sub>H<sub>6</sub> it is three and half-times. The differences, though appreciable, are not very big and will be exhibited in gas properties in still smaller proportions and extremely accurate data will be required over a wide enough temperature range where dispersion energy plays an important role to throw light on the relative appropriateness of the different potentials. The repulsive energy is appreciably different on these three potentials, the (28-7) potential is the steepest and then are in order the (18-6) and the (12-6) potentials.

The potential parameters of Table II in conjunction with the  $F(T^*)$  values of Table I are used to calculate  $B(T)$  as a function of temperature where experimental data are available. The computed values are shown as continuous curves in Fig. 1 for neo-C<sub>5</sub>H<sub>12</sub>, C<sub>2</sub>N<sub>2</sub>, C<sub>3</sub>H<sub>4</sub>, SiF<sub>4</sub>, SF<sub>6</sub>, C<sub>2</sub>H<sub>6</sub> and CH<sub>4</sub> as a function of temperature. Also shown are the experimental points. The agreement between the theoretical and experimental values is excellent, the departure being well within the experimental errors. In the case of the (12-6) and the (28-7) potentials also the theoretically computed values are equally good and reproduce the experimental data satisfactorily except for neo-C<sub>5</sub>H<sub>12</sub> on the (12-6) potential. The reason for this is that in all cases we are well below the Boyle temperature and the main contribution to the molecular interaction is due to the attraction energy, which as shown above is not much different for the three potentials. At sufficiently high temperatures the repulsive energy will be of importance and these potentials will yield sufficiently different values. Consequently, one of the real test of the appropriateness of the potential will actually lie at such-high temperatures. Unfortunately, at present no such experimental data exist to warrant this test. In the case of neo-C<sub>5</sub>H<sub>12</sub> we find that the (18-6) potential gives a superior reproduction than the (12-6) potential and very much in conformity with the potentials (28-7) and the one suggested by Pollara and Funke (1959).

A more conclusive test of the potential is possible if some other properties could be calculated for which the experimental data are available. Zero pressure Joule-Thomson coefficient is one such property and will be discussed in this paper.



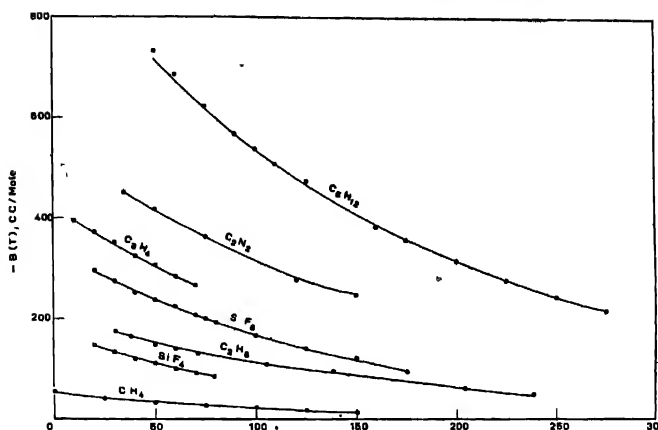


Fig. 1 Plot of  $B(T)$  versus  $T$ ;  $\bullet$  experimental points; continuous curve, calculated according to the (18-6) potential.

Experimental  $\mu^0 C_p^0$  values are available for  $\text{CH}_4$  and  $\text{C}_2\text{H}_6$  as a function of temperature. Calculated values of  $\mu^0 C_p^0$  for these two gases according to the (12-6) and (18-6) potentials are recorded in Table IV only at those temperatures

TABLE IV

Theoretical and experimental values of  $\mu^0 C_p^0$  (cc/mole) as a function of temperature

Temperature °K	Exp <sup>a</sup>	Methane Cal (12-6)	Cal (18-6)	Exp <sup>b</sup>	Ethane Cal (12-6)	Cal (18-6)
294.3	144.2	158.6	159.4	507.4	397	541.8
311.0	130.3	146.0	144.8	463.5	363.5	496.6
327.6	117.7	133.3	132.6	411.0	333.8	453.4
344.3	106.9	122.1	121.2	392.6	308.1	417.7
361.1	97.7	112.3	110.8	356.3	286.0	384.3
387.6	89.0	103.1	104.7	317.7	266.7	354.7

(a) Budenholzer, *et al.* (1939).

(b) Sage, *et al.* (1937).

where experimental data are reported. In the case of methane the two sets of calculated values agree very well, though these are approximately 10% greater than the experimental values. A somewhat similar situation exists for the case of ethane except that the calculated values, according to the (18-6) potential, are in much agreement with the experimental values than those on the (12-6) potential. The experimental data for ethane correspond to one atmosphere.

The Lennard-Jones type (18-6) potential has also been extended to evaluate the second virial coefficient by Saxena and Joshi (1962), and the zero pressure Joule-Thomson coefficient by Saxena, Joshi and Ramaswami (1962) for polar gases. The extended (18-6-3) potential seems to be somewhat superior to the conventional (12-6-3) potential. Thus, on the basis of all this work and evidences, both theoretical and experimental, we propose this new (18-6) potential, tentatively for the prediction of properties of quasi-spherical molecules at high temperatures till more measurements become available to confirm or reveal the form of an adequate intermolecular potential.

#### REFERENCES

- Ammo, R. C. and Legvold, S., 1959, *J. Chem. Phys.* **30**, 163; 1960, *ibid.* **33**, 91.
- Bird, R. B. and Spotz, E. L., 1950, University of Wisconsin, CM-599; See also Hirschfelder, J. O., Curtiss, C. F. and Bird, R. B., 1954, *Molecular Theory of Gases and Liquids*, John Wiley & Sons, Inc., New York, p. 1114.
- Budenholzer, R. A., Sage, B. H. and Lacey, W. N., 1939, *Ind. Eng. Chem.*, **31**, 369.
- Hamann, S. D., Mc Manamey, W. J. and Pearso, J. F., 1953, *Trans. Faraday Soc.* **49**, 351.
- Hamann, S. D., and Lambert, J. A., 1954, *Australian J. Chem.* **7**, 1.
- Hirschfelder, Curtiss and Bird, 1954, *Molecular Theory of Gases and Liquids*, p. 1112.
- Keesom, W. H., 1912, *London Comm. Suppl.* 25; See also Lennard-Jones, J. E., 1924, *Proc. Roy. Soc. (London)* **A106**, 463.
- Margenau, H. and Murphy, G. M., 1950, *The Mathematics of Physics and Chemistry*, D. Van Nostrand Co. Inc., New Jersey, p. 473; See also Rutledge, G., 1932, *Phys. Rev.* **40**, 262.
- McCoubrey, J. C. and Singh, M. N., 1957, *Trans. Faraday Soc.* **53**, 877; 1959, *ibid.* **55**, 1826; 1960, *ibid.* **56**, 486.
- Pollara, L. Z. and Funke, P. T., 1959, *J. Chem. Phys.* **31**, 855.
- Reamer, H. H., Olds, R. H., Sage, B. H. and Lacey, W. N., 1944, *Ind. Eng. Chem.* **36**, 950.
- Rice, W. E. and Hirschfelder, J. O., 1954, *J. Chem. Phys.* **22**, 187.
- Rowlinson, J. S., 1954, *Trans. Faraday Soc.* **50**, 647.
- Sage, B. H., Webster, D. C. and Lacey, W. N., 1937, *Ind. Eng. Chem.*, **29**, 658.
- Saxena, S. C. and Joshi, K. M., 1962, to be published. in *Phys. Fluids*.
- Saxena, S. C., Joshi, K. M. and Ramaswami, S., 1962, to be published.
- Schamp, H., Mason, E. A., Richardson, A. C. B., and Altman, A., 1958, *Phys. Fluids* **1**, 329.
- Tanczos, F. J., 1956, *J. Chem. Phys.*, **25**, 439.
- Wohl, K. Z., 1931, *Physik. Chem.*, **B14**, 36.

# Letters to the Editor

*The Board of Editors will not hold itself responsible for opinions expressed in the letters published in this section. The notes containing reports of new work communicated for this section should not contain many figures and should not exceed 500 words in length. The contributions must reach the Assistant Editor not later than the 15th of the second month preceding that of the issue in which the letter is to appear. No proof will be sent to the authors.*

6

## EFFECT OF SURFACE RECOMBINATION VELOCITY ON CARRIER LIFETIME FOR CYLINDRICAL GEOMETRY

P. DAS

INSTITUTE OF RADIO PHYSICS AND ELECTRONICS, UNIVERSITY OF CALCUTTA

(Received January 17, 1962)

The effective lifetime of excess carriers in semiconductors as obtained by the photoconductive decay method is a function of the bulk lifetime as well as the surface recombination velocity. The samples which have been employed for such measurements are usually taken in the rectangular form. For such rectangular samples, the contribution of the surface recombination has been calculated by Shockley (1951).

Recently, Jacobs *et al.* (1959), Larabee (1960) and some other workers have proposed a microwave method for the measurement of lifetime of excess carriers in semiconductors, in which the sample is mounted inside the wave-guide and the photoconductive decay is detected by the change in microwave power absorption. In carrying out some measurements on Si samples in cylindrical form by this method in our laboratory, need was felt for estimating the contribution of surface recombination to the effective lifetime for cylindrical geometry. In the present note an analysis is made to determine the effective lifetime in terms of the bulk lifetime and the surface recombination velocity for different sizes of the sample having cylindrical geometry. The general continuity equation for excess carriers is

$$\frac{\partial \delta}{\partial t} = -\frac{\delta}{\tau} + D \nabla^2 \delta + G \quad \dots (1)$$

where  $\delta$  = excess carrier density,  
 $\tau$  = bulk lifetime,

$G$  = number of carriers generated per unit time per unit volume,

$D$  = diffusion constant for the carriers.

In the problem considered here the cylindrical sample is illuminated in a region far away from the ends. The continuity equation then may be reduced to

$$\frac{\partial \delta}{\partial t} = -\frac{\delta}{\tau} + D \frac{1}{r} \frac{\partial}{\partial r} \left( r \frac{\partial \delta}{\partial r} \right) \quad (2)$$

Let

$$\delta(r, t) = R(r) T(t) \quad (3)$$

where  $R$  and  $T$  are two functions to be determined.

Putting Eq. (3) into Eq. (2) one gets

$$\frac{d^2 R}{dr^2} + \frac{1}{r} \frac{dR}{dr} + \frac{R}{\lambda^2} = 0 \quad (4)$$

$$\frac{1}{T} \frac{dT}{dt} + \nu = 0 \quad (5)$$

where  $\nu$  gives the inverse of effective lifetime.

and

$$\frac{1}{\lambda^2} = \frac{1}{D} \left( \nu - \frac{1}{\tau} \right) \quad (6)$$

The solution of (4) and (5) are respectively

$$R = A J_0(r/\lambda) + B Y_0(r/\lambda) \quad (7)$$

$$T = e^{-\nu t} \quad (8)$$

where  $A$  and  $B$  are arbitrary constants.

At  $r = 0$ , the solution (7) must be finite and at  $r = a$ , i.e., at the boundary one has

$$-eD \left( \frac{\partial \delta}{\partial r} \right)_{r=a} = S\delta$$

where  $S$  = surface recombination velocity,

$e$  = electronic charge.

Putting the boundary conditions into (7) one obtains —

$$P(a/\lambda) = \frac{J_0(a/\lambda)}{J_1(a/\lambda)} \quad (9)$$

where

$$P = D/(as)$$

The complete solution is

$$\delta(r, t) = \sum_f A e^{-\nu_f t} \frac{J_0(r/\lambda_f)}{J_1(a/\lambda_f)} \quad (10)$$

where  $\nu_f$  is related to  $(a/\lambda_f)$  by Eq. (6) and  $(a/\lambda_f)$  is determined by Eq. (9).

The plots giving the roots of Eq. (6) for different values of  $P$  are shown in Fig. 1.

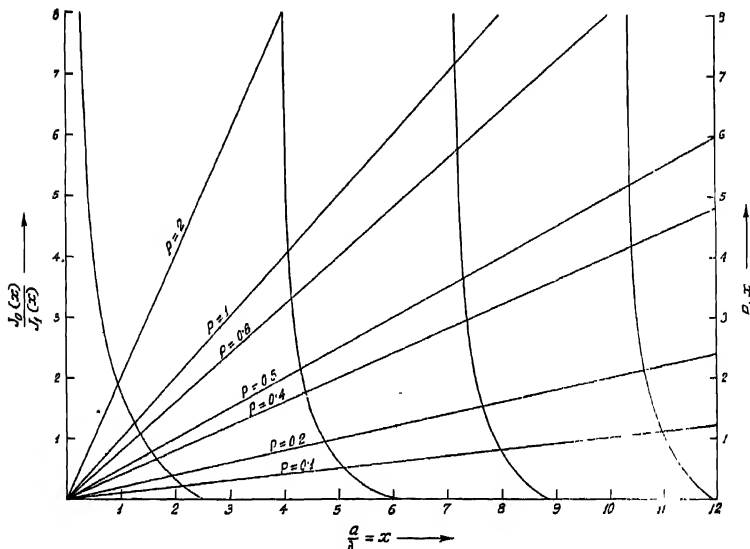


Fig. 1. Plots of the two functions of the equation  $p.a/\lambda = \frac{J_0(a/x)}{J_1(a/\lambda)}$  versus  $(a/\lambda)$ . The solutions  $(a/\lambda)$  of the equations are the points of intersection of the two families of plots.

It is evident from Eq. (10) that the decay of excess carriers will be different from exponential for small values of  $t$ . However, the higher order modes characterised by higher values of  $\nu$  die out quicker than the fundamental mode. The effective lifetime as determined by the photoconductive decay method is that corresponding to the fundamental mode and is given by

$$\nu_1 = \frac{1}{\tau_s} = \frac{1}{\tau} + \frac{D}{\lambda_1^2}$$

where  $\lambda_1$  is the largest root of Eq. (9).

It may be interesting to determine the values of  $\nu_1$  for two limiting cases for which  $S$  is either infinity or very small,

The values of  $\lambda_1$  in the two limiting cases are as given below :

(i) For  $S \rightarrow \infty$  i.e.  $P \rightarrow 0$

$$\frac{a}{\lambda_1} \rightarrow 2.5 \quad \text{or} \quad v_1 = \frac{1}{\tau} + 6.25 \frac{D}{a^2}$$

(ii) For  $S \rightarrow 0$  i.e.  $P \rightarrow \infty$

$$\frac{a}{\lambda_1} \rightarrow \sqrt{\frac{1}{P}} \quad \text{or} \quad v_1 = \frac{1}{\tau} + \frac{S}{a}$$

The author expresses his sincere gratitude to Prof. J. N. Bhar, D.Sc., F.N.I. for his kind interest and to Dr. B. R. Nag for his helpful suggestions.

#### REFERENCES

- Jacobs, H., Ramisa, A. P. and Brand, F. A., 1959, *J. Appl. Phys.*, **30**, 1054-1060.  
 Larabee, R. D., 1960, *RCA Rev*, **21**, March, 124.  
 Shockley, 1951, 'Electrons and Holes in Semiconductors', 319.

# A COMPOSITE MODULATOR FOR COMPATIBLE SINGLE SIDEBAND

N. B. CHAKRABARTI

INSTITUTE OF RADIO PHYSICS AND ELECTRONICS, UNIVERSITY OF CALCUTTA

(Received January 4, 1962)

A technique for generation of compatible single sideband signals that employs a transmitted carrier single sideband signal as the primary source will be very briefly described below.

It can be easily shown that a combination of AM and PM, the phase modulation of which is represented by  $\phi = 2 \tan^{-1} \frac{r \sin \omega_s t}{1 + r \cos \omega_s t}$  and the amplitude modulation by  $A(t) = 1 + m \cos \omega_s t$ , at a modulation frequency  $\omega_s$  radians/sec., results in a one-sided spectrum provided  $m = \frac{2r}{1+r^2}$ . The spectrum contains, for a single tone modulation, the carrier, the first order upper sideband and the second order upper sideband of magnitudes  $\frac{1}{1+r^2}$ ,  $\frac{2r}{1+r^2}$  and  $\frac{r^2}{1+r^2}$  respectively. This follows from the identity

$$e^{j\omega_c t} \left( \frac{1 + r e^{j\omega_s t}}{1 + r^2} \right)^2 = (1 + m \cos \omega_s t) e^{j \left( \omega_c t + 2 \tan^{-1} \frac{r \sin \omega_s t}{1 + r \cos \omega_s t} \right)}$$

The phase modulation  $\phi$  is easily obtained by doubling and limiting a TSSB signal of index  $r$ . The required relationship between  $m$  and  $r$  is established by controlling the carrier amplitude from detected r.m.s. audio level. A simple way of achieving this is to combine in right amplitude and phase the TSSB signal and the carrier frequency output of a narrowband carrier amplifier driven from the TSSB signal. It is found that if the resultant index can be represented by  $r = \frac{m}{2 - 0.625m^2}$ , the required relationship  $m = \frac{2r}{1+r^2}$  is quite well satisfied up to a modulation index of 90%.

Experimental results show that the undesired side components can be kept less than 1% and the total distortion less than 3% at a modulation index of 85%.

It should be mentioned that the presence of the second order upper sideband is not exceptionable, for the energy content is ordinarily low for high modulation frequencies. In fact, its presence causes crowding rather than spreading of the spectrum.

## BOOK REVIEWS

**FLUCTUATION, RELAXATION AND RESONANCE IN MAGNETIC SYSTEMS.** Edited by D. ter Haar, Price 63s net. Published by Oliver and Boyd Ltd., Edinburgh.

The volume consists of a full report of the lecture given at the 1961 Summer School of the Scottish Universities, on the different theoretical aspects of the behaviours of a magnetic system under the usual internal and external potential fields perturbations tending to reach equilibrium conditions with thermal agitations. As Professor Wyllie, the Director of the School tells in his preface the lectures aim at the "evolution of a physical system with a statistically specified Hamiltonian" with special reference to magnetic systems since "they can be easily brought to a condition far from thermal equilibrium, but still rather simply specified." The underlying fundamental assumption is that the perturbed systems can be treated to behave linearly or at best the departure from linearity is small, in other words the principle of superposition of responses to low enough stimuli holds good. On this basis the introductory lecture by Prof. Wyllie deals with some of the fundamentally important definitive functions and theorems of the magnetic behaviour under an oscillating field, the phenomena of relaxation and dispersion, fluctuations in physical properties constituting noise and their autocorrelation function and spectra density, damping and fluctuation dissipation, line broadening etc., finally leading to the crux of the problem, namely, a complete dynamics of the spin-lattice interactions and the equilibrium conditions involving irreversible thermodynamical processes.

The subsequent papers by a number of well known workers in the field expand upon some of the intricate and interesting topics, introduced by Prof. Wyllie. The starting point is a lecture by Callen in which he deals in details with the fluctuation-dissipation theorem, and the irreversible thermodynamical processes which lead to the similar results as by the density matrix and Green function theories, details of which are given in the lectures by Dr. ter Haar. The stochastic (i.e. random fluctuational) theory of line-shape and relaxation phenomenon is dealt with by Prof. Kubo. The mechanism of line broadening is further dealt with by Callen under assumption that the driving force fails to disturb the thermal equilibrium distribution, when the response of a system to a long continued oscillation is considered. The relaxation in paramagnetics and ferromagnetics are treated exhaustively by Gorter and Callen respectively while Orbach gives the general theory of spin-lattice relaxation in solids and the Statistical mechanics of ferromagnetism is dealt with by Callen. The problem of space and time correlation in crystals is dealt with by Davies. The behaviour of a fluctuating photon



field and its equilibrium with fluctuating lattice fields is discussed by Mc. Combie to illustrate the successful use of the Master Equation. There are other interesting articles on neutron scattering and correlation in liquids, nuclear precession in metals at low temperatures, nuclear double resonance, study of rate process by n.m.r. technique, and nuclear relaxation in alkali halides. Finally, the more general problem of nonlinear relaxation and irreversible thermodynamics is treated as a generalization of Ousager's theory of nonlinear dissipative systems, by Uhlhorn.

The discussions are mainly of a very high level theoretical nature but is judiciously moderated by the inclusion of experimental materials to show up the uncertainties or plausibilities of the theory. The book provides much food of thought to the specialist in the line and is invaluable as index of the recent position in respect of a most interesting and yet little understood range of phenomena.

A. Bose

#### PROGRESS IN ELEMENTARY PARTICLE AND COSMIC RAY PHYSICS.

Vol. V. Edited by T. G. Wilson and S. A. Wouthuysen, Pp 461+xii. North Holland Publishing Co., Amsterdam 1960)

Some of the earlier volumes of this series appeared under the title "Progress in Cosmic Ray Physics". The change in the title of the present volume, embracing the developments in the physics of the elementary particles, seems to be judicious considering the contribution of cosmic ray studies in the field of elementary particles since Anderson's discovery of positron upholding Dirac's picture of anti-particle of electron.

The discovery of the non-conservation of parity in weak interactions in the realm of elementary particles has given a great impetus to the study of the subject, both in its theoretical and experimental aspect, which is being reviewed by A. Lundby in the first article in this volume, narrating our state of knowledge from 1958. Relevant questions on parity, charge conjugations, time reversal symmetries in different experimental cases are discussed adequately.

In the second article Gammel and Thaler discuss the nucleon-nucleon interaction and the experimental result of  $p$ - $p$  and  $n$ - $p$  scattering with its bearing to charge independence of nuclear forces. Present theories and potential models describing nucleon-nucleon interactions up to about 300 Mev are presented.

In the third article J. McConnell reviews the history of the subject of anti-particles since Dirac's prediction of positron. Different theories for the production of anti-nucleon and its annihilation are given, however, in the words of the author "theoretical physicists are greatly hampered by the scarcity of reliable experimental data concerning anti-nucleons". Some experimental results on 'anti-proton'-proton interactions are presented briefly.

In the next article on "Observation on Cosmic ray 'Jet' interactions in Nuclear Emulsions", D. H. Perkins discusses the exploitation of the emulsion technique of Bristol fame in recording directly, at high altitudes, the detailed features of individual interactions due to the primaries in the ultra-high-energy region (above 1000 Gev). The nature of the secondary particles, their energies and angular distributions, inelasticity in high energy nucleon-nucleon, nucleon-nucleus collisions and current theories of meson production are also discussed. The masterly presentation of the subject, mentioning also the disadvantages of the technique, is well illustrated with many plates of the photomicrograph of various interactions.

In the last article entitled, "The absorption and decay of negative muons" R. M. Tennant presents the experiments and results of the absorption and decay of cosmic ray and machine-derived meson. A comparison of the experimental results and theories is also given.

The authors of five different well chosen articles have covered their respective subjects in detail, including also hitherto unpublished data from private sources. The book will no doubt serve useful purpose not only to research workers in the field of cosmic ray and elementary particle physics but also to students undergoing advanced studies in Physics.

B. N. Bhar

## INDIRECT SPIN COUPLING IN MAGNETIC GARNETS\*

K. P. SINHA AND M. K. SINHA

NATIONAL CHEMICAL LABORATORY, POONA-8 (INDIA)

(Received November 17, 1961; Resubmitted April 9, 1962)

**ABSTRACT.** The indirect exchange mechanisms arising through empty excited orbitals are applied for a theoretical study of the spin coupling in magnetic garnets. The unit chosen for detailed calculations is a five-centre (AA'OBC with A, A', B, C standing for the magnetic ions and O for the anion) and six-electron system.

It is found that for the model chosen the most stable state, within the framework of these mechanisms and physical situations assumed to be existing, is one of the singlets which involves anti-ferromagnetic interactions between the various magnetic ions. Thus the paramagnetic ions tend to compensate each other's spins. This conclusion is supported by the observed magnetic moments for such systems.

## INTRODUCTION

Like ferrosinels, the magnetic garnets are ferrimagnetic (Geller 1960) and it is expected that the spin coupling between the magnetic ions is achieved in some form of indirect exchange interaction involving the diamagnetic ions. Theoretically, various mechanisms for this basically antiferromagnetic interaction are possible but their relative importance has been difficult to assess. We shall, however, investigate the indirect spin coupling in magnetic garnets following a mechanism recently developed by one of the authors and co-workers (Koide, Sinha and Tanabe 1959), which has been successfully applied to rocksalt, perovskite, zinc blende and spinel-like magnetic compounds (Sinha and Koide 1960, Sinha 1961).

The central theme of this mechanism resides in choosing the appropriate model for the crystalline system and studying the perturbations caused by certain spin dependent transitions of the anion electrons to excited orbitals, on the zero order ground eigenstates of the  $S^2$  operator for the unit chosen. This furnishes the relevant interaction terms which lead to the spin coupling of the various states. The state whose energy suffers maximum depression owing to this perturbation is most stable and should correspond to the ground state. Additional perturbations are also provided by two electron transitions from the magnetic ions to the empty excited orbitals and strengthen the former effects (Sinha 1961). In what follows, we give a detailed calculations for these processes after selecting a unit appropriate for garnet-like compounds. For this we must briefly discuss the relevant features of the magnetic garnets.

\*Communication No. 482 from National Chemical Laboratory, Poona-8.

## DESCRIPTION OF MODEL

The garnets are represented by the general formula  $\{A_3\}[B_2](C_3)O_{12}$  and crystallize in a cubic lattice (space group  $1a\ 3d$ ) with eight formula units per unit cell (Bertaut and Forrat 1956; Geller and Gilleo 1957). The ions in  $\{ \}$  occupy 'c' sites and are surrounded dodecahedrally by 8 oxygen ions, in  $[ \ ]$  occupy 'a' sites (the octahedral), and those in  $( \ )$  occupy the 'd' sites (the tetrahedral), each surrounded by the respective numbers of oxygen ions. Since the cations are situated in these special positions we must bear in mind the dispositions of the electronic orbitals under the influence of the respective ligand configurations. The oxygen ions are placed in  $h$  sites and possess the advantage of some degree of freedom. However, we shall not be concerned about the refinement in their positions. Nevertheless, it is of great importance to understand the disposition of the metal ions relative to the oxygen ions. On examining the structure, it is found that the octahedral, tetrahedral and dodecahedral ions are linked with each other only through oxygen ions. If we consider one such oxygen ion there are four nearest metal ions, namely, two  $A$  ions at  $c$  positions at distances  $2.37\text{ \AA}$  and  $2.43\text{ \AA}$ , one ion at  $a$  site at  $2.00\text{ \AA}$  and one  $C$  ion at  $d$  sites at  $1.88\text{ \AA}$  from the central oxygen ions (See Geller and Gilleo 1957 data for  $Y_3F_2(FeO_4)_3$  for corresponding angles).

The geometry of this unit is a distorted tetrahedron and clearly lacks all symmetry elements. Although, the  $A$  and  $A'$  are located at slightly larger distances, magnetic study on a system where  $A$ 's are paramagnetic in addition to the  $B$  and  $C$  reveals the presence of exchange interaction involving them (Geller 1960). Thus if we consider a system, which contains magnetic ions at all the  $a$ ,  $d$  and  $c$  sites e.g.  $\{Gd_3\}[Sc_{1.75}Fe_{0.25}](Fe_3)O_{12}$ , we might expect all the interactions to be present, specifically  $a-d$ ,  $a-c$ ,  $d-c$ , and possibly  $c-c'$ . We shall, therefore, first select our model as the unit with the oxygen ion lying centrally and surrounded by two  $A$  ions and a  $B$  and a  $C$  ion. This will provide us a general model for studying the interaction noted above in a collective scheme. The unit may be further broken down and studied if some of the metal ions are taken to be non-magnetic.

## ORBITALS AND WAVE FUNCTIONS

In the earlier papers, we have considered the influence of the crystal field while choosing the wave functions of the cations at the appropriate sites. In the present case also, we are guided by similar considerations and the choice for orbital wave functions of tetrahedral and octahedral cation electrons remains the same, i.e., we choose that wave function which has maximum overlap with the oxygen ion. For the ions at  $c$ , i.e., the dodecahedral sites, the field is of a distorted cubal type. For cubal field, we know that the splitting of an ion with  $d$ -electrons is similar to that when in a tetrahedral field (McClure 1959). More specifically the triplets  $t_{2g}$  ( $dxy$ ,  $dyz$  and  $dxz$ ) lie higher than the doublets  $e_g$ . ( $d_{z^2}-x^2-y^2$ ,  $d_{x^2-y^2}$ ).

For  $f$  electrons the splitting in the cubal field is such that there is one non-degenerate orbital  $\psi(f\beta) = \psi_{xyz}$  and two triply degenerate sets, namely,

$$\psi(f\delta_1) = \psi_z(5z^2 - 3r^2), \quad \psi(f\delta_2) = \psi_x(5x^2 - 3r^2), \quad \psi(f\delta_3) = \psi_y(5y^2 - 3r^2)$$

and

$$\psi(fe_1) = \psi(x^2 - y^2)z, \quad \psi(fe_2) = \psi(z^2 - y^2)x, \quad \psi(fe_3) = \psi(z^2 - x^2)y.$$

Hence, in the case of ions having  $f$  electrons also it is better to select the orbital which has the appropriate disposition.

However, some magnetic garnets are known in which all the magnetic ions in  $a$ ,  $c$  and  $d$  sites belong to the iron series. A typical example is  $\{MnY_2\}$  [ $Fe_{1.70}Ge_{0.28}$ ] ( $Fe_{2.30}Ge_{0.72}O_{12}$ ). For simplicity, we shall confine our calculations to such systems, i.e., magnetic ions at all the three distinct sites ( $a$ ,  $d$ ,  $c$ ) having  $d^5$  ( $^6S_{5/2}$ ) configurations.

As before, we take one representative electron from each of the magnetic ions  $A$ ,  $A'$ ,  $B$ ,  $C$ . We denote the orbital wave functions of the electrons belonging to  $A'$  and  $A$  (i.e., of  $C$  sites) by  $u_1$  and  $u_2$  and of  $B$  ( $a$  site) and  $C$  ( $d$  site) by  $w$  and  $v$  respectively. If we include the  $\alpha$  and  $\beta$  spin functions with each of the orbital function, we shall have sixteen Slater determinants (antisymmetrized product functions). In the present case, the system lacks any symmetry and there are no symmetry considerations to help us in the classification of the wave functions of the system. We shall be content with such linear combinations of the Slater determinants which are the eigen functions of the  $S^2$  operator; these are:

Quintet:

$$|5\phi(2)\rangle_c = [u_1 u_2 v w] \quad (3.1)$$

Triplets

$$|^3\phi_1(1)\rangle_c = {}^3\{u_1 u_2\}^1(vw) = \frac{1}{\sqrt{2}} \{[u_1 u_2 v \bar{w}] - [u_1 u_2 \bar{v} w]\} \quad (3.2)$$

$$|^3\phi_2(1)\rangle_c = {}^3\{1(u_1 u_2)^3(vw)\} = \frac{1}{\sqrt{2}} \{[u_1 \bar{u}_2 v w] - [\bar{u}_1 u_2 v w]\} \quad \dots \quad (3.3)$$

$$|^3\phi_3(1)\rangle_c = {}^3\{u_1 u_2\}^3(vw) = \frac{1}{2} \{[u_1 \bar{u}_2 v w] + [\bar{u}_1 u_2 v w] - [u_1 u_2 v \bar{w}] - [u_1 u_2 \bar{v} w]\} \quad \dots \quad (3.4)$$

Singlets :

$$|^1\phi_1(0)\rangle_c = {}^1\{u_1 u_2\}^3(vw) = \frac{1}{\sqrt{12}} \{[u_1 \bar{u}_2 v \bar{w}] + [u_1 \bar{u}_2 \bar{v} w] + [\bar{u}_1 u_2 v \bar{w}] + [\bar{u}_1 u_2 \bar{v} w] - 2[u_1 u_2 v \bar{w}] - 2[u_1 u_2 \bar{v} w] - \dots \} \quad (3.5)$$

$$|^1\phi_2(0)\rangle_c = {}^1\{u_1 u_2\}^1(vw) = \frac{1}{2} \{[u_1 \bar{u}_2 v \bar{w}] - [u_1 \bar{u}_2 \bar{v} w] - [\bar{u}_1 u_2 v \bar{w}] + [\bar{u}_1 u_2 \bar{v} w]\} \quad \dots \quad (3.6)$$

(The bracket notation represents the usual Slater determinant multiplied by appropriate normalizing factor (in this case  $(4!)^{-1/2}$ ). The orbitals without bar include up spin functions of the electrons in them and with bar down spin functions).

The above six states are obtained by the straight forward application of the branching diagram technique. However, certain physically distinguishable alternative states are also possible.  $|^3\phi_1(1)\rangle_e$  represents a state where the  $(u_1 u_2)$  has triplet and  $(vw)$  singlet spin configurations;  $|^3\phi_2(1)\rangle_e$  belongs to the reverse situation. In view of the differences in the orbitals  $u_1, u_2, v, w$ , it may be required to consider such states where, for example,  $(u_1, v)$  are in singlet and  $(u_2 w)$  in triplet and similar such combinations. In all, there will be six such combinations including (2) and (3). Likewise, there will be alternative states for singlets.

From the oxygen ion, we consider two coupled electrons in the ground state. These two may belong to any of the  $s, p_x, p_y$ , or  $p_z$  orbitals or such a linear combination of these which has a fair degree of overlap with all the magnetic ions. We shall formally denote these orbitals by  $\phi$ . The ground singlet states is:

$$[\phi \bar{\phi}] \quad \dots \quad (3.7)$$

The excited electronic configurations of the oxygen ion and the magnetic ion are assumed to arise, in the present mechanism, through the lowest lying available empty orbitals. This is denoted by  $\chi$ . Excited triplet states of the two oxygen ion electron will be described by

$$\left. \begin{array}{l} [\chi\phi] \\ \{[\chi\bar{\phi}] + [\bar{\chi}\phi]\}/\sqrt{2} \\ [\bar{\chi} \bar{\phi}] \end{array} \right\} \quad \dots \quad (3.8)$$

The above states involve single electron transition to  $\chi$ . States arising due to two electron transition to  $\chi$ , one each from two magnetic ions will be described later.

Thus, the ground states of the total system are taken as the products of the four cation electron wave functions and the singlet wave function of the two anion electrons. These are described below:

Ground states

$$\text{Quintet :} \quad |^5\psi(2)\rangle = {}^5\{^4(u_1 u_2 vw) {}^1(\phi^2)\} \quad \dots \quad (3.9)$$

$$\text{Triplets :} \quad |^3\psi_1(1)\rangle = {}^3\{^3(u_1, u_2) {}^1(vw) {}^1(\phi^2)\} \quad \dots \quad (3.10)$$

$$|^3\psi_2(1)\rangle = {}^3\{^1(u_1 u_2) {}^3(vw) {}^1(\phi^2)\} \quad \dots \quad (3.11)$$

$$|^3\psi_3(1)\rangle = {}^3\{^3(u_1 u_2) {}^3(vw) {}^1(\phi^2)\} \quad \dots \quad (3.12)$$

*Singlets*

$$|^1\psi_1(0)\rangle = \{^1(^3(u_1 u_2) \ ^3(vw))\}^1(\phi^2)\} \quad \dots \quad (3.13)$$

$$|^1\psi_2(0)\rangle = \{^1(^1(u_1 u_2) \ ^1(vw) \ ^1(\phi^2))\} \quad \dots \quad (3.14)$$

In addition, we also write down the alternative ways of expressing triplet and singlet states.

*Alternative Triplets*

$$|^3\psi_{a1}(1)\rangle = \{^3(^3(u_1 v) \ ^1(u_2 w) \ ^1(\phi^2))\} \quad (3.15)$$

$$|^3\psi_{a2}(1)\rangle = \{^3(^1(u_1 v) \ ^3(u_2 w) \ ^1(\phi^2))\} \quad (3.16)$$

$$|^3\psi_{a3}(1)\rangle = \{^3(^3(u_1 w) \ ^1(u_2 v) \ ^1(\phi^2))\} \quad (3.17)$$

$$|^3\psi_{a4}(1)\rangle = \{^3(^1(u_1 w) \ ^3(u_2 v) \ ^1(\phi^2))\} \quad (3.18)$$

$$|^3\psi_{a5}(1)\rangle = \{^3(^3(u_1 v) \ ^3(u_2 w))\}^1(\phi^2)\} \quad (3.19)$$

$$|^3\psi_{a6}(1)\rangle = \{^3(^3(u_1 w) \ ^3(u_2 v))\}^1(\phi^2)\} \quad (3.20)$$

*Alternative singlets*

$$|^1\psi_{a1}(0)\rangle = \{^1(^3(u_1 v) \ ^3(u_2 w))\}^1(\phi^2)\} \quad (3.21)$$

$$|^1\psi_{a2}(0)\rangle = \{^1(^3(u_1 w) \ ^3(u_2 v))\}^1(\phi^2)\} \quad (3.22)$$

$$|^1\psi_{a3}(0)\rangle = \{^1(^1(u_1 v) \ ^1(u_2 w) \ ^1(\phi^2))\} \quad (3.23)$$

$$|^1\psi_{a4}(0)\rangle = \{^1(^1(u_1 w) \ ^1(u_2 v) \ ^1(\phi^2))\} \quad (3.24)$$

First we write the excited states involving two electron transition to  $\chi$ , one each from two paramagnetic ions. It is to be noted that there are no quintet states in this process. These triplets and singlets are given below :

*Triplets :*

$$|^3\psi_{e1}\chi^2(1)\rangle = \{^3(^1(\chi^2) \ ^3(vw) \ ^1(\phi^2))\} = [\chi\bar{\chi} \ vw \ \phi\bar{\phi}] \quad (3.25)$$

$$|^3\psi_{e2}\chi^2(1)\rangle = \{^3(^3(u_1 u_2) \ ^1(\chi^2) \ ^1(\phi^2))\} = [u_1 u_2 \ \chi \bar{\chi} \ \phi\bar{\phi}] \quad (3.26)$$

$$|^3\psi_{e3}\chi^2(1)\rangle = \{^3(^1(\chi^2) \ ^3(u_2 w) \ ^1(\phi^2))\} = [\chi u_2 \ \bar{\chi} \ w\phi\bar{\phi}] \quad (3.27)$$

$$|^3\psi_{e4}\chi^2(1)\rangle = \{^3(^1(\chi^2) \ ^3(u_2 v) \ ^1(\phi^2))\} = [\chi u_2 v \ \bar{\chi} \ \phi\bar{\phi}] \quad (3.28)$$

$$|^3\psi_{e5}\chi^2(1)\rangle = \{^3(^1(\chi^2) \ ^3(u_1 v) \ ^1(\phi^2))\} = [u_1 \chi \ v\bar{\chi} \ \phi\bar{\phi}] \quad (3.29)$$

$$|^3\psi_{e6}\chi^2(1)\rangle = \{^3(^1(\chi^2) \ ^3(u_1 w) \ ^1(\phi^2))\} = [u_1 \chi \bar{\chi} \ w\phi\bar{\phi}] \quad (3.30)$$

$$|^1\psi_{e1}\chi^1(0)\rangle = \{^1(^1(\chi^2) \ ^1(vw) \ ^1(\phi^2))\} = \frac{1}{\sqrt{2}} \{[\chi\bar{\chi} \ v\bar{w}\phi\bar{\phi}] - [\chi\bar{\chi} \ v\bar{w}\phi\bar{\phi}]\} \quad (3.31)$$

$$|^1\psi_{e_3}\chi^2(0)\rangle = {}^1\{({}^1\chi^2) {}^1(u_1u_2) {}^1(\phi^2)\} = \frac{1}{\sqrt{2}} [u_1\bar{u}_2\chi\bar{\chi}\phi\bar{\phi}] - [\bar{u}_1u_2\chi\bar{\chi}\phi\bar{\phi}] \dots \quad (3.32)$$

$$|^1\psi_{e_3}\chi^2(0)\rangle = {}^1\{({}^1\chi^2) {}^1(u_2w) {}^1(\phi^2)(\phi^2)\} = \frac{1}{\sqrt{2}} [\chi u_2\bar{\chi}w\phi\bar{\phi}] - [\chi\bar{u}_2\bar{\chi}w\phi\bar{\phi}] \dots \quad (3.33)$$

$$|^1\psi_{e_4}\chi^2(0)\rangle = {}^1\{({}^1\chi^2) {}^1(u_2v) {}^1(\phi^2)\} = \frac{1}{\sqrt{2}} \{[\chi u_2\bar{v}\bar{\chi}\phi\bar{\phi}] - [\chi\bar{u}_2v\bar{\chi}\phi\bar{\phi}]\} \dots \quad (3.34)$$

$$|^1\psi_{e_5}\chi^2(0)\rangle = {}^1\{({}^1\chi^2) {}^1(u_1v) {}^1(\phi^2)\} = \frac{1}{\sqrt{2}} \{(u_1\chi\bar{v}\bar{\chi}\phi\bar{\phi}) - [\bar{u}_1\chi v\bar{\chi}\phi\bar{\phi}]\} \dots \quad (3.35)$$

$$|^1\psi_{e_6}\chi^2(0)\rangle = {}^1\{({}^1\chi^2) {}^1(u_1w) {}^1(\phi^2)\} = \frac{1}{\sqrt{2}} \{[u_1\chi\bar{w}\bar{\chi}\phi\bar{\phi}] - [\bar{u}_1\chi w\bar{\chi}\phi\bar{\phi}]\} \dots \quad (3.36)$$

We now consider the excited states which involve a transition of one anion electron to the excited orbital  $\chi$ .

*Excited states involving one electron transition to  $\chi$  :—*

$$|^5\psi_{e_1}\chi^1(2)\rangle = {}^5\{({}^3(u_1u_2) {}^1(vw) {}^3(\chi\phi)\} = \frac{1}{\sqrt{2}} \{[u_1u_2v\bar{w}\chi\phi] - [u_1u_2\bar{v}w\chi\phi]\} \dots \quad (3.37)$$

$$|^5\psi_{e_2}\chi^1(2)\rangle = {}^5\{({}^1(u_1u_2) {}^3(vw) {}^3(\chi\phi)\} = \frac{1}{\sqrt{2}} \{[u_1\bar{u}_2vw\chi\phi] - [\bar{u}_1u_2vw\chi\phi]\} \dots \quad (3.38)$$

$$|^5\psi_{e_3}\chi^1(2)\rangle = {}^5\{({}^3(u_1u_2) {}^3(vw) {}^3(\chi\phi)\} = \frac{1}{2} \{[u_1\bar{u}_2vw\chi\phi] + [\bar{u}_1u_2vw\chi\phi] - [u_1u_2v\bar{w}\chi\phi] - [u_1u_2\bar{v}w\chi\phi]\} \dots \quad (3.39)$$

As before we can have the alternative quintet excited states also. These six are obtained from (3.15) to (3.20) by substituting  ${}^3(\chi\phi)$  in place of  ${}^1(\phi^2)$ .

We will have yet another quintet excited states which is obtained below:

$$\begin{aligned} \text{i.e.} \quad |{}^5\psi_{e_4}\chi^1(2)\rangle &= {}^5\{({}^5(u_1u_2vw) {}^3(\chi\phi)\} \\ &= \frac{1}{\sqrt{12}} \{[u_1u_2v\bar{w}\chi\phi] + [u_1u_2\bar{v}w\chi\phi] + [u_1\bar{u}_2vw\chi\phi] + [\bar{u}_1u_2vw\chi\phi] - 2[u_1u_2vw\bar{\chi}\phi] \\ &\quad - 2[u_1u_2vw\chi\bar{\phi}]\} \dots \quad (3.40) \end{aligned}$$

*Triplets :*

$$|^3\psi_{e_1}\chi^1(1)\rangle = {}^3\{({}^3(u_1u_2) {}^3(vw)) {}^3(\chi\phi)\} \dots \quad (3.41)$$

$$|^3\psi_{e_2}\chi^1(1)\rangle = {}^3\{({}^1(u_1u_2) {}^3(vw) {}^3(\chi\phi)\} \dots \quad (3.42)$$



Also we have four alternative states of these types obtained from (3.21) to (3.24) by putting  ${}^3(\chi\phi)$  in place of  ${}^1(\phi^2)$ . Then we have triplets obtained from the triplets of cation electrons and triplets of anion electrons

$$\begin{aligned} |{}^3\psi_{e3}\chi^1(1)\rangle &= {}^3\{({}^3u_1u_2) {}^1(vw) {}^3(\chi\phi)\} \\ &= \frac{1}{\sqrt{8}} \{ [\bar{u}_1\bar{u}_2 v\bar{w}\chi\phi] + [\bar{u}_1\bar{u}_2 v\bar{w}\chi\phi] - [\bar{u}_1\bar{u}_2 \bar{v}w\chi\phi] - [\bar{u}_1\bar{u}_2 v\bar{w}\chi\phi] - [u_1u_2 v\bar{w}\chi\phi] \\ &\quad + [u_1u_2 \bar{v}w\chi\phi] - [u_1u_2 v\bar{w}\chi\phi] + [u_1u_2 \bar{v}w\chi\phi] \} \dots \quad (3.43) \end{aligned}$$

$$\begin{aligned} |{}^3\psi_{e4}\chi^1(1)\rangle &= {}^3\{({}^3u_1u_2) {}^3(vw) {}^3(\chi\phi)\} \\ |{}^3\psi_{e5}\chi^1(1)\rangle &= {}^3\{({}^3u_1u_2) {}^3(vw) {}^3(\chi\phi)\} \end{aligned} \quad (3.44)$$

$$\begin{aligned} &= \frac{1}{\sqrt{16}} \{ [u_1\bar{u}_2 v\bar{w}\chi\phi] + [\bar{u}_1\bar{u}_2 v\bar{w}\chi\phi] - [u_1u_2 v\bar{w}\chi\phi] - [u_1u_2 \bar{v}w\chi\phi] - \\ &\quad - [u_1u_2 v\bar{w}\chi\phi] + [\bar{u}_1\bar{u}_2 v\bar{w}\chi\phi] - [u_1u_2 v\bar{w}\chi\phi] - [u_1u_2 \bar{v}w\chi\phi] \\ &\quad - 2([u_1\bar{u}_2 v\bar{w}\chi\phi] - [u_1u_2 \bar{v}w\chi\phi]) \} \end{aligned} \quad (3.45)$$

We will have six alternative similar states three for the orbital set  $(u_1v)$   $(u_2w)$  and another three for the set  $(u_1w)$   $(u_2v)$ . These can be formulated in exactly the same fashion as (3.43) to (3.45). The last triplet excited state is obtained from quintet cation electron state and the triplet anion electron states. Symbolically,

$$\begin{aligned} |{}^3\psi_{e6}\chi^1(1)\rangle &= {}^3\{({}^3u_1u_2) {}^3(vw) {}^3(\chi\phi)\} \\ &= \sqrt{6/10} \{ |2\rangle_c {}^3|-1\rangle_a - \sqrt{3/10} \{ |1\rangle_c {}^3|0\rangle_a + \sqrt{1/10} \{ |0\rangle_c {}^3|1\rangle_a \dots \} \} \quad (3.46) \end{aligned}$$

Singlets :

$$\begin{aligned} |{}^1\psi_{e1}\chi^1(0)\rangle &= {}^1\{({}^3u_1u_2) {}^1(vw) {}^3(\chi\phi)\} \\ &= \{2^3|1\rangle_c {}^3|-1\rangle_a - {}^3|0\rangle_c {}^3|0\rangle_a + 2^3|-1\rangle_c {}^3|1\rangle_a\} / \text{normalization} \\ &= \frac{1}{\sqrt{24}} \{ 2[u_1u_2 v\bar{w}\chi\phi] - 2[\bar{u}_1\bar{u}_2 \bar{v}w\chi\phi] - ([\bar{u}_1\bar{u}_2 v\bar{w}\chi\phi] + [u_1u_2 \bar{v}w\chi\phi] - [\bar{u}_1\bar{u}_2 \bar{v}w\chi\phi] \\ &\quad - [\bar{u}_1\bar{u}_2 v\bar{w}\chi\phi] + [\bar{u}_1u_2 v\bar{w}\chi\phi] + [u_1\bar{u}_2 v\bar{w}\chi\phi] - [\bar{u}_1u_2 \bar{v}w\chi\phi] \\ &\quad - [u_1u_2 \bar{v}w\chi\phi] + 2[\bar{u}_1\bar{u}_2 v\bar{w}\chi\phi] - 2[\bar{u}_1\bar{u}_2 \bar{v}w\chi\phi] \} \dots \quad (3.47) \end{aligned}$$

$$|{}^1\psi_{e2}\chi^1(0)\rangle = {}^1\{({}^3u_1u_2) {}^3(vw) {}^3(\chi\phi)\} \dots \quad (3.48)$$

(3.48) is obtained in the same fashion as (3.47) except that now we have  ${}^1(u_1u_2)$ ,  ${}^3(vw)$  in place of  ${}^3(u_1u_2)$ ,  ${}^1(vw)$ . Likewise we will have four alternative excited singlets obtained for the combinations  ${}^3(u_1v)$   ${}^1(u_2w)$ ,  ${}^3(u_1w)$   ${}^1(u_2v)$ ,  ${}^1(u_2v)$   ${}^3(u_2w)$ ,  ${}^1(u_1w)$   ${}^3(u_2w)$ .

$$\begin{aligned}
|{}^1\psi_{a_3}\chi^i(0)\rangle &= \frac{1}{\sqrt{3}} \{ |0\rangle_e |0\rangle_a - |1\rangle_e |-1\rangle_a - |-1\rangle_e |1\rangle_a \} \\
&= \frac{1}{\sqrt{12}} \{ [u_1 u_2 \bar{v} \bar{w} \chi \bar{\phi}] - [\bar{u}_1 \bar{u}_2 v w \chi \bar{\phi}] + [u_1 u_2 \bar{v} \bar{w} \bar{\chi} \phi] - [\bar{u}_1 \bar{u}_2 v w \bar{\chi} \phi] - [u_1 u_2 v \bar{w} \bar{\chi} \phi] \\
&\quad - [\bar{u}_1 \bar{u}_2 \bar{v} w \bar{\chi} \phi] + [\bar{u}_1 \bar{u}_2 v w \bar{\chi} \phi] + [\bar{u}_1 u_2 v w \bar{\chi} \phi] - [\bar{u}_1 u_2 \bar{v} \bar{w} \chi \phi] - [u_1 \bar{u}_2 \bar{v} \bar{w} \chi \phi] \\
&\quad + [\bar{u}_1 \bar{u}_2 \bar{v} w \chi \phi] + [\bar{u}_1 u_2 v \bar{w} \chi \phi] \} \quad \dots \quad (3.49)
\end{aligned}$$

We will have two more alternative excited singlets like (3.49) obtained from the combinations  ${}^1\{{}^3({}^3(u_1 v) {}^3(u_2 w)) {}^3(\chi \phi)\}$  and  ${}^1\{{}^3({}^3(u_1 w) {}^3(u_2 v)) {}^3(\chi \phi)\}$

#### THE ENERGY MATRIX

We now proceed to calculate the energy matrix of the Hamiltonian of the system within the manifold considered in the previous section. As before, we describe the Hamiltonian in atomic units ( $e = \hbar = m = 1$ ):

$$H = \sum_i H_i + \sum_{i,j} 1/r_{ij} \quad \dots \quad (4.1)$$

where  $H_i = -\frac{1}{2}\nabla_i^2 + V(r_i)$ , with  $V(r_i)$  standing for the potential acting on the electron due to the five nuclei and all other electrons except the six under consideration. The orbitals involved in the calculation are assumed to be orthogonal or appropriately orthogonalized in certain cases, to each other.

#### Diagonal Elements

Ground states :

We write down the diagonal matrix elements of the ground states in a compact master formula

$$\begin{aligned}
\langle {}^{2s+1}\psi(S_{m_1} S_{m_2}) | H | {}^{2s+1}\psi(S_{m_1} S_{m_2}) \rangle &= Q_0 + (-1)^{S_{m_1}} J(a_1 a_2) + (-1)^{S_{m_2}} J(a_3 a_4) \\
&- \frac{1}{2} \left( 1 + \frac{S(S+1) - S_{m_1}(S_{m_1}+1) - S_{m_2}(S_{m_2}+1)}{2} \right) (J(a_1 a_3) + J(a_1 a_4) + J(a_2 a_3) \\
&\quad J(a_2 a_4)) \quad \dots \quad (4.2)
\end{aligned}$$

The various symbols used in (4.2) stand for the following :

$$Q_0 = \left[ \sum_i \epsilon(a_i) + 2\epsilon(\phi) + \frac{1}{2} \sum_{i,j} k(a_i a_j) + 2 \sum_i k(a_i \phi) + k(\phi \phi) - \sum_i J(a_i \phi) \right] \quad (4.3)$$

where  $K$  and  $J$  represent the well-known coulomb and exchange integrals respectively and  $\epsilon(a)$  stands for the one electron term  $\langle a | -\frac{1}{2}\nabla^2 + V | a \rangle$  (Sinha 1961a). The suffixes  $i$  and  $j$  run over 1 to 4 and the orbitals  $a_1, a_2, a_3, a_4$  stand for  $u_1 u_2$  or any other combination eg.  $(u_1 v)$  ( $u_2 w$ ) etc.  $S_{m_1}, S_{m_2}$  stand for the resultant spin

of the two magnetic electrons in  $a_1a_2$  and  $a_3a_4$  etc. For example, in the set  ${}^5(u_1u_2vw)$ ,  $S_{m1} = 1$ ,  $S_{m2} = 1$ , for  ${}^3(u_1u_2) {}^1(vw)$   $S_{m1} = 1$  and  $S_{m2} = 0$ .  $S$  is the resultant spin of the total system. With the aid of formula (4.2) and keeping the above facts in mind, the diagonal matrix elements of all the ground quintet, triplet, singlet and their alternative states can be easily derived.

Excited states involving two electron transition to  $\chi$

$$\begin{aligned} < {}^{2s+1}\psi_e \chi^2(S_{ak}a_l) | H | {}^{2s+1}\psi_e(S_{ak}a_l) > = \sum_k \epsilon(a_k) + 2\epsilon(\phi) + 2\epsilon(\chi) + K(\chi\chi) + K(\phi\phi) \\ & + 4K(\chi\phi) + 2\sum_k K(u_k\phi) + 2\sum_k K(a_k\chi) + K(a_1a_l) - 2J(\chi\phi) - \sum_k J(a_k\phi) \\ & - \sum_k J(a_k\chi) + (-1)^{S_{ak}a_l} J(a_ka_l) = Q\chi^2 + (-1)^{S_{ak}a_l} J(a_ka_l) \end{aligned} \quad (4.4)$$

In the above  $k$  runs over 1 to 2, i.e.,  $a_1a_2$  stand for  $u_1u_2$  or  $vw$ , or  $u_1$  vetc. as the case may be. Equation (4.4) furnishes another master formula with the aid of which the diagonal matrix elements of all the triplet and singlet excited states, involving two electron transition to  $\chi$ , can be obtained.

*Excited states involving one electron transition to  $\chi$ .* For these diagonal elements it is difficult to summarise the results in one master formula. We have to take recourse to two or three  
First we have

$$\begin{aligned} < {}^{2s+1}\psi(S_mS_{m1}S_{m2}S_x) | H | {}^{2s+1}\psi(S_mS_{m1}S_{m2}S_x) > = Q_1 + (-1)^{S_{m1}} J(a_1a_2) \\ & + (-1)^{S_{m1}} J(a_3a_4) + (-1)^{S_x} J(a_5a_6) \\ & - \frac{1}{2} \left( 1 + \frac{[S_m(S_m+1) - S_{m1}(S_{m1}+1) - S_{m2}(S_{m2}+1)]}{2} \right) \\ & \quad (J(a_1a_3) + J(a_1a_4) + J(a_2a_3) + J(a_2a_4)) \\ & - \frac{1}{2} \left( 1 + \frac{[S_{m1x}(S_{m1x}+1) - S_{m1}(S_{m1}+1) - S_x(S_x+1)]}{2} \right) \\ & \quad (J(a_1a_5) + J(a_1a_6) + J(a_2a_5) + J(a_2a_6)) \\ & - \frac{1}{2} \left\{ 1 + \frac{S_{m2x}(S_{m2x}+1) - S_{m2}(S_{m2}+1) - S_x(S_x+1)}{2} \right\} \\ & \quad (J(a_3a_5) + J(a_3a_6) + J(a_4a_5) + J(a_4a_6)) \\ & - \frac{1}{2} \left\{ 1 + \frac{S_{m2x}(S_{m2x}+1) - S_{m2}(S_{m2}+1) - S_x(S_x+1)}{2} \right\} \\ & \quad (J(a_3a_5) + J(a_3a_6) + J(a_4a_5) + J(a_4a_6)) \end{aligned}$$

Here

$$Q\chi^i = \sum_m \epsilon(a_m) + \frac{1}{2} \sum_{\substack{m \\ m_i \neq n}} K(a_m a_n) \quad \dots \quad (4.5)$$

where  $m$  and  $n$  each run over 1 to 6,  $S_m$  indicates the resultant spin of the magnetic electrons in  $a_1 a_2 a_3 a_4$ ,  $Sx$  in  $a_5 a_6$ ,  $S m_1 x$  in  $a_1 a_2 a_5 a_6$  and  $S n_2 x$  in  $a_3 a_4 a_5 a_6$ ,  $a_1 a_2 a_3 a_4 a_5 a_6$  stand for  $u_1 u_2 v w \chi \phi$  or any other combination

With the help of the formula (4.5), the diagonal matrix elements of the following excited states involving one electron transition to  $\chi$  can be obtained. These are

$$\begin{aligned} & |^5\psi_{e1}\chi^1(2)\rangle, |^5\psi_{e2}\chi^1\rangle \\ & |^3\psi_{e2}\chi^1\rangle, |^3\psi_{e3}\chi^1\rangle, |^3\psi_{e4}\chi^1\rangle \text{ and} \\ & |^1\psi_{e1}\chi^1\rangle, |^1\psi_{e2}\chi^1\rangle \end{aligned}$$

However, the diagonal matrix elements of the excited states which involve the cation electron configuration as in  $(2S_m+1) (^3(u_1 u_2) ^3(vw))$  have to be obtained by the master formula given below.

$$\begin{aligned} \langle ^{2s+1}\psi(S S_m S_x) | H | ^{2s+1}\psi(S S_m S_x) \rangle &= Q\chi^1 + (-1)^{S_{m1}} J(a_1 a_2) + (-1)^{S_{m2}} J(a_3 a_4) \\ &+ (-1)^{S_x} J(a_5 a_6) - \frac{1}{2} \left( 1 + \frac{[S_m(S_m+1) - S_{m1}(S_{m1}+1) - S_{m2}(S_{m2}+1)]}{2} \right) \\ &\quad (J(a_1 a_3) + J(a_1 a_4) + J(a_2 a_3) + J(a_2 a_4)) \\ &- \frac{1}{2} \left( 1 + \frac{[S(S+1) - S_m(S_m+1) - S_x(S_x+1)]}{2} \right) \\ &\quad \left\{ \begin{array}{l} J(a_1 a_5) + J(a_1 a_6) + J(a_2 a_5) + J(a_2 a_6) \\ + J(a_3 a_5) + J(a_3 a_6) + J(a_4 a_5) + J(a_4 a_6) \end{array} \right\} \quad \dots \quad (4.6) \end{aligned}$$

The above furnishes the matrix elements of

$$|^5\psi_{e3}\chi^1\rangle, |^5\psi_{e4}\chi^1\rangle, |^3\psi_{e1}\chi^1\rangle, |^3\psi_{e5}\chi^1\rangle, |^3\psi_{e6}\chi^1\rangle \text{ and } |^1\psi_{e3}\chi^1\rangle.$$

*Off-diagonal Elements :*

Since we are interested in the depressions of the various ground states owing to the interaction with the corresponding excited states, we shall consider off-diagonal elements between these. The matrix elements between two different excited states are of no importance. We summarise the results below :

*Those involving two electron transition to  $\chi$*

In this situation, we have seen that there are no excited quintet states. There are six triplet and six singlet excited states of this type involving transition

for  $u_1 u_2$  or  $u_1 v$  or  $vw$  etc. to  $\chi$ . With three ground triplets and two ground singlets, we require thirty off-diagonal elements. Fortunately, all these can be easily derived from the master formula given below :

$$\begin{aligned} & \langle {}^{2s+1}\psi_n(S_{ij}(M_s) \dots) | H | {}^{2s+1}\psi_m \chi^2(a_i \rightarrow \chi) \rangle \\ &= \left\{ \left[ 1 - \frac{S_{ij}(S_{ij}+1)}{2} \right] \sum_{terms} (1 - |(M_s)_{ij}|) \right\} \langle a_i \chi^i | g_{1z} | a_j \chi^j \rangle / N_0 N_e \dots \quad (4.7) \end{aligned}$$

In the above equation  $N_0$  and  $N_e$  represent the normalization of ground and excited wave functions in question,  $S_{ij}$  is the resultant spin of electrons in  $a_i a_j$  orbitals of the ground state.  $S_{ij}$  is to be taken unity for triplet and zero for singlet as well as when the electrons in  $a_i a_j$  are not in definite resultant spin (i.e., when they are not eigen functions of the  $S^2$  operator).  $(M_s)_{ij}$  is the magnitude of the  $M_s$  values ( $z$  component) of the spins in  $a_i$  and  $a_j$ . The summation is to be carried out for all the Slater determinants occurring as many times in the ground state wavefunctions.  $a_i a_j$  stand for  $u_1 u_2$ ,  $vw$  or  $u_1 v$ , etc. The integrals of the form  $\langle a_i \chi^i | g_{1z} | a_j \chi^j \rangle \equiv {}^x J a_i a_j$  have the following significance,

$$\langle ab | g_{1z} | cd \rangle = \int a^*(r_1) b(r_1) \frac{1}{r_{12}} c^*(r_2) d(r_2) dr_1 dr_2 \quad (4.8)$$

As illustrations, we have

$$\begin{aligned} \langle {}^3\psi_1 | H | {}^3\psi_{e2} \chi^1 \rangle &= \sqrt{2} \langle v\chi | g_{1z} | w\chi \rangle = \sqrt{2} {}^x J_{vw} \\ \langle {}^3\psi_1 | H | {}^3\psi_{e3} \chi^2 \rangle &= 1/\sqrt{2} \langle u_1 \chi | g_{1z} | v\chi \rangle = 1/\sqrt{2} {}^x J_{u_1 v} \\ \langle {}^1\psi_2 | H | {}^1\psi_{e1} \chi^2 \rangle &= \sqrt{2} \langle u_1 \chi | g_{1z} | u_2 \chi \rangle = \sqrt{2} {}^x J_{u_1 u_2} \\ \langle {}^1\psi_1 | H | {}^1\psi_{e3} \chi^2 \rangle &= \sqrt{3/2} \langle u_1 \chi | g_{1z} | v\chi \rangle = \sqrt{3/2} {}^x J_{u_1 v} \end{aligned}$$

For states involving one electron transition to  $\chi$ :

Since there are several ways in which the excited wave functions in this scheme are derived, it is not possible to get one or two compact master equations for the off-diagonal elements. Thus, wherever necessary we shall give the appropriate explicit expressions.

To include the off-diagonal elements involving alternative states also, we describe the wavefunctions by the following notations.

$$| {}^{2s+1}\psi(S_{m_1} S_{m_2} S_m S_x) \rangle \quad \text{where } S_{m_1}, S_{m_2}, S_m, S_x, \text{ as before}$$

are the resultant spins in the sets  $(a_1 a_2)$ ,  $((a_3 a_4)(a_1 a_2), (a_3 a_4))\{\phi\phi\}$  or  $\{\chi\phi\}$  respectively. Further, the hybrid exchange integrals of the type  $\langle a\chi | g_{12} | a\phi \rangle$  will be denoted by  ${}^a J_{\chi\phi}$ . The various off-diagonal elements are described below :

*Quintets :*

$$\langle {}^5\psi(1120) | H | {}^5\psi(1011) \rangle = \{a_3 J_{\chi\phi} - a_4 J_{\chi\phi}\} / \sqrt{2} \quad \dots (4.9)$$

$$\langle {}^5\psi(1120) | H | {}^5\psi(0111) \rangle = \{a_1 J_{\chi\phi} - a_2 J_{\chi\phi}\} / \sqrt{2} \quad \dots (4.10)$$

$$\langle {}^5\psi(1120) | H | {}^5\psi(1111) \rangle = \{a_1 J_{\chi\phi} + a_2 J_{\chi\phi} - a_3 J_{\chi\phi} - a_4 J_{\chi\phi}\} / 2 \quad \dots (4.11)$$

$$\langle {}^5\psi(1120) | H | {}^5\psi(1121) \rangle = 3\{a_1 J_{\chi\phi} + a_2 J_{\chi\phi} + a_3 J_{\chi\phi} + a_4 J_{\chi\phi}\} / \sqrt{12} \quad \dots (4.12)$$

*Triplets :*

These are given in sets corresponding to the respective three ground states :

$$\langle {}^3\psi(1010) | H | {}^3\psi(1101) \rangle = \{a_3 J_{\chi\phi} - a_4 J_{\chi\phi}\} / \sqrt{6} \quad \dots (4.13)$$

$$\langle {}^3\psi(1010) | H | {}^3\psi(0001) \rangle = \{a_1 J_{\chi\phi} - a_2 J_{\chi\phi}\} / \sqrt{6} \quad \dots (4.14)$$

$$\langle {}^3\psi(1010) | H | {}^3\psi(1011) \rangle = \{a_1 J_{\chi\phi} + a_2 J_{\chi\phi}\} \quad \dots (4.15)$$

$$\langle {}^3\psi(1010) | H | {}^3\psi(0111) \rangle = 0 \quad \dots (4.16)$$

$$\langle {}^3\psi(1010) | H | {}^3\psi(1111) \rangle = \{a_3 J_{\chi\phi} - a_4 J_{\chi\phi}\} / 2\sqrt{2} \quad \dots (4.17)$$

$$\langle {}^3\psi(1010) | H | {}^3\psi(1121) \rangle = \sqrt{\frac{5}{6}} \{a_3 J_{\chi\phi} - a_4 J_{\chi\phi}\} \quad \dots (4.18)$$

$$\langle {}^3\psi(0110) | H | {}^3\psi(1101) \rangle = \frac{1}{\sqrt{6}} \{a_3 J_{\chi\phi} - a_4 J_{\chi\phi}\} \quad \dots (4.19)$$

$$\langle {}^3\psi(0110) | H | {}^3\psi(0001) \rangle = \frac{1}{\sqrt{2}} \{a_3 J_{\chi\phi} - a_4 J_{\chi\phi}\} \quad \dots (4.20)$$

$$\langle {}^3\psi(0110) | H | {}^3\psi(1011) \rangle = 0 \quad \dots (4.21)$$

$$\langle {}^3\psi(0110) | H | {}^3\psi(0111) \rangle = \{a_3 J_{\chi\phi} + a_4 J_{\chi\phi}\} \quad \dots (4.22)$$

$$\langle {}^3\psi(0110) | H | {}^3\psi(1111) \rangle = \{a_1 J_{\chi\phi} - a_2 J_{\chi\phi}\} / 2\sqrt{2} \quad \dots (4.23)$$

$$\langle {}^3\psi(0110) | H | {}^3\psi(1121) \rangle = \sqrt{\frac{5}{6}} \{a_1 J_{\chi\phi} - a_2 J_{\chi\phi}\} \quad \dots (4.24)$$

$$\langle {}^3\psi(1110) | H | {}^3\psi(1101) \rangle = \{a_1 J_{\chi\phi} + a_2 J_{\chi\phi} - a_3 J_{\chi\phi} - a_4 J_{\chi\phi}\} / \sqrt{12} \quad \dots (4.25)$$

$$\langle {}^3\psi(1110) | H | {}^3\psi(0001) \rangle = \{a_1 J_{\chi\phi} + a_2 J_{\chi\phi} - a_3 J_{\chi\phi} - a_4 J_{\chi\phi}\} / 2 \quad \dots (4.26)$$

$$\langle {}^3\psi(1110) | H | {}^3\psi(1011) \rangle = \{a_3 J_{\chi\phi} - a_4 J_{\chi\phi}\} / \sqrt{2} \quad \dots (4.27)$$

$$\langle {}^3\psi(1110) | H | {}^3\psi(0111) \rangle = \{a_1 J_{X\varphi} - a_2 J_{X\varphi}\} / \sqrt{2} \quad \dots \quad (4.28)$$

$$\langle {}^3\psi(1110) | H | {}^3\psi(1111) \rangle = \{a_1 J_{X\varphi} + a_2 J_{X\varphi} + a_3 J_{X\varphi} + a_4 J_{X\varphi}\} / 4 \quad \dots \quad (4.29)$$

$$\langle {}^3\psi(1110) | H | {}^3\psi(1121) \rangle = \sqrt{\frac{5}{12}} \{a_1 J_{X\varphi} + a_2 J_{X\varphi} - a_3 J_{X\varphi} - a_4 J_{X\varphi}\} \quad \dots \quad (4.30)$$

*Singlets :*

$$\langle {}^1\psi(1100) | H | {}^1\psi(1011) \rangle = \{a_3 J_{X\varphi} - a_4 J_{X\varphi}\} / \sqrt{2} \quad \dots \quad (4.31)$$

$$\langle {}^1\psi(1100) | H | {}^1\psi(0111) \rangle = \{a_1 J_{X\varphi} - a_2 J_{X\varphi}\} / \sqrt{2} \quad \dots \quad (4.32)$$

$$\langle {}^1\psi(1100) | H | {}^1\psi(1111) \rangle = a_1 J_{X\varphi} + a_2 J_{X\varphi} - a_3 J_{X\varphi} - a_4 J_{X\varphi} / 3 \quad \dots \quad (4.33)$$

$$\langle {}^1\psi(0000) | H | {}^1\psi(1011) \rangle = \sqrt{\frac{3}{2}} \{a_1 J_{X\varphi} - a_2 J_{X\varphi}\} \quad \dots \quad (4.34)$$

$$\langle {}^1\psi(0000) | H | {}^1\psi(0111) \rangle = \sqrt{\frac{3}{2}} \{a_3 J_{X\varphi} - a_4 J_{X\varphi}\} \quad \dots \quad (4.35)$$

$$\langle {}^1\psi(0000) | H | {}^1\psi(1111) \rangle = 0 \quad \dots \quad (4.36)$$

With the help of the above equations, we can easily write down the off-diagonal matrix elements involving alternative ground states and the corresponding excited states also. In fact, one has only to change the definitions of  $a$ 's.

#### PERTURBATIONS STUDY OF INTERACTION

As is well known for such systems, owing to the presence of the intervening non-magnetic ions, the direct exchange interactions between the magnetic ions is extremely negligible. Thus, if we neglect the appropriate exchange integrals in (4.2) namely  $J(a_i a_j)$  etc. we find that the ground quintet, triplet and singlet states are degenerate. In this section we study the splitting of these due to the perturbations caused by the corresponding excited states which result in different degrees of depressions of the various zeroth order eigen states of  $S^2$  operator.

First consider the excited state diagonal matrix elements. For these also the exchange integrals  $J(a_i a_j)$  etc. are much too feeble compared to the common dominant terms  $Q_{X^2}$ ,  $Q_{X'}$  occurring in (4.4) and (4.5). Thus retaining only the dominant terms, we use the approximation that the mean energy of the excited states involving two cation electron transition to  $\chi$  is

$${}^{2s+1}E_{X^2} = E_{X^2} \simeq Q_{X^2} \quad \dots \quad (5.1)$$

and those involving one anion electron transition to  $\chi$  by

$${}^{2s+1}E_{X'} = E_{X'} \simeq Q_{X'} \quad \dots \quad (5.2)$$

Likewise, for the degenerate ground states, we use the notation

$${}^{2s+1}E_{\varphi} = E_{\varphi} \simeq Q_{\varphi} \quad \dots \quad (5.3)$$

As shown in the previous papers (Sinha, Koide and Tanabe 1959, Koide and Sinha 1960, Sinha 1961) the spin dependent energy depressions of the various lower states will appear in the second order perturbation treatment for both the mechanisms (Sinha 1961).

We denote it by

$$\delta(^{2x+1}E_i) = \Sigma < \dots S_{m_j} | H | S_{m_i} = 0 > < S_{m_j} = 0 | H | \dots S_{m_j} > / E_{X^2} - E_{\phi} \\ + \Sigma < \dots S_{x^1} = 0 | H | S_{x^1} = 1 > < S_{x^1} = 1 | H | S_{x^1} = 0 > / E_{X^1} - E_{\phi} \quad (5.4)$$

In order to evaluate the depressions of the various zeroth order ground states, we must first determine the nature of the orbitals of the magnetic ion as well as the anion for the physical model chosen. If we choose the oxygen ion as the origin and  $OC$  as the  $Z$  axis then  $OA'$  will be nearly the  $X$  axis and normal to the plane defined by  $COA'$ , we take the  $Y$  axis passing through  $O$ . On examining the geometry of the model further we find that the magnetic ions  $C$  and  $A'$  lie in the positive octant and the ions  $A$  and  $B$  more or less in the negative octant. We have taken orbitals belonging to  $C$  and  $A'$  as  $v$  and  $u_1$  and those of  $A$  and  $B$ ,  $u_2$  and  $w$  respectively. These have been chosen in view of their  $\sigma$  type overlap with oxygen ion. For  $d$  orbitals these are either  $t_{2g}$  or  $e_g$  type. Thus on inverting to the negative octant, they would not change sign.

Now for the choice of  $\phi$ , we have to be guided by the overlap of the oxygen orbitals with all the cations as well as the vector nature of the  $p$  orbitals, i.e., instead of taking one of these, we take one of the hybridized  $p^3$  orbitals namely,  $\phi = (p_x + p_y + p_z)/\sqrt{3}$  ... (5.5), which will have maximum overlap with the cations. On inversion this orbital changes sign.

For the choice of  $\chi$  either we choose a  $3s$  function on the oxygen ion or a linear combination of the lowest empty cation orbitals, i.e., out of  $4s$  or a symmetrical hybridized orbital of the cations. Thus  $\chi$  also would not change sign.

In that we are interested in the absolute magnitude of the off-diagonal matrix elements, we must see their values as evaluated in one octant. Taking the nature of  $\phi$  into account when we carry out this evaluation, we have to be guided by the following relations.

$$(u_1 J_{\chi\phi} \mp u_2 J_{\chi\phi}) = (|u_1 J_{\chi\phi}| \pm |u_2 J_{\chi\phi}|) \quad (5.6)$$

$$(v J_{\chi\phi} \mp w J_{\chi\phi}) = (|v J_{\chi\phi}| \pm |w J_{\chi\phi}|) \quad (5.7)$$

The hybrid exchange integrals of the type  ${}^x J_{a_i a_j} \equiv \langle \chi a_i | g_{12} | \chi a_j \rangle$  do not change sign.



We now show the calculations for the choice of sets as  $(a_1 a_2)$   $(a_3 a_4) = (u_1 u_2)$  ( $vw$ ). For the quintet we do not have any excited states involving two cation electron transition to  $\chi$ . Now the orbitals  $u_1$  and  $u_2$  are centered at ions about  $2.40\text{\AA}$  from the oxygen and  $v$  and  $w$  at ions about  $2\text{\AA}$  from the same. The magnitude of the exchange integrals  $|u_1 J_{\chi\varphi}|$  and  $|u_2 J_{\chi\varphi}|$  are about the same and those of  $|v J_{\chi\varphi}|$  and  $|w J_{\chi\varphi}|$  likewise comparable. In view of the relations (5.6) and (5.7) and the above rough estimates the absolute magnitude of the off-diagonal matrix elements where  $u_1 J_{\chi\varphi}$  and  $u_2 J_{\chi\varphi}$  and also  $v J_{\chi\varphi}$  and  $w J_{\chi\varphi}$  occur with the same sign are negligible compared with those where these occur as  $(u_1 J_{\chi\varphi} - u_2 J_{\chi\varphi})$ ,  $(v J_{\chi\varphi} - w J_{\chi\varphi})$ . We neglect those negligible terms in our perturbation study. For rigorous estimates they can easily be included, however, without altering the qualitative conclusions derived. In what follows, we give the energy depressions of the various states for  $(a_1 a_2)$   $(a_3 a_4) = (u_1 u_2)$  ( $vw$ ).

*Quintet :*

$$\delta(^5E) : \frac{1}{2} \{ (|u_1 J_{\lambda\varphi}| + |u_2 J_{\lambda\varphi}|)^2 + (|v J_{\lambda\varphi}| + |w J_{\lambda\varphi}|)^2 / (E_{\chi^1} - E_{\varphi}) \dots \quad (5.8)$$

*Triplets :*

$$\begin{aligned} \delta(^3E_1) : & \left\{ \frac{1}{2} (|u_1 J_{\lambda\varphi}| + |u_2 J_{\lambda\varphi}|)^2 + \frac{3}{8} (|v J_{\lambda\varphi}| + |w J_{\lambda\varphi}|)^2 / (E_{\chi^1} - E_{\varphi}) \right. \\ & + \{ 2 |x J_{vw}|^2 + \frac{1}{2} (|x J_{u_1 v}|^2 + |x J_{u_1 w}|^2 + |x J_{u_2 v}|^2 \\ & \left. + |x J_{u_2 w}|^2) / (E_{\chi^2} - E_{\varphi}) \right\} \dots \quad (5.9) \end{aligned}$$

$$\begin{aligned} \delta(^3E_2) : & \left\{ \frac{3}{8} (|u_1 J_{\lambda\varphi}| + |u_2 J_{\lambda\varphi}|)^2 + \frac{1}{2} (|v J_{\lambda\varphi}| + |w J_{\lambda\varphi}|)^2 / (E_{\chi^1} - E_{\varphi}) \right. \\ & + \{ 2 |x J_{u_1 u_2}|^2 + \frac{1}{2} (x J_{u_1 v}|^2 + |x J_{u_1 w}|^2 + |x J_{u_2 v}|^2 \\ & \left. + |x J_{u_2 w}|^2) / (E_{\chi^2} - E_{\varphi}) \right\} \dots \quad (5.10) \end{aligned}$$

$$\begin{aligned} \delta(^3E_3) : & \frac{1}{2} \{ (|u_1 J_{\chi\varphi}| + |u_2 J_{\chi\varphi}|)^2 + (|v J_{\chi\varphi}| + |w J_{\chi\varphi}|)^2 / (E_{\chi^1} - E_{\varphi}) \} \\ & + \{ |x J_{u_1 v}|^2 + |x J_{u_1 w}|^2 + |x J_{u_2 v}|^2 + |x J_{u_2 w}|^2 / (E_{\chi^2} - E_{\varphi}) \dots \quad (5.11) \end{aligned}$$

*Singlets :*

$$\begin{aligned} \delta(^1E_1) : & \frac{1}{2} \{ (|u_1 J_{\chi\varphi}| + |u_2 J_{\chi\varphi}|)^2 + (|v J_{\chi\varphi}| + |w J_{\chi\varphi}|)^2 / (E_{\chi^1} - E_{\varphi}) \} \\ & + \frac{3}{8} \{ |x J_{u_1 v}|^2 + |x J_{u_1 w}|^2 + |x J_{u_2 v}|^2 + |x J_{u_2 w}|^2 / (E_{\chi^2} - E_{\varphi}) \dots \quad (5.12) \end{aligned}$$

$$\begin{aligned} \delta(^1E_2) : & \frac{3}{8} \{ (|u_1 J_{\chi\varphi}| + |u_2 J_{\chi\varphi}|)^2 + (|v J_{\chi\varphi}| + |w J_{\chi\varphi}|)^2 / (E_{\varphi^1} - E_{\varphi}) \} \\ & + \{ 2 |x J_{u_1 u_2}|^2 + 2 |x J_{vw}|^2 + \frac{1}{2} (|x J_{u_1 v}|^2 + |x J_{u_1 w}|^2 + |x J_{u_2 v}|^2 \\ & + |x J_{u_2 w}|^2) / (E_{\chi^2} - E_{\varphi}) \dots \quad (5.13) \end{aligned}$$

An examination of the equations (5.8) to (5.13) shows that the depression of the quintet state is least and that of singlet  $1E_2$  is the maximum. The lowering of the various states relative to  ${}^5E$  is given below :

$$\delta({}^5E) - \delta({}^3E_1) = \frac{2}{3} (|{}^vJ_{\chi\varphi}| + |{}^wJ_{\chi\varphi}|)^2 / (E_{\chi^1} - E_{\varphi}) + \{2|{}^xJ_{vw}|^2 + \frac{1}{2} (|{}^xJ_{u_1v}|^2 + |{}^xJ_{u_1w}|^2 + |{}^xJ_{u_2v}|^2 + |{}^xJ_{u_2w}|^2) / (E_{\chi^2} - E_{\varphi}) \dots \quad (5.14)$$

$$\delta({}^5E) - \delta({}^3E_2) = \frac{2}{3} (|{}^{u_1}J_{\chi\varphi}| + |{}^{u_2}J_{\chi\varphi}|)^2 / (E_{\chi^1} - E_{\varphi}) + \{2|{}^xJ_{u_1u_2}|^2 + \frac{1}{2} (|{}^xJ_{u_2v}|^2 + |{}^xJ_{u_1w}|^2 + |{}^xJ_{u_2w}|^2 + |{}^xJ_{u_1v}|^2) / (E_{\chi^2} - E_{\varphi}) \dots \quad (5.15)$$

$$\delta({}^5E) - \delta({}^3E_3) = \{ |{}^xJ_{u_1v}|^2 + |{}^xJ_{u_1w}|^2 + |{}^xJ_{u_2v}|^2 + |{}^xJ_{u_2w}|^2 + |{}^xJ_{u_1w}|^2 / (E_{\chi^2} - E_{\varphi}) \dots \quad (5.16)$$

$$\delta({}^5E) - \delta({}^1E_1) = \frac{2}{3} \{ |{}^xJ_{u_1u_2}|^2 + |{}^xJ_{u_2v}|^2 + |{}^xJ_{u_2w}|^2 + |{}^xJ_{u_1w}|^2 / (E_{\chi^2} - E_{\varphi}) \dots \quad (5.17)$$

$$\delta({}^5E) - \delta({}^1E_2) = \{ (|{}^{u_1}J_{\chi\varphi}| + |{}^{u_2}J_{\chi\varphi}|)^2 - (|{}^vJ_{\chi\varphi}| + |{}^wJ_{\chi\varphi}|)^2 / (E_{\chi^1} - E_{\varphi}) + \{2|{}^xJ_{u_1u_2}|^2 + 2|{}^xJ_{vw}|^2 + \frac{1}{2} (|{}^xJ_{u_1v}|^2 + |{}^xJ_{u_1w}|^2 + |{}^xJ_{u_2v}|^2 + |{}^xJ_{u_2w}|^2) / (E_{\chi^2} - E_{\varphi}) \dots \quad (5.18)$$

From the above the energy sequence can be roughly indicated as :

$${}^1E_2 < {}^3E_2 \leq {}^3E_1 < {}^1E_1 < {}^3E_3 < {}^5E \dots \quad (5.19)$$

Let us look at the spin coupling arrangement in the various states with reference to the spins in  $(u_1 u_2) (vw)$

$${}^1E_2 \rightarrow {}^1\{({}^1u_1 u_2) {}^1(vw)\}$$

$${}^3E_2 \rightarrow {}^3\{({}^3u_1 u_2) {}^1(vw)\}$$

$${}^3E_1 \rightarrow {}^3\{({}^1u_1 u_2) {}^3(vw)\}$$

$${}^1E_1 \rightarrow {}^1\{({}^3u_1 u_2) {}^3(vw)\}$$

$${}^3E_3 \rightarrow {}^3\{({}^3u_1 u_2) {}^3(vw)\}$$

$${}^5E \rightarrow {}^5\{({}^3u_1 u_2) {}^3(vw)\}$$

Thus the most stable state is obtained when in both  $(u_1 u_2)$  and  $(vw)$  the spins are in the singlet state, i.e.,  ${}^1E_2$ . The next ones arise when only one of them either  $(vw)$  or  $(u_1 u_2)$  is in singlet state, i.e.,  ${}^3E_2$ ,  ${}^3E_1$ . When the states are formed from the configuration  $(2S+1)\{({}^3u_1 u_2) {}^3(vw)\}$  they lie higher up. One can, therefore, safely conclude that the dominant couplings are always anti-ferromagnetic.

We now give a brief discussion about the choice of  $\chi$ . The physical basis about the choice of the lowest excited empty orbital relative to  $\phi$  has been considered in earlier papers (Koide, Sinha and Tanabe 1959, Sinha 1961).

For the present purpose also the appropriate description of  $\chi$  is given by

$$\chi = (\sum_{i=1}^{\infty} |a_i| \sigma_i) / \text{Normalisation} \quad (5.20)$$

where  $\sigma_i$  are the cation empty orbitals, namely,  $4s$  or an appropriate symmetrical hybrid having maximum charge density towards the anion. The  $|a_i|$  are the coefficients (positive numbers) which can in principle be determined by variation. The other combination with  $a_i$ 's have negative sign will have higher energy because of mixing with  $\phi$  which is an odd function. In fact the combination as given by (5.20) has the lowest non-orthogonally integral with  $\phi$  (Sinha 1961).

The magnitude of the hybrid exchange integrals of the type occurring in (5.14) and (5.18) and the energy denominators have been assessed earlier. Here too, they would be of the same order of magnitude.

In view of the fact that we do not have any pure magnetic garnets in the sense that all the  $\{A\}$   $\{B\}$   $\{C\}$  sites are occupied by the same type of transition metal ions, there is no point in calculating the transition temperature from our model and compare with results. It may, however, be remarked that the general features are correctly predicted. The fact that the singlet state is the lowest one suggests that the magnetic moments of the paramagnetic ions tend to compensate each other. Thus for the system  $\{\text{Mn}_2 \text{ Y}_2\} [\text{Fe}_{1.7} \text{ Ge}_{0.3}] (\text{Fe}_{2.3} \text{ Ge}_{0.7}) \text{O}_{12}$  (Goller 1960) one would predict on our model a magnetic moment of  $2\mu_B$ . This is the observed value and is consistent with the above formulae which was suggested by Tauber *et al.* (1958).

Instead of discussing specific examples, we shall point out certain general conclusions as derived from the foregoing analysis.

## DISCUSSION

In this paper we have explained the nature of indirect spin coupling in garnet like magnetic compounds on the basis of mechanisms suggested earlier (Koide, Sinha and Tanabe 1959). The model chosen is a six electron and five centre system appropriate for garnets. Unfortunately, the geometry of the system lacks symmetry and hence the calculations have been quite involved. Nevertheless, the model does incorporate the possible types of interactions namely,  $a-d$ ,  $c-c$ ,  $c-d$ ,  $c-a$ , etc., in a composite way. Taking one electron from each paramagnetic ions ( $A' ACB$ ) and two from central anion it has been shown for the set ( $u_1 u_2$ ) ( $vw$ ) that the singlet state where all the spins are mutually compensated is the most stable state. In other words, the coupling is predominantly anti-ferromagnetic.

In view of the fact that the 'a' and 'd' ions are closer to the anion compared to the c ions, the hybrid exchange integrals for them will be correspondingly larger. One can, therefore, conclude that a-d interaction is definitely the strongest. The c-c interaction is weaker compared to this. On our model c-d and c-a interactions also exist.

Specific cases can be analysed from the above calculations by choosing the sets  $(a_1 a_2)$   $(a_3 a_4)$  according to the symmetry of the wave functions in the actual crystals.

That YIG, i.e.,  $\{Y_3\} [Fe_2] (Fe_3)O_{12}$  is ferrimagnetic (with  $5\mu_B$  per formula unit) is in agreement with strong a-d interaction. This system can, however, be analysed by the earlier models (three centre four electrons, Koide, Sinha and Tanabe 1959, Sinha 1961).

In conclusions, it can be emphasized that the broad indication of the calculations are that the singlet is the lowest i.e., the ions tend to compensate the spins of each other. Thus even when some of the sets do not contain paramagnetic ions, paramagnetic ions at other sites interact antiferromagnetically. This is supported by  $\{Gd_3\} [Mn_2] (GaGe_2)O_{12}$  with spontaneous magnetization  $9.6\mu_B$ . In this case the appropriate electrons wave functions of Gd are taking part in the interactions.

It may be remarked finally that in the present mechanism the spatial dispositions of both occupied and empty orbitals are important and hence interactions are possible even where angles are not appropriate for their mechanisms.

#### ACKNOWLEDGMENT

We are grateful to Dr. A. B. Biswas for his interests in this work and discussions. One of the authors (MKS) is indebted to C.S.I.R. for the award of Research Fellowship.

#### REFERENCES

- Bortaut F. and Forrat F., 1956, *C. R. Acad. Sci. (Paris)*, **242**, 382.  
 Geller S. and Gilloow M. A., 1957, *J. Phys. Chem. Solid* Vol. **3**, Nos. 1-2, 30-36.  
 Geller S., 1960, *Int. J. Phys. Chem. Solid (Paris)* Vol. **16**, Nos. 1/2 pp. 21-29.  
 Koide S, Sinha K. P., Tanabe, Y., 1959, *Prog. of Theo. Phys.* **22**, 647.  
 McClure, D. S. 1959, *Solid State Physics*, Vol. 9, Ed. Seitz and Turnbull, 399.  
 Sinha K. P., Koide S., 1960, *Sci. Pap. Coll Gen Education University of Tokyo*, **10**, 195.  
 Sinha K. P., (1961a), *Ind. J. Phys.*, **35**, 127.  
 Sinha K. P., 1961b, *Ind. J. Phys.*, **35**, 484.  
 Tauber A, Banks E and Kodosy H. H., 1958, *J. Appl. Phys.*, **29**, 385.

# INFRARED STUDY OF HYDROGEN BONDING IN ISOMERIC TOLUIDINES IN DIFFERENT ENVIRONMENTS

K. C. MEDHI, S. B. BANERJEE AND G. S. KASTHA

OPTICS DEPARTMENT, INDIAN ASSOCIATION FOR THE CULTIVATION OF  
SCIENCE, CALCUTTA-32

(Received July 5, 1962)

**ABSTRACT.** The changes in the frequencies of N-H symmetric and asymmetric stretching vibrational bands of the three isomeric toluidines in different environments relative to the frequencies observed in the respective  $\text{CCl}_4$  solutions have been studied with a Perkin-Elmer Model 21 spectrophotometer. The results indicate the existence of intermolecular association between toluidine molecules in the case of pure liquids and between toluidine molecules and polar solvents in the case of solutions. Attempt has been made to account for the difference in the N-H stretching frequencies of the three isomers in solution in  $\text{CCl}_4$  and the changes in the frequencies observed in other solvents.

## INTRODUCTION

Flett (1948) discussed the variations of characteristic  $\text{NH}_2$  group stretching frequencies of substituted anilines in relation to the reactivity of the group in question and suggested a correlation of the observed variations with the electronic nature of the bond involved. Later, Krueger and Thompson (1957) also studied the dependence of the intensity and frequency of stretching vibrations of  $\text{NH}_2$  group attached to the aromatic ring on the Hammett  $\sigma$  factor of the substituent group. Solvent effect on N—H stretching frequencies in substituted anilines has also been reported by Cutmore and Hallam (1962).

In an earlier work, Gordy and Stanford (1940) had suggested that the molecules of *o*- and *p*-toluidines might remain in polymeric groups in the liquid state. Recently, Zanker and Wittwer (1959), from a study of the infrared spectra of toluidines in  $\text{CCl}_4$  solutions, proposed that the  $\text{NH}_2$  and  $\text{CH}_3$  groups in *o*-toluidine molecule are either involved in steric interaction or are weakly bonded through C—H...N bond. More recently, Whetsel (1961) compared the infrared spectra of toluidines in solutions in  $\text{CCl}_4$  and  $\text{CHCl}_3$  in the first overtone region and postulated the existence of weak hydrogen bond between the N-atom of the  $\text{NH}_2$  group and the proton of the  $\text{CHCl}_3$  molecule.

It was not known, however, whether other solvents also produce such changes in the N—H stretching frequencies of the toluidine molecule and whether such changes are dependent on the relative positions of the substituent groups in the

aromatic ring of the three isomers. An investigation of the infrared spectra of the toluidines in the liquid state and in solution in a number of polar and non polar solvents was, therefore, undertaken and in the present paper the results have been presented with probable interpretations.

## EXPERIMENTAL

Chemically pure samples of the toluidines supplied by E. Merck were further purified by fractional and vacuum distillation. In the case of the para compound the purity was tested by its melting point. The solvents were carefully purified and dried before use. A Perkin Elmer Model 21 spectrophotometer provided

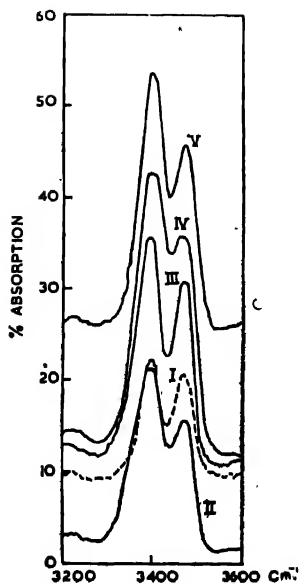


Fig. 1a—Infrared absorption spectra of *o*-toluidine

- I 4% solution in carbon tetrachloride
- II " " in cyclohexane
- III " " in carbon disulphide
- IV " " in chloroform
- V " " in benzene

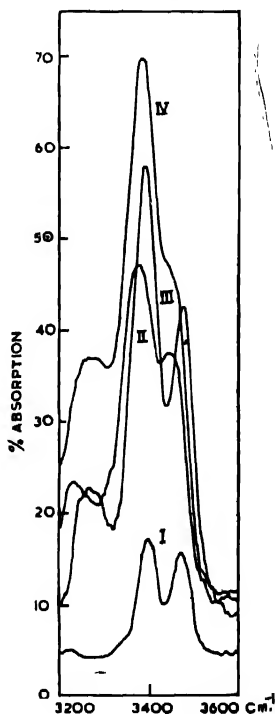


Fig. 1b—Infrared absorption spectra of *o*-toluidine

- I 4% solution in carbon tetrachloride
- II Pure liquid (thin film)
- III 4% solution in ether
- IV " " in acetone

with rock salt optics was used to record the infrared absorption bands of the compounds in the pure state and in solutions with the arrangements described in an earlier paper (Banerjee and Kastha, 1962).

## RESULTS AND DISCUSSION

The infrared absorption curves are reproduced in Figs. 1, 2 and 3. The symmetric and asymmetric N—H stretching frequencies in  $\text{cm}^{-1}$  for *o*-, *m*- and *p*-toluidine in the liquid state and in solutions are given in Tables I, II and III. The corresponding frequencies for the para compound in the solid state have been included in Table III.

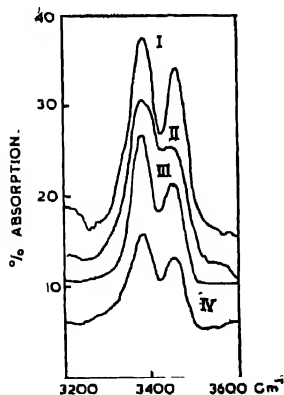


Fig. 2a—Infrared absorption spectra of *m*-toluidine

- I 4% solution in carbon tetrachloride
- II " " in chloroform
- III " " in benzene
- IV " " in cyclohexane

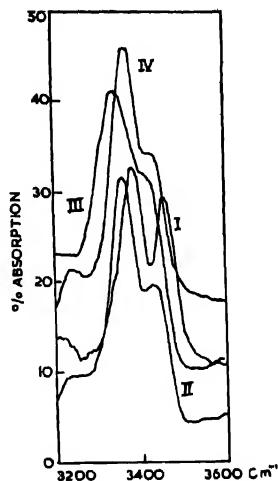


Fig. 2b—Infrared absorption spectra of *m*-toluidine

- I 4% solution in carbon tetrachloride
- II " " in other
- III Pure liquid (thin film)
- IV 4% solution in acetone

It can be seen that the observed N—H stretching frequencies in *o*-toluidine molecule in solution in  $\text{CCl}_4$  are higher than the corresponding frequencies in the molecules of the meta and the para isomer in  $\text{CCl}_4$  solution and are closer to the N—H frequencies in the parent compound aniline. The lowering of the frequencies in the case of *p*- and *m*-toluidine may be due to retardation of migration of charge from the  $\text{NH}_2$  group due to the presence of the slightly electro-positive  $\text{CH}_3$  group in the meta and para positions. This makes the N-atom slightly more negative than that in aniline molecule and causes a weakening of the N—H bond strength.

It may be noted here for comparison, that the presence of highly electronegative  $\text{NO}_2$  group in the para position in *p*-nitrotoluene causes a large migration of negative charge from the  $\text{NH}_2$  group thus increasing the N—H bond strength so that

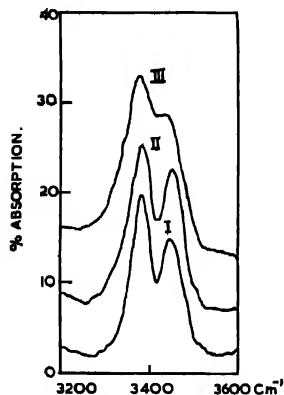


Fig. 3a—Infrared absorption spectra of *p*-toluidine

- I 4% solution in benzene  
 II „ „ in carbon tetrachloride  
 III „ „ in chloroform

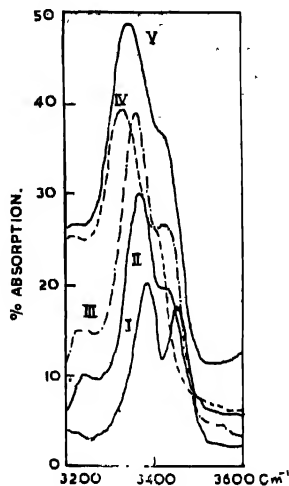


Fig. 3b—Infrared absorption spectra of *p*-toluidine

- I 4% solution in carbon tetrachloride  
 II „ „ in acetone  
 III „ „ in ether  
 IV Pure solid (thin film)  
 V Pure liquid (thin film)

the N—H frequencies are even higher than those in aniline molecule (Flett, 1948). The presence of  $\text{CH}_3$  group in the ortho position in *o*-toluidine does not apparently affect the migration of charge from the  $\text{NH}_2$  group to the benzene ring, because of the possibility of deflection of electronic charge cloud towards the meta position.

TABLE I

*o*-Toluidine,

N—H stretching frequencies

	Liquid	Solution in						
		$\text{CCl}_4$	$\text{CS}_2$	$\text{C}_6\text{H}_6$	$\text{C}_6\text{H}_5$	$\text{CHCl}_3$	$(\text{CH}_3)_2\text{CO}$	$(\text{C}_2\text{H}_5)_2\text{O}$
$\nu_{\text{sym.}}$ ( $\text{cm}^{-1}$ )	3382s	3390s	3399s	3398s	3398s	3397s	3390s	
$\nu_{\text{asym.}}$ ( $\text{cm}^{-1}$ )	3449ms	3472ms	3470ms	3470ms	3472ms	3464ms	3458ms	3468ms



TABLE II  
*m*-Toluidine,  
 N—H stretching frequencies

	Liquid	Solution in					
		CCl <sub>4</sub>	C <sub>6</sub> H <sub>12</sub>	C <sub>6</sub> H <sub>6</sub>	CHCl <sub>3</sub>	(CH <sub>3</sub> ) <sub>2</sub> CO	(C <sub>2</sub> H <sub>5</sub> ) <sub>2</sub> O
$\nu_{sym}(\text{cm}^{-1})$	3340s	3382s	3383s	3380s	3378ms	3368s	3362ms
$\nu_{asym}(\text{cm}^{-1})$	3418ms	3460ms	3459ms	3450ms	3445m	3440ms	3435ms

TABLE III  
*p*-Toluidine  
 N—H stretching frequencies

	Crystals	Liquid	Solution in				
			CCl <sub>4</sub>	C <sub>6</sub> H <sub>6</sub>	CHCl <sub>3</sub>	(CH <sub>3</sub> ) <sub>2</sub> CO	(C <sub>2</sub> H <sub>5</sub> ) <sub>2</sub> O
$\nu_{sym}(\text{cm}^{-1})$	3332s	3345s	3380s	3382s	3380s	3370s	3365m
$\nu_{asym}(\text{cm}^{-1})$	3407m	3427ms	3450m	3445ms	3440m	3435m	3425ms

In the absence of data for the frequencies of symmetric and asymmetric N—H stretching bands of free molecules of all the three isomers in the gaseous state, the frequencies of these bands in CCl<sub>4</sub> solutions of the compounds have been taken to be the normal frequencies. As regards the general behaviour of these vibrations in different environments, it can be seen from the tables that the frequencies are reduced in the polar solvents and in pure liquids and the reduction in the frequencies is the largest in the case of the respective pure liquids. Moreover, the lowering of frequencies is larger for the meta compound than for the other isomers, and for all the three isomers the asymmetric vibration is, in general, more affected than the symmetric vibration.

The considerable lowering of the N—H vibrational frequencies with respect to those observed in CCl<sub>4</sub> solutions may be attributed to formation of weak intermolecular N—H...N bonds in the case of pure liquids. In the case of the para compound in the solid state, the molecules come closer together and as a result the N—H...N bond becomes stronger causing a further reduction in the N—H frequencies. It may be mentioned here that Gordy and Stanford (1940) proposed the existence of toluidine molecules in polymeric groups in the liquid state. But it should be noted that the half-width of the bands observed in the present investigation is much less than that of the O—H vibrational bands due to crystals of *p*-nitrophenol (Banerjee and Kastha, 1962). This shows that perhaps the intermolecularly associated molecules of *p*-toluidine are not present as long polymeric

chain. The relatively smaller change in the N—H vibrational frequencies observed in the case of *o*-toluidine in the liquid state indicates a weaker N—H...N bond due to partial shielding of the N atom by the CH<sub>3</sub> group in the pure liquid.

In studying the influence of solvents on the frequencies, the relative shifts of the symmetric and asymmetric N—H stretching frequencies of the compounds in non-polar solvents like benzene, cyclohexane and carbon disulphide, with respect to those observed in CCl<sub>4</sub> solutions are found to lie approximately on a

straight line when plotted against the difference of the value of  $\frac{n^2-1}{2n^2+1}$  for the

solvent in question and that for CCl<sub>4</sub>. But in the case of solutions in polar solvents like acetone, ether and chloroform wide deviations are observed. From this it can be inferred that though the observed shifts in non-polar solvents could be satisfactorily explained as due to an electrostatic effect, some other effects should be considered to explain the changes in the other cases. The deviations in solutions in acetone and ether can be attributed to the formation of N—H...O bond between toluidine molecules and the solvent molecules. Incidentally, it may not be out of place to point out here that the percentage lowering in the N—H frequencies in solutions of these compounds in acetone and ether is much smaller than that observed in O—H stretching vibrational frequencies in corresponding solutions of nitrophenols (Banerjee and Kastha, 1962), from which it is evident that the N—H...O bonds are much weaker than the O—H...O bonds. Evidence of the formation of weak hydrogen bond between the N-atom of the toluidine molecule and the proton of the chloroform molecule has been furnished by Whetsel (1961) who observed two bands for the asymmetric N—H stretching vibration in chloroform solution in place of only one band in CCl<sub>4</sub> solution, in the first overtone region. In the present investigation a marked increase in the strength of absorption in the region between the two bands due to the symmetric and antisymmetric vibrations is observed, but due to the close proximity of the two bands no splitting could be detected.

As has been pointed out above, the change in the N—H frequencies is more pronounced in the meta compound than in the para compound while it is the least in the ortho compound. The smaller influence of environments on the N—H vibrations in *o*-toluidine may be due to partial shielding of the N-atom of the NH<sub>2</sub> group by the CH<sub>3</sub> group in the ortho position from the influence of the surrounding solvent molecules. The difference in the behaviour of *m*- and *p*-toluidine molecules may be understood in terms of the effect of the Hammett  $\sigma$  factor of the substituent group in the two compounds on the force constant of the N—H bond. The Hammett  $\sigma$  for *m*-toluidine is  $-0.069$  and that for *p*-toluidine is  $-0.170$  (Jaffé, 1953) which indicates that the negative charge on the N-atom is larger in the latter compound than in the former. Accordingly, the H-atom in the NH<sub>2</sub> group of the meta compound would be more positive than that in the para compound and, therefore, the N—H...N linkage in the pure liquid and the

N—H...O linkage in solution in acetone would be stronger in the case of the meta isomer. It can, however, be seen from Tables II and III that the lowering of the N—H frequencies for *m*- and *p*-toluidine is almost the same in the case of the ether solution. It has been pointed out by Jaffé (1953) that the Hammett  $\sigma$  of para toluidine changes to  $-0.105$  in alcohol-ether solution, approaching thereby the value for the meta compound. This change in  $\sigma$  may account for the equality in the strength of N—H...O bonds in the cases of meta and para toluidine in ether solution.

#### ACKNOWLEDGMENT

The authors' thanks are due to Professor S. C. Sirkar, D.Sc., F.N.I., for his kind interest in the work.

#### REFERENCES

- Banerjee, S. B. and Kastha, G. S., 1962, *Ind. J. Phys.*, **36**, 163.  
Cutmore, E. A. and Hallam, J., 1962, *Trans. Farad. Soc.*, **58**, 40.  
Flett, M. St. C., 1948, *Trans. Farad. Soc.*, **44**, 767.  
Gordy, W. and Stanford, O. T., 1940, *J. Am. Chem. Soc.*, **62**, 497.  
Jaffé, H. H., 1953, *Chem. Rev.*, **53**, 244.  
Krueger, P. J. and Thompson, H. W., 1957, *Proc. Roy. Soc.*, **243A**, 143.  
Whetsel, K. B., 1961, *Spectrochim. Acta.*, **17**, 614.  
Zankor, V. and Wittwer, A., 1959 *Hydrogen Bonding* (Pergamon Press).

# MULTICOMPONENT DIFFUSION IN THE SYSTEMS <sup>85</sup>Kr-Ne-Kr AND <sup>85</sup>Kr-A-Kr

RANJIT PAUL

INDIAN ASSOCIATION FOR THE CULTIVATION OF SCIENCE, CALCUTTA-32

(Received July, 7, 1962).

**ABSTRACT.** The diffusion coefficient of radio-active isotope <sup>85</sup>Kr in trace quantities in mixtures of neon-krypton and argon-krypton as well as in pure neon, argon and krypton has been determined using an all metal apparatus. The diffusion takes place inside a precision bore capillary joining two gas chambers. For analysis one of the chambers has a thin cellophane window with a scintillation counter placed close to it. First, both the chambers were filled with the desired gas mixture and then a small amount of <sup>85</sup>Kr added to the analysis chamber and the pressure equalised. Diffusion was then started by opening a bellows valve constructed at the middle of the capillary and counting rate was determined at regular intervals, from which diffusion coefficient was calculated. The diffusion coefficient  $D_{1 \rightarrow 23}$  of <sup>85</sup>Kr in mixture of krypton and the other gas is found to be accurately given by the theoretically predicted formula

$$\frac{C_2}{D_{1 \rightarrow 23}} = \frac{C_2}{D_{12}} + \frac{C_3}{D_{13}}$$

where  $C_2$ ,  $C_3$  are the concentration of ordinary krypton and that of the other gas respectively, and  $D_{12}$  and  $D_{13}$  are the binary diffusion coefficients. As expected a plot of the experimental values of  $1/D_{1 \rightarrow 23}$  against  $C_3$  is found to be a straight line from which  $D_{12}$  and  $D_{13}$  are calculated.

## INTRODUCTION

The study of diffusion of gases by radioactive tracer is by now a well known technique. Hirst and Harrison (1939) have determined the mutual diffusion coefficient of Radon with air, H<sub>2</sub>, He, Ne and A. Hutchinson (1949) measured the self-diffusion coefficient of argon using <sup>41</sup>A, which is β active as tracer. Drickamer *et al.* (Timmerhaus and Drickamer, 1951, 1953; Robb and Drickamer, 1951; Jeffries and Drickamer 1953, 1954) have measured diffusion coefficients at high pressures using scintillation counter. Amdur and others (Amdur, Irvine, Mason and Ross, 1952; Amdur and Schatzki, 1957) have studied CO<sub>2</sub>-CO<sub>2</sub>, CO<sub>2</sub>-N<sub>2</sub>O, A-Xe using an ionization chamber in Loschmidt type apparatus. Amdur and Schatzki (1958) used the same technique to determine the diffusion coefficient at limiting concentrations in the system A-Xe using <sup>37</sup>A and <sup>131m</sup>Xe as tracers. Recently, some workers (Lonsdale and Mason, 1957; Saxena and Mason, 1959, Weissman, Saxena and Mason, 1960, 1961) have used the rate of approach to steady state in thermal diffusion to measure both thermal and ordinary diffusion coeffi-

cients. They studied the systems having one component as  $\text{CO}_2$  and used  $^{14}\text{CO}_2$  as tracer. Using an apparatus similar to that of Hutchinson (1949) we have already studied the multi-component system  $^{86}\text{Kr}-\text{He}-\text{Kr}$  (Srivastava and Paul, 1962). In the present paper we have used the same arrangement to study the multi-component diffusion in two other systems.

So far there has been a dearth of multicomponent diffusion data in the literature. Hellund (1940) developed the theory of multicomponent gas mixtures by using a variational procedure. Curtiss and Hirschfelder (1949) have given simpler expressions by neglecting quantum corrections. Recently, Larenjeira and Kistemaker (1960) have given a somewhat elementary theory of thermal diffusion in three component system and obtained much simpler expressions, which they appear to have verified experimentally.

Fairbanks and Wilke (1950) were first to investigate three component diffusion experimentally. Using stefan's technique, they measured the diffusion coefficient of ethyl propionate in  $\text{H}_2$ -air mixtures and toluene in  $\text{H}_2$ -A mixtures, treating the organic vapour, as trace and found the results in substantial agreement with the theory. Recently, Walker, de Haas and Westenberg (1960) have used a point source technique to study the diffusion of  $\text{CO}_2$  in mixtures of helium and nitrogen. Treating  $\text{CO}_2$  as trace and neglecting the separation of the two components during the experiment, they obtained results in agreement with the theory. They used a rather complicated arrangement to analyse the gas with the help of a thermal conductivity analyser by freezing out the  $\text{CO}_2$ . Our method is much simpler which enables us to carry on investigations with any radioactive gas with considerable ease.

#### APPARATUS AND EXPERIMENTAL PROCEDURE

The description of the apparatus and the experimental procedure have been dealt with in detail in the previous paper (Srivastava and Paul, 1962). Exactly the same procedure was followed.

#### RESULTS

The thermostatic bath was maintained at  $301.6^\circ\text{K}$ . The values of diffusion coefficients were determined from the plots of  $\log(N_1^t - N_1^\infty)$  against 't' as indicated in the previous paper. The values of the diffusion coefficients at atmospheric pressure are tabulated in Tables I and II.

The  $D_{exp}$  values are believed to be accurate to about  $\pm 1\%$ .  $D_{cal}$  value in column 5 have been calculated on Lennard-Jones (12:6) model from force constants available in the literature and applying mass corrections. The agreement between the experimental and the calculated values is satisfactory. The values of  $1/D_{exp}$  have been plotted against the concentration of the lighter gas (Fig. 1) resulting in a straight line within the limits of experimental accuracy. The values of

TABLE I  
<sup>15</sup>Kr-A-Kr System

% of Argon	Pressure in cm.	Relaxation time in mins.	D <sub>exp</sub> cm <sup>2</sup> /sec	D <sub>cal</sub> cm <sup>2</sup> /sec	D <sub>cal</sub> cm <sup>2</sup> /sec
0	5.872	133.1	0.101	0.0986	0.101
19.46	6.730	144.2	0.107	0.1047	0.107
39.51	4.907	99.5	0.113	0.1117	0.113
63.90	5.050	95.1	0.122	0.1217	0.122
79.43	5.292	94.2	0.129	0.1290	0.128
100	4.844	80.3	0.138	0.1403	0.138

TABLE II  
<sup>86</sup>Kr-Ne-Kr system

% of Neon	Pressure in cm.	Relaxation time in mins.	D <sub>exp</sub> cm <sup>2</sup> /sec	D <sub>cal</sub> cm <sup>2</sup> /sec	D <sub>cal</sub> cm <sup>2</sup> /sec
0	5.872	133.1	0.101	0.0986	0.101
22.04	4.689	91.4	0.117	0.1143	0.117
42.63	5.753	95.5	0.138	0.1342	0.137
60.41	6.911	84.4	0.160	0.1580	0.161
78.10	5.884	69.5	0.194	0.1919	0.194
100	4.987	43.6	0.262	0.261	0.262

TABLE III

Gas Pairs	D from graph	D after mass correction	D other workers
Kr—Kr	.101	.1014	.093 (a) at 293°K
Kr—A	.138	.1383	.140 (b) at 303°K
Kr—Ne	.202	.2025	.206 (b) at 303°K

(a) Groth and Harteck (1941)

(b) Srivastava and Srivastava (1959).

diffusion coefficient read from the graph are given in column 6 of the Tables I and II. The values of multicomponent diffusion coefficients at limiting concentrations give the ordinary binary diffusion coefficient with  $^{85}\text{Kr}$  as one component and are tabulated in column 2 of Table III. These values are then

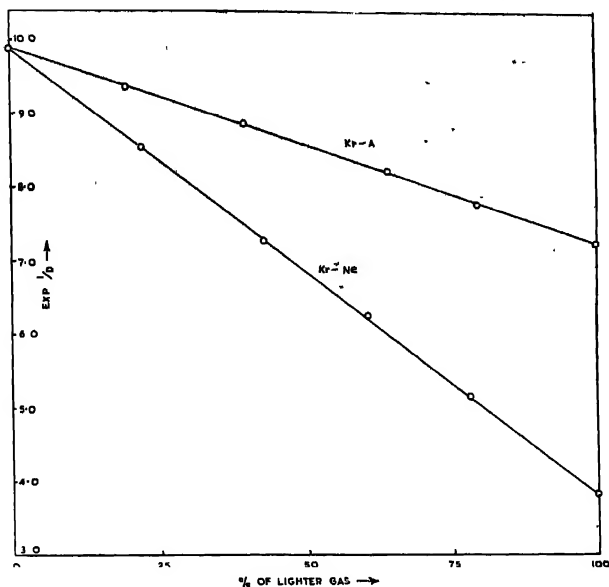


Fig. 1. Plot of  $1/D_{exp}$  against concentration of lighter gas.

used to obtain the binary diffusion coefficient with ordinary krypton by applying the mass corrections and are given in column 3. In column 4, the experimental values of other workers at nearest temperature available, are recorded with corresponding temperatures. The agreement is quite good.

#### ACKNOWLEDGMENT

The author is grateful to Prof. B. N. Srivastava, D.Sc., F.N.I., for his keen interest in the work and for valuable discussions. He is also thankful to Council of Scientific and Industrial Research, New Delhi, for financial assistance.

#### REFERENCES

- Amdur, I., Irvine, J. W., Mason, E. A. and Ross, J., 1952, *J. Chem. Phys.*, **20**, 436.  
 Amdur, I., and Schatzki, T. F., 1957, *J. Chem. Phys.*, **27**, 1049.  
 Amdur, I., and Schatzki, T. F., 1959, *J. Chem. Phys.*, **29**, 1425.  
 Curtiss, C. F., and Hirschfelder, J. O., 1949, *J. Chem. Phys.*, **17**, 550.

- Fairbanks, D. F. and Wilke, C. R., 1950, *Ind. Eng. Chem.*, **42**, 471.  
Groth, W. and Harteck, P., 1941, *Z. Electrochem.*, **37**, 167.  
Hellund, E. J., 1940, *Phys. Rev.*, **57**, 319, 328.  
Hirst, W., and Harrison, G. E., 1939, *Proc. Roy. Soc.*, **A169**, 572.  
Hutchinson, F., 1949, *J. Chem. Phys.*, **17**, 1031.  
Jeffries, Q. R., and Drickamer, G. H., 1953, *J. Chem. Phys.*, **21**, 1358.  
Jeffries, Q. R., and Drickamer, H. G., 1954, *J. Chem. Phys.*, **22**, 436.  
Larenjoira, M. F. and Kistemaker, J., 1960, *Physica*, **26**, 431.  
Lonsdale, H. K., and Mason, E. A., 1957, *J. Chem. Phys.*, **61**, 154.  
Robb, W. L., and Drickamer, H. G., 1951, *J. Chem. Phys.*, **19**, 1504.  
Saxena, S. C., and Mason, E. A., 1959, *Mol. Phys.*, **2**, 264, 379.  
Srivastava, B. N., and Paul, R., 1962, *Physica*, **28**, 646.  
Srivastava, B. N. and Srivastava, K. P., 1959, *J. Chem. Phys.*, **30**, 984.  
Timmerhaus, K. D., and Drickamer, H. G., 1951, *J. Chem. Phys.*, **19**, 1242.  
Timmerhaus, K. D., and Drickamer, H. G., 1952, *J. Chem. Phys.*, **20**, 981.  
Walker, R. E., de Haas, N., and Westenberg, A. A., 1960, *J. Chem. Phys.*, **32**, 1314.  
Weissman, S., Saxena, S. C., and Mason, E. A., 1960, *Phys. Fluids*, **3**, 510.  
Weissman, S., Saxena, S. C. and Mason, E. A. 1961, *Phys. Fluids*, **4**, 643.



# A METHOD OF DETERMINING THE TERMINAL IMPEDANCES AND TRANSFER FUNCTION OF GENERAL MULTIMESH LADDER NETWORKS CONTAINING TWO KINDS OF ELEMENTS ONLY

S. C. DUTTA ROY\*

ELECTRONICS SECTION, RIVER RESEARCH INSTITUTE, MOHANTPUR,  
NADIA

(Received December 20, 1961)

**ABSTRACT.** A technique is presented for finding the input impedance ( $Z_i$ ), output impedance ( $Z_o$ ), and the transfer function ( $\beta$ ) of general multimesh ladder networks containing two kinds of elements only, viz., resistance and capacitance or resistance and inductance or inductance and capacitance. Each of the above functions is expressed as a ratio of two polynomials in  $p^j$  where  $p$  is the complex frequency and  $j = 1, -1, 2$  or  $-2$ . The coefficients of powers of  $p^j$  in one of the polynomials are obtained by following an empirical procedure; the coefficients of the other polynomial are derived from those of the first by using a simple formula.

## INTRODUCTION

The case of an  $n$ -mesh  $RC$  ladder in which the elements of similar kind are equal has been treated by Tehudi (1950) and also by Bhattacharya (1952). If instead, the elements composing the various meshes are completely arbitrary, the situation becomes extremely complicated. No general formulae for this general case have yet been developed.

A procedure has been described in this paper for finding the expressions for the input impedance  $Z_i$ , output impedance  $Z_o$  and the transfer function  $\beta$  of a general  $n$ -mesh ladder network containing two kinds of elements only, viz., resistance  $R$  and capacitance  $C$ , resistance  $R$  and inductance  $L$ , and capacitance  $C$  and inductance  $L$ . Each of these functions are rational and in general, can be expressed as  $N(p^j)/D(p^j)$  where  $p$  is the complex frequency and  $j = 1, -1, 2$  or  $-2$ . The coefficients of  $p^j$  in either  $N$  or  $D$  are found by empirical rules formulated in the paper. The coefficients of the other polynomial are obtained from those of the first by using a simple formula given in the paper.

The above empirical rules have been formulated by observation from simple meshes and it has been shown by induction that if the procedure is correct for  $k$  meshes, then it applies to  $(k+1)$  meshes also.

\* Present address: Dept. of Physics, University of Kalyani, Kalyani, Nadia.

The procedure will first be explained with reference to the *RC* case; the modifications required for extension to the *RL* and *LC* cases will then be indicated.

#### RC CASE—LADDER CONFIGURATIONS AND SYMBOLS

The two forms of general resistance capacitance ladder networks, to be designated as the *R-C* and *C-R* forms are shown in Figs. 1(a) and (b) respectively. It will be assumed that the source and the load impedances in either configuration are respectively zero and infinite. The following symbols will be used :

$E_i$ ...input voltage,

$(E_o)_k$ ...output voltage with  $k$  number of meshes,

$n$ ...total number of meshes,

$k$ ...designation of an arbitrary mesh (i.e.  $k = 1, 2, \dots, n-1, n$ )

$(Z_i)_k$ ...impedance looking to the right from the points  $T_k, t_k$  (Fig. 1) ( $\neq$  the input impedance with  $k$  number of meshes),

$(Z_o)_k$ ...impedance looking to the left from the points  $T_k, t_k$  (= the output impedance with  $k$  number of meshes)

$\beta_k$ ...transfer function of the ladder with  $k$  number of meshes,

$B$ ... a coefficient in the denominator polynomial,

$A$ ... a coefficient in the numerator polynomial.

Without any loss of generality, it can be assumed that

$$R_1 = u_1 R, R_2 = u_2 R, \dots R_k = u_k R, \dots R_n = u_n R \quad \dots (1a)$$

and

$$C_1 = v_1 C, C_2 = v_2 C, \dots C_k = v_k C, \dots C_n = v_n C \quad (1b)$$

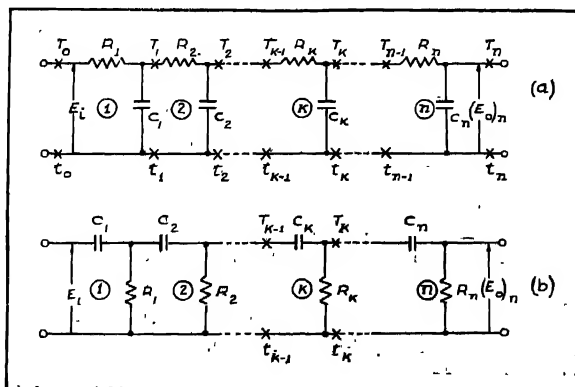


Fig. 1. Showing (a) *R-C* and (b) *C-R* forms of general resistance capacitance ladder networks. Encircled figures denote the designations of the meshes.

where  $R$  is a resistance parameter,  $C$  a capacitance parameter and  $u_1, u_2, \dots, u_k, \dots, u_n$  and  $v_1, v_2, \dots, v_k, \dots, v_n$  are constants. The quantity  $pCR$  may be called a modified complex frequency and will be denoted by  $q$ . The symbol  $(B_{l-r})_k$  will be used to mean the coefficient of  $q^{k-r}$  in the denominator polynomial  $(D_0)_k$  of the function  $(Z_0)_k$ .

# RECURRENCE FORMULAE

A recurrence formula for each of the functions  $(Z_i)_k$ ,  $(Z_0)_k$  and  $\beta_k$  can be deduced for either network in Fig. 1 as follows.

## R-C Case

$(Z_i)_k$  can be calculated in terms of  $(Z_i)_{k+1}$  from the equivalent circuit of Fig. 2(a) as

$$(Z_i)_k = R \frac{(u_{k+1}v_{k+1}q+1)(Z_i)_{k+1}/R+u_{k+1}}{v_{k+1}q(Z_i)_{k+1}/R+1} \quad \dots (2)$$

Fig. 2(b) gives the equivalent circuit for calculation of  $(Z_0)_k$  in terms of  $(Z_0)_{k-1}$ . We have

$$(Z_0)_k = R \frac{(Z_0)_{k-1}/R+u_k}{v_kq(Z_0)_{k-1}/R+u_kv_kq+1} \quad \dots (3)$$

The Thevenin equivalent circuit for the network to the left of the points  $T_{k-1}$ ,  $t_{k-1}$  consists of an ideal generator of voltage  $E_i\beta_{k-1}$  and a series impedance of value  $(Z_0)_{k-1}$ , as shown in Fig. 2(c). From this figure,  $\beta_k$  can be calculated as

$$\beta_k = \frac{(E_0)_k}{E_i} = \frac{\beta_{k-1}}{v_kq(Z_0)_{k-1}/R+u_kv_kq+1} \quad \dots (4)$$

## C-R case

The equivalent circuits for this case are shown in Figs. 3(a) to 3(c). The recurrence relations in this case are :

$$(Z_i)_k = R \frac{(u_{k+1}v_{k+1}q+1)(Z_i)_{k+1}/R+u_{k+1}}{v_{k+1}q(Z_i)_{k+1}/R+u_{k+1}v_{k+1}q} \quad \dots (5)$$

$$(Z_0)_k = R \frac{u_kv_kq(Z_0)_{k-1}/R+u_k}{v_kq(Z_0)_{k-1}/R+u_kv_kq+1} \quad \dots (6)$$

$$\beta_k = \frac{\beta_{k-1}u_kv_kq}{v_kq(Z_0)_{k-1}/R+u_kv_kq+1} \quad \dots (7)$$

The recurrence formulae given above will be found much useful in deducing expressions for  $(Z_i)_0$ ,  $(Z_0)_n$  and  $\beta_n$  in terms of  $u$ 's,  $v$ 's and  $q$  for the  $n$ -mesh network.

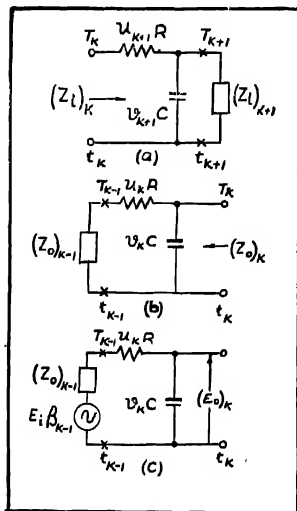


Fig. 2. Equivalent circuits for deducing the recurrence relations for (a)  $Z_i$ , (b)  $Z_0$  and (c)  $\beta$  for the R-C case.

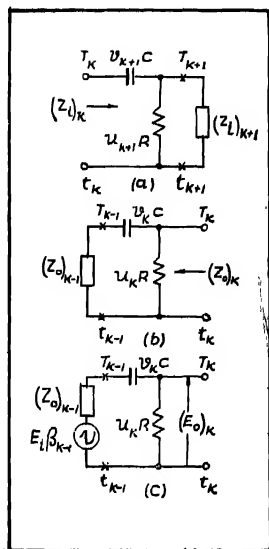


Fig. 3. Equivalent circuits corresponding to those of Fig. 2 for the C-R case.

### OUTPUT IMPEDANCE

Putting  $k = 1$  in Eq. (3) and noting that  $(Z_0)_0$ , the source impedance is zero, we have

$$(Z_0)_1 = R \frac{u_1}{u_1 v_1 q + 1} = R \frac{(A_0)_1}{(B_1)_1 q + (B_0)_1} = R \frac{(N_0)_1(q)}{(D_0)_1(q)} \quad \dots (8)$$

Putting  $k = 2$  in (3) and substituting for  $(Z_0)_1$  from Eq. (8), we have

$$(Z_0)_2 = R \frac{(N_0)_2(q)}{(D_0)_2(q)} \quad \dots (9a)$$

where

$$\begin{aligned} (N_0)_2(q) &= u_1 v_1 u_2 q + (u_1 + u_2) \\ &= (A_1)_2 q + (A_0)_2 \end{aligned} \quad (9b)$$

and

$$\begin{aligned}(D_0)_2(q) &= u_1 v_1 u_2 v_2 q^2 + (u_1 v_1 + u_1 v_2 + u_2 v_2) q + 1 \\ &= (B_2)_2 q^2 + (B_1)_2 q + (B_0)_2\end{aligned}\quad (9c)$$

Similarly, for  $K = 3$ ,

$$(Z_0)_3 = \frac{R(N_0)_3(q)}{(D_0)_3(q)} \quad (10a)$$

where

$$\begin{aligned}(N_0)_3(q) &= u_1 v_1 u_2 v_2 u_3 q^2 + (u_1 v_1 u_2 + u_1 v_1 u_3 \\ &\quad + u_1 v_2 u_3 + u_2 v_2 u_3) q + (u_1 + u_2 + u_3) \\ &= (A_2)_3 q^2 + (A_1)_3 q + (A_0)_3\end{aligned}$$

and

$$\begin{aligned}(D_0)_3(q) &= u_1 v_1 u_2 v_2 u_3 v_3 q^3 + (u_1 v_1 u_2 v_2 + u_1 v_1 u_2 v_3 \\ &\quad + u_1 v_1 u_3 v_3 + u_1 v_2 u_3 v_3 + u_2 v_2 u_3 v_3) q^2 \\ &\quad + (u_1 v_1 + u_1 v_2 + u_1 v_3 + u_2 v_2 + u_2 v_3 + u_3 v_3) q + 1 \\ &= (B_3)_3 q^3 + (B_2)_3 q^2 + (B_1)_3 q + (B_0)_3\end{aligned} \quad \dots \quad (10c)$$

Proceeding in this way,  $(E_0)_4$ ,  $(E_0)_5$  etc., can be calculated. But as the number of meshes increases, the calculations grow unmanageably both in length and complexity.

It will be shown that the expression for the output impedance for any number of meshes can be found directly from the circuit diagram with the help of the following procedure.

For the denominator coefficients,  $(B_{k-r})_k$ , ( $k = 1, 2, \dots, n$  and  $r = 0, 1, 2, \dots, k$ ), the rules to be followed are :

*Rule 1 :*  $(B_0)_k$  is unity, whatever  $k$  equals to.

*Rule 2 :* Each coefficient,  $(B_{k-r})_k$  is, in general, the sum of a number of terms, in which no term occurs more than once.\*

*Rule 3 :* Each term is the product of  $(k-r)$  number of  $u$ 's and the same number of  $v$ 's, in which no  $u$  or  $v$  occurs more than once.

*Rule 4 :* Each term must begin with  $u$  and end in  $v$ .

*Rule 5 :*  $u$ 's and  $v$ 's must alternate, i.e., no two  $u$ 's or  $v$ 's can be juxtaposed.

*Rule 6 :* Each term must be written such that if the subscript of an  $u$  be  $s_1$  and that of the next  $v$  be  $s_2$ , then

$$0 \leq (s_2 - s_1) \leq r$$

\* The number of terms in  $(B_{k-r})_k$  is  $(2k-r) ! / \{r!(2k-2r)!\}$

Also, if the subscript of a  $v$  be  $s'_1$  and that of the next  $u$  be  $s'_2$ , then

$$1 \leq (s'_2 - s'_1) \leq (r+1)$$

The sum of all possible terms obeying these rules gives  $(B_{k-r})_k$ . It may be easily verified that for  $k = 1, 2$  and  $3$  and  $r = 0, 1, 2$  and  $3$ , the coefficients obtained by following the above procedure are the same as those given by (8), (9c) and (10c).

The coefficients  $(A_{k-r-1})_k$  occurring in  $(N_0)_k(q)$  can be very simply obtained if those in  $(D_0)_k(q)$  are known. We note from (8), (9) and (10) that

$$\begin{aligned}(A_0)_1 &= \frac{(B_1)_1}{v_1}, \\(A_1)_2 &= \frac{(B_2)_2}{v_2}, \quad (A_0)_2 = \frac{(B_1)_2 - T_2}{v_2}, \\(A_2)_3 &= \frac{(B_3)_3}{v_3}, \quad (A_1)_3 = \frac{(B_2)_3 - T_3}{v_3}, \\(A_0)_3 &= \frac{(B_1)_3 - \Sigma T_3}{v_3}.\end{aligned}$$

where  $T_k$  denotes a term not containing  $v_k$ . The above results can be put in the general form :

$$(A_{k-r-1})_k = \frac{(B_{k-r})_k - \Sigma T_k}{v_k} \quad \dots \quad (11)$$

where  $k = 1, 2, 3$  and  $r = 0, 1, 2, 3$ .

The above procedure has been formulated with reference to values of  $k$  upto 3. We shall now show that it holds for  $k = 4$  also. For  $k = 4$ , we can write,

$$(Z_0)_4 = \frac{(A_3)_4 q^3 + (A_2)_4 q^2 + (A_1)_4 q + (A_0)_4}{(B_4)_4 q^4 + (B_3)_4 q^3 + (B_2)_4 q^2 + (B_1)_4 q + (B_0)_4}$$

For  $(B_4)_4$ ,  $k = 4$  and  $r = 0$ . Applying rule 3 we note that each term will have 4  $u$ 's and 4  $v$ 's with no  $u$  or  $v$  occurring more than once. Combining this with rule 2, we note that  $(B_4)_4$  will be given by a single term involving all  $u$ 's and  $v$ 's. Thus,

$$(B_4)_4 = u_1 v_1 u_2 v_2 u_3 v_3 u_4 v_4 \quad \dots \quad (12a)$$

For  $(B_3)_4$ ,  $k = 4$  and  $r = 1$ . Each term will now have 3  $u$ 's and 3  $v$ 's in which no  $u$  or  $v$  can be repeated. Beginning with  $u_1$  and obeying rules 2 to 6, the possible terms are

$$\begin{array}{ll}u_1 v_1 u_2 v_2 u_3 v_3, & u_1 v_1 u_2 v_2 u_3 v_4, \\u_1 v_1 u_2 v_2 u_4 v_4, & u_1 v_1 u_2 v_3 u_4 v_4, \\u_1 v_1 u_3 v_3 u_4 v_4, & u_1 v_2 u_3 v_3 u_4 v_4.\end{array}$$

Let the sum of these terms be called  $b_1$ . It may be observed that in each term,

$$0 \leq (s_2 - s_1) \leq 1 \quad \text{and} \quad 1 \leq (s'_2 - s'_1) \leq 2$$

Because of the requirement of 3  $u$ 's and 3  $v$ 's and because of rule 6, there can be only a single term beginning with  $u_2$ . This is

$$b_2 = u_2 v_2 u_3 v_3 u_4 v_4$$

Because of rule 6, there cannot be a term beginning with  $u_3$  or  $u_4$ . Thus, ,

$$(B_3)_4 = b_1 + b_2 \tag{12b}$$

Proceeding in a similar manner,

$$\begin{aligned} (B_2)_4 = & u_1 v_1 u_2 v_2 + u_1 v_1 u_2 v_3 + u_1 v_1 u_2 v_4 \\ & + u_1 v_1 u_3 v_3 + u_1 v_1 u_3 v_4 + u_1 v_1 u_4 v_4 \\ & + u_1 v_2 u_3 v_3 + u_1 v_2 u_3 v_4 + u_1 v_2 u_4 v_4 \\ & + u_1 v_3 u_4 v_4 + u_2 v_2 u_3 v_3 + u_2 v_2 u_3 v_4 \\ & + u_2 v_2 u_4 v_4 + u_2 v_3 u_4 v_4 + u_3 v_3 u_4 v_4 \end{aligned} \tag{12c}$$

and

$$\begin{aligned} (B_1)_4 = & u_1 v_1 + u_1 v_2 + u_1 v_3 + u_1 v_4 + u_2 v_2 + u_2 v_3 \\ & + u_2 v_4 + u_3 v_3 + u_3 v_4 + u_4 v_4 \end{aligned} \tag{12d}$$

The remaining coefficient,  $(B_0)_4$  is unity by rule 1. The  $A$ -coefficients can be obtained by applying formula (11).

$$(A_3)_4 = u_1 v_1 u_2 v_2 u_3 v_3 u_4 \quad \dots \tag{12e}$$

$$\begin{aligned} (A_2)_4 = & u_1 v_1 u_2 v_2 u_3 + u_1 v_1 u_2 v_2 u_4 + u_1 v_1 u_2 v_3 u_4 \\ & + u_1 v_1 u_3 v_3 u_4 + u_1 v_2 u_3 v_3 u_4 + u_2 v_2 u_3 v_3 u_4 \end{aligned} \quad \dots \tag{12f}$$

$$\begin{aligned} (A_1)_4 = & u_1 v_1 u_2 + u_1 v_1 u_3 + u_1 v_1 u_4 + u_1 v_2 u_3 \\ & + u_1 v_2 u_4 + u_1 v_3 u_4 + u_2 v_2 u_3 + u_2 v_2 u_4 + u_2 v_3 u_4 + u_3 v_3 u_4 \end{aligned} \quad \dots \tag{12g}$$

and

$$(A_0)_4 = u_1 + u_2 + u_3 + u_4 \tag{12h}$$

Putting  $k = 4$  in (3) and substituting for  $(Z_0)_3$  from (10a) through (10c), we get the same values of the coefficients as given by (12a) through (12h). Thus the method gives correct results for  $k = 4$ . For generalisation, it remains to show that if the procedure is correct for  $k$  meshes, it is so for  $(k+1)$  meshes also.

Writing

$$(Z_0)_k = R \frac{(N_0)_k(q)}{(D_0)_k(q)} \quad \text{and} \quad (Z_0)_{k+1} = R \frac{(N_0)_{k+1}(q)}{(D_0)_{k+1}(q)}$$

we have from (3),

$$(N_0)_{k+1} = (N_0)_k + (D_0)_k u_{k+1} \quad \dots (13a)$$

$$(D_0)_{k+1} = v_{k+1} q(N_0)_k + u_{k+1} v_{k+1} q(D_0)_k + (D_0)_k \quad \dots (13b)$$

Equating the coefficients of powers of  $q^{k-r}$  on either side of equation (13a) and of  $q^{k+1-r}$  on either side of equation (13b), we have,

$$(A_{k-r})_{k+1} = (A_{k-r})_k + u_{k+1} (B_{k-r})_k \quad \dots (14a)$$

$$(B_{k+1-r})_{k+1} = v_{k+1} (A_{k-r})_k + u_{k+1} v_{k+1} (B_{k-r})_k + (B_{k+1-r})_k \quad \dots (14b)$$

$(B_{k+1-r})_k$  is a coefficient of  $(D_0)_k$  and as such, does not involve  $v_{k+1}$ . Thus from equation (14b),

$$\frac{(B_{k+1-r})_{k+1} - \Sigma T_{k+1}}{v_{k+1}} = (A_{k-r})_k + u_{k+1} (B_{k-r})_k$$

The right hand side is just  $(A_{k-r})_{k-1}$ ; thus formula (11) applies to  $(k+1)$  meshes also.

From formula (11),  $(A_{k-r})_k$  in equation (14b) can be replaced by

$$\frac{(B_{k+1-r})_k - \Sigma T_k}{v_k}$$

Thus,

$$(B_{k+1-r})_{k+1} = \frac{v_{k+1}}{v_k} \left[ (B_{k+1-r})_k - \Sigma T_k \right] + u_{k+1} v_{k+1} (B_{k-r})_k + (B_{k+1-r})_k \quad \dots (15)$$

Now, terms contributing to the coefficient  $(B_{k+1-r})_k$  may be classified into three groups :

Group I—Terms containing neither  $u_{k+1}$  nor  $v_{k+1}$ ,

Group II—Terms containing both  $u_{k+1}$  and  $v_{k+1}$ ,

Group III—Terms containing  $v_{k+1}$  but not  $u_{k+1}$ .

There cannot be a term containing  $u_{k+1}$  but not  $v_{k+1}$  because of rule 4.

Group I terms are the same as those contributing to the coefficient  $(B_{k+1-r})_k$  of  $(D_0)_k$ . The third term on the right hand side of equation (15) gives these terms.

Since any term contributing to  $(B_{k+1-r})_{k+1}$  must have  $(k+1-r)$  number of  $u$ 's and the same number of  $v$ 's, terms of Group II must be those contributing to  $(B_{k-r})_k$  each being multiplied by  $u_{k+1} v_{k+1}$ . Thus the second term on the right hand side of equation (15) takes account of all such terms.

Terms of Group III will be those contributing to  $(B_{k+1-r})_k$ , which would normally end in  $v_k$ , with  $v_k$  replaced by  $v_{k+1}$ . If in a term of  $(B_{k+1-r})_k$  normally ending in  $v_{k-s}$  ( $s > 0$ ),  $v_{k-s}$  is replaced by  $v_{k+1}$ , we shall obtain a duplication of



a term previously considered; this is not permitted because of rule 2. Thus the first term on the right hand side of Eq. (15) accounts for Group III terms.

Thus the procedure formulated for finding a coefficient in the denominator polynomial is correct for  $(k+1)$  meshes and the generality of the method is established.

Finally, the expression for the output impedance of an  $n$ -mesh  $R$ - $C$  ladder can be written as

$$(Z_0)_n = \frac{(N_0)_n(q)}{(D_0)_n(q)} = \frac{\sum_{r=0}^{n-1} (A_{n-r-1})_n q^{n-r-1}}{\sum_{r=0}^n (B_{n-r})_n q^{n-r}} \quad \dots (16)$$

where  $(B_0)_n = 1$ ,  $(B_{n-r})_n$  is to be obtained by following the rules 2 to 6 with  $k$  replaced by  $n$  and  $(A_{n-r-1})_n$  is to be obtained from formula (11) with  $k$  replaced by  $n$ .

*C-R Case :*

In the recurrence relation (6), let us put

$$u_k = \frac{1}{V_k}, \quad v_k = \frac{1}{U_k} \quad \text{and} \quad q = \frac{1}{Q}$$

Then (6) transforms to

$$(Z_0)_k = \frac{1}{pC} \frac{pc(Z_0)_{k-1} + U_k}{V_k(Z_0)_{k-1} + R + U_k V_k Q + 1} \quad \dots (17)$$

This is of the same form as (3) with  $u$  replaced by  $U$ ,  $v$  by  $V$ ,  $q$  by  $Q$  and  $R$  by

$\frac{1}{pC}$ . Putting  $k = 1$  in (17), we have

$$(Z_0)_1 = \frac{1}{pC} \frac{U_1}{U_1 V_1 Q + 1} \quad \dots (18)$$

since  $(Z_0)_0 = 0$ . Putting  $k = 2$  in (17) and substituting for  $(Z_0)_1$  from (18), we have

$$(Z_0)_2 = \frac{1}{pC} \frac{U_1 V_1 U_2 Q + (U_1 + U_2)}{U_1 V_1 U_2 V_2 Q^2 + (U_1 V_1 + U_1 V_2 + U_2 V_2) Q + 1} \quad \dots (19)$$

Similarly,

$$(Z_0)_3 = \frac{1}{pC} \frac{(N_0)_3(Q)}{(D_0)_3(Q)} \quad \dots (20a)$$

where

$$(N_0)_3(Q) = U_1V_1U_2V_2U_3Q^2 + (U_1V_1U_2 + U_1V_1U_3 + U_1V_2U_3 + U_2V_2U_3)Q + (U_1 + U_2 + U_3) \quad \dots (20b)$$

and

$$(D_0)_3(Q) = U_1V_1U_2V_2U_3V_3Q^3 + (U_1V_1U_2V_3 + U_1V_1U_2V_3 + U_1V_1U_3V_3 + U_1V_2U_3V_3 + U_2V_2U_3V_3)Q^2 + (U_1V_1 + U_1V_2 + U_1V_3 + U_2V_2 + U_2V_3 + U_3V_3)Q + 1 \quad \dots (20c)$$

(18), (19) and (20) are of the same form as (8), (9) and (10) respectively with the small letter symbols replaced by capital letters and  $R$  by  $\frac{1}{pC}$ . Thus for this case,

$$(Z_0)_n = \frac{1}{pC} \frac{(N_0)_n(Q)}{(D_0)_n(Q)} = \frac{1}{pC} \frac{\sum_{r=0}^{n-1} (A_{n-r-1})_n Q^{n-r-1}}{\sum_{r=0}^n (B_{n-r})_n Q^{n-r}} \quad \dots (21)$$

where  $(B_0)_n = 1$ ,  $Q = 1/(pCR)$  and the other coefficients are calculated exactly as in the previous case or obtained from those results by replacements as stated above.

#### TRANSFER FUNCTION

Putting  $k = 1$  in Eq. (4), we have

$$\beta_1 = \frac{1}{u_1v_1q + 1} \quad \dots (22)$$

since  $\beta_0$ , the source transfer function is unity. Putting  $k = 2$  in Eq (4), substituting for  $\beta_1$  from (22) and simplifying, we have

$$\beta_2 = \frac{1}{u_1v_1u_2v_2q^2 + (u_1v_1 + u_1v_2 + u_2v_2)q + 1} \quad \dots (23)$$

Similarly,

$$\begin{aligned} \frac{1}{\beta_3} = & u_1v_1u_2v_2u_3v_3q^3 + (u_1v_1u_2v_2 + u_1v_1u_2v_3 + u_1v_1u_3v_3 + u_1v_2u_3v_3 + u_2v_2u_3v_3)q^2 \\ & + (u_1v_1 + u_1v_2 + u_1v_3 + u_2v_2 + u_2v_3 + u_3v_3)q + 1 \quad \dots (24) \end{aligned}$$

Comparing (22) to (24) with (8) to (10) in order, we note that

$$\beta_k = \frac{1}{(D_0)_k}, \quad k = 1, 2, 3$$

Proceeding similarly, it can be shown that  $\beta_k = 1/(D_0)_k$ . For generalisation, it is necessary to prove that if  $\beta_k = 1/(D_0)_k$ , then  $\beta_{k+1} = 1/(D_0)_{k+1}$ . From (4), replacing  $k$  by  $(k+1)$ , we have

$$\beta_{k+1} = \frac{\beta_k}{v_{k+1}q(Z_0)_k/R + u_{k+1}v_{k+1}q + 1}$$

Since  $\beta_k = \frac{1}{(D_0)_k}$  and  $(Z_0)_k = R \frac{(N_0)_k}{(D_0)_k}$ ,

$$\begin{aligned}\beta_{k+1} &= \frac{1}{v_{k+1}q(N_0)_k + (D_0)_k(u_{k+1}v_{k+1}q + 1)} \\ &= \frac{1}{(D_0)_{k+1}} \quad \text{from equation (13b).}\end{aligned}$$

Thus, in general,

$$\beta_n = \frac{1}{(D_0)_n}$$

The above is true for all the cases. Thus if  $(Z_0)_n$  is known,  $\beta_n$  is simply obtained as the inverse of the denominator polynomial.

## VI. INPUT IMPEDANCE

Putting  $k = n-1$  in Eq. (2) and noting that  $(Z_i)_n = \infty$  we have

$$\begin{aligned}(Z_i)_{n-1} &= \frac{1}{pC} \frac{u_n v_n q + 1}{v_n} = \frac{1}{pC} \frac{(A_1)_{n-1}q + (A_0)_{n-1}}{(B_0)_{n-1}} \\ &= \frac{1}{pC} \frac{(N_i)_{n-1}(q)}{(D_i)_{n-1}(q)} \quad \dots (26)\end{aligned}$$

Putting  $k = n-2$  in (2) and substituting for  $(Z_i)_{n-1}$  from Eq. (26), we have

$$(Z_i)_{n-2} = \frac{1}{pC} \frac{(N_i)_{n-2}(q)}{(D_i)_{n-2}(q)} \quad \dots (27a)$$

where

$$\begin{aligned}(N_i)_{n-2}(q) &= u_{n-1}v_{n-1}u_n v_n q^2 + (u_{n-1}v_{n-1} + u_{n-1}v_n + u_n v_n)q + 1 \\ &= (A_2)_{n-2}q^2 + (A_1)_{n-2}q + (A_0)_{n-2} \quad \dots (27b)\end{aligned}$$

and

$$\begin{aligned}(D_i)_{n-2}(q) &= v_{n-1}u_n v_n q + (v_{n-1} + v_n) \\ &= (B_1)_{n-2}q + (B_0)_{n-2}\end{aligned}\quad \dots \quad (27c)$$

Similarly,

$$(Z_i)_{n-3} = \frac{1}{pC} \frac{(N_i)_{n-3}(q)}{(D_i)_{n-3}(q)} \quad \dots \quad (28a)$$

where

$$\begin{aligned}(N_i)_{n-3}(q) &= u_{n-2}v_{n-2}u_{n-1}v_{n-1}u_n v_n q^3 \\ &\quad + (u_{n-2}v_{n-2}u_{n-1}v_{n-1} + u_{n-2}v_{n-2}u_{n-1}v_n \\ &\quad + u_{n-2}v_{n-2}u_n v_n + u_{n-2}v_{n-1}u_n v_n \\ &\quad + u_{n-1}v_{n-1}u_n v_n)q^2 + (u_{n-2}v_{n-2} + u_{n-2}v_{n-1} \\ &\quad + u_{n-2}v_n + u_{n-1}v_{n-1} + u_{n-1}v_n + u_n v_n)q + 1 \\ &= (A_3)_{n-3}q^3 + (A_2)_{n-3}q^2 + (A_1)_{n-3}q + (A_0)_{n-3}\end{aligned}\quad \dots \quad (28b)$$

and

$$\begin{aligned}(D_i)_{n-3}(q) &= v_{n-2}u_{n-1}v_{n-1}u_n v_n q^2 + (v_{n-2}u_{n-1}v_{n-1} \\ &\quad + v_{n-2}u_{n-1}v_n + v_{n-2}u_n v_n + v_{n-1}u_n v_n)q + (v_{n-2} + v_{n-1} + v_n) \\ &= (B_2)_{n-3}q^2 + (B_1)_{n-3}q + (B_0)_{n-3}\end{aligned}\quad \dots \quad (28c)$$

Expressions (26) to (28) bear some similarity with the corresponding expressions (8) to (10) for  $Z_0$ . In this case, however, the numerator coefficients are to be regarded as the basic quantities and the denominator coefficients are to be derived from them. Proceeding in a manner exactly similar to that in deriving the expression for  $Z_0$ , it can be shown that the input impedance of an  $n$ -mesh  $R$ - $C$  ladder is given by

$$(Z_i)_0 = \frac{1}{pC} \frac{\sum_{r=0}^n (A_{n-r})_0 q^{n-r}}{\sum_{r=0}^{n-1} (B_{n-r-1})_0 q^{n-r-1}} \quad \dots \quad (29)$$

where  $(A_0)_0 = 1$ ,  $(A_{n-r})_0$  is to be obtained by following rules 2 to 6, with  $(B_{k-r})_k$  replaced by  $(A_{n-r})_0$ , and  $k$  by  $n$ , and  $(B_{n-r-1})_0$  is to be calculated by the following formula :

$$(B_{n-r-1})_0 = \frac{(A_{n-r})_0 - \sum T_1}{\dots} \quad \dots \quad (30)$$

The input impedance for the  $C-R$  case is given by a formula similar to (29) with  $u$  replaced by  $U$ ,  $v$  by  $V$ ,  $q$  by  $Q$  and  $1/(pC)$  by  $R$ , where  $U$ ,  $V$  and  $Q$  are respectively the inverse of  $v$ ,  $u$  and  $q$ .

# RL LADDER NETWORKS

The two forms of ladder networks containing resistance and inductance only are shown in Fig. 4; the element values are chosen as follows :

$$R_k = u_k R \quad \text{and} \quad L_k = L/v_k$$

for the  $R-L$  case (Fig. 4a) and

$$L_k = U_k L \quad \text{and} \quad R'_k = R/V_k$$

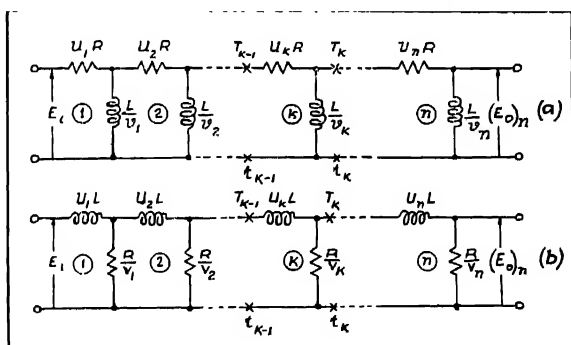


Fig. 4. Showing forms of general resistance-inductance ladder networks ; (a)  $R-L$  form  
(b)  $L-R$  form.

for the  $L-R$  case, (Fig. 4b). Then the recurrence relations for the output impedance are given by

$$(Z_0)_k = R \frac{(Z_0)_{k-1}/R + u_k}{v_k(Z_0)_{k-1}/(pL) + u_k v_k q + 1} \quad \dots \quad (31)$$

$$(Z_0)_k = pL \frac{(Z_0)_{k-1}/(pL) + U_k}{V_k(Z_0)_{k-1}/R + U_k V_k Q + 1} \quad \dots \quad (32)$$

where  $q = R/(pL)$  and  $Q = pL/R$ . Now computing  $(Z_0)_k$  for  $k = 1, 2$  and  $3$  for both the cases, it will be easily seen that the  $R-L$  and the  $L-R$  cases have become identical with  $R-C$  and  $C-R$  cases respectively, except for replacement of  $1/(pC)$  by  $pL$  and the interpretations of  $q$  and  $Q$ . Once  $(Z_0)_n$  is found,  $\beta_n$  and  $(Z_i)_0$  can be easily obtained as in the previous cases.

## L-C LADDER NETWORKS

The two forms of inductance capacitance ladder networks are shown in Fig. 5, where the elements have been chosen as follows :

$$L_k = u_k L \quad \text{and} \quad C_k = v_k C$$

for the  $L$ - $C$  case and

$$L_k = L/v_k \quad \text{and} \quad C_k = C/u_k$$

for the  $C$ - $L$  case. The recurrence relations for the output impedance can be found to be given by

$$\frac{(Z_0)_k}{L-C \text{ case}} = pL \frac{(Z_0)_{k-1}/(pL) + u_k}{pCv_k(Z_0)_{k-1} + u_kv_kq + 1} \quad \dots (33)$$

$$\frac{(Z_0)_k}{C-L \text{ case}} = \frac{1}{pC} \frac{pC(Z_0)_{k-1} + U_k}{V_k(Z_0)_{k-1}/(pL) + U_kv_kQ + 1} \quad \dots (34)$$

where  $q = p^2LC$  and  $Q = 1/(p^2LC)$ . Relation (33) is the same as (3) with  $R$  replaced by  $pL$  and  $q$  interpreted as  $p^2LC$ . Similarly, relation (34) is the same as (17) with  $R$  replaced by  $pL$  and  $Q$  interpreted as  $1/(p^2LC)$ . With these modifications, the  $L$ - $C$  and  $C$ - $L$  cases become identical with  $R$ - $C$  and  $C$ - $R$  cases respectively.

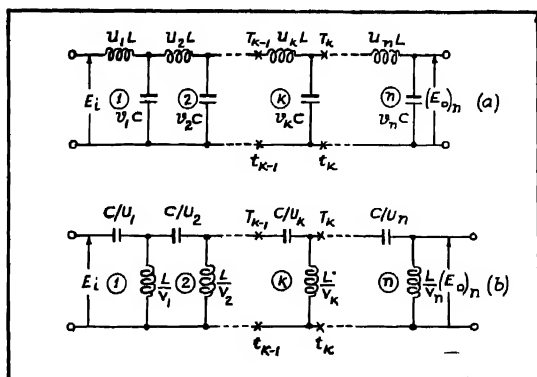


Fig. 5. Showing forms of general inductance capacitance ladder networks : (a)  $L$ - $C$  form and (b)  $C$ - $L$  form.

## CONCLUSION

A technique has been presented for finding the terminal impedances and transfer function of general two element ladder networks; the final expressions

are obtained as a ratio of polynomials in  $pCR$  or  $1/(pCR)$  ( $RC$  ladder),  $pL/R$  or  $R/(pL)$  ( $RL$  ladder), and  $p^2LC$  or  $1/(p^2LC)$  ( $LC$  ladder) where  $R$ ,  $L$  and  $C$  are normalising parameters. It has been shown that the coefficients in one of the polynomials can be obtained in terms of known constants  $u_k$  or  $U_k$  and  $v_k$  or  $V_k$  by empirical rules; the coefficients of the other polynomial are obtained from those of the first by using a simple formula.

#### ACKNOWLEDGMENTS

The author is deeply indebted to Prof. J. N. Bhar, Head of the Department of Radio Physics and Electronics, Calcutta University, for his constant help and guidance in the work. Grateful thanks are due to Dr. A. K. Choudhury and Dr. B. R. Nag of the above Department for their helpful criticism and suggestions. The author is also thankful to Shri B. Maitra, Director, River Research Institute, West Bengal, for his kind permission to publish this work.

#### REFERENCES

- Bhattacharya, B. K., 1952, *Ind. J. Phys.*, **28**, 563.  
Tehudi, E. W., 1950, *Proc. I.R.E.*, **38**, 309.

## A NATURAL OCCURRENCE OF BETA FORM OF IRON OXY HYDROXIDE\*

K. C. CHANDY

MINERALOGIST, GEOLOGICAL SURVEY OF INDIA, CALCUTTA, INDIA

(Received May, 17, 1962)

**ABSTRACT.** The heavy mineral fractions of a natural coke (Jhama) from borehole JK-5 at Kirkend, Jharia coal field, India, have been investigated by X-ray diffraction methods. In addition to the minerals feldspars, calcite, siderite, apatite, ilmenite, dolomite, goethite, hematite, magnetite, and quartz, it was found that one sample of coke from depth 3785'-4" in the borehole contained the beta form of iron oxyhydroxide which is not reported to occur in the natural state. This occurrence is described and discussed in the light of existing knowledge on the conditions of formation of beta iron oxyhydroxide.

Natural coke (Jhama) formed by contact action of intrusive lamprophyre sill is common in the coal fields of the Damodar Valley. As part of a programme of research on natural coke conducted by the Petrology Division of the Geological Survey of India, the heavy mineral fractions of the natural coke from borehole JK-5 at Kirkend, Jharia coal field, India, have been investigated by X-ray diffraction methods. Of these, one sample showed the presence of the Beta form of Iron Oxy hydroxide. This note gives the details of the occurrence.

The coke from depth 3785'-4" in the borehole was powdered and the heavy fraction separated in Bromoform. The yield was very poor, consisting of a few dark coloured opaque grains. Under the binocular microscope, many similar as well as different types of grains could be discerned. There were many clear and transparent crystal fragments. Some brownish black grains with patches of brownish red on them were highly magnetic as tested by a hand magnet.

In view of the limited material available and to facilitate X-ray identification, the following procedure was adopted :

- (1) The heavy mineral fraction separated in bromoform was powdered and the brick red powder was coated on a thin glass fibre. X-ray diffraction pattern recorded in a philips 114.6 mm camera using filtered iron radiation yielded the spacings recorded in column II of Table I.
- 2) After separating the heavy fraction as in 1 above, the highly magnetic grains were removed by a hand magnet. The few grains obtained were carefully crushed in an agate mortar and loaded into a Lindemann

---

\* Published with the approval of the Director General, Geological Survey of India, Calcutta.



glass capillary. A pattern recorded under same conditions as above gave the spacings listed in column III of Table 1.

- 3) The material remaining after operation 2 was placed on the stage of a binocular microscope. By means of a hypodermic needle attached to an India rubber bulb, similar looking grains were picked out and mounted at the tip of a tapered drop of canada balsam formed at the end of a stiff glass fibre. The X-ray beam was allowed to penetrate the tip of the globule in order to record the pattern of the grains. As a result of this investigation, the following minerals were found to be present in the heavy fraction of this natural coke :—feldspars, calcite, siderite, apatite, ilmenite, dolomite, goethite, hematite, magnetite, and quartz. In the course of this work, a few brownish red grains which appeared like broken bits of brownish red sealing wax under the microscope were encountered. Two of these grains could be mounted. Column IV of Table 1 gives the diffraction spacings recorded with this specimen.

TABLE I

Line No.	Heavy fraction	Magnetic grains	Non-magnetic grains	Sample III heat treated	Hematite A.S.T.M. 1-1053	Magnetite A.S.T.M. 1-1111	Goethite A.S.T.M. 2-0272
I	II	III	IV	V	VI	VII	VIII
1	7.43(m)	7.43(m)	7.42(m)				
2	5.25(w)	5.24(vw)	5.25(w)				
3			5.00(vw)				5.00(20N)
4	4.84(vvw)	4.82(vw)		4.84(vvw)		4.85(6)	
5			4.63(vw)				4.6(40B)
6	4.20(w), b	4.19(m)	4.19(vs)	4.22(vvw), b			4.18(100)
7			3.71(vw)				
8	3.68(vw)	3.68(w)		3.09(m)	3.68(18)		
9	3.56(vvw), a, d			3.58(vvw)			
10			3.36(vvw)				3.36(30)
11	3.33(mbsp), b	3.33(m)	3.32(s)	3.34(wsp), b			
12	3.18(wsp), f		3.19(w)				
13	3.03(m), c	3.03(w), c		3.03(m), e			
14	2.96(vw)	2.96(m)	2.97(vvw)	2.96(w)		2.97(28)	2.98(20B)
15	2.81(vw), g, d	2.82(m), g, d		2.81(w), g, d			
16		2.74(vvw), e					
17	2.69(mb)	2.69(s)	2.70(m)	2.70(m)	2.69(100)		2.69(80)
18	2.62(vvw)	2.62(vw)	2.627(vw)				
19			2.585(w)				2.57(20N)
20	2.52(vsb)	2.53(vsb)	2.539(m)	2.52(vs)	2.51(75)	2.53(100)	
21	2.41(vvw)	2.45(w)	2.45(s)	2.42(vvw)		2.42(11)	2.45(80)
22	2.35(vvw)	2.378(vvw)					

TABLE I (contd.)

Line No.	Heavy fraction	Magnetic grains	Non-magnetic grains	Sample III heat treated	Hematite A.S.T.M. 1-1053	Magnetite A.S.T.M. 1-1111	Goethite A.S.T.M. 2-0272
23	2.28(vvw) c.	2.285(w),	2.289(w)	2.29(vvw),			
24			2.25(w)				2.25(30)
25	2.197(vw)	2.20(m)	2.19(w)	2.20(w)	2.20(18)		2.18(50)
26	2.153(w)	2.158(vw)		2.15(vw)			
27	2.092(vw)	2.096(m)	2.096(vvw)	2.00(w)		2.10(32)	2.09(5P)
28	2.058 (vw)	2.052(vw)					
29	2.01(vvw) e	2.02(vw),					2.00(10N)
30	1.939 (vw)	1.943(w)	1.952(vw)				
31	1.853(wb)	1.838(m)		1.85(w)	1.84(63)		
32			1.81(vw)				1.80(40)
33	1.748 (vw), d	1.774(w)	1.75(vw)				
34		1.718(m)	1.724(mb)			1.71(16)	1.72(70)
35	1.696(nb)	1.692(s)		1.696(w)	1.69(63)		1.69(30N)
36	1.637(vw)	1.636(m)	1.639(w)				
37	1.612(vw)	1.613(m)	1.61(vvw)	1.605(w)	1.60(13)	1.61(64)	1.60(30)
38	1.59(vw)						
39		1.56(w)	1.567(w)				1.56(50)
40	1.519 (vw)	1.51(w)	1.515(m)				1.51(40)
41	1.482(mb)	1.484(s)	1.479 (vw)	1.486(mb)	1.491(50)	1.48(80)	* 1.47(40B)
42	1.45(mb)	1.452(m)	1.453(w)	1.452(w)	1.45(50)		1.45(50)
43		1.418(vw)	1.423 (vw)				1.42(20N)
44	1.378 (vw)	1.376(vw)	1.380(vw)				1.39(20N)
45							1.36(30N)
46	1.316 (vw)	1.311(w)	1.318 (vw)	1.318 (vw)	1.31(18)	1.33(6)	1.32(30)
47	1.28(vvw)	1.278(vw)				1.28(20)	1.29(20N)
48	1.144 (vw)	1.148(w)	1.149(w)		1.14(13)		
49	1.092 (vw)	1.092(w)		1.09(vvw)		1.09(32)	

II Heavy fraction of the natural coke (sinking in Bromoform).

III Magnetic grains picked out from II by a hand magnet.

IV Non-magnetic grains picked out from fraction II.

V A portion of sample of II after heat treatment at 280°-300°C.

B Broad

sp spots superposed/spotty line

a line due to anatase

b line due to quartz

c line due to calcite

d line due to siderite

e line due to Ilmenite

f line due to feldspar

g line due to Apatite

Other symbols have usual meanings.

All spacings are in Angstrom Units and the intensities are given within parentheses.

A study of Columns II, III, and IV of Table I shows that in all the three patterns there are certain prominent lines common to them, which have not been accounted for as due to any mineral. These lines have been picked out and recorded in column II of Table II. An attempt was made to account for these lines. It was interesting to note that these lines were always present with one or more of the iron minerals goethite, hematite, magnetite, and siderite, suggesting incidentally, that they may belong to an iron compound. A comparison of these spacings with those of known iron compounds showed that they agreed closely with those of Beta iron oxy hydroxide. The X-ray data for this compound as obtained from literature are given in columns III to VII of Table II. It may be noted from Table I that the other lines of Beta form of iron oxy hydroxide are also present in the X-ray patterns though overlapped by lines with similar spacings of other constituents.

The presence of Beta iron oxy hydroxide was further confirmed by heating experiments. It is reported in literature that all the known iron oxy hydroxides transform into oxides of iron at a temperature around 250°C. A portion of the sample used in taking the pattern for data of column II of Table I was heated between 280-300°C for about 3 hours. The spacings obtained from this heated sample are recorded in column V of Table I. Though the lines were diffuse, the new spacings are consistent with the transformation of beta iron oxy hydroxide and goethite to hematite. The presence of the other components in the heated sample shows that they remain unchanged at this temperature.

Further attempts to get a purer fraction of Beta iron oxy hydroxide alone were not successful. However, it may be noted that the sample concerned with the data of column IV of Table I (this is repeated in column VIII of table 2) contains practically goethite and beta iron oxy hydroxide only.

A recent study (Das Gupta and Mackay, 1959) has shown that  $\text{Cl}^-$  or  $\text{F}^-$  ions (but not  $\text{Br}^-$  ions) are necessary for the formation of Beta iron oxy hydroxide which can be prepared artificially by the hydrolysis of any ferric compound in the presence of the above ions. In the present case, the amount of heavy fraction was so small that no chemical analysis could be conducted. However, it may be noted that  $\text{Cl}^-$  and  $\text{F}^-$  ions are readily available in the volatiles from the lamprophyre which causes natural coke formation. So the presence of beta iron oxy hydroxide in the natural coke is consistent with its conditions of formation. It is interesting to note here that this form of iron oxy hydroxide is not reported to occur in the natural state\*\*, though van Schuylenborgh (1949) has concluded from his study that it may occur along with limonites (goethite); an association borne out by this study.

#### ACKNOWLEDGMENT

The author gratefully acknowledges the kind encouragement and keen interest shown by Dr. M. V. N. Murthy, Superintending Geologist in-charge,

TABLE II

Line No.	Some Common Lines	X-ray data for Beta FeO.OH.					Non-mag-netic grains††
		A.S.T.M. 1-0662	A.S.T.M. 3-0440	A.S.T.M. 3-0430	A.S.T.M. 5-0480	Das Gupta† (1960)	
I	II	III	IV	V	VI	VII	VIII
1	7.43	7.4(63)	7.45(80)	7.46(90)	7.6(85)	7.403(vs)	7.42(m)
2	5.25	5.26(5)	5.26(80)	5.20(70)	5.3(75)	5.249(m)	5.25(w)
3				3.71(30)		3.704(vw)	3.71(vw)
4		3.33(100)	3.32(100)	3.33(100)	3.33(100)	3.311(vs)	3.32(S)
5	2.627	2.64(15)	2.64(40)	2.63(60)	2.62(45)	2.616(m)	2.627(vw)
6		2.55(75)	2.54(100)	2.55(90)	2.55(80)	2.543(s)	2.539(m)
7		2.37(5)	2.36(10)	2.36(40)		2.343(w)	
8		2.29(25)	2.28(80)	2.29(80)	2.28(40)	2.285(m)	2.289(w)
9		2.10(5)	2.10(20)	2.10(40)	2.09(15)	2.097(w)	2.096 (vw)-G
10				2.06(30)	2.05(15)	2.064(w)	
11	1.952	1.96(25)	1.94(40)	1.95(70)	1.94(35)	1.944(ms)	1.952(vw)
12		1.87(5)	1.85(10)	1.86(20)	1.84(15)	1.854(vw)	
13		1.75(10)		1.76(45)	1.74(25)	1.746(m)	1.75(vw)
14			1.71(10)	1.73(15)		1.719(vw)	1.724 (mB)-G
15	1.639	1.65(45)	1.63(100)	1.64(80)	1.63(55)	1.635(vs)	1.639(w)
16			1.55(10)				
17		1.51(15)	1.51(50)	1.52(55)	1.51(15)	1.513(m)	1.515 (m)-G
18		1.49(5)	1.48(40)	1.49(30)	1.483(10)	1.497(w)	1.479 (vw)-G
19						1.480(w)	
20		1.45(25)	1.44(60)	1.45(60)	1.434(30)	1.438(s)	1.453 (w)-G
21		1.38(15)	1.38(60)	1.38(50)	1.373(20)	1.374(m)	1.380 (vw)-G
22		1.32(5)	1.31(40)	1.31(40)	1.310(8)	—	1.318 (vw)-G
23		1.24(5)			1.221(5)		
24		1.15(5)	1.14(60)	1.142(10)			1.149(w)

†† Data from column IV, Table I, after eliminating lines due to Goethite only.

α Overlapped by lines due to Goethite.

NOTE: All spacings are in Angstrom units, and intensity estimation are given within brackets.

Petrology Division, during the course of this investigation. My thanks are due to my colleagues in the Mineral Physics section, specially to Dr. D. R. Das Gupta for very interesting and stimulating discussions, and to Mr. S. P. Sanyal, Asst. Geologist, who has helped me with the heavy mineral separation.

#### R E F E R E N C E S

Das Gupta, D. R., and Mackay, A. L., (1959), *Jour. Phys. Soc., Japan*, **14**, 932.

Das Gupta, D. R. Ph.D. (1960) Thesis, University of London.

Van Schuylenborgh, J., and Sanger, A. M. H., (1949), *Rec. Trav. Chim. Pays-Bas*, **68**, 999-1010.

\*\* In a paper entitled "Strengite, Phosphosiderite, Cacoenite et apatite fibroradice de Richelle" Van Tassel, R., has recorded an earlier occurrence of Beta  $\text{FeO.OH}$  in the Journal "Bull De La Soc. Belge De Geologie, **68**, 360-67, 1959". According to him, small cavities in Phosphate rich breccias in Paleozoic limestone at Richelle, Belgium are frequently lined with a brown coating composed of amorphous iron phosphate (delvauxite,, goethite, and Beta  $\text{FeO.OH}$  which were identified by their X-ray patterns. The author is indebted to Dr. A. L. Mackay, Birkbeck College, London, for this reference which was received after announcement of the present occurrence in Indian minerals, Vol. 15, No. 12, p. 197 1961. The association of Beta  $\text{FeO.OH}$  with Goethite is clear in both cases.

# THE CORRELATION OF SPREAD ON ONE NIGHT AND THE SUCCESSIVE NIGHTS

M. S. V. GOPAL RAO AND B. RAMACHANDRA RAO

(IONOSPHERIC RESEARCH LABORATORIES, PHYSICS DEPARTMENT, ANDHRA  
UNIVERSITY, WALTAIR)

(Received April 30, 1962)

**ABSTRACT.** A correlation coefficients of spread  $-F$  on one night and the successive nights were estimated and it was found that it is positive and significant for 24-hour time shift for Waltair data. Data for first half night showed better correlation both for 24- and 48-hour time shifts. There is a distinct seasonal variation in the correlation. The correlation for Kodalkanal data is not significant for most part of the year.

In his study of radio star scintillations Hewish (1952) observed that days with large fluctuations tended to occur in groups. Because of the close correlations between these scintillations and spread  $F$  observed on ionograms it is possible that nights of large spread  $F$  index may also tend to occur in groups. Briggs (1958) investigated this aspect by finding correlation coefficients between the mean spread  $F$  index for one night and successive nights for Slough and Inverness stations. He obtained significant positive correlation coefficients for some months for time shifts of 24 hours and positive coefficients of reduced significance were obtained for 48 hours time shifts. In view of the gross differences in the spread  $F$  characteristics between high and low latitudes it will be of interest to examine this recurrence tendency of spread  $F$  on successive nights at equatorial latitudes. Spread  $F$  index data collected at Waltair utilising the 0-10 index scheme of Gopal Rao *et al.*, (1960) and that of Kodalkanal reduced from the regular  $f_oF_2$  data bulletins following Briggs (1958) 0-3 index system have been used in this study.

As the phenomenon of spread  $F$  is predominant during the pre-midnight period, the data for the months of January and February, 1959 is taken throughout night and the first and second half night data are analysed separately with a view to find if there is any difference in behaviour. For this purpose the mean spread  $F$  index is obtained separately for the first half and second half night time data and correlation coefficients are obtained for 24 and 48 hours time shifts. The results thus obtained are shown in Table I along with the values obtained for the full night data. Similar analysis is carried out over an extended period of one year from March 1959 to February, 1960 using the first half night data.

TABLE I  
Waltair (First half night) 1959-1960

Period	Time shift							
	24 hrs.				48 hrs.			
	<i>r</i>	<i>s</i>	<i>P</i> =0.01	<i>P</i> =0.05	<i>r</i>	<i>s</i>	<i>P</i> =0.01	<i>P</i> =0.05
Jan., 10 to Feb., 10, 1959 (Full night)	+0.57	±0.12			+0.28	±0.17		
First half night	+0.49	±0.14			±0.26	±0.17		
Second half night	+0.36	±0.16			+0.07	±0.17		
South Solstice	+0.47	±0.13			+0.04	±0.13	—	—
Vernal equinox	+0.08	±0.12	—	—	+0.21	±0.12	—	—
North Solstice	-0.14	±0.14	—	—	-0.41	±0.14	*	
Autumnal equinox	+0.22	±0.13	—	—	+0.03	±0.14	—	—

In view of the distinct seasonal characteristics of spread F at Waltair (Rao and Rao 1961), the data is divided into four parts, two corresponding to equinoctial and the other two to solstitial seasons. The correlation coefficients thus obtained for each season are shown in Table I along with the value. The significance of the coefficients is tested at  $P = 0.01$  level and indicated by asterisk if significant and dash if not significant. Results of a similar analysis for Kodaikanal are shown in Table II.

TABLE II  
Kodaikanal, 1955-1956

Period	Time shift							
	24 hrs (first half night)				24 hrs. (full night)			
	<i>r</i>	<i>s</i>	<i>P</i> =0.01	<i>P</i> =0.05	<i>r</i>	<i>s</i>	<i>P</i> =0.01	<i>P</i> =0.05
South Solstice	-0.08	±0.12	—	—	+0.02	±0.12	—	—
Vernal equinox	-0.06	±0.11	—	—	+0.03	±0.11	—	—
North Solstice	-0.08	±0.11	—	—	-0.27	±0.10	*	
Autumnal equinox	+0.21	±0.10	—	—	+0.06	±0.11	—	—

Considering the results for the full night data for January—February, 1959, it will be seen from the results presented in Table I that the correlation coefficients are in general significant and positive for 24 hour time shift and positive but less significant for 48 hours time shift, a result which is in agreement with that reported

by Briggs. The data for the first half night showed better correlation both for 24 hour and 48 hours time shifts compared to the second half night time data.

The results of Waltair for the various seasons using first half night data indicate that the day to day recurrence tendency of spread F is strongest only during south solstice and is moderate during autumnal equinox and poor during rest of the year. Further, during north solstice the coefficients turned negative also. For 48 hours time shift it is significantly negative during north solstice indicating large variations in the spread F on alternate nights. The coefficients at Kodaikanal are in general not significant during most part of the year except during north solstice when it is found to be significantly negative, using the full night data. The overall picture seems to suggest that at these equatorial latitudes the day to day recurrence tendency of spread F is observable, if any, during local winter only and is completely reversed during local summer months. Examining these results in the light of the results reported by Briggs<sup>2</sup> (1958) for high latitudes, it appears that this recurrence tendency of spread F on successive or alternate nights will be stronger at higher latitudes than at equatorial stations.

It is becoming well known that equatorial spread F is inhibited during magnetic storms. If a severe magnetic storm commences and remains for a few days, it will cause high spread F activity at high latitudes and keeps calm conditions without spread F at equatorial stations. Thus at low latitudes it is quite likely that nights without spread F may occur in groups than those of high or low spread F as observed at high latitudes.

#### ACKNOWLEDGMENT

We are indebted to the Council of Scientific and Industrial Research (India) for the financial support of these investigations. One of the authors (M.S.V.G. Rao) is thankful to the Council for the award of Senior Research Fellowship.

#### REFERENCES

- Briggs, B. H. 1958. *J. Atmos. Terr. Phys.*, **12**, 34.  
 Howish, A. 1952, *Proc. Roy. Soc.*, **A-214**, 494.  
 Rao, M. S. V. G. Gopal, Rao, B. Ramachandra and Ramachandra Rao Pant, P. 1960. *J. Atmos. Terr. Phys.*, **17**, 345.  
 Rao M. S. V. G. Gopal, and Rao B. Ramachandra, 1961. *J. Atmos. Terr. Phys.*, **22**, 12.



# Letters to the Editor

*The Board of Editors will not hold itself responsible for opinions expressed in the letters published in this section. The notes containing reports of new work communicated for this section should not contain many figures and should not exceed 500 words in length. The contributions must reach the Assistant Editor not later than the 15th of the second month preceding that of the issue in which the letter is to appear. No proof will be sent to the authors.*

## 8

### UNIT CELL AND SPACE GROUP OF THIODIGLYCOLLIC ACID

SUKLA ROY

DEPARTMENT OF GENERAL PHYSICS AND X-RAY, INDIAN ASSOCIATION FOR THE  
CULTIVATION OF SCIENCE, CALCUTTA 32

(Received May 4, 1962)

Thiodiglycollic acid,  $\text{HO}_2\text{C}-\text{H}_2\text{C}-\text{S}-\text{CH}_2-\text{CO}_2\text{H}$ , is of interest because of its use as a precipitating organic reagent for zirconium (Sant and Sant, 1959). It is also used for the detection of copper, lead, mercury and silver and for the estimation of cadmium.

Recently, we have started studying the crystal structures of various organic analytical reagents and their metal derivatives and the investigation of the crystal structure of thiodiglycollic acid was undertaken in this connection.

Satisfactory single crystals were obtained by evaporation at room temperature of a concentrated aqueous solution of the compound. The crystals appeared as plates elongated in a direction subsequently designated as the 'a' axis.

Oscillation, zero- and first-layer Weissenberg pictures were taken along both the 'a' and the 'b' axis, using copper X-ray radiation. The crystal is found to be orthorhombic with

$$a = 5.03 \pm .03 \text{ \AA}$$

$$b = 6.6 \pm .03 \text{ \AA}$$

$$c = 17.74 \pm .03 \text{ \AA}$$

The observed density is 1.66 gm/cc. The calculated density for four molecules is 1.70 gm/cc. Therefore, there are 4 molecules per unit cell.

On indexing the Weissenberg photograph the following extinction conditions were observed.

$o\ o\ l$	absent for $l \neq 2n$
$o\ k\ o$	absent for $k \neq 2n$
$h\ o\ o$	absent for $h \neq 2n$
$o\ k\ l$	absent for $k+l \neq 2n$
$h\ o\ l$	absent for $h \neq 2n$
$h\ k\ o$	no systematic absence.
$h\ k\ l$	no systematic absence.

The space group is thus either  $Pna2_1$  or  $Pnam$ . It may be seen that the axes have been so assigned as to conform to the space group symbol  $Pna2_1$  rather than conform to the convention  $c < a < b$ . Further work is in progress.

The author is thankful to Prof. B. N. Srivastava, D.Sc., F.N.I., for his keen interest in the problem and to Dr. Sankar K. Dutta for suggesting the problem and guidance throughout the piece of work.

#### REFERENCE

Sant, S. B., and Sant, B. R., 1959, *Anal. Chem. Acta*, 21, 221-3.

## BOOK REVIEW

**THE ABUNDANCE OF THE ELEMENTS.** By Lawrence H. Aller. Pp. 283 + xi; Interscience Monographs and Texts in Physics and Astronomy, Vol. VII. Interscience Publishers. New York, London, 1961. \$ Price 10.00.

In this book the author presents our knowledge on the quantitative distribution of the elements in the 'Universe' at the present age. The contributions to elemental abundance from different sources such as the sun and stars, the gaseous nebulae, the interstellar medium, cosmic rays, the earth's crust and the meteorites have been discussed in five different chapters, where a good deal of astrophysics is summarised.

The discussion on abundance of isotopes of different elements is given in Chapter 7, which is followed by a chapter wherein a revised Suess-Urey compilation of abundances is presented. Stress has been laid on the experimental data and the theory of the formation of isotopes and of stability of nuclei has been dealt with in brief. In the chapter on 'Composition Differences between Stars' the author presents an well informative discussion on difference of elemental abundance in stars of different ages and based on deductions of spectroscopical observations, and accordingly explains the nomenclature of 'helium stars', 'carbon stars', heavy metal stars, etc.

In the last chapter the author discusses in detail different theories and hypotheses of nucleogenesis, especially of Burbidges, Fowler and Hoyle and their bearings on the problem of elemental abundances.

The book is full of up-to-date information from various sources, the clarity and scholarly presentation of the subject matter will be appreciated both by research workers and students and by people interested in cosmogony.

*B. N. Bhar.*



# PERIODICITY AND STRUCTURAL DEVELOPMENT IN NUCLEI

A. K. DUTTA, B. PAL, A. DAS GUPTA AND N. CHAUDHURY

PALIT LABORATORY OF PHYSICS, CALCUTTA UNIVERSITY.

(Received June 1, 1962)

**ABSTRACT.** The deviations of the stable nuclear masses from the Bethe-Weizsacker relation have been determined with the help of the constants previously determined by Green (1954) as well as by a new set of constants determined now. The masses were taken from Everlings (1960) data. The deviations fall on a number of periodic curves connected through the isotopes on excess neutron basis. The minima of the periodic curves show a nearly constant charge variation and a liquid crystal structure has been suggested for the nuclei, composed of different subgroups of elementary nuclei Li, Be and B. The number of subgroups in a composite structure explains the observed periodicity. The cohesion energy between the subgroups obtains a nearly constant value per unit.

## INTRODUCTION

In a short note, one of us (Dutta, 1961) has shown on a number of periodic curves, the distribution of the experimental deviations of stable nuclear masses from the Bethe-Weizsacker relation. The experimental mass values were taken from Duckworth's compilation (1958). There were only few data available beyond the element 62, and the curves were, therefore, limited to that extent. The constants used for the Bethe-Weizsacker relation were those suggested by Green. They had been determined on an indirect procedure of evaluation (Green, 1954), with stages of approximation.

We have taken now the more complete data of Everling (1960), which are not always identical with Duckworth's values. We have plotted with the help of Green's constants, the deviations  $\Delta M$  of the stable nuclei against mass number, in Fig. 1(a), with the oxygen mass scale as the standard. We have also redetermined the constants of the Bethe-Weizsacker relation by the method of least squares. We have used for the purpose the complete summation over the 250 stable isotopes, the relevant binding energy data being taken from Everling's table. The constants of the relation,

$$E = -a_1 A + a_2 A^{2/3} + a_3 Z^2 A^{-1/3} + a_4 (N-Z)^2 / 4A,$$

so determined, modify those suggested by Green, as shown in Table I below.

TABLE I  
Constants of the Bethe-Weiszacker relation

	$a_1$	$a_2$	$a_3$	$a_4$
Green	16.918	19.120	0.763	101.78
New Value	16.719	18.505	0.751	96.856

We have plotted, again, the  $\Delta M$  values, calculated with the new constants, in a second set of graphs, shown in the same diagram, (Fig. 1b). (Our thanks are due to the Director, Statistical laboratory for the calculation of some of the necessary data by electronic computers.)

We would now discuss the procedure for plotting the points and would try to understand the implications. We consider here the deviations  $\Delta M$ , from the Bethe-Weiszacker relation, to be accounted for by the structural energy, a minor addition on account of the structural configuration. This is a generally accepted idea by workers in this line. Such deviations from the Bethe-Weiszacker relation were calculated by other workers also (Green 1958, Seeger 1961). The haphazardly distributed  $\Delta M$  plots against mass number always exhibit a periodic character of the distribution of excess mass or energy in a general way. This is shown in the plots of Green, incorporated here, in Fig 2, to make the periodic character self-evident. The sorting out of the individual curves has not been attempted before, as a general procedure. Moser (1959), however, had connected the  $\Delta M$  values for odd nuclei. In effect, this actually picks out one periodic curve from the superposition of a number of them.

In the process of sorting out of individual curves, based on structural correlation, we would be justified in correlating or joining up, all odd charge nuclei and even charge odd nuclei separately in two curves. They are expected to be structurally allied from the point of view of symmetry. The curves would indicate the corresponding structural energy fluctuation against nuclear development or mass number. In Fig. 1, we have indicated the points on these curves by crosses and solid circles, respectively. We are, thus, left with the even-even nuclei to be structurally correlated and they form the bulk of the multitude of points. From the element  $Z = 10$ ,  $N = 10$  to the element  $Z = 82$ ,  $N = 126$ , we have in all 150 stable even-even nuclei. The set gives us 37 possible elements, with a number of isotopes for each element and 59 possible variations in neutron numbers, associated with different isotones. We would, thus, have a larger number of curves run through the isotopes of different elements, than through the isotones, on any systematic basis of running through the points. It is expected to require a larger number of curves through all the 150 points to bring out the periodic nature of the individual curves and thus the curves through the isotopes

of different elements are more rational, from the desired point of view. We have, however, attempted to draw the periodic curves through the isotones; also, in spite of the limitations. To force a periodic character to the curves through the isotones, we have, at many places, given a wave form to the irregular fluctuations in consecutive points, which is without any real significance. The curves through the isotones are drawn separately in Fig. 1(c).

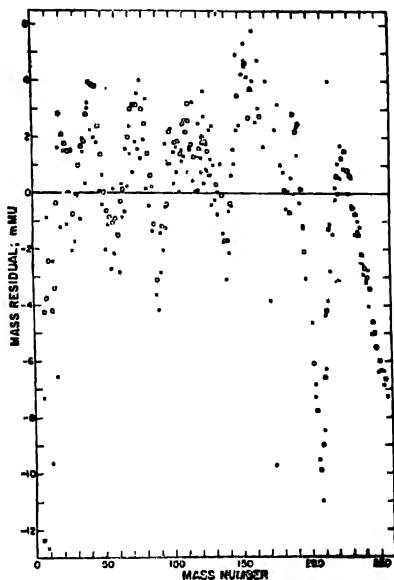


Fig. 2. Deviations  $\Delta M$  against mass number from Green, (1958),

We come, now, to the choice of even-even isotopes, as also of the isotones to be joined in a sequence. In an attempt to explain the structural periodicity of the nuclei, on the basis of the shell model, Seeger (1961) had modified the Bethe-Weizsacker relation and had incorporated a structural term in the relation,

$$\Delta M = \Delta M_{\text{seeger}} - S_{jk}(N', Z'),$$

where the structural term  $S_{jk}(N', Z')$  is to be determined by the relation,

$$S_{jk}(N', Z') = \zeta_j \sin N'\pi + \zeta_k \sin Z'\pi + \nu_j \sin 2N'\pi + \nu_k \sin 2Z'\pi \\ + (\phi_j + \phi_k) \sin N'\pi \sin Z'\pi + \chi.$$





of nucleons for the different periodicity loops. This is also satisfied by the magic numbers. Further, in order to satisfy the basic requirement of a balanced distribution of protons and neutrons in the nuclear space, it is necessary for the shell structure to have both the neutron and the proton numbers increasing simultaneously in periodicity loops, with increasing nuclear size. Otherwise, undue preponderance of one or the other constituent would occur in comparatively large regions of nuclear space, and this is against the basic conception of balanced nuclear composition. The findings, therefore, go against any shell model, in spite of the occurrence of some magic numbers.

We have already observed that the periodic minima are separated by approximately 14 units of charge with increasing number of neutrons, for sizes of the nuclei containing at least 130 nucleons. We have also noted that the periodicity numbers fails to satisfy the requirement of a shell structure. We have, therefore, to look for other alternative possibilities. Addition of small and nearly fixed amount of charge for periodicity, tends to suggest the growth in the form of a liquid crystal structure, and, naturally, with gradually more composite type of crystal configuration for larger nuclei. In order to explain the periodic curves on this basis, we must visualise the growth of the nuclei within a particular structure group, in such a way, that with increasing number of nucleons in that structure, they become at initial stages more strongly bound and on further addition of nucleons tend to be unstable. A more composite form of structure would, then set in, to accommodate more nucleons. Repetitions of this process would give us the periodicity curves.

We should realise that when a structure grows by addition of protons and neutrons in the same structural pattern, as in a classical procedure of two adjacent layers, we would be involving the nucleus to a gradually larger surface area. On account of the tendency of a nucleus to obtain a minimum surface area with constant spacings, we would expect with larger number of nucleons, a larger number of groups, each with a smaller nucleon number to make the structure more compact. This would cause a smaller surface area. The properties of minimum surface area and constant spacing are recognised for nuclei.

Further, for the formation of the nucleus, the major divisions composing a particular structure, should have mutual attraction between them. In order that this is ensured, we may further consider the major divisions, when they are large, to be divided into subgroups and examine them for mutual cohesivity. A strongly bound subgroup like that of a closed configuration, would have a minimum attraction towards other segments and would not have a tendency to be associated with others to form a bigger structure. Thus, each of these subgroups, when visualised separately, must be, by themselves loosely bound and in such divisions into subgroups no portion should be left out, which by itself is strongly knit. These subgroups do not imply that the nuclei are built with these smaller

units, in a process of addition. They are only visualised here in parts, as a help to understanding cohesivity throughout the entire nuclear structure.

Let us now proceed to divide the nuclear crystal space into subgroups that are liable to be strongly bound by association. This signifies that they are themselves weakly bound. It will be observed from the study of the masses of all small nuclei, given in Table III below, that the group Li,

TABLE III  
Elements and masses of small nuclei in aMU

${}_3\text{Li}^6 - 6.017$	${}_4\text{Be}^8 - 8.008$	${}_5\text{B}^{10} - 10.016$	${}_6\text{C}^{12} - 12.0038$	${}_7\text{N}^{14} - 14.0075$
${}_2\text{He}^4 - 4.0039$	${}_3\text{Li}^7 - 7.018$	${}_4\text{Be}^9 - 9.015$	${}_5\text{B}^{11} - 11.013$	${}_6\text{C}^{13} - 13.0075$
${}_3\text{Li}^8 - 8.025$	${}_4\text{Be}^{10} - 10.017$	${}_5\text{B}^{12} - 12.018$	${}_7\text{N}^{15} - 15.0050$	

Be and B, with their variations of neutron numbers have large excess masses, compared to He or C and N nuclei. They are, thus, weakly bound themselves and would tend to be more strongly bound by association. We would, therefore, propose that it is necessary to visualise a nucleus, as composed of subgroups of neutron proton arrangements which correspond to associations of these elements only, in order that cohesion is ensured throughout the nucleus. Any surplus group corresponding to associations of  ${}_2\text{He}^4$  nuclei would not tend towards close binding. The unstable  ${}_4\text{Be}^8$  nucleus also points towards that direction. This does not imply that the nuclei are actually built by the elementary nuclei Li, Be and B. It is only a way of testing the cohesive character of the entire nucleus, by parts. In fact, on disintegration, we would expect a strongly bound unit like  ${}_2\text{He}^4$  to come out of the composite structure, with a redistribution in the arrangement of the remaining nucleons. The entity corresponding to the  ${}_2\text{He}^4$  nucleus, would be less strongly bound to the other regions of the nucleus, if somehow, the entity becomes differentiated in the nuclear structure.

The periodic character of the nuclear structural curves may now be explained in the following way. The first set of maxima, with even-even nuclei, at  $Z = 10$ ,  $A = 20, 21, 22$ , correspond to nuclei association, equivalent to the sets,  $({}_5\text{B}^{10}, {}_5\text{B}^{10})$ ;  $({}_5\text{B}^{10}, {}_5\text{B}^{11})$  and  $({}_5\text{B}^{11}, {}_5\text{B}^{11})$ . The structure then changes over to a more composite character, to minimise the surface area and we get a decrease in the binding energy curve. The minima, in the following structural groups, with 14, 28, 42 and 56 units of charge correspond respectively to 4, 8, 12 and 16 subgroups arranged in a composite form. These units may be looked upon as corresponding to the Li, Be or B nuclei, having charge values of 3, 4 or 5 units, with the necessary neutron numbers to give stability to the structure. It is apparent from the data that the larger nuclei require more neutrons in each of the subgroups. Such structural rearrangement would satisfy minimum surface area. The variation of

the charges corresponding to the minima may be accounted for by slight modification of the subgroups. The occurrence of maxima in the region of charge values 20, with 4 subgroups, at 32, 34 with 8 subgroups and again in the region of 46, 48 with 12 subgroups would indicate, on this basis that the 4 subgroups structure changes to a more composite structure when they are saturated with Boron nuclei configurations. For 8 and 12 units the structure changes to a more composite form much earlier than they are saturated with the larger subgroup units. The want of a pronounced minimum in the region of 70 charge units, expected from the periodic point of view, implies that the structure with 20 subgroups are comparatively weakly bound, throughout their range of combinations. The nuclei tend to become more strongly bound again from the charge value of 78, when the structural composition of 24 units operate. This is indicated from the  $\Delta M$  curves in fig.1.

A similar consideration for the odd charge nuclei with an odd number of subdivisions, to have a basic symmetry explains the maxima and minima for the odd charge curve. The even charge odd nuclei would have an even number of subgroups, an odd number of which would contain odd neutron numbers to satisfy symmetry. The scheme appears to explain the observed periodic structure and their anomalies. At the same time it gives a tentative scheme of nuclear structure

We may further have a measure of the cohesional energy between the subgroups in a nucleus, from the data of the subgroup masses given in Table III and the mass of the nucleus. The mutual binding energy between the subgroups is derivable from the relation,

$$\text{Mutual subgroup energy} = \frac{\text{Total mass of subgroups} - \text{mass of nucleus}}{\text{number of subgroups}}$$

This gives us as an approximately constant value of the order of 19 mev for the mutual cohesion energy between the subgroups, except for few small nuclei, where the value comes down to nearly 14 Mev. The calculated values are given in Table IV below. The approximate constancy of the binding energy between the sub-groups, in all nuclei, satisfy the fundamental nuclear property of a uniform binding strength for the nucleons in all nuclei. It also justifies the structural groupings for the different composite nuclei, on which basis the values have been calculated. Automatically, therefore, it justifies the liquid crystal structure model of the nuclei, the basis of such subgroups associations. Some peculiarities of the subgroup cohesional energy data may be noted. The fission product nuclei like Ye, Kr, Sr, Zr, tend to obtain the cohesional energy values per subgroup, a little on the higher side. The nuclei in the 20 subgroup units corresponding mainly to the Rare earth group, have a tendency to obtain smaller cohesional energy. Of the smaller nuclei  ${}_8\text{O}^{16}$  may be considered to be a combination of  ${}_3\text{Li}^6$ ,  ${}_5\text{B}^{10}$  rather than of two  ${}_4\text{Be}^8$  subgroups to obtain a reasonable cohesional energy.

TABLE IV

Element	Number of subgroups	Subgroup elements	Energy per subgroup
${}^6\text{C}^{12}$	2	2 $Li^0$	14.0
${}^8\text{O}^{16}$	2	$Li^0$ , $B^{10}$	15.4
${}^8\text{O}^{16}$	2	2 $Be^8$	7.4
${}^{10}\text{Ne}^{20}$	2	2 $B^{10}$	15.4
${}^{14}\text{Si}^{28}$	4	2 $Li^0$ , 2 $Be^0$	18.6
${}^{16}\text{P}^{31}$	5	4 $Li^0$ , $Li^7$	19.0
${}^{18}\text{Ar}^{40}$	4	2 $Be^8$ , 2 $B^{12}$	17.9
${}^{10}\text{K}^{41}$	5	2 $Li^0$ , $Li^7$ , 2 $B^{11}$	19.2
${}^{27}\text{Co}^{50}$	7	2 $Li^0$ , $Li^7$ , 2 $Be^0$ , 2 $B^{11}$	20.7
${}^{28}\text{Ni}^{58}$	8	4 $Li^0$ , 2 $Be^8$ , 2 $Be^0$	18.6
${}^{32}\text{As}^{75}$	7	2 $Be^{10}$ , 5 $B^{11}$	20.3
${}^{34}\text{Se}^{74}$	8	2 $Be^8$ , 4 $Be^0$ , 2 $B^{11}$	18.2
${}^{35}\text{Br}^{70}$	11	2 $Li^0$ , 8 $Li^7$ , $B^{11}$	19.5
${}^{36}\text{Kr}^{80}$	12	4 $Li^0$ , 8 $Li^7$	20.1
${}^{40}\text{Kr}^{82}$	12	2 $Li^0$ , 10 $Li^7$	21.1
${}^{38}\text{Sr}^{88}$	12	2 $Li^0$ , 8 $Li^7$ , 2 $Be^{10}$	21.5
${}^{39}\text{Y}^{89}$	11	5 $Li^7$ , 6 $Be^0$	20.9
${}^{40}\text{Zr}^{90}$	12	2 $Li^0$ , 8 $Li^7$ , 2 $B^{11}$	21.02
${}^{42}\text{Mo}^{92}$	12	2 $Li^0$ , 4 $Li^7$ , 2 $Be^8$ , 4 $Be^0$	19.0
${}^{48}\text{Cd}^{111}$	12	9 $Be^0$ , 3 $Be^{10}$	19.0
${}^{54}\text{Xe}^{130}$	16	4 $Li^7$ , 6 $Li^0$ , 6 $Be^{10}$	21.7
${}^{50}\text{Ba}^{138}$	16	6 $Li^7$ , 2 $Li^0$ , 8 $Be^{10}$	20.1
${}^{64}\text{Gd}^{155}$	16	5 $Be^0$ , 11 $Be^{10}$	18.7
${}^{74}\text{W}^{182}$	20	2 $Li^7$ , 8 $Li^0$ , 6 $Be^{10}$ , 4 $B^{11}$	17.9
${}^{76}\text{Os}^{188}$	20	8 $Li^0$ , 8 $Be^{10}$ , 4 $B^{11}$	17.4
${}^{82}\text{Pb}^{208}$	24	4 $Li^7$ , 14 $Li^0$ , 2 $Be^{10}$ , 4 $B^{12}$	18.9

The average value of 19 mev. as the cohesional energy per subgroup, consisting of 9 nucleons, in the mean, gives us an approximate value of 2 mev. as the cohesional energy per nucleon. For the weakly bound subgroup elements considered above, the mean binding energy is of the order of a little more than 6 Mev. per nucleon. The sum total of the binding energy per nucleon for the subgroup elements and the cohesional energy per nucleon, gives us 8 Mev. as the total energy per nucleon, corroborating an already known fact. In the nuclear composition, there is, however, no particular distinction between the binding energy of the nucleons in a subgroup and the cohesional energy between subgroups. The subgroup divisions are a little artificial, as already stated and this may be done in more than one possible way. The significance of binding energy between the nucleons in a subgroup and between the different subgroups is thus lost and we are left with the total binding energy per nucleon as 8 Mev.

When, however, by some probable adjustment, a smaller subgroup becomes less affected by neighbours and more strongly bound into a helium like structure, with about 7 Mev as the binding energy per nucleon, the subgroup will be left with less cohesional energy for neighbouring subgroups. Out of the total expected 8 Mev cohesional energy for the four nucleons, 4 Mev or somewhat less has been used up for the extra binding energy of the  $4\text{He}$  nucleons. This arises from the difference of 7 Mev as the binding energy for the helium-like nucleons and 6 Mev or a little more for the weakly bound subgroup elements nucleons. We are thus left with energies of the order of 4 Mev or somewhat more as the cohesional energy to bind the 4 nucleons with other nucleons. The amount is much too small to keep the  ${}_2\text{He}^4$  group within the larger nucleus. The particle together with the extra cohesional energy, of the order of 4 mev or somewhat more is thus expected to be liberated, by such probable adjustment. The  $\alpha$ -disintegration energy is generally of this order. In the case of the  $\beta$ -disintegration involving a change in charge number by one unit, a readjustment of the subgroup number from even to odd values, with other associated changes, would be expected.

Lastly, we may state that the dynamic liquid drop model for the Bethe-Weiszacker relation from which we have started and a constant disposition of the crystalline structure considered finally are not necessarily contradictory. We presume that on account of the neutron proton exchange, there will be a rapid fluctuation of charge distribution inside the nucleus. On account of the balanced distribution of neutron and protons in the overall picture, however, there will be a superposed streaming motion of the charge and hence apparently of the nucleons, throughout the nucleus. This will give rise to a fluidity as well as a presentation of constant relative character between the neighbouring subgroups of the crystal structure to ensure cohesion.

#### A C K N O W L E D G M E N T

It is a pleasure to thank Dr. B. D. Nagchaudhuri Dr. S. Dutta Mazumdar and Dr.D. Basu, for critical discussions.

## R E F E R E N C E S

- Duckworth, H. E., 1958, *Mass Spectroscopy*, Appendix (Cambridge University Press).  
Dutta, A. K., 1961, *Ind. J. Phys.*, **35**, 591.  
Everling, F., Konig, L. A. Mattauch, J. H. and Wapstra, A. H., 1960, *Nuclear Physics*, **18**, 519.  
Green, A. E. S., 1954, *Phys. Rev.*, **95**, 1006.  
Green, A. E. S., 1958, *Rev. Mod. Phys.*, **30**, 569.  
Mozar, F. S., 1959, *Phys. Rev.*, **116**, 970.  
Seeger, P. A., 1961, *Nuclear Physics*, **25**, 1.

# LUMINESCENCE SPECTRA OF 2,4-DECHLORO- AND 3,4-DICHLOROTOLUENE IN THE SOLID STATE AT $-180^{\circ}\text{C}^*$

J. K. ROY

OPTICS DEPARTMENT,

INDIAN ASSOCIATION FOR THE CULTIVATION OF SCIENCE, CALCUTTA-32.

(Received July 19, 1962)

## Plate V

**ABSTRACT.** The luminescence spectra of 2,4- and 3,4-dichlorotoluene in the solid state at  $-180^{\circ}\text{C}$  have been investigated using mainly the group of Hg lines at 3650 Å as the exciting radiation. An analysis of the bands due to the crystals of the substances has been made. It has been observed that the two vibration frequencies  $1478$  and  $1590\text{ cm}^{-1}$  and three frequencies  $1376$ ,  $1483$  and  $1594\text{ cm}^{-1}$  are coupled with the electronic transitions giving rise to the luminescence spectra of 2,4- and 3,4-dichlorotoluene respectively. Further, it has been concluded from a comparison of the absorption spectra due to singlet $\rightarrow$ triplet transition of these substances that the luminescence bands owe their origin to a preliminary process of absorption due to a spin-forbidden transition from the singlet to the triplet state of the molecules and that the degree of violation of the selection rule forbidding the transition between the states of different multiplicity depends markedly on the nature of the substituent

## INTRODUCTION

Lewis and Kasha (1944) first suggested that the phosphorescence exhibited by many pure substances are due to transitions from the lowest triplet state of the molecules to the lowest singlet state and studied such phosphorescence bands in a large number of organic compounds in rigid glass media. Sanyal (1953) observed similar luminescence bands in the visible region in ortho- and parachlorotoluene in the solid state at  $-180^{\circ}\text{C}$ . Later, Biswas (1954; 1955a and b) observed that many substituted benzene compounds irradiated with 3650 Å group of Hg at  $-180^{\circ}\text{C}$  give rise to similar luminescence in the visible region. Biswas (1956a) and Sirkar and Biswas (1956) also observed that the intensity of this luminescence increases rapidly with lowering of temperature of the solidified mass and the relative intensities of the bands are altered considerably when the substance is dissolved in different solvents such as benzene, *n*-heptane, cyclohexane, methyl alcohol, etc. Using suitable light filters, Biswas (1956b) also observed that the group of Hg lines at 3650 Å and other lines of shorter wavelengths upto 3000 Å are responsible for the production of this luminescence. He also observed (Biswas, 1958) that part of the luminescence is pro-

\*Communicated by Prof. S. C. Sirkar

duced by delayed emission. Recently, while investigating the Raman spectra of 2,4- and 3,4-dichlorotoluene in the solid state at  $-180^{\circ}\text{C}$ , Deb and Banerjee (1960) observed that each of these two disubstituted toluenes gives rise to a number of luminescence bands at low temperature. The experimental arrangement in these cases were not, however, suitable for determining the wavelengths of the radiation responsible for the excitation of the luminescence spectra at low temperature, as the mercury lines in the near ultraviolet region were largely absorbed by the glass condensers used in these experiments and also some of the mercury lines were overexposed. The luminescence bands reported by these authors were therefore, probably incomplete. It was thought worth while to find out the complete spectrum and to analyse it if possible, because such data might throw some light on the origin of these luminescence spectra. The investigation of the luminescence spectra of these two disubstituted toluenes in the solid state at  $-180^{\circ}\text{C}$  was, therefore, undertaken and the results obtained in these investigations have been discussed in the present paper.

#### EXPERIMENTAL

The compounds 2,4-dichlorotoluene and 3,4-dichlorotoluene used in the present investigation were supplied by Fisher Scientific Company, U.S.A. and they were of chemically pure quality. The liquids were again repeatedly fractionated at reduced pressure before use.

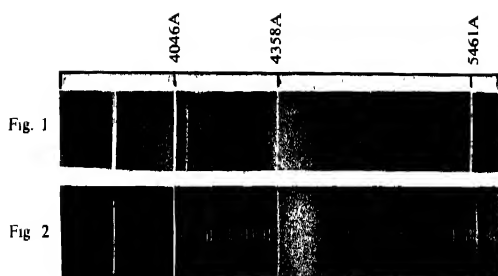
The experimental arrangement and procedure adopted in the present investigation were the same as those used previously by Biswas (1956a). The substance under investigation was sealed under reduced pressure in a Pyrex glass tube provided with a long narrow stem and the tube containing the specimen was put inside a Dewar vessel made of fused silica and the specimen was always kept completely immersed in the liquid oxygen contained in the Dewar. Liquid oxygen was replenished from time to time to keep it at a proper level in the vessel. Light from a mercury arc filtered through a Wood's filter and having lines in the region 3000-3700 Å was used as the exciting radiation. The luminescent radiation coming out at right angles to the exciting radiation was then focussed on the slit of the spectrograph with another lens and its spectrum was photographed.

A Fuess glass spectrograph having a dispersion of about 11 Å/mm in the 4046 Å region was used for recording the luminescence spectra in the visible region. The slit width of the spectrograph was kept at 0.7 mm and the time of exposure was 6 to 8 hours. Spectrograms were taken on Ilford Zenith plates. On each spectrogram an iron arc spectrum was superposed as comparison.

#### RESULTS AND DISCUSSION

The wave numbers with the estimated relative intensities of the luminescence bands due to pure 2,4- and 3,4-dichlorotoluene excited by the 3650 Å group of mercury lines in the solid state at  $-180^{\circ}\text{C}$  are reproduced in Plate 1, Figs. 1 and 2





## Luminescence Spectra

Fig. 1 2,4—dichlorotoluene at  $-180^{\circ}\text{C}$ Fig. 2. 3,4—dichlorotoluene at  $-180^{\circ}\text{C}$



and the tentative assignments of the bands are given in Tables I and II respectively.

It can be seen from the spectrograms reproduced in Fig. 1 that 2, 4-dichlorotoluene in the solid state at  $-180^{\circ}\text{C}$  produces four groups of broad luminescence bands in the region 4090Å, 4401Å, 4757Å and 5100Å respectively, but closer examination reveals that each of these groups consists of more than one band touching each other. By estimating the frequencies of the constituent bands with the help of the iron arc spectrum photographed on the spectrograms and carrying out analysis in terms of ground state vibrational frequencies, the results shown in Table I are obtained. The first group on the shorter wavelength side appears to consist of three bands at 24752, 24306 and 24194  $\text{cm}^{-1}$  respectively. Each of the second and the third groups also seems to consist of three bands and the fourth group shows two bands. The analysis shows that the vibrational frequencies 382, 1478 and 1590  $\text{cm}^{-1}$  are involved in the luminescence due to this substance. These frequencies also correspond to some of the Raman frequencies of the molecule (Deb and Banerjee, 1960). The frequency 1478  $\text{cm}^{-1}$  appears to represent a component of the  $\nu_{14}$  mode of frequency 1485  $\text{cm}^{-1}$  in benzene and the frequency 1590  $\text{cm}^{-1}$  corresponds in all probability to a component of  $\nu_{22}$  mode in benzene of frequency 1596  $\text{cm}^{-1}$ . The frequency 382  $\text{cm}^{-1}$  was assigned by Deb and Banerjee (1960) to the mode  $\nu_{20}$  of frequency 606  $\text{cm}^{-1}$  in benzene. It is observed that the modes coupled with the electronic transition giving rise to the luminescence spectra exhibited by 2, 4-dichlorotoluene involve asymmetric stretching and contraction of the C = C bond of the benzene ring.

TABLE I  
Luminescence bands of 2, 4-dichlorotoluene

$\nu$ in $\text{cm}^{-1}$	Assignment
24572 (w)	$\nu_1$
24306 (w)	$\nu_2$
24194 (w)	$\nu_3$
22982 (vs)	$\nu_1 - 1590$
22716 (vs)	$\nu_2 - 1590$ or $\nu_3 - 1478$
22604 (vs)	$\nu_3 - 1590$
21392 (s)	$\nu_1 - (2 \times 1590)$
21238 (s)	$\nu_2 - (1590 + 1478)$ or $\nu_3 - 2 \times 1478$
21014 (s)	$\nu_3 - 2 \times 1590$
19424 (vw)	$\nu_3 - 3 \times 1590$
19154 (vw)	$\nu_3 - (2 \times 1590 + 1478 + 382)$

TABLE II

Luminescence bands of 3, 4-dichlorotoluene

$\nu$ in $\text{cm}^{-1}$	Assignment
24206 (m)	$\nu_1$
24066 (m)	$\nu_2$
22830 (vs)	$\nu_1 - 1376$
22612 (vs)	$\nu_1 - 1594$
22470 (s)	$\nu_2 - 1596$
21452 (s)	$\nu_1 - 2 \times 1376$
21239 (s)	$\nu_1 - 2 \times 1483$
21020 (m)	$\nu_1 - 2 \times 1593$
20874 (m)	$\nu_2 - 2 \times 1596$
19718 (m)	$\nu_2 - (2 \times 1483 + 1382)$
19243 (m)	$\nu_2 - (3 \times 1483 + 374)$

## (b) 3, 4-Dichlorotoluene

It can be seen from the spectrograms reproduced in Fig. 2 that 2, 4-dichlorotoluene in the solid state at  $-180^\circ\text{C}$  also produce four groups of broad luminescence bands in the region 4130Å, 4378Å, 4660Å and 5070Å respectively and these groups of bands are found to consist of more than one band lying adjacent to each other. In Table II the results obtained by analysing the bands carried out with the help of the iron arc spectrum photographed on the spectrogram have been given. The examination of the structure of the broad bands shows that the first group on the shorter wavelength side consists of two band at 24206 and 24066  $\text{cm}^{-1}$  respectively, the second group consists of three bands, third group of four bands and the fourth group consists of two bands. The analysis shows that the vibrational frequencies 374, 1376, 1483 and 1594  $\text{cm}^{-1}$  are involved in the emission of the luminescence spectrum. These frequencies also correspond to some of the Raman frequencies of the molecule (Deb and Banerjee, 1960). The frequency 1483  $\text{cm}^{-1}$  corresponds to  $e_{1u}$  mode of frequency 1485  $\text{cm}^{-1}$  benzene and 1594  $\text{cm}^{-1}$  correspond to  $e_{2g}$  mode of frequency 1596  $\text{cm}^{-1}$  in benzene.

It is thus observed that the frequencies 378, 1480 and 1592  $\text{cm}^{-1}$  are coupled with the electronic transition giving rise to the luminescence spectra of both 2, 4-dichlorotoluene and 3, 4-dichlorotoluene. The singlet  $\rightarrow$  triplet absorption spectra due to these two dichlorotoluenes in the liquid state were also studied earlier (Roy, 1961). It might be pointed out that in the case of 2, 4-dichlorotoluene the position of the 0, 0 band in the continuous absorption spectrum may

be taken to be at  $29750\text{ cm}^{-1}$  in the liquid state. In the solid state this position is expected to be shifted towards longer wavelengths. If the shift were of the order of  $400\text{ cm}^{-1}$  the frequency of the 0,0 band could be taken as  $29350\text{ cm}^{-1}$ . The difference between the frequency of this band and the frequency of the luminescence band at  $24572\text{ cm}^{-1}$  is of the order of  $4800\text{ cm}^{-1}$  and this difference may be due to the vibration transition of frequency  $3 \times 1590\text{ cm}^{-1}$ . Similarly, the 0,0 band in the absorption spectra of 3,4-dichlorotoluene in the solid state would be found to be at about  $28350\text{ cm}^{-1}$  and the first luminescence band in the shorter wavelength side in the solid state is at  $24206\text{ cm}^{-1}$  and this difference of about  $4190\text{ cm}^{-1}$  may be due to the vibration transition of frequency  $3 \times 1376\text{ cm}^{-1}$ .

A comparison of the intensity and the position of the luminescence bands due to the two dichlorotoluenes in the solid state at  $-180^\circ\text{C}$  given in Tables I and II shows that the positions of the bands of the 3,4 isomer are displaced towards longer wavelengths with respect to those of the 2,4-isomer and the bands of the former compound are slightly stronger than those of the latter. Also, the bands of the two isomers are displaced as a whole to the longer wavelength region with respect to those of parachlorotoluene. Since it has been suggested earlier that the luminescence bands in the case of *p*-chlorotoluene are produced through absorption of energy by transition from the singlet to the triplet state and the consequent re-emission of the absorbed energy the results obtained in the cases of the two dichlorotoluenes show that substitution of another chlorine atom in the benzene ring produces further perturbation of the  $\pi$ -electron energy levels and thereby decreases the energy differences of the two states, this decrease depending to some extent on the relative positions of the two chlorine atoms in the ring of the aromatic molecule. The fact that the bands of 3,4-dichlorotoluene are slightly stronger than these due to 2,4-dichlorotoluene indicates that in the solid state the strength of absorption is greater in the former compound than in the latter.

Thus all the results discussed above point to the fact that the luminescence bands observed in the halogen substituted toluenes owe their origin to a preliminary process of absorption due to a spin-forbidden transition from singlet to triplet state of the molecules, the latter state being rather broad and that the degree of violation of the selection rule forbidding the transition between states of different multiplicity depend markedly on the nature of the substituent. It is well known that the substitution of chlorine atoms in the aromatic molecule brings about some migration of the electron from the substituent into the ring. This distortion of the orbitals is evidently responsible for the singlet  $\rightarrow$  triplet absorption, but the association of the vibrational modes  $e_{2g}$  and  $e_{1u}$  with this electronic transition shows that the perturbation depends largely on the relative interatomic distances in the adjacent segments of the benzene ring.

## ACKNOWLEDGMENT

The author is highly indebted to Professor S. C. Sirkar, D.Sc., F.N.I. for his kind interest and for guidance throughout the progress of the work.

## REFERENCES

- Biswas, D. C., 1954, *Ind. J. Phys.*, **28**, 423.  
Biswas, D. C., 1955a, *Ind. J. Phys.*, **29**, 257.  
Biswas, D. C., 1955b, *Ind. J. Phys.*, **29**, 503.  
Biswas, D. C., 1956a, *Ind. J. Phys.*, **30**, 143.  
Biswas, D. C., 1956b, *Ind. J. Phys.*, **30**, 255.  
Biswas, D. C., 1956, *Ind. J. Phys.*, **32**, 301.  
Deb, K. K. and Banerjee, S. B., 1960, *Ind. J. Phys.*, **34**, 554.  
Lewis, G. N. and Kasha, M., 1944, *J. Am. Chem. Soc.*, **66**, 2100.  
Roy, J. K., 1961, *Ind. J. Phys.*, **35**, 628.  
Sanyal, S. B., 1953, *Ind. J. Phys.*, **27**, 447.  
Sirkar, S. C. and Biswas, D. C., 1956, *J. Chem. Phys.*, **24**, 470.

# F<sup>19</sup> FREE INDUCTION DECAY IN POLYCRYSTALLINE MgF<sub>2</sub>

S. K. SINHA, S. K. GHOSH, J. LAHIRI AND  
A. ROYCHOUDHURY

Saha Institute of Nuclear Physics, CALCUTTA.

(Received May 21, 1962)

**ABSTRACT.** The F<sup>19</sup> free-induction decay in polycrystalline MgF<sub>2</sub> has been recorded and it agrees satisfactorily with the real part of complex fourier transform of the steady F<sup>19</sup> absorption line from the same sample. The use of the free induction decays in the experimental analysis of nuclear magnetic resonance line shapes in solids has been discussed.

## INTRODUCTION

The pulse technique (Hahn, 1950) in nuclear magnetic resonance (nmr) method has been subsequently found to supplement and extend the steady technique in the study of various aspects of liquid state properties (Hahn-Maxwell, 1952; Carr and Purcell, 1954; Crawford and Foster, 1956; Douglass and McCall, 1958, Ghosh and Sinha, 1960; Woessner, 1961). In solids, on the other hand, no such extensions have so far been made. The investigation of the free-induction decay mechanism in solids (Herzog and Hahn, 1956; Lowe and Norberg 1957) and the experimental work on CaF<sub>2</sub> single crystals (Lowe and Norberg, 1957) has, however, established that the free-induction decay shapes in solids is identical with the real part of the complex fourier transform of the steady state unsaturated line shape observed for the same sample. This suggests that one can analyse the properties of the fourier transform of the steady line shape to see if the free-induction decay shapes can be used to extend or refine the steady line shape studies in solids.

In section II, the apparatus for recording the free-induction decays has been described together with the recorded F<sup>19</sup> free-induction decay shape in polycrystalline MgF<sub>2</sub>. In section III, the use of free induction decay shapes in the experimental analysis of nmr line shapes in solids has been discussed.

## F<sup>19</sup> FREE-INDUCTION DECAY IN MgF<sub>2</sub> POWDER

The apparatus used is a conventional spin-echo apparatus, and the block diagram is shown in Fig. 1. The pulsed oscillator and the detector part together with the electromagnet have been described previously (Banerjee, Ghosh and Saha, 1957). In the present set-up, the Bloch-head and the rf preamplifier have

been redesigned, and a gated integrator has been used to record the free-inductions signal.

In the Bloch-head, the transmitter and the receiver coils are wound over hollow cylindrical formats of ergon (a refractory material, containing no hydrogen atoms) on which grooves can be cut. This was done to eliminate the back-ground proton signal coming from perspex formats and the adhesive resins that were previously used to place the transmitter and the receiver coils in position. The transmitter coil is split up into two equal sections connected in series, and were placed on the two sides of the receiver coil. Some amount of isolation of the receiver coil from the transmitter coils is desirable in pulse technique also in order to prevent overdriving of the detecting system during the pulse period. For V-mode control, there is a copper paddle and provision for adjusting the position of one section of the transmitter coil; and for U-mode control, the capacitors used to resonate the transmitter coils were used to reduce the centre-voltage at the transmitter coil.

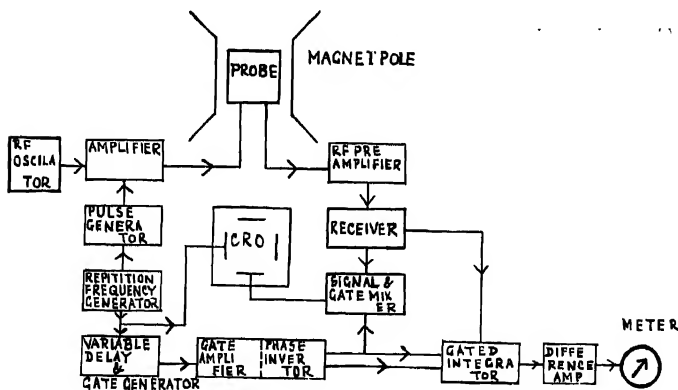


Fig. 1. Block diagram of the experimental arrangement.

The *nmr* signal before being fed to the detecting circuit was fed to an *rf* pre-amplifier to improve the signal-to-noise ratio. The circuit diagram for the *rf* preamplifier is shown in Fig. 2. The 3db band width of the preamplifier is  $\sim 10$  Mc/sec., centered at 14 Mc/sec. and the minimum centre-band gain is  $\sim 10$ .

The circuit diagram for the gated integrator (Holcomb and Norberg, 1955) is shown in Fig. 3. Essentially it is a switch arrangement, and the detected *nmr* signal is fed to it. The switching is done by means of the "gate-pulses" and the out-put voltage charges some capacitors arranged in such a way that the R.C. element retains that voltage until the signal repeats again. After a few repetitions the integrated voltage, which is subsequently amplified in a difference



amplifier, gives a measure of the signal amplitude which is time-averaged over the duration of the gate-pulse. By shifting the position of the gate-pulse with respect to the exciting  $rf$  pulse, one can get the signal voltage as a function of time. To measure the time of application of the gate pulse (with respect to the

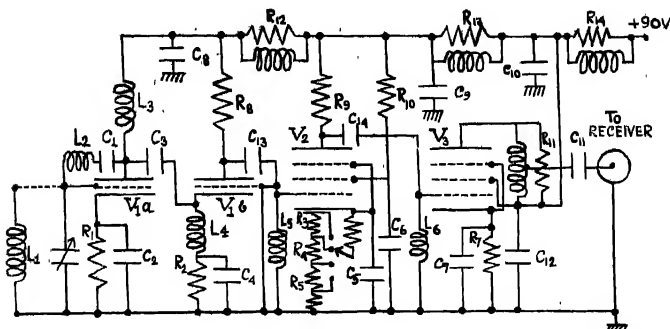


Fig. 2. Circuit diagram of the  $rf$  preamplifier.  $L_1$  is the receiver coil,  $L_2 = 40$ ,  $L_3 = 25$ ,  $L_4 = 45$ ,  $L_5 = 15$ ;  $R_1 - 7 = 100$ ,  $R_8, 11, 14 = 1K$ ,  $R_9 = 1.5 K$ ,  $R_{10} = 4.7 K$ ;  $C_{1-2, 4, 7-14} = 0.01$ ,  $C_3 = 0.02$ ,  $C_{11-6} = 0.001$ . The values of inductances, resistances and capacities are in microhenry, ohm and microfarad respectively.

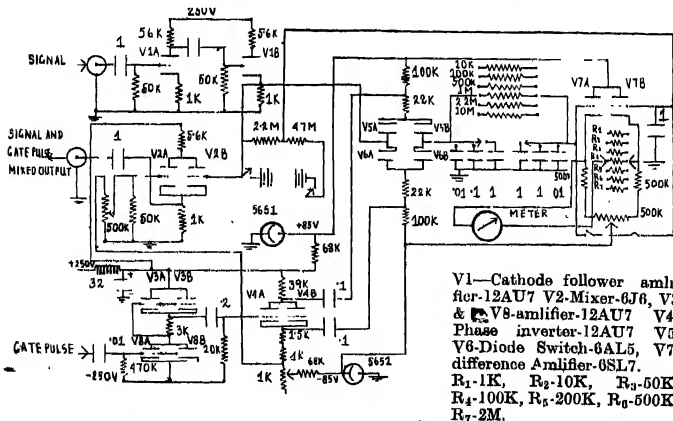


Fig. 3. Circuit diagram of the gated Integrator.  $V_1, V_3, V_4, V_8 = 12 AU 7$ ,  $V_2 = 6J6$ ,  $V_5, V_6 = 6AL5$ ,  $V_7 = 6SL7$ .  $R_1 = 1 K$ ,  $R_2 = 10 K$ ,  $R_3 = 50 K$ ,  $R_4 = 100 K$ ,  $R_5 = 200 K$ ,  $R_6 = 500 K$ ,  $R_7 = 1M$ .

Resistances and capacities are in ohm and microfarad respectively.

exciting  $rf$  pulse), it is mixed together with the n.m.r. signal and presented on a cathode ray oscilloscope with a calibrated trace.

This method is alternative to the photographic method and is somewhat equivalent to the narrow-band integration technique used in steady *nmr* studies. Integration at each points of the signal improves the signal to noise ratio considerably.

Experimental record of the fluorine free induction n.m.r. signal from polycrystalline  $\text{MgF}_2$  (BDH analar grade) is shown in Fig. 4. The exciting *rf* pulse was approximately a  $90^\circ$ -pulse and the resonance frequency was 14Mc/sec. The oscilloscope trace was calibrated by time markers from a harmonic generator whose fundamental frequency was locked to 1Kc/sec output of a standard low frequency function generator (HP 202 A model). The real part of the complex fourier transform of the unsaturated steady state fluorine n.m.r. line shape from the same sample is also shown in figure 4 by the dotted curve. All numerical integrations were performed by Filon's method (Filon, 1928-29). The steady state line shape gave a second moment of  $8.5 \pm 0.5$  gauss which agreed (Ghosh, Lahiri and Sinha, 1961) with the computed second moment from the known crystal structure of  $\text{MgF}_2$ . The agreement between the free-induction shape and the fourier transform of the steady line shape is satisfactory as seen in Fig. 4. The free induction signal prior to 35  $\mu$ -seconds could not be recorded because of receiver saturation, and attempts are being made to reduce this paralysis time of the receiver.

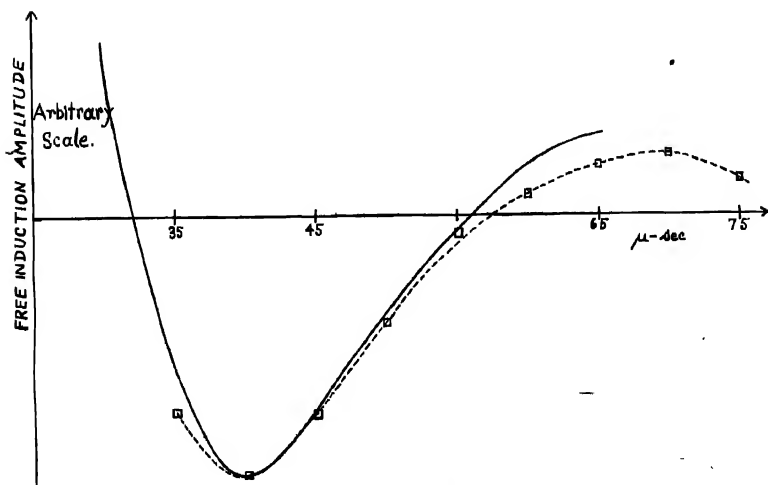


Fig. 4.  $\text{F}^{19}$  free induction decay in polycrystalline  $\text{MgF}_2$  (solid curve). The Fourier transform of the corresponding steady absorption line is also shown (dotted curve).

FREE INDUCTION SIGNAL SHAPE AND THE  
STRUCTURAL STUDIES IN SOLIDS

If the free induction shape is always the real part of the complex fourier transform of the unsaturated steady state n.m.r. line shape it is clear that no extra information can be obtained from the free induction signals (Abragam, 1961). We, however, note that the correspondence is true only for unsaturated steady state absorption line shape. Thus the inverse fourier transform of the free induction signal will yield an absorption line shape free from saturation broadening and other instrumental broadenings like modulation broadenings etc. (Perlman and Bloom, 1952, Andrew, 1953; Spry, 1957; McCall, 1957).

We discuss below the use of free induction signals for structural studies in solids.

(a) Single line absorption spectrum, broadened by neighbours :

If the absorption peak occurs at frequency  $\omega_1$  the steady state line shape function can be written as

$$g(\omega) = A_0 \int_{-\infty}^{+\infty} \delta(\omega' - \omega_1) B(\omega - \omega') d\omega' = A_0 B(\omega - \omega_1) \quad \dots (1)$$

Therefore, the complex fourier transform  $F(t)$  comes out as

$$F(t) = F_0 \exp \left( -\frac{t^2}{4b} \right) \exp (i\omega_1 t) \quad \dots (2)$$

where we have taken

$$B(\omega - \omega') = a \exp \{ -b(\omega - \omega')^2 \} \quad \dots (3)$$

and  $F_0$  stands for  $aA_0\sqrt{\pi/b}$ .

The free induction signal will then be given by

$$S(t) = F_0 \exp \left( -\frac{t^2}{4b} \right) \quad \dots (4)$$

and from any two points on the free induction signal shape, the second moment of the steady state absorption signal can be obtained. Much of the labour of crystal structure study by McCall and Hamming (McCall and Hamming, 1959) method can thus be eliminated.

(b) Two line absorption spectrum, broadened by neighbours :

If the absorption lines are at  $\pm\omega$ , and they are broadened by a function like (3), the free induction signal will be given by

$$S(t) \simeq F_0 \exp \left( -\frac{t^2}{4b} \right) \cos \omega t \quad \dots (5)$$

The first zero will occur at

$$t = \frac{\pi}{2\omega} \quad \dots (6)$$

from which the value of  $\omega$ , and hence the second-moment of the close group of nuclei giving rise to the two-line absorption spectrum can be obtained. It is always easier to locate the zeroes in free induction signals as compared to the location of peaks in steady absorption signals. The free induction method is, therefore, expected to be more convenient in studying two-member groups of nuclei by Pake's (Pake, 1948) procedure.

(c) Absorption spectrum in polycrystalline samples: For polycrystalline samples we can write

$$g(\omega) = \int_{-\infty}^{+\infty} f(\omega_0) B(\omega - \omega_0) d\omega_0 \quad \dots (7)$$

where  $f(\omega_0)$  is the normalized polycrystalline shape for a close group of resonating nuclei, relatively isolated from their neighbours and  $B(\omega - \omega_0)$  represents line broadening due to those neighbours. The corresponding free induction signal will be

$$\begin{aligned} S(t) &= \int_{-\infty}^{+\infty} d\omega \cdot \exp(i\omega t) \int_{-\infty}^{+\infty} f(\omega_0) B(\omega - \omega_0) d\omega_0 \\ &= B(t) \cdot \sum_{n=0}^{\infty} \frac{(-it)^n}{n!} <\omega_0^n> \quad \dots (8) \end{aligned}$$

where

$$B(t) = \int_{-\infty}^{+\infty} B(\omega - \omega_0) \exp\{i(\omega - \omega_0)t\} d(\omega - \omega_0). \quad \dots (9)$$

and  $<\omega_0^n>$  is the  $n^{\text{th}}$  moment of  $f(\omega_0)$ . Usually  $B(\omega - \omega_0)$  is taken as an exponential function of  $(\omega - \omega_0)^2$ , and therefore  $B(t)$  is also an exponential function of  $t^2$ . From the zeroes of  $S(t)$  as given in (8) we can, therefore, calculate  $<\omega_0^n>$ 's exclusively. However, because of the exponential nature of  $B(t)$ , one will observe experimentally only a few zeroes of  $S(t)$ , and in using (8) one must note that in

the series  $\sum_{n=0}^{\infty} \frac{(-it)^n}{n!} <\omega_0^n>$  positive and negative terms appear alternately.

For example, in polycrystalline  $\text{CaSO}_4 \cdot 2\text{H}_2\text{O}$  the first and the second zeroes of  $S(t)$  when computed from Pake's (Pake, 1948) steady state line shape occurs at  $t = 15.2$  and  $40 \mu\text{-sec.}$  respectively, as shown in Fig. 5. Computing  $<\omega_0^2>$  and  $<\omega_0^4>$  from Van Vleck's (Van Vleck, 1948) formula we can write

$$\begin{aligned} \sum_{n=0}^{\infty} \frac{(-it)^n}{n!} <\omega_0^n> &= 0 = 1 - 0.95 + 1.024 \times 10^3 - \dots, \quad t = 15.2 \times 10^{-8} \text{ sec.} \\ &= 0 = 1 - 6.59 + 49.104 \times 10^3 - \dots, \quad t = 40 \times 10^{-8} \text{ sec.} \end{aligned}$$

and the above series show that in general it would be difficult to decide as to how many zeroes will be necessary for extracting reliable values of  $\langle \omega_0^2 \rangle$  and  $\langle \omega_0^4 \rangle$  etc.

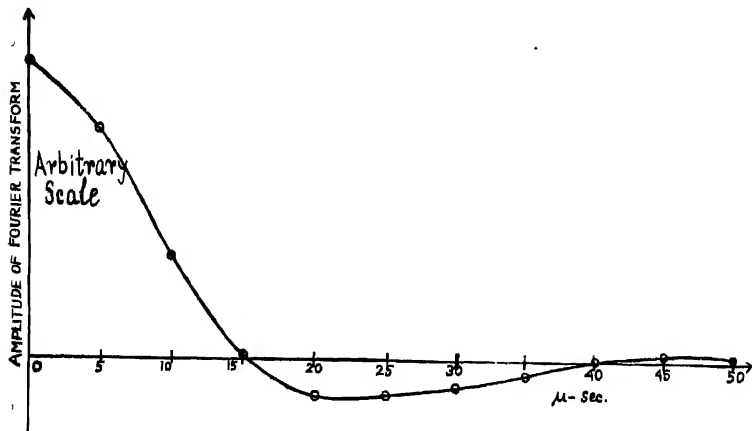


Fig. 5. Fourier transform of the proton absorption line (Pake, 1948) from polycrystalline  $CaSO_4 \cdot 2H_2O$ .

The above discussion shows that the free induction method will be more convenient for the study of one line and two line n.m.r. absorption spectra. These will correspond to solids with isolated nuclei, and single crystals with close group of two interacting nuclei respectively. On the other hand, the free induction method appears to offer no simplification in the experimental study of polycrystal line samples or single crystals having more than two closely interacting nuclei, except helping to avoid instrumental broadenings etc. as indicated at the beginning of this section.

#### ACKNOWLEDGMENT

The authors thank Prof. A. K. Saha for his interest in the study and for going through the manuscript. They are also thankful to Dr. M. Bose for some discussions.

#### REFERENCES

- Abraham, A. 1961, *The Principles of Nuclear Magnetism*, The Clarendon Press, Oxford, p. 63.
- Andrew, E. R., 1953, *Phys. Rev.*, **91**, 425.
- Banerjee, B. M., Ghosh, S. K. and Saha, A. K., 1957, *Ind. J. Phys.*, **31**, 211.
- Crawford, G. J. R. and Foster, J. S., 1950, *Canad. J. Phys.*, **34**, 653.
- Carr, H. Y. and Purcell, E. M., 1954, *Phys. Rev.*, **94**, 630.

- Douglas, D. C. and McCall, D. W., 1958, *J. Phys. Chem.*, **62**, 1102.  
Filon, L. N. G., 1928-29, *Proc. Roy. Soc. Edin.*, pp. 38-47.  
Ghosh, S. K. and Sinha, S. K., 1960, *Ind. J. Phys.*, **34**, 339.  
Ghosh, S. K., Lahiri, J. and Sinha, S. K., 1961, *Ind. J. Phys.*, **35**, 236.  
Hahn, E. L., 1950, *Phys. Rev.*, **80**, 580.  
Hahn, E. L. and Maxwell, D. E., 1952, *Phys. Rev.*, **88**, 1070.  
Herzog, B. and Hahn, E. L., 1956, *Phys. Rev.*, **103**, 148.  
Lowe, I. J. and Norberg, R. E., 1957, *Phys. Rev.*, **107**, 46.  
McCall, D. W., 1958, *Jour. Applied Phys.*, **29**, 739.  
McCall, D. W. and Hamming, R. W., 1959, *Acta. Cryst.*, **12**, 81.  
Pake, G. E., 1948, *J. Chem. Phys.*, **16**, 327.  
Portman, M. M. and Bloom, M., 1952, *Phys. Rev.*, **88**, 1290.  
Spry, W. J., 1957, *J. Appl. Phys.*, **28**, 660.  
Van Vleck, J. H., 1948, *Phys. Rev.*, **74**, 1168.  
Woessner, D. E., 1961, *J. Chem. Phys.*, **35**, 41.

# ON ADAPTATION OF THE GROUPING CHART AND SIMPLIFICATION OF MULTIPLE OUTPUT SWITCHING FUNCTIONS

A. K. CHOUDHURY, M. S. BASU AND SUNIL RANJAN DAS

INSTITUTE OF RADIO PHYSICS AND ELECTRONICS,  
UNIVERSITY OF CALCUTTA

(Received February 16, 1962)

**ABSTRACT.** The mechanised grouping chart is a powerful aid in minimisation as it renders possible very quick determination of the prime implicants and the essential prime implicants of any switching function. In this paper a method is first described by which a mechanised chart for a certain number of variables can be adapted for handling problems involving a larger number of variables. The method is then extended for simplifications of multiple output switching functions.

## INTRODUCTION

In all the available methods of finding out the minimal two stage form of switching functions, two important steps to be carried out are determination of the prime implicants and identification of the essential prime implicants, if any. In an earlier paper, the grouping chart (Choudhury and Basu, 1962) was shown to be a valuable aid in performing the above mentioned tasks. It was also shown that the labour involved in having vertical and horizontal lines drawn on the chart every time a new function is handled, can be eliminated by having the chart mechanised. An apparent limitation to the utility of this device is set by the number of variables for which the chart is mechanised. A method will be described here by which a mechanised grouping chart designed for a certain number of variables can be adapted for minimising switching functions involving a larger-number of variables. If the number of variables in a given function be  $(r+n)$ , it can be decomposed into  $2^r$  different functions involving  $n$ -variables. The prime implicants of each of these functions can be found out by the available  $n$ -variable mechanised grouping chart and the essential prime implicants may be identified. Then by a procedure suggested in this paper, the prime implicants of the original function in  $(n+r)$ -variables are determined and the essential prime implicants identified. This method of adaptation of the grouping chart is then extended for simplification of multiple output switching functions.

## GENERAL OUTLINE OF THE METHOD

If  $f(x_n, x_{n-1}, x_{n-2}, \dots, x_1)$  be any switching function of  $n$  binary variables, it can be split up into a number of functions of smaller number of variables by partitioning the variables into two groups. Thus, if a partition is made so as to include  $p$  variables viz.,  $x_n, x_{n-1}, x_{n-2}, \dots, x_{n-p+1}$  in one group and other  $q$  variables in the other group,  $p+q$  being equal to  $n$ , then the original function of  $n$ -variables can be expressed as sum of  $2^p$  different functions each involving  $q$  (i.e.  $n-p$ ) variables. For example, if we make  $p = 2$ , then we can write

$$\begin{aligned} f(x_n, x_{n-1}, x_{n-2}, \dots, x_1) = & \bar{x}_n \bar{x}_{n-1} f_1(x_{n-2}, x_{n-3}, \dots, x_1) \\ & + \bar{x}_n x_{n-1} f_2(x_{n-2}, x_{n-3}, \dots, x_1) + x_n \bar{x}_{n-1} f_3(x_{n-2}, x_{n-3}, \dots, x_1) \\ & + x_n x_{n-1} f_4(x_{n-2}, x_{n-3}, \dots, x_1) \end{aligned} \quad \dots (1)$$

The component functions  $f_1, f_2$  etc. are easily derived from the original  $n$ -variable function by well-known procedure.

If the terms of the given function are written in the decimal mode, then the said operation is simply equivalent to writing the terms as numbers modulo  $2^q$ . In other words, we divide each decimal number representing the terms by  $2^q$ . The quotients may be  $0, 1, 2, 3 \dots 2^p - 1$ . The remainders form corresponding groups which are simply the component functions each of  $q$  (i.e.,  $n-p$ ) variables (Singer, 1957). If we combine the terms of group 0 with those of group 1, we get a  $(q-1)$  variable function. This is simply the remainder corresponding to quotient 0 if we express the terms of the original  $n$ -variable function as numbers modulo  $2^{q+1}$ . From Eqn. (1) it is clear that if any term occurs in the component function  $f_1$  and the same term occurs in  $f_2$ , then when we take the sum  $\bar{x}_n \bar{x}_{n-1} f_1 + \bar{x}_n x_{n-1} f_2$ , those two terms will differ by one change of variable and will form a 1-cell making elimination of one variable possible. In general, it may be stated that if terms  $a_1, a_2, a_3, \dots, a_k$  form a  $k$ -cell in any one of the component functions and the same terms are found to occur in some other component function and if the corresponding quotients are found to form a 1-cell, then those  $2^{k+1}$  terms will form a cell of next higher dimension viz.,  $k+1$ , when the said component functions are combined. A scrutiny of the grouping chart will reveal that this very same principle is utilised there for seeking out the grouping of terms and consequent cell formation in any switching function. From what has been said above, it follows that if a term " $a$ " is found to occur in two different component functions whose corresponding quotients form a 1-cell, and if the weight of the term " $a$ " be  $\omega_1$  in one function and  $\omega_2$  in the other, then in the combined function the two terms will have their weights enhanced by 1 and it will be  $(\omega_1+1)$  and  $(\omega_2+1)$  respectively.

## SUGGESTED PROCEDURE FOR FINDING OUT THE PRIME IMPLICANTS

Utilising the above mentioned ideas, one can proceed according to the following steps for finding out the prime implicants and identifying the essential prime



implicants of an  $(r+n)$  variable function with the help of an available  $n$ -variable mechanised grouping chart.

(1) The decimal numbers corresponding to the terms of the given function are divided by  $2^n$  so as to get numbers modulo  $2^n$ . Thus the original function is split up into  $2^n$  different functions each of  $n$ -variables, corresponding to quotients  $0, 1, 2, 3 \dots 2^n - 1$ .

(2) With the help of the grouping chart the weights of the different terms and the prime implicants of each of the above  $2^n$  functions are found out.

(3) The functions corresponding to quotients 0 and 1 are now combined to form a function of  $(n+1)$  variables. If any term occurs in both the functions, then weight of each of such terms should be increased by 1. If terms  $p, q, r, s, \dots$  form a  $k$ -cell in one function and the same terms form a similar  $k$ -cell in the other, then those two  $k$ -cells are combined and the resulting  $2^{k+1}$  terms form a  $(k+1)$  cell. In this way all the different groupings and hence prime implicants of the  $(n+1)$  variable function are found out.

(4) The procedure mentioned in step (3) is repeated for functions corresponding to quotients 2 and 3, 4 and 5, etc. and a set of  $(n+1)$  variable functions is found out.

(5) The first two of this set are again combined, new weights are assigned to terms and new prime implicants are found out. The same thing is done for other pairs as before.

(6) In this way ultimately we get the terms of the original  $(r+n)$  variable function. As all the prime implicants are known and the weight of each term is also known, the essential prime implicants can be identified. Most economic coverage of the terms not covered by the essential prime implicants now remains to be found out, which can be done by any of the available methods. (McCluskey, 1956; Mukhopadhyay 1962; Quine, 1952; Urbano and Mueller, 1956) The method may be illustrated by the following example.—

### *Example*

The prime implicants and the essential prime implicants, if any, of the following 7-variable switching function are to be found out with the help of a 5-variable grouping chart :

$$T = \Sigma(0, 2, 5, 8, 10, 12, 13, 16, 18, 21, 24, 26, 28, 29, \\ 30, 32, 34, 37, 39, 40, 42, 45, 46, 48, 50, 53, 55, \\ 56, 58, 61, 64, 65, 67, 72, 73, 77, 78, 79, 80, 81, \\ 83, 88, 89, 91, 95, 100, 102, 106, 107, 111, 114, 116, \\ 120, 122, 126, 127)$$

Dividing each term by 32, we get the following 4 functions corresponding to quotients 0, 1, 2, and 3 respectively :

$$A = \Sigma(0, 2, 5, 8, 10, 12, 13, 16, 18, 21, 24, 26, 28, 29, 30)$$

$$B = \Sigma(0, 2, 5, 7, 8, 10, 13, 14, 16, 18, 21, 23, 24, 26, 29)$$

$$C = \Sigma(0, 1, 3, 8, 9, 13, 14, 15, 16, 17, 19, 24, 25, 27, 31)$$

$$D = \Sigma(4, 6, 10, 11, 15, 18, 20, 24, 26, 30, 31).$$

With the help of the grouping chart the weights of each term and the prime implicants of each function are found out. Then  $A$  and  $B$  are combined to form a six variable function  $P$ . It is found that a 3-cell is formed in  $A$  by the terms (0, 2, 8, 10, 16, 18, 24, 26) and the same 3-cell is present in  $B$ . So in  $P$  the terms (0, 2, 8, 10, 16, 18, 24, 26, 32, 34, 40, 42, 48, 50, 56, 58) form a 4-cell. Similarly the other prime implicants are found out. Table I(a) and (b) give the terms of the functions  $A$  and  $B$  respectively with weights of the different terms and respective prime implicants of the functions. In Table I(c) are shown the terms of the function  $P$  along with their new weights and the prime implicants found out by combining those of  $A$  and  $B$ .

TABLE I(a)

$$A = \Sigma(0, 2, 5, 8, 10, 12, 13, 16, 18, 21, 24, 26, 28, 29, 30)$$

Terms	Weights	Prime implicants
0	3	
2	3	
8	4	1. (0, 2, 8, 10, 16, 18, 24, 26)
16	3	
5	2	2. (24, 26, 28, 30)
10	3	
12	3	3. (12, 13, 28, 29)
18	3	
24	4	4. (5, 13, 21, 29)
13	3	
21	2	5. (8, 12, 24, 28)
26	4	
28	4	
29	3	
30	2	

TABLE I(b)

$B = \Sigma(0, 2, 5, 7, 8, 10, 13, 14, 16, 18, 21, 23, 24, 26, 29)$

Terms	Weight	Prime implicants
0	3	
2	3	
8	3	1. (0, 2, 8, 10, 16, 18, 24, 26)
16	3	
5	3	2. (5, 13, 21, 29)
10	4	
18	3	3. (5, 7, 21, 23)
24	3	
7	2	4. (10, 14)
13	2	
14	1	
21	3	
26	3	
23	2	
29	2	

TABLE I(c)

$P = \Sigma(0, 2, 5, 8, 10, 12, 13, 16, 18, 21, 24, 26, 28, 29, 30, 32, 34, 37, 39, 40, 42, 45, 46, 48, 50, 53, 55, 56, 58, 61)$

Terms	Original weight	Weight to be added	Total weight	Prime implicants
0	3	1	4	
2	3	1	4	
5	2	1	3	
8	4	1	5	1. (0, 2, 8, 10, 16, 18, 24, 26, 32, 34, 40, 42, 48, 50, 56, 58)
10	3	1	4	
12	3	0	3	2. (24, 26, 28, 30)
13	3	1	4	3. (12, 13, 28, 29)
16	3	1	4	
18	3	1	4	4. (8, 12, 24, 28)
21	2	1	3	5. (5, 13, 21, 29, 37, 45, 53, 61)
24	4	1	5	
26	4	1	5	6. (37, 39, 53, 55)
28				7. (42, 46)

TABLE 1(c)—*contd.*

Terms	Original weight	Weight to be added	Total weight	Prime implicants
29	3	1	4	
30	2	0	2	
32(0)	3	1	4	
34(2)	3	1	4	
37(5)	3	1	4	
39(7)	2	0	2	
40(8)	3	1	4	
42(10)	4	1	5	
45(13)	2	1	3	
46(14)	1	0	1	
48(16)	3	1	4	
50(18)	3	1	4	
53(21)	3	1	4	
55(23)	2	0	2	
56(24)	3	1	4	
58(26)	3	1	4	
61(28)	2	1	3	

In a similar manner functions  $C$  and  $D$  are combined to get function  $Q$ . Finally  $P$  and  $Q$  are combined to regain the original 7 variable function. In Table II are shown the terms of this function along with their weights and the prime implicants as found out by the process of combination mentioned. From inspection of the weights, ten of the prime implicants are identified to be essential ones which are marked by asterisk.

TABLE II  
Combined seven-variable function

Terms	Original weight	Weight to be added	Total weight	Prime implicants
0	4	1	5	1. (0, 2, 8, 10, 16, 18, 24, 26, 32, 34, 40, 42, 48, 50, 56, 58)*
2	4	0	4*	2. (5, 13, 21, 29, 37, 45, 53, 61)*
5	3	0	3	3. (04, 65, 72, 73, 80, 81, 88, 89)
8	5	1	6	4. (0, 8, 16, 24, 64, 72, 80, 88)
10	4	0	4	5. (79, 95, 111, 127)
12	3	0	3	6. (81, 83, 89, 91)
13	4	1	5	7. (56, 58, 120, 122)
16	4	1	5	8. (50, 58, 114, 122)*
18	4	0	4	9. (42, 58, 106, 122)
21	3	0	3	10. (37, 39, 53, 55)*
24	5	1	6	11. (65, 67, 81, 83)*
26	5	0	5	12. (24, 56, 88, 120)
28	4	0	4	13. (24, 26, 38, 30)*
29	4	0	4	14. (12, 13, 28, 29)
30	2	0	2	15. (8, 12, 24, 28)
32	4	0	4	16. (120, 127)

TABLE II—*contd.*

Terms	Original weight	Weight to be added	Total weight	Prime implicants
34	4	0	4	17 (122, 126)
37	4	0	4	18 (107, 111)
39	2	0	2	
40	4	0	4	
42	5	1	6	19. (91, 95)
45	3	0	3	20. (106, 107)
46	1	0	1	21. (78, 79)*
48	4	0	4	22. (77, 79)
50	4	1	5	23. (100, 116)*
53	4	0	4	24. (100, 102)*
55	2	0	2	25. (73, 77)
56	4	1	5	26. (42, 46)*
58	4	1	5	27. (13, 77)
61	3	0	3	
64(0)	3	1	4	
65(1)	4	0	4	
67(3)	2	0	2	
72(8)	3	1	4	
73(9)	4	0	4	
77(13)	2	1	3	
78(14)	1	0	1	
79(15)	4	0	4	
80(18)	3	1	4	
81(17)	4	0	4	
83(19)	3	0	3	
88(24)	4	1	5	
89(25)	1	0	4	
91(27)	3	0	3	
95(31)	3	0	3	
100(36)	2	0	2	
102(38)	1	0	1	
106(42)	2	1	3	
107(43)	2	0	2	
111(47)	3	0	3	
114(50)	1	1	2	
116(52)	1	0	1	
120(56)	2	1	3	
122(58)	4	1	5	
126(62)	2	0	2	
127(63)	3	0	3	

SIMPLIFICATION OF MULTIPLE OUTPUT  
SWITCHING FUNCTIONS

Often it may be required to realise a number of switching functions all of which are functions of the same set of variables. Instead of generating the functions independently, it becomes advantageous to use a multiple output circuit. If the number of variables be  $n$  and the number of switching functions to be realised be  $t$ , then  $n$ -input and  $t$ -output terminals will be used in the circuit if we want to realise the functions in two stages. If any particular term occurs in all the  $t$  different functions, this means that for a particular combination of the input

variables, output will be present for each of the  $t$ -functions. So this condition can be generated once and is shared by all the output terminals. The problem of simplification of multiple output switching functions to get the minimal two stage form which will require the least number of diodes can be effectively handled by extending the application of the principles mentioned in connection with the adaptation of the grouping chart. Let  $f_1, f_2, f_3, \dots$  be different single output functions each involving the same set of  $n$ -variables viz.,  $x_n, x_{n-1}, x_{n-2}, \dots, x_1$ . These different functions can be combined into one multiple output function  $F$  which is given by

$$F = af_1 + bf_2 + cf_3 + \dots$$

where  $a, b, c, \dots$  is a set of  $t$  auxiliary binary variables.

So the multiple output function which combines the  $t$  different single output functions involves  $(n+t)$  variables when  $n$  is the number of input variables of the component functions and  $t$  is the number of auxiliary variables introduced. Our problem is to find out the minimal form of the multiple output function when the component single output functions are specified, economy in the number of components being the criterion of minimality.

The different transmission functions  $f_1, f_2$ , etc. may be expressed in the decimal mode. For example, we can say,  $f_1 = \Sigma(0, 1, 6, 10, 12, 15)$  which means that the function  $f_1$  is the Boolean sum of the terms within the brackets. We can call this as the transmission  $a$ . Similarly let transmission  $b$  be  $f_2 = \Sigma(0, 1, 2, 3, 4, 5, 8, 9)$  and transmission  $c$  be  $f_3 = \Sigma(0, 1, 2, 7, 11, 13, 14)$ .  $f_1, f_2$  and  $f_3$  have been chosen here to be 4-variable functions. The multiple output function which incorporates these three individual transmissions may be written as

$$F = a\Sigma(0, 1, 6, 10, 12, 15) + b\Sigma(0, 1, 2, 3, 4, 5, 8, 9) + c\Sigma(0, 1, 2, 7, 11, 13, 14)$$

where  $a, b$ , and  $c$  are binary in nature, i.e., can assume values 0 or 1.

If we want to find out the minimal form of any switching function from its topological concept, we first of all find out the weights of each term of the function. The weight of any term gives the number of other terms in the function with which it can form a 1-cell. This concept of weight is slightly modified when we consider the terms of a multiple output switching function. If we consider the different transmissions individually, every term will have a certain weight associated with it. Now if a particular term is found to occur in two different transmissions we can say that the terms form a 1-cell in the sense that they can be combined and jointly realised in the output. So "1" will be added to the weight of each of them. In general, if any term is found to occur in  $p$  different transmissions, weight of that term in each of the individual transmission functions should be increased by " $p$ ".

Similar modifications will be made in the concept of  $k$ -cells present in a multiple output function. If a  $k$ -cell is found to be present in an individual transmission function which is a component of a multiple output function, we know that  $k$ -variables can be eliminated with corresponding economy in the number of diodes. But if the same  $k$ -cell occurs in  $q$  different component functions, a further economy can be effected by the sharing of the same output by those  $q$  different transmissions. If we consider an  $n$ -variable multiple output function in which the same  $k$ -cell is present in  $q$  different transmissions, it is easy to see that the net reduction in cost is equivalent to  $(n-k)(q-1)$  diodes. Thus when the question of minimisation of the multiple output function as a whole is considered, we can say that a cell of dimension  $(k+q-1)$  is present. This dimension is derived partly from the cell structure present and partly from the number of transmissions in which that cell structure occurs and both of these considerations are important regarding economy.

The idea of assigning new weights to terms and new dimensions to cell formations is prompted by the consideration that while aiming at the most economic realisation of a multiple output switching function we should not only explore the possibility of elimination of variables by seeking out the cell formations but also see how many times repetition can be avoided while realising the individual transmissions in the output.

Utilising the above mentioned ideas, simplification of a multiple output switching function can be done according to the following procedure :

#### Step 1

The weights of the different terms and the prime implicants of each individual transmission functions are found out. This can be done easily with the help of a mechanised grouping chart.

#### Step 2

All the different transmission functions are examined and the weights to be added to each term are found out. The new weights are thus determined.

#### Step 3

Prime implicants of the different functions are combined and total prime implicants of the multiple output switching function are found out.

#### Step 4

The essential prime implicants are identified and marked. If any term is found to be included in a prime implicant whose dimension is equal to the new weight of the term, then that prime implicant is an essential one with respect to the term. By dimension of the prime implicant its new dimension (i.e.,  $k+q-1$ ) is to be understood. The terms that are covered by essential prime implicants are cancelled.

*Step 5.*

We are now left with a number of non-essential prime implicants and a number of terms to be covered by them. Most economic way or ways of doing this are found out following a systematic procedure.

The suggested method is illustrated by the following example.

*Example.*

Find out the most economic multiple output two stage realisation of the following three 4-variable output functions :

$$f_1 = \Sigma(0, 1, 2, 4, 7, 9, 14)$$

$$f_2 = \Sigma(0, 1, 2, 5, 6, 13, 14, 15)$$

$$f_3 = \Sigma(0, 1, 2, 3, 4, 8, 12, 15)$$

Let us call  $f_1$ ,  $f_2$  and  $f_3$  as transmissions  $a$ ,  $b$  and  $c$  respectively.

The following table is made and entries in the different columns are do as suggested in the procedure.

TABLE III

Terms	Weight	Weight to be added	Total weight	Prime implicants	Combined Prime implicants	Essential Prime implicants
<i>a</i>						
0	3	2	5	(0-1)	abc (0-1)	
1	2	2	4	(0-2)	abc (0-2)	
2	1	2	3	(0-4)	ac (0-4)	ab $c'$ (0-2)
4	1	1	2	(1-9)	a (1-9)	$a$ $\bar{c}$ (0-4)
7	0	0	0	(7)	a (7)	a (7)]
9	1	0	1	(14)	ab (14)	a (1-9)
14	0	1	1			ab (14)
<i>b</i>						
0	2	2	4	(0-1)	b (1-5)	
1	2	2	4	(0-2)	b (2-6)	
2	2	2	4	(1-5)	b (5-13)	
5	2	0	2	(2-6)	b (6-14)	
6	2	0	2	(5-13)	b (13-15)	
13	2	0	2	(6-14)	b (14-15)	
14	2	1	3	(13-15)	bc (15)	
15	2	1	3	(14-15)		
<i>c</i>						
0	4	2	6	(0-1-2-3)	c (0-1-2-3)	
1	2	2	4		c (0-4-8-12)	
2	2	2	4	(0-4-8-12)		
3	2	0	2			c (0-1-2-3)
4	2	1	3			
8	2	0	2	(15)		c (0-4-8-12)
12	2	0	2			
15	0	1	1			bc (15)

In the last column it is found that  $abc(0-2)$  is an essential prime implicant with respect to  $a(2)$ . As  $c(0-2)$  is included in another essential prime implicant



$c(0-1-2-3)$  which is a cell of higher dimension we cancel the letter  $c$  from  $abc(0-2)$  to avoid unnecessary repetition and keep  $ab(0-2)$  as an essential prime implicant. Such cancellations are to be done whenever possible.

After cancelling the terms which are covered by the essential prime implications, we are left with the following terms, viz.,  $b(1)$ ,  $b(5)$ ,  $b(6)$  and  $b(13)$ . These are to be covered by the following non-essential prime implicants :

$\bar{a}\bar{b}\bar{c}(0-1)$ ,  $b(1-5)$ ,  $b(2-6)$ ,  $b(5-13)$ ,  $b(6-14)$ ,  $b(13-15)$  and  $b(14-15)$ . The most economic coverage or coverages can be easily found out.  $b(1-5) + b(13-15) + b(6-14)$  is one such minimal coverage. In Fig. 1 the circuit for realising the given functions  $f_1$ ,  $f_2$  and  $f_3$  in a minimal two stage form is shown.

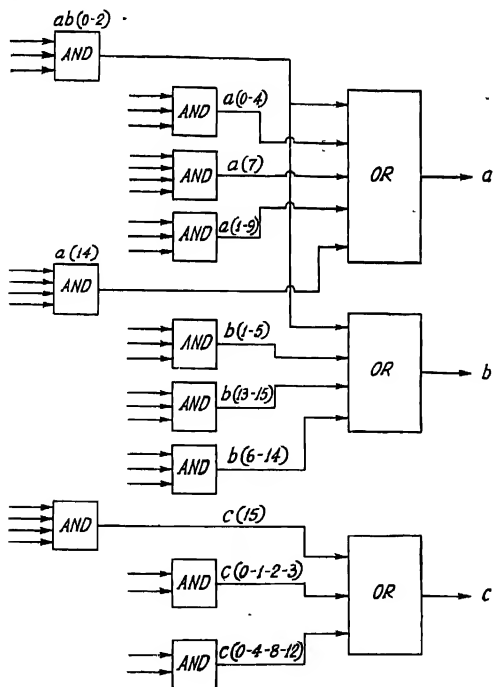


Fig. 1—Circuit for realising functions,  $f_1$ ,  $f_2$  and  $f_3$  in minimal two-stage form;

### CONCLUSION

A method has been described for extending the utility of a mechanised grouping chart. This is a distinct advantage because it avoids the necessity of mechanising a chart for large number of variables. Also the strain involved in considering

too many intersection points on a chart is avoided. The suggested procedure for simplification of multiple output switching functions presents no difficulty and the determination of the prime implicants and the identification of the essential ones for a given multiple output function can be done in a very straightforward manner.

#### ACKNOWLEDGMENT

The authors wish to express their indebtedness to Prof. J. N. Bhar, D.Sc., F.N.I., for guidance and keen interest in the work.

#### REFERENCES

- Bartee, C. T., 1961, *I. R. E. Transactions on Electronic Computers*, EC-10, 1, 21-30.  
 Caldwell, S. H., 1958, *Switching Circuits and Logical Design*, John Wiley & Sons, New York.  
 Calingaert, P., 1959, *Proceedings of an International Symposium on the Theory of Switching*, 1957, Part II, 59-73.  
 Choudhury, A. K. and Basu, M. S., 1962, *Ind. J. Phys.*, 36, 317.  
 McCluskey, E. J. (Jr.), 1956, *Bell System Tech. Jour.*, 35, 1417-1444.  
 Mukhopadhyay, A., 1961, (December), *I. E. E. Monograph*, No. 487E.  
 Urbano, R. H. and Mueller, R. K., 1956, *I. R. E. Transactions on Electronic Computers*, EC-5.  
 Vandling, G. C., 1960, *I. R. E. Transactions on Electronic Computers*, EC-9, 4, 447-486.  
 Singer, T., 1959, *Proceedings of an International Symposium on The Theory of Switching*, April, 1957, Part I, 125-133.  
 Warfield, J. N., 1958, *I. R. E. Transactions on Electronic Computers*, EC-7, 2, 180-181.

# ON THE ABSORPTION OF 3.18-CM MICROWAVES IN ANILINE AND SUBSTITUTED ANILINES\*

T. J. BHATTACHARYYA

OPTICS DEPARTMENT,  
INDIAN ASSOCIATION FOR THE CULTIVATION OF SCIENCE, CALCUTTA-32

(Received July 11, 1962)

**ABSTRACT.** The absorption of 3.18-cm microwaves in aniline, *o*- and *m*-chloroaniline and *o*-, *m*- and *p*-toluidine in the liquid state and also in their solutions in diphenyl ether at different temperatures has been studied. A maximum in the temperature vs. absorption curve has been observed and the time of relaxation has been determined in each case. The data for calculating the radius of the rotor in each case have been determined and the radius of the rotor has been calculated. The radius of the rotor in each case has been found to be 1.1 Å approximately and the rotor has been identified with the NH<sub>2</sub> group.

It has been concluded that the CNH<sub>2</sub> group retains its pyramidal structure as in the case of the NH<sub>3</sub> molecule even when one of the three H atoms is substituted by the benzene ring. These conclusions are compared with those drawn from results of investigation on the determination of permanent moments of the molecules.

## INTRODUCTION

It was concluded from the results of investigations on the absorption of microwaves in the 3-cm region in some aromatic alcohols by previous workers (Ghosh, 1954; Bhattacharya, 1960) that the OH group is capable of orienting freely about the C-O bond in the absence of any electro-negative element in the ortho position in the molecule, but such rotational motion is restricted when there is a strong electro-negative atom like chlorine in the ortho-position with respect to OH group (Ghosh, 1955b) because of formation of intramolecular weak linkages of the type OH...Cl. In the case of solutions of *o*-chlorophenol in suitable solvents these weak bonds break up and the OH group can orient freely about the C-O bond, exhibiting thereby an absorption in the 3-cm region (Bhattacharya, 1958).

The influence of different environments on the absorption of microwaves in similar compounds having the NH<sub>2</sub> group as a substituent was not studied by any previous worker. It was, therefore, thought worthwhile to investigate the absorption of 3.18-cm microwaves in aniline, *o*-chloroaniline, *m*-chloroaniline and *o*-, *m*- and *p*-toluidines and in their solutions in benzene, carbon tetrachloride and diphenyl ether and to find out to what extent the NH<sub>2</sub> group has freedom of orientation in the different environments.

\*Communicated by Prof S. C. Sarkar

## EXPERIMENTAL

The liquids were first dehydrated carefully with anhydrous magnesium sulphate and were then subjected to fractional distillation to get rid of traces of absorbed moisture which might show absorption in the 3-cm region. The solvents were also purified to get rid of moisture and finally they did not show any absorption in the 3-cm region.

The experimental arrangement used for studying the absorption of micro-waves in the pure liquids and in their solutions in diphenyl ether was the same as those described in an earlier paper (Bhattacharyya, 1958).

The data required to calculate  $a$ , the radius of the rotor in the case of aniline were obtained from the International Critical Tables. The values of  $\eta$ , the coefficient of viscosity of the liquids and solutions at different temperatures were determined with a viscometer by comparing the time of flow of a volume of the solution and that of a standard liquid. A temperature viscosity graph for each liquid was drawn and the viscosity of the liquid at the required temperature was obtained from the graph.

The dielectric constants,  $c$ , were measured by the resonance method developed by Hartshorn and Ward (1936). The refractive indices of the pure liquids were obtained from the International Critical Tables and those of the solutions were measured in the laboratory with Abbe's refractometer. Square of the index was taken as equal to  $\epsilon_0$ . In calculating the attenuation coefficient of the solutions the index thickness of the liquid in the solvent was used.

## RESULTS AND DISCUSSION

The attenuation coefficients of the pure substances at different temperatures are shown graphically in Fig. 1, and those of the solutions of the substances in diphenyl ether are shown in Fig. 2. No absorption maximum was found in the cases of the solutions of the substances in benzene and carbon tetrachloride. In these cases the absorption was found to increase continuously with the lowering the temperature but before the maximum could be reached the mixtures froze.

The concentration of the solution in each case was 30% by volume.

It can be seen from Fig. 1 that pure aniline shows maximum absorption at 23°C. In the cases of pure *o*-chloroaniline and *m*-chloroaniline the maxima occur at 30°C. Ortho- and *m*-toluidines show absorption maxima at 20°C and 25°C respectively. The liquid *p*-toluidine like its solutions in benzene and CCl<sub>4</sub> shows increasing absorption with lowering of temperature till it freezes.

The radius of the rotor in the cases in which absorption maxima were found were calculated by using Debye's formula as discussed in an earlier paper (Bhattacharyya, 1960). The data required for the calculation of the radius of the rotor along with the values of the radius thus calculated are given in Table I.

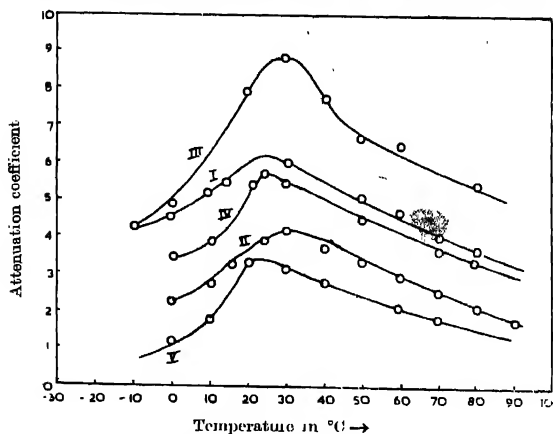


Fig. 1. Temperature-attenuation curves for absorption of 3.18-cm. microwaves:  
I. Aniline II. *o*-Chloroaniline III. *m*-Chloroaniline IV. *m*-Toluidine V. *o*-Toluidine.

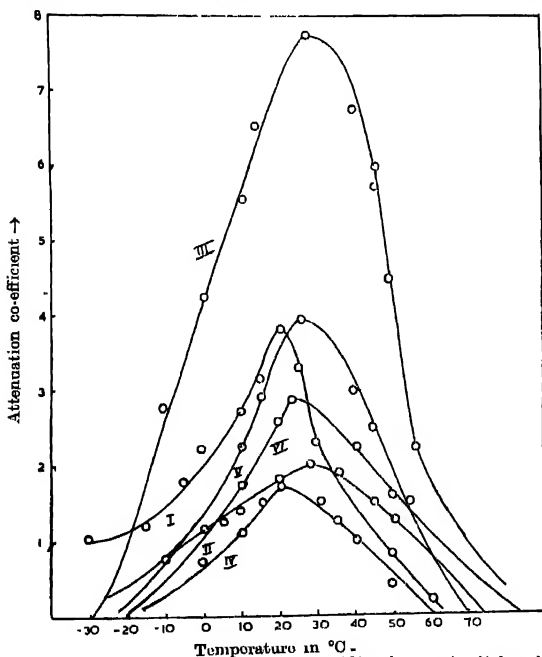


Fig. 2. Temperature-attenuation curves for 30% solutions in diphenyl ether:  
I. Solution of aniline II. Solution of *o*-chloroaniline III. Solution of *m*-chloroaniline  
IV. Solution of *o*-toluidine V. Solution of *p*-toluidine VI. Solution of *m*-toluidine.

TABLE I  
Frequency = 9415 Mc/sec

Substance	$\epsilon$	$\epsilon_0$	T°K	$\eta \times 10^{-2}$	$\tau \times 10^{11}$ sec	$\alpha \times 10^{18}$ cm
Aniline	7.2	= 2.52	296	4.02	1.405	1.043
<i>o</i> -Chloroaniline	11.0	= 2.53	303	3.10	1.228	1.097
<i>m</i> -Chloroaniline	11.2	= 2.53	303	3.30	1.249	1.080
<i>o</i> -Toluidine	6.4	= 2.47	298	3.80	1.450	1.071
<i>m</i> -Toluidine	6.0	= 2.47	293	3.75	1.473	1.081
30% Aniline in diphenyl ether	5.1	= 2.47	293	4.4	1.529	1.038
30% <i>o</i> -Chloroaniline in diphenyl ether	5.83	= 2.4963 = 2.50	301	3.3	1.3922	1.1054
30% <i>m</i> -Chloroaniline in diphenyl ether	5.9	= 2.4963 = 2.50	301	3.35	1.3852	1.1023
30% <i>o</i> -Toluidine in diphenyl ether	5.01	= 2.465 = 2.47	293	3.80	1.535	1.0914
30% <i>m</i> -Toluidine in diphenyl ether	4.86	= 2.465 = 2.47	296	3.7	1.5449	1.093
30% <i>p</i> -Toluidine in diphenyl ether	5.0	= 2.465 = 2.47	298	3.75	1.5357	1.1064

The radius of the rotor calculated for the different substances were found to be 1.1A approximately both in the pure liquids and in the solutions. The same value of the radius of the rotor in all these cases suggests that the rotor in all these cases must be a substituent group common to all. As the  $\text{NH}_2$  group is the only group common to the molecules of all the substances the rotor is assumed to be the  $\text{NH}_2$  group. These investigations give us interesting information regarding the structure of this substituent group. If the  $\text{NH}_2$  group would possess a planar structure we would not expect any absorption, because of the cancellation of the components of the dipole moments of each N-H bond perpendicular to C-N bond. If the  $\text{NH}_2$  group would be supposed to retain its pyramidal structure as in the  $\text{NH}_3$  molecule even when one of the H atoms is substituted by the benzene ring the dipole moment would be inclined at an angle  $\theta$  to the C-N bond and it could orient under the influence of the incident microwaves and we might expect absorption of the microwaves. Thus the presence of absorption of microwaves in aniline and substituted anilines suggests the pyramidal structure of  $\text{NH}_2$  group in these molecules. This conclusion is in agreement with the results obtained by Tiganik (1931) in his investigations on the dielectric behaviour of chloroanilines and toluidines. He found that though the calculations of dielectric constants based on both planar and non-planar structure of  $\text{NH}_2$  group in meta substituted anilines yield results in agreement with the experimental results yet in the cases

of ortho substituted compounds calculations based on pyramidal structure give results more in agreement with the experiments than those calculated on the basis of planar structure of  $\text{NH}_3$ .

The absence of any absorption maxima in the cases of the solutions in benzene and carbon tetrachloride may be due to the low viscosity of these solutions. From Table I it will be evident that for maximum absorption a viscosity of the order of  $3 \times 10^{-2}$  is necessary, but such a high viscosity cannot be obtained in the cases of solutions in benzene and carbon tetrachloride. To verify whether the low viscosity of the solutions was responsible for the full transmission of the microwaves through these solutions diphenyl ether, which is more viscous than either carbon tetrachloride or benzene, was chosen as the solvent and the absorption maxima were found to lie in the temperature region  $20^\circ\text{C}$ - $30^\circ\text{C}$  in these cases. The radius of the rotor calculated from the observed values of  $\tau$  was found to be 1.1A approximately. This is fairly in agreement with the values obtained in the cases of the pure substances.

Thus it can be concluded that the N-H bond makes a fairly large angle with the direction of the C-N bond so as to make the radius of the rotor about 1.0A and this method is useful in finding such angles at least approximately.

#### ACKNOWLEDGMENT

The author is indebted to Professor S. C. Sirkar, D.Sc., F.N.I for his constant guidance throughout the progress of the work. Thanks are also due to Dr. S. B. Banerjee for his helpful discussion.

#### REFERENCES

- Bhattacharyya, T. J., 1958, *Ind. J. Phys.*, **32**, 573.  
 Bhattacharyya T. J., 1960, *Ind. J. Phys.*, **34**, 358.  
 Ghosh, D. K., 1954, *Ind. J. Phys.*, **28**, 191.  
 Ghosh, D. K., 1955, *Ind. J. Phys.*, **29**, 450.  
 Hartshorn, L. and Ward, W. H., 1930, *J. Inst. Elec. Engr. (London)*, **79**, 597.  
 Tigaruk, L., 1931, *Zeit. f. Physikalische Chemie*, **14B**, 135.

## Letters to the Editor

The Board of Editors will not hold itself responsible for opinions expressed in the letters published in this section. The notes containing reports of new work communicated for this section should not contain many figures and should not exceed 500 words in length. The contributions must reach the Assistant Editor not later than the 15th of the second month preceding that of the issue in which the letter is to appear. No proof will be sent to the authors.

9

### A GENERAL METHOD OF FINDING THE PRINCIPAL CRYSTALLINE SUSCEPTIBILITIES OF TRICLINIC CRYSTALS

U. S. GHOSH AND R. N. BAGCHI

DEPARTMENT OF MAGNETISM, INDIAN ASSOCIATION FOR THE CULTIVATION OF SCIENCE, JADAVPUR, CALCUTTA-32

(Received August 3, 1962)

The existing methods (Mathur, 1960, Krishnan and Mookherji 1936, 1938) to determine the principal crystalline susceptibilities of triclinic crystals are considered to be difficult, approximate and extremely tedious. We shall indicate a new method of finding the principal susceptibilities and their directions in such a crystal. The method is quite general, comparatively easier and involves no approximation or trial and error. Its accuracy depends only upon that of the measuring apparatus employed.

Let us take any one of the three principal crystallographic axes of a triclinic crystal as the  $x$ -axis. The perpendicular to this axis lying in any adjacent principal crystallographic plane is taken as the  $y$ -axis and a line perpendicular to both  $x$  and  $y$  axes is the  $z$ -axis. Consider any crystallographic plane whose Millerian indices are  $h, k, l$ . The normal to this plane ( $hkl$ ) has direction cosines  $\xi, \eta, \zeta$  relative to the  $x, y, z$  axes respectively. The above choice of co-ordinate axes enables us to express the direction cosines  $\xi, \eta, \zeta$  in terms of Millerian indices, axial length ratios, triclinic angles and a dihedral angle between two principal planes (these are not all independent parameters but are retained for convenience of expression and calculation).

The equation of the ellipsoid of crystalline susceptibility (per gm-molecule) referred to the  $x, y, z$  system is

$$K_{xx}x^2 + K_{yy}y^2 + K_{zz}z^2 + 2K_{xy}xy + 2K_{xz}xz + 2K_{yz}yz = 1$$



where  $K_{xx}$ ,  $K_{yy}$ ,  $K_{zz}$ ,  $K_{xy}$ ,  $K_{yz}$ ,  $K_{xz}$  are the six independent components of the susceptibility tensor (per gm-molecule) referred to the  $x, y, z$  system. If the values of the above six tensor components are determined, the three principal crystalline susceptibilities are given by the three roots of  $\chi$  of the following determinantal equation

$$\begin{vmatrix} K_{xx}-\chi & K_{xy} & K_{xz} \\ K_{xy} & K_{yy}-\chi & K_{yz} \\ K_{xz} & K_{yz} & K_{zz}-\chi \end{vmatrix} = 0 \quad \dots \quad (1)$$

The direction cosines of any one of the principal crystalline susceptibilities, say,  $\chi_i$ , relative to  $x, y, z$  axes respectively, are given by

$$\left. \begin{aligned} f_i &= [K_{xy}K_{yz} - K_{xz}(K_{yy} - \chi_i)]Q \\ g_i &= [K_{xy}K_{xz} - K_{yz}(K_{xx} - \chi_i)]Q \\ h_i &= [(K_{xx} - \chi_i)(K_{yy} - \chi_i) - K_{xy}^2]Q \end{aligned} \right\} \quad \dots \quad (2)$$

$$\text{where } Q = \pm \{ [K_{xy}K_{yz} - K_{xz}(K_{yy} - \chi_i)]^2 + [K_{xy}K_{xz} - K_{yz}(K_{xx} - \chi_i)]^2 + [(K_{xx} - \chi_i)(K_{yy} - \chi_i) - K_{xy}^2]^2 \}^{-\frac{1}{2}}$$

To find the values of the 6 tensor components, we have to measure  $\chi_{max} + \chi_{min}$  along six non-parallel planes of the crystal where  $\chi_{max}$  and  $\chi_{min}$  are the maximum and minimum susceptibilities (per gm-molecule) respectively in a plane. The value of  $\chi_{max} + \chi_{min}$  in a plane whose normal has direction cosines  $\xi, \eta, \zeta$  has been calculated by us to be

$$\chi_{max} + \chi_{min} = K_{xx}(1 - \xi^2) + K_{yy}(1 - \eta^2) + K_{zz}(1 - \zeta^2) - 2K_{xy}\xi\eta - 2K_{xz}\xi\zeta - 2K_{yz}\eta\zeta \quad (3)$$

Hence working with six planes we shall have six linear equations of the type (3) and the six unknowns  $K_{xx}$ ,  $K_{yy}$ ,  $K_{zz}$ ,  $K_{xy}$ ,  $K_{xz}$  and  $K_{yz}$  can be determined.

The maximum and minimum susceptibilities in any plane can be measured as follows. (1) Measure the anisotropy ( $\chi_{max} - \chi_{min}$ ) in the plane. (2) The crystal is then suspended freely in a horizontal type susceptibility balance (Ghosh, P. K., to be published) so that the plane in question is horizontal. With a flexible and twistable suspension the maximum susceptibility automatically sets itself in the direction of magnetic field. Measurement of susceptibility under this condition gives  $\chi_{max}$  in the given plane. In this way both  $\chi_{max}$  and  $\chi_{min}$  in six different planes can be obtained with a good degree of accuracy, and hence the magnitude and directions of the principal crystalline susceptibilities from equations (1), (2) and (3).

Measurements on  $\text{CuSO}_4 \cdot 5\text{H}_2\text{O}$  and  $\text{CuSeO}_4 \cdot 5\text{H}_2\text{O}$  are in progress in this laboratory. The details of the theory of the method and experimental results will be published shortly.

The authors are grateful to Professor A. Bose, D.Sc., F.N.I., for his guidance and valuable suggestions throughout the progress of the work.\*

## REFERENCES

- Ghosh, P. K., 1961, *Ind. J. Phys.*, **35**, 319  
 Krishnan, K. S. and Mookherji, A., 1936, *Phys. Rev.*, **50**, 860.  
 1938, *Phys. Rev.*, **54**, 534.  
 Mathur, S. C., 1960, *Proc. Nat. Inst. Sc. India*, **A26**, 581.

\*After we had sent the paper for publication, Dr. D. Neogi of Agra College who participated in our Seminar lecture in which this problem was worked out, informed us, (Private communication) that we could have taken an arbitrary set of orthogonal axes ( $x, y, z$ ) and the 5 measurements of  $\chi_{max}$  to  $\chi_{min}$  with the following conditions together with the measurement of mean susceptibility: (1)  $y$ -axis vertical, (2)  $z$ -axis vertical, (3)  $z$ - $x$  plane vertical and  $z$  inclined to the vertical, (4)  $x$ - $y$  plane vertical and  $x$  inclined to the vertical, (5),  $y$ - $z$  plane vertical and  $y$  inclined to the vertical, to determine  $\chi_1$ . This method essentially does not differ from that of ours. But in practice his method involves some very tedious angular settings of the crystals which are very likely to cause large errors in measurement and are very time consuming. Further, it will be extremely difficult to correlate the principal tensor axes with the crystal axes without which the determination of the magnitudes of the principal tensors alone will have little significance or use.

# ELECTRON TEMPERATURE IN AIR UNDER LOW FREQUENCY ELECTRIC DISCHARGES EXCITED BY EXTERNAL SLEEVE ELECTRODES

D. P. JATAR AND K. R. CHANDRAKAR

DEPARTMENT OF PHYSICS, UNIVERSITY OF SAUGAR, SAUGAR, M.P.

(Received July 24, 1961, Resubmitted March 15, 1962)

The knowledge of electron energies is essential for understanding the mechanism of any type of electric discharge. So far there has been no attempt to study this quantity in low frequency discharges excited by external sleeve electrodes. In the present work, the floating double probe method of Johnson and Malter (1950) was used. A cylindrical tube of 32 mm diameter, filled with air at 2 mm Hg., was excited by low frequency (50 c/s) potentials. Two probes made of tungsten wire of 0.15 mm diameter were sealed in the tube 2 mm apart. The inter-sleeve distance,  $ds$ , was varied over the range from 2 to 5 cm. The distance,  $d_p$ , of the probes from a given sleeve was also varied.

The probe characteristics obtained were similar to those reported by Johnson and Malter. A typical characteristic is shown in Fig. 1. The values of the electron temperature calculated by the 'equivalent resistance method' were found to be smaller than those calculated by the other methods. There was an appreciable variation in the values of the electron temperature for different sleeve distances and probe positions. Considering the mean value of the electron temperature for each sleeve distance and probe position, the electrons can be divided into three groups of average temperature 3.0, 5.0, and  $7.5 \times 10^4$  °K.

In the negative glow of d.c. discharges, three groups of electrons, termed the fast, the medium and the slow electrons, have been reported (Francis, 1956), their energies varying from 25 to 0.5 eV. The recent results of Okuda and Yamamoto (1956) indicate that the fast electrons are observed only as a discrepancy in single probe measurements and are absent in multiple probe measurements. The absence of electron energies beyond about 10 ev may be attributed to this. However, the present glow did not exhibit regions corresponding to the negative glow and the positive column and a different mechanism for this type of discharge may be necessary.

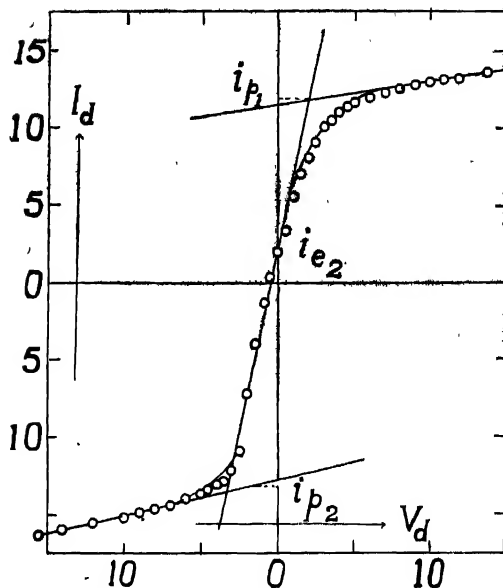


Fig. 1. Double probe potential-current characteristic.

$I_d$ —Probe current in arbitrary units.

$V_d$ —Probe potential in volts.

$$i_{p1} = 11.8; \quad i_{p2} = 13.4; \quad i_{e2} = 15.5$$

$$R_0 = \frac{dV_d}{dI_d} = \frac{2.0}{11.5}; \quad G = \frac{i_{e2}}{\Sigma i_p} = \frac{15.5}{25.2}$$

$i_{p1}$ ,  $i_{p2}$ ,  $i_{e2}$ , and  $R_0$  measured at  $V_d = 0$

$$T_0 = 11600(-C^2) R_0 \Sigma i_p \\ = 1.203 \times 10^4 \text{ } ^\circ\text{K.}$$

Grateful thanks of the authors are due to the Council of Scientific and Industrial Research, New Delhi, for awarding the Junior Research Fellowship to one of the authors. (K.R.C.)

#### REFERENCES

- Johnson, E. O. and Malter, L., 1950, *Phys. Rev.*, **80**, 58.  
 Francis, Gordon, 1956, 'Handbook of Physics', Springer Verlag, Berlin.  
 Okuda, T. and Yamamoto, K., 1960, *J. Appl. Phys.* **31**, 158,  
 Chandrakar, K. R., 'Probe Studies under low frequency electric discharges in air',  
 Ph.D. Thesis, University of Saugar, (1960).

# THE INFRA-RED SPECTRUM OF CYCLOHEXYL BENZENE

R. N. BAPAT

PHYSICS DEPARTMENT, COLLEGE OF SCIENCE, NAGPUR

(Received June 9, 1962)

The infrared spectrum of cyclohexyl benzene was recorded on the Perkin-Elmer infrared spectrophotometer using sodium chloride optics. The substance was introduced directly in between the sodium chloride plates and the thickness of the film was 0.1 m.m. This was kept in front of one of the apertures. In front of the second aperture only one plate of sodium chloride having the same thickness as the total thickness of these two plates was kept. In case of broad bands, in order to define them further the plates were pressed together to include a very thin film. In Fig. 1 the infrared spectrum of cyclohexyl benzene is given.

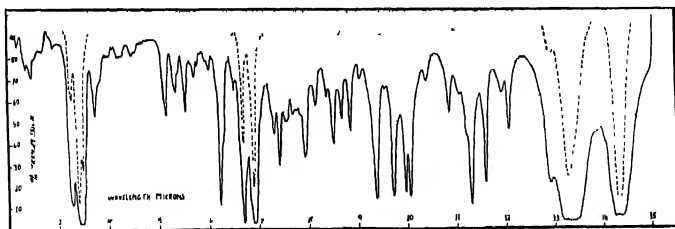


Fig. 1. Infrared absorption spectrum of cyclohexyl benzene.

## RESULTS

All the bands observed in case of cyclohexyl benzene are given below, with the intensities for the same (v<sub>vw</sub>-very very weak, v<sub>w</sub>-very weak, m<sub>w</sub>-medium weak, w-weak, s-strong, v<sub>s</sub>-very strong, v<sub>vs</sub>-very very strong). Infrared spectrum of cyclohexyl benzene.

4545 v.v.w.

4201 v.v.w.

4016 w.

3424 v<sub>w</sub>.

3039 s

2932 v<sub>s</sub>

2865 v<sub>s</sub>

2666 m<sub>w</sub>

1941 mw	1273
1886	1264 mw
1869 vw	1228 w
1851	1197 vvw
1801 mw	1177 m
1769	1154 mw
1748 vvw	1131 m
1727	1104 mw
1694	1068 s
1680	1047
1661 vvw	1029 s
1644	1005 s
1607 s	996 s
1588 m	961 vvw
1563	922 mw
1538 vw	904
1495 vs	892
1461	884 s
1449 vs	863 ms
1369 w	840 vvw
1350 mw	829 m
1328 vvw	775 ms
1298 vvw	753 vvs
1290 vvw	696 vvs

The discussion and other details will be published elsewhere.

## BOOK REVIEWS

**LECTURES ON FLUID MECHANICS.** By Sydney Goldstein. Pp. i-xvi+309. Interscience Publishers Ltd., London; Interscience Publishers Inc, New York, 1960. Price \$ 6.60.

This is the second of the four volumes in which the proceedings of the Summer Seminar on Applied Mathematics held at the University of Colorado in June 1957 were to be published. The object of the Seminar "was to give mature mathematicians an opportunity to become familiar with some of the major sectors in applied mathematics". The present volume contains twelve lectures on Fluid Mechanics by the author and two special lectures by J. M. Burgers.

The first Chapter deals with Kinematics. Starting with an explanation of Lagrangian and Eulerian specifications, it deals with acceleration, equation of continuity, boundary conditions, the rate-of-strain component, the vorticity, vortex lines and tubes, irrotational motions, vector potentials and stream functions. Vector notation has been used in all these treatments. Chapter 2 dealing with Dynamics of the General Fluid starts with the stress tensor and gives successively the equations of momentum, angular momentum and energy. Chapter 3 deals with electric and magnetic forces in a fluid and the discussions are based on Minkowski's theory of the electrodynamics of moving media. The theory of motion of inviscid fluids is given in Chapter 4. The conditions for steady motion, the equation for velocity potential in the irrotational motion of a gas, the theorems of Kelvin, Helmholtz and Lagrange, Cauchy's vorticity equations and shock waves are dealt with in this Chapter.

The properties of viscous fluids, and Navier-Stokes equations are discussed in Chapter 5 and exact solutions of Navier-Stokes equations are given in the next Chapter. The boundary-layer theory and its extension to incompressible fluids are discussed in Chapters 7 and 8 respectively. Chapter 9 deals with boundary layers in gases, and dynamics of inviscid gases are given in Chapter 11. The next two chapters deal respectively with mixture and high temperature effects in gases and longitudinal (electrostatic) waves in a gas. There are four appendices and two special lectures by J. M. Burgers on some problems of magneto-gasdynamics.

References to journals and books have been given whenever necessary in the text and a list of books and monographs has also been included.

As indicated earlier, the volume is meant for advanced students as well as for research workers in Applied Mathematics who will find the volume to be extremely useful to them. The get up of this cloth-bound volume is quite good.

S. C. S.

INTERNATIONAL DIRECTORY OF RADIOISOTOPES VOLUME I. Pp. i-xiii+264. International Atomic Energy Agency, Vienna, 1959. Price not stated.

As indicated in the preface of this volume, it has been published in accordance with the recommendations of the Preparatory Commission of the International Atomic Energy Agency with the object of assisting the Member States to acquire the knowledge and skills needed to make full use of radioisotopes and radiation sources. It is acknowledged that the Member States have co-operated in this attempt by providing the information required for the peaceful uses of atomic energy.

The first thirteen pages of the volume deal with (1) Safe handling of radioactive materials, (2) Suppliers of radioisotopes, (3) Additional information on radioisotope production, (4) Definition of terms and (5) Information on tables. The tables of Radioisotopes run through 263 pages and give data for 185 radioisotopes. Each table gives the information about the radio isotope in six columns, giving respectively the description, the supplier and code, the unit weight, the specific and total activity, the price and some remarks about fission product, purity, etc.

It is needless to point out that it was possible to collect such a valuable store of information only with the help of international cooperation. Every scientist who is engaged either in research work or in any other humanitarian work in which the use of radio isotopes is indispensably necessary will find the Directory immensely useful to him. In the opinion of the reviewer this volume should find a place in the library of every scientific institution.

S. C. S.

ADVANCES IN SPECTROSCOPY, VOLUME II. Edited by H. W. Thompson. i-xi+479 Interscience Publishers Inc., New York, 1961. Price \$ 13.00

This is the second volume of the series of volumes proposed to be published annually and it contains articles on nine different topics contributed by different authors.

In the first article on Application of Atomic Absorption Spectra to chemical Analysis by A. Walsh the author has discussed the characteristics of the atomic absorption spectra, experimental techniques for measuring peak absorption, advantages and limitation of this method of analysis and the present status of the method.

The second article contributed by A. C. Gaydon deals with Spectra of Flames. After describing typical burners used for producing suitable flames, this article gives information about the use of flames in absorption and emission spectroscopy in the qualitative as well as quantitative estimation of molecules.



The third article on X-ray Spectroscopy contributed by Herbert Friedman deals with the details of technique required for the method of analysing minerals by X-ray spectroscopy. Various difficulties encountered in the method and the means of overcoming them have been discussed in detail.

The fourth article on Nuclear Magnetic Resonance by R. E. Richards deals with the theory of the phenomenon including derivation of Bloch equations. The discussions on N.M.R. in solids include those on dipole-dipole coupling, nuclear electric quadrupole interaction and effect of molecular motion in the solid. Next, the chemical shifts, spin-spin coupling and spin-lattice relaxation in liquid and gases have been discussed. Finally, the experimental techniques have been described in detail.

In the fifth article W. Vedder and D. F. Hornig have discussed the Infrared Spectra of Crystals. The method of calculating normal vibrations of three dimensional lattice with the help of group theory has been explained and discussions on the spectra of a few typical molecules in the crystalline state have also been included.

The sixth article by J. H. Jaffe deals with Refraction of Gases in the Infrared and gives the details and principles of the Rehovoth refractometer.

The seventh article by K. P. Norris gives an account of the Infrared Spectra of Microorganisms, and the eighth article by G. H. Beaven deals with the spectra of proteins and related compounds. The methods and the results of investigations on the ultraviolet absorption spectra, fluorescence and phosphorescence spectra of proteins have been discussed in detail.

The last article on "Some recent developments in the Theory of Molecular Energy Levels" has been contributed by H. C. Longuet-Higgins. The theory deals mainly with the coupling between the vibrational and electronic motions of the molecules and the significance of the Jahn-Teller and Renner effects has been discussed in detail.

Each of the articles includes an exhaustive list of references. Research workers interested in the various topics discussed in the volume will be greatly benefited by the publication of this volume.

S. C. S.

—

# RESPONSE FUNCTION OF A DEGENERATE ELECTRON GAS

P. MISRA AND D. MISRA

DEPARTMENT OF PHYSICS, RAVENSHAW COLLEGE, CUTTACK

(Received November 13, 1961)

**ABSTRACT.** The electrical behaviour of a homogeneous electron gas is best described by the 'Response function'  $\vec{K}(k\omega)$  defined by the relation  $\vec{J}_a(k, \omega) = K_{a\beta}(k, \omega) \vec{E}_\beta(k, \omega)$  which in space time configuration becomes a nonlocal and acausal relation  $\vec{J}_a(\vec{r}, t) = \int_{-\infty}^{+\infty} \int d\vec{r}' dt' K_{a\beta}(\vec{r}-\vec{r}', t-t') \vec{E}_\beta(\vec{r}', t')$ ,  $\vec{J}$  and  $\vec{E}$  being the current density and electric field respectively and  $\vec{J}$  and  $\vec{E}$  their Fourier transforms. This function is analogous to the inverse of 'Impedance' in electric circuits and determines how an electrical disturbance propagates in the electron gas and under what circumstances the disturbance becomes oscillatory. The expression for the energy loss and scattering of charged particles involve this response function. For these reasons the function is a very important parameter for an electron gas. So far, this function has been evaluated for an electron gas at absolute zero temperature. In this paper we have evaluated this function at temperatures in the neighbourhood of absolute zero temperature by using the Boltzmann-Vlasov equations and Fermi-Dirac distribution law of electron energies. Causality condition has been invoked on  $K_{a\beta}(\vec{r}-\vec{r}', t-t')$  to make the current-electric field relation causal. Condition under which the electrical disturbance becomes oscillatory are discussed. It is found that these conditions are the dispersion formulae for the Plasma oscillations of the electron gas.

## RESPONSE FUNCTION FROM BOLTZMANN-VLASOV EQUATION

The linearised Boltzmann-Vlasov equation

$$\frac{\partial f_1}{\partial t} + \vec{u} \cdot \vec{\nabla}_r f_1 = \frac{n_0 e \vec{E}}{m} \cdot \vec{\nabla}_u f_0, \quad (1)$$

(where  $f_0$  is the equilibrium distribution function and  $f_1$  represents the departure from this equilibrium value and  $\vec{E}$ , the electric field resulting thereby) can be solved with the help of the Green's function  $B(\vec{r}, \vec{u}, t)$  defined by

$$\left( \frac{\partial}{\partial t} + \vec{u} \cdot \vec{\nabla}_r \right) B(\vec{r}, \vec{u}, t) = \delta(\vec{r}) \delta(t) \quad \dots \quad (2)$$

This solution is

$$f_1(\vec{r}, t) = \frac{n_0 e}{m} \int \vec{dr}' \int_{-\infty}^{+\infty} dt' B(\vec{r}-\vec{r}', t-t', \vec{u}) \vec{\nabla}_u f_0 \cdot \vec{E}(\vec{r}', t') \quad \dots (3)$$

and gives the following expression for the current density  $\vec{J}(\vec{r}, t)$ :

$$\begin{aligned} J_\alpha(\vec{r}, t) &= -e \langle u_\alpha f_1(\vec{r}, t) \rangle = -\frac{n_0 e^2}{m} \int \vec{dr}' \int_{-\infty}^{+\infty} dt' \langle u_\alpha B(\vec{r}-\vec{r}', t-t', \vec{u}) \frac{\partial f_0}{\partial u_\beta} \rangle E_\beta(\vec{r}', t') \\ &= \int \vec{dr}' \int_{-\infty}^{+\infty} dt' K_{\alpha\beta}(\vec{r}-\vec{r}', t-t') E_\beta(\vec{r}', t'), \quad \dots (4) \end{aligned}$$

where

$$\begin{aligned} K_{\alpha\beta}(\vec{r}, t) &= -\frac{\omega_0^2}{4\pi} \int \vec{du} B(\vec{r}, t, \vec{u}) u_\alpha \frac{\partial f_0}{\partial u_\beta}, \\ \omega_0^2 &= \frac{4\pi n_0 e^2}{m} \quad \text{and} \quad \langle F(\vec{u}) \rangle = \int \vec{du} F(\vec{u}). \end{aligned}$$

In energy-momentum space, equation (4) reads

$$\vec{J}_\alpha(\vec{k}, \omega) = \vec{K}_{\alpha\beta}(\vec{k}, \omega) \vec{E}_\beta(\vec{k}, \omega), \quad \dots (5)$$

where the curly letters stand for the Fourier transforms of their ordinary counterparts.  $\vec{K}_{\alpha\beta}(\vec{k}, \omega)$  is the 'response function' of the electron gas, and is given by

$$\vec{K}_{\alpha\beta}(\vec{k}, \omega) = \frac{-\omega_0^2}{4\pi} \int \vec{du} \vec{B}(\vec{k}, \omega, \vec{u}) u_\alpha \frac{\partial f_0}{\partial u_\beta} \quad \dots (6)$$

The value of  $\vec{B}(\vec{k}, \omega, \vec{u})$  can be found by solving Eqn. (2). This solution is obtained by taking Fourier transforms of both sides of Eq. (2). One gets

$$\vec{B}(\vec{k}, \omega) = \frac{i}{\omega - \vec{k} \cdot \vec{u}} \quad \dots (7)$$

which on substitution in (6) gives for

$$\begin{aligned} \vec{k} &= (0, 0, k), \quad \vec{u} = (u_1, u_2, u) \\ \vec{K}_{\alpha\beta}(\vec{k}, \omega) &= \frac{-i\omega_0^2}{4\pi} \int \vec{du} \frac{u_\alpha}{\omega - \vec{k} \cdot \vec{u}} \frac{\partial f_0}{\partial u_\beta} \Big|_{(\omega - ku)} \\ &= \frac{-i\omega_0^2}{4\pi} \int \vec{du} \frac{u_\alpha \partial f_0 / \partial u_\alpha}{\omega - ku} \delta_{\alpha\beta} = \frac{-i\omega_0^2}{4\pi} I_\alpha(k, \omega) \delta_{\alpha\beta} \quad \dots (8) \end{aligned}$$

It will be seen that the integrand of  $I(k, \omega)$  is singular at  $u = \omega/k$ . It has been shown by Pradhan that the prescription for integration across this singular point can be obtained by invoking the causality condition:

$$K_{\alpha\beta}(\vec{r}-\vec{r}', t-t') = 0 \quad \text{for } t < t' \quad (9)$$

This condition will be satisfied if we give a small positive imaginary part to  $\omega$  in Eq. (8) in which case we have

$$I_{\alpha}(\vec{k}, \omega) = \int d\vec{u} \frac{u_{\alpha} \frac{\partial f_0}{\partial u_{\alpha}}}{\omega - k\vec{u} + i\epsilon}, \quad \bar{K}_{\alpha\beta}(\vec{k}, \omega) = \frac{-i\omega_0^2}{4\pi} \delta_{\alpha\beta} I_{\alpha}(\vec{k}, \omega) \dots \quad (10)$$

Explicit expressions for  $\bar{K}_{\alpha\beta}(\vec{k}, \omega)$  have been obtained by Lindhard (1954) for a degenerate electron gas at absolute zero temperature in which the imaginary part is arbitrary due to lack of proper treatment of the singularity in Eq. (8). Expressions for this same function for oscillatory disturbance† both at absolute zero and in the neighbourhood of absolute zero temperature with correct treatment of the singularity have been obtained by Pradhan and one of the present authors (1960). It is the purpose of the present work to find expressions for all the com-

ponents of  $\bar{K}_{\alpha\beta}(\vec{k}, \omega)$  at absolute zero as well as in the neighbourhood of absolute zero temperature using Eq. (10). Since exact evaluation which should be valid for all temperatures, is not possible, we employ Sommerfeld approximation (Sommerfeld, 1928).

#### COMPUTATION OF $\bar{K}_{tr}(k, \omega)$

In this section we shall make a computation of  $\bar{K}_{tr}(k, \omega) = \bar{K}_{11,22}(k, \omega)$  for temperatures in the neighbourhood of absolute zero by employing Sommerfeld's approximation for evaluation of the integral on the R.H.S. of Eq. (10). The zero temperature value can be obtained from this expression by letting temperature go to zero. According to Eq. (10)

$$\begin{aligned} \bar{K}_{tr}(k, \omega) &= \frac{-i\omega_0^2}{4\pi} \int d\vec{u} \frac{u_1 \frac{\partial f_0}{\partial u_1}}{\omega - k\vec{u} + i\epsilon} = \frac{-i\omega_0^2}{4\pi} \int_{-\infty}^{+\infty} du \frac{F(u)}{\omega - ku + i\epsilon} \\ &= \frac{-i\omega_0^2}{4\pi} P \int_{-\infty}^{+\infty} du \frac{F(u)}{\omega - ku} - \frac{\omega_0^2}{4k} F\left(\frac{\omega}{k}\right) = K_{tr}^{(1)} + iK_{tr}^{(2)} \dots \quad (11) \end{aligned}$$

---

†For oscillatory disturbance  $\bar{K}_{33}(\vec{k}, \omega)$  takes such a value that the dielectric constant  $\epsilon_{33}(\omega) = 1 - \frac{4\pi k_{33}(\omega)}{\omega}$  is identically zero for all temperatures. This will be discussed in section 4 of this paper.

where for a Fermi distribution :

$$F(u) = \int_{-\infty}^{+\infty} du_1 \int_{-\infty}^{+\infty} du_2 \cdot u_1 \frac{\partial f_0}{\partial u_1} = -\frac{4\pi}{n_0} \left(\frac{m}{h}\right)^3 \left[ \frac{1}{m\beta} \log(1 + e^{-v + \frac{1}{2}m\beta u^2}) \right]$$

Therefore :

$$\begin{aligned} K_{tr}^{(2)}(k, \omega) &= -\frac{\omega_0^2}{4\pi} P \int_{-\infty}^{+\infty} du \frac{F(u)}{\omega - ku} \\ &= -\frac{\omega_0^2}{mn_0\beta} \left(\frac{m}{h}\right)^3 P \int_{-\infty}^{+\infty} du \frac{\log(1 + e^{-v + \frac{1}{2}m\beta u^2})}{\omega - ku} = \frac{\omega_0^2 m^2}{n_0 h^3 \beta k} I(u) \end{aligned} \quad \dots (12)$$

where

$$I(u) = \int_0^\infty dx \frac{d\phi/dx}{1 + e^{-v+x}} \dots \text{ with } d\phi/dx = \log \left| \frac{\omega/k + u}{\omega/k - u} \right|.$$

According to Sommerfeld,

$$I(u) = \phi(x=v) + 2 \sum_{n=1}^{\infty} C_{2n} \left( \frac{\partial^{2n} \phi}{\partial x^{2n}} \right)_{x=v}$$

where

$$C_n = \sum_{s=1}^{\infty} (-1)^{s+1} \cdot S^{-n}$$

so that

$$C_2 = \pi^2/12$$

We shall compute up to terms  $n=1$  in this expansion and at the same time make Taylor expansion of  $\phi(v)$  and  $\left(\frac{d^2\phi}{dx^2}\right)_{x=v}$  about  $v=v_0$  retaining terms up to first order in  $(v-v_0)$ . In that case we get

$$\begin{aligned} I(u) &= \phi(x=v) + \frac{\pi^2}{6} \left( \frac{\partial^2 \phi}{\partial x^2} \right)_{x=v} \\ &= \phi(x=v_0) + (v-v_0) \left( \frac{\partial \phi}{\partial v} \right)_{v=v_0} + \frac{\pi^2}{6} \left( \frac{d^2 \phi}{dx^2} \right)_{x=v_0} + (v-v_0) \frac{\pi^2}{6} \left\{ \frac{\partial}{\partial v} \left( \frac{d^2 \phi}{dx^2} \right)_{x=v} \right\}_{v=v_0} \\ &= m\beta \left[ \frac{\omega v_0}{k} + \frac{1}{2} \left( v_0^2 - \frac{\omega^2}{k^2} \right) \log \left| \frac{\omega/k + v_0}{\omega/k - v_0} \right| \right] \\ &\quad + \frac{\pi^2}{12m\beta v_0^2} \log \left| \frac{\omega/k + v_0}{\omega/k - v_0} \right| + \frac{\pi^2}{3} \frac{\omega/k}{m\beta v_0} \frac{1}{\omega^2/k^2 - v_0^2} + O\left(\frac{1}{\beta^4}\right) \end{aligned}$$

where  $v_0$  = velocity at the top of Fermi distribution and which on substitution in Eq. (12) gives

$$\begin{aligned} \widetilde{K}_{tr}^{(2)}(k, \omega) = & \frac{\omega_0^2}{n_0 k} \left( \frac{m}{\hbar} \right)^3 \left[ \frac{\omega v_0}{k} + \frac{1}{2} \left( v_0^2 - \frac{\omega^2}{k^2} \right) \log \left| \frac{\omega/k + v_0}{\omega/k - v_0} \right| \right] \\ & + \frac{\pi^2 \omega_0^2}{12 m^2 \beta^2 v_0^3} \left( \frac{m}{\hbar} \right)^3 \frac{1}{n_0 k} \log \left| \frac{\omega/k + v_0}{\omega/k - v_0} \right| + \frac{\pi^2 \omega_0^2 \omega}{3 m^2 \beta^2 k^2 n_0 v_0} - \left( \frac{m}{\hbar} \right)^3 \frac{1}{\omega^2/k^2 - v_0^2} + O \left( \frac{1}{\beta^4} \right) \end{aligned}$$

... (13)

To this approximation  $\widetilde{K}_{tr}^{(1)}$  has the value as obtained from Eq. (11) by Taylor's expansion

$$\begin{aligned} \widetilde{K}_{tr}^{(1)}(k, \omega) = & - \frac{\omega_0^2}{4k} F \left( \frac{\omega}{k} = - \frac{\omega_0^2}{4k} \left\{ F_0 \left( \frac{\omega}{k} \right) + (v - v_0) \left( \frac{\partial F(v, \omega/k)}{\partial v} \right) \right\}_{v=v_0} \right\} \\ = & + \frac{\omega_0^2}{4k} \left\{ \frac{2\pi}{n_0} \left( \frac{m}{\hbar} \right)^3 \left( v_0^2 - \frac{\omega^2}{k^2} \right) \theta \left( v_0^2 - \frac{\omega^2}{k^2} \right) + \frac{\pi^2}{8 m^2 \beta^2 v_0^5} \theta \left( v_0^2 - \frac{\omega^2}{k^2} \right) \right\} \dots \end{aligned} \quad (14)$$

At absolute zero temperature  $\beta = \infty$  whence  $\widetilde{K}_{tr}^{(1)}$  and  $\widetilde{K}_{tr}^{(2)}$  take the values

$$\widetilde{K}_{tri(\omega)}^{(1)} = \frac{\pi \omega_0^2}{2 k n_0} \left( \frac{m}{\hbar} \right)^3 (v_0^2 - \omega^2/k^2) \theta (v_0^2 - \omega^2/k^2) \quad \dots \quad (14a)$$

$$\widetilde{K}_{tr(0)}^{(2)} = \frac{\omega_0^2}{n_0 k} \left( \frac{m}{\hbar} \right)^3 \left[ \frac{\omega v_0}{k} + \frac{1}{2} (v_0^2 - \omega^2/k^2) \log \left| \frac{\omega/k + v_0}{\omega/k - v_0} \right| \right] \quad \dots \quad (13a)$$

#### COMPUTATION OF $\widetilde{K}_l(k, \omega)$

Now we shall perform analogous computations for  $\widetilde{K}_l(k, \omega) = \widetilde{K}_{33}(k, \omega)$ . From Eq. (10) we have

$$\begin{aligned} \widetilde{K}_l(k, \omega) = & \frac{-i \omega_0^2}{4\pi} \int_{-\infty}^{\infty} \frac{du}{\omega - ku + i\epsilon} \frac{u \partial f_0 / \partial u}{\omega - ku + i\epsilon} = \frac{-i \omega_0^2}{4\pi} \int_{-\infty}^{\infty} du \frac{G(u)}{\omega - ku + i\epsilon} \\ = & - \frac{i \omega_0^2}{4\pi} P \int_{-\infty}^{\infty} du \frac{G(u)}{\omega - ku} - \frac{\omega_0^2}{4k} G(\omega/k) \end{aligned} \quad \dots \quad (15)$$

where

$$G(u) = u \frac{\partial}{\partial u} \int_{-\infty}^{\infty} du_1 \int_{-\infty}^{\infty} du_2 f_0(u_1, u_2, u) = - \frac{4\pi}{n_0} \left( \frac{m}{\hbar} \right)^3 \frac{u^2}{1 + e^{-v + \frac{1}{4} m \beta u}}$$

for the Fermi distribution. Therefore,

$$\begin{aligned}\widetilde{K}_I^{(2)}(k, \omega) &= \frac{\omega_0^2}{n_0} \left( \frac{m}{\hbar} \right)^3 P \int_{-\infty}^{\infty} du \frac{u^2/1 + e^{-\nu + i m \beta u^2}}{\omega - ku} \\ &= - \frac{2\omega_0^2 \omega}{\sqrt{2m\beta} k^2 n_0} \left( \frac{m}{\hbar} \right)^3 \int_0^{\infty} dx \frac{d\phi/dx}{e^{-\nu+x} + 1}\end{aligned}\quad (16)$$

with

$$\frac{d\phi}{dx} = \frac{\sqrt{x}}{x - m\beta\omega^2/2k^2}$$

Performing integrations in a manner similar to the previous section we get

$$\begin{aligned}\widetilde{K}_I^{(2)}(k, \omega) &= - \frac{2\omega_0^2}{n_0 k} \left( \frac{m}{\hbar} \right)^3 \left[ \frac{v_0 \omega}{k} + \frac{\omega^2}{2k^2} \log \left| \frac{\omega/k - v_0}{\omega/k + v_0} \right| \right] \\ &+ \frac{\pi^2 \omega_0^2 \omega}{6m^2 \beta^2 k^2 n_0 v_0} \left( \frac{m}{\hbar} \right)^3 \frac{(v_0^2 + 3\omega^2/k^2)}{v_0^2 - \omega^2/k^2}\end{aligned}\quad \dots (17)$$

For  $\widetilde{K}_I^{(1)}(k, \omega)$  Eq. (15) gives, to this order of approximation,

$$\widetilde{K}_I^{(1)}(k, \omega) = + \frac{\pi \omega_0^2 \omega^2}{n_0 k^3} \left( \frac{m}{\hbar} \right)^3 \theta \left( v_0^2 - \frac{\omega^2}{k^2} \right) \quad \dots (18)$$

The zero temperature values are obtained by letting  $\beta = \infty$  in Eq. (17) and and Eqn. (18).

#### CONDITIONS FOR OSCILLATORY RESPONSE

Maxwell's electromagnetic field equation

$$\vec{\nabla}_r \times (\vec{\nabla}_r \times \vec{E}) - \frac{1}{C^2} \frac{\partial^2 \vec{E}}{\partial t^2} = - \frac{4\pi}{C^2} \frac{\partial \vec{J}}{\partial t} \quad \dots (19a)$$

which is equivalent to the following component-wise equations

$$\left( \frac{\partial^2}{\partial t^2} + k^2 c^2 \right) E_{tr} = -4\pi \frac{\partial J_{tr}}{\partial t}, \quad \frac{\partial^2 E_t}{\partial t^2} = -4\pi \frac{\partial J_t}{\partial t} \quad \dots (19b)$$

tells us that the response will be oscillatory if

$$\tilde{J}_{tr}(k, \omega) = \frac{i(\omega^2 - k^2 c^2)}{4\pi \omega} \tilde{E}_{tr}(k, \omega), \quad \tilde{J}_t(k, \omega) = \frac{i\omega}{4\pi} \tilde{E}_t(k, \omega)$$



which is equivalent to the statement

$$\tilde{K}_{tr}^{osc}(k, \omega) = \frac{i}{4\pi\omega} (\omega^2 - k^2c^2), \quad \tilde{K}_l^{osc}(k, \omega) = \frac{i\omega}{4\pi} \quad \dots (20)$$

For damped oscillations  $\omega$  will be complex in these relations. For small imaginary component of  $\omega$  i.e., for small damping, Eq. (20) takes the form ( $\bar{\omega} = \omega - ir$ )

$$\tilde{K}_{tr}^{osc}(k, \bar{\omega}) = \tilde{K}_{tr}^{osc}(k, \omega) - ir \frac{d\tilde{K}_{tr}^{osc}(k, \omega)}{d\omega} = \frac{i(\omega^2 - 2ir\omega - k^2c^2)(1 + ir/\omega)}{4\pi\omega} \quad \dots (21a)$$

$$\tilde{K}_l^{osc}(k, \bar{\omega}) = \tilde{K}_l^{osc}(k, \omega) - ir \frac{d}{d\omega} \tilde{K}_l^{osc}(k, \omega) = \frac{i(\omega - ir)}{4\pi} \quad \dots (21b)$$

Now we can use the expressions (11) and (15) for  $\tilde{K}_{tr}(k, \omega)$  and  $\tilde{K}_l(k, \omega)$  on the left hand side of these equations and equating real and imaginary parts we obtain the following conditions for oscillations:

Transverse :

$$\frac{\omega_0^2}{4\pi} P \int_{-\infty}^{+\infty} du \frac{F(u)}{\omega - ku} + \frac{\omega_0^2 r}{4k} \frac{d}{d\omega} F(\omega/k) = \frac{\omega^2 - k^2c^2}{4\pi\omega} + O(r^2) \quad (22a)$$

$$\frac{\omega_0^2}{4k} F(\omega/k) + \frac{\omega_0^2 r}{4\pi} \frac{d}{d\omega} \left\{ P \int_{-\infty}^{+\infty} du \frac{F(u)}{\omega - ku} \right\} = -\frac{r}{2\pi} + \frac{r}{4\pi\omega^2} (\omega^2 - k^2c^2) \quad \dots (22b)$$

Longitudinal :

$$\frac{\omega_0^2}{4\pi} P \int_{-\infty}^{+\infty} du \frac{G(u)}{\omega - ku} + \frac{\omega_0^2 r}{4k} \frac{d}{d\omega} G(\omega/k) = \frac{\omega}{4\pi} \quad \dots (22c)$$

$$\frac{\omega_0^2}{4k} G(\omega/k) + \frac{\omega_0^2 r}{4\pi} \frac{d}{d\omega} \left\{ P \int_{-\infty}^{+\infty} du \frac{G(u)}{\omega - ku} \right\} = -\frac{r}{4\pi} \quad \dots (22d)$$

These conditions are actually the dispersion formulae for the oscillations and agree with those obtained with reference (1) and other works quoted in reference (1).

## ACKNOWLEDGMENTS

The authors are grateful to Dr. T. Pradhan for suggesting the problem and for guidance. They would like to acknowledge a number of clarifications by way of discussions with Dr. B. Deo and Dr. S. P. Misra.

## REFERENCES

- Pradhan, T. (to be published)  
Lindhard, J. 1954, *Kgl. Danske, Videnskab, selskab, Mat-fys. Medd.*, **28** No. 8.  
Pradhan T. and P. Misra, 1960, *Phys. Rev*, **119**, 1878.  
Sommerfeld, A. 1928, *Z. Physik*, **47**, 1.

# RAMAN AND INFRARED SPECTRA OF ISOQUINOLINE, $\alpha$ -FLUORO -AND $\alpha$ -CHLORONAPHTHALENE IN DIFFERENT STATES\*

KRISHNA KUMAR DEB

DEPARTMENT OF OPTICS,  
INDIAN ASSOCIATION FOR THE CULTIVATION OF SCIENCE  
JADAVPUR, CALCUTTA-32

(Received August 20, 1962)

Plate VI A and VI B

**ABSTRACT.** The Raman spectra of isoquinoline,  $\alpha$ -fluoro- and  $\alpha$ -chloronaphthalene in the liquid state and in the solid state at  $-180^{\circ}\text{C}$  and also their infrared spectra in the liquid state and in solution have been investigated and probable assignment of the vibrational frequencies has been made. It has been pointed out from the observed results that in the liquid state the molecules of  $\alpha$ -fluoronaphthalene exist mostly as dimers and those of  $\alpha$ -chloronaphthalene as a mixture of dimers and monomers. Some changes also take place in the spectra of the compounds on solidification. All these results have been explained on the hypothesis that molecular association takes place at low temperatures.

## INTRODUCTION

The assignment of the vibrational frequencies of the naphthalene molecule to its different modes was made earlier by Lippincott and O'Reilly (1955) and also more exhaustively by Mc Clellan and Pimental (1955). Recently, Scully and Whiffen (1960) made a revised assignment by calculating the vibrational frequencies of naphthalene and the planar vibrational frequencies have been calculated independently by Freeman and Ross (1960). Since there is a disagreement between some of the assignments proposed by different workers, an attempt was made to arrive at correct assignments of some of the vibrational modes of naphthalene by comparing its Raman and infrared spectra with those of quinoline (Deb, 1961), because some of the vibrational frequencies of the naphthalene molecule were expected to be almost equal to those of quinoline. On the other hand, when some of the hydrogen atoms of naphthalene are substituted by heavier atoms certain vibrational frequencies of the molecule diminish to a great extent. Hence, a comparison of the Raman spectra of such substituted compounds with the spectrum due to naphthalene might also be helpful in the assignment of the vibrational frequencies of these molecules.

\*Communicated by Prof. S. C. Sirkar

The Raman spectra of naphthalene crystals at different low temperatures were studied earlier by many workers and certain explanation of the origin of new low frequency lines was made (Sirkar and Ray, 1950; Ray 1950). Recently, the Raman spectra of quinoline and tetralin in the solid state at  $-180^{\circ}\text{C}$  were studied (Deb 1961) and the results were compared with those due to naphthalene and benzene. It was not known, however, how the spectra of substituted naphthalenes in the solid state depend on the nature and the position of the substituent atom. In order to find out such influence, the Raman spectra isoquinoline,  $\alpha$ -fluoro- and  $\alpha$ -chloronaphthalene in the liquid state and in the solid state at  $-180^{\circ}\text{C}$  and also their infrared spectra in the liquid phase and in solutions in the region  $607\text{ cm}^{-1}$  to  $3200\text{ cm}^{-1}$  have been studied in the present investigation and the results have been discussed in this paper.

#### EXPERIMENTAL

The liquids were supplied by Eastman Kodak Co., U.S.A, and were of chemically pure quality. They were further purified by distillation under reduced pressure. The arrangements for studying the Raman spectra of the substances in the liquid state and in the solid state at  $-180^{\circ}\text{C}$  were the same as those used in earlier investigations (Deb, 1960). The state of polarisation of the Raman lines was also determined by recording simultaneously the horizontal and vertical components of the spectra of the scattered light using a double image prism. The spectra were recorded on Ilford Zenith plates with the help of a Fuess glass spectrograph having a dispersion of about  $11\text{ \AA}/\text{mm}$ . in the region  $4047\text{ \AA}$ :

The infrared spectra of the liquids and their solutions in  $\text{CCl}_4$ ,  $\text{CS}_2$ , *n*-hexane,  $\text{CHCl}_3$  and ether in the region from  $607\text{ cm}^{-1}$  to  $3200\text{ cm}^{-1}$  have been recorded with the help of a Perkin-Elmer Model 21 spectrophotometer with NaCl optics. Absorption cells of thickness  $0.05\text{ mm}$  were used in recording the spectra due to the solutions while much thinner films pressed between two NaCl discs were used in the case of pure liquids. Suitable compensation cells were used in the reference beam while recording the absorption spectra due to the solutions.

#### RESULTS

The Raman spectra of isoquinoline,  $\alpha$ -fluoro- and  $\alpha$ -chloro naphthalene in the liquid and solid states are reproduced in figures 1, 2 and 3. Plate (VIA and VIB) and the infra-red absorption curves for the three compounds in the liquid state are shown in figs. 4, 5 and 6. The Raman shifts observed for the three substances are given in Tables I, II and III. The Raman frequencies of the compounds reported by previous workers have been included in the Tables for comparison. The state of polarisation of the Raman lines are indicated by the usual letters "P" and "D" which mean polarised and totally depolarised respectively. The infrared frequencies observed in the cases of the three liquids are given in Table IV.

TABLE I  
Raman spectra of isoquinoline.  $\Delta\nu$  in  $\text{cm}^{-1}$

(Pure liquid)		
Jatkar (1936)	Present Author	(Solid at $-180^\circ\text{C}$ ) Present author
		76(4)
		122(2)
		142(2)
	181(2b)D	
	382(1)D	
499(10)	507(8)P	502(4)
517(10)	523(4)P	517(2)
	638(1)P	
778(10)	786(10)P	785(5)
	967(0b)D?	
1008(4)	1010(4)P	1006(0)
1030(5)	1034(6)P	1024(2)
1132(0)	1139(2)D	
	1177(0)P	
	1213(1)P	
1252(1)	1260(1)D	
1278(2)		
1321(5)	1318(3)P	1318(0)
1378(10)	1383(15)P	1383(10)
1428(5)	1430(6)P	1432(1)
1457(5)	1462(6)P	1458(1)
1491(0)		
1551(2)	1556(2)P	1554(0)
1580(6)	1586(6b)P	1581(1)
	1627(0)P	
2448(0)		
2490(1)		
3047(8)	3055(6b)P	3055(1b)

TABLE II  
Raman spectra of  $\alpha$ -fluoronaphthalene.  $\Delta\nu$  in  $\text{cm}^{-1}$

Pure liquid		
Gookel (1935)	Present author	Solid at $-180^\circ\text{C}$ Present author
150(3b)	150(6b)D	104(4b)
273(2b)	270(6)D	163(2b)
	410(0)D	275(0)
465(2b)	462(5)P	462(1)
	473(5)D	473(1)
526(0)	529(3)D	
565(3)	568(6)P	566(1b)
705(6)	703(12)P	706(6)
873(2)	874(4)P	874(0)
	956(0)P	
1012(0)	1010(2)P	1010(0)
1036(4)	1037(2)P	
1076(1)	1073(4)P	1075(1)
1160(0)	1146(2)D	1146(1b)
1232(0)	1220(1)P	
	1261(1)P	
1385(10)	1380(15)P	1382(12)
	1411(0)P	
1441(3)	1442(8b)P	1441(4b)
1509(2)	1572(8b)D	1572(4b)
	1635(0)P	
3065(4)	3003(6b)P	3007(4b)

TABLE III  
Raman spectra of  $\alpha$ -chloronaphthalene  
 $\Delta\nu$  in  $\text{cm}^{-1}$

Pure liquid		
Landolt-Börnstein Tables (1951)	Present author	Solid at - 180°C Present author
		56(2b)
	132(6)D	140(1)
174(1)		
221(6)	221(6)D	
247(4)	242(2)D	
287(1)		
355(3)	350(1)P	
	384(1)P	
393(4)	397(0)P	
426(4)	426(2)P	
458(2)		
515(6)	511(8)D	523(0)
535(5)	533(10)P	532(4)
590(1)		
665(7)	664(8)P	663(1)
731(2)	727(0)P	
	760(3)P	
787(2)	782(0)P	
828(7)	825(8)P	825(3)
861(2)	858(0)P	
897(3)	901(0)P	
954(4)	957(0b)P	
937(4)	967(0)P	
1021(5)	1014(4)P	1012(0)
	1044(4)P	1044(1)
1058(6)	1062(4)P	1062(0)
1140(5)	1137(4)D	1137(0)
1159(2)	1156(2)P	
1202(4)	1201(0)P	
1257(5)	1250(1)P	
1368(10)	1367(15)P	1367(12)
1435(8)	1428(8)P	1427(2)
1462(6)	1456(3)P	1458(0)
1565(9)	1563(10)D	1566(6)
	1586(0) P	
1622(2)	1622(0)P	
2874(2)	2878(2b)P	
2932(1)		
3002(3)	2998(1)P	
3060(10)	3058(8b)P	3060(4b)
3075(0)		

TABLE IV

Infrared bands of isoquinoline,  $\alpha$ -fluoro and  $\alpha$ -chloronaphthalene.  
 $\nu$  in  $\text{cm}^{-1}$

Isoquinoline	$\alpha$ -Fluoronaphthalene	$\alpha$ -Chloronaphthalene
640(ms)		
742(vs)	702(ms)	660(w)
	760(vs)	742(ms)
		765(vs)
780(ms)	790(vs)	790(vs)
800(s)	840(w)	806(ms)
825(vs)	852(w)	814(ms)
		850(w)
860(s)	870(ms)	880(vw)
930(ms)		
942(s)	950(w)	942(ms)
970(w)	960(w)	962(s)
1008(ms)	1010(ms)	1000(vw)
1035(ms)	1030(ms)	1020(vw)
	1070(s)	1060(vw)
		1070(vw)
1140(ms)	1150(w)	1135(w)
1180(w)		1160(vw)
1220(ms)	1212(w)	1200(ms)
1240(w)	1230(s)	
1260(s)	1260(s)	1250(ms)
1280(s)		
		1340(w)
1380(s)	1390(s)	1380(s)
1440(w)	1440(w)	1430(vw)
1460(w)	1460(ms)	1458(vw)
1500(s)	1510(ms)	1500(ms)
1550(w)		
1562(ms)	1570(ms)	1562(w)
1580(s)		1590(w)
1590(s)	1600(s)	
1628(s)	1635(w)	1620(vw)
	2840(w)	
		2870(w)
2945(w)	2920(w)	2930(w)
2990(ms)	3002(w)	
3060(s)	3060(ms)	3060(ms)
	3100(w)	

## DISCUSSION

(a) *Probable assignment*

The molecules of isoquinoline,  $\alpha$ -fluoro- and  $\alpha$ -chloro naphthalene belong to the point group  $C_{2v}$ . The first molecule should have thirty one in-plane and fourteen out-of-plane modes of vibration and each of the latter two compounds would give rise to thirty-three in-plane and fifteen out of plane vibrations. All these vibrations would be active both in Raman scattering and in infrared absorption. The in-plane vibrations belonging to the symmetry class  $a'$  are expected to give rise to polarised Raman lines while the out of plane vibrations giving rise to depolarised lines would belong to the symmetry class  $a''$ . An attempt can now be made to assign the frequencies by comparing the Raman and infrared frequencies of the three compounds with each other and with those of naphthalene.

*Isoquinoline.* It can be seen from Table I that isoquinoline gives sixteen polarised and five totally depolarised lines. Thus the number of Raman lines observed is smaller than that expected. This may be due partly to the feebleness of some of the lines and also the frequencies of some other vibrational modes may be too close to each other to be resolved.

In the case of naphthalene there are nine planar modes of symmetry  $A_g$ . As pointed out previously (Deb 1961) the most probable frequencies of these modes are 512, 763, 1025, 1144, 1380, 1460, 1580, 3025, and 3060  $\text{cm}^{-1}$ . The corresponding frequencies in isoquinoline seem to be 523, 786, 1034, 1177, 1383, 1462, 1586 and 3055 (b)  $\text{cm}^{-1}$  respectively. The last broad line may actually represent two frequencies. Of the remaining eight polarised Raman lines of isoquinoline some are due to modes corresponding to those of symmetry  $B_{3g}$  of naphthalene. In the latter case such frequencies are (Scully and Whiffen 1960) 506, 936, 1168, 1340, 1436, 1624 and 3055  $\text{cm}^{-1}$ . The corresponding frequencies in the present case may be 507, 1010, 1213, 1318, 1430, 1556 and 3055  $\text{cm}^{-1}$  respectively. The remaining lines are depolarised and they are due to out of plane vibrations. It may be pointed out that in this case there are two equally strong and polarised Raman lines 507 and 523  $\text{cm}^{-1}$  respectively. In the case of quinoline, only one such strong line at 519  $\text{cm}^{-1}$ , was observed. Judging from the fact that the frequency 512  $\text{cm}^{-1}$  of naphthalene increases to 519  $\text{cm}^{-1}$  in quinoline and in other naphthalene derivatives the line 523  $\text{cm}^{-1}$  of isoquinoline can be assigned to a mode which corresponds to one of  $A_g$  class and the line 507  $\text{cm}^{-1}$  to another of  $B_{3g}$  class is naphthalene (Scully and Whiffen 1960). There are two weak Raman lines at 1260 and 1627  $\text{cm}^{-1}$  respectively. They appear strongly in the infrared absorption. Hence they may be assigned to modes corresponding to those of  $B_{1u}$  class of frequencies 1268 and 1600  $\text{cm}^{-1}$  respectively in naphthalene (Scully and Whiffen 1960). The moderately strong Raman line 1010  $\text{cm}^{-1}$  having a counterpart in the medium infrared absorption band at 1008  $\text{cm}^{-1}$  may be identified with the mode 1010  $\text{cm}^{-1}$  of  $B_{2u}$  class in naphthalene (Scully



and Whiffen 1960). Besides, the very strong infrared absorption bands at 742 and 825  $\text{cm}^{-1}$  may be identified with the modes corresponding to vibrations in naphthalene belonging to class *u*.

*$\alpha$ -Fluoro and  $\alpha$ -Chloro naphthalene.* It can be seen from Table II and III that the number of Raman lines due to  $\alpha$ -Chloronaphthalene is much larger than that due to  $\alpha$ -fluoronaphthalene. This may be due to presence of both monomeric and associated dimeric molecules in the former liquid and of only associated dimeric molecules in the latter liquid. In the, case of  $\alpha$ -fluoronaphthalene twenty-two lines are observed. Of these, fifteen are polarised and seven are totally depolarised. On the other hand, in the case of  $\alpha$ -Chloronaphthalene, out of the thirty-four observed lines twenty-eight are polarised and the remaining six lines are totally depolarised. As in the case of quinoline (Deb 1961) and isoquinoline, the frequencies of the two compounds corresponding to those of  $A_g$  and  $B_{3g}$  modes of naphthalene are listed in Table V. They will represent the in-plane vibrations of the molecules.

TABLE V  
Raman frequencies

Symmetry class in naphthalene	$\alpha$ -Fluoronaphthalene $\Delta\nu$ in $\text{cm}^{-1}$	$\alpha$ -Chloronaphthalene $\Delta\nu$ in $\text{cm}^{-1}$
$A_g$	568	533
	703	664
	1010	825
	1073	1014
	1380	1367
	1442	1428
	1572	1503
	3055	3055
$B_{3g}$	462	426
	874	760
	1037	1044
	1229	1250
	1442(b)	1456
	1635	1622
	3055	3058

It can be seen from Tables II, III and IV that in the case of  $\alpha$ -fluoronaphthalene there is a weak Raman line  $1260\text{ cm}^{-1}$  having a strong infra-red counterpart at  $1260\text{ cm}^{-1}$ . This frequency and that corresponding to the strong infrared absorption at  $1600\text{ cm}^{-1}$  may respectively correspond to the lines 1268 and  $1600\text{ cm}^{-1}$  due to naphthalene (Scully and Whiffen 1960) belonging to the  $B_{1u}$  class. There is a strong infrared band at about  $790\text{ cm}^{-1}$  in the spectrum due to each of the liquids. This band may correspond to the  $780\text{ cm}^{-1}$  band due to naphthalene belonging to the  $B_{3u}$  class (Scully and Whiffen 1960).

(b) *Changes in the Raman spectra with the solidification of the liquids*

It can be seen from Tables I, II and III that the spectra due to all the liquids undergo some changes when the liquids are solidified and cooled to  $-180^\circ\text{C}$ .

In the case of isoquinoline the broad line  $181\text{ cm}^{-1}$  appears to be split up into three components at 76, 122 and  $142\text{ cm}^{-1}$  respectively. The corresponding line  $150\text{ cm}^{-1}$  of  $\alpha$ -fluoronaphthalene appears to be split up into a doublet with the components at 104 and  $163\text{ cm}^{-1}$ . Similarly, the line  $132\text{ cm}^{-1}$  of  $\alpha$ -chloronaphthalene splits up into two components at 56 and  $140\text{ cm}^{-1}$  respectively. Such splitting of the Raman lines was also observed in the case of fluorinated toluenes (Deb, 1962). The lines 181, 150 and  $132\text{ cm}^{-1}$  given respectively by the three molecules may be assigned to the mode of  $B_{3u}$  class having the frequency  $176\text{ cm}^{-1}$  in the case of naphthalene (Scully and Whiffen 1960). Also the lines  $270\text{ cm}^{-1}$  of  $\alpha$ -fluoronaphthalene and  $221\text{ cm}^{-1}$  of  $\alpha$ -chloronaphthalene become too weak to be observed with solidification. This line probably corresponds to the line  $285\text{ cm}^{-1}$  of naphthalene and is due to an out of plane vibration of the skeleton. The disappearance of the line as well as the splitting up of each of the lines 181, 150 and  $132\text{ cm}^{-1}$  due respectively to isoquinoline,  $\alpha$ -fluoro- and  $\alpha$ -chloronaphthalene may indicate strong association of the molecules in the crystal as in the case of fluorotoluenes (Deb, 1962).

There are some other changes in the spectra which also corroborate the above views. The lines  $523$  and  $1034\text{ cm}^{-1}$  due to isoquinoline shift to 517 and  $1024\text{ cm}^{-1}$  respectively. Also the line  $511\text{ cm}^{-1}$  due to  $\alpha$ -chloronaphthalene shifts to  $523\text{ cm}^{-1}$  and becomes very weak. This latter line may correspond to that of frequency  $581\text{ cm}^{-1}$  belonging to  $A_u$  class in the case of naphthalene and probably arises from an out of plane vibration of the skeleton.

(c) *Effect of solvent on infrared spectra*

It can be seen from Table IV that there are three strong infrared bands at about 1260, 1380 and  $3060\text{ cm}^{-1}$  in the spectra due to isoquinoline,  $\alpha$ -fluoro- and  $\alpha$ -chloronaphthalene respectively. These may correspond to the modes of frequencies 1268, 1386 and  $3056\text{ cm}^{-1}$  belonging to  $B_{1u}$  class in the case of naphthalene. Similarly, the infra-red bands at about 942 and  $790\text{ cm}^{-1}$  given by the three compounds may correspond to the modes of frequencies 955 and  $780\text{ cm}^{-1}$

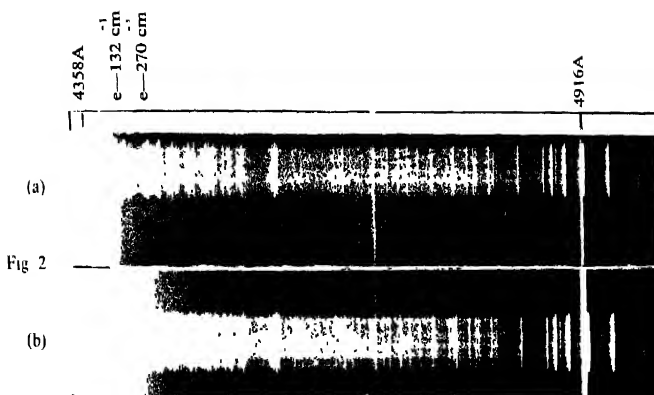
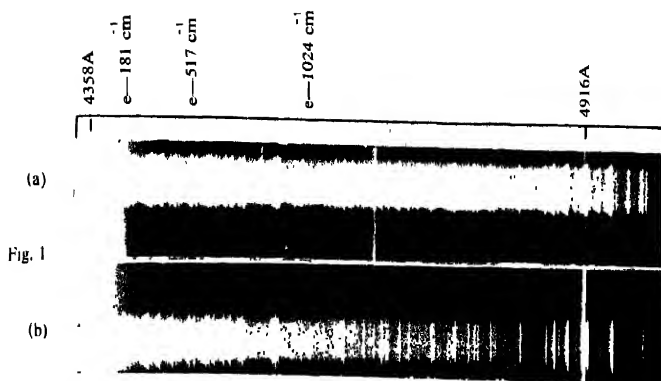


Fig. 1 (a) Raman spectrum of isoquinoline, liquid at  $30^\circ\text{C}$  (with Rhodamine 6 GBN filter)

(b) " " " " solid at  $-180^\circ\text{C}$

Fig. 2 (a) " " of  $\alpha$ -fluronaphthalene, liquid at  $30^\circ\text{C}$

(b) " " " " solid at  $-180^\circ\text{C}$

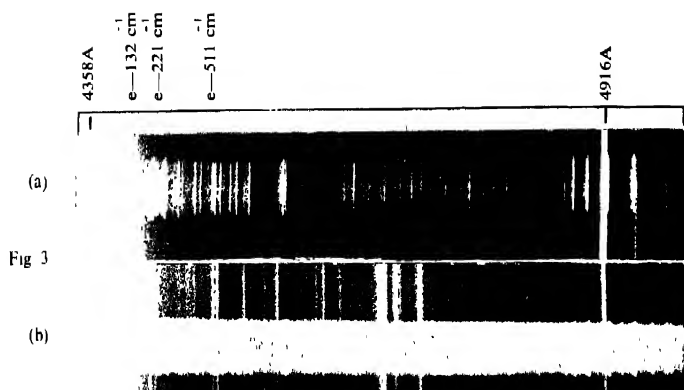


Fig. 3 (a) Raman spectrum of  $\alpha$ -chloronaphthalene, solid at  $-180^{\circ}\text{C}$

(b) " " " " liquid at  $30^{\circ}\text{C}$  (with Rhodamine 6 GBN filter)

belonging to  $B_{2u}$  class in the case of naphthalene. There is also a strong band at about  $1500\text{ cm}^{-1}$  in the spectra of the three compounds. This may correspond to the mode of frequency  $1510\text{ cm}^{-1}$  belonging to  $B_{2u}$  class in the case of naphthalene. Besides these, the strong infra-red band at 860, 870 and  $814\text{ cm}^{-1}$  given respectively by the three compounds may correspond to the frequency  $878\text{ cm}^{-1}$  belonging to  $B_{1u}$  class in the case of naphthalene calculated by Scully and Whiffen (1960).

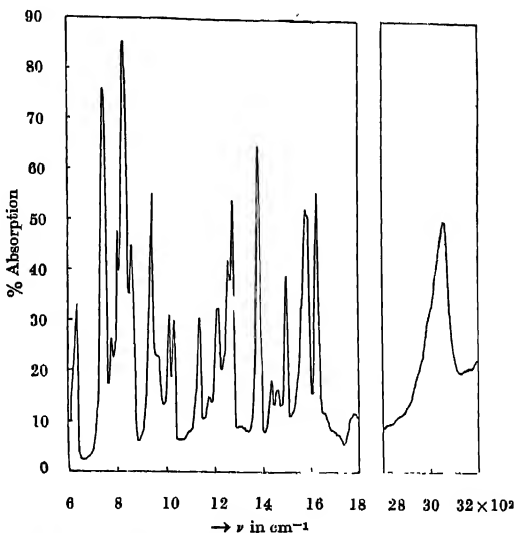


Fig. 4. Infrared spectrum of pure isoquinoline at 26°C.

The infra-red band  $640\text{ cm}^{-1}$  due to isoquinoline shifts to  $630\text{ cm}^{-1}$  when the substance is dissolved in either  $\text{CHCl}_3$  or  $\text{CS}_2$ . This band may correspond to the mode  $B_{2u}$  of naphthalene having the frequency  $818\text{ cm}^{-1}$ . In the case of other two compounds this band is absent which shows that the substitution in  $\alpha$ -position changes the frequency of this mode which may be identified with No. 8 of the  $B_{2u}$  class given by Freeman and Ross (1960). It can be seen from Fig. 7 that the band  $3060\text{ cm}^{-1}$  is split up into two bands at  $2980\text{ cm}^{-1}$  and  $3070\text{ cm}^{-1}$ , respectively, the former being stronger. These changes indicate an interaction between the hydrogen atom of the molecule with the chlorine atom of the chloroform molecule. In fact, the frequencies of many of the bands diminish a little when the compound is dissolved in either  $\text{CHCl}_3$  and hexane.

In discussing the results obtained in the Raman spectra of  $\alpha$ -fluoro- and  $\alpha$ -chloronaphthalene it has been pointed out that the molecules of the former

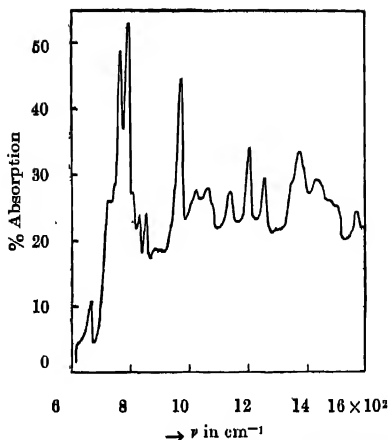


Fig 9. Infrared spectrum of 5% solution of  $\alpha$ -chloronaphthalene in hexane.

These changes also corroborate the conclusion that the liquid consists of monomers and dimers and the latter are reduced in number in dilute solution.

#### ACKNOWLEDGEMENT

The author wishes to acknowledge his ever grateful indebtedness to Professor S. C. Sirkar, D.Sc., F.N.I., for his kind help and inspiring guidance throughout the progress of the work. Thanks are also due to Dr. Kastha, D.Sc., for his helpful discussions in connection with this work.

#### REFERENCES

- Deb, K. K., 1960, *Ind. J. Phys.*, **34**, 247.  
 Deb, K. K., 1961, *Ind. J. Phys.*, **35**, 535.  
 Deb, K. K., 1962, *Ind. J. Phys.*, **36**, 59.  
 Freeman, D. E. and Ross, I. G., 1960, *Spectrochimica Acta*, **16**, 1393.  
 Gockel, H., 1935, *Z. Physik. Chem., B* **29**, 79, 912.  
 Jatkari, S. K. K., 1936, *Ind. J. Phys.*, **10**, 23.  
 Landolt-Bornstein, 1961, *Zahlenwerte und Funktionen*, 1 Band, Atom und Molekular Physik, p 525.  
 Lippincott, E. R. and O'Reilly, E. J., 1955, *J. Chem. Phys.*, **23**, 238.  
 McClellan, A. L. and Pimental, G. C., 1955, *J. Chem. Phys.*, **23**, 245.  
 Ray, A. K., 1950, *Ind. J. Phys.*, **24**, 549.  
 Scully, D. B. and Whiffen, D. H., 1960, *Spectrochimica Acta* **16**, 1409.  
 Sirkar, S. C. and Ray, A. K., 1950, *Ind. J. Phys.*, **24**, 189.

# LINEAR POLARIZATION OF $5.12\text{mc}^2$ GAMMA RAYS RAYLEIGH SCATTERED FROM K-ELECTRONS IN MERCURY

B. S. SOOD

PHYSICS DEPARTMENT, PUNJAB UNIVERSITY, CHANDIGARH-3

(Received February 26, 1962)

**ABSTRACT.** The linear polarization of  $5.12\text{mc}^2$  gamma rays Rayleigh scattered from K-electrons in mercury has been evaluated by using the amplitudes of scattering obtained from refined numerical and approximate form factors calculations respectively. It is seen that the two calculations predict quite different percentage polarization at some scattering angles. The contribution of Nuclear Thomson Scattering has been taken into account.

## INTRODUCTION

Rayleigh scattering was originally calculated for the gamma ray region by Franz (1935) using Fermi-Thomas electron distributions, and more recently by Bethe using Dirac functions for the K-electrons. These calculations commonly known as form-factor calculations, assume some non-relativistic approximations and neglect the electron binding in the intermediate state of the scattering process. Later a formalism for calculating Rayleigh scattering of gamma rays by the K-electrons in heavy atoms was developed (Brown, Peierls and Woodward, 1954). Refined numerical calculations for the scattering of gamma rays of energy  $0.32\text{mc}^2$  (Brenner, Brown and Woodward 1954),  $0.64\text{mc}^2$  (Brown and Mayers, 1956),  $1.28$  and  $2.56\text{mc}^2$  (Brown and Mayers, 1957) by K-electrons in mercury were done by using this formalism. Recently, these calculations have been extended to gamma rays of energy  $5.12\text{mc}^2$  (Cornille and Chapdelaine, 1959). At low energies ( $0.32$  and  $0.64\text{mc}^2$ ) the scattering cross sections calculated by the form factor method do not differ appreciably from those given by refined calculations, but at higher energies the refined calculations show smaller scattering cross sections than those calculated by the form factor method. Experimentally measured values of cross sections of Rayleigh scattering at various angles show somewhat better agreement with the predictions of refined calculations. Unfortunately, considerably large errors are associated with the experimental values because of the estimation of large corrections for the counter efficiency, the absorption of the incident and scattered radiation in the scatterer, the determination of the source-scatterer and scatterer-detector solid angles and the contribution of incoherent scattering.

This makes the results rather ambiguous, especially when the difference between the predictions of the two theories is small. However, another important feature of the refined calculations which markedly differs from those of the form factor method has been suggested and successfully used by Sood (1958) to compare the two theories for 411 Mev, 662 Mev and 1.25 Mev gamma rays. This is with respect to the predictions of the polarization of the elastically scattered gamma rays. The percentage polarization of 5.12mc<sup>2</sup> gamma rays elastically scattered from mercury has been calculated in the following section.

#### POLARIZATION OF RAYLEIGH SCATTERING

It is much easier to analyse experimentally the scattered radiation in terms of linear than circular polarization, the results of Cornille *et al.* (1959) giving circular polarization of the scattered radiation are modified to give linear polarization. The circularly polarized radiation can be regarded to result from two equal plane polarized parts, polarized at right angle and differing in phase by 90°. If  $\langle X |$  and  $\langle Y |$  denote polarizations along unit vectors parallel and perpendicular to the scattering plane respectively then the amplitude  $M(1' 1)$  for the scattering of a right handed incoming photon into a right handed outgoing photon can be expressed in terms of the linear polarization parallel and perpendicular to the scattering plane as  $\frac{1}{2} \langle X + iY | X + iY \rangle$ . Similarly  $M(2' 2)$ ,  $M(1' 2)$  and  $M(2' 1)$  can be written as  $\frac{1}{2} \langle X - iY | X - iY \rangle$ ,  $\frac{1}{2} \langle X + iY | X - iY \rangle$  and  $\frac{1}{2} \langle X - iY | X + iY \rangle$ . It is now easy to show that the amplitudes  $\langle X | X \rangle$  and  $\langle Y | Y \rangle$  of the linear polarization with the electric vector parallel and perpendicular to the scattering plane are equal to

$$\langle X | X \rangle = [M(1' 1) + M(2' 2)] + [M(1' 2) + M(2' 1)]$$

$$\langle Y | Y \rangle = [M(1' 1) + M(2' 2)] - [M(1' 2) + M(2' 1)]$$

The percentage linear polarization defined as  $\frac{J_1 - J_{11}}{J_1 + J_{11}}$  is equal to

$$\frac{|\langle Y | Y \rangle|^2 - |\langle X | X \rangle|^2}{|\langle Y | Y \rangle|^2 + |\langle X | X \rangle|^2}$$

where  $J_1$  and  $J_{11}$  are the intensities of linear polarization with electric vector perpendicular and parallel to the scattering plane respectively. The percentage polarization at various scattering angles has been evaluated using the values of  $[M(1' 1) + M(2' 2)]$  and  $[M(1' 2) + M(2' 1)]$  as given by Cornille *et al.* The results are shown in Fig. 1. Curve A which gives the percentage polarization using refined numerical calculations is to be compared with curve C which is calculated from the form factor data. It is seen that the two calculations give quite different variation of polarization with scattering angle. Therefore, the measurement of



polarization rather than the differential scattering cross section will provide more sensitive and better check of the existing calculations of Rayleigh scattering.

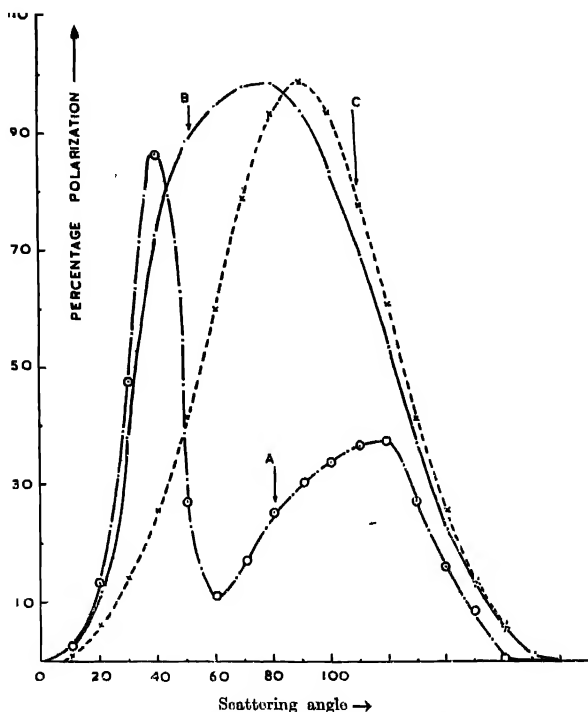


Fig. 12 Linear polarization of  $5.12mc^2$  gamma rays elastically scattered from mercury at various scattering angles. Curve A. Rayleigh scattering from refined numerical calculations. Curve B. Nuclear Thomson and Rayleigh from refined calculations. Curve C. Rayleigh from form-factor calculations.

The contributions of Nuclear Thomson and Delbrück scattering which cannot be energetically distinguished from Rayleigh scattering has to be taken into account. Thomson scattering is known to interfere constructively with Rayleigh scattering. (see, for example, Sood, 1962). The theory of Thomson scattering is well-known and fully established; the amplitudes of scattering from mercury atom in the plane of scattering and perpendicular to it are  $0.01237 \cos \theta$  and  $0.01237$  in units of  $r_0$ , the classical electron radius, respectively. Curve B shows the percentage polarization when Thomson scattering is also taken into account

along with the refined calculations. The form factor predictions of polarization remain unaffected due to the contribution of Thomson component since both the form factor Rayleigh and Thomson scattering have the same percentage polari-

zation given by  $\frac{\sin^2 \theta}{1 + \cos^2 \theta}$  where  $\theta$  is the angle of scattering.

The contribution of Delbrück scattering has not been considered since at present very little is known about the Delbrück amplitudes at large angles. It may, however, be possible to derive some useful information about Delbrück scattering and its interference with Rayleigh-Thomson component, from the measurements of the polarization of elastic scattering at different angles and its comparison with the curve B.

#### ACKNOWLEDGMENTS

I am grateful to Prof. B. M. Anand for providing facilities for carrying out this work.

#### REFERENCES

- Brenner, S., Brown, G. E. and Woodward, J. B., 1954, *Proc. Roy. Soc.*, **A227**, 59.  
 Brown, G. E. and Mayers, D. F., 1955, *Proc. Roy. Soc.*, **A234**, 387.  
 Brown, G. E. and Mayers, D. F., 1957, *Proc. Roy. Soc.*, **A242**, 89.  
 Brown, G. E., Peierls, R. E. and Woodward, J. B., 1954, *Proc. Roy. Soc.*, **A227**, 51.  
 Cornillo, H. and Chapdelaine, M., 1959, *Nuovo Cim.*, **14**, 1386.  
 Franz, W., 1935, *Phys. Z.*, **98**, 314.  
 Sood, B. S., 1958, *Proc. Roy. Soc.*, **A247**, 375.  
 Sood, B. S., 1962, Communicated to *Ind. J. Phys.*

# ELECTRON CAPTURE BY ALPHA-PARTICLE PASSING THROUGH HELIUM ATOM

S. C. MUKHERJEE AND N. C. SIL

DEPARTMENT OF THEORETICAL PHYSICS,  
INDIAN ASSOCIATION FOR THE CULTIVATION OF SCIENCE,  
JADAVPUR, CALCUTTA-32.

(Received September 11, 1962)

**ABSTRACT.** The expressions for the single and double electron capture by  $\alpha$ -particle passing through normal helium atoms have been derived by applying a variational method.

Single electron charge exchange phenomenon has been extensively studied both theoretically and experimentally by several authors (for references vide review article by Bates and McCarroll (1962)). Recently Fogel, Krupnik and Cafranov (1955) have observed experimentally the cross section of capture of two electrons in the rearrangement collision:  $H^+ + H_2 \rightarrow H^- + H_2^{1+}$ . Rosentsveig and Gerasimenko (1955) have studied theoretically the reaction  $H^+ + He \rightarrow H^- + He^{++}$  for very small incident ion energy using perturbed stationary states method. Gerasimenko and Rosentsveig (1957) have calculated the cross section for the capture of two electrons by a fast  $\alpha$ -particle colliding with a helium atom in its ground states by using simple Born approximation method. For high energy region Alison (1958) experimentally measured the cross section for the capture of two electrons by  $\alpha$ -particles passing through helium atom.

In this paper we have derived expressions for the cross section of single and double electron capture by  $\alpha$ -particles passing through normal helium atoms. We have used a simple variational treatment and we have restricted our theory to low energy of the incident ion. However, the extension of this method to high energy of the incident ion is also under progress.

We consider the capture of electrons (1 and 2) by the alpha particle  $A$  from the ground state of the helium atom.  $B$ . We assume that  $A$  and  $B$  move with

$\xrightarrow{\quad} \xrightarrow{\quad} \xrightarrow{\quad}$   
velocities  $\frac{1}{2}v$  and  $-\frac{1}{2}v$  respectively. Let  $R$  be the position vector of  $B$

$\xrightarrow{\quad} \xrightarrow{\quad} \xrightarrow{\quad}$   
relative to  $A$  and  $ra_1, ra_2; rb_1, rb_2$  are the position vectors of electrons 1 and 2 from  $A$  and  $B$ . Initially at  $t = -\infty$  we have the two electrons attached to the nucleus  $B$  in its ground state.

The time rate of change of the electron state wave function is given by the time dependent Schrödinger equation.

$$H\psi = i\hbar \frac{\partial \psi}{\partial t} \quad \dots (1)$$

This equation may be obtained by making stationary the following variational integral  $I$

$$I = - \int \left( \bar{\psi} H \psi - \frac{1}{2} \hbar \bar{\psi} \frac{\partial \psi}{\partial t} + \frac{1}{2} i \hbar \psi \frac{\partial \bar{\psi}}{\partial t} \right) dv_1 dv_2 dt \quad \dots (2)$$

with respect to small arbitrary variations of  $\psi$  and  $\bar{\psi}$ . The Hamiltonian  $\hat{H}$ , corresponding to the motion of the electrons in the Coulomb field of two nuclei is taken as

$$H = - \frac{\hbar^2}{2m} \Delta_1^2 - \frac{\hbar^2}{2m} \Delta_2^2 - \frac{Ze^2}{r_{a1}} - \frac{Ze^2}{r_{a2}} - \frac{Ze^2}{r_{b1}} - \frac{Ze^2}{r_{b2}} + \frac{e^2}{r_{12}} \quad \dots (3)$$

(neglecting the nucleus-nucleus interaction).

For a suitable approximation to  $\psi$ , we choose a trial wave function  $\psi_T$  which is a linear combination of the two ground state wave functions of helium atom around the two nuclei and a system of two ionised helium atoms.

$$\text{Thus} \quad \psi_T = A(t)\phi_A + B(t)\phi_B + C(t)\chi \quad \dots (4)$$

the coefficients being left free as function of time.

Performing the space integration, we may write

$$I = \int L dt \quad \dots (5)$$

$$\text{where} \quad L = (E + g_1) \bar{A}A + \left( Ef_{AB} + \frac{\hbar_1}{2} + \frac{\hbar_2}{2} \right) \bar{A}B + \frac{1}{2} (\epsilon(R)f_{AC} + Ef_{AC} + l_2) \bar{A}C$$

$$+ \left( Ef_{AB} + \frac{\hbar_1}{2} + \frac{\hbar_2}{2} \right) \bar{B}A + (E + g_2) \bar{B}B + \frac{1}{2} (\epsilon(R)f_{BC} + Ef_{BC} + l_1) \bar{B}C$$

$$+ \frac{1}{2} (\epsilon(R)f_{AC} + Ef_{AC} + l_2) \bar{C}A + \frac{1}{2} (\epsilon(R)f_{BC} + Ef_{BC} + l_1) \bar{C}B + \epsilon(R) \bar{C}C$$

$$+ \frac{1}{2} i\hbar \{ \dot{\bar{A}}\dot{A} + \dot{\bar{A}}\dot{B}f_{AB} + \dot{\bar{A}}\dot{C}f_{AC} + \dot{\bar{B}}\dot{A}f_{AB} + \dot{\bar{B}}\dot{B} + \dot{\bar{B}}\dot{C}f_{BC} + C\dot{\bar{A}}f_{AC} + C\dot{\bar{B}}f_{BC} + \dot{\bar{C}}\dot{C} \}$$

$$- \frac{1}{2} i\hbar \{ A\dot{\bar{A}} + A\dot{\bar{B}}f_{AB} + A\dot{\bar{C}}f_{AC} + B\dot{\bar{A}}f_{AB} + B\dot{\bar{B}} + B\dot{\bar{C}}f_{BC} + C\dot{\bar{A}}f_{AC} + C\dot{\bar{B}}f_{BC} + \dot{C}\dot{\bar{C}} \}$$

where

$$\int \phi_A \phi_B = f_{AB}, \quad \int \phi_A \chi = f_{AC}, \quad \int \phi_B \chi = f_{BC}, \quad Ze^2 \int \left( \frac{1}{rb_1} + \frac{1}{rb_2} \right) \phi_A \phi_A = g_1$$

$$Ze^2 \int \left( \frac{1}{ra_1} + \frac{1}{ra_2} \right) \phi_B \phi_B = g_2, \quad Ze^2 \int \left( \frac{1}{ra_1} + \frac{1}{ra_2} \right) \phi_A \phi_B = h_1$$

$$Ze^2 \int \left( \frac{1}{rb_1} + \frac{1}{rb_2} \right) \phi_A \phi_B = h_2, \quad Ze^2 \int \left( \frac{1}{ra_1} + \frac{1}{ra_2} \right) \phi_B \chi = l_1,$$

$$Ze^2 \int \left( \frac{1}{rb_1} + \frac{1}{rb_2} \right) \phi_A \chi = l_2$$

We have neglected the terms which tend to zero with velocity  $v$  and as such our calculation is valid only for low velocity.

Finally from the variational principle, by making  $I$  stationary with respect to small arbitrary variations of  $A$  and  $B$ , we get the following three equations:

$$(a_{11} - a_{12})(A - B) + i\hbar(1 - f_{AB}) \frac{d}{dt}(A - B) = 0 \quad (6)$$

$$(a_{11} + a_{12})D + 2a_{13}C + i\hbar(1 + f_{AB})\dot{D} + 2i\hbar f_{AC}\dot{C} = 0 \quad (7)$$

$$a_{13}D + e(R)C + i\hbar f_{AC}\dot{D} + i\hbar\dot{C} = 0 \quad (8)$$

where  $D = A + B, \quad a_{11} = E + g_1, \quad a_{12} = Ef_{AB} + \frac{h_1}{2} + \frac{h_2}{2}$

$$a_{13} = \frac{1}{2} [e(R)f_{AC} + Ef_{AC} + l_2]$$

From the above three equations, we get the values of  $A$ ,  $B$  and  $C$  where  $|B_{t=\infty}|^2$  indicates the double electron capture probability and  $|C_{t=\infty}|^2$  indicates the single electron capture probability.

Neglecting the influence of  $C$  in the equation (7) we can write equation (7) for sufficiently good approximation as

$$2f_1 D + i\hbar(1 + f_{AB})\dot{D} = 0 \quad \dots \quad (9)$$

where

$$2f_1 = a_{11} + a_{12}$$

which can be easily solved.

Substituting the values of  $D$  and  $\dot{D}$  from equation (9) to equation (8), we get

$$\epsilon(R)C + i\hbar \dot{C} = - \left( a_{13} - \frac{2f_1}{1+f_{AB}} f_{AC} \right) \exp \left[ \frac{i}{\hbar} \int_{-\infty}^t \frac{2f_1}{1+f_{AB}} dt \right] \quad \dots (10)$$

Applying the initial condition i.e. at  $t = -\infty$ ,  $A = 1$ ,  $B = 0$ ,  $C = 0$  we finally get

$$|C_{t=\infty}|^2 = \left| \int_{-\infty}^{\infty} dt \left( a_{13} - \frac{2f_1 f_{AC}}{1+f_{AB}} \right) \exp \left[ \frac{i}{\hbar} \int_{-\infty}^t \left( \frac{2f_1}{1+f_{AB}} - \epsilon(R) \right) dt \right] \right|^2 \quad \dots (11)$$

$$\text{and} \quad 4|B_{t=\infty}|^2 = \left| \exp \frac{i}{\hbar} \int_{-\infty}^{\infty} \frac{a_{11} + a_{12}}{1+f_{AB}} dt - \exp \frac{i}{\hbar} \int_{-\infty}^{\infty} \frac{a_{11} - a_{12}}{1-f_{AB}} dt \right|^2 \quad \dots (12)$$

which on further simplification gives

$$|B|^2 = \sin^2 \frac{1}{\hbar} \int_{-\infty}^{+\infty} \frac{a_{12} - a_{11} f_{AB}}{1 - f_{AB}^2} dt \quad \dots (13)$$

For the present, to make the calculation simpler, we calculate the values of the coefficient by using ordinary Hylleraas type of He-atom wave functions for  $\phi_A$  and  $\phi_B$  and London-Fleischer type of hydrogen molecular wave function for  $\chi$ ,

$$\text{i.e. } \phi_A = \frac{\lambda^3}{\pi} e^{(\lambda a_1 + \lambda a_2)} \phi_B = \frac{\lambda^3}{\pi} e^{-\lambda(r b_1 + r b_2)}; \lambda = \frac{27}{16}$$

$$\text{and } \chi = \frac{[e^{-2(\lambda a_1 + \lambda b_1)} + e^{-2(\lambda a_2 + \lambda b_2)}]}{N} \quad ; \quad N = (2)^3 \sqrt{2(1 + e^{-4R}[1 + 2\bar{R} + \frac{1}{3}\bar{R}^2])}$$

From the equation (13), expression for double capture, we can expect resonance structure with changes of energy which is under computation. The details of calculation will be published soon.

#### ACKNOWLEDGEMENT

We wish to thank Professor D. Basu for many valuable discussions.

#### REFERENCES

- Alison S. K., 1958, *Phys. Rev.*, **109**, 76.  
 Bates, D. R., Mc Carroll, R., 1962, *Advances in Physics*, **11**, 39.  
 Fogel, Krupnik, Cafranov, 1955, *Soviet Phys. JETP*, **1**, 415.  
 Gerasimanko, V. I., Rosentsveig, L. N., 1957, *Soviet Phys. JETP*, **4**, 509.  
 Rosentsveig, L. N., Gerasimanko, V. I., 1955, Works of the Physics Division of the Physico-Mathematical Faculty, Kharkov State University, **6**, 89.

## ULTRASONIC VELOCITY IN LIQUID BINARY MIXTURES

M. V. KAULGUD\*

DEPARTMENT OF CHEMISTRY, UNIVERSITY OF POONA

(Received June 16, 1961, Resubmitted November 13, 1961)

**ABSTRACT.** Measurements of ultrasonic velocity and density at different concentrations have been reported at 1.9 Mc for the following systems. carbontetrachloride-benzene, chloroform-*n*-heptane, ethylenedichloride-benzene and ethylenedichloride-*n*-heptane.

The author's earlier treatment (Kaulgud, 1960) for explaining the velocity deviations in binary mixtures has been extended to the following six mixtures, carbontetrachloride-benzene, heptane-benzene, chloroform-benzene, and ethylene-dichloride-benzene. The nature of the velocity-concentration curves is in accordance with the observations made earlier, viz., when the intermolecular free length in solution is greater than the ideal value (calculated) then the velocity-concentration curves are concave upwards and vice-versa. The agreement between the observed and calculated velocities is good. The velocity deviations for a given substance in heptane solution are more than in the benzene solution. The system carbon-tetrachloride-*n*-heptane is an exception.

## INTRODUCTION

In the previous paper (Kaulgud 1960) the author had made use of the relation of Jacobson (1952) viz.

$$UL\rho^{1/2} = K \text{ (constant)} \quad (1)$$

in order to calculate the velocity in binary mixtures. Here  $U$  is ultrasonic velocity in m/sec.,  $\rho$  = density in gm/cc and  $L_f$  is the intermolecular free length in Å defined as :

$$\frac{2 \times \text{available volume}}{\text{surface}} = \frac{2V_a}{Y}. \text{ The available volume is the molar volume at room}$$

temperature less the molar volume at absolute zero, the latter being estimated by the Sugden's equation :  $V_0 = V_T(1 - T/T_c)^{0.3}$  ( $T_c$  = critical temperature). The surface area of the molecules is estimated by assuming the molecules to be spherical and calculating the radius from the volume at absolute zero ( $V_0 = \frac{4}{3} \times \pi NR^3$ ). Equation (1) has been found to hold in the case of many liquids (Jacobson loc. cit.). In order to calculate the velocity in binary mixtures the definition of the free lengths in the case of pure liquids could be extended to binary mixtures thus :

---

\*Now at the Institute of Technical Acoustics, TU Berlin

$$L_{mix} = \frac{2 \times \text{available volume}}{\text{surface}} = \frac{2 \left[ \frac{1}{\rho_{mix}} - \left( \frac{\omega_1 V_{01}}{M_1} + \frac{\omega_2 V_{02}}{M_2} \right) \right]}{\frac{\omega_1 Y_1}{M_1} + \frac{\omega_2 Y_2}{M_2}} \quad \dots (2)$$

where  $\rho_{mix}$  is the experimentally measured density and  $\omega_1, \omega_2; V_{01}, V_{02};$  and  $M_1, M_2$  are respectively the weight fractions, volume at absolute zero and the molecular weights of the component 1 and 2. It was shown (Kaulgud loc. cit.) that in the expression (2) if we put for  $1/\rho_{mix}$  its ideal value  $\left( = \frac{\omega_1}{\rho_1} + \frac{\omega_2}{\rho_2} \right)$  and make use of the relation  $L_f = 2V_a/Y$  for both the components 1 and 2, it could be written as :

$$L_{mix, ideal} = L_1 \cdot \frac{\omega_1 Y_1 / M_1}{\omega_1 \frac{Y_1}{M_1} + \frac{\omega_2 Y_2}{M_2}} + L_2 \cdot \frac{\omega_2 Y_2 / M_2}{\frac{\omega_1 Y_1}{M_1} + \frac{\omega_2 Y_2}{M_2}} \quad \dots (3)$$

or as  $L_1 S_1 + L_2 S_2$  if we define  $\frac{\omega_1 Y_1 / M_1}{\omega_1 Y_1 / M_1 + \omega_2 Y_2 / M_2}$  etc.

as the surface fraction ' $S_1$ ', of the component '1' etc.. It was established in the previous paper (Kaulgud loc. cit.) by calculations done on ten binary systems of polar-polar, polar-nonpolar and nonpolar-nonpolar type, that if  $L_{mix}$  given by exp. (2) is greater than  $L_{mix, ideal}$  (exp. 3) then the velocity-concentration curves are concave upwards (-ve deviation) and vice versa. The object of the present paper is to extend these calculations to the following six binary mixtures in order to confirm the earlier findings. In the brackets are given the source of velocity and density data :

- (1) Benzene-Carbonditetrachloride (This work; Tuomikoski and Nurmi 1940)
- (2) Benzene-Heptane (Tuomikoski and Nurmi, 1940)
- (3) Benzene-Chloroform (Gabrielli and Poianni, 1951)
- (4) Carbonditetrachloride-Chloroform (Gabrielli and Poianni, 1951)
- (5) Benzene-Methylene chloride (Tuomikoski and Nurmi, 1940)
- (6) Benzene-Ethylendichloride (This work).

The method of calculations indicated already (Kaulgud loc. cit.) is briefly as follows : The values of  $K$  in eq. (1) have been given by Jacobson (1952). ( $K = 618$  at  $20^\circ$ ,  $625$  at  $25^\circ$ ,  $631$  at  $30^\circ$  and so on). In the application of the relation :

$$L_f = \frac{2V_a}{Y} = \frac{2(V_T - V_0)}{(36\pi N V_0^2)^{1/3}} \quad \dots (4)$$

to a pair of liquids, the value of  $(V_T - V_0)$  is assumed to be known sufficiently accurately and the small difference in  $L_f$  value demanded by eqn. (1) and that given



by eqn. (4) is attributed to nonspherical nature of the molecules so that the actual surface area  $Y' = F(36\pi NV_0^2)^{1/3}$  where  $F$  is a form factor. This modified  $Y'$  value gives a free length value which satisfies relation (1) exactly. Values of  $F$  have been found to lie between 0.9 and 1.09 in the extreme cases. For the solutions,  $L_{mix}$  is calculated from eq. (2) by using the experimentally measured density  $\rho_{mix}$ , and is used to calculate the velocity from relation (1). This velocity value is compared with the experimentally measured value. Values of  $L_{mix, ideal}$  are also calculated from relation (3) and compared with  $L_{mix}$ . The results of the calculations are given below.

### EXPERIMENTAL

The measurements of velocity in systems (1) and (6) were made in this laboratory by the author at 1.9Mc frequency by using the Hiedemann's method. The standing wave pattern was obtained by oscillating the quartz crystal kept outside the cell, and the wavelength directly measured by a micrometer microscope. The frequency was measured by a heterodyne beat method. The temperature was controlled by enclosing the cell in a double walled rectangular jacket having transparent windows, through which water thermostated at 25° was circulated. All the liquids were purified by standard methods given in Weissberger's book on Organic Solvents. The velocities values are accurate to  $\pm 1.5$ m/sec. The densities were measured by a *ca.* 6c c. Lypkin's pycnometer. In addition to the two systems 1 and 6, measurements were also made for the system ethylenedichloride-*n*-heptane (at 25°) and chloroform-*n*-heptane (at 20°) for the sake of comparison of the data with the corresponding system in benzene solution.

### RESULTS AND DISCUSSION

The results of the above calculations have been represented graphically. The results of the calculations done on the systems ethylene-dichloride-*n*-heptane, and chloroform-*n*-heptane published already in graphical form (Kaulgud loc. cit.), have been given in tabular form (Tables 1 and 2 respectively) in this paper to bring out certain points to be discussed shortly.

It can be seen that in all the cases  $L_{expt} > L_{ideal}$  and hence as expected the velocity curves are concave upwards (negative deviations). This confirms the conclusions drawn in the previous paper that in binary mixtures the velocity is governed by the intermolecular free lengths. This is true of non-polar : non-polar and non-polar : polar systems as well. Another feature which emerges from the free length deviation for the same substance dissolved in benzene and heptane, is that it is less in the former than in the latter. The velocity deviations are correspondingly less and more respectively. A comparison of the free length and velocity deviations at any specified concentration can be done to show the above fact clearly.

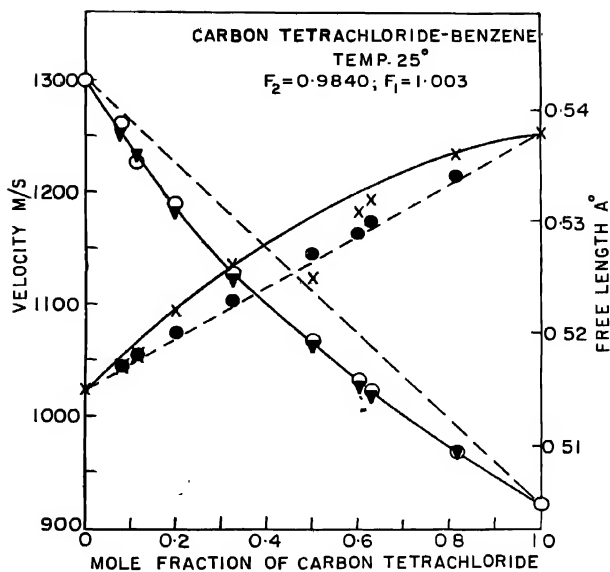


Fig. 1. O—O Experimental velocity.

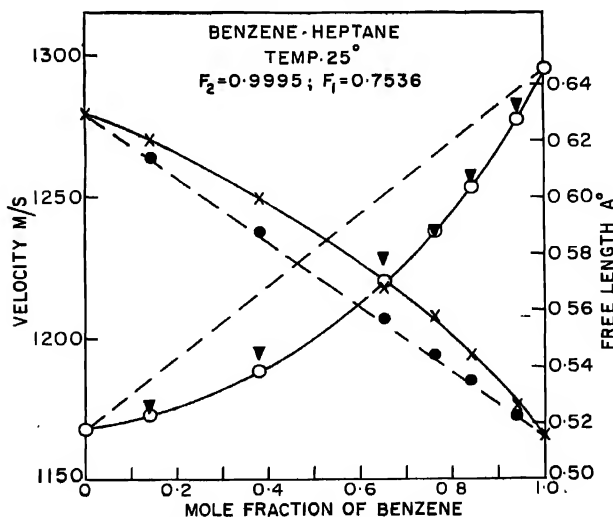


Fig. 2. ▽—▽ Calculated velocity.

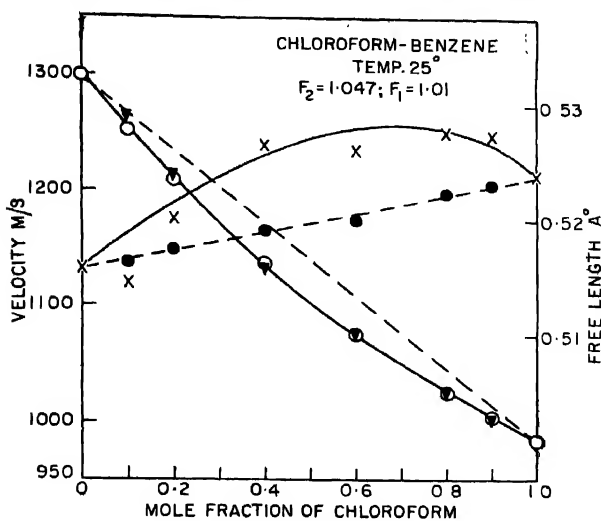


Fig. 3. ●—● Ideal free lengths

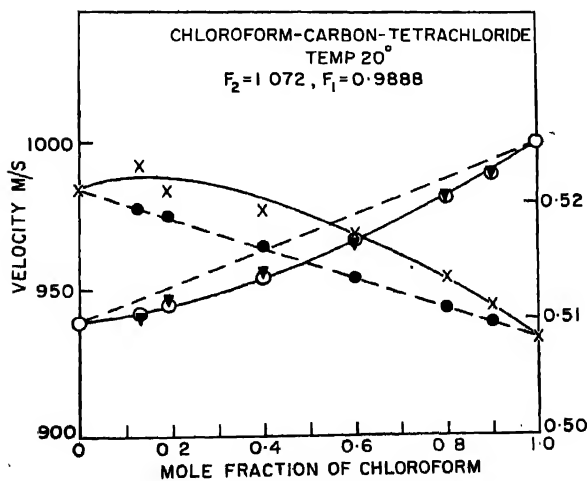


Fig. 4. x—x Experimental free lengths

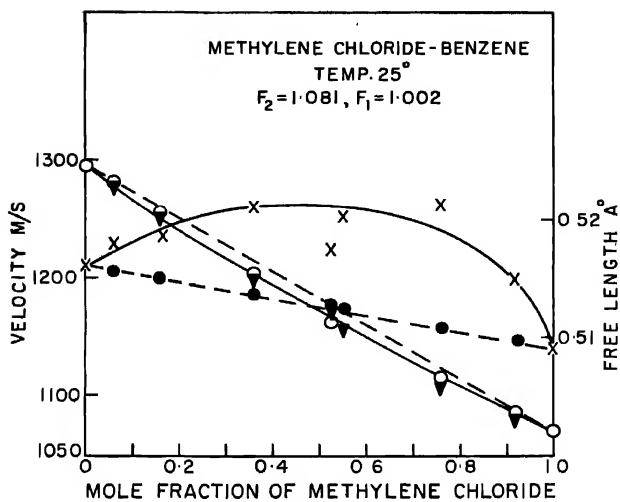
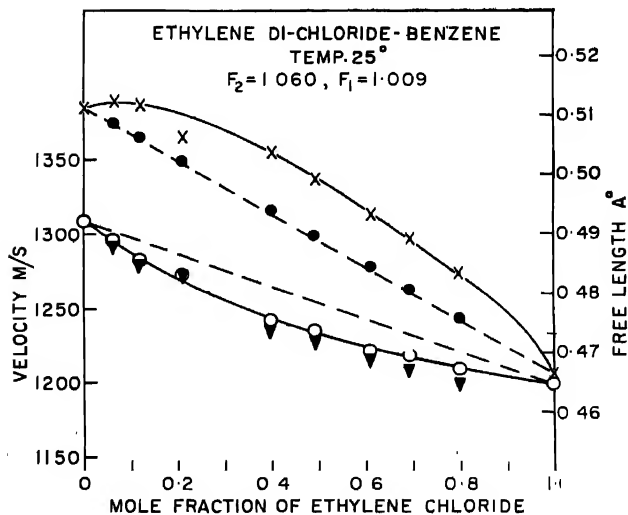
Fig. 5.  $F_2 = Y'_2/Y_2$ Fig. 6.  $F_1 = Y'_1/Y_1$

TABLE I

System : Ethylenedichloride-*n*-heptane  
(Temp. 25°C)

$$Y_2' = 68.98 \times 10^8 \text{ sq.cm./mole.} \quad Y_1' = 95.21 \times 10^8 \text{ sq.cm./mole.}$$

$$Y_2 = (36\pi N V_{02}^2)^{1/3} = 64.86 \times 10^8 \text{ sq.cm./mole.}$$

$$Y_1 = (36\pi N V_{01}^2)^{1/3} = 96.96 \times 10^8 \text{ sq.cm./mole}$$

Mole fraction of ethylene di-chloride	Density gm/cc.	$U_{obs}$ m/s	$U_{calc}$ m/s eq. 1	$L_{mix}$ Å eq. 2	$L_{ideal}$ Å eq. 3	$S_2$
0.000	0.6793	1135	1135	0.6680	0.6680	0.000
0.06053	0.6986	1126	1122	0.6664	0.6581	0.04911
0.1262	0.7174	1125	1111	0.6642	0.6489	0.09479
0.2457	0.7591	1111	1107	0.6483	0.6296	0.1908
0.3992	0.8220	1106	1106	0.6236	0.6027	0.3248
0.5430	0.8927	1108	1108	0.5974	0.5750	0.4626
0.6991	0.9870	1123	1117	0.5633	0.5418	0.6273
0.8474	1.099	1152	1151	0.5181	0.507	0.8007
1.000	1.247	1199	1199	0.4669	0.4669	1.000

This work

TABLE II

System : Chloroform-*n*-heptane  
(Temp. 20°C)

$$Y_2' = 66.76 \times 10^8 \text{ sq.cm./mole.} \quad Y_1' = 96.01 \times 10^8 \text{ sq.cm./mole.}$$

$$Y_2 = (36\pi N V_{02}^2)^{1/3} = 64.86 \times 10^8 \text{ sq.cm./mole}$$

$$Y_1 = (36\pi N V_{01}^2)^{1/3} = 96.96 \times 10^8 \text{ sq.cm./mole.}$$

mole fraction of chloroform	Density gm/cc.	$U_{obs}$ m/s	$U_{calc}$ m/s eq. 1	$L_{mix}$ Å eq. 2	$L_{ideal}$ Å eq. 3	$S_2$
0.000	0.6833	1158	1158	0.6459	0.6459	0.000
0.1811	0.7667	1111	1103	0.640	0.6272	0.1332
0.4035	0.8943	1057	1049	0.6230	0.6011	0.320
0.5859	1.029	1027	1034	0.5892	0.5765	0.4957
0.7944	1.226	1006	1012	0.5517	0.5439	0.7285
0.9132	1.368	1002	1006	0.5267	0.5227	0.8800
1.000	1.489	1001	1001	0.5059	0.5059	1.000

This work

Although equations (3) and (1) demand that the velocity and free lengths be linear functions of surface fraction, the deviations in Table III below have been reckoned on the basis of mole fraction, carefully noting cases in which due to a large difference in  $Y_1$  and  $Y_2$ , (and hence in mole fraction and surface fraction) the deviations on the two scales differ very much. All the deviations in Table III are at 0.5 mole fraction.

TABLE III

Deviations of free length and velocity in binary mixtures. Temp. 25°

System	$-\Delta U$ m/s	$+\Delta L_f$ Å	Ref.
(1) $C_2H_4Cl_2(1:2)-C_6H_6$	22	0.01	
(2) $C_2H_4Cl_2(1:2)-n-C_7H_{16}$	60	0.02	This work
(3) $CH_2Cl_2-C_6H_6$	10	0.009	Tuomikoski and
(4) $CH_2Cl_2-C_7H_{16}$	27	0.026	Nurmi, 1940.
(5) $CHCl_3-C_6H_6$	40	0.007	Gabrielli and
			Poisson, 1951.
(6) $CHCl_3-n-C_7H_{16}$	40	0.022*	This work
	(52)		
(7) $CH_3COCH_3-C_6H_6$	(+12)	(-0.003)	Tuomikoski and
			Nurmi, 1940
(8) $CH_3COCH_3-C_7H_{16}$	35	0.03	"
(9) $CCl_4-C_6H_6$	45	0.004	This work,
			Tuomikoski and
(10) $CCl_4-C_7H_{16}$	37	0.01	Nurmi, 1940.
	(38)		

\*20°C

As can be seen from the table, the free length and the corresponding velocity deviations are more in heptane solution than in benzene solution. In the system chloroform-*n*-heptane\*\*, the velocity when plotted versus surface fraction shows a deviation of 52m/s as against 40m/s when reckoned on mole fraction basis. This can be verified by plotting the data in Table II. The velocity data for the system ethylenedichloride-*n*-heptane when plotted in the same manner, does not show any such variation in the value of  $\Delta U$ , because of the peculiar nature of velocity concentration curve. In the system acetone-benzene we get a small positive velocity deviation instead of negative as in others. This appears to be due to a small contraction of volume after mixing, resulting from a weak interaction between benzene and acetone through the hydrogen bonding tendency of oxygen atom. Consequently the free length is slightly decreased giving a slightly positive velocity deviation. The system heptane-carbontetrachloride is an exception. This was

\*\* The effect of temp. on  $\Delta U$  will be very small and hence it is neglected in comparing  $\Delta U$  of  $CHCl_3$ - $\Delta U$ -heptane at 20° with  $\Delta U$  of  $CHCl_3$ -Benzene at 25°.

thought to be due to the impure sample of heptane (petroleum fraction) used by Tuomikoski and Nurni (1940) in their measurements. Repetition of the velocity measurements in this laboratory using pure-*n*-heptane shows a velocity deviation of only 38 m/s at 0.5 mole fraction. There is also not much difference between mole fraction and surface fraction in this case. Therefore the rule of greater velocity deviation in system having a larger difference ( $L_{exptl.} - L_{ideal}$ ) appears to break down in this case.

#### CONCLUSION

The earlier finding that the velocity deviations are governed by the non-ideality in free length is confirmed. It is found that more the difference ( $L_{exptl.} - L_{ideal}$ ) the greater is the velocity deviation. The system heptane-carbon-tetrachloride appears to be an exception to this general rule of greater velocity deviation for larger free lengths difference.

#### ACKNOWLEDGMENT

Thanks are due to Prof. S. K. K. Jatkar for his keen interest and valuable help during the course of the present work.

#### REFERENCES

- Gabriel, J., and Poirani, G., 1951, *Chem. Abstr.*, **48**, 42751.  
 Jacobson, B., 1952, *Acta Chem. Scand.*, **6**, 1485.  
 Kaulgud, M. V., 1960, *Acustica*, **10**, 316.  
 Tuomikoski, P. and Nurni, V., 1940, *Comment. Phys. Maths. Helvingh*, **10**, 11.

# SOME PECULIARITIES IN CURRENT CONDUCTION DURING ELECTROLYSIS OF A FLOWING ELECTROLYTE

SANTI R. PALIT

INDIAN ASSOCIATION FOR THE CULTIVATION OF SCIENCE, JADAVPUR,  
CALCUTTA 32, INDIA.

(Received August 31, 1962)

**ABSTRACT.** The current passing through an electrolyte at a given voltage has been found to change considerably on making the electrolyte flow. For salts the current decreases on flow, whereas for acids and alkalis the current increases on flow except at very low concentrations. The magnitude of this change depends strongly on the geometry of the electrodes. For most electrolytes the maximum change of current on streaming is observed at a concentration just above .0001N. Electrolytes show a dyssymmetry of current conduction which is found to be linked up with the above behaviour. As an explanation it is suggested that an 'electrolysis layer' builds up on an electrode during electrolysis which in effect either increases or decreases the effective area of the electrode depending on whether this layer is conducting or non-conducting. Streaming of the electrolyte merely removes this layer and gives rise to the observed change of current on flow.

## EXPERIMENTAL

The electrical conductivity of an electrolyte has been found to depend on whether it is flowing or stationary and under certain conditions a large difference between these two values which may be as high as one hundred per cent or even more has been observed and reported (Palit, 1962). The behaviour appears to be rather unexpected and some preliminary results are presented here.

The arrangements shown in Fig. 1 have been utilised for these experiments. The electrodes are platinum wires 0.5–5 mm in length with inter-electrode separation of 2 to 10 mm; these dimensions are neither optimum nor critical. The tubes *a* and *b* serve for inlet and outlet of the electrolyte, though actually the flow may be in any direction provided it sweeps past the vicinity of the electrodes. To minimise disturbances due to gas evolution, heating effect, etc., the current has been kept quite low, usually below one milliampere, sometimes at a value as low as a few microamperes. The observations are however essentially similar at all amperage, provided that the current is low enough.



## RESULTS

*Current-voltage (D.C.) curves*—It has been observed that the applied voltage remaining constant, the current changes if the electrolyte is made to flow past the electrodes. The current generally attains a limiting value with increasing rate of flow of the electrolyte, and this limiting current strength being attained it does not change any more by any further increase of flow of the electrolyte. Further, when the electrolyte is streaming with sufficient speed, the current is usually quite steady and reproducible, whereas under the usual stationary conditions the current beyond the decomposition potential is somewhat non-steady and erratic, and is often quite slow to reach the final value unless current density, voltage and other conditions are properly adjusted. Consequently, by making the electrolyte flow a totally different but, on the other hand, quite reproducible current-voltage curve is obtained. Since these results are quite reproducible we call these curves the 'true' current-voltage curve ( $i-V$  curve).

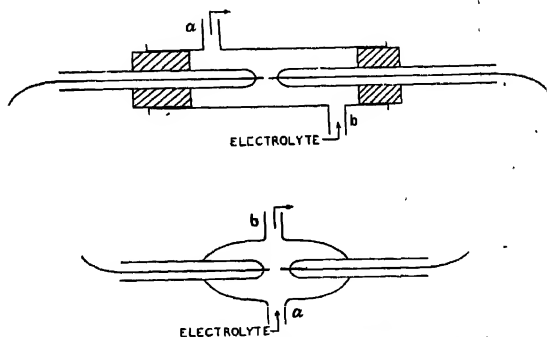


Fig. 1. Cells for electrolysis of flowing electrolytes.

Normally the current decrease on making the electrolyte flow. This is true for almost all salts at ordinary concentrations and acids and alkalies at very low concentrations. Acids and alkalies, however, show the reverse behaviour (i.e. the current increase on making the electrolyte flow) at ordinary concentrations (i.e. from about  $N/1000$  upwards). A typical current voltage curve with D.C. using  $5 \times 10^{-4}N$  KCl as the electrolyte and an apparatus as shown in Fig. 1 is shown in Fig. 2. It would be observed from Fig. 2 that beyond the decomposition potential the D.C. current voltage curve ( $i-V$  curve) for potassium chloride ( $5 \times 10^{-4}N$ ) under flowing condition runs much below the usual  $i-V$  curve though the general shape is more or less the same. It should be further noted that the 'true'  $i-V$  curve tends to be linear from somewhat beyond the so-called decomposition potential. In Fig. 3 is shown the linear portion of the 'true'  $i-V$  curves for various concentrations of a few electrolytes wherein it would be observed that

the extrapolated potential is almost independent of concentration. All these lines in Fig. 3 extrapolate to 2.8–3 volts. This value however may change with the geometry of the cell and other imposed conditions. The matter is receiving further study.

*Relative change of current on streaming*—To avoid circumlocution, we shall call the electric current, when the electrolyte is stationary, the 'non-flow' current or 'normal' current and denote it by  $i'$ ; and we shall call the corresponding steady

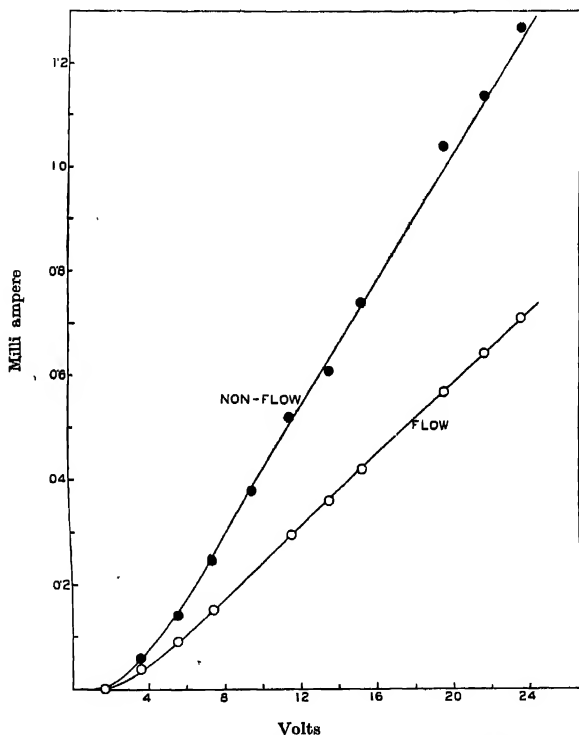


Fig. 2. Current—voltage curve of N/2000 KCl solution

electric current when the electrolyte is made to flow past the electrodes at sufficient speed, the 'flow' current and denote it by  $i$ . At a given voltage,  $R_i$ , the relative change of current strength on making the electrolyte flow  $\left(R_i = \frac{\Delta i}{i} = \frac{i - i'}{i'}\right)$

may be quite high, even exceeding one hundred per cent, under suitable conditions. Of the various factors which have influence on  $\Delta i$ , the most impor-

tant ones appear to be (i) the applied voltage, (ii) the size and shape of the electrodes and their disposition, and (iii) the nature and concentration of the electrolyte.

Of these three factors the voltage needs only be a little beyond the decomposition potential to produce a fairly well-defined  $R_s$  value and this changes only slightly with increasing voltage. All  $R_s$  values in this paper are in this voltage range. At voltages in the non-linear portion of the  $i$ - $V$  curve (i.e. near the bend

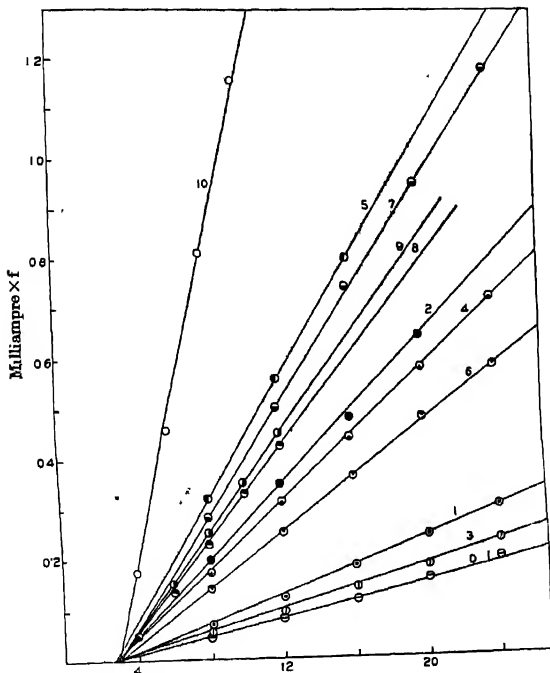


Fig. 3. Linear portion of  $I$ - $V$  curve of flowing electrolytes [curve 0:—water used for 1 & 2; 1 & 2:— $10^{-4}$  and  $5 \times 10^{-4}$   $\text{NH}_4\text{SO}_4$ ; 3, 4 & 5:— $2 \times 10^{-4}$   $\text{N}$ ,  $10^{-3}$   $\text{N}$  and  $2 \times 10^{-3}$   $\text{N}$   $\text{CH}_3\text{COONa}$ ; 6 & 7:— $5 \times 10^{-4}$   $\text{N}$  &  $10^{-3}$   $\text{N}$   $\text{NaOH}$ , 8, 9 & 10:— $10^{-4}$   $\text{N}$ ,  $2 \times 10^{-3}$   $\text{N}$  and  $5 \times 10^{-4}$   $\text{N}$   $\text{BaCl}_2$  (for 8 and 10, multiply ordinate by 0.2 and for 9 by 0.02)].

and below) the  $R_s$  value is somewhat erratic and is quite sensitive to voltage change; with decreasing voltage,  $i$  approaches  $i'$  and exceeds  $i'$  at sufficiently low voltage, presumably due to elimination of polarization.

As regards geometry of the cell, for maximum effect the electrodes should be fairly close but not too close to each other, and they should be well in the line of flow of the electrolyte. The determination of the 'flow' current does not normally pose any problem, but the normal current,  $i'$  may sometimes take some time to reach its final value, and unfortunately is a little erratic. This time lag and erratic nature can be very much reduced by choosing the right dimension, etc., of the electrodes as also by working in the right voltage range. The electrodes may be wires or foils of platinum or any other unattackable material including graphite or carbon.

As regards nature and concentration of the salt it has been already pointed out that  $R_i$  is negative for salts (i.e. current decreases on flow), but is positive for acids and bases except at very low concentrations (ca. N/1000 and below). The variation of  $R_i$  with concentration of an electrolyte at a given voltage using the same cell appears to be qualitatively similar for all electrolytes. The  $R_i$  versus concentration plot shows a steep peak in the  $10^{-4}$  to  $10^{-3}$ N range and from then on continuously falls downwards with concentration. For salts this curve generally remains in the negative region of  $R_i$  and tends to meet the concentration axis with increase in concentration. Two typical curves for salts (KCl and  $\text{MgSO}_4$ ) are shown in Fig. 4 to illustrate this behaviour. The shape of Fig. 4 is of course voltage-dependent as mentioned in the previous para and may be materially changed at low voltage.

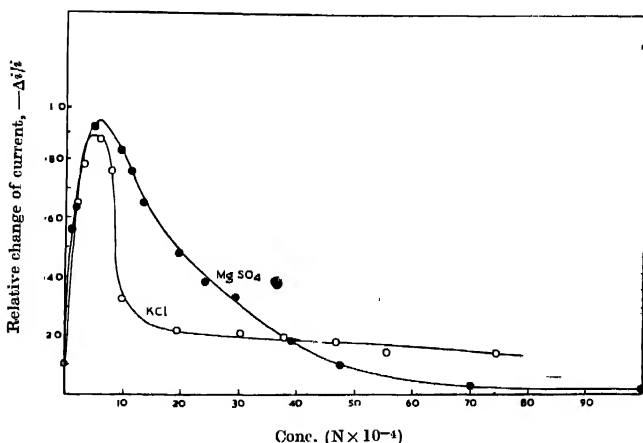


Fig. 4. Relative change of current on making at electrolyte flow versus concentration for KCl and  $\text{MgSO}_4$  ( $V = 12$  volts).

Acids (and also bases) as already mentioned may show positive value of  $R_i$  and so the  $R_i$  versus  $c$  plot easily extends right up to the positive  $R_i$  region. This

is shown in Fig. 5 for sulphuric acid. It shows a steeper peak at a somewhat lower concentration in comparison with the aforementioned electrolytes; but at higher concentration it shows just the opposite behaviour, the 'flow' current being higher than the 'stationary' current. Furthermore, this positive behaviour (i.e. positive  $R_i$  values) persists over quite a long range, whereas for many neutral salts  $R_i$  tends to zero with increasing concentration of the salt. Hydrochloric acid and caustic soda behave like sulphuric acid except that they have a stronger tendency towards positive  $R_i$  values (Fig. 5).

As to apportioning the individual share of each electrode to the observed  $\Delta i$  which is the net effect of the two electrodes, this has been experimentally

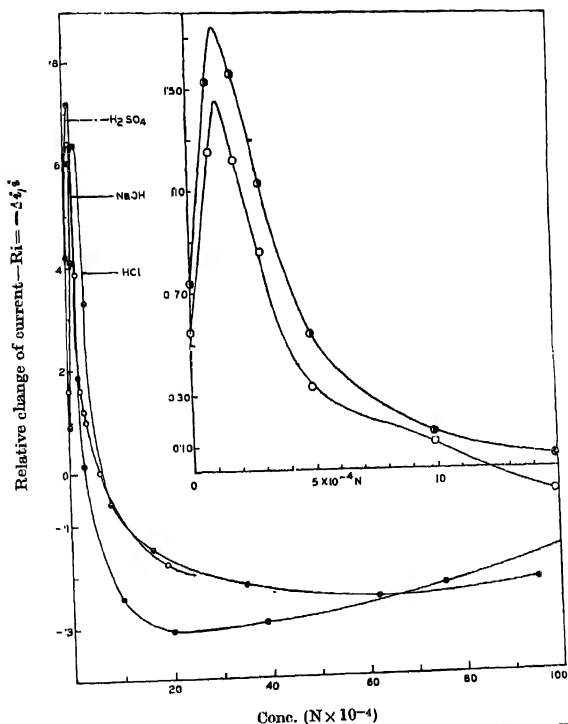


Fig. 5.  $R_i$  versus concentration for  $H_2SO_4$ ,  $NaOH$  and  $HCl$  (12 volts). [Inset is for  $H_2SO_4$  in a different cell; the upper curve is for 12 volts and the lower one for 8 volts.]

investigated by making the flow at only one electrode. It has been observed that both the electrodes are usually sensitive to electrolyte flow, and the behaviour of the cathode may be opposite to that of the anode. Flow at cathode has been

generally found to give negative  $\Delta i$ , i.e. the current decreases on electrolyte flow. The flow at anode may produce positive as well as negative  $\Delta i$  depending on the electrolyte and its concentration; positive  $\Delta i$  has been observed at sufficiently high concentration of those electrolytes which show an overall positive  $\Delta i$ . A detailed investigation of this aspect is in progress. Evidently, any theory must take cognizance of these facts.

*A.C. Current*—This peculiar behaviour is shown not only by D.C. but also by A.C. It is, however, easier to study it with D.C. than with A.C. as this is easily observed with D.C. at quite a low voltage just beyond the decomposition potential in the millampere or the microampere range, where complications due to heating effect of the current are negligible. With A.C. such behaviour is observable at a higher voltage and the magnitude of  $\Delta i$  under otherwise identical conditions is much smaller. However, it is useful to study this behaviour with A.C. because of the remarkable fact that the current voltage curve is linear and passes through the origin (Palit, 1962). The passage of current being ohmic it becomes rather easy to determine the resistance of an electrolyte by this method. Evidently, this technique would be easier than the existing methods for determining the conductivity of very weakly conducting solutions, and particularly in non-aqueous media.

## DISCUSSION

*Mechanism*—Any suggested explanation for the above behaviour has to account for the large magnitude of  $\Delta i$ , its negative character for salts and positive character for acids and bases, and the peculiar concentration dependence of  $\Delta i$  or  $R_i$ . The large magnitude of  $\Delta i$  discounts any explanation based on polarisation. It appears that the observed behaviour is primarily due to the formation of a layer or region on and near the electrodes due to migration of ions on electrolysis, this layer strongly influencing the conduction of current. For salts, either or both these layers are layers of much higher conductivity whose net effect is an increase of the effective area of the electrodes, or decrease in effective distance between the two electrodes. On making the electrolyte flow this layer is swept off which causes the current to decrease. For acids and bases at least one of the two layers is a less conducting layer whose net effect is a decrease of the effective area of the electrodes. On making the electrolyte flow these very poorly conducting layers get swept off with consequent increase of current.

The formation of some kind layer near the electrodes can be demonstrated by a number of simple experiments. For example, the simple device of mechanically disturbing the regions quite close to the electrodes shows conclusively the existence of a sensitive region near each electrode. The following simple experiment is also highly instructive. Two platinum wires are placed horizontally one above the other separated by a few millimeters, and a small D.C. current

(of the order of one milliamperere or so) is passed through them using a flow-sensitive electrolyte (say,  $3 \times 10^{-4}N$  KCl) at a voltage of about 8 volts or higher. It is observed that the current depends considerably on which of the electrodes is the cathode and the anode respectively. Surprisingly, the current is much less when the lower electrode is made the cathode, other conditions remaining the same. The explanation is that when the lower one is the cathode, the evolved bubbles of hydrogen gas as they rise up stir up the vicinity of the anode and interferes with the formation of the 'active' layer by mechanical agitation and may be also by some kind of chemical action. When the lower electrode is the anode, the disturbance at the anode is much smaller, and the cathode is also less disturbed because of the much less volume of the uprising gas from the anode. Such dissymmetry of current due to difference in mechanical disturbance due to gas evolution is almost the rule in electrolysis beyond the decomposition potential, and appears to have received little careful study.

It is difficult to make any surmise about the species present in these layers near the electrodes which are responsible for the change of current on making the electrolyte flow past the electrodes (for brevity, we shall call these layers electrolysis-layers). The obvious suggestion would be that these electrolysis-layers are merely 'concentration'-layers or 'depletion'-layers due to ionic migration. This however cannot be the true explanation because in that event 'conductivity' water should show no such decrease on streaming whereas actually it does so fairly well. Further, with dilute sulphuric acid as the electrolyte the electrolysis-layer near the cathode will be a depletion layer and so should show an increase of current with streaming (i.e. positive  $\Delta i$ ), whereas the observed cathodic behaviour is just the reverse.

It is hence tentatively suggested that a build-up of free radicals takes place in the electrolysis-layers, and these radicals being highly conducting like metals increases the effective area of the electrodes and so show the usual behaviour of decrease of current on flow of the electrolyte. The positive behaviour (i.e. increase of current on streaming) for acids and bases is probably due to the formation on the anode of a thin layer of non-conducting gas, usually oxygen, along with the free radicals.

That something of high electrical conductivity is being continuously formed on the electrodes during electrolysis is convincingly demonstrated by the following experiment. A small third electrode is placed very near a large cathode (or an anode) in a flow-sensitive electrolyte and a small D.C. current is sent for a few seconds so that gas bubbles are coming out freely. If the D.C. current is stopped and a small voltage is applied between the cathode (or the anode as the case may be) and the small third electrode it is observed that the current is very much higher than the normal value before the electrolysis and it rapidly decreases with time to reach the original value. This happens at a cathode even with

dilute sulphuric acid as the electrolyte and at the anode with distilled water or dilute caustic soda as the electrolyte. Since no conducting ionic species are formed near the cathode in the above experiment, the reasonable conclusion appears to be that a layer of free radicals is formed in the electrolysis layer which is a good conductor of electricity. An alternative explanation based on the formation of a highly conducting layers of water ( $\text{H}_2\text{O}^-$  and  $\text{H}_2\text{O}^+$ ) near the cathode and anode respectively is also possible. The true explanation however remains an open question. Further work is in progress.

#### ACKNOWLEDGMENT

Thanks are due to Dr. K. S. G. Doss for helpful discussions.

#### REFERENCE

Palit, S. R., 1902, *Indian J. Phys.*, **36**, 55.



# THE TOTAL CROSS-SECTIONS FOR THE NUCLEAR SCATTERING OF HIGH ENERGY NUCLEONS

G. Z. SHAH AND B. M. THAKER

DEPARTMENT OF PHYSICS, BHAVAN'S COLLEGE, ANDHERI, BOMBAY-58.

(Received September 27, 1961)

**ABSTRACT.** Using the characteristic nuclear density distribution obtained by Gatha, Shah and Patol (1954) for light elements, an expression for the total cross-sections has been derived. The parameters of the complex refractive index have been determined from Jastrow's Hard Core nucleon model and the scattering cross-sections for  $(n,n)$  and  $(n,p)$  scattering respectively. Using these parameters theoretical values of total cross-sections have been calculated for all the light elements for the energies ranging between 200 Mev to 1400 Mev. These values of  $\sigma_t$  are then compared with the experimental values of  $\sigma_t$  at the corresponding energies. A reasonably good agreement is obtained between the theoretical and the experimental total cross-sections.

## INTRODUCTION

The optical model of the nucleus was first introduced by Fernbach, Serber and Taylor (1949). In this model a nucleus is regarded as a distribution of nuclear matter, characterised by a complex refractive index, determined by the interaction of the nucleons within the nucleus with the particular elementary particle. This model is convenient for an analysis of the nuclear scattering of high energy nucleons. The assumption of a uniform nuclear density distribution is inadequate for a correct interpretation of the nuclear scattering of high energy nucleons, firstly, because the nuclear radii required to correlate the experimental data at various energies appear to diminish with the increase in energies and secondly, the theoretical  $\sigma(\theta)$  vanishes at the minima in contrast to the experimental observations. Therefore, Gatha, Shah, and Patel (1954) have carried out an analysis of the nuclear scattering of high energy nucleons for light elements on the basis of this model for the nucleus with non-uniform nuclear density distribution.

Extensive measurements are available for  $\sigma_t$  for various elements for energies ranging between 14 Mev to 1400 Mev. In the present investigation a theoretical formula for total cross-sections has been derived in the Born approximation using the characteristic nuclear density distribution derived by Gatha, Shah and Patel (1954). The theoretical values of total cross-sections are then compared with the experimental values at 208 Mev (Carvalho, Private communication), 270 Mev (De Juran and Knable, 1950), 300 Mev (W. Ball, Private communication), 350 Mev. (Ashmore, Jarvish, Mather and Sen, 1958), 380 Mev (Dzhelepov *et al*,

1955), 410 Mev (Nedzel, 1954), 590 Mev (Dzhelepove *et al*, 1956), 860 Mev (Chen *et al*, 1955), 910 Mev, (Law *et al*, 1958), and 1400 Mev (Coor *et al*, 1955).

#### OPTICAL MODEL OF THE NUCLEUS

In the optical model of the nucleus, the nuclear scattering of an incident high energy particle is described by means of an interaction potential which is independent of the co-ordinates of the individual nucleons within the nucleus but depends only on the co-ordinates of the incident particle with respect to the nucleus as a whole. Using impulse approximation introduced by Chew (1950), the multiple scattering formalism is reduced to a two body problem.

The nuclear potential  $U$  on this approximation has been correlated with the nuclear density distribution  $\rho(\vec{r})$  by Gatha, and Shah (Private communication) considering the spin effect negligible and neglecting the quadratic terms whose contributions to total cross-section  $\sigma_t$  as small, as

$$U = -2k\bar{n}\rho(\vec{r}) \quad \dots (1)$$

where

$k$  = propagation vector of the incident particle within the nucleus.

$\rho(\vec{r})$  = characteristic nuclear density distribution. This is defined as that function of  $\vec{r}$  to which the nuclear density distribution  $\rho(r)$  for any nucleus reduces when the independent variable  $r$  is transformed to  $\vec{r}$  where  $\vec{r} = r \times A^{-1/3}$ ,

$$\text{and} \quad \bar{n} = \bar{n}_1 + i\bar{n}_2$$

$$\text{with} \quad \bar{n}_1 = \pi/k [f_{nn}(0) + f_{np}(0)]$$

$$\text{and} \quad \bar{n}_2 = \epsilon/4 [\sigma_{nn} + \sigma_{np}]$$

where  $f_{nn}(0)$  and  $f_{np}(0)$  represent the forward scattering amplitudes for  $(n, n)$  and  $(n, p)$  scattering respectively.  $\epsilon$  is a factor included for the exclusion principle which becomes unity at such high energies. One can also write the nuclear complex refractive index  $n$  as

$$n = 1 + \{n_1 + in_2\}/k \quad \dots (2)$$

where

$$n_1 = \bar{n}_1\rho \quad \text{and} \quad n_2 = \bar{n}_2\rho \quad \text{with } \rho$$

as the nuclear density

#### CHARACTERISTIC NUCLEAR DENSITY DISTRIBUTION

Gatha, Shah and Patel (1954) have analysed the nuclear differential scattering of 340 Mev nucleons on the basis of the Born approximation. As a result, they

have derived a characteristic nuclear density distribution for light elements given by

$$\rho(\vec{r}) = N \sum_{q=1}^3 \alpha_q \exp(-\beta_q \vec{r}^2) \quad \dots (3)$$

where

$$\begin{aligned} \alpha_1 &= 3.77 \times 10^{26} \text{ cm}^{-2}, & \beta_1 &= 28.94 \times 10^{26} \text{ cm}^{-2}, \\ \alpha_2 &= 2.94 \times 10^{26} \text{ cm}^{-2}, & \beta_2 &= 3.83 \times 10^{26} \text{ cm}^{-2}, \\ \alpha_3 &= 1.50 \times 10^{26} \text{ cm}^{-2}, & \beta_3 &= 0.75 \times 10^{26} \text{ cm}^{-2}, \end{aligned}$$

and  $N = 0.066 \times 10^{13} \text{ cm}^{-1},$

The total cross-section  $\sigma_t$  can be expressed in the form

$$\sigma_t = -\frac{1}{k} \int_m \{ \int e^{-ikz} U \psi d\vec{r} \} \quad \dots (4)$$

where  $\psi$  is the exact wave function. Morse and Feshbach (1953) have shown that to evaluate  $\sigma_t$  up to the first Born approximation it is necessary to evaluate the above integral up to the second Born approximation. On this basis the expression for the total cross-section is given by

$$\sigma_t = 2\bar{n}_2 A + C[\bar{n}_1^2 - \bar{n}_2^2] A^{4/3} \quad \dots (5)$$

where

$$C = 8\pi \int_0^\infty \chi^2(\tilde{S}) \frac{d\tilde{S}}{\tilde{S}}$$

and

$$\chi(\tilde{S}) = \int_0^\infty \rho(\vec{r}) \sin(\tilde{S} \cdot \vec{r}) \vec{r} d\vec{r}$$

with

$$S = 2k \sin(\theta/2)$$

and

$$\tilde{S} = S \times A^{1/3}.$$

#### TOTAL CROSS-SECTIONS

In the present investigation we have calculated the theoretical values of  $\sigma_t$  using equation (5) for large number of elements at various energies. Since the nucleon-nucleon scattering experiments do not provide the forward scattering amplitudes, we obtain them by correlating some model for the process with the angular distributions within the experimental range. One model is based on tensor interaction (Christian and Hart, 1950; Christian and Noyes, 1950) while another model is based upon a hard-core nucleon (Jastrow, 1951). It has been shown by Gatha and Shah (Private communication) that for high energy nuclear scattering Jastrow's model is more reliable than the other one. The Jastrow's

TABLE I  
Comparison of Theoretical and Experimental total Cross-Sections

	208 Mev		270 Mev		300 Mev		350 Mev		380 Mev	
	Theor. (mbn)	Exptl. (mbn)	Theor. (mbn)	Exptl. (mbn)	Theor. (mbn)	Exptl. (mbn)	Theor. (mbn)	Exptl. (mbn)	Theor. (mbn)	Exptl. (mbn)
Li	177.3	192 $\pm$ 3	—	—	—	—	—	—	—	—
Be	226.3	247 $\pm$ 6	214.6	229 $\pm$ 3	—	—	—	—	—	—
B	267.3	276 $\pm$ 9	—	—	—	—	—	—	—	—
C	294.3	296 $\pm$ 3	281.4	288 $\pm$ 3	277.6	282	273.8	285.3 $\pm$ 1.6	273.1	286 $\pm$ 2
N	338.4	350 $\pm$ 10	—	—	—	—	—	—	—	—
O	381.6	385 $\pm$ 10	366.5	372 $\pm$ 7	—	—	357.6	366 $\pm$ 3	356.7	376 $\pm$ 6
Al	607.3	592 $\pm$ 10	588.9	555 $\pm$ 8	583.4	577	577.5	565 $\pm$ 4.5	576.4	582 $\pm$ 8
S	705.8	680 $\pm$ 20	—	—	—	—	—	—	—	—
Cl	769.9	740 $\pm$ 20	—	—	—	—	—	—	—	—

TABLE I (contd.)  
Comparison of Theoretical and Experimental total Cross-Sections

	410 Mev		580 Mev		860 Mev		910 Mev		1400 Mev	
	Theor. (mbn)	Exptl. (mbn)	Theor. (mbn)	Exptl. (mbn)	Theor. (mbn)	Exptl. (mbn)	Theor. (mbn)	Exptl. (mbn)	Theor. (mbn)	Exptl. (mbn)
Li	—	—	—	—	—	—	—	—	—	—
Be	208.5	231 $\pm$ 4	233.8	261 $\pm$ 4	254.3	316 $\pm$ 16	—	—	261.0	308 $\pm$ 13
B	—	—	—	—	—	—	—	—	—	—
C	272.8	297 $\pm$ 3	303.1	319 $\pm$ 2	326.4	405 $\pm$ 23	328.2	362 $\pm$ 2.4	333.7	378 $\pm$ 10
N	—	—	—	—	—	—	—	—	—	—
O	356.5	378 $\pm$ 5	391.8	407 $\pm$ 5	—	—	418.9	469 $\pm$ 10	—	—
Al	576.1	587 $\pm$ 8	618.5	631 $\pm$ 9	640.8	750 $\pm$ 50	—	—	643.6	703 $\pm$ 18
S	673.9	672 $\pm$ 9	—	—	—	—	—	—	—	—
Cl	738.0	742 $\pm$ 10	—	—	—	—	—	—	—	—

curve for  $\bar{n}_1$  against energy is practically constant and levels off beyond 340 Mev. We have, therefore, taken in the present investigation the value  $\bar{n}_1 = 8$  units at 340 Mev as the constant value for  $\bar{n}_1$  for all higher energies.

Recently, an extensive data on scattering cross-sections for  $(n, n)$  or  $(p, p)$  and  $(n, p)$  scattering is available for various high energies. We have plotted smooth curves passing through all the experimental points and used these curves for determining  $\bar{n}_2$  at different energies.

The theoretical values of  $\sigma_t$ , calculated, using equation (5), are compared with the corresponding experimental values of  $\sigma_t$  at various energies. Such a comparison is shown in Table I.

#### CONCLUSION

It is clear from the above comparison that there is a close agreement between the theoretical and experimental values of  $\sigma_t$  up to about 600 Mev. Beyond this energy the agreement is approximate. The deviations between the theoretical and experimental values of  $\sigma_t$  above 600 Mev may perhaps be due to the meson production at high energies or systematic errors in experimental observations. However, the close agreement between the experimental and theoretical values of  $\sigma_t$  indirectly confirms the existence of a characteristic nuclear density distribution. A similar analysis based on Glauber approximation (Glauber, 1952) is under investigation, details of which will be published later on.

#### REFERENCES

- Ashmore, A., Jarvish, R. G., Mather, D. S. and Sen, S. K., 1957, *Proc. Phys. Soc.*, **70A**, 745.
- Ball, W. (Private communication)
- Carvalho (Private communication)
- Chew, G. F., 1950, *Phys. Rev.*, **80**, 196.
- Chen, F. F., Leavitt, C. P. and Shapiro, A. M., 1955, *Phys. Rev.*, **99**, 867.
- Christian, R. S., and Hart, E. W., 1950, *Phys. Rev.*, **77**, 441.
- Christian, R. S., and Noyes, H. P., 1950, *Phys. Rev.*, **79**, 85.
- Coor, T., Hill, D. A., Hornyak, W. F., Smith, I. W., and Show, G., 1955, *Phys. Rev.*, **98**, 1369.
- DeJuren, J. and Knable, N., 1950, *Phys. Rev.*, **80**, 27.
- Dzhelelov, V. P., Satarov, V. I. and Galovin, B. M., 1955, *Doklady Akad. Nauk. S. S. S. R.*, **104**, 717.
- Ibid, 1956 *Sov. Phys., JETP*, **2**, 349.
- Fernbach, S., Serber, R., and Taylor, T. B., 1949, *Phys. Rev.*, **75**, 1352.
- Gatha, K. M., Shah, G. Z., and Patel, N. J., 1954, *Proc. Phys. Soc.*, **76A**, 773.
- Gatha, K. M., and Shah, G. Z., (Private communication)
- Glauber, R. J., 1953, *Phys. Rev.*, **91**, 459.
- Jastrow, R., 1951, *Phys. Rev.*, **81**, 636.
- Phys. Rev.*, **82**, 261.
- Law, Hutchisson and White., 1958, *Nucl. Phys.*, **9**, 600.
- Morse, P. M., and Feshbach, H., 1953, *Methods of Theoretical Physics* (New York, McGraw Hill), pp 1073.
- Nedzel, V. A., 1954, *Phys. Rev.*, **94**, 174.

# PRELIMINARY X-RAY STUDY OF CRYSTAL STRUCTURE OF CEDRELONE

B. CHAUDHURI, I. M. DAS, AND A. N. TALUKDAR

DEPARTMENT OF PHYSICS, GAULATI UNIVERSITY

(Received March 3, 1962)

Cedrelone (m.p.  $207^{\circ}\text{C}$ ) was isolated by Parihar and Dutt (1950) from the heartwood of Indian Mahogany (Cedrella Toona Roxb) well known for its commercial and medicinal importance. Of late there had been some controversy about its constitution. The above authors proposed  $\text{C}_{25}\text{H}_{30}\text{O}_5$  as its molecular formula with presence of lactone and phenolic hydroxyl groupings in the molecule. A reinvestigation of its constitution by Aghoramurthy, Das, Mukherjee and Rao (1962) based on spectroscopic data and relevant chemical evidences had led to  $\text{C}_{26}\text{H}_{30}\text{O}_5$  as its chemical formula with the structure as shown in the Fig. 1, containing primarily, one diosphenol group, one unsaturated six-membered ring with a carbonyl group and a furan ring. Conventional

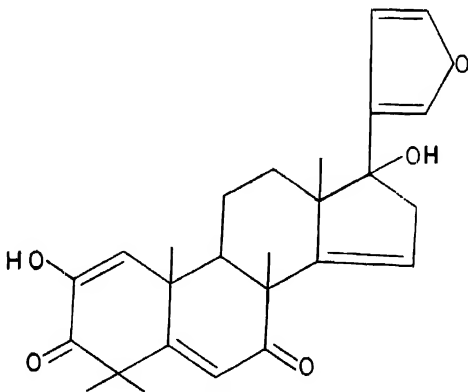


Fig. 1

methods of molecular weight determination such as acetyl estimation and cryscopic measurements may perhaps be considered unsuitable for unique confirmation of this small difference of 12 units in the molecular weights of these two alternative formulae. X-ray study of crystal structure of cedrelone was undertaken with the ultimate aim of complete structure determination

by Fourier method and also to determine its molecular weight from unit cell and density measurements.

No suitable single crystal was found in the original sample of cedrelone supplied by Prof. T. R. Sheshadri. Recrystallisation from dilute solution in alcohol yielded colourless pinacoids belonging to monoclinic holosymmetric  $2/m$  class showing forms  $\{001\}$  and  $\{100\}$ . Oscillation and Weissenberg photograph gave the following monoclinic unit cell :

$$\begin{aligned}a &= 18.75 \text{ \AA} \\b &= 13.07 \text{ \AA} \\c &= 18.78 \text{ \AA} \\\beta &= 102^{\circ}15'(101^{\circ})\end{aligned}$$

No correction due to film-shrinkage was made.  $\beta$  was determined by the method of  $\omega$  separation from zero-level Weissenberg photograph (The corresponding value obtained from goniometric measurement is given in the parenthesis). Redetermination of the unit cell dimensions by  $\theta$ -method (Weiss, Cochran and Cole, 1948) gave the following values.

$$\begin{aligned}a &= 18.595 \pm .002 \text{ \AA} \\b &= 12.956 \pm .001 \text{ \AA} \\c &= 18.619 \pm .002 \text{ \AA} \\\beta &= 101^{\circ}49' 30''\end{aligned}$$

Density of the crystals determined by floatation method in aqueous solution of strontium chloride and also of potassium iodide, aided by centrifugation was found to be  $1.273 \pm .002$  gm/cc. The molecular weight calculated with the refined unit cell dimensions was 420.7 with 8 molecules in the unit cell, supporting formula  $C_{26}H_{30}O_5$  proposed by Aghoramurthy and others (1962). Calculated density based on this formula (molecular weight 422) was 1.277 gm/c.c.

Oscillation as well as  $b$  and  $c$  axis Weissenberg photographs were indexed. Reflexions of type  $hol$  with  $h+l$  odd,  $oko$  with  $k$  odd,  $hoo$  with  $h$  odd and  $ool$  with  $l$  odd were systematically absent. These absences uniquely established the space group to be  $P2_1/n$  (equivalent to  $P2_1/c$  with appropriate axial transformation). Symmetry elements of this space group permit only four equivalent positions. Assuming that all atoms are in general positions, the asymmetric structural unit therefore comprises two molecules of cedrelone.

An interesting pseudo-symmetric feature is exhibited by  $hol$  Weissenberg photograph. Distribution of intensities is found to be nearly identical on either side of the  $[101]^*$  and  $[10\bar{1}]^*$  directions. A pseudo orthorhombic cell can be constructed with  $a' = 11.72 \text{ \AA}$ ,  $b' = b$  and  $c' = 14.95 \text{ \AA}$ ,  $a'$  and  $c'$  being parallel

to 101 and  $10\bar{1}$  planes. This pseudo-symmetry in *hol* zone of reflexions indicates that in projection there are pseudo planes of symmetry parallel to the trace of 101 and  $10\bar{1}$  planes. A clue to the approximate structure may perhaps lie on this observation. Further work on obtaining an approximate structure by optical transform method (Lipson and Taylor, 1951) using "Optical Diffractometer" (Hughes and Taylor, 1953) is in progress.

We are indebted to Prof. T. R. Sheshadri for supplying cedrelone crystals and for his interest in the work. We also wish to thank Prof. P. C Mahanta, Head of the Department of Physics, Gauhati University for his encouragement and Mr. M. G. R. Nair, Chemistry Department, Gauhati University, for his help in recrystallising the cedrelone sample.

#### REFERENCES

- Aghoramurthy, K., Dass, I., Mukherjee, S. K. and Rao, M. M., 1962, To be published.  
Hughes, W. and Taylor, C. A., 1953, *J. Sci. Instrum.*, **30**, 105.  
Lipson, H. and Taylor, C. A., 1951, *Acta Cryst.*, **4**, 458.  
Parihar, D. B. and Dutt, S. B., 1950, *J. Ind. Chem. Soc.*, **27**, 77.  
Weiss, O., Cochran, W. and Colo, W. F., 1948, *Acta Cryst.*, **1**, 83.



# A NOTE ON KIHARA'S THEORY OF RADIOFREQUENCY DISCHARGE

S. N. SEN AND A. K. GHOSH

DEPARTMENT OF PHYSICS, JADAVPUR UNIVERSITY, CALCUTTA-32

(Received July 14, 1962)

Starting from a molecular model, the breakdown voltage in case of a radio frequency discharge is given by Kihara (1952)

$$eB_0P/2E = A_1PL \left[ 1 - \frac{E/B_0P}{C_2L/\lambda} \right]$$

Kihara in his paper has only plotted the values of  $E$  against  $P$  for different values of  $P$  and compared the results thus obtained with the values obtained by Githens (1940). But it is evident that  $P_{min}$ , the value of  $P$  at which the breakdown voltage becomes a minimum can be obtained from the above equation and is given by

$$P_{min} = \frac{2E_{min}}{B_0} \log \frac{2A_1LE_{min}}{B_0\lambda} \quad (1)$$

where  $E_{min}$  is the minimum breakdown voltage.

TABLE I

Frequency of applied field in Mc/sec	Gas	$P_{min}$ in mm. from eqn (1)	$P_{min}$ in mm. experimental values	Reference
0	H <sub>2</sub>	1.4	0.9	Thomson (1937)
2.83	H <sub>2</sub>	3.5	2.6	
3.73	H <sub>2</sub>	2.594	1.7	
6.33	H <sub>2</sub>	1.58	1	
15.6	H <sub>2</sub>	1.002	0.46	
7.1	N <sub>2</sub>	0.121	0.136	Sen & Ghosh (unpublished data)
7.1	Air	0.152	0.200	
9.5	H <sub>2</sub>	19.00	12.00	Prowse and Clark (1958) Townsend and Williams (1958)
30	H <sub>2</sub>	4.799	4.8	

To test the accuracy of the above expression we have calculated the values of  $P_{min}$  from Eq. (1) from the data available in literature and compared them with the values of  $P_{min}$  obtained experimentally.

It is thus evident that the values of pressure at which the breakdown voltage will be minimum as deduced from Kihara's theory agree quite well in some cases investigated and also there is wide divergence in others. The discrepancy may be ascribed partly to the approximate values of the molecular constants which modify the values of  $A_1$ .

Kihara in his theory has introduced two constants  $A_0$  and  $B_0$  which are given by

$$A_0 = \frac{N}{P} \cdot \frac{\sigma}{U_i} \cdot \left( \frac{3\lambda}{\rho} \right)^{\frac{1}{2}}$$

$$B_0 = \frac{N}{P} \cdot \frac{mc^2}{2e} \cdot (3\lambda\rho)^{\frac{1}{2}} \quad \dots (2)$$

and further he has shown that they are identical with the constants  $A$  and  $B$  in Townsend's equation where

$$A = \frac{1}{\lambda_1} \quad \text{and} \quad B = \frac{v_i}{\lambda_1} \quad \dots (3)$$

where  $v_i$  is the ionization potential of the gas and  $\lambda_1$  is the mean free path of electrons in the gas at a pressure of 1 m.m. Equating  $A_0$  and  $B_0$  in Eq. (2) with  $A_1$  and  $B_1$  in Eq. (3) respectively we obtain

$$\frac{C_d}{\sigma} \rho \times .64 = 1. \quad \dots (4)$$

Further  $\lambda$  can be calculated independently from the relation

$$C_d = .05 \left( \frac{E}{P} \right) \frac{1}{\lambda} \quad \dots (5)$$

where  $C_d$  is the drift velocity of electrons in the gas. The values of  $C_d$  and  $\sigma$  have been obtained by Kihara quite independently and consequently  $\rho$  can be calculated from Eq. (4). From the values of  $\rho$  and  $\lambda$  thus obtained  $A_0$  can be calculated from Eq. (2) and from  $A_0$  and  $B_0$ ,  $v_i$  can be obtained. The values of  $v_i$  obtained from Townsend's coefficients  $A$  and  $B$  have also been entered into the Table 2 for comparison.

Consequently, it is evident that the values of  $v_i$  as derived from Kihara's theory are closer to actual  $v_i$  values than the values obtained from Townsend's coefficients. But Kihara has calculated the values of the molecular constants

TABLE II

Gas	$\rho \times 10^{24}$ from Eqn(4)	$\lambda \times 10^8$ from eqn(5)	$v_i$ in volts (Ionization potential)			
			from Kihara's theory.	from Townsend's coefficients	Literature values	
H <sub>e</sub>	0.133	4.0	2.877	13.0	11.93	24.5
H <sub>2</sub>	0.487	7.7	7.6	17.1	26	15.4
N <sub>2</sub>	1.03	15.4	15.67	21.8	28.5	15.5
A	1.43	13.63	14.00	13	15.0	15.7
CH <sub>4</sub>	0.95	16.7	15.67	7.3	5.7	14.5

in his theory from Townsend's coefficients. It is thus concluded that better agreement with experimental results will be obtained if the values of the molecular constants are obtained independently and not from Townsend coefficients. To investigate these points, we are undertaking the breakdown voltage measurements over a wide range of frequencies and pressure and in different gases in order to determine  $P_{min}$  and the results will be reported in future.

The present work forms part of a programme of the scheme on "Electrical discharge through gases and vapours and its investigation by microwave probe and optical method" and the authors are indebted to C.S.I.R., Government of India, for financing the project.

## REFERENCES

- Othens, S., 1940, *Phys. Rev.*, **57**, 822.  
 Kihara, T., 1952, *Rev. Mod. Phys.*, **24**, 43.  
 Prowse, W. A. and Clark, J. L., 1958, *Proc. Phys. Soc.*, **72**, 625.  
 Sen, S. N. and Ghosh, A. K., (Unpublished data)  
 Thomson, J., 1937, *Phil. Mag.*, **23**, 1.  
 Townsend W. G. and Williams G. C., 1958, *Proc. Phys. Soc.*, **72**, 823.



## THE SPECTRUM OF CoBr IN THE VISIBLE

( $\lambda$  4300— $\lambda$  4700 Å)

S. V. KRISHNA RAO AND P. TIRUVENGANNA RAO

PHYSICS DEPARTMENT, ANDHRA UNIVERSITY, WALTAIR.

(Received May, 21, 1962).

## Plate VII

**ABSTRACT.** High dispersion spectrograms of CoBr in the visible ( $\lambda$  4390— $\lambda$  4700 Å) have shown the existence of characteristic band systems designated as *A*, *B*, *C* and *D*. The *A*, *B* and *C* systems consist of single-headed bands while the *D* system consists of double-headed bands. Approximate vibrational constants have been determined from the vibrational analysis. The observed bromine isotope effect in the *B* and *C* systems confirms the vibrational analysis.

## INTRODUCTION

Mesnage (1939), reported characteristic bands of CoBr in the region  $\lambda$ 4300— $\lambda$ 5650 Å, in emission in a high frequency discharge, but no analysis was presented for any of the bands. Recently, Krishnamurty (1952) investigated the spectrum of CoBr excited in a heavy current discharge and proposed the analysis of three systems of bands in the region  $\lambda$ 4300—4700 Å and interpreted them as belonging to an electronic triplet of the type  ${}^3\Pi$ — ${}^3\Sigma$ . In addition, Krishnamurty proposed the analysis of a weaker system of bands in the region  $\lambda$ 5418— $\lambda$ 5975 Å, on the basis of a  ${}^5\Pi_{(a,b)}$ — ${}^5\Sigma$  transition. However, the analysis of the different band systems of CoBr, proposed by Krishnamurty, were based on spectra taken under the low dispersion of the Glass Littrow spectrograph. As the spectra are superposed by strong atomic lines of Cobalt and Bromine, the classification of the different systems and the identification of the different heads are uncertain.

In continuation of our work on NiCl and CoCl, we have examined the spectrum of CoBr both under low and high dispersion. The experimental procedure and the method of photographing the spectra were similar to those employed by us in the case of CoCl.

## RESULTS AND ANALYSIS

In the spectrum of CoBr, excited in a high frequency discharge from a 100-Watt oscillator, four discrete band systems in the visible region  $\lambda$ 4300— $\lambda$ 4700 Å have been definitely identified from a close scrutiny of both low and high dispersion spectrograms. Starting from the violet side, these systems were designated as

A, B, C and D respectively. The structure and analyses of these systems are described below.

In the region  $\lambda 4700\text{--}\lambda 6000\text{\AA}$ , the weaker system of bands obtained by Krishnamurty could not be photographed under the high dispersion of the grating. In the photographic infrared region  $\lambda 6800\text{--}\lambda 8000\text{\AA}$  although some bands were observed as in the case of  $\text{CoCl}$ , the band heads are diffuse and ill-defined for measurement.

#### *The A system*

This system is easily identified even under low dispersion as shown in strip (a). Under high dispersion, (strip b) the bands of the strong  $\Delta v = 0$  sequence appear line-like and single-headed. The weaker  $\Delta v = -1$  sequence consists of only two bands. The line-like appearance of the bands is due to the close values of  $\omega_e'$  and  $\omega_e''$ .

#### *The B and C systems*

The two strong  $\Delta v = 0$  sequences of these two systems are shown in strip (c). In each of the two strong sequences, the heads appear single-headed. The (1, 1) and (2, 2) bands of system B seem to be accompanied by fortuitous heads, which are formed by unresolved rotational lines. The bands of the  $\Delta v = +1$  sequences of these two systems show double heads corresponding to  $\text{CoBr}^{79}$  and  $\text{CoBr}^{81}$  species. The observed splittings fit well as shown in Table II, with the splittings expected according to the equation.

$$\Delta v = (\rho - 1)[\omega_e'(v' + 1/2) - \omega_e''(v'' + 1/2)] \\ - (\rho^2 - 1)[x e' \omega_e' (v' + 1/2)^2 - x e'' \omega_e'' (v'' + 1/2)^2] \quad \dots (1)$$

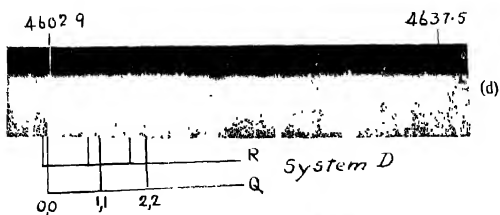
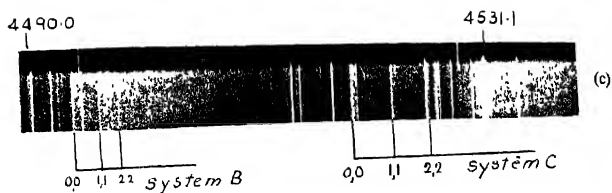
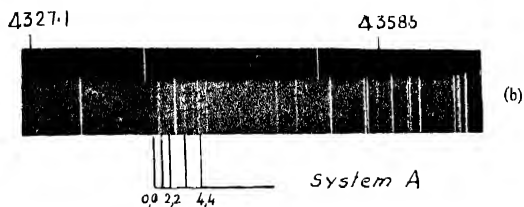
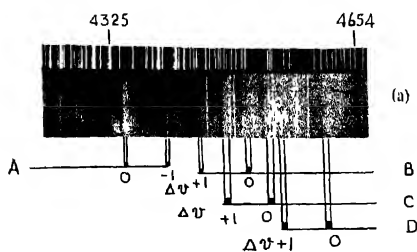
#### *The D system*

The strong bands of the  $\Delta v = 0$  sequence are shown in strip (d). Each of the bands (0, 0) (1, 1) and (2, 2) are double headed, consisting of *R* and *Q* heads. The *Q* heads of the weaker  $\Delta v = +1$  sequence are also identified from grating spectrograms. The band heads of this system could be represented by the following quantum formula.

$$v = 21731.1 + 300.2(v' + 1/2) + 0.72(v' + 1/2)^2 - \\ - 322.8(v'' + 1/2) + 0.15(v'' + 1/2)^2 \quad \dots (2)$$

A peculiar feature of this system is that the anharmonic constant for the upper state is negative, so that the spacings of the vibrational levels are anomalous over the observed range.

The data and classifications of the different heads are given in Table I.



The spectrum of CoBr in the visible region  $\lambda 4300\text{--}\lambda 4700\text{\AA}$

- (a) :—Fuess spectrogram
- (b) :— $\Delta\nu=0$  sequence of system A (21 ft. grating 2nd order spectrogram)
- (c) :— $\Delta\nu=0$  sequences of systems B and C (21 ft. grating 2nd order spectrogram)
- (d) :— $\Delta\nu=0$  sequence of system D (21 ft. grating 2nd order spectrogram).





TABLE I

Band heads of CoBr in the region  $\lambda$  4300-4700 Å

Wavenumber	Intensity	Classification
<i>System—A</i>		
23048.4	5	0,0
23045.0	8	1,1
23040.7	4	2,2
23034.1	3	3,3
23026.4	6	4,4
22776.7	4	0,1
22773.2	5	1,2
<i>System—B</i>		
22548.7	4	1,0
22546.9	4	1,0 <sub>1</sub>
22535.9	6	2,1
22534.5	6	2,1 <sub>1</sub>
22527.3	5	3,2
22525.9	5	3,2 <sub>1</sub>
22245.9	10	0,0
22234.6	5	1,1
22226.0	3	2,2
<i>System—C</i>		
22427.0	5	1,0
22425.5	5	1,0 <sub>1</sub>
22407.0	3	2,1
22405.5	3	2,1 <sub>1</sub>
22385.8	3	3,2
22384.4	3	3,2 <sub>1</sub>
22123.5	10	0,0
22105.9	7	1,1
22088.9	4	2,2
<i>System—D</i>		
22021.7	5	1,0 Q
22002.6	5	2,1 Q
21984.4	4	3,2 Q
21722.4	5	0,0 R
21720.0	10	0,0 Q
21703.3	7	1,1 R
21698.6	7	1,1 Q
21685.8	5	2,2 R
21679.8	5	2,2 Q

The heads of CoBr<sup>81</sup> are marked with i.

TABLE II

Isotope effect in systems B and C of CoBr

$\nu', \nu''$	Calc	Obs
<i>System—B</i>		
1,0	—1.0	—1.8
2,1	—1.5	—1.4
3,2	—1.4	—1.4
<i>System—C</i>		
1,0	—1.6	—1.5
2,1	—1.4	—1.5
3,2	—1.3	—1.4

TABLE III  
Vibrational constants of band systems of CoBr

System	(0,0)	$\nu'$	$\nu_0'\nu'$	$\nu''$	$\nu_0''\nu''$
A	23048.4	269.1	0.4	271.6	-0.05
B	22245.9	304.3	0.75	318.3	2.1
C	22123.5	306.8	1.05	324.0	1.5
D	21720.0 Q	300.2	-0.72	322.8	0.15

## DISCUSSION

Table III summarizes the vibrational constants of the CoBr molecules. The lower state vibrational frequency  $318.3\text{ cm}^{-1}$  of the B system is entirely in keeping with the ground state frequency  $316\text{ cm}^{-1}$  of NiBr.

The A, B, C systems of CoBr, consisting of single-headed bands appear to be analogues of some of the single-headed band systems of CoCl. (A, B, C, D and E.)

Each of the systems A, B, C, D and E in CoCl was previously attributed to a transition in which  $\Delta\Omega = 0$  corresponding to case (c). As CoBr is a heavier molecule than CoCl, we may expect even a greater tendency towards case (c). Thus each of the A, B and C systems may be interpreted as arising from a transition in which  $\Delta\Omega = 0$  in Hund's case (c). The D system consisting of double-headed bands may be attributed to a case (c)—case (c) transition in which  $\Delta\Omega = \pm 1$ .

## ACKNOWLEDGMENT

The authors wish to express their thanks to Prof K. R. Rao for his interest in this work. One of the authors (S.V.K. Rao) is grateful to the Council of Scientific and Industrial Research, (Delhi) for the award of Senior Research Fellowship.

## REFERENCES

- Krishnamurthy, V. G. 1952, Thesis for Doctorate, Andhra Univ., Waltair.  
 Mesnager, P. 1939, *Ann. De. Phys., Paris. (Tome)* **12**, 5.  
 Rao, S. V. K. and Rao, P. T., 1961, *Ind. J. Phys.* **35**, 556.  
 Rao, et al., 1962, *Z. f. Physik*, **166**, 261.

# ULTRASONIC STUDIES IN AQUEOUS SOLUTIONS OF ELECTROLYTES

M. G. SESHAGIRI RAO AND B. RAMACHANDRA RAO

ULTRASONIC RESEARCH LABORATORIES, PHYSICS DEPARTMENT., ANDHRA  
UNIVERSITY, WALTAIR.

(Received January 22, 1962, Re-submitted July 1962)

**ABSTRACT.** Ultrasonic velocity measurements are carried out in aqueous solutions of some nitrates and the variation of ultrasonic velocity, adiabatic compressibility, apparent molal compressibility and molar sound velocity with concentration is studied. The results are interpreted in terms of Gucker's limiting laws. The hydration numbers are estimated for all the electrolytes and compared with the data obtained by other methods. The molar sound velocity values are estimated for 100% of the electrolyte and the values are compared with the computed values known for some of the metallic radicals.

## INTRODUCTION

Considerable work has already been done on the study of ultrasonic velocity and hence adiabatic compressibility and apparent molal compressibility in aqueous solutions of electrolytes. The calculation of apparent molal compressibility and adiabatic compressibility forms the basis for the verification of Gucker's (1933) limiting laws, derived from the well-known Debye-Huckel's theory of electrolyte solutions. It is also possible to estimate the number of water molecules associated with the ions, known as the hydration number, from the apparent molal compressibility value at infinite dilution. Gucker himself verified his limiting laws by the piezometric method of measuring compressibilities. Later Bachem (1936), Scott, Obenhaus and Wilson (1934), Krishnamurthy (1950, 1951) Rao and Rao (1958) studied the apparent molal compressibilities in several solutions of electrolytes of different valence types and reported deviations from the limiting laws. While investigating the variation of ultrasonic velocity with concentration in solutions of electrolytes some authors (Barthel, 1954, Murthy and Murthy 1958, Balachandra, 1960; Padmini and Rao, 1960) reported unusual features like decrease of ultrasonic velocity with increase of concentration of the salt, in electrolytes having heavy metallic and acid radicals. Marks (1960) has calculated the hydration numbers of certain sulphates and hydroxides of alkali metals, Lithium, Sodium, Potassium and Ammonium. Following the same lines Padmini and Rao (1960) studied some acetates and halides; and Bhimasenachar and Subrahmanyam (1960) investigated some nitrates.

As very little work has been done especially on the study of molar sound velocity and hydration numbers of electrolytes, the authors have taken up the present

investigation of studying ultrasonic velocity, adiabatic compressibility, apparent molal compressibility, and molar sound velocity in some nitrates. The salts Ag NO<sub>3</sub> (Rao and Rao, 1961) and UO<sub>2</sub>(NO<sub>3</sub>)<sub>2</sub> (Rao and Rao, 1962) have already been reported, but included in this paper for a comparative study.

#### EXPERIMENTAL DETAILS

The following is the list of nitrates whose aqueous solutions are studied in the present investigation.

- |                      |        |  |        |
|----------------------|--------|--|--------|
| 1. Lithium nitrate.  | (1-1). | 5. Cadmium nitrate. 4H <sub>2</sub> O.   | (2-1). |
| 2. Silver nitrate.   | (1-1). | 6. Uranyl nitrate. 6H <sub>2</sub> O.    | (2-1). |
| 3. Beryllium nitrate |        | 7. Aluminium nitrate. 9H <sub>2</sub> O. | (3-1). |
| 3H <sub>2</sub> O    | (2-1). |  |        |
| 4. Calcium nitrate.  |        | 8. Lanthanum nitrate. 3H <sub>2</sub> O. | (3-1). |
| 4H <sub>2</sub> O    | (2-1). |  |        |

The samples used are of either of B.D.H or E. Merck, Analar quality. The ultrasonic velocities are measured at 30°C by using the double crystal, fixed path interferometer of Rao and Rao (1957). The densities are determined accurate to 1 mg. by means of a specific gravity bottle. The velocity measurements are accurate to 1 m/sec. The parameters, adiabatic compressibility, apparent molal compressibility and molar sound velocity are calculated by using the usual relations

$$\beta_{ad} = \frac{1}{\rho V^2}, \quad R = \frac{M}{\rho} (V)^{1/3}$$

$$\phi(K_2) = \frac{1000\beta}{C} - \beta_0 \left\{ \frac{1000\rho}{C} - M_2 \right\}$$

where  $\rho$  and  $\rho_0$  are the densities of the solution and the solvent;

$C$  = molal concentration expressed in moles/litre of the solvent.

$M_1$  and  $M_2$  = molecular weights of the solvent and solute.

$V$  = ultrasonic velocity.

$\beta_{ad}$  = adiabatic compressibility of the solvent.

$\bar{M}$  = average molecular weight of the solutions given by

$$M = \frac{n_1 M_1 + n_2 M_2}{n_1 + n_2}$$

where  $n_1$  and  $n_2$  are respectively the number of moles of the solute and the solvent.

The molar concentration  $C$  is calculated using the formula

$$C = \frac{n_1}{n_1 + n_2} \times 100.$$

The results are presented graphically in Figs. 1 to 6.

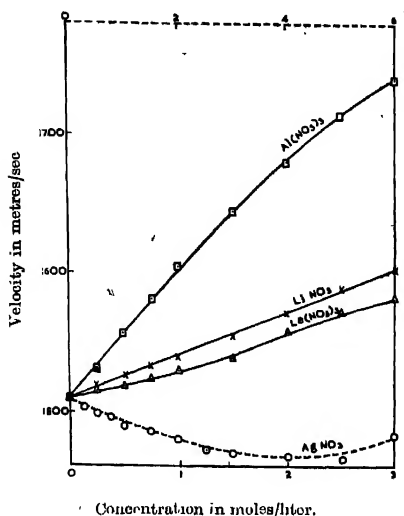


Fig. 1. Variation of ultrasonic velocity with molal concentration in  $\text{LiNO}_3$ ,  $\text{AgNO}_3$ ,  $\text{Al(NO}_3)_3$ , and  $\text{La(NO}_3)_3$ .

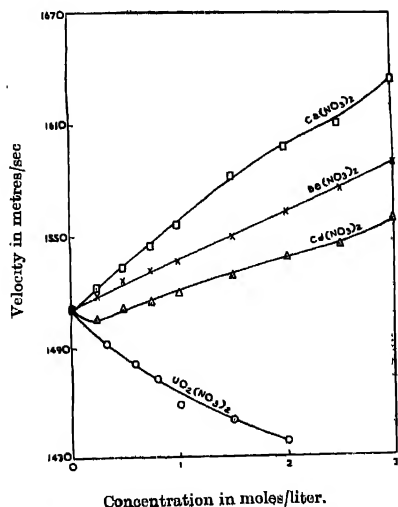


Fig. 2. Variation of ultrasonic velocity with molal concentration in  $\text{Ca(NO}_3)_2$ ,  $\text{Be(NO}_3)_2$ ,  $\text{Cd(NO}_3)_2$  and  $\text{UO}_2(\text{NO}_3)_2$ .

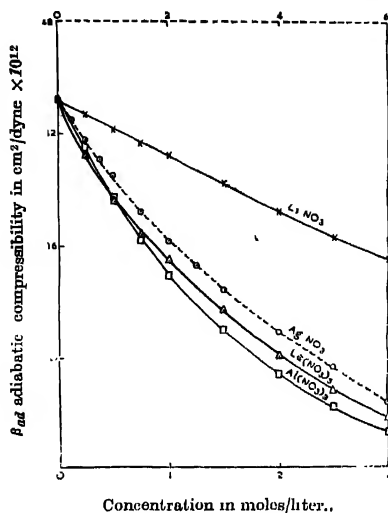


Fig. 3. Variation of adiabatic compressibility with molal concentration in  $\text{LiNO}_3$ ,  $\text{AgNO}_3$ ,  $\text{AlNO}_3$  and  $\text{La(NO}_3)_3$ .

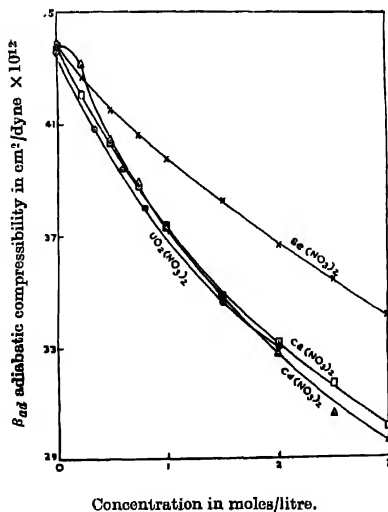


Fig. 4. Variation of adiabatic compressibility with molal concentration in  $\text{Ca(NO}_3)_2$ ,  $\text{Be(NO}_3)_2$ ,  $\text{Cd(NO}_3)_2$  and  $\text{UO}_2(\text{NO}_3)_2$ .

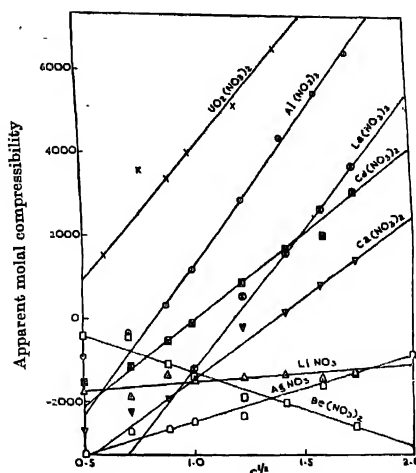


Fig. 5. Variation of apparent molal compressibility ( $\bar{\kappa}(K_2)$ ) with square-root of molal concentration.

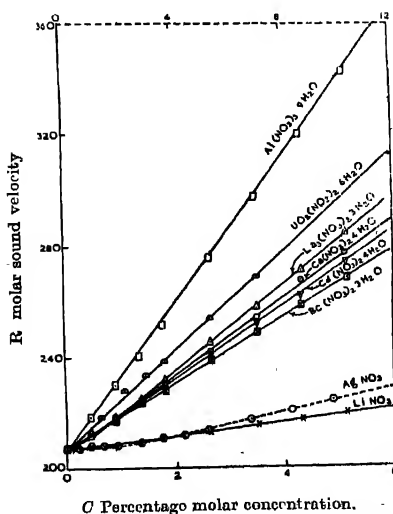


Fig. 6. Variation of molar sound velocity ( $R$ ) with molar concentration ( $C$ ).

VARIATION OF ULTRASONIC VELOCITY AND  
ADIABATIC COMPRESSIBILITY WITH  
CONCENTRATION

From a study of the Figs. 1 and 2 it is evident that the ultrasonic velocity exhibits peculiar variation in the case of some salt solutions. In the case of silver nitrate solutions the ultrasonic velocity decreased upto a concentration of 4M and then showed an increasing tendency while uranyl nitrate showed only a decreasing tendency even at the maximum concentration studied. The cadmium nitrate solution exhibited the same behaviour of cadmium acetate (Padmini and Rao, 1960) in that the ultrasonic velocity showed first a slight decrease and then an increase with further increase of concentration. It is evident from the Figs. 1 and 2 that in all types of electrolytes having a common anion, the heavier the metallic radical, the less is the velocity gradient, the only exception being beryllium nitrate (2-1).

In spite of the unusual variations in the case of ultrasonic velocity, the adiabatic compressibility showed a decrease with increase of concentration in all the salts as can be seen from Fig. 3 and 4 following closely Gucker's equation

$$\beta = \beta_0 + AC + BC^{1/2}.$$

From a systematic study of a series of aqueous solutions of some sulphates Marks (1959), has drawn the conclusion that for a fixed anion the compressibility at a particular concentration decreases with increasing ionic radius of the cation. This rule was verified and confirmed by Padmini and Rao taking all the available data from literature and the deviations observed in some hydrated salts are explained. Table I contains the compressibility data at 1 mole concentration together with the ionic radii for the different cations, the theoretical and experimental slopes of apparent molal compressibility graphs and the hydration numbers estimated for the different salts of the present investigation. It can be seen that the Marks rule applies satisfactorily for these salts. Taking  $\text{Li NO}_3$  and  $\text{Ag NO}_3$  both of which are of (1-1) type and are anhydrous, silver nitrate which has a large cation exhibits lower compressibility. In the (3-1) type salts the compressibility of lanthanum nitrate solution is higher than aluminium nitrate solution although the radius of its cation is higher than the latter. This discrepancy may be due to the excess of six water molecules in the water of crystallisation of aluminium salt whose tendency is to lower the compressibility. Among the (2-1) type salts, beryllium which has the smallest radius shows the higher compressibility in accordance with the above rule. Cadmium nitrate and uranyl nitrate having the same cationic radius should have the same compressibility but uranyl nitrate shows slightly less compressibility. This may be due to the two extra molecules of water of crystallisation associated with the uranyl salt. Calcium which is having a slightly higher radius than cadmium and having the same number of water molecules, should have lower compressibility compared to cadmium salt but the experimental result



is actually the reverse. This may be associated with the peculiar behaviour of cadmium nitrate at low concentrations.

#### APPARENT MOLAL COMPRESSIBILITY AND HYDRATION NUMBERS

As can be seen from Fig. 5 the apparent molal compressibility  $\phi(K_2)$  varies almost linearly with square-root of concentration in all the electrolyte solutions. The value of  $\phi(K_2)$  for most of the salt solutions is positive at higher concentrations and negative at lower concentrations. The values of the gradients  $\partial\phi(K_2)/\partial C^{1/2}$  are determined and presented in Table I along with the theoretically computed values. It is interesting to note that while all other nitrates showed a positive gradient for the apparent molal compressibility beryllium nitrate showed a negative gradient. In the (1-1) type electrolytes the experimental slope of  $\text{LiNO}_3$  showed good agreement with the theoretical value whereas the silver nitrate showed a large deviation. For the (2-1) electrolytes except beryllium nitrate whose experimental slope is negative and less than the theoretical slope, and uranyl nitrate whose slope is very much larger than the theoretical slope, the other salts calcium and cadmium nitrates showed reasonably good agreement with the theoretical slope. The gradients for both the (3-1) types of salts, showed some amount of divergence from the theoretical slope, the experimental values being lower in both cases, but the agreement may be considered as fairly satisfactory. It may, therefore, be concluded that the experimental data can be explained qualitatively on the basis of Gucker's limiting laws. The negative gradient in the case of beryllium nitrate is yet to be explained.

The study of apparent molal compressibility at infinite dilution enables the calculation of hydration number of electrolyte. The hydration number represents the number of water molecules bound to either the cation or anion or the molecules as a whole. The first layer of molecules attached to the ion is known as the primary water of hydration and is incompressible compared to the free solvent molecules, Wada, Shimbo and Oki (1950) have given the following relation for the calculation of the primary hydration numbers.

$$\lim_{C \rightarrow 0} \phi(K_2) = \beta_0 V_h$$

where  $V_h$  is the volume of the primary water of hydration for the whole of the electrolyte. The limiting value  $\phi(K_2)$  can be arrived at by extrapolating  $\phi(K_2)$  versus  $C^{1/2}$  graph to zero concentration. Using the experimental value of  $\phi(K_2)$  and  $\beta_0$ , the values of  $V_h$  are estimated. By making the further assumption that the molar volume of the solvent molecules in the primary hydration sheath is the same as that of the pure solvent, the combined primary hydration number for the electrolyte is obtained by dividing  $V_h$  by the molecular weight of water. The

experimental values thus obtained for all the nitrates investigated are presented in the last column in Table I. The authors have also studied the anhydrous samples of some salt solutions and found that the hydration number of anhydrous salt is equal to the sum of the hydration number of the hydrated salt and the number of water molecules attached to it. The hydration numbers thus transformed for the anhydrous salt are reported in the last column of Table I.

TABLE I

Name of the salt	Chemical formula	Adiabatic compressibility at 1 Mole concentration	Ionic radius of the cation in Å	$\delta z(K_2)/\delta \sqrt{c}$		Hydration number for	
				Theoretical	Experimental	Hydrated salt	anhydrous salt
1. Lithium nitrate (1—1)	$\text{LiNO}_3$	40.90	0.60	6.3	5.0	2.24	2.24
2. Silver nitrate (1—1)	$\text{AgNO}_3$	39.77	1.25	6.3	16.4	5.10	5.10
3. Beryllium nitrate (2—1)	$\text{Be}(\text{NO}_3)_2 \cdot 3\text{H}_2\text{O}$	39.79	0.34	32.6	-18.5	-0.62	2.4
4. Calcium nitrate (2—1)	$\text{Ca}(\text{NO}_3)_2 \cdot 4\text{H}_2\text{O}$	37.42	0.99	32.6	38.7	6.7	10.7
5. Cadmium nitrate (2—1)	$\text{Cd}(\text{NO}_3)_2 \cdot 4\text{H}_2\text{O}$	37.30	0.97	32.6	41.5	5.3	9.3
6. Uranyl nitrate (2—1)	$\text{UO}_2(\text{NO}_3)_2 \cdot 6\text{H}_2\text{O}$	37.18	0.97	32.6	61.3	2.5	8.5
7. Aluminium nitrate (3—1)	$\text{Al}(\text{NO}_3)_3 \cdot 9\text{H}_2\text{O}$	34.34	0.50	92.4	72.0	7.07	16.07
8. Lanthanum nitrate (3—1)	$\text{La}(\text{NO}_3)_3 \cdot 3\text{H}_2\text{O}$	35.30	1.15	92.4	66.7	9.9	12.9

TABLE II

Name of the salt	Chemical formula	R for hydrated salt	R for anhydrous salt	R for the metal computed	R for metal available in literature
1. Lithium nitrate	$\text{LiNO}_3$	430	430	181	55
2. Silver nitrate	$\text{AgNO}_3$	422.5	422.5	173.5	—
3. Beryllium nitrate	$\text{Be}(\text{NO}_3)_2 \cdot 3\text{H}_2\text{O}$	1382.5	762.4	264.4	—
4. Calcium nitrate	$\text{Ca}(\text{NO}_3)_2 \cdot 4\text{H}_2\text{O}$	1615.5	788.7	290.7	436
5. Cadmium nitrate	$\text{Cd}(\text{NO}_3)_2 \cdot 4\text{H}_2\text{O}$	1406.0	579	81	315
6. Uranyl nitrate	$\text{UO}_2(\text{NO}_3)_2 \cdot 6\text{H}_2\text{O}$	1986.7	746.7	100.7	—
7. Aluminium nitrate	$\text{Al}(\text{NO}_3)_3 \cdot 9\text{H}_2\text{O}$	2894.2	1034	287	319
8. Lanthanum nitrate	$\text{La}(\text{NO}_3)_3 \cdot 3\text{H}_2\text{O}$	1723.5	1103.5	356.5	—

The values of hydration numbers for lithium and calcium are taken as 4, 18 and 10 respectively as reported by Bell<sup>17</sup>. Assuming the above values, the hydration number for the nitrate radical in lithium and lanthanum nitrates comes out to be the same and equal to  $-1.7$  whereas the same value in calcium nitrate is  $+0.35$ . The negative value of hydration for the nitrate radical is in accordance with the concept of negative hydration put forth by Wang<sup>(18)</sup>. Taking the value of  $-1.7$  as the contribution due to the nitrate radical, hydration numbers for the cations  $\text{Ag}^+$ ,  $\text{Be}^{++}$ ,  $\text{Cd}^{++}$ ,  $\text{UO}_2^{++}$  and  $\text{Al}^{+++}$  have been calculated and the values are 6.8, 5.8, 12.7, 11.9 and 21.2 respectively. These values of hydration numbers for these cations are reported for the first time.

#### MOLAR SOUND VELOCITY AND ASSOCIATION

It is interesting to note from Fig. 6 that the molar sound velocity varied linearly with concentration expressed in percentage molar concentration. Extrapolating these linear graphs to 100% molar concentration, the  $R$  value for the pure salt is obtained. Taking the contribution of the nitrate radical towards  $R$  as 249 (by assuming individual values of  $N$  and 0) and taking the experimental value of 206.7 for water, the  $R$  values for the metallic radicals are calculated and compared with those available in literature. The results are presented in Table II and as can be seen from the table there is no agreement between the values of  $R$  for the metals estimated from the aqueous electrolyte solutions and those from the other methods. This may be due to the highly associated nature of the solvent water.

#### ACKNOWLEDGMENT

One of the authors (M.G.S. Rao) is indebted to the Council of Scientific and Industrial Research, New Delhi, for financial assistance.

#### REFERENCES

- Bachem, Ch., 1936, *Zeits. fur. Physik.*, **101**, 541.
- Balachandran, C. G., 1960, *Nature*, **187**, 130.
- Barthol, R., 1954, *J. Acous. Soc. Amer.*, **260**, 227.
- Bell, R. P., 1958, *Endavour*, **17**, 31.
- Bhimasenachar, J. and Subrahmanyam, S. V., 1960, *Jour. Acous. Soc. Amer.*, **32**, 703.
- Gucker, F. T., 1933, *Jour. Amer. Chem. Soc.*, **55**, 2709.
- Krishnamurthy, Bh. 1950, *Jour. Sci. Ind. Res.* **9B**, 215 and 1951, *Jour. Sci. Ind. Res.* **10B**, 140.
- Marks, G. W., 1959, *Jour. Acous. Soc. Amer.*, **31**, 936.
- Marks, G. W., 1960, *Jour. Acous. Soc. Amer.*, **32**.
- Murthy, M. S. and Murthy, Bh. K., 1958, *Jour. Sci. Ind. Res.*, **17B**, 216.
- Padmini P. R. K. L and Rao, B. R., 1960, *Ind. Jour. Phys.*, **35**, 505.
- Rao, K. S. and Rao, B. R., 1958, *Jour. Sci. Ind. Res.*, **17B**, 444.
- Rao, M. G. S and Rao, B. R., 1961, *Nature*, **191**, 164.
- Rao, M. G. S and Rao, B. R., 1962, *Curr. Sci.*, **31**, 9.
- Rao, K. S. and Rao, B. R., 1957, *Jour. Sci. Ind. Res.*, **16B**, 483.
- Scott, A. F., Obenhaus and Wilson, R. W., 1934, *Jour. Phys. Chem.*, **38**, 937.
- Wada, Shimbo and Oda, 1950, *Jour. Acous. Soc. Amer.*, **22**, 880.
- Wang, 1954, *Jour. Phys. Chem.*, **58**, 686.

# RESONANCE IN ELECTRON CAPTURE BY PROTON PASSING THROUGH HYDROGEN ATOMS

S. C. MUKHERJEE AND N. C. SIL

DEPARTMENT OF THEORETICAL PHYSICS,  
INDIAN ASSOCIATION FOR THE CULTIVATION OF SCIENCE,  
JADAVPUR, CALCUTTA-32

(Received September 26, 1962)

**ABSTRACT.** The recent experimental results of Lockwood and Everhart (1962) on the capture probability of an electron by a proton passing through hydrogen atom shows that at an angle of scattering of  $3^\circ$ , the capture probability when plotted against the reciprocal of the proton velocity reveals resonant structure with maxima and minima. It is found that the application of the variational method of Sil (1960), in the low energy region reproduces this structure fairly well. The theoretical results begin to differ from the experimental findings at 3 Kev and thereafter the difference goes on increasing with higher energies. As in the method of Sil, the proton-proton interaction has been neglected.

## INTRODUCTION

Lockwood and Everhart (1962) have studied the probability of an electron capture by a proton passing through hydrogen atoms for a particular impact parameter corresponding to  $3^\circ$  angle of scattering of the incident proton; their findings reveal a resonant variation of the capture probability with the reciprocal of the proton velocity corresponding to the energy of 0.75 Kev to 30 Kev. In this energy range the maxima occur at 20.1, 3.92, 1.57 and 0.78 Kev, and the minima at 7.69, 2.39 and 1.11 Kev.

Applying the impact parameter method of Bates, Massey and Stewart (1953), Ziemba and Russek (1959) have tried to explain the resonance peaks that occur at  $5^\circ$  scattering angle in the electron capture probability of  $\text{He}^+$  passing through He at different energy values (1 Kev-200 Kev) of the incident  $\text{He}^+$ . The theoretical values of the capture probability oscillate between 1 and 0, whereas the experimental values fluctuate between 0.6 and 0.2. The positions of the maxima and minima agree well with the experimental findings at high energies; the method is not quite satisfactory at lower energies and as such the agreement between theory and experiment is poor. Bates and McCarroll (1962) have recently reported the results of Ferguson (1961) and McCarroll (1961) for the positions of maxima and minima in the electron capture cross section for  $\text{H}^+ - \text{H}$  atom collision at  $3^\circ$  scattering angle. The calculation of Ferguson is based on an expansion in molecular eigenfunction whereas that of McCarroll on an expansion in atomic eigenfunction.

Sil (1960) has applied a variational method to calculate the total capture cross section of electrons by protons incident on hydrogen atoms at low energies of the incident protons and has found good agreement with the experimentally observed values of Fite, Brackmann and Snow (1958) and with the theoretical findings of Dalgarno and Yadav (1953), who have used the perturbed stationary states method. A perusal of the paper of Sil shows that the matrix element for the capture process contains a term similar to the proton-proton interaction term included by Jackson and Schiff (1953). though the Hamiltonian form, which Sil has taken, does not contain proton-proton interaction.

In this paper we have calculated for low energies of the incident proton, using the same variational method, the capture probability of an electron by the incident proton which gets scattered at an angle of  $3^\circ$  in the Laboratory system. Our theoretical results also show the resonant structure with the maxima and minima and agree with the experimental values of Lockwood and Everhart (1962), specially when the incident proton energy is 3Kev or less.

#### THEORY

When a proton passes by a hydrogen atom and captures the electron from the atom, the incident proton is scattered by the Coulomb interaction of the atomic proton. The variational method which we apply here consists of the determination of the transition probability of an electron from a bound state of the hydrogen atom to a similar state of the moving proton under the influence of the Coulomb field of the proton. This probability is obtained as a function of the relative energy and the impact parameter and is calculated from the classical scattering of the two protons in their mutual field. For the calculations of the electron capture probability we assume that the centre of mass of the incident proton and the proton of the target atom is at rest, while the protons move in a straight line with uniform velocities  $-\frac{1}{2}v$  and  $+\frac{1}{2}v$  respectively. In the Coulomb field of the two protons, the paths of the two protons are hyperbolas, but in the calculation of the capture probability, we assume the paths to be straight lines and the error involved in this assumption is negligible.

Let  $R$  be the position vector of the incident proton relative to the atomic proton at any time  $t$ ,  $t = 0$  is the instant when the two protons are nearest to each other with  $p$ , the impact parameter, as the distance.

The electron capture probability as given by the variational method of Sil (1960) is

$$|B|^2 = \sin^2 \left[ \frac{1}{\hbar} \int_{-\infty}^{\infty} f(R) dt \right] \quad \dots (1)$$

where

$$f(R) = \frac{f_2 - f_1 f_3}{1 - f_3^2}$$

$$\begin{aligned} f_1(R) &= \int \frac{e^2}{r_2} \bar{\psi}_1 \psi_1 dV \\ &= e^2 \left[ \frac{1}{R} - \frac{1}{a_0} \exp\left(-\frac{2R}{a_0}\right) - \frac{1}{R} \exp\left(-\frac{2R}{a_0}\right) \right] \end{aligned}$$

where  $a_0$  is the first Bohr radius of the hydrogen atom.

$$f_2(R) = \frac{e^2}{2} \int \left( \frac{1}{r_1} + \frac{1}{r_2} \right) \bar{\psi}_1 \psi_2 dV$$

$$f_3(R) = \int \bar{\psi}_1 \psi_2 dV$$

$\psi_1$  and  $\psi_2$  are the initial and final wave functions and  $f_2$  and  $f_3$  for low incident proton energies become,

$$f_2 = \frac{e^2}{a_0} \left( 1 + \frac{R}{a_0} \right) \exp\left(-\frac{R}{a_0}\right)$$

$$f_3 = \left( 1 + \frac{R}{a_0} + \frac{1}{3} \frac{R^2}{a_0^2} \right) \exp\left(-\frac{R}{a_0}\right)$$

In the laboratory system of coordinates the scattering angle and the impact parameter are connected by the Rutherford's formula (vide Ziembra and Russek, 1959)

$$p = \frac{e^2}{\tan \theta \cdot E} \quad \dots (2)$$

where  $E$  is the energy of the incident proton in the laboratory system. From the relation (2) we get

$$\int_{-\infty}^{\infty} f(R) dt = \frac{2}{v} \phi(p)$$

where

$$\phi(p) = \int_p^{\infty} \frac{f(R) R dR}{\sqrt{R^2 - p^2}} \quad \dots (3)$$

and  $\phi(p)$  is evaluated by a numerical method as shown in the Appendix. For each value of  $E$ , we get the corresponding values of  $p$  and  $\phi(p)$  from relations (2) and (3) respectively and substituting these values in Equation (1) we get the

corresponding capture probability. We compare our theoretical values with the experimental results of Lockwood and Everhart (1962) as shown in the Figure.

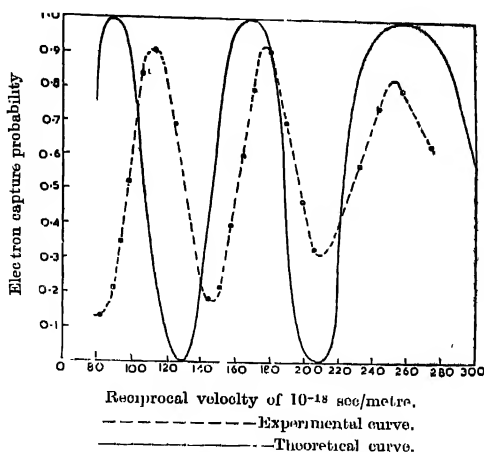


Fig. 1. The electron capture probability  $p$  for collisions of  $H^+$  on  $H$  is plotted against the reciprocal of the incident proton velocity. These data are for collisions in which the scattered particle emerges at  $3^\circ$  in laboratory system.

In Table I we have given our results for the values of the incident proton energy at which the maximum and minimum values of the capture probability occur together with the results of Ferguson and McCarroll and have compared the theoretical findings with the experimental values of Lockwood and Everhart. Both Ferguson and McCarroll have given results with and without the neglect of the translatory motion of the electron.

The effect of the translatory motion of the electron is ignored in (I) and taken into account in (II).

## DISCUSSION

Our results give fair agreement with the experimental values when the incident proton energy is small. With the increase of incident proton energies we find marked deviations from observed values. This is due to the fact that  $f_2$  and  $f_3$  have been calculated in the approximation of zero value of the translatory velocity of the ion. Moreover, in our calculations we have considered only two main possibilities for the electron state, i.e., either the electron remains attached to the atomic proton or it is captured by the incident ion in the ground state. Besides the above two possibilities, the electron may be left in the original atom in an excited state, it may be captured by the incident ion in any of its excited orbits or it may be knocked off the original atom without being captured by the

Positions of maxima and minima of differential electron capture cross section for  $H^+-H$  atom collisions at  $3^\circ$  scattering angle

TABLE I

Energy (Kev units) at which maxima and minima occur										
Theory						Experiment				
Present Authors		Ferguson (1961)				McCarroll (1961)				Lockwood & Everhart (1962)
(I)		(I)		(II)		(I)		(II)		
Max	Min	Max	Min	Max	Min	Max	Min	Max	Min	Max
0.772		1.19		—		1.00		—		0.780
	1.183		1.63		1.15		1.42		1.03	1.11
1.80	3.08	2.34	3.65	1.96	2.70	2.20	3.55	1.40	2.03	1.57
										2.39
6.44		6.48		4.06		6.48		3.12		3.92
			14.6		6.95		14.8		5.63	7.69
	58.4		16.9		59.6		14.2		20.1	



incident ion. All these effects may give rise to additive or destructive interference in the capture probability by affecting the energy of the incident particle.

A perusal of the table shows that the positions in the energy scale of the maxima and minima according to our calculations which neglect the translatory motion of the electron agree closely with the experimental values at low energies where the above neglect is justified. The influence of the translatory motion of the electron is to make the maxima and minima occur at correspondingly lower values as can be seen from the results of Ferguson and McCarroll who have given two sets of results, one of which takes into account the above influence. If we had not neglected the translatory motion our agreement with experiment would have been still better. Somehow or other the calculations of Ferguson and McCarroll which incorporates the translatory motion do not show as good agreement as expected; at energies greater than 7 Kev the positions of the maxima and minima fall considerably below the experimental findings.

From the experimental results we find that the resonance peaks at energy of the order of 8 Kev to 0.78 Kev remain almost equally spaced and the peaks and valleys lie between 0.9 and 0.1, but the amplitudes of the peaks become smaller with decreasing energy, whereas from our theoretical results we find that when the incident proton energy is small, the spacings of the peaks are broad and with the increase of energy it shrinks and becomes narrow but the peaks and valleys reach the values 1 and 0. Zienba and Russok in their calculation for resonance electron capture in  $5^\circ$  scattering angle of  $\text{He}^+$  on He has also found the oscillation of the maxima and minima between unity and zero, which is the characteristic feature of the impact parameter method. According to this method for small values of impact parameter the probability for resonance electron capture oscillates between unity and zero.

#### ACKNOWLEDGMENT

Authors are indebted to Prof. D. Basu for many valuable discussions.

#### APPENDIX

$$\text{Evaluation of } \phi(p) = \int_p^\infty \frac{f(R)RdR}{\sqrt{R^2 - p^2}}$$

We split up  $f(R)$  into two parts

$$f(R) = f_1(R) + f_2(R)$$

where  $f_2(R) = 2/3 R e^{-R}$  being the asymptotic form of  $f(R)$  and  $f_1(R)$  is the residual part after subtracting  $f_2(R)$  from  $f(R)$ . For the purpose of evaluation of  $\phi(P)$  we suitably approximate  $f_1(R)$  by two exponential functions of  $R$ .

i.e.  $f_1(R) \simeq A_1 e^{-\lambda_1 R} + A_2 e^{-\lambda_2 R}$ .  $A_1$ ,  $A_2$ ,  $\lambda_1$ ,  $\lambda_2$  are found to be complex numbers.

Finally, we may write

$$f(R) \simeq e^{-\alpha R} (a \cos \beta R + b \sin \beta R) + \frac{a}{\beta} R e^{-R}$$

where  $\alpha = 1.346, \quad \beta = 0.3558$

and  $a = 1, \quad b = -0.7832$

The numerical values of the above expression on the right hand side were compared with  $f(R)$  and except for a small range near  $R = 0.2$ , the relative error was found to be less than 1% over the entire range of  $R$  from 0 to  $\infty$ .

It is convenient to express  $f_1(R)$  in the form

$$f_1(R) \simeq A \exp(-\rho e^{-i\theta} R) + \bar{A} \exp(-\rho e^{i\theta} R)$$

where  $A = \frac{1}{2}(1 + i \cdot 0.7832), \quad \bar{A} = \frac{1}{2}(1 - i \cdot 0.7832)$

and  $\rho = 1.3935, \quad \theta = 15^\circ$

Let us now consider the integral

$$I_0 = \int_p^\infty \frac{e^{-ZR} dR}{\sqrt{R^2 - p^2}}$$

which on substitution of  $R = p \times U$  becomes

$$I_0 = \int_1^\infty \frac{e^{-(pz)U} dU}{\sqrt{U^2 - 1}} = K_1(pZ)$$

where  $|\arg pZ| < \pi/2$  (Watson 1944, P. 142).

The integral  $I_1 = \int_p^\infty \frac{e^{-ZR} R dR}{\sqrt{R^2 - p^2}}$  is obtained by differentiating with respect to  $Z$ .

Thus  $I_1 = - \left( \frac{\partial I_0}{\partial z} \right) = -p K'_0(pZ)$

where the dash denotes the differentiation with respect to the argument.

Now since  $K'_0(\zeta) = -K_1(\zeta)$  (Watson, 1954, P. 79)

$$I_1 = pK_1(pZ)$$

$$\text{Thus} \quad \phi_1(p) = \int_p^\infty \frac{f_1(R)RdR}{\sqrt{R^2-p^2}} = pAK_1(ppe^{-\theta}) + p\bar{A}K_1(ppe^{i\theta})$$

The integral

$$I_2 = \int_p^\infty \frac{e^{-R}R^2dR}{\sqrt{R^2-p^2}}$$

may be obtained by differentiating  $I_1$  with respect to  $Z$  and putting  $Z = 1$  the derivative.

$$\begin{aligned} \text{Thus} \quad I_2 &= - \left( \frac{\partial I_1}{\partial Z} \right)_{Z=1} = p^2 [K_1'(pZ)]_{Z=1} \\ &= pK_1(p) + p^2 K_0(p) \end{aligned}$$

$$\text{Since} \quad ZK_1'(Z) + K_1(Z) = -ZK_0(Z)$$

$$\text{Hence} \quad \phi_2(p) = \frac{2}{3} \int_p^\infty \frac{e^{-R}R^2dR}{\sqrt{R^2-p^2}} = \frac{2}{3} [pK_1(p) + p^2 K_0(p)]$$

$$\text{Finally} \quad \phi = \phi_1 + \phi_2$$

#### REFERENCES

- Bates, D. R., Massey, H. S. W. and Stewart, A. L., 1953, *Proc. Roy. Soc.*, **A216**, 437.  
 Bates, D. R. and McCarroll, A., 1962, *Advances in Physics*, **11**, 39.  
 Dalgarno, A. and Yudav, H. N., 1953, *Proc. Phys. Soc.*, **A66**, 173.  
 Ferguson, A. F., 1961, *Proc. Roy. Soc.*, **A264**, 540.  
 Fite, W. L., Brackmann, T., and Snow, W. R., 1958, *Phys. Rev.*, **112**, 1161.  
 Grant, J., Lockwood and Edger Everhart, 1962, *Phys. Rev.*, **125**, 567.  
 Jackson, J. D. and Schiff, H., 1953, *Phys. Rev.*, **89**, 359.  
 McCarroll, R., 1961, *Proc. Roy. Soc.*, **A264**, 547.  
 Sil, N. C., 1960, *Proc. Phys. Soc.*, **LXXV**, 194.  
 Watson, G. N., 1944, *Theory of Bessel Functions*, Cambridge University Press.  
 Ziemba, F. P. and Russek, A., 1959, *Phys. Rev.*, **115**, 922.

# INTENSITY MEASUREMENT IN BANDS AND ROTATIONAL TEMPERATURE

N. R. TAWDE AND M. I. SAVADATTI

DEPARTMENT OF PHYSICS, KARNATAK UNIVERSITY, DHARWAR.

(Received May 9, 1962)

**ABSTRACT.** Rotational temperatures for OH ( $2\Sigma - 2\pi$ ), excited in the inner cone of methyl alcohol-air flames have been measured at various air/fuel ratios of combustible mixture. At these air/fuel ratios, intensity of OH (0-0) at the  $R_1$  head ( $I_p$ ) is measured simultaneously with the corresponding integrated intensity ( $I_{v'v''}$ ). The ratio  $I_{v'v''}/I_p$  is found to follow the rotational temperature ( $T$ ) of OH.

## INTRODUCTION

The measurement of intensities of molecular band system is often complicated by the partial overlapping of neighbouring bands, making the direct measurement of integrated total band intensities extremely difficult, if not impossible. Hence many times intensity at the band head is preferred to integrated intensities. It has been shown by Tawde and others (1961) that band head (peak) intensities represent fairly satisfactorily the whole band intensities.

Floyd and King (1955) have developed a method of correcting peak intensities. This method is applicable to singlet systems and systems that can be approximated to singlet systems. The fractional band intensity method of Robinson and Nicholls (1958) is suitable for all types of bands. In both of these developments, knowledge of rotational temperature is essential. It has been observed (Gaydon 1957), and is a well established fact also, that higher rotational temperatures would increase the total intensity of band out of proportion to the intensity increase at the band head. This would introduce errors, if peak intensities are taken as a measure of band intensities in experiments where rotational temperatures are changing.

So, it was thought worthwhile to study the relationship between peak and integrated intensities as rotational temperature is varied. Theoretically it is possible to calculate the relationship, which, according to Robinson and Nicholls (1958), comes out as

$$\frac{I_p}{I_{v'v''}} = \frac{B_{v'}}{kT} \exp \left[ \frac{B_{v'}}{kT} \right] \sum_{J_A}^{J_B} S_J' \exp \left[ - \frac{E_{J'}}{kT} \right] \quad \dots \quad (A)$$

where,

$I_p$  —Intensity at the peak

$I_{v'v''}$ —Total band intensity

- $B_{v'}$  —Rotational constant  
 $k$  —Boltzmann's constant  
 $T$  —Rotational temperature  
 $E_{J'}$  —Rotational term value  
 $S_{J'}$  —Line strength factor  
 $J_A, J_B$  —Limits of upper level rotational quantum numbers giving lines forming fraction of the band whose intensity is measured.

## EXPERIMENTAL

An experimental study of the variation of band-head and total intensities with rotational temperature has been undertaken with a view to see whether an empirical rule for correcting peak intensities could be obtained.

OH( $^2\Sigma-^2\pi$ ) bands emitted from the methyl alcohol-air flames were chosen and subjected to intensity and rotational temperature measurements. Rotational temperature was varied by varying the air supply to the flame. OH bands have open rotational structure with two prominent band heads. Intensities have been measured with the help of photoelectric automatic scanning unit attached to a medium quartz spectrograph. Scanning speed was adjusted to smooth out the open rotational structure so that the intensity record gave just two peaks  $R_1, R_2$  of the (0—0) band of OH. The  $R_1$  peak has been taken as the relative peak intensity. The area under the entire contour, after properly accounting for overlapping, is taken as total band intensity.

Rotational temperatures were determined by measuring intensities of rotational lines  $R_2^3, R_2^4, R_2^{14}$  and  $R_2^{16}$  with the help of Littrow (large) quartz spectrograph at the various air/fuel ratios.

## RESULTS AND DISCUSSION

The observed results have been collected in Table I.

TABLE I  
Intensities and rotational temperatures of OH

Air fuel	Integrated intensity $I_{v'v''}$	Peak Inten- sity $I_p$	$\frac{I_{v'v''}}{I_p}$	Rotational temp. T °K
4.40	9.0	11.8	0.763	2908
4.80	16.8	20.6	0.813	2936
5.20	23.5	28.0	0.840	2962
5.54	29.5	33.2	0.885	2979
5.67	35.5	39.8	0.893	2988
6.48	25.0	36.4	0.685	2852

Graph of  $I_{v'v''}/I_p$  against  $T$  is plotted in Fig. 1 and it is found that a straight line could be fitted. So it might be concluded that  $I_{v'v''}$  increases faster than  $I_p$  and hence  $I_p$  ( $mT+c$ ) should be used to represent band intensity where  $m$  and  $c$  need be determined.

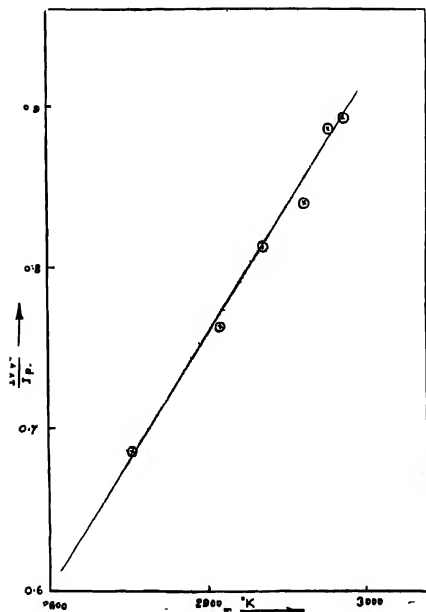


Fig. 1

For small range of temperature variations equation (A) can be transformed to an approximate equation

$$I_{v''}/I_p \approx KT \exp [E_J/kT]$$

$$\approx KT \left[ 1 + \frac{E_J}{kT} \right]$$

$$\approx KT + \frac{E_J K}{k}$$

where  $E_J$  is an average over all possible  $E_J$  and  $K$  is a constant. Hence we may infer that the result gives qualitative agreement with the expression given by Robinson and Nicholls. No exact quantitative agreement should be expected because of the fact that the open rotational structure of OH and the heavy overlapping from adjacent bands make the determination of integrated intensity approximate.

#### REFERENCES

- Floyd and King, 1955, *J. Opt. Soc. Am.*, **45**, 249.  
 Gaydon, 1957, "Spectroscopy of Flames"  
 Robinson and Nicholls, 1958, *Scientific Report No. 3 Contract AF 19(604)* 1718  
 Tawde, Jyoti and Savadatti, 1962, *Ind. J. Phys.*, **35**, 307..

# ELASTIC SCATTERING OF FAST PROTONS BY SPHEROIDAL NUCLEAR POTENTIAL WITH DIFFUSE BOUNDARY\*

S. K. DUTTA AND N. C. SIL

DEPARTMENT OF THEORETICAL PHYSICS

INDIAN ASSOCIATION FOR THE CULTIVATION OF SCIENCE,  
JADAVPUR, CALCUTTA-32

(Received March 31, 1962; Resubmitted on Sept. 3, 1962)

**ABSTRACT.** In this paper the cross section of elastic scattering of fast protons by a deformed nucleus has been calculated using the Born's approximation method. The nuclear interaction is represented by the optical model potential of Woods-Saxon type which comprises both the prolate spheroidal shape and the diffusivity of the boundary of the potential. The Coulomb potential is taken to be that due to a uniform charge distribution within the deformed nucleus. The theoretical results for the case of tantalum nucleus ( $A = 171$ ,  $Z = 73$ ) obtained with a prolate spheroidal potential having diffuse boundary agree quite well with the experimental findings and the agreement is much better than that obtained with the same potential having a sharp cut-off.

## INTRODUCTION

In a previous investigation by Dutta and Sil (1962) hereafter referred to as paper 1, the elastic scattering cross section of 96 Mev protons by prolate spheroidal nucleus has been calculated with a constant depth and sharp cut-off nuclear potential. According to that calculation the theoretical results are in overall agreement with the experimental findings; the theory predicts the correct positions of the maxima and minima in the differential cross section curve, however the theoretical cross section obtained is very large at large angles in comparison with the experimental findings. Similar result of very large scattering at large angles has been obtained for the elastic scattering of protons by a spherically symmetric potential well with a sharp cut-off boundary. In order to obtain a better fit of the theory with the experiment, Woods and Saxon (1954) have introduced the idea of rounding off the edge of the nuclear potential well and subsequently various authors have confirmed better agreement with experimental results for the scattering of protons for various energy values. For the purpose of reducing the very high values of the theoretical cross sections at large angles obtained in paper 1 we introduce here the idea of diffusivity of Woods and Saxon type in the nuclear potential at the boundary of the spheroidal nucleus. The spin-orbit

---

\*The contents of the paper were presented at the Symposium on Collisional Processes held in Dehradun from March 10 to 12, 1962.

coupling term has been neglected. The Coulomb field is generated by a uniform distribution of protons within the nucleus.

The scattering amplitude is calculated by the Born's approximation method. The differential scattering cross section is obtained for the case of a nucleus oriented in a particular direction which is then averaged over all possible orientations. We suppose that the nucleus has not suffered any rotation during the time it is in interaction with the incident particle (adiabatic approximation). It is assumed that the volume of the deformed nucleus remains the same as that of a conventional sphere with the same mass. The values of the semi-major axis  $a$  and the semi-minor axis  $b$  of the prolate spheroid are calculated from the constant volume consideration and the value of the electric quadrupole moment of the nucleus concerned. The values of the parameters,  $R$ -the nuclear radius of equivalent sphere,  $V_1$  and  $V_2$  the depth of the real and imaginary part respectively of the complex nuclear potential are taken from the paper by Saxon (1960). For comparison with experiment we choose the tantalum nucleus, since it possesses a large electric quadrupole moment and hence an appreciable prolate spheroidal deformation.

#### MATHEMATICAL FORMULATION

We write the nuclear potential in elliptic coordinates as

$$V = -\frac{(V_1 + iV_2)}{1 + e(\xi - \xi_0)/a'}$$

where  $\xi = \xi_0$  gives a prolate spheroid of rotation around the  $Z$ -axis with the semi-axes  $a = c\xi_0$  and  $b = c\sqrt{\xi_0^2 - 1}$ ,  $c$  being half the distance between the foci of the prolate spheroid.

The coulomb potential is given by

$$U(\mathbf{r}) = \int_{\text{spheroid}} \frac{\rho_1 d^3 \mathbf{r}'}{|\mathbf{r} - \mathbf{r}'|}$$

$\rho_1/e$  being the charge density due to the uniform distribution of the protons.

The scattering amplitude by the Born's approximation method is given by

$$\begin{aligned} f &= \frac{1}{4\pi} \cdot \frac{2\mu}{\hbar^2} \int \{V(\mathbf{r}) + U(\mathbf{r})\} e^{i\mathbf{k} \cdot \mathbf{r}} d^3 \mathbf{r} \\ &= f_1 + f_2 \end{aligned}$$

where  $f_1$  and  $f_2$  are the scattering amplitudes due respectively to  $V(\mathbf{r})$  and  $U(\mathbf{r})$ , and  $K = K_i - K_f$ ,  $K = |K| = 2k \sin \frac{\theta}{2}$ ,

$$|K_i| = |K_f| = k, \quad k^2 = \frac{2\mu E}{\hbar^2}.$$



$\mu$  being the reduced mass and  $E$  the energy of the incident proton. For the convenience of calculation it is assumed that the axis of symmetry of the prolate spheroid is the  $Z$ -axis and that the vector  $K$  lies in the  $XZ$ -plane. Let  $\alpha$  be the angle of orientation, the angle between the vector  $K$  and the  $Z$ -axis.

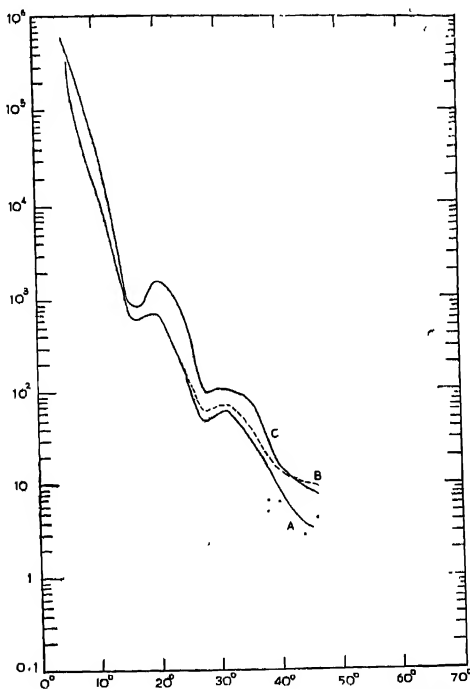


Fig. 1 The dashed curve B represents an 'upper limit' to the experimental value of the elastic scattering cross-section and the solid curve A represents the 'extrapolated' elastic scattering cross-section (Gerstein *et al.*). The solid curve C represents the theoretical values of the elastic scattering cross-section as calculated in this paper.

In paper I, it is shown that the amplitude of scattering due to the Coulomb potential, when the nucleus is oriented at an angle  $\alpha$  with respect to the vector  $K$ , is given by

$$f_2 = \frac{2\mu\rho_1}{\hbar^2 K^2} \cdot \frac{(2\pi)^{3/2} b^2 a}{(a^2 K^2 \cos^2 \alpha + b^2 K^2 \sin^2 \alpha)^{3/4}} \quad J_{3/2}(\sqrt{a^2 K^2 \cos^2 \alpha + b^2 K^2 \sin^2 \alpha}).$$

The amplitude of scattering due to the nuclear potential may be written in elliptic coordinates as

$$f_1 = \frac{-\mu}{2\pi\hbar^2} \int_1^\infty \int_{-1}^1 \int_0^{2\pi} \exp \{ i c K [\xi \eta \cos \alpha + \sqrt{(1-\eta^2)(\xi^2-1)} \cdot \cos \phi \sin \alpha] \} \\ \times \frac{(V_1 + iV_2)}{1 + e(\xi - \xi_0)/a'} \cdot C^3(\xi^2 - \eta^2) d\xi d\eta d\phi.$$

Now making use of the relation (Watson, Pp-20)

$$J_n(Z) = \frac{1}{2\pi} \int_a^{2\pi+a} \exp\{i(n\theta - 2 \sin \theta)\} d\theta.$$

and putting

$$\eta = \cos \psi, N = \frac{\mu C^3}{\hbar^2} (V_1 + iV_2)$$

$$KC\sqrt{\xi^2-1} \cdot \sin \alpha = Z \sin \beta, \quad KC\xi \cos \alpha = Z \cos \beta$$

we get

$$f_1 = -N \int_1^\infty \int_0^{2\pi} \exp(iZ \cos \beta \cos \psi) J_0(Z \sin \beta \sin \psi) \frac{(\xi - \cos^2 \psi)}{1 + e(\xi - \xi_0)/a'} \sin \psi d\xi d\psi$$

With the help of the following relation (Watson, Pp-379),

$$\int_0^\pi \exp(iZ \cos \theta \cdot \cos \psi) J_{\nu-1/2}(Z \sin \theta \sin \psi) C_{\nu}^{\nu}(\cos \theta) \sin \theta^{\nu+1/2} \cdot d\theta.$$

$$= \left( \frac{2\pi}{Z} \right)^{1/2} i^{\nu} \sin^{\nu-1/2} \psi \cdot C_{\nu}^{\nu}(\cos \psi) \cdot J_{\nu+1/2}(Z).$$

we obtain

$$f_1 = - \int_1^\infty \frac{d\xi}{1 + e(\xi - \xi_0)/a'} \left[ N \left( \frac{2\pi}{KC} \right)^{1/2} \left( \frac{1}{\sqrt{\xi^2 - \sin^2 \alpha}} \right)^{1/2} \right. \\ \left. \left\{ \left( \xi^2 - \frac{1}{3} \right) J_{1/2}(KC\sqrt{\xi^2 - \sin^2 \alpha}) + \frac{1}{3} \left( \frac{2\xi^2 - \sin^2 \alpha (3\xi^2 - 1)}{\xi^2 - \sin^2 \alpha} \right) \right. \right. \\ \left. \left. \times J_{3/2}(KC\sqrt{\xi^2 - \sin^2 \alpha}) \right\} \right]$$

Integrating by parts, we get

$$f_1 = \frac{(-1)\sqrt{2\pi} \cdot N}{a} \int_1^{\infty} \frac{e(\xi - \xi_0)/a'}{[1 + e(\xi - \xi_0)/a']^2} \cdot \xi(\xi^2 - 1) \frac{J_{3/2}(KC\sqrt{\xi^2 - \sin^2 \alpha})}{(KC\sqrt{\xi^2 - \sin^2 \alpha})^{3/2}} \cdot d\xi$$

$$= \frac{(-2)N}{K^2 C^2 a} \int_1^{\infty} \frac{\sin(KC\sqrt{\xi^2 - \sin^2 \alpha})}{KC\sqrt{\xi^2 - \sin^2 \alpha}} \cdot \frac{d}{d\xi} \left[ \frac{(\xi^2 - 1)e(\xi - \xi_0)/a'}{\{1 + e(\xi - \xi_0)/a'\}^2} \right] d\xi.$$

This is the scattering amplitude due to the nuclear potential when the nucleus is oriented at an angle  $\alpha$  and the integral is numerically evaluated. The differential cross section for the nucleus oriented at an angle  $\alpha$  is obtained by taking the modulus square of the sum of the scattering amplitudes due to the nuclear and coulomb potentials. The averaging over all orientations of the nucleus is carried out by integrating numerically the differential cross section with respect to  $\cos \alpha$  from 0 to 1.

The theoretical values of the elastic scattering cross section of 96 Mev protons by tantalum nucleus are compared with the experimental findings of Gerstein, Niederer and Strauch (1957).

We have used the values of the parameters given by Saxon (1960).

$$R = r_0 A^{1/3}, \quad r_0 = 1.25 \text{ Fermi}$$

$$V_1 = 45 \text{ Mev}, \quad V_2 = 20 \text{ Mev}, \quad E = 96 \text{ Mev}$$

the value of the diffusivity parameter for spherically symmetric potential is 0.65, from which we have  $a' = 0.1434$ .

## RESULTS AND DISCUSSION

In the previous calculation of scattering of protons by tantalum nucleus in paper I, it has been pointed out that the differential cross section shows less pronounced minima when a spheroidal deformation is introduced in a rectangular potential. However, beyond the scattering angle of  $10^\circ$  the predicted values of the cross section obtained with a spheroidal well are considerably large compared with the experimental results. Our calculations show that the diffusivity of the boundary of the spheroidal nuclear potential reduces the values of the scattering cross section considerably and more so at large angles. Further according to our present calculation the maxima and minima of the theoretical curve for the scattering cross section are less pronounced than what has been obtained in paper I, and the curve agrees quite closely with the experimental findings. Our calculations have been done up to the scattering angle of  $45^\circ$  since the experimental data are available up to that angle only.

Because of the very form of the potential, the conservation of angular momentum is ensured only by transfer of angular momentum from the incident particle to the target nucleus: this transfer sets the latter into slow precessional motion. However, the precession is so slow that one is justified in considering the nucleus as stationary for the scattering process as pointed out by Margolis (1959).

#### ACKNOWLEDGMENT

The authors wish to record their deep sense of gratitude to Prof. D. Basu, for his kind interest in the problem and many valuable discussions during the progress of the work.

#### REFERENCES

- Dutta, S. K. and Sil, N. C., 1962, *Ind. J. Phys.*, **36**, 408.  
Gerstein, G., Niederer, J. and Strauch, K., 1957, *Phys. Rev.*, **108**, 427.  
Margolis, B., Proceedings of the International Conference on the Nuclear Optical Model, 1959, Florida, Pp. 34  
Saxon, D. S., Proc. of the Int. Conf. on Nuclear Structure, 1960, Kingston Canada, Pp 197.  
Watson, G. N., A Treatise on the theory of Bessel Function, Cambridge University Press, 1944  
Woods and Saxon, 1954, *Phys. Rev.*, **95**, 577.

# ON THE RELATION BETWEEN DISSOCIATION ENERGY AND MOLECULAR CONSTANTS

B. B. LAUD

DEPARTMENT OF PHYSICS, UNIVERSITY OF POONA, POONA-7

(Received July, 30 1962).

**ABSTRACT.** The general relation between potential energy and internuclear distance, recently proposed by Lippincott has been tested for its efficacy in relation to Morse function. One of the important features of Lippincott's relation is that it leads to a simple relation connecting dissociation energy, equilibrium internuclear distance, force constant and a parameter  $n$ . A comparative study of this relation and the one similar to it, evolved recently by Somayajulu, is presented. It has been shown that the empirical relation suggested by Lippincott for the evaluation of  $n$  is not valid, nor is  $n$  a constant for similar molecules in the same electronic state as suggested by Somayajulu.

## INTRODUCTION

In the course of the development of subject of band spectra, the problem of finding suitable mathematical functions for approximating potential energy curves has occupied a good deal of attention. Of the several expressions that have been suggested so far, the most widely used is Morse (1929) function, perhaps because of the simplicity of its form and the convenience of obtaining the energy levels in closed form. However, although Morse model has been found to represent adequately the vibrational energy levels for some electronic states, for others it appears to be seriously in error. Several refinements of the Morse type of functions have, therefore, been suggested. A critical assessment of the relative merits of some of these functions has been made by Hulbert and Hirschfelder (1941) and by Varshni (1957). Of the functions of recent origin, the one developed by Lippincott (1953) promises to be valuable, but has not yet been given adequate trial. One of the important features of this function is that, on imposing conditions for stability, it leads to a simple relation connecting dissociation energy with internuclear distance and force constant. This provides a useful method for predicting dissociation energies, and if its validity is established, it may aid in resolving some of the controversies currently existing in this field. It was, therefore, thought worthwhile to undertake a study, on the above lines, of the Lippincott's function and of the relation arising from it.

Curiously enough Somayajulu (1960) has evolved empirically a relation similar to the one deducible from Lippincott's function. A comparative study of these relations is yet another objective of this communication.

LIPPINCOTT'S FUNCTION AND THE RELATION  
BETWEEN  $D_e$ ,  $k_e$  AND  $r_e$ .

Lippincott proposed the following relation between potential energy and internuclear distance :

$$V = D_e[1 - e^{-n(\Delta r)^2/2r}][1 + a f(r)] \quad (1)$$

where  $D_e$  is the dissociation energy referred to the bottom of the potential curve,  $r_e$  the equilibrium bond distance,  $r$  the bond distance,  $a$  and  $n$  are constants,  $\Delta r = r - r_e$  and  $f(r)$  is a function of the internuclear distance chosen such that,  $f(r) = \infty$  when  $r = 0$  and  $f(r) = 0$  when  $r = \infty$ .

This function satisfies most of the criteria desirable of a good potential function and according to Lippincott, has found extensive application in quantitatively predicting and correlating the bond properties of a large number of diatomic and polyatomic molecules.

For many purposes the  $f(r)$  term is unimportant and the function assumes a simple three parameter form :

$$V = D_e [1 - e^{-n(\Delta r)^2/2r}] \quad \dots (2)$$

By imposing the conditions for stability that

$$\left( \frac{\partial V}{\partial r} \right)_{r=r_e} = 0$$

and

$$\left( \frac{\partial^2 V}{\partial r^2} \right)_{r=r_e} = k_e$$

the following relation may be readily derived from (2).

$$D_e (\text{ergs/molecule}) = k_e r_e / n \quad \dots (3)$$

$k_e$  and  $r_e$  are fairly accurately known for a large number of molecules. For the evaluation of parameter  $n$ , Lippincott suggests the following empirical relation.

$$n = n_0 (I/I_0)_A^{1/2} (I/I_0)_B^{1/2} \text{ cm}^{-1} \quad \dots (4)$$

where  $n_0 = 6.32 \times 10^8$  and  $(I/I_0)_A$  and  $(I/I_0)_B$  are the ionization potentials of atoms A and B respectively, relative to those of the corresponding atoms in the same row and the first column of the periodic table. For H atoms  $I/I_0$  has been assigned the value 0.88 rather than 1. Justification for the relations (2) and (4) has been obtained by Lippincott in subsequent papers (1955, 1957) by showing

that these may be derived from a simple quantum mechanical model through the use of perturbed delta functions.

Using relations (3) and (4), Lippincott calculated the dissociation energies of 22 molecules. The results were quite reasonable when compared with the experimentally determined values, the average percent deviation being 4.5. As has been pointed out by Lippincott, this percent deviation is considerably larger than the experimental error in obtaining  $r_e$ ,  $k_e$  and  $(I/I_0)$ , which is of the order of 0.1 per cent; but it is quite reasonable and is considerably better than the per cent error obtained for the same set of molecules using the Morse function.

However, a good potential function should be general and represent the potential energy curves for large class of diatomic molecules and not just for a few favourable examples. In order to test the merits of relation (3), it would be desirable, therefore, to check it with a wider selection of molecules for which experimentally determined dissociation energies, bond lengths and force constants are accurately known.

Following Lippincott's method, we computed the dissociation energies of 16 molecules, the constants for which are reliably known. The experimental data for  $\omega_e$ ,  $\omega_e x_e$ ,  $\mu$ ,  $r_e$  and  $I$  have been taken from Herzberg (1944, 1950), unless otherwise specified. The dissociation energies have been taken from Cottrell (1958). The results are presented in Table 1. Values calculated using Morse function are also given side by side for comparison.

The agreement, it will be seen, is extremely poor. Some of the calculated values are in utter disagreement with the observed values. Major discrepancies are noticed in the cases of CdH, HgH and ZnH. Mulliken (1937) has indicated the possibility of a maximum in the potential curves for these molecules due to tendential approach of two interacting states. Since equation (2) does not lead to these maxima, it may be argued, that the dissociation energies calculated from it will not agree with the observed values. However, excellent agreement is obtained in the case of BeH, which is analogous to HgH and in which we have almost certainly tendential crossing.

It is quite obvious, therefore, that the large discrepancies must be attributed to the approximate nature of the relations used rather than to the uncertainties associated with the observed dissociation energies. If it is assumed that relation (2) represents correctly the actual potential energy function, the discrepancies may be traced to relation (4). This relation was intuitively arrived at by Lippincott by realizing that the wave function for the hydrogen-like atom involves an exponential in  $I^{\frac{1}{2}}$  and that this form should carry over approximately to an exponential in the product  $(I)^{\frac{1}{2}}\bar{A} (I)^{\frac{1}{2}}\bar{B}$  for the wave function for a molecule AB. This further implies that the potential energy function should also involve an exponential in  $(I)^{\frac{1}{2}}\bar{A} (I)^{\frac{1}{2}}\bar{B}$ . The dependence of parameter  $n$  on the ionization poten-

tials, therefore, seems to be well founded, and hence the cause for the large errors is to be sought in the nature of  $n_0$ .

TABLE I

Dissociation energies (in e.v.) of some diatomic molecules :

Molecule	Observed $D_0$	Relations (3) and (4)		Morso		Relation (6)	
		$D_0$	Devia- tion %	$D_0$	Devia- tion %	$D_0$	Devia- tion %
AgH	2.5 2.3 (G)	2.19	12.4 4.7	2.71	8.4 17.8	2.17	13.2 5.6
BaO	5.637	3.90	30.8	6.74	19.5	5.35	5.0
BeH	2.3	2.31	0.4	3.57	55.2	2.99	30.0
CdH	0.678	1.43	110.9	1.28	88.7	0.99	46.0
CuF	3.0	2.35	20.7	3.00	0.0	2.33	22.3
CuCl*	3.7(H) 4.99(G)	2.10	43.2 57.0	3.73	0.8 25.2	2.04	20.5 41.0
GeO*	6.8	5.58	17.9	6.94	2.0	5.41	20.0
HgH	0.372	1.19	220.4	0.63	72.0	0.47	26.3
ICl	2.15	2.15	0.0	3.10	44.1	2.39	11.1
InCl	4.5	2.00	55.6	3.07	31.8	2.40	46.6
LiI*	3.5	1.43	59.1	4.05	15.7	3.50	0.0
NaI*	3.16 (H) 3.07 (G) 3.11	1.27	59.8 58.6 59.1	3.36	6.3 9.5 8.1	2.72	13.9 11.4 12.5
PO	5.4	5.72	5.9	7.12	31.8	5.56	2.9
SeO*	3.5 (G) 5.4 (H)	4.27	22.0 20.9	5.47	56.3 1.3	4.26	21.7 21.1
SiN	4.5	5.40	20.0	6.19	37.5	4.83	7.3
ZnH	0.85	1.62	90.5	1.35	58.8	1.04	22.3

\*The values of  $n_0$  for these molecules are taken from Somayajulu (1960).

H. Herzberg.

G. Gaydon, (1947)

In a later paper Lippincott and Schroeder (1955) have suggested that  $n_0$  may have a characteristic value for each group of similar molecules. Thus, for alkali metals and alkali hydrides  $n_0$  has the value  $4.21 \times 10^8$ , while for most molecules, where the binding is primarily covalent and including all the molecules of the fourth, fifth, sixth and seventh columns of the periodic table  $n_0$  has the value  $6.32 \times 10^8$ .

With a view to ascertaining whether  $n_0$  has a fixed value for a group of similar molecules, we computed, using accurately known experimental data and relation



(4), the value of  $n_0$  for some molecules which will give an exact agreement with the observed  $D_0$  values. The values thus computed are given in Table II.

TABLE II

Values of  $n_0$  calculated from the known values of  $D_e$ ,  $k_e$ ,  $r_e$  and ionization potentials :

Hydrides		Oxides		Halides	
Molecule	$n_0/10^8$	Molecule	$n_0/10^8$	Molecule	$n_0/10^8$
CdH	11.74	BaO	4.45	AlBr	3.16
HgH	16.30	GeO	5.17	ClF	6.06
KH	4.36	PO	6.78	CaF	4.98
LiH	4.19	TiO	5.23	ICl	6.31
NaH	4.91	VO	6.95	InCl	2.74
ZnH	10.76	SeO	4.99		
			7.68*		
AgH					

\*Corresponding to the  $D_0$  values 5.4 and 3.5 e.v. suggested by Herzberg (1950) and Gaydon (1947) respectively.

As is readily apparent,  $n_0$  is not a constant for a group of molecules such as hydrides or oxides or halides, but differs from molecule to molecule. It varies appreciably also for molecules, the constituent atoms of which belong to the same column of the periodic table. Even for alkali hydrides the value of  $n_0$  changes from  $4.19 \times 10^8$  to  $4.91 \times 10^8$ ; and for SeO, though it belongs to sixth column of the periodic table, for an exact agreement  $n_0$  should be either  $4.99 \times 10^8$  or  $7.68 \times 10^8$  and not  $6.32 \times 10^8$ . These observations tend to show that  $n_0$  is not a constant as suggested by Lippincott, but is perhaps a function of certain parameters associated with the molecules.

#### SOMAYAJULU'S RELATION

It will be interesting to consider at this stage, a relation similar to relation (3), but arrived at empirically by Somayajulu (1960).

Somayajulu finds the following relationship between dissociation energy and internuclear distance :—

$$\frac{k_e r_e}{D_0} = S \quad (5)$$

where  $S$  is a constant for similar molecules in the same electronic state and  $D_0$  is the dissociation energy measured from the lowest vibrational level,  $V = 0$ ,

The main difference between Lippincott's relation and that of Somayajulu is that the latter assumed a characteristic value for the constant of equation (5) for different sequences of molecules, whereas Lippincott evaluated the constant from ionization potentials by means of an empirical rule. Somayajulu's method is to calculate  $S$  from accurately known values of  $D_0$ ,  $k_s$  and  $r_s$  of a molecule and use it in computing the dissociation energies of the other molecules in the same group. A curious feature of his method is that generally the first member of the group comes out to be an exception. In order to illustrate Somayajulu's method, we shall now discuss in brief the way in which the dissociation energies of  $O_2$ -type molecules were calculated by him.  $D_0$  for  $O_2$  is now well established from the convergence limit to be 5.1148 e.v.. Taking  $O_2$  as the reference compound, one can obtain the dissociation energies of  $S_2$ ,  $Se_2$ ,  $Te_2$ ,  $SO$ ,  $SeO$  and  $TeO$ . These have been given in Table III along with the experimental values. There appears to be a general agreement between the calculated values and some of the values suggested for these molecules. However, as "the general consensus now in the literature is that  $D_0$  for  $SO$  should be 5.358 e.v.", he calculated the dissociation energies of the molecules of the above group compatible with the value 5.358 e.v. for  $D_0(SO)$ . These are given in column 4 of Table III.

The results are quite satisfactory for  $S_2$ ,  $Se_2$  and  $Te_2$ , but less satisfactory in the case of  $SeO$  and  $TeO$ .  $O_2$  constitutes an exception as a first member.

TABLE III  
 $D_0$  calculated by Somayajulu's relation -

Molecule	With $O_2$ as the reference compound	Experimental value	With $SO$ as the reference compound
$O_2$	5.1148	5.1148	6.433
$S_2$	3.37	3.3 3.6 4.4	4.243
$Se_2$	2.8	2.8 3.55	3.52
$Te_2$	2.2	2.3 3.18	2.78
$SO$	4.26	4.2 5.358	5.358
$SeO$	3.76	3.5 5.4	4.725
$TeO$	3.46	2.728 3.453	4.372

Leaving aside the question whether such a procedure is justifiable or not, one should expect that since both Lippincott and Somayajulu use similar

relationship they should lead to identical conclusions. Although the constants of the two relations have been arrived at by entirely different procedures, if it is assumed that such a relationship exists between  $k$ ,  $r_e$  and  $D_e$ , the constants (allowing for the fact that one relation involves  $D_e$ , while the other involves  $D_0$ ) should differ only to the extent of the order of experimental errors in obtaining quantities involved in their evaluation. Hence the relations should allow an unambiguous selection when two or more widely differing alternative values are proposed. It would be interesting to examine the dissociation energies of some such molecules in the light of the above argument.

There has been some controversy about the dissociation energy of BrF and the suggested values are 2.16, 2.384 and 2.6 e.v.. Somayajulu's relation gives 2.637 e.v. supporting the value 2.6; while the value obtained from Lippincott's relation is 2.336 e.v. which is close to the value 2.384. Similar observations have also been made in the case of AgH, AuH, and SeO and have been tabulated in Table IV.

**TABLE IV**  
*D<sub>0</sub> calculated by Lippincott's and Somayajulu's relations :—*

Molecule	Experimental values		Lippincott	Somayajulu
BrF	2.16	2.38	2.34	2.64
	2.60			
SeO	3.5	5.4	4.27	4.73
AgH	2.3	2.5	2.19	2.53
AuH	3.1	4.1	3.12	4.12

Thus although the relation (3) and (5) are identical in some respects, the conclusions arrived at from these, are diverse. We, therefore, conclude from the above analysis that the relations (3) and (5) with the constants defined in the manner suggested by the respective authors do not have universal application and the agreement observed by them seems to be somewhat accidental. The true relation probably depends upon parameters which will require detailed knowledge about molecular force fields.

#### RELATION INDEPENDENT OF $n$

Although relation (3) which is derived from relation (2), fails to give correct dissociation energies, one must not hasten to conclude that Lippincott's function (2) is in any way inferior to Morse's. On the contrary, as will be shown in the following lines, in some respects it may be considered to be a desirable advance-

ment over Morse function. The failure of relation (3) must be attributed, as shown above, to the lack of knowledge regarding the nature of the parameter  $n$ .

By expanding  $V$  in a power series to the quartic term in  $\Delta r$ , followed by the comparison of the corresponding terms with those expected for the solution of the Schrodinger equation for an anharmonic oscillator, the following relation is obtained :

$$D_e \text{ (ergs/molecule)} = \frac{k_e}{(64\pi^2c \mu \frac{k_e}{\omega_e x_e / 3h}) - 1/r_e^2} \quad \dots (6)$$

This equation offers a check on the potential function independent of the empirically evaluated constant  $n$ .  $D_0$  values calculated using relation (6) are given in Table I. The calculated values, in general, represent a marked improvement over those calculated from the Morse relation  $D_e = \omega_e^2/4\omega_e x_e$  or from relation (3). The error is significantly lower than that due to Morse. Even in the cases of CdH, HgH and ZnH, the gulf between observed and calculated values is considerably narrowed down by relation (6). This promotes confidence in Lippincott's relation.

#### POTENTIAL CURVES

The validity and usefulness of a potential energy function, however, must not be judged merely by its behaviour at its extreme limits. The function may satisfy the requisite criteria at  $r = 0$ ,  $r = r_e$  and  $r = \infty$  and yet may be away from the actual curve in the intermediate positions. It is, therefore, necessary to examine Lippincott's function from this point of view also.

With this end in view, we have constructed potential curves for  $A^3\pi_g$ ,  $X^3\pi_u$  states of  $C_2$  and  $C^3\pi_u$  and  $B^3\pi_g$  states of  $N_2$ , from Lippincott's as well as Morse functions (Figs. 1 and 2). The curves correspond to the electronic states giving rise to the transitions corresponding to Swan system and second positive system respectively. The worst practical defect of the Morse function is that it generally gives too great an asymmetry as compared to the actual cases. It rises too steeply for  $r < r_e$  and too slowly for  $r > r_e$ . This defect has been considerably reduced in the case of Lippincott's function as is apparent from the figures.

The intermediate behaviour of the function may be judged by considering the role, the curves play in predicting the most probable vibrational transitions. The course of the most probable transitions obtained from the curves on the basis of the Franck-Condon principle, should closely fit with the Condon parabola obtained experimentally.

In Table V and VI we give some of the most probable transitions for the aforementioned two systems predicted from the two sets of curves. For comparison for  $C_2$  (Swan) system we give the experimental data obtained by Tawde and Laud (1954) for the stabilized alcohol-air flames, and for  $N_2$  (second positive) system,

the data obtained by Tawde and Patankar (1953) using d.c. discharge as the source for excitation.

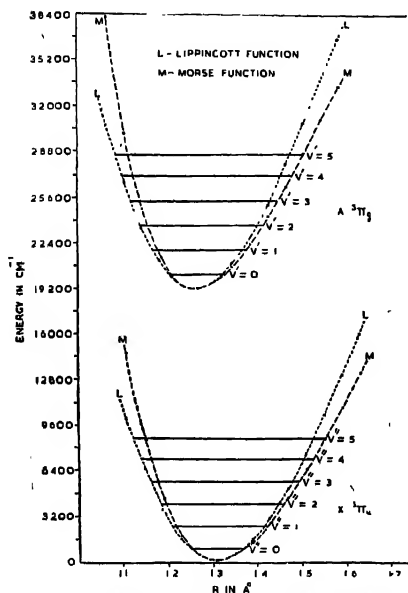


FIG. 1. POTENTIAL ENERGY CURVES FOR  $C_2$  [SWAN] SYSTEM

TABLE V

Some of the most probable transitions:  $C_2$  (Svan) system

$r_{min} \longleftrightarrow r_{min}$			$r_{max} \longleftrightarrow r_{max}$		
Morse	Lippincott	Experimental	Morse	Lippincott	Experimental
0, 1	0, 1	0, 1	1, 0	1, 0	1, 1
1, 3	1, 3	1, 2	2, 1	2, 0 2, 1	2, 1
2, 4	2, 4	2, 3	3, 2	3, 1 3, 2	3, 2
3, 6	3, 5	3, 4	4, 2 4, 3	4, 2	4, 3

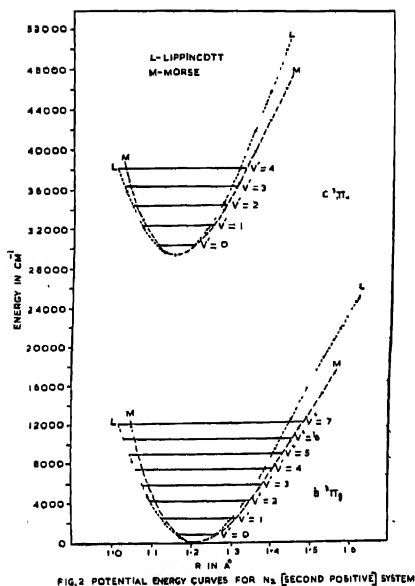
FIG.2 POTENTIAL ENERGY CURVES FOR  $N_2$  (SECOND POSITIVE) SYSTEM

TABLE VI

Some of the most probable transitions :  $N_2$  (second positive) system

$r_{min} \longleftrightarrow r_{min}$			$r_{max} \longleftrightarrow r_{max}$		
Morse	Lippincott	Experimental	Morse	Lippincott	Experimental
0, 3	0, 2	0, 1	2, 0	2, 0	2, 1
1, 5	1, 4	1, 3	3, 1	3, 0 3, 1	3, 1
2, 7	2, 5	2, 4	4, 1 4, 2	4, 1	4, 2

In both the cases, on the  $r_{max} \longleftrightarrow r_{max}$  side, the experimental distribution is more in accord with the Morse distribution than with Lippincott's. On the other side, however, the Morse distribution is seriously off. Lippincott's curves give a slightly broader Condon parabola than the experimental one, deviation on either side being approximately the same.

The relative positions of the three parabolae reveal that the behaviour of Lippincott's function is better than Morse's, particularly in the region  $r < r_e$  and it is, therefore, concluded that it can be considered to be a significant improvement over Morse's.

One of the disadvantages of relation (2) is that it predicts  $\alpha_e = 0$  for all diatomic molecules. Although the values of  $\alpha_e$  are small for the ground states of diatomic molecules, they are definitely not zero. This suggests that in (1) ' $\alpha$ ' is not zero. With this, the internuclear potential function assumes a five-parameter form. Lippincott, Steele and Caldwell (1961) assumed that, for large values of  $r$ , the  $f(r)$  term takes the form of a Lennard-Jones 6-12 attraction potential, which is compatible with the conditions that  $f(r)$  is expected to satisfy. Using this they calculated dissociation energies for a number of molecules. A close scrutiny of the values reported by them shows that although the five-parameter function brings about an improvement in some cases, it causes a further deterioration in others and hence it is concluded that no further advantage can be obtained by using it for the calculation of  $D_0$ .

#### REFERENCES

- Cottrell, T. L., 1958, *The strengths of Chemical bonds*, 2nd Edition, Butterworths Scientific Publications, London.
- Gaydon, A. G., 1947, *Dissociation Energies and Spectra of Diatomic Molecules*, Chapman and Hall Ltd., London.
- Herzberg, G., 1944, *Atomic spectra and Atomic structure*, Dover publication, New York.
- Herzberg, G., 1950, *Spectra of Diatomic Molecules*. D. Van Nostrand Co., Inc. Princeton, New Jersey.
- Hulburt, H. M. and Hirschfelder, J. O., 1941, *J. Chem. Phys.*, **9**, 61.
- Lippincott, E. R., 1953, *J. Chem. Phys.*, **21**, 2070.
- Lippincott, E. R., 1955, *J. Chem. Phys.*, **23**, 603.
- Lippincott, E. R., 1957, *J. Chem. Phys.*, **26** 1078.
- Lippincott, E. R. and Schroeder, R., 1955, *J. Chem. Phys.*, **23**, 1131.
- Lippincott, E. R., Steele, D. and Caldwell, P., 1961, *J. Chem. Phys.*, **35**, 123.
- Morse, P. M., 1929, *Phys.*, *Rev.* **34**, 57.
- Mulliken, R. S., 1937, *J. Phys. Chem.*, **41**, 5.
- Somayajulu, G. R., 1960, *J. Chem. Phys.*, **33**, 1541.
- Tawde N. R. and Laud, B. B., 1954, *Proc. Nat. Inst. Sci. India*, **20**, 259.
- Tawde, N. R. and Patankar, V. S., 1943, *Proc. Phys. Soc. London*, **55**, 396.
- Varshni, V. P., 1957, *Rev. Mod. Phys.*, **29**, 664.

# THE CRYSTAL STRUCTURE OF 3,5-DIBROMO PARA-AMINO BENZOIC ACID

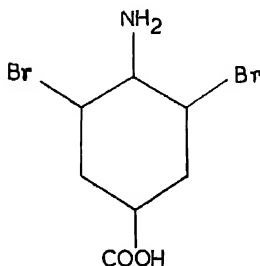
A. K. PANT

INDIAN ASSOCIATION FOR THE CULTIVATION OF SCIENCE, JADAVPUR,  
CALCUTTA-32.

(Received August 24, 1962)

**ABSTRACT.** 3,5-dibromo para-amino benzoic acid crystallizes in orthorhombic system with  $a = 22.46$ ,  $b = 19.47$ ,  $c = 3.94\text{\AA}$  with eight molecules per unit cell. From extinction conditions possible space groups were  $P_{ma}$  and  $P_{2an}$ . The statistical test of Howells *et al.* to the (001) projection showed the presence of centre of symmetry thereby proving it to be  $P_{2an}$ . (001) and (010) Patterson projections gave the approximate co-ordinates of bromine atoms and thus a trial structure was obtained which was subsequently refined by Fourier syntheses.

The structural formula of 3,5-dibromo *p*-amino benzoic acid is



No goniometric or X-ray data are available for this compound. Good single crystals were obtained by slow evaporation of a saturated solution of the substance in a mixture of equal amounts of ethyl alcohol and acetone at room temperature. The crystals are orthorhombic and grow in the form of needles elongated along the *c*-axis.

The approximate unit cell dimensions were determined from the rotation photographs about the three crystallographic axes. More accurate values were obtained from the high angle reflexions, for which  $\alpha_1$  and  $\alpha_2$  were resolved, in the zero layer Weissenberg photographs along the *a* and *c*-axes, using the method



of Farquhar and Lipson (1946). Film shrinkage correction was applied (Srivastava, 1959). The cell dimensions are :

$$a = 22.46 \text{ \AA}$$

$$b = 19.47 \text{ \AA}$$

$$c = 3.94 \text{ \AA}$$

The observed density at 25°C, measured by flotation in a mixture of ethylene dibromide and mercury diethyl is  $2.26 \text{ g.cm}^{-3}$ . The calculated density for eight molecules per unit cell is  $2.27 \text{ g.cm}^{-3}$ .

Zero layer Weissenberg photographs along the  $a$ ,  $b$  and  $c$ -axes and the first and second layer-line equi-inclination Weissenberg photographs along the  $c$ -axis were taken using  $\text{Cu K}\alpha$  radiation. The systematic absences are consistent with the space groups  $P_{mnn}$  (centrosymmetric) and  $P_{2nn}$  (non-centrosymmetric). The  $N(z)$  statistical test (Howells, Phillips and Rogers, 1950) was applied for the  $[001]$  zone for which the projection is centric for  $P_{mnn}$  and acentric for  $P_{2nn}$ . The  $N(z)$  values for different values of  $z$  are plotted in Fig. 1. The continuous curves are the theoretical ones. It is clearly seen that the experimental values of  $N(z)$  agree very well with the theoretical curve for the centro-symmetric case, thereby implying the space group is  $P_{mnn}$ . This conclusion was confirmed by  $(001)$  Patterson and electron density projections.

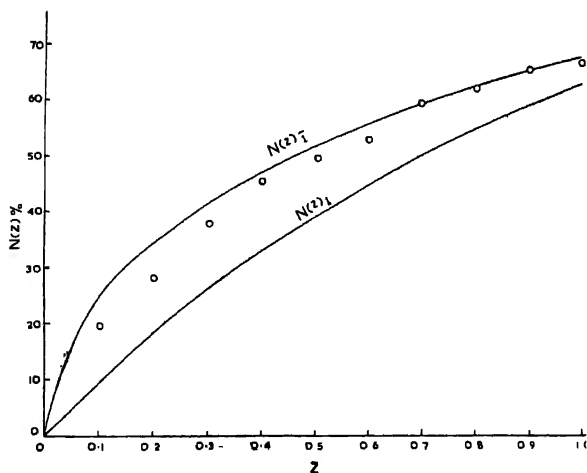


Fig. 1

The  $(001)$  Patterson projection gave the approximate  $x$  and  $y$  co-ordinates of the bromine atoms. Assuming the usual bond lengths and angles and a plane

molecule, a trial structure was postulated. Signs of the structure factors, obtained on the basis of the trial structure were then used to compute the (001) electron density projection. The  $x$  and  $y$  co-ordinates were refined by the usual iterative process. The (010) Patterson projection gave the  $z$ -co-ordinates of the bromine atoms. The  $z$ -co-ordinates of the other atoms were fixed from standard bond length considerations. Using the observed structure amplitudes and the calculated phases (signs), the (010) electron density projection was obtained.

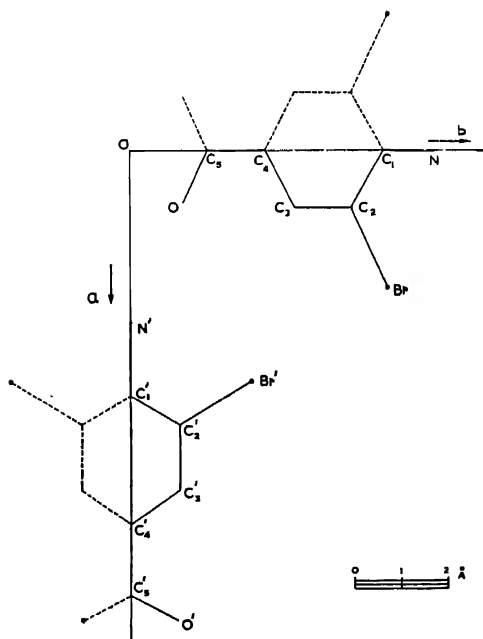


Fig. 2

Fig. 2 shows the projection of the molecules on the (001) plane. The asymmetric unit consists of two half molecules. The atomic parameters obtained at this stage are listed in Table 1. The  $z$ -parameters have rather large errors at this stage.

TABLE I

Atom	$x/a$	$y/b$	$z/c$	Atom	$x/a$	$y/b$	$z/c$
Br	0.1284	0.2826	0.1642	Br'	0.2164	0.1320	0.8200
N	0	0.3330	-0.0066	N'	0.1629	0	0.5000
C <sub>1</sub>	0	0.2789	0.1924	C <sub>1</sub> '	0.2204	0	0.5000
C <sub>2</sub>	0.0539	0.2428	0.2865	C <sub>2</sub> '	0.2564	0.0538	0.6264
C <sub>3</sub>	0.0539	0.1808	0.4746	C <sub>3</sub> '	0.3179	0.0538	0.6264
C <sub>4</sub>	0	0.1483	0.5688	C <sub>4</sub> '	0.3494	0	0.5000
C <sub>5</sub>	0	0.0844	0.7680	C <sub>5</sub> '	0.4161	0	0.5000
O	0.0498	0.0578	0.8594	O'	0.4388	0.0523	0.6223

The reliability index, which was obtained with unobserved reflexions taken as half the minimum observable value, is 0.177 for ( $hk0$ ) reflexions and 0.193 for ( $h0l$ ) reflexions. In the calculation of structure factors, the atomic-scattering factor curves of Berghuis *et al.* (1955) for carbon, nitrogen and oxygen and that of Thomas and Umeda (1957) for bromine have been used. The overall temperature factor, obtained by Wilson's method (1942), used for ( $hk0$ ) reflexions is  $1.5 \text{ \AA}^2$ . The same temperature factor was used for the other projection as well. Further refinement of the structure is in progress. Details of the investigation will be published shortly.

## ACKNOWLEDGMENT

The author is thankful to Prof. K. Banerjee, D.Sc., F.N.I., and to Dr. R. K. Sen, D.Sc., for their keen interest and guidance throughout the progress of this work. He is also thankful to his brother Dr. L. M. Pant and to Dr. U. C. Sinha for many valuable suggestions. The financial assistance from the C.S.I.R. is gratefully acknowledged.

## REFERENCES

- Berghuis, J., Haanapel, IJbertha M., Loopstra, B. O., MacGillavary, Caroline H., and Voencendaal, A. L., 1955, *Acta Cryst.* **8**, 478.  
 Farquhar, M. C. M., and Lipson, H., 1946, *Proc. Phys. Soc.* **58**, 200.  
 Howells, E. R., Phillips, D. C., and Rogers, D., 1950, *Acta. Cryst.* **3**, 210.  
 Srivastava, S. N., 1959, *Acta. Cryst.* **12**, 412.  
 Thomas, L. H., and Umeda, K., 1957, *J. Chem. Physics*, **26**, 293.  
 Wilson, A. J. C., 1942, *Nature*, **150**, 152.

# Letters to the Editor

The Board of Editors will not hold itself responsible for opinions expressed in the letters published in this section. The notes containing reports of new work communicated for this section should not contain many figures and should not exceed 500 words in length. The contributions must reach the Assistant Editor not later than the 15th of the second month preceding that of the issue in which the letter is to appear. No proof will be sent to the authors.

15

## THE CRYSTAL STRUCTURE OF 1,8-DIHYDROXY ANTHRAQUINONE ANAND PRAKASH

INDIAN ASSOCIATION FOR THE CULTIVATION OF SCIENCE,  
JADAVPUR, CALCUTTA-32

(Received September 9, 1962)

The space group of 1,8-dihydroxyanthraquinone along with the other crystallographic data was given earlier by Jagannadham (1957). The axial lengths are :-

$$a = b = 5.86 \text{ \AA}, \quad c = 31.33 \text{ \AA}.$$

The crystal belongs to the tetragonal class. The space group is  $C_4^2-P_{41}$ , or its enantiomorphic equivalent  $C_4^3-P_{43}$  and contains four molecules per unit cell. It is noncentrosymmetric and has four equivalent points.

In the present investigation the space group was confirmed and the axial lengths were found to be correct within the accuracy of rotation method. For intensity measurement of  $(0kl)$  reflections, zero-layer normal beam Weissenberg photographs were taken about the  $[100]$  axis, using the  $\text{Cu } K_\alpha$ -radiation from a Radon House sealed unit run at 40 KV and 15 mA. The different times of exposure varied from 12 minutes to about 50 hours. Relative integrated intensity measurements were made with the Moll recording microphotometer. They were placed on absolute scale by Wilson's method (1942) and thus the structure amplitudes of  $(0kl)$  reflections were evaluated assuming the crystal to be ideally imperfect.

In deducing the trial structure, the molecule of 1,8-dihydroxyanthraquinone was assumed to be planar with bond lengths and bond angles of anthraquinone (Murty, 1960) and standard bond length of C—O bond. A reasonably accurate

structure was obtained mainly by the method of trial and error. Using these trial co-ordinates, the structure factors of all the observed (0kl) reflections were

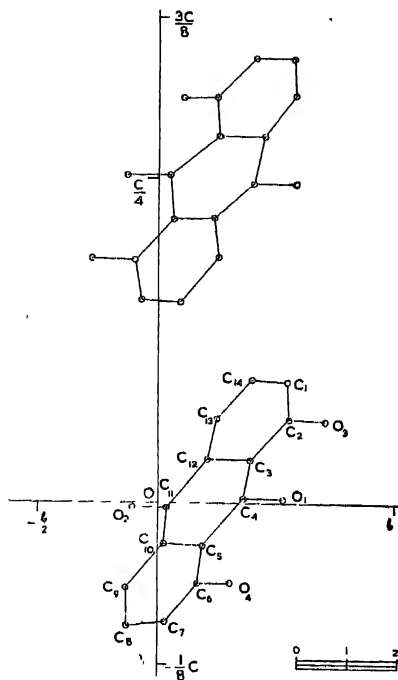


Fig. 1

calculated. This showed a  $R$  value 40.5%. The atomic scattering factors of carbon and oxygen were taken from Berghuis *et al* (1955) and an isotropic  $B$  factor of  $3.0\text{\AA}^2$  and  $3.5\text{\AA}^2$  was used for carbon and oxygen respectively. The preliminary structure was refined by successive Fourier projections on (100) in which the molecule is well resolved. As the equivalent points for (100) are  $(y, z; x, \frac{1}{4}+z, \bar{y}, \frac{1}{2}+z; \bar{x}, \frac{3}{4}+z)$ , the projection of the first and second molecule on (100) gave all the  $(xyz)$  co-ordinates.

The co-ordinates of 1,8-dihydroxyanthraquinone after fourth Fourier projection on (100) are given in Table I. The projection of the molecules on (100) is shown in the Fig. 1.

## Fractional co-ordinates

Atom	<i>x</i>	<i>y</i>	<i>z</i>	Atom	<i>x</i>	<i>y</i>	<i>z</i>
C <sub>1</sub>	+0.441	+0.545	+0.0948	C <sub>10</sub>	+0.233	+0.031	+0.0324
C <sub>2</sub>	+0.248	+0.556	+0.0648	C <sub>11</sub>	+0.404	+0.044	-0.0031
C <sub>3</sub>	+0.260	+0.392	+0.0342	C <sub>12</sub>	+0.431	+0.207	+0.0333
C <sub>4</sub>	+0.055	+0.360	+0.0036	C <sub>13</sub>	+0.584	+0.253	+0.0660
C <sub>5</sub>	+0.067	+0.200	-0.0342	C <sub>14</sub>	+0.583	+0.404	+0.0961
C <sub>6</sub>	-0.098	+0.167	-0.0626	O <sub>1</sub>	-0.129	+0.529	+0.0025
C <sub>7</sub>	+0.061	+0.033	-0.0932	O <sub>2</sub>	+0.578	-0.101	-0.0029
C <sub>8</sub>	+0.097	-0.130	-0.0955	O <sub>3</sub>	+0.112	+0.710	+0.0632
C <sub>9</sub>	+0.259	-0.128	-0.0658	O <sub>4</sub>	-0.269	+0.308	-0.0620

The reliability factor  $R$  is 25.0% for ( $0kl$ ) reflections, leaving out the unobserved reflections. The high  $R$  value in spite of good general agreement is due to large number of weak reflections. Further refinement by (Fo-Fc) synthesis and other standard methods is in progress.

Author is indebted to Dr. R. K. Sen, D.Sc., for suggesting the problem and guidance and to Prof. K. Banerjee for his keen interest and encouragement. The author is also grateful to Dr. U. C. Sinha for the valuable suggestions and to C.S.I.R. for financial assistance.

## REFERENCES

- Berghuis, J., Haanappel, I. J. M., Potters, M., Loopstra, B. O., Mac-Gillavry, C. H., and Veenendaal, A. L., (1955), *Acta Cryst.*, **8**, 478.  
 Jagannadham, A. V., 1957, *Zeit Fur Krist.* Bd. **108**, 457-458.  
 Murty, B. V. R., 1960, *Zeit fur Krist.*, Bd. **113**, 445.  
 Wilson, A. J. C., 1942, *Nature, London*, **150**, 152.

## STUDY OF SILVER FULMINATE BY X-RAY DIFFRACTION

S. N. PANDEY

DEFENCE RESEARCH FELLOW, D.R.L. (S), KANPUR.

*(Received January, 17, 1962, Resubmitted April 24, 1962)*

## Plate VIIIA and VIIIB

Singh (1959) has calculated the unit cell dimensions from Weissenberg X-ray diffraction photograph of silver fulminate and has shown that it has got orthorhombic body centred structure. ASTM X-ray card index gives the powder pattern of silver fulminate. The analysis of the ASTM X-ray data did not confirm the previous findings. It is, therefore, desirable to study further the structure of silver fulminate crystals.

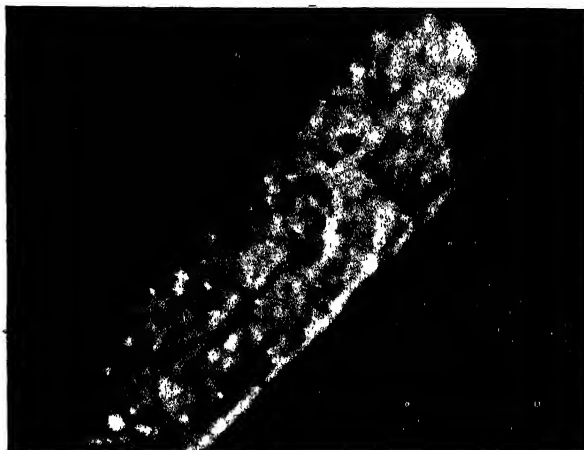
Crystals of silver fulminate have been prepared by two different methods.

- (a) 20 c.c. of  $\text{AgNO}_3$  (40% in  $\text{HNO}_3$  of s.p. gr. 1.2) solution was added to 30 cc of 95% ethyl alcohol, heated up to  $70^\circ\text{C}$ . It was purified by washing. This was further crystallised out from 20% of freshly prepared ammonium acetate solution, containing a little amount of acetic acid, so as to bring the pH of the solution to 4.5 to 6, which was heated to  $65^\circ\text{C}$ . The crystals were obtained by controlled cooling. After washing white, pale, hard and transparent crystals were found; this is referred as sample A.
- (b) The procedure was similar to above except that 10%  $\text{HNO}_3$  was used. Crystallisation was done in absence of Acetic Acid. The pH of the solutions was 7.7–8. Crystals were white, opaque, fragile. This is referred to as sample B. A Microphotograph of the sample B is shown in Fig. 1.

X-ray diffraction pattern was taken using filtered  $\text{Cu-K}_\alpha$  radiation at 40kv–20ma. About 20 crystals of sample B were examined. Plate VII A & B gives the X-ray diffraction pattern of the samples A and B.

Sample A gave layer line photographs and sample B always gave a powder diffraction pattern in spite of the fact that crystals having well defined edges were used. The unit cell dimension were calculated from A, which were approximately the same as those found by Singh' ( $a = 6.04\text{\AA}$ ,  $b = 3.88\text{\AA}$ ,  $c = 11.2\text{\AA}$ ).

From these known values of cell dimensions, the powder diffraction pattern of sample B was analysed. Table 1 gives the values of  $\theta$ ,  $\sin^2\theta$  (observed), possible indices and calculated values of  $\sin^2\theta_{hkl}$  on the above basis of sample B.



Fig/ 1. The microphotograph of sample B. The edges of the crystals are well defined.

TABLE I

Lines	Observed $\theta^\circ$	$\sin^2 \theta$	Indices	$\sin^2\theta_{hkl}$	I (obs)	I (cal)
1	2	3	4	5	6	7
1	8.15	0.0202	002	0.0160	100	100
2	12.15	0.0443	011	0.0400	85	73
3	14.39	0.0617	111	0.0603	39	91
4	15.16	0.0684	201	0.0697	40	40
5	16.70	0.0826	013	0.0818	33	39
6	17.15	0.0870	202	0.0840	53	29
7	17.50	0.0904	104	0.0917	41	27
8	19.80	0.1147	014	0.1149	70	25
9	23.40	0.1577	015	0.1579	00	12
10	23.60	0.1600	120	0.1630	35	11.6
11	24.25	0.1687	121	0.1677	33	10.9
12	24.95	0.1780	214	0.1799	34.8	19.8
13	25.25	0.1830	205	0.1820	28	9.5
14	29.07	0.2359	206	0.2349		
15	29.97	0.2493	107	0.2475		
16	30.20	0.2530	305	0.2542		
17	31.70	0.2761	402	0.2780		
18	32.60	0.2903	320	0.2930		
19	33.95	0.3119	322	0.3126		
20	34.75	0.3257	108	0.3186		
21	36.89	0.3613	031	0.3593		



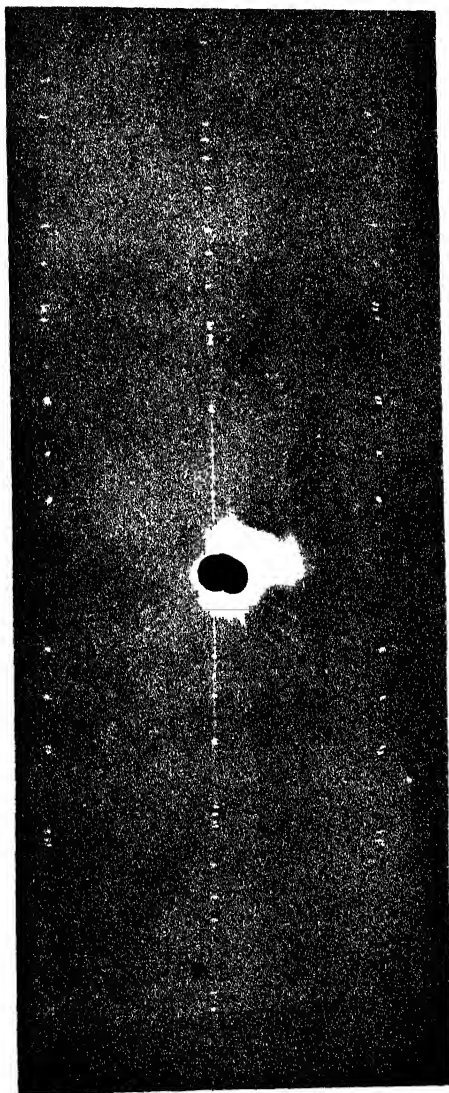


Fig. 2. The X-ray rotation photograph of sample A with  $c$  as zone axis of rotation. The layer lines are clearly shown.

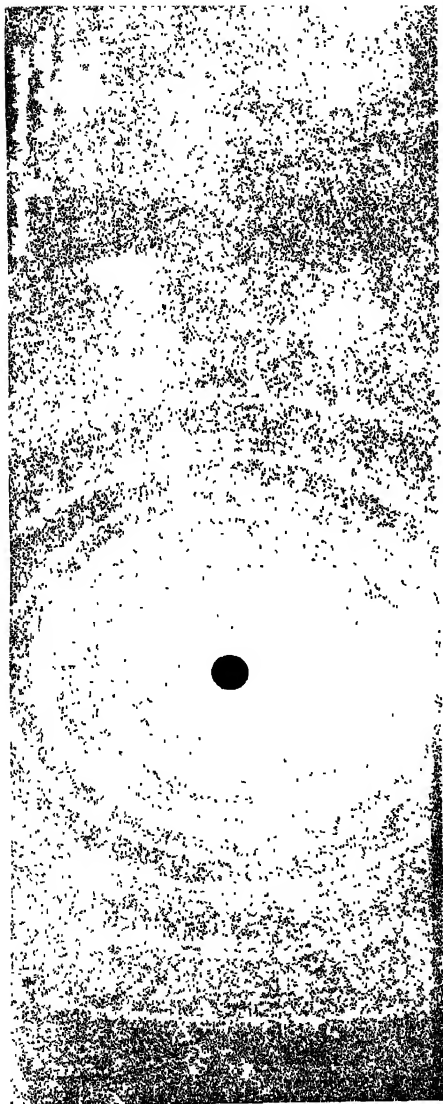


Fig. 3. The X-ray rotation photograph of sample B with  $c$  as zone axis of rotation. This shows, a polycrystalline nature of substance B.

It may be noted that odd values of  $h, k, l$  have been found. Therefore it is indicated that sample B differs in crystal structure from that of A. This has been further found true by intensity measurements. It is found that observed intensities of the lines are quite different from the calculated values, assuming it as body centered.

From the above study it is seen that the structures of samples A and B are different. Though sample B has got all external features of a single crystal, X-ray diffraction studies show that it is a poly-crystalline sample. The exact nature is not known and requires further investigation. It is pointed out that unless chemical processing for obtaining the crystals of silver fulminate is properly controlled, one may obtain an unknown poly-crystalline form whose structure may be quite different from the known body centered form. Further work for determining the space group of sample B is being undertaken.

The author is grateful to Dr. Kartar Singh, Dy. Dean of Institute of Armament Studies, Kirkee, for suggesting the problem. The author also wishes to thank Shri D. D. Mangain, SSA, for helping in the experimental work. The work was done with the cooperation of Shri W.J. John, Group Officer (Optics and X-ray) in the Physics Division of Defence Research Laboratory (Stores) Kanpur.

## R E F E R E N C E

Singh K., 1959, *Acta crystallographica* **12p.** 1053,

# A SHORT NOTE ON THE NATURE OF THE CRYSTALLINE ELECTRIC FIELD IN TRIVALENT VANADIUM ALUM

R. CHATTERJEE

MAGNETISM DEPARTMENT,

INDIAN ASSOCIATION FOR THE CULTIVATION OF SCIENCE,  
CALCUTTA-32.

(Received August 14, 1962).

Siebert's theory (1937) of magnetic susceptibility of vanadium ammonium alum, has been modified by Chakravorty (1959) who used Abragam and Pryce's Hamiltonian and wave functions. This theory is on the whole, more reasonable than the earlier and gives a much better fit with the experimental results. An empirical reduction in the value of spin-orbit coupling  $\zeta$  of about 40% from the free ion value  $+104 \text{ cm}^{-1}$  for  $\text{V}^{3+}$  has to be assumed owing to overlap of 3d-charge cloud with  $s$  and  $p$ -charge of neighbouring oxygen atoms. It appears, therefore, more reasonable to apply to the problem the more general method of the molecular orbitals. We have started with the molecular orbital for  $\text{XY}_6$  complexes, Stevens (1953) and Bosc *et al.* (1960), with the assumption that the magnetic electrons are partly in the central  $d$ -orbitals and partly in  $p$ -orbitals round the outer nuclei. Under a cubic ligand field the  $3d^2 \text{ } ^3F$  free ion ground state of  $\text{V}^{3+}$  ion, splits into a degenerate orbital triplet  $(de)'$  lying lowest and another triplet  $(de)''$  and an orbital singlet lying successively above it separated to the order of  $10^4 \text{ cm}^{-1}$ . The comparatively small trigonal component of the field now splits up each of the two triplets into a singlet and a doublet with the assumption that lowest singlet is at  $+2/3$  and upper doublet  $-1/3$ .

There is another term  ${}^3P$  arising from the same configuration  $3d^2$  for the free ion, about  $9300 \text{ cm}^{-1}$  above  ${}^3F$  (Owen 1955). So the lowest triplet state contains an admixture of  ${}^3P$  through the effective "Lande splitting factors"  $\alpha, \alpha'$  which are greater than unity for F-state ions (Abragam and Pryce, 1951). Including the three-fold spin degeneracy of each of the lowest three orbital states we get a ninth order secular determinant for spin-orbit interaction and trigonal distortion, and solving the determinant, we finally get the eigenvalues and the corresponding eigen-states. Applying the first order and second order magnetic perturbations we get the principal  $g$ -values and susceptibilities. The  $g$ -values for  $\text{V}^{3+}$  alums are not available directly from the paramagnetic resonance measurements. Zverev and Prokhorov (1958) have measured the paramagnetic resonance spectrum for vanadium corundum with structure similar to the alum, giving  $g_{||} = 1.92$ ,  $D \sim 10 \text{ cm}^{-1}$ , at  $4^\circ\text{K}$ , while calculated indirectly



## BOOK REVIEW

**MODERN MAGNETISM**--by L. F. Bates, Pp. 514. Cambridge University Press, 4th Edition, 45s. net.

Whether to a student or to a research worker on Magnetism Professor Bates's "Modern Magnetism" needs no introduction and this is its fourth edition, revised with meticulous care to make it up-to-date. Professor Bates is one of the outstanding figures in the field of Magnetism and his writings on the subject are inimitable for their lucidity and depth. Standard text books on Magnetism covering a wide range of the different aspects of the subject can indeed be counted at the fingers' end, and the present book supplies to a considerable extent the ever growing demand of the beginners as also the more advanced students in the field. Also, the research workers find it a compendium of references covering a very wide range of magnetic phenomena.

The present edition contains plenty of additions and alterations particularly, in respect of the chapters on ferromagnetism. It is, however, felt that the addition of sections on magneto-optic effects, and magnetic behaviours of semiconductors, in general, in relation to their other properties would have been very welcome. In the chapter on paramagnetic resonance some discussions on the spin-Hamiltonian representation would have made it complete.

*A. Bose*